# The Matuyama-Brunhes geomagnetic field reversal: a global and temporal perspective

Thesis submitted in accordance with the requirements of
the University of Liverpool for the degree of Doctor in Philosophy
by
Maxwell Christopher Brown

May 2008

# Abstract

Understanding the global and temporal evolution of the geomagnetic field during reversals can provide important constraints on conditions at the core-mantle boundary and on geodynamo processes. However, the behaviour of the geomagnetic field during reversals is unclear. Many palaeomagnetic studies from both volcanic and sedimentary sequences have aimed to uncover details of the reversal processes; however, a paucity of data has made robust conclusions about reversal behaviour difficult.

The model CALS7K.2 has been used to explore the possible influence of the time-varying non-dipole components of the geomagnetic field during field reversals. Results generated by the model suggest that non-dipole components could add significant structure to the field during the reversal processes. Globally, the main polarity reversal is variable in duration and rapid reversals on sub-decadal time-scales are seen for a small number of locations. The model generates variable reversal paths; however, there is a longitudinal preference for certain longitudinal paths, both spatially and, more weakly, temporally. Directional reversal features are not globally synchronous: some polarity changes finish before they start elsewhere; however, variations in intensity appear more coherent.

The Matuyama-Brunhes reversal is the most recent geomagnetic field reversal (~780 ka) and is recorded in numerous sedimentary and volcanic sequences. It provides our best chance to characterise a reversal globally. Volcanic sequences from La Palma and Guadeloupe that record the Matuyama-Brunhes boundary, possible precursors, and fluctuations in the magnetic field prior to the main polarity reversal, have been investigated. Absolute palaeointensity was determined using the microwave technique and palaeodirectional results were obtained from thermal demagnetisation. Ten flows from the twenty-nine flows studied gave reliable mean palaeointensities; however, only one of the ten flows records a transitional direction. The VDM determined from this flow is 1.9 $\pm$ 0.6 ($\pm\sigma$) x $10^{22}$ $Am^2$. Analysis of all Matuyama-Brunhes data suggests that the main directional changes occurred once the VDM was reduced below 3 x $10^{22}$ $Am^2$ (~40% of the present field value). Further comparisons with palaeointensity data compiled from all reversals younger than 20 Ma supports this conclusion; however, the lack of transitional data does not allow us to make any truly robust statements about the transitional field behaviour.

# Acknowledgement

My supervisors, John Shaw and Richard Holme, are especially thanked for their time, patience and encouragement throughout this thesis. Martin Gratton is thanked for his help with experimentation and with fieldwork on La Palma and Guadeloupe, without whom the work presented in this thesis would be much poorer. The staff and students at the Geomagnetism Laboratory are thanked for experimental assistance, scientific discussion and their friendship - John Share, John Hakes, John Piper, Ceri Davies, Neil Suttie and Andy Herries. Mimi Hill and Yuhji Yamamoto are greatly thanked for many interesting scientific discussions and help during my time at the laboratory. Edward Horncastle is thanked for his support and help regarding coding problems. Amy Chen is thanked for her help with all things to do with FORC diagrams and rock magnetism and also for making my stay at the Institute for Rock Magnetism, University of Minnesota, very enjoyable. Roman Leonhardt and Karl Fabian are thanked for their time and for providing code for IMMAB4; Monkia Korte is thanked for providing code for CALS7K.2. Leó Kristjánsson is thanked for sending me pilot samples, Iceland data sets and for general discussions on the palaeomagnetism of Iceland. Vicente Soler is acknowledged for assistance during field work on La Palma. The staff at the Institute for Rock Magnetism, University of Minnesota, are thanked for their help during my time there, especially Mike Jackson and Peat Sølheid. Cathy Constable and Mathieu Dumberry are thanked for their insightful comments on the results presented in Chapter 5.

Work presented in this thesis was supported by NERC grants NER/S/J/2004/13080 and NERC/A/S/2003/00330 and a visiting fellowship to the Institute for Rock Magnetism, University of Minnesota. The microwave instrumentation at the University of Liverpool was funded by NERC grant NE/B50572X/1. The Institute for Rock Magnetism is supported by a grant from the Instruments and Facilities program, Earth Science Division, the National Science Foundation.

I would also like to thank everybody who has taken the time to discuss my research over the last three and a half years; the sum of your help has been invaluable. Finally, I would like to thank my Mum and Dad for supporting me throughout my studies.

# Contents

# List of Figures

# List of Tables

# Abbreviations

$^{40}Ar/^{39}Ar$ - Argon-40/Argon-39

AF - Alternating Field

AGFM - Alternating Gradient Force Magnetometer

AN - Barranco (Gorge) del Aqua northern section, La Palma (also called TN (Singer et al., 2002) and LS (Quidelleur & Valet, 1996))

AS - Barranco (Gorge) del Aqua southern section, La Palma (also called TS (Singer et al., 2002) and LL (Quidelleur & Valet, 1996))

CALS7K.2 - Continuous global geomagnetic field model for the last 7000 years based on archaeomagnetic and palaeomagnetic data (Korte & Constable, 2005a)

CR - Camino Réal section, El Time, La Palma (ET section (Valet et al., 1999))

CMB - Core Mantle Boundary

D or Dec - Declination

*dm* - Confidence limit for VGP latitude

*dp* - Confidence limit for VGP longitude

FORC - First Order Reversal Curve

G - Prefix for lava flows from Guadeloupe, French West Indies

GPTS - Global Polarity Time Scale

GUFM - Continuous global geomagnetic field model from 1590 to 1990 based on historical data (Jackson et al., 2000)

$H_c$ - Coercivity

$H_{cr}$ - Remanent coercivity

I or Inc - Inclination

IMMAB4 - Continuous global geomagnetic field model based on a iterative Bayesian approach for the MB reversal (Leonhardt & Fabian, 2007)

IRM[1] - Iosthermal Remanent Magnetisation

IRM[2] - Institute for Rock Magnetism, University of Minnesota

ka - Thousand years ago

kyr - Thousand years

K/Ar - Potasium-40/Argon-40

LT - Low Temperature

Ma - Million years ago

M.A.D. - Maximum Angular Deviation

MB - Matuyama-Brunhes

MD - Multidomain

ME - Main El Time section, La Palma

MMVFTB - Magnetic Measurements Variable Field Translation Balance

MPMS - Magnetic Properties Measurement System

$M_{rs}$ - Saturation remanence

$M_s$ - Saturation magnetisation

Myr - Million years

NRM - Natural Remanent Magnetisation

OVP - Orthogonal Vector Plot

pNRM - Partial Natural Remanent Magnetisation

PSD - Pseudo Single Domain

pTRM - Partial Thermal Remanent Magnetisation

$pT_MRM$ - Microwave produced pTRM

RS - Ratio between susceptibility at -196°C and 10°C

SD - Single Domain

SP - Super Paramagnetic

SQUID - Superconducting Quatumn Interference Device

SV - Secular Variation

$T_c$ - Curie Temperature

Ti - Titanium

TM - Titanomagnetite

TRM - Thermal Remanent Magnetisation

$T_MRM$ - Microwave produced TRM

VADM - Virtual Axial Dipole Moment

VDM - Virtual Dipole Moment

VFTB - Variable Field Translation Balance

VGP - Virtual Geomagnetic Pole

VRM - Viscous Remanent Magnetisation

VSM - Vibrating Sample Magnetometer

$\alpha_{95}$ - Radius of 95 confidence cone

$\chi$ - Susceptibility

$\chi$' - In-phase AC susceptibility

$\chi$" - Quadrature AC susceptibility

$\chi'_{fd}$ - Frequency dependent susceptibility

$\kappa$ - Precision parameter

# Chapter 1

# Introduction

On 21st April 1906, at a meeting of the Société Française de Physique, Bernard Brunhes presented an important discovery concerning the magnetisation of several formations in the volcanic Massif Central, France (Laj et al., 2002). The talk was later published in November 1906 in the *Journal de Physique* under the title "Recherches sur la direction de l'aimantation des roches volcaniques" (Brunhes, 1906). It was the first study to report reversed magnetisation in natural samples and to suggest that the Earth's magnetic field had reversed in the geological past.

Brunhes followed the work of Guiseppe Folgheraiter (1894), who showed that ordinary bricks and pottery carried a strong stable remanent magnetisation that was aligned in the direction of the field in which they were baked. Following the work of Delesse in 1849 and Melloni in 1853 (who were the first to observe that certain rocks were magnetised parallel to the Earth's magnetic field (Merrill et al., 1996)) Folgheraiter suggested that recent lavas erupted from Vesuvius would have also recorded the direction of the magnetic field as they cooled. Brunhes realised that, given the magnetic stability of clays baked by lavas, if the direction of the field recorded in baked clays is different to that of the present field, then this is direction of the geomagnetic field when the lava flows were emplaced and heated the clays.

Brunhes investigated several sites of baked clays and volcanic rocks with the aid of Pierre David (Didier & Roche, 1999). At Pont Farein near Saint-Flour, Cézens, Brunhes found a Miocene outcrop of 100 m and sampled both the clay and the overlying basaltic lava flow. Three inclinations of $-69°$, $-74°$ and $-78°$ were obtained from the clay and an inclination of $-76°$ from the lava flow. This was the first reported evidence that the geomagnetic field had been reversed in the past.

Mercanton (1926a,b) realised that if the geomagnetic field had reversed in the past, then reversely magnetised rocks should be found in all parts of the world. He studied samples from Spitsbergen, Greenland, Iceland, the Faroe Islands, Mull, Jan Mayen and Australia, and found both normal and reversed magnetisation, confirming Brunhes initial observations. Around this time Motonori Matuyama (1929) studied volcanic

sequences covering the last 2 Myr from Japan, Korea and Manchuria and noticed that reversed lavas were always older than those with the normal polarity of the present field. Matuyama was the first to suggest a time sequence associated with reversely magnetised rocks. Hans Gelletich (1934) surveyed the 1.2 Ga Pilansberg dyke system in South Africa (the largest in the world). Although he performed no laboratory experiments he observed reversed remanence throughout its 100-mile length, in contrast to the surrounding normally magnetised rocks. Reversals in dyke systems were also seen in tholeiite dykes in northern England (Bruckshaw & Robertson, 1949).

The 1950s saw an impressive increase in reversal studies, providing formidable evidence for the existence of geomagnetic field reversals (Glen, 1982). However, during the 1950s there was much debate over the origin of reversely magnetised rocks. Many favoured a self-reversal mechanism in the magnetic minerals rather than global scale changes in the Earth's magnetic field.

Detailed studies in the Massif central, France, by Roche (1951, 1953, 1956, 1958) confirmed the observation of Matuyama and in addition found an alternating pattern of polarities through time. Until 1960, Roche's palaeomagnetic stratigraphy was the only correlation between a sequence of reversals of thermoremanent magnetisation and a previously defined stratigraphic column.

Similar patterns were observed in Icelandic lava sequences by Hospers (1953, 1954), and this important work stimulated Icelanders' interest in reversals (Kristjánsson, 1993). Trausti Einarsson and Thörbjorn Sigurgeirsson began systematic measurements of thousands of samples from across Iceland. In total they studied approximately 21 km of stratigraphy and found that samples were almost equally divided into normal and reversed polarities (Einarsson & Sigurgeirsson, 1955). They were the first to propose transoceanic magnetostratigraphic correlation by suggesting that their sequence could be compared with Roches's from France. Einarsson (1957) noted that the polarity observed was independent of rock type (a very important observation in the validation of geomagnetic field reversals, discussed later in this introduction), reversal duration is geologically very short (10,000 years), and that periods of stable polarity were uneven in duration: observations that appear accurate and portentous over 50 years later.

Thörbjorn Sigurgeirsson and Ari Brynjolfsson expanded on this work and began to analyse long cores (up to 600m (Kristjánsson, 1993)) in more sophisticated ways. Instead of measuring the primary remanence with a compass, they used alternating field (AF) demagnetisation to isolate the components of remanent magnetisation. The magnetometer used for this work was designed by Brynjolfsson, on Sigurgeirsson's initiative, and measured both intensity and direction of magnetic moments. Although AF treatment had been tried by Graham (1953), Brynjolfsson's initial study (Brynjolfsson, 1956) was the first to show successful isolation of stable primary remanence directions using AF demagnetisation. Both Sigurgeirsson (1957) and Brynjolfsson (1957) found gradual

changes in direction of the field between reversed and normal polarities, and noted definite paths followed by the magnetic pole during reversals. Sigurgeirsson (1957) was the first paper to describe pole paths. Brynjolfsson (1957) also noted that the magnitude of moment of the transitional rocks was about one fifth of that found in Tertiary basalts. One of the most pertinent conclusions from Brynjolfsson (1957) was: "The direction of magnetisation changes gradually from reversed to normal....The clockwise traces of the variation remind one of the present clockwise traces of the secular variation....Perhaps the similarity indicates that reversals took place during a period of 1,000-3,000 years. It is difficult to understand how such changes could be caused by some self-reversal during the cooling process or during the time passed, as we would then expect random variations in the direction of magnetism." (cf. Glen, 1982, p. 116). The work of Einarsson, Sigurgeirsson, and Brynjolfsson was pioneering, providing strong evidence for geomagnetic field reversals, and also developing new palaeomagnetic techniques, which are still used today.

Reversals were also found in sedimentary sequences at this time. Aleksei Khramov carried out extensive studies in western Turkmenistan (Khramov, 1955, 1957, 1958). Khramov was an outspoken member of a small community of Soviet scientists who believed in continental drift, and called for a palaeomagnetic correlation of sediments and a palaeomagnetic time-scale. Khramov's work and ideas were influential on the first polarity time-scales of Cox, Doell and Dalrymple in the U.S. and McDougall and Tarling in Australia, during the 1960s (Glen, 1982).

Despite this evidence, there was still skepticism about geomagnetic field reversals. The main counter-evidence was proposed by those who favoured a self-reversal mechanism within the magnetic minerals that hold the remanence. In 1951, Louis Néel (the future Nobel laureate), after inquiry by John W. Graham, proposed four theoretical self-reversal mechanisms; starting a debate that would last throughout the 1950s.

Although not known at this time, examples of self-reversals are rare in nature (Merrill et al., 1996), and have only been seen in a limited number of rarer compositions. No self-reversals have been found in magnetite, titanomagnetite or pure hematite; the three minerals that give rise to most remanent magnetisations in almost all sedimentary and igneous rocks (Glen, 1982).

Many important scientists of the time proposed theoretical mechanisms for self-reversal (Néel, 1951, 1955; Verhoogen, 1956; Uyeda, 1958) and carried out laboratory experiments (Nagata et al., 1951; Kawai, 1954; Balsley & Buddington, 1954; Uyeda, 1957). The stature of Néel, Nagata and Verhoogen, and the ideas that they proposed, gave the mechanism of self-reversal more weight than was perhaps justified, especially when the experimental data were so scant. However, this was a time of great change in Earth Sciences, and the idea that the geomagnetic field could reverse was a huge change in thinking. The idea of self-reversal provided an escape from such a massive change.

The radiometric dating of lava sequences with different polarities indicated that rocks of the same age do have the same polarity. With the development of the first land-based globally correlated geomagnetic polarity time scale (GPTS) for the last 5 Myr by Cox et al. (1963), it was shown that reversed magnetisation was a global phenomena and was not caused by a self-reversal process. With the discovery of alternating bands of reversed and normally magnetised sea floor basalts (Vine & Matthews, 1963) a GPTS could be established back to 160 Ma (e.g., Vine (1966) and Heirtzler et al. (1968)) and the idea of geomagnetic reversals was now robust. It also provided an explanation for why giant sea floor anomalies are banded parallel to the ridge axis, and was key in the understanding and development of sea-floor spreading and plate tectonics.

The development of new technologies from the 1960s onwards enabled a much greater understanding of the transitional field. Starting in the mid 1960s, development of sensitive rock magnetometers using superconducting quantum interference devices (Deaver & Goree, 1967; Goree & Fuller, 1976; Goree, 2007) allowed increasingly precise measurements of very weakly magnetised transitional samples (often not possible with astatic, induction coil spinner, or fluxgate spinner magnetometers). This greatly increased the number and the precision of palaeomagnetic measurements of the transitional field.

Our increased understanding of the present day field has also also enabled a greater understanding of the reversal process, which again has been helped enormously by the development of new technologies. The use of satellites and the development of powerful computers has allowed global modelling of the today's geomagnetic field and identification of global geomagnetic features that may persist through geological time and influence the reversal process (see Chapter 2). From 1979-1980 the MAGSAT satellite made the first precise globally distributed measurements of the vector field near the Earth and in recent years two new satellites, Ørsted (1999) and CHAMP (2000), have been launched and continue to make high resolution vector measurements (Purucker, 2007). These measurements are crucial to further our understanding of the geomagnetic field on all time scales.

The development of powerful computers also enabled the development of reversing numerical geodynamo simulations (see Chapter 2). The geodynamo being the mechanism within the Earth's interior that continually generates the geomagnetic field. It is thought that convection in the outer core is driven by thermal and compositional bouyancy sources at the inner core boundary and this drives the dynamo. The simulation of Glatzmaier & Roberts (1995) was the first three-dimensional dynamo model to produce several reversals. Since this initial simulation many groups have created their own simulations with different parameters; all far from the Earth's true regime. The continuing development of more powerful computers means that new simulations can have more Earth-like parameters (Takahashi et al., 2005). In conjuction, palaeomagnetic data, satellite data, geomagnetic field models and numerical dynamo simulations

have provided great insight into the behaviour of the geomagnetic field through time at the Earth's surface and at the core-mantle boundary.

## 1.1 Research aims

The aim of the research conducted for this Ph.D. is to further our understanding of geomagnetic field reversals through careful palaeomagnetic and rock magnetic observations, simple mathematical modelling, and basic statistical analysis. Developing a better understanding of the global temporal evolution of the geomagnetic field during reversals will provide important constraints on conditions at the core-mantle boundary and on the geodynamo processes. To characterise the behaviour of the geomagnetic field during reversals the full magnetic vector must be calculated, requiring both palaeodirectional and palaeointensity data at multiple global locations. Determining palaeodirections is relatievly easy; however, obatining palaeointensities is much more difficult and a large part of this research concentrates on obtaining high quality palaeointensity results using the microwave technique at the University of Liverpool. These results are then combined with palaeodirections obtained by thermal demagnetisation at the University of Liverpool or from published studies. Two locations that record the Matuyama-Brunhes (MB) reversal were chosen for further research: La Palma (Canary Islands) and Guadeloupe (West Indies). Field work was carried out on La Palma and Guadeloupe and a suite of samples collected. Palaeodirectional and palaeointensity results are compared with previously published data from the MB reversal and from other reversals, a simple mathematical reversal model, and a model of the MB reversal by Leonhardt & Fabian (2007). Possibly erroneous palaeointensity determinations have also been investigated through detailed rock magnetic experiments.

## 1.2 Thesis layout

The thesis can be separated into four parts: introductory chapters; a description of a simple mathematical reversal model; studies of palaeointensity, palaeodirection and rock magnetism; a statistical assessment of reversal data. The thesis ends with an overall conclusion and suggestions for further research (Chapter 8).

### 1.2.1 Introductory chapters

Chapter 2 outlines some key observations of reversals from previous palaeomagnetic studies of the MB reversal and from reversals in numerical dynamo models. Features of present day secular variation are described and linked to theories and observations of the reversing field. Chapter 3 describes sampling methods, experimental details, and techniques used for analysis of palaeomagnetic data. There are now many excellent text books which cover the basics of palaeomagnetism (Butler, 1992; Tauxe, 1998) and rock

magnetism (Dunlop & Özdemir, 1997). With the publication of the *Encyclopedia of Geomagnetism and Palaeomagnetism (Eds. D. Gubbins and E. Herrero-Bervera, Springer, 2007)* many fundamentals of geomagnetism, palaeomagnetism and rock magnetism are all comprehensively addressed, so a reiteration in this thesis of many of these principles is not necessary. Only a brief summary of the most important points is given, with the reader being referred to the above texts.

### 1.2.2 Simple mathematical reversal model

Chapter 4 describes a simple reversal model based upon CALS7K.2 (Korte & Constable, 2005a). The aim of the model is to test the possible level of complexity generated at the Earth's surface when only the most simple reversal or excursion scenarios are considered. Duration, reversal onset time, virtual geomagnetic pole paths, directional and intensity variations are all investigated and compared with published palaeomagnetic observations. The results from this research are published in Brown et al. (2007) (a reprint of this paper is enclosed in the back cover).

### 1.2.3 Palaeomagnetic studies

Chapters 5 and 6 describe detailed palaeomagnetic and rock magnetic results from La Palma (Chapter 5 and 6) and Guadeloupe (Chapter 5). Chapter 5 shows new microwave palaeointensity and thermal palaeodirectional results. In Chapter 5 palaeointensity and palaeodirectional results are compared with previous MB studies, the simple mathematical reversal model presented in Chapter 4, and a model of the Matuyama-Brunhes reversal by Leonhardt & Fabian (2007). Chapter 6 further investigates three lava flows from La Palma with possibly erroneous palaeointensity determinations. First-order reversal curves have primarily been used to assess variations in magnetic domain state on different sample scales. An attempt is made to link the results of the first-order reversal curve measurements and the palaeointensity results. Adaptations of Chapters 5 and 6 have been submitted to *Physics of the Earth and Planetary interiors* (reprints are enclosed in the back cover).

### 1.2.4 Statistical assessment of reversal data

Chapter 7 presents a statistical analysis of palaeodirection and palaeointensity data from all reversals. This chapter focuses on the relationship between palaeointensity variations and palaeodirectional variations and the transitional behaviour of virtual geomagnetic poles. MB data is highlighted and compared with data from all other reversals.

### 1.2.5 Conclusions

Chapter 8 presents the main conclusions of the thesis and are drawn from chapters 4, 5, 6 and 7. The chapter ends with ideas for future work and how the members of the

palaeomagnetic community are trying to overcome some of the problems highlighted in this thesis.

# Chapter 2

# Introduction to geomagnetic field reversals

In this chapter some key palaeomagnetic observations of the Matuyama-Brunhes (MB) reversal will be outlined. In Section 2.2, reversal theory is briefly addressed and results from numerical dynamo models are described. The final section reports some features of the today's geomagnetic field and how they may relate to polarity reversals.

## 2.1 The Matuyama-Brunhes geomagnetic field reversal

The Matuyama-Brunhes (MB) reversal is the most recent geomagnetic field reversal and is recorded in numerous sedimentary sequences and by 16 volcanic sequences at seven locations globally (Fig. 2.1 and Table A.1, Table A.2, Table A.3, Table A.4 and Table A.5). Until recently it was believed that a sequence of lavas at Tjörnes Peninsula, Iceland, recorded the MB transitional field; however, new $^{40}Ar/^{39}Ar$ dating of the flows recording transitional directions suggests that they are 862 $\pm$ 41 ka and record an excursion approximately 80 kyr before the main polarity change (B. Singer *pers comm.*).

The MB reversal provides our best chance to characterise globally a reversal. Astronomical dating, using tuned oxygen isotopes from sediments, places the main polarity change at 781 $\pm$ 2 ka in the Atlantic and at 775 $\pm$ 2 ka from cores from the Indian-Pacific-Caribbean (Tauxe et al., 1996a). A significant reduction in intensity approximately 15 kyr before the main polarity change is also recorded (Fig. 2.2a) (Hartl & Tauxe, 1996). Astronomical dates from Yamazaki & Oda (2001) from South Atlantic anoxic sediments agree with the 781 ka estimate of Tauxe et al. (1996a). They also date a number of large geomagnetic field fluctuations before the main polarity change to be between 788 ka and 795 ka. Channell et al. (2004) using Atlantic sediments south of Iceland have dated the mid-point of the reversal to be between approximately 772.5 ka and 773.5 ka, younger than the mean estimates of previous estimates; however, within the range of results obtained by Tauxe et al. (1996a): 769.9 $\pm$ 3.8 ka to 784.2 $\pm$ 19.4 ka (from 18 sites). The variations in dating could be caused by problems with the sedimen-

tary recording process and/or by real global offsets in the timing of directional changes (Coe et al., 2000; Brown et al., 2007; Leonhardt & Fabian, 2007).

$^{40}Ar/^{39}Ar$ dating of lava flows has identified features relating to the reversal process at between 776 ka and 798 ka (Singer et al., 2002; Brown et al., 2004; Coe et al., 2004a; Singer et al., 2005). $^{40}K/^{40}Ar$ dating of lava flows has identified features that could belong to the MB reversal process at between approximately 777 ka and 825 ka (Valet et al., 1999; Carlut et al., 2000; Carlut & Quidelleur, 2000; Quidelleur et al., 2002, 2003). Many flows dated by $^{40}Ar/^{39}Ar$ method record a change in direction and intensity at 795 $\pm$ 7 ka (Singer et al., 2005) (Fig. 2.2b). This fluctuation in the geomagnetic field is commonly called the MB precursor and the current data suggest that this is a real feature as it is concordant with variations recorded in sedimentary records by Hartl & Tauxe (1996) (Fig. 2.2). $^{10}Be$ records from Antarctic ice cores have also been used to calculate variations in the virtual axial dipole moment (VADM) at the time of the MB reversal. Raisbeck et al. (2006) calculated two intensity lows, one related to the main polarity change at approximately 780 ka and another at approximately 800 ka, which is again believed to be the MB precursor.

Accurate dating of both sedimentary and volcanic reversal sequences is required to correlate geomagnetic field variations globally and to constrain the core processes that generate the magnetic field (Singer et al., 2005; Leonhardt & Fabian, 2007). Fig. 2.2 demonstrates that there are still considerable inaccuracies in radiometric dating and that errors are of the same magnitude as the possible reversal duration. This makes it very difficult to correlate features globally and determine the duration of directional and intensity variations (even if the field is assumed to behave uniformally globally). This problem is compounded when the possible complexity and global non-uniformity of the field during a reversal is considered (Coe & Glen, 2004). Reversals in direction may well be offset in their onset and may vary in duration. This problem is investigated further in Chapter 4.

The MB reversal records many characteristics that have been observed in other reversals and determined from statistical analysis of multiple reversal records; the behaviour of VGP paths and clustering of VGPs being two of the most interesting and controversial. Early studies of MB sedimentary sequences from Lake Tecopa, California (Hillhouse & Cox, 1976) and the Boso Peninsula, Japan (Niitsuma, 1971) provided different VGP paths, which suggested that the field was not dipolar during the reversal. The Lake Tecopa dry sediments were re-examined by Valet et al. (1989) and a much more complex VGP path was determined, with a portion including the path determined by Niitsuma (1971). The results of Valet et al. (1989) still suggested significant non-dipole contributions to the transitional field, but highlighted the need for multiple contemporaneous records if conclusions about the geometry of the transitional field are to made. Clement (1991) analysed multiple marine sedimentary records recording the

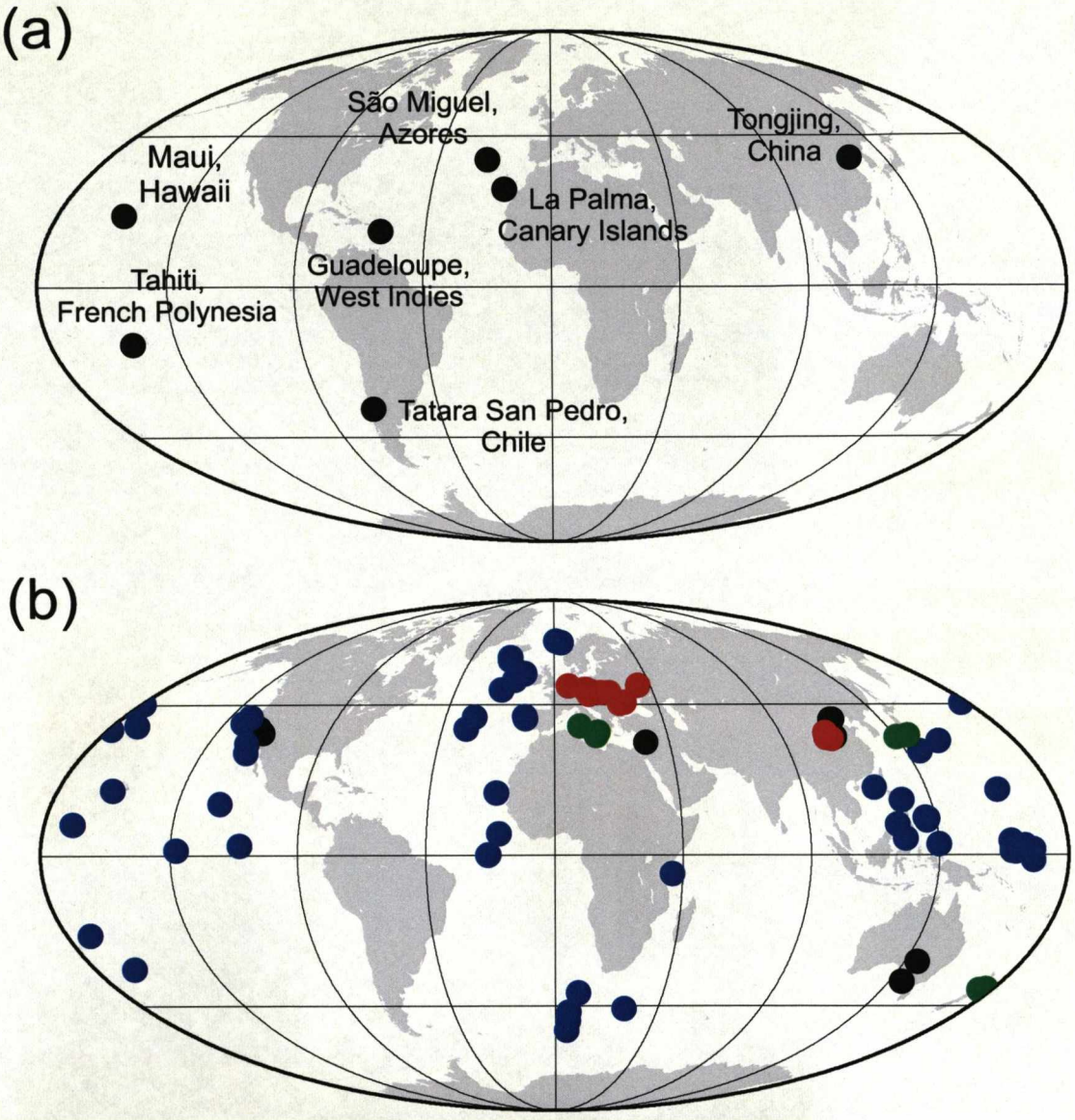


Figure 2.1: (a) Location map for lava flows that record the MB reversal. La Palma (Quidelleur & Valet, 1996; Valet et al., 1998, 1999; Quidelleur et al., 1999; Singer et al., 2002; Quidelleur et al., 2002, 2003), Guadeloupe (Carlut et al., 2000; Carlut & Quidelleur, 2000),Tahiti (Chauvin et al., 1990; Mochizuki et al., 2005), Tatara San Pedro(Brown et al., 1994, 2004; Gratton et al., 2007), Maui (Coe et al., 2004a), Tongjing (Zhu et al., 1991), São Miguel (Johnson et al., 1998). (b) Locations of sedimentary sequences recording the MB reversal. Black = lake sediments, red = loess, green = marine and blue = oceanic. Details of all locations can be found in Appendix A.

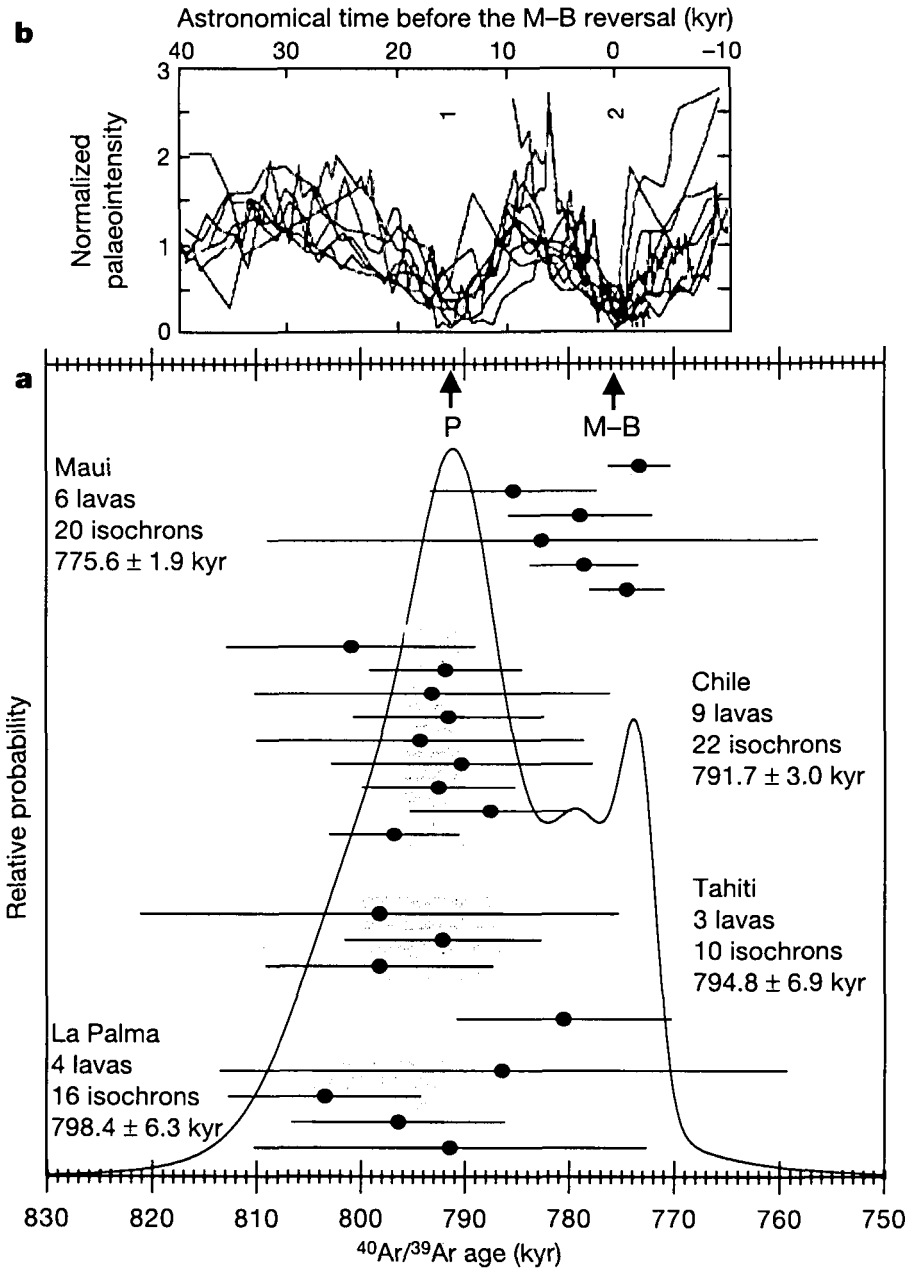


Figure 2.2: Figure from Singer et al. (2005). (a) Relative palaeointensity records from 12 marine sedimentary records (Hartl & Tauxe, 1996). (b) $^{40}Ar/^{39}Ar$ ages of 23 transitionally magnetised lava flows from La Palma, Hawaii and Tahiti. Grey bands show the weighted mean age and $\pm 2\sigma$ uncertainty for each lava sequence. The uppermost lava from La Palma is younger than the underlying four La Palma lavas but of the same age as the lavas from Maui. The probability density curve determines that the lavas span a minimum of 18 kyr. **P** indicates the time of the precursor. **M-B** indicates the time of the MB main directional reversal.

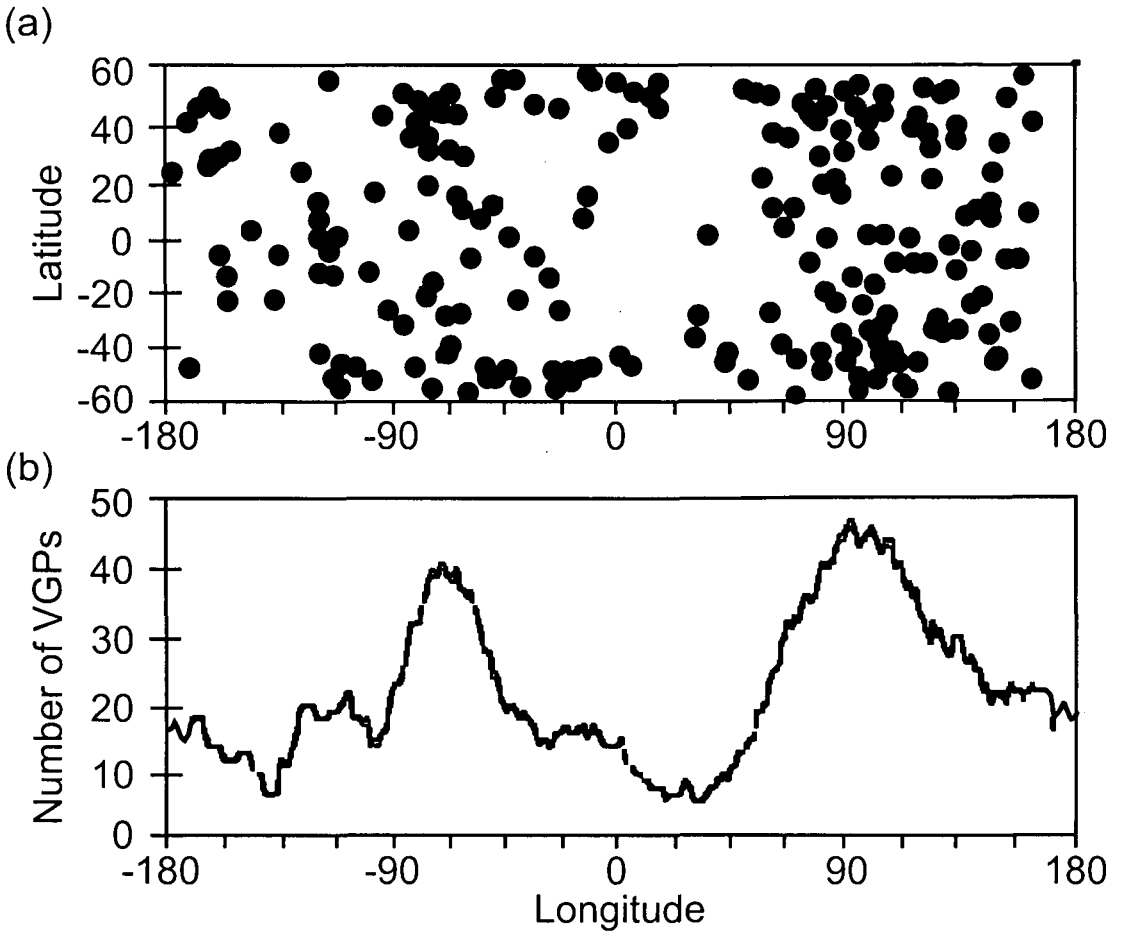


Figure 2.3: (a) Geographical distribution of MB transitional records from a selection of sedimentary records (adapted from Clement (1991)). (b) Longitudinal distribution of transitional VGPs in a sliding 30° longitude window (Clement, 1991).

MB reversal and determined that there was a bimodal distribution of VGP longitudes (Fig. 2.3), a suggestion that was supported by the statistical analysis of all MB data by Love & Mazaud (1997). There appeared to be two sets of preferred VGP paths that traced over the Americas and over East Asia/Australia. Similar results were determined from multiple records back to the Miocene (Laj et al., 1991). Analysis of all available sedimentary and volcanic data by Hoffman (2000) again showed a preference for these two paths. Love (1998, 2000) assessed all transitional VGPs obtained from volcanic sequences from the last 20 Myr and suggested that these paths persisted through this time. The idea of VGP paths is controversial, with many sedimentary records not recording such paths (e.g. Valet et al. (1992) and Prévot & Camps (1993)) and others being affected by problems with acquisition of remanence (Rochette, 1990; Valet et al., 1992; Langereis et al., 1992). The origins of preferred VGP paths are further investigated in Chapter 4 and all transitional data from volcanic sequences are statistically assessed in Chapter 7.

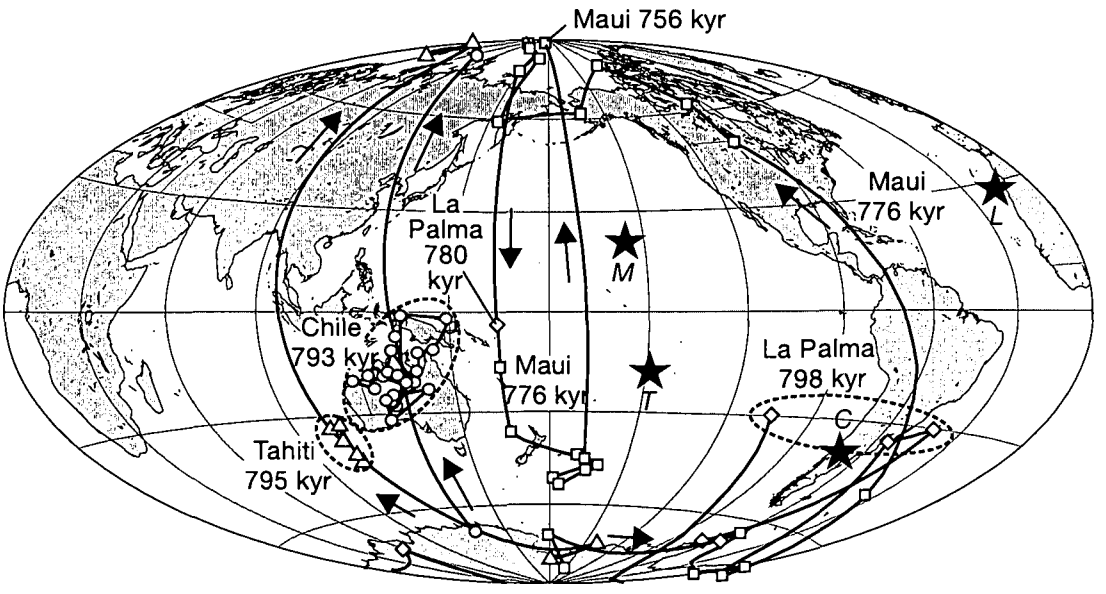


Figure 2.4: MB VGPs from La Palma ($L$) (Singer et al., 2002) (diamonds), Tahiti ($T$) (Chauvin et al., 1990) (triangles), Chile ($C$) (Brown et al., 2004) (circles) and Maui ($M$) (Coe et al., 2004a) (squares). Stars mark sample locations. Figure after Singer et al. (2005).

Another interesting observation during the MB transition is clustering of VGPs. Both sedimentary and volcanic sequences record VGP clusters over the South Atlantic and near Australia. VGP clusters are recorded in volcanic sequences from Tahiti (Chauvin et al., 1990; Singer et al., 2005) and Chile (Brown et al., 2004; Singer et al., 2005) (Fig. 2.4). More recent studies of sedimentary records (Channell & Lehman, 1997; Channell et al., 2004) have revealed very detailed records of the MB transition and show VGP clustering over north east Asia and the South Atlantic, but do not show any clustering over Australasia. Clusters are also coincident with the location of the preferred paths. VGP clusters are discussed further in Section 2.3, Section 5.4 and Chapter 7. The most detailed volcanic record to date from the MB reversal is from Maui (Coe et al., 2004a) and shows a large looping VGP path dated at 775.6 $\pm$ 1.9 ($\pm\sigma$) ka (Fig. 2.4). More specific details of individual MB reversal studies are discussed in Chapter 5.

Global modelling of the MB reversal has been attempted by Shao et al. (1999) and Leonhardt & Fabian (2007) with the IMMAB4 model of Leonhardt & Fabian (2007) being particularly impressive in its approach and its reproducibility of some features of the MB transitional field; however, as the authors note, more detailed palaeomagnetic records of transitional fields are required to gain further insight into the reversal process. Except for the palaeointensity record of Valet et al. (1999) from La Palma, only 36 flow mean palaeointensities have been determined and data are often of low quality. This research aims to provide new reliable microwave palaeointensity and ther-

mal palaeodirection data for the reversal, with the hope that subsequent models can be further improved.

## 2.2 Reversal theory and results from numerical dynamo simulations

Once established, through palaeomagnetic observations, that geomagnetic field reversals had occurred in the past, it was necessary to develop a theoretical understanding of the processes that controlled the geomagnetic field during these events. Within the theory of magnetohydrodynamics the sign of the magnetic field is not important (Merrill et al., 1995; Stevenson, 1983). The dynamo can be viewed as a "bistable" system where fields of both normal or reversed polarity states are equally probable and relatively stable (Sarson, 2007) and the sense of the field is irrelevant Gubbins & Coe (1993). The theoretical problem is to describe how and why one state changes to another and why this occurs in such an irregular way. In trying to understand this problem many important questions arise. Are reversals isolated events triggered by exceptional scenarios in the core, or are they the product of normal dynamical variations of the geodynamo? Is a fundamentally different regime of dynamo behaviour required or are reversals just a minor variation in the normal dynamo behaviour? What are the differences between the transitional field behaviour and normal field behaviour? Are the process that generate excursions the same as those that cause reversals, or are there a range of events caused by different process? To gain insight into these problems numerical dynamo models have been created to simulate how the geodynamo may behave through time.

There are a number of self-consistent, three-dimensional dynamo models that have recurring polarity reversals. Although all numerical dynamos have input parameters that are far from those of the geodynamo they still provide valuable insight into the processes that could generate and control reversals. Merrill & McFadden (1999), Dormy et al. (2000), Wicht & Olson (2004) and Sarson (2007) provide good reviews of these models. The key features from these simulations will be briefly describe here.

The model of Glatzmaier & Roberts (1995) was the first three-dimensional dynamo model to produce several reversals. Their dynamo model was very chaotic and the polarity reversals occurred at irregular intervals. In comparison, the models of Kida et al. (1997) and Wicht & Olson (2004) produced regular reversals that were almost periodic. This frequency is thought to be controlled by boundary conditions, especially boundary heterogeneity and is sensitive to the Rayleigh number of the convection (Wicht & Olson, 2004). Kutzner & Christensen (2002) found that the Rayleigh number had that greatest control on secular variation and reversal frequency. By increasing the Rayleigh number (and holding the rotation rate constant) the dynamo behaviour changes from being non-reversing and dominantly axially dipolar to a configuration no longer dominated by the dipole and more variable through time. There is an intermediate configuration in which

the dynamo will switch between these two regimes, the switches being polarity reversals. In some cases the reversals were abrupt and similar to palaeomagnetic records. In other cases the reversals happened during long periods of non-dipolar transitional field states.

Glatzmaier et al. (1999) generated a variety of reversing dynamos using different patterns of boundary heat flow heterogeneity. Coe et al. (2000) compared the surface fields from these simulations with palaeomagnetic records and concluded that some were comparable to geomagnetic reversals; however, they found that more than one type of reversal existed and not all of them were Earth like.

Sarson & Jones (1999) attributed their reversals to fluctuations in the strength of a polar upwelling plume. Wicht & Olson (2004) also identified plume upwellings as the critical fluid dynamic element in reversals. Convective upwellings in the outer core, generate magnetic upwellings that overwhelm the normal rotationally generated dipole field and cause an initial intensification of the field, seen as flux patches in equatorial areas in the tangent cylinder. The turbulent fluid motions can bend or twist toroidal field lines into poloidal field loops that have a north-south orientation. If the magnetic upwelling is strong enough, the top of the poloidal loop pierces the core-mantle boundary and creates a pair of flux patches. One flux patch is of the same polarity as the the pole in that hemisphere while the other is reversed. If the twisting causes the reversed patch to lie closer to the normal pole than the normal flux patch the dipole field will weaken (Glatzmaier & Olson, 2005). If the reversed flux patches become sufficiently intense the dipole field will then collapse, causing a reduction in the overall field strength. Gradually, the dipole will re-establish itself with an overall reversed polarity.

Takahashi et al. (2005), using one of the worlds most powerful supercomputers, the Earth Simulator, have created the most Earth-like model of the dynamo. It is the first model to run in a quasi-Taylor state, where viscosity plays a negligibly small role in the core dynamics. This was achieved by using parameters that although still far from the Earth's, they are closer than in previous simulations. Polarity reversals occurred when normal magnetic flux patches at high latitudes moved polewards and disappeared, and reversed field patches at low and mid-latitudes then moved polewards. Unlike Sarson & Jones (1999) and Wicht & Olson (2004), reversals or excursions were not generated within the tangent cylinder (an imaginary cylinder aligned with the rotation axis of the Earth in contact with the inner core at the equator).

Recent work of Aubert et al. (2008) has used Dynamical Magnetic Field line Imaging (DMFI) to represent the time evolution of relevant magnetic field lines in numerical dynamos. DMFI animations of Earth-like numerical dynamos were then used to highlight the possible field line mechanism of simulated polarity excursions and reversals. They determined that while magnetic anticyclones are responsible for the regeneration of a stable axial dipole, excursions and reversals of the dipole axis are caused by the emergence of magnetic upwellings (generated within buoyancy driven upwellings in the

outer core, but with little or no dramatic change in fluid flow (Wicht & Olson, 2004)), which amplify and transport a generally multipolar magnetic field from the inner to the outer boundary of the models.

## 2.3 Link between reversals and present day secular variation

Although the historical geomagnetic field is dominated by a stable axial dipole, there are characteristics of the secular variation that may relate to the reversal mechanism. Flux patches are seen in historical and archaeomagnetic field models (Bloxham & Gubbins, 1989; Bloxham & Jackson, 1992; Jackson et al., 2000; Korte & Constable, 2005a), often showing reversed flux spots at the core mantle boundary at mid to high latitudes. The largest concentration of locally reversed field directions at the core mantle boundary is beneath the South Atlantic, where a group of reversed flux spots extend from South Africa to South America. Other flux patches are seen at high latitudes within the tangent cylinder, where a purely geocentric axial dipole would have maximum intensity. Flux patches are also seen to vary in strength and location through time. Core field models from satellite data have also revealed changing flux spot behaviour. A comparison of the 1980 Magsat model with the 2000 Ørsted model revealed growth of several new reversed flux patches, most notably beneath the Western Atlantic near Bermuda (Hulot et al., 2002).

It has been suggested by Hoffman & Singer (2004) that clustering of VGPs observed in the reversal record are coincident with areas of the most intense vertical flux of the present day field after synthetic removal of the axial dipole component. Hoffman & Singer (2004) also calculated synthetic VGPs from the present day non-dipole field and determined that the South Atlantic and Australasia regions are preferred.

Recent observations of the geomagnetic field have recorded a decrease in its intensity. Is this decrease related to the onset of the reversal process or to normal secular variation? Gubbins et al. (2006), using the GUFM model of Jackson et al. (2000) (constrained by direct observations after 1840 of the geomagnetic field (Jonkers et al., 2003), with additional palaeointensity measurements from the database of Korte et al. (2005) for the period 1590 to 1840), assessed the variation in dipole strength from 1590 to 1990. They calculated that from 1590 to 1840 the strength decreased very gradually at approximately 2.28 nT/year (0.7% per century), but after 1840 there was a sudden increase in the change to 5% per century (using the data from Gubbins et al. (2006) it is approximately 4.7% per century). This rapid decrease in the field is attributed to growth of reversed flux patches in the Southern Hemisphere around 1780 A.D., which continue to grow and drift south. This could suggest that the recent field shows the onset of a reversal process and at the current rate of decay the exponential decay time of the axial dipole is approximately 1600 years (Wicht & Olson, 2004).

Korte & Constable (2005b, 2006) using the model CALS7K.2 (Korte & Constable, 2005a) assessed the rate of decrease of the dipole moment since its maximum value at 320 A.D. (black line, Fig. 2.5a), and calculated a fall of 1.5% per century. This is only slightly higher than the free decay rate of 1% per century. Although the present decrease at approximately 5% per century is strong, it is comparable to other decreases over the last 7000 years (Korte & Constable, 2006). Although the field at the present time is lower than at 320 A.D., it has been as low as this in the past 7000 years, with similar rates of change of the dipole moment and has not reversed (Fig. 2.5b). Korte & Constable (2006), therefore, suggest that the present decrease in the dipole field is part of normal secular variation.

## 2.4 Summary

This chapter has described some key observations of the palaeomagnetic field during the Matuyama-Brunhes reversal and some important concepts such as preferred VGP longitudes and VGP clusters have been outlined. Some features of the recent field have also been described and it has been suggested that the occurrence of present day flux patches may influence the transitional field during a reversal and cause preferred VGP paths or VGP clusters. Whether these features are a geomagnetic phenomena is currently debated and as part of the following chapters these ideas will be explored further by simple mathematical modelling (Chapter 4), showing new palaeomagnetic data for the MB reversal (Chapter 5) and by creating and assessing a global data base of reversal studies (Chapter 7).

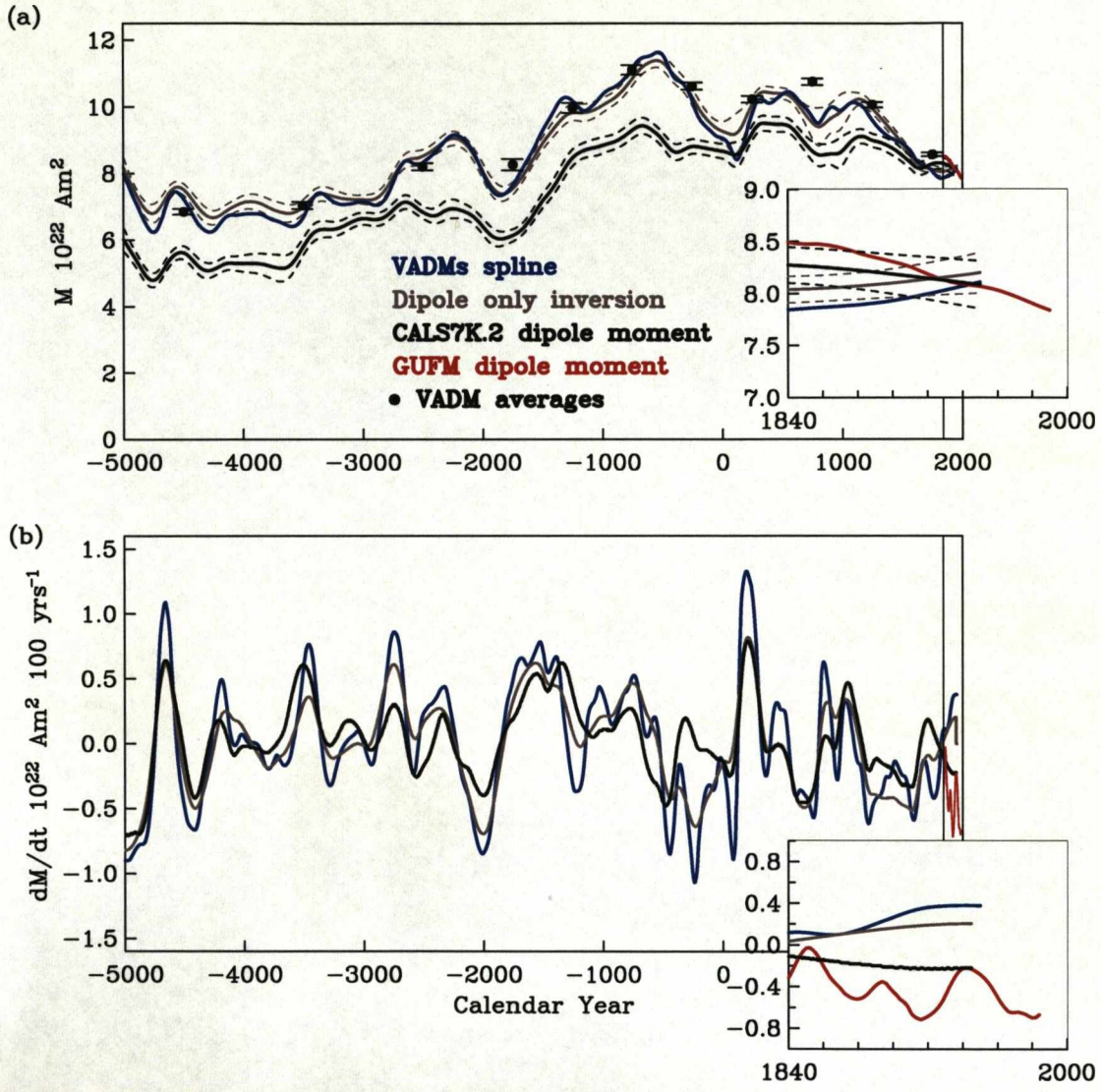


Figure 2.5: From Korte & Constable (2006). (a) Dipole moment estimates (M) and (b) their rates of change for the past 7000 yr obtained from the same data by different methods: average VADMs (black dots) and a weighted spline fit (blue line); a spherical harmonic inversion of intensity and directional data for a dipole-only (grey line); dipole moment estimate from CALS7K.2 (Korte & Constable, 2005a) (black line) and in the expanded right-hand part also from the historical model GUFM (Jackson et al., 2000) (red).

# Chapter 3

# Methodology

This chapter describes all field and laboratory methods. Rock magnetic methods, palaeodirection determination and the microwave absolute palaeointensity technique are all described along with details of the methods used to analyse the data.

## 3.1 Sampling techniques and sample preparation

Field work in Guadeloupe was undertaken in March 2005 by Martin Gratton and the author. Field work was carried out on La Palma in March 2006 by Martin Gratton, Vicente Soler and the author. Details specific to individual studies are given Chapter 5. The initial stage of the field work was reconnaissance. Geological notes and sketches were made of all lava flows and stratigraphies were established. Global Positioning System (GPS) coordinates and altitude measurements were taken using two hand held systems. Where previous studies had been made on the same sections core holes were also noted. Photos of the main sections can be found in Appendix B.

A STIHL BT 45 drill adapted by John Shaw with attached water pump was used to drill sample holes. Care was taken to apply a constant water supply, so not to heat the samples and remagnetise them in anyway. 25 mm cylindrical cores were encircled using a diamond tipped drill bit in a non-magnetic matrix. Samples were oriented both magnetically and with a suncompass. Y-east of true north (YETN) and the dip of the core were recorded (Fig. 3.1). Samples were gently extracted using an aluminium nail. They were then scored and marked with black pen. Photographs were taken of all sampled flows and sample holes were labelled. Spacing between sample holes and their height from the base of the flows were measured. Any notes from previous studies were adhered to. At least three cores were extracted per flow.

In the laboratory, 25 mm cores were sliced into ~25 mm long cylinders (Fig. 3.2). The different 25 mm cores were labelled a, b, c, etc, depending on the length of the original core. The tops of all the cores were removed and were not used for any experiments in case any surface weathering had caused low-temperature oxidation of the sample and production of a chemical remanent magnetisation. The bottoms of the cores were also

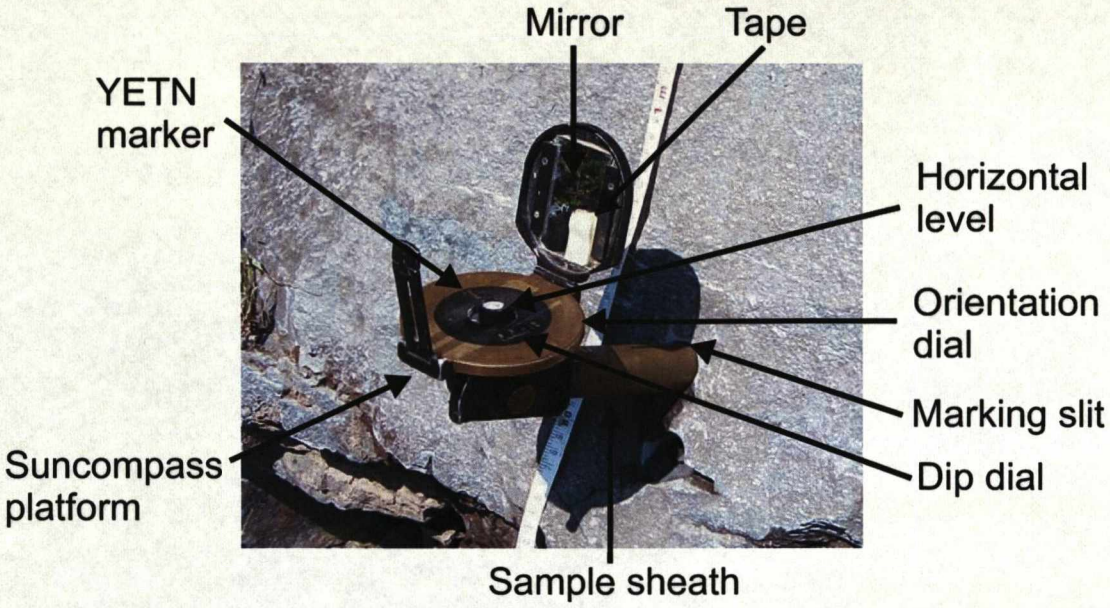


Figure 3.1: Suncompass. The sample sheath is placed over the sample in the gap removed by the drill bit. The suncompass is made horizontal with the aid of the horizontal level. The dip of the sample is then recorded. A mirror is attached to the orientation dial and the dial is rotated until the contrast between the reflection and shadow caused by the tape is maximised. The YETN is then recorded. The sample is marked with copper wire in the marking slit.

removed and were suitable for further experimentation. Bottoms of cores have the suffix BOT. 25 mm cores were used for thermal demagnetisation. 5 mm cylindrical samples were drilled in a zero field at the Geomagnetism Laboratory, University of Liverpool. 5 mm cylindrical cores were encircled using a diamond tipped drill bit in a non-magnetic matrix and examples are shown in Fig. 3.2. All rock magnetic and palaeointensity experiments used 5 mm cores.

## 3.2 Rock-magnetic techniques

A number of magnetic property measurements were made to evaluate samples suitability for palaeointensity experiments and to identify those samples which might be expected to give the most accurate palaeomagnetic results. Multiple measurements were made on 5 mm sub-samples from 25 mm cores and from multiple 25 mm cores per flows. All samples were weighed so that absolute magnetisations could be calculated.

### 3.2.1 Hysteresis, isothermal remanent magnetisation and back field coercivity measurements

Hysteresis and back field coercivity measurements were carried out on a Variable Field Translation Balance (MMVFTB) at the University of Liverpool and on a Princeton


Figure 3.2: (a) 25 mm core samples with 5 mm sub-samples extracted. (b) Examples of 5 mm sub-samples.

Measurement Corporation MicroMag 2900 vibrating sample magnetometer (VSM) at the Institute for Rock Magnetism, University of Minnesota. Hysteresis measurements made using the VFTB used a maximum field of 0.75 T and measurements made using the VSM used a maximum field of 1.5 T.

Various diagnostic rock magnetic parameters can be calculated from hysteresis loops (Fig. 3.3). High field susceptibility, $\chi_{hf}$, is the gradient of the closed linear part of the loop at high fields and is a measure of the paramagnetic component of a sample. Saturation magnetisation, $M_s$, is the maximum magnetisation obtained in response to the applied field. To remove the paramagnetic contribution $\chi_{hf}$ is extended back to the $H = 0$ axis and this intersection is $M_s$. $M_{rs}$ is the magnetisation that the sample retains in a zero field once the saturating field is removed and is a measure of magnetisation at $H = 0$. The coercive force, $H_c$, is a measure of the ease at which particles can be magnetised in a new direction. It is defined as the field required to reduce the magnetisation (in field) from saturation to zero. Multi domain (MD) particles require only a small applied field to drive the MD domain walls back to a zero moment position, so the coercive force of MD particles is small. The field required to reverse single domain (SD) particles' moments to zero is much greater (≈300mT for elongate SD magnetite (Butler, 1992)). $H_{cr}$ is the coercivity of remanence and is the reverse field required to remove any net remanence of the sample after it has been saturated. The low field susceptibility, $\chi_{lf}$, is the gradient of the reversible part of the magnetisation, for a demagnetised sample, taken through the origin.

Hysteresis parameters are used to determine bulk magnetic domain state. Ratios of $M_{rs}/M_s$ and $H_{cr}/H_c$ are plotted as a Day et al. plot (Day et al., 1977). Different regions of the Day et al. plot delimit SD, pseudo-single domain (PSD) and MD bulk domain states. For SD particles, when the applied field is reduced to zero after saturation, the magnetisation of each SD grain rotates to the nearest easy direction.

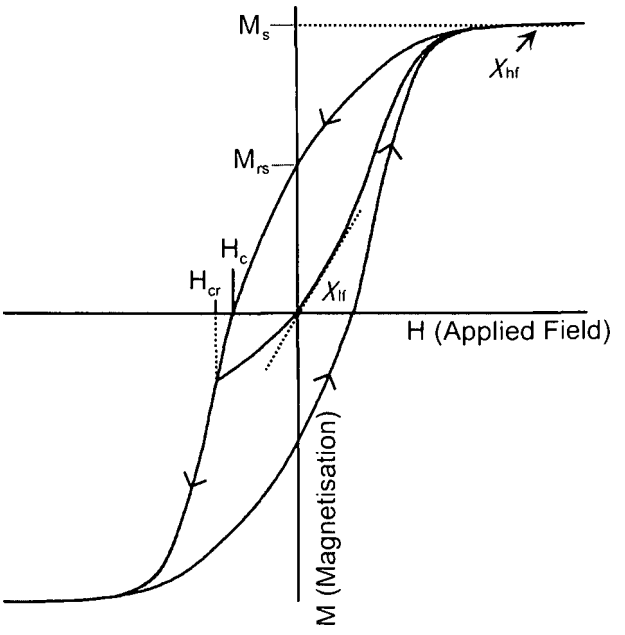


Figure 3.3: Hysteresis loop for randomly oriented SD or MD particles. Calculated parameters from hysteresis loops include the saturation magnetisation, $M_s$, the saturation remanent magnetisation ,$M_{rs}$, the coercive force, $H_c$, the coercivity of remanence, $H_{cr}$, the high field susceptibility $\chi_{hf}$ and the low field susceptibility $\chi_{lf}$.

For uniaxial SD particles $M_{rs}/M_s \geq 0.5$ (Dunlop & Özdemir, 1997) and $H_{cr}/H_c \leq 2$ Dunlop (2002). When a field is applied to MD particles domain walls are destroyed and the magnetisation reaches saturation. Domains re-form on the removal of the applied field, but because of lattice imperfections and internal strains domain wall energy is a function of position. Domain walls therefore do not return to their original position but settle in energy minima near their initial positions. This results in a small remanent magnetisation. Ideal MD particles have $M_{rs}/M_s \leq 0.05$ (Dunlop & Özdemir, 1997) and $H_{cr}/H_c \geq 5$ (Dunlop, 2002). $M_{rs}/M_s$ and $H_{cr}/H_c$ particle size boundaries from (Dunlop, 2002) are plotted on all Day et al. plots shown in this thesis. The majority of natural samples plot in a broad transitional area of the Day et al. plot, between SD and MD, which is attributed to pseudo-single domain (PSD) behaviour. The reasons for this behaviour are numerous and discussed well in the literature (Dunlop & Özdemir, 1997; Dunlop, 2002). Possible explanations include SD-like moments in larger MD particles caused by dislocations or surface defects such as vortex structures (Krása & Fabian, 2007), mixtures of SD and MD particles (Dunlop, 2002; Carter-Stiglitz et al., 2001), and mixtures of SD and superparamagnetic (SP) particles (Tauxe et al., 1996b), as well as particles that are PSD. In addition, the hysteresis experiments of Day et al. (1977) were performed on crushed magnetic particles which behave differently to un-crushed particles, so the grain size delimitations on the Day et al. plot may not apply to many

natural samples (Tauxe et al., 2002).

Hysteresis parameters can also be plotted as $M_{rs}/M_s$ against $H_c$, as a so called Tauxe plot (Tauxe et al., 2002). It was noted by Nagata (1953) that $H_c$ varies linearly with $M_{rs}/M_s$ for igneous rocks. The relationship between $M_{rs}/M_s$ and $H_c$ does not give independent grain size information as the slope is strongly dependent on $M_s$ and therefore the samples mineralogy (Wasilewski, 1973). The inclusion of $H_{cr}/H_c$ on the Day et al. (1977) plot is to define grain size distributions that are independent of composition. Plots of $M_{rs}/M_s$ against $H_c$ are therefore useful to determine different compositional trends and the gradient of the linear relationship being diagnostic of different compositions (Wang et al., 2004). It can also distinguish magnetic particles with different sizes and shapes (Tauxe et al., 2002).

It is noted that accurate determinations of $M_{rs}/M_s$ require full saturation at the highest applied field. Fabian (2006) determined, using his approach to saturation analysis, that young mid-ocean basalts with variable ülvospinel content did not reach full saturation in many samples when a field of 1 T was applied. This led to an underestimation of $M_s$ and an overestimation of $M_{rs}/M_s$. Approach to saturation analysis has not been carried out as part of this research, so caution is warranted over the accuracy of all $M_{rs}/M_s$ determinations, especially as different maximum applied fields were used for VFTB and VSM measurements.

Isothermal remanent magnetisation (IRM) measurements were made using the VTFB. An IRM is acquired by applying a pulsed direct field and particles with coercivities less than the applied field become magnetised in the applied field direction. An applied field of 0.75 T was chosen for all experiments. The gradient of the IRM acquisition curve can be diagnostic of domain state and magnetic mineralogy. MD magnetite will saturate at a lower field than SD magnetite. The maximum saturation field for magnetite is 300 mT. For haematite saturation occurs at higher fields (Dunlop & Özdemir, 1997). Backfield coercivity measurements were made using the VFTB and the VSM after the hysteresis measurement had finished. $H_{cr}$ is determined at the backfield from which the saturation remanence is reduced to zero.

### 3.2.2 First-order reversal curves

First-order reversal curves (FORC) (Mayergoyz, 1986), represented as a two-dimensional FORC diagram (Pike et al., 1999), allow analysis of the statistical distribution of both coercivities, $H_c$, and bias fields (switching fields), $H_u$. FORC measurements were performed on selected 5 mm samples (explicitly described in text) and were measured using a Princeton Measurements Corporation MicroMag 2900 VSM or alternating gradient force magnetometer (AGFM) at the Institute for Rock Magnetism, University of Minnesota. FORC diagrams were obtained from partial hysteresis curves using a maximum field of 300 mT, with 1 mT incremental field step between partial hysteresis curves and

an averaging time of 100 ms. The range of $H_a$ and $H_b$ (Fig. 3.4) and the number of curves varied for each sample; however, as the field step used in each experiment was the same, the resolution of each diagram was also the same. This allowed a consistent comparison of FORC diagrams.

The FORC measurement starts by applying user-defined high positive field. The field is then decreased to a reversed field, $H_a$ (Fig. 3.4a). The induced magnetisation is measured at defined fields, $H_b$, as the applied field is increased back to the user defined high positive field. A set of FORCs is obtained by repeating the process for increasing values of $H_a$ (Fig. 3.4b) . Each magnetisation measurement is denoted as $M(H_a, H_b)$ (Fig. 3.4a), where $H_b > H_a$. The FORC distribution $\rho(H_a, H_b)$ is defined as the mixed second derivative:

$$\rho(H_a, H_b) = -\frac{1}{2}\frac{\partial^2 M(H_a, H_b)}{\partial H_a \partial H_b} \tag{3.1}$$

A FORC diagram is a contour plot of the FORC distribution on a transformed coordinate system: $H_c = (H_b - H_a)/2$ and $H_u = (H_b + H_a)/2$ (Fig. 3.4d). All FORC distributions were calculated using the FORCLAB MATLAB code (Winklhofer & Zamanyi, 2006). $H_b > H_a$, therefore, $H_c > 0$, and a FORC diagram is confined to the right-hand half plane. An isolated particle with a constant field applied along the easy axis of magnetisation and with a switching field, $H_{sw}$, contributes to a FORC distribution at $\{H_c = H_{sw}, H_u = 0\}$ (Fig. 3.4e). When placed in a constant local interaction field, $H_{int}$, parallel to the applied field the particle contributes to the FORC distribution at $\{H_c = H_{sw}, H_u = H_{int}\}$ (Fig. 3.4f).

Plotting the raw distribution of $\rho(H_a, H_b)$ produces a very noisy FORC diagram. It is therefore necessary to smooth the data. As field increments are equal all data are equally spaced in the $\{H_a, H_b\}$ coordinate system (Fig. 3.4d). To evaluate the point at the centre of a square grid (e.g. Fig. 3.4d), the magnetisation at each point on the grid is fitted using a polynomial surface of the form: $a_1 + a_s H_2 + a_3 H_a^2 + a_4 H_b + a_5 H_b^2 + a_6 H_a H_b$, where $-a_6$ represents $\rho(H_a, H_b)$ at the centre of the grid. The grid size can be changed, with increasing points causing a greater smoothing of the data. A smoothing factor (SF) is used to define the level of smoothing, where the number of points = $(2SF+1)^2$. Individual smoothing factors are shown on the FORC diagrams. The smoothing factor is not important in this study as the field steps used for each sample are the same.

### 3.2.3 Thermomagnetic measurements

Thermomagnetic measurements were carried out in air using a Magnetic Measurements variable field translation balance (VFTB) at the Geomagnetism Laboratory, University of Liverpool. Magnetisation in an applied field of 0.75 T was measured as temperature was increased from room temperature to 700°C and then allowed to cool back to room temperature.

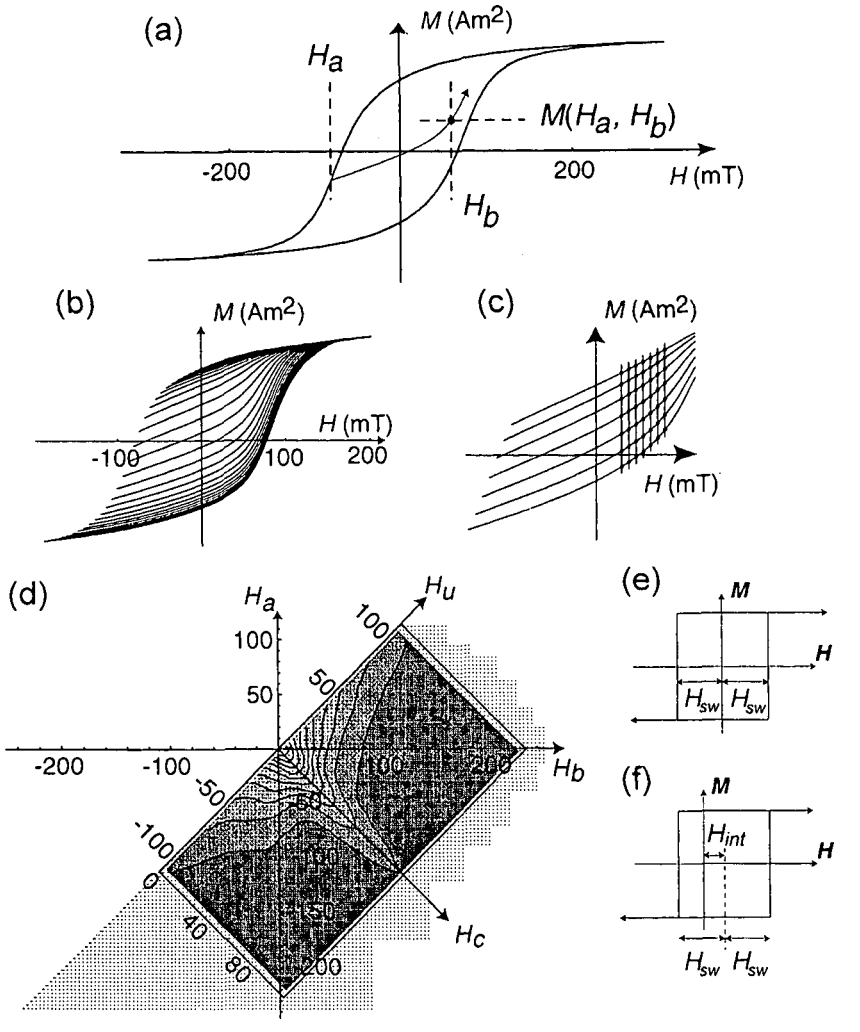


Figure 3.4: From Roberts et al. (2000). Illustration of construction and interpretation of a FORC diagram. (a) A major hysteresis loop with reversal point at $H_a$ and magnetisation point $M(H_a, H_b)$. (b) Example of a set of FORCs. (c) A subset of FORCs from Fig. 3.4b. Dots represent a 7 x 7 array of equally spaced points in $H_a$ and $H_b$, corresponding to a smoothing factor of 3. (d) FORC distribution plotted in $\{H_a, H_b\}$ coordinate system, with transformed coordinate system $\{H_c, H_b\}$ superimposed. (e) Hysteresis loop for an isolated SD particle, with a field applied along along the easy axis of magnetisation. $H_{sw}$ is the switching field for the particle. (f) Hysteresis loop for the same SD particle with a constant location interaction field acting parallel to the applied field and magnetic easy axis of the the grain. $H_{int}$ is a constant local interaction field.

All thermomagnetic curves are corrected for their paramagnetic content, calculated from hysteresis measurements on the same sample prior to heating using the VFTB. Curie temperature is determined using the extrapolation method (Moskowitz, 1981). Curie temperatures can be used to determine the composition of the magnetic minerals within the sample. The titanium content of the titanomagnetite is estimated using a polynomial fit to experimental data for synthetic titanomagnetites (Bleil & Petersen, 1982). This approach only allows rough estimates of the composition of natural titanomagnetites, with uncertainties of $\pm$ 0.1 for the mole fraction of the ülvospinel end-member. This uncertainty comes from variations in Curie temperature determined from synthetic titanomagnetites with the same apparent composition (Lattard et al., 2006).

Thermomagnetic curves can also assess the amount of alteration (caused by oxidation of the magnetic minerals on heating in the laboratory) of the sample and whether inversion of titanomaghemite to titanomagnetite has occurred (Dunlop & Özdemir, 1997). As experiments have been performed in air and not in a vacuum or reduced environment, it is difficult to distinguish inversion from oxidation during laboratory heating for samples with a low Curie Temperature, as an increase in induced magnetisation will occur on cooling (Dunlop & Özdemir, 1997). The amount of irreversibility has been assessed by calculating the percentage difference in induced magnetisation between the heating and cooling curves at 100°C. All data determined from thermomagnetic experiments can be found in Appendix C.

### 3.2.4 Low-temperature measurements

Low temperature susceptibility was measured on a small number of samples using a Quantum Design MPMS susceptometer or a Lakeshore susceptometer at the Institute for Rock Magnetism, University of Minnesota. Experiments conducted on the MPMS measured in-phase ($\chi'$) and quadrature ($\chi''$) AC susceptibilities while increasing temperature from 5 K to 300 K at 5 frequencies (1, 5.6, 31.6, 177.6 and 997.3 Hz) and at 239 A/m. Measurement made on the Lakeshore measured in-phase ($\chi'$) and quadrature ($\chi''$) AC susceptibilities while increasing temperature from 20 K to 300 K at 5 frequencies (40, 140, 400, 1000 and 4000 Hz) and at 200 A/m. Multiple samples per flow were measured on a Bartington MS2 susceptibility meter at the Geomagnetism Laboratory, University of Liverpool, which operates at 465Hz. 1 mm x 5 mm discs of the cores were placed in liquid nitrogen for twenty minutes and then removed from the liquid nitrogen and allowed to heat up in the ambient conditions of the laboratory while susceptibility was continuously measured. Discs were made thin to minimise the temperature lag between the sample and the thermocouple. Each sample was wrapped in blue tack and marked along its long axis, so that the sample can be reoriented between the two stages of measurement: the initial room temperature measurement and measurement during

warming. This precaution was taken in case the sample was magnetically anisotropic.

The temperature dependence of magnetic susceptibility can be diagnostic of titanomagnetite composition (Moskowitz et al., 1998; Carter-Stiglitz et al., 2006; Yamamoto, 2006) and can indicate whether low temperature oxidation has occurred in nature (Özdemir et al., 1993; Cui et al., 1994; Dunlop & Özdemir, 1997) due to the suppression of the Verwey transition (Verwey, 1939). The susceptibility of MD or equidimensional SD particles is dependent upon magnetocrystalline anisotropy, and exhibit abrupt changes in susceptibility around the Verwey transition (Özdemir et al., 1993). For magnetite the Verwey transition has been reported to be between 110 to 120 K and is the temperature at which magnetite undergoes a first-order crystallographic transition from an inverse cubic spinel structure to monoclinic symmetry. Oxidation depresses, broadens and can totally suppresses the susceptibility peak. Particle size in does not appear to be a factor: smaller particles are more susceptible to surface oxidation resulting in an apparent particle size dependence (Özdemir et al., 1993). Variations in composition also affect the position of the Verwey transition, and for titanomagnetite ($Fe_{3-x}Ti_xO_4$) where x > 0.04 (i.e. TM04) then the Verwey transition no longer exists (Moskowitz et al., 1998); however, isotropic points still exist over the whole compositional range ( x < 0.6) for naturally occurring titanomagnetites (Radhakrishnamurty & Likhite, 1993; Moskowitz et al., 1998).

The ratio of susceptibility at 77K (the temperature of liquid nitrogen) to susceptibility at room temperature is defined as the RS value (Radhakrishnamurty et al., 1977) and has been calculated for all samples (see Appendix C). For purely paramagnetic material the maximum RS value is 3.5. If RS values are higher than 3.5, this indicates a magnetic mineral such as titanohematite is present with a Curie temperature between 77 K and room temperature. SD particles are dominated by shape anisotropy, which is not strongly temperature dependent and only small changes are expected between room and liquid nitrogen temperatures; however, MD particles are dominated by magnetocystalline anisotropy and susceptibility decreases as temperature decreases. RS values are considered to increase in response to decreasing magnetic particle size (Thomas, 1993).

The frequency dependence of susceptibility can indicate super-paramagnetic (SP) contributions (Mullins & Tite, 1973; Dearing et al., 1996; Worm & Jackson, 1999) or can show possible particle size variations, which could be related to the degree of high-temperature oxidation (Yamamoto, 2006). Frequency dependence can be calculated using

$$\chi_{fd} = \frac{\chi_{lf} - \chi_{hf}}{\chi_{lf}} \tag{3.2}$$

where $\chi_{lf}$ is the susceptibility at the lowest frequency and $\chi_{hf}$ is the susceptibility at highest frequency. However, it is difficult to decompose the frequency dependence of susceptibility signal and results are often difficult to interpret.

## 3.3 Thermal demagnetisation and directional data analysis

Thermal demagnetisation was used to obtain palaeodirections from 25 mm samples. A Magnetic Measurements thermal demagnetiser was used to demagnetise the samples and magnetic measurements were made using a Molspin spinner magnetometer. Samples were demagnetised in 50°C steps up to 500°C and then in 20°C steps until the remanent magnetisation was lost.

All data were analysed using PLOTCORE by Alan McCormack. Palaeodirections were determined using principal component analysis. Orthogonal vector plots (OVP) (or Zijderveld plots Zijderveld (1967)) are used to illustrate changes in the magnetic vector with increasing demagnetisation. OVPs use a projection to represent orthogonal vertical and horizontal planes. The intensity of the vector is related to the distance from the origin with the demagnetisation of a single component of magnetisation producing a linear trend towards the origin on both planes of projection. If there is more than one component of magnetisation then there will be the equivalent number of linear segments on the OVP. If the components comprise magnetic particles with discrete blocking temperature spectra then the distinction between the different components will be sharp. If the spectra of different components overlap then there will be a smoother variation between the linear sections. The isolation of the individual linear components allows a best-fit direction to be determined for each of the components of magnetisation and the maximum angular deviation (M.A.D.) (Kirschvink, 1980) is used to assess the accuracy of the best fit. Directional data can also be plotted on a stereonet, with declination values on the circumference and inclination data along the radius. Individual components of magnetisation are seen as clusters of points on the stereonet.

Fisher statistics (Fisher, 1953) were used to determine the mean palaeodirection for a flow. To assess the dispersion of the individual results, both $\kappa$ and $\alpha_{95}$ were calculated. $\kappa$ is the precision parameter, where $\kappa = 0$ implies random grouping, and $\kappa = \infty$ indicates no dispersion. $\alpha_{95}$ is the angle from the true mean within which 95% of directions lie. The minimum acceptance for a site mean is generally regarded as $\kappa > 30$ and $\alpha_{95} < 15$ (Butler, 1992). Fisher statistics were calculated by FISH95 by Alan McCormack.

Virtual geomagnetic poles (VGP) have been calculated using equations from Butler (1992) (page 122). The circular confidence limit $\alpha_{95}$ has been transformed in to an ellipse of confidence about the VGP. The angular length of the semi-axis of the ellipse along the site to pole great circle, *dp*, and the semi-axis of the ellipse perpendicular to the great circle, *dm*, have been calculated using equations from Butler (1992) (pages 231-232).

## 3.4 Absolute palaeointensity determination

All palaeointensity determinations have been made using the microwave technique. Detailed descriptions of the microwave equipment and methodology can be found in Hill (2000) and Gratton (2004), so only brief outlines of the general theory, equipment and protocols used are given here. The acceptability criteria for all palaeointensity results shown in this thesis are described at the end of this section.

### 3.4.1 Basic microwave theory

The microwave method is an alternative to thermal techniques and can substantially limit thermochemical alteration of magnetic particles during experimentation; such alteration is the main reason for the failure of palaeointensity experiments with thermal techniques such as the Thellier (Thellier & Thellier, 1959; Coe, 1967a) and Shaw techniques (Shaw, 1974a; Rolph & Shaw, 1985). Thermal methods involve bulk heating samples, creating phonons (lattice vibrations) that then generate magnons (electron spin waves) causing the magnetic particles to demagnetise in a zero field. The microwave procedure does not use bulk heating of the sample matrix, but instead uses high-frequency microwaves that are resonant with the magnetic particles exciting the magnons within those particles directly (Walton, 2002, 2004a,b; Walton et al., 2004). It has been shown by Hill et al. (2002) and Biggin et al. (2007b) that in most cases where both methods are successful, microwave-thermoremanent magnetisation ($T_M$RM) is equivalent to conventional thermoremanent magnetisation (TRM).

### 3.4.2 Microwave equipment

From January 2007, two 14 GHz microwave systems with 80 W microwave amplifiers have been in operation at the Geomagnetism Laboratory, University of Liverpool: one with a liquid-nitrogen FIT SQUID magnetometer and another with a more sensitive three axis liquid-helium Tristan Technologies SQUID magnetometer. The two systems have different microwave resonant cavities and both have programmable field coils (up to 100 $\mu$T) surrounding the microwave cavity and a microwave TRM ($T_M$RM) can be induced in any specified direction. Both systems are semi-automated and computer controlled. The microwave cavity is tuned by computer (fine tuning can be done by hand with the 14 GHz microwave system with F.I.T. SQUID magnetometer) and the power into the cavity and reflected out of the cavity is monitored. A calculation is made for the total energy imparted into the cavity and is displayed graphically during the experiment. More specific details of the two systems are described below.

### 14 GHz microwave system with F.I.T. SQUID magnetometer

This system has a horizontal design (Fig. 3.5a). The sample is moved between the load position, the resonant microwave cavity and the magnetometer by a set of air-rams. Microwaves are generated at ~14 GHz by a Hewlett -Packard 8673M synthesised signal generator (operational range, 2-18 GHz) and amplified via a custom built set of solid state Microwave Amplifiers Ltd. 80W microwave amplifiers (operational range between 13.5 - 14.5 GHz). Microwaves are directed into the cavity by a vertical waveguide. A mu-metal shield encloses the waveguide, microwave resonant cavity, field coils, and magnetometer. During the experiment the sample remains in the zero field mu-metal shield.

The magnetometer used in this system is a "high" temperature liquid nitrogen F.I.T. SQUID magnetometer, with sensitivity of 13 $\pm$ 10 x $10^{-10}$ $Am^2$. This magnetometer uses a loop that super-conducts around 77 K (liquid nitrogen temperature). When a magnetised sample is placed in this loop a constant current is induced which is proportional to the magnetic moment along the loop axis. In this magnetometer the loop is oriented at 45° to the rotation axis of the sample (Shaw et al., 1984) and the total magnetic moment is measured by rotating the sample 360° and measuring the moment every 90°. This rotation and measurement is computer controlled. Before the experiment a background field measurement is taken to remove any small background field effects.

Positioning of the sample in the magnetometer is critical because of the 45° SQUID setup. The sample should be 8 mm from the magnetometer sensor in the horizontal direction (details of this calibration are in Gratton (2004)). The sample is correctly positioned at the beginning of the experiment. After the sample rod is loaded, the air ram moves the sample rod to the measuring position, the sample rod is gently pushed into the system until it touches the casing of the magnetometer and a marker ring is tightened on the sample rod at the end of the sample carriage sheath. The sample rod is then moved back, and a ring 8mm long that lies over the sample carriage sheath is then moved on to the sample rod so that it abuts the sample carriage sheath. The sample rod is pushed in again until the marker ring touches the 8mm long ring. The sample now lies 8 mm from the magnetometer sensor.

### 14 GHz microwave system with Tristan Technologies SQUID magnetometer

This system has a vertical design (Fig. 3.5b). The sample is moved vertically by a step-motor controlled by a computer. Microwaves are generated at ~14 GHz by MG3692B 20GHz synthesised signal generator and again amplified via a custom built set of solid state Microwave Amplifiers Ltd. 80W microwave amplifiers (operational range between 13.5 - 14.5 GHz). These amplifiers are of the same design as those used in the other 14 GHz microwave system. Microwaves are directed into the cavity by a vertical waveguide.

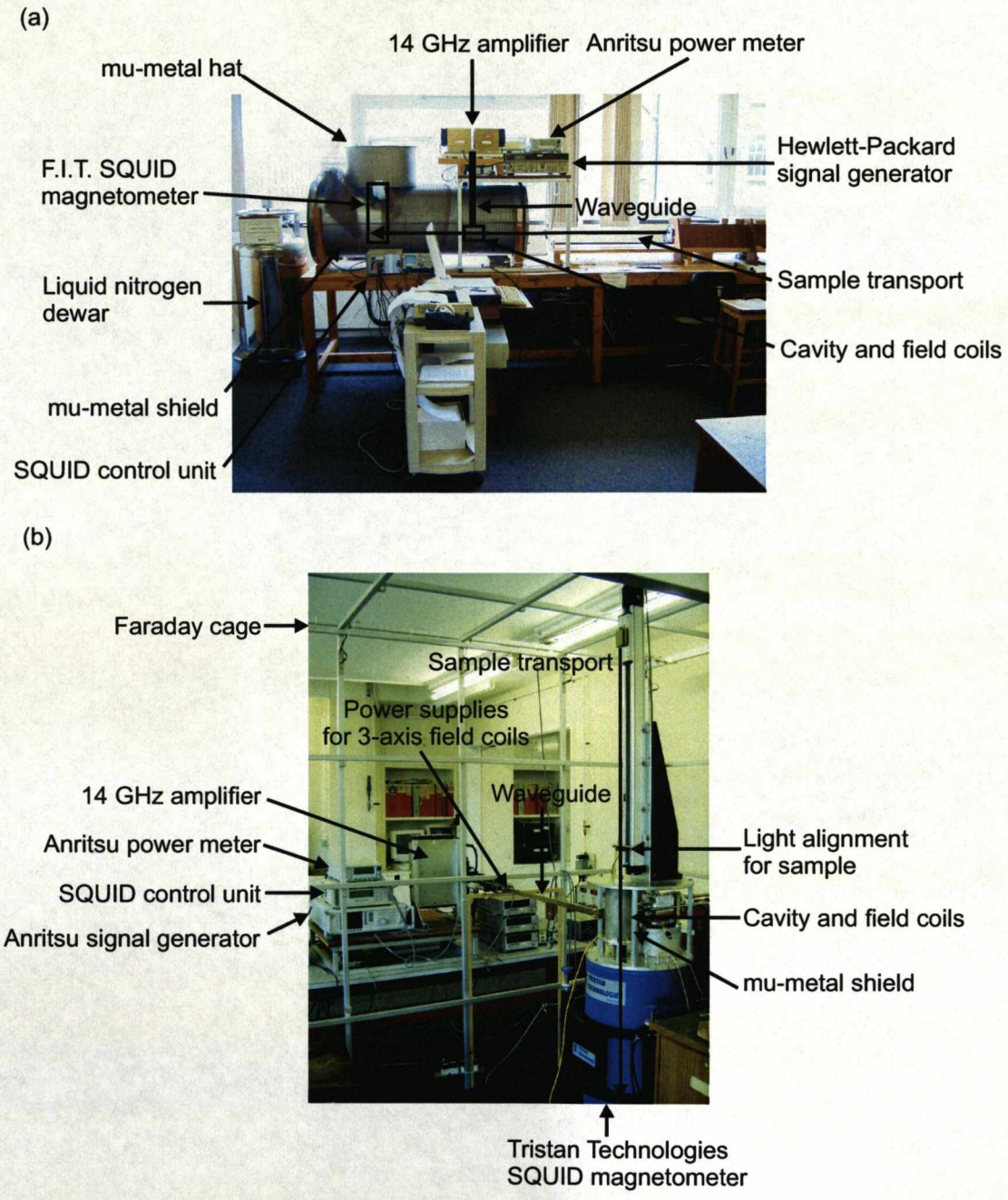


Figure 3.5: University of Liverpool, Geomagnetism Laboratory 14 GHz microwave systems. (a) Older horizontal system with liquid nitrogen SQUID magnetometer. (b) Newer vertical system with Tristan Technologies liquid helium SQUID magnetometer.

The magnetometer, microwave cavity, field coils and sample transport sit in a Faraday cage. An additional mu-metal shield encloses the microwave cavity and field coils.

The magnetometer is a Tristan technologies "low" temperature liquid helium SQUID magnetometer, with maximum sensitivity $\sim$ 1x10$^{-11}$ Am$^2$ (Shaw & Share, 2007)). The sensitivity of the magnetometer can be changed to suite the how strongly magnetised the samples are. The first time the sample is measured a sensitivity test is performed and one of the six sensitivity ranges chosen. Any range can be chosen and the magnitude of the X, Y and Z components as well as the background measurement are displayed on the computer screen. This allows the most suitable range to be selected. The sample is measured three times (with background readings pre- and post- measurement), once in X, once in Y and once in Z.

### 3.4.3 Microwave resonant cavity and tuning

The microwave cavity is cylindrical with internal length 18.5 mm and diameter 15 mm. These dimensions correspond to a resonant frequency of $\sim$14 GHz when operating in the chosen mode with no sample present in the cavity. For the cavity to work at optimum efficiency the sample must be placed exactly in the centre of the cavity, as the cavity dimensions are such that that the length of the cavity equals two half wavelengths of the operating frequency of the microwaves. The cavity is designed to resonate at a specific frequency when it is empty. When a sample is put into the cavity it changes the cavities resonant characteristics. This requires the length of the cavity to be shortened to increase the resonant frequency of the empty cavity, so that when a sample is placed in the centre of the cavity, the resonant frequency is reduced and lies in the operating range of the microwave amplifiers. In practice this only needs to be done once (or on the odd occasion) as lava samples have similar resonant characteristics. For each experiment the exact resonant frequency must be determined. This is done by placing the sample in the centre of the cavity. As sample rods and samples vary very slightly in length, the position of the sample must be adjusted from experiment to experiment. This done by moving the cavity carriage by hand in the 14 GHz microwave system with F.I.T. SQUID magnetometer and by moving the stepper-motor by a computer controlled stepping command in the 14 GHz microwave system with Tristan Technologies SQUID magnetometer.

To assess whether the optimum frequency has been achieved a computer controlled sweep is made between two user defined frequencies while applying 1 W of microwave power. The amount of reflected power is recorded and plotted against frequency (Fig. 3.6). The computer automatically chooses the frequency where reflected power is at a minimum (Fig. 3.6a and c). The position of the sample is adjusted to reduce the reflected power as much as possible. In addition to the position within the cavity reflected power is affected by asymmetry in the sample geometry or to other anisotropic effects that

are not understood. Rotating the sample can therefore affect the amount of reflected power. Care was taken to make the samples as geometrically symmetrical as possible. Sample size is also of concern. If the samples are very large reflected power is often large and changing the sample size is seen to affect the characteristics of the resonant cavity. However, with weakly magnetised samples it is necessary to make larger than average samples as the F.I.T. SQUID magnetometer is not sensitive enough to measure samples with a low NRM (details of the magnetometer are given above).

If the reflected power is not minimised unwanted heating effects occur, caused by heating of the cavity walls and by other field effects within the cavity that are currently being researched. Two scenarios are described in Fig. 3.6 that emphasise the need to correctly tune the cavity. Fig. 3.6a shows an ideal frequency sweep; reflected power is $\approx$0. Fig. 3.6b shows an idealised associated response through time during the microwave experiment from the scenario in Fig. 3.6a. Reflected power remains low throughout the experiment (red line) and therefore the difference between the forward power (black line) and the reflected power is small (blue line). If this scenario is maintained for all power steps throughout the experiment then when consistency checks (see Section 3.4.6) are performed the sample should absorb the sample amount of energy and the checks are valid. In practice there are small variations in tuning throughout the experiment and the relationship between forward and reflected power changes slightly for each power step, even for a scenario close to this idealised situation. These small variations in the total energy absorbed are recorded and used to assess whether consistency checks are valid.

In the second scenario, there is a non-ideal frequency response (Fig. 3.6c) . Reflected power is not zero and the associated situation during the experiment can look like Fig. 3.6d. There is a large amount of reflected power throughout the experiment. Unwanted heating effects often occur in this situation. The frequency response is also variable from step to step (possibly caused by thermochemical alteration of the magnetic minerals), producing an inconsistent relationship between forward and reflected power during the experiment. This makes it difficult to perform valid consistency checks, as the power during a repeated step is not equal to the power of the original step.

### 3.4.4 Experimental procedure

$\sim$5 mm by $\sim$3 mm samples were drilled from 25 mm cores and were attached by glue to the sample rod. Exact sample size varied due to a sample's NRM and care was taken to maximise the NRM measured, but also retain good tuning characteristics. Samples were trimmed using a rotating diamond tipped blade (water was applied throughout the process) and made as geometrically symmetrical as possible. The glue used to attach the sample to the sample rod is set by ultra-violet (UV) light. Samples were placed in a closed box with UV lights for between 5 to 10 minutes.

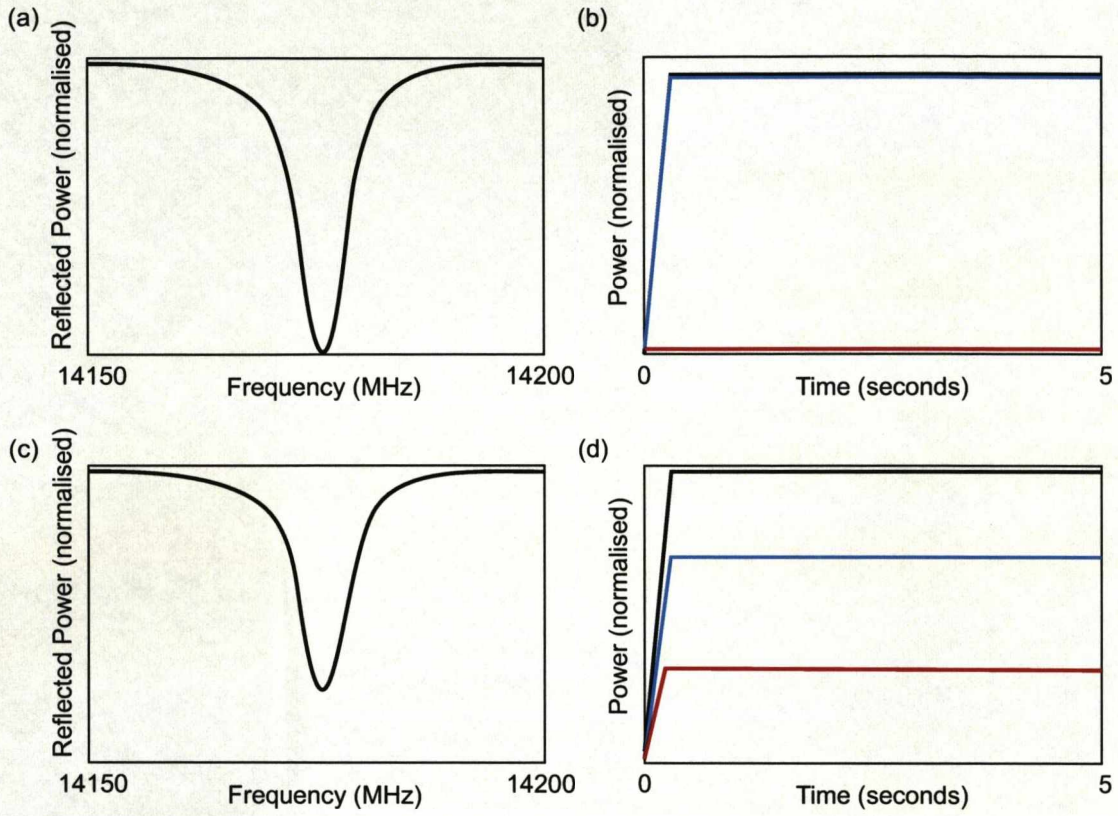


Figure 3.6: Schematic representation of the graphical output from microwave control computers. Examples of idealised frequency sweeps from samples (a) in the correct cavity position and with good resonant characteristics, (c) not in the centre of the cavity or have non-ideal resonant characteristics. (b) Example of the power response of the cavity through time for a scenario producing (a). (d) The same as (b) but for a scenario producing (c). Black = forward power, red = reflected power, blue = the difference between the input power and reflected power.

Before each microwave palaeointensity experiment a microwave demagnetisation experiment was performed on a sister sample from the same core. Both microwave demagnetisation and palaeointensity experiments are directly analogous to conventional thermal experiments (Hill et al., 2002). The demagnetisation experiment allows all components of magnetisation to be resolved and is very important in defining the power range for which the primary component of magnetisation is retained. At the beginning of both demagnetisation and palaeointensity experiments low power steps (between 1 W for 1 second and 16 W for 5 seconds) were applied to make sure that any secondary components were identified and the power a which the primary component became isolated was well defined. This tentative approach allowed for the maximum amount of NRM to be used in the palaeointensity experiment.

During the experiments microwave power was applied for 5 seconds for each step. Ideally the microwave application time would be as short as possible as alteration is time and temperature dependent (Walton, 1988). 5 seconds was chosen experimentally as it allows the greatest flexibility in power steps that could be used. Low powers applied for less than 5 seconds were often ineffective at demagnetising the sample. At higher powers an application time of 10 seconds often greatly increased the amount the sample was demagnetised from one power step to the next. This made it difficult to control the NRM-$T_M$RM spacing. Before each power application the cavity was tuned as described in Section 3.4.3. Microwave power was increased in steps at the discretion of the operator following the protocols described in Section 3.4.5. The increase in power applied in the next step was determined based on the result of the previous step. Once the maximum power of 80 W was reached, the time of microwave power application was increased until a maximum of 20 seconds and the experiment stopped when the sample was fully demagnetised or became detached from the sample rod.

### 3.4.5 Microwave protocols

The applied field coil setup used in the two microwave systems allows any palaeointensity protocol based on the original Thellier & Thellier (1959) method to be used. Three different protocols were chosen: the double-heating method (Coe, 1967a), the perpendicular method (Kono & Ueno, 1977; Hill & Shaw, 2007), and the quasi-perpendicular method (Biggin et al., 2007b). The majority of experiments used the perpendicular method. The microwave system with the Tristan Technologies SQUID magnetometer was only used for the quasi-perpendicular experiments.

All absolute palaeointensity methods follow the same basic principles, and relate to the relationship between NRM and the acquired TRM in the laboratory (in this case a $T_M$RM), and the relationship between the field at the time of formation ($F_{anc}$) and the field applied in the laboratory ($F_{lab}$). The NRM intensity of a sample (if

thermoremanent) is related to the magnitude of the palaeofield ($F_{anc}$) by

$$NRM = k_1 F_{anc} \tag{3.3}$$

The same relationship applies in the laboratory between the produced TRM from any palaeomagnetic technique and the applied field, so that

$$T_{\mathrm{M}}RM = k_2 F_{lab} \tag{3.4}$$

where $k_1$ and $k_2$ are constants relating to the state of the sample, and are only equal if the magnetic properties of the sample have not changed since formation. This means that the NRM should have not decayed since formation and the sample should not have gained any secondary components of magnetism or undergone physiochemical alteration. $k_1$ and $k_2$ only remain equal if no alteration occurs during the experiment, as any alteration due to heating changes the rocks magnetic susceptibility, therefore making $F_{lab}$ void in (3.5).

$$\frac{F_{anc}}{F_{lab}} = \frac{NRM}{TRM} \tag{3.5}$$

The magnitude of $F_{lab}$ is chosen to be as close as possible to the magnitude of $F_{anc}$ (Kono & Tanaka, 1984) and if it is unclear which field to apply, a low field is chosen so that $F_{lab} < F_{anc}$ (Yu et al., 2004). These precautions are taken to minimise errors in the final palaeointensity determination.

### Double-Heating method

The so called double-heating method proposed by Coe (1967a) is a modification of the original method of Thellier & Thellier (1959). The general goal of the Thellier & Thellier (1959) method is to compare (3.5) for multiple partial TRM (pTRM) segments and is based upon the laws of reciprocity, independence and additivity (Thellier, 1938). In the microwave version of the double-heating method the sample is demagnetised in a zero field at a certain microwave power and the remaining NRM is measured. It is then remagnetised at the same power step and then measured. The field is applied in the Z-direction and is left on until the sample leaves the microwave cavity to be measured. The magnetometer records all X, Y and Z values and NRM and $T_{\mathrm{M}}$RM values at each power step ($i$) are calculated in the following way:

$$NRM_i = \sqrt{X_{NRM}^2 + Y_{NRM}^2 + Z_{NRM}^2} \tag{3.6}$$

$$T_M RM_i = \sqrt{(X_{NRM} - X_{T_M RM})^2 + (Y_{NRM} - Y_{T_M RM})^2 + (Z_{NRM} - Z_{T_M RM})^2} \tag{3.7}$$

All values of NRM and $T_{\mathrm{M}}$RM are normalised to the initial NRM measurement and plotted on an Arai-Nagata plot (Nagata et al., 1963) (Fig, 3.9). p$T_{\mathrm{M}}$RM checks and

$pT_MRM$ tail checks are generally applied after the third remagnetisation and subsequently after every two remagnetisation steps (Fig. 3.9). Consistency checks are explained in Section 3.4.6.

In the double heating method, the amount of energy given to the magnetic minerals needs to be accurately reproduced. In the thermal variation of the experiment this is not a problem as temperature can be controlled accurately in thermal demagnetisers. In the microwave technique reproducing the energy the sample absorbs is more difficult and is not determined by the power that is supplied by the microwave amplifiers alone(discussed in Section 3.4.3. If the tuning characteristics change (Fig. 3.6) then the energy absorbed by the sample in the demagnetisation and remagnetisation steps will be different. The need for accurate power absorption reproducibility is especially important for samples that have a narrow blocking spectrum and demagnetise over a small power range. This is often the case for many lavas. The development of better cavities and monitoring of the forward and reflected power has increased the applicability of this method.

### Perpendicular method

This method is particularly suited to the microwave system and overcomes problems of reproducing the same power steps (as seen in some microwave double-heating experiments). The perpendicular method was conceived by Kono & Ueno (1977) and was subsequently developed for the microwave technique (see Hill & Shaw (1999), Hill (2000) and Hill & Shaw (2007)). This method only requires one microwave power application at each step (rather than a demagnetisation step followed by an applied field step, as in the double-heating method). With the exception of the consistency checks, all steps during the experiment are applied field steps (Section 3.4.6). The applied laboratory field is directed perpendicular to the NRM, and therefore the fully remagnetised $T_MRM$ is acquired perpendicular to the NRM. The reduced number of steps, compared with the double heating method, also reduces any possible alteration.

The first step is to remove all secondary components (see below). The characteristic remanent magnetisation (ChRM) remains and the applied field ($F_{lab}$) direction is calculated perpendicular to this. Unlike the original Kono & Ueno (1977) method, the samples are not rotated 90° to their NRM direction, but remain static. Instead the $F_{lab}$ is applied perpendicular to the NRM. Two methods are used to calculate NRM and $T_MRM$. The first method assumes the resulting total vector of magnetisation (RM) lies in the plane defined by the direction of the applied field ($F_{lab}$) and the ChRM. The NRM is the scalar product of RM and the ChRM direction unit vector (3.8). $T_MRM$ is the scalar product of RM and the $F_{lab}$ direction unit vector (3.9). Bold type face are vectors, italics are scalars.

$$NRM = \mathbf{RM} \cdot \mathbf{ChRM} \tag{3.8}$$

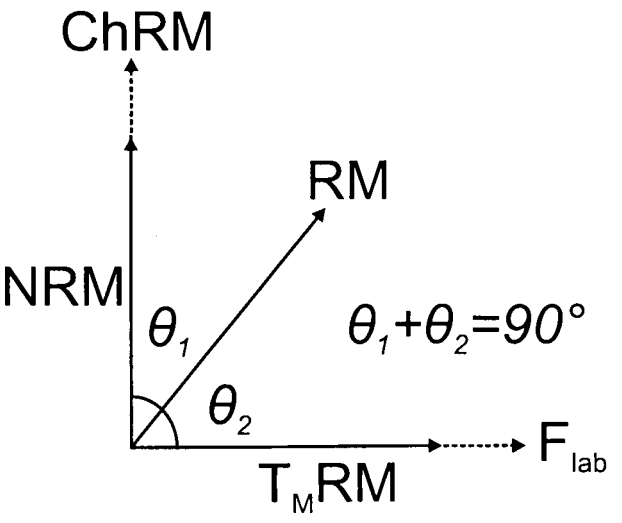


Figure 3.7: After Hill & Shaw (2007). Representation of **NRM** and $\mathbf{T_M RM}$ components and the **RM**, as well as the directions of $F_{lab}$ and ChRM.

$$T_M RM = \mathbf{RM} \cdot \mathbf{F_{lab}} \tag{3.9}$$

The second method does not assume that RM is in the {NRM, $T_M$RM} plane or that the ChRM and Flab directions are perpendicular. The angles between the direction of RM and ChRM ($\theta_1$) vectors, and RM and Flab ($\theta_2$) vectors are calculated. These angles are then used to calculate NRM (3.10) and $T_M$RM (3.11) (Fig. 3.7).

$$NRM = RM \frac{sin\theta_2}{sin\phi} \tag{3.10}$$

$$T_M RM = RM \frac{sin\theta_1}{sin\phi} \tag{3.11}$$

where

$$\theta_1 = cos^{-1}\left(\frac{\mathbf{RM} \cdot \mathbf{ChRM}}{RM}\right) \tag{3.12}$$

$$\theta_2 = cos^{-1}\left(\frac{\mathbf{RM} \cdot \mathbf{F_{lab}}}{RM}\right) \tag{3.13}$$

$$\phi = 180 - (\theta_1 + \theta_2) \tag{3.14}$$

If $\theta_1$ and $\theta_2 \neq 90°$ then RM does not lie in the {ChRM, $F_{lab}$} plane. This can result if the ChRM is not stable (cases 2 and 3 Fig. 3.8), the sample is anisotropic (case 4 Fig. 3.8), there is an error in the direction of Flab, or the magnetometer is not measuring correctly. It is vital that the applied field steps are only performed on the primary component of magnetisation (Hill & Shaw, 2007). If the secondary components are not removed and they in the plane of the applied field, then relationship between between NRM and $T_M$RM will be non-linear. If the secondary components lie outside of the plane of the applied field then the sum of $\theta_1$ and $\theta_2$ is not equal to 90° (Fig. 3.7)

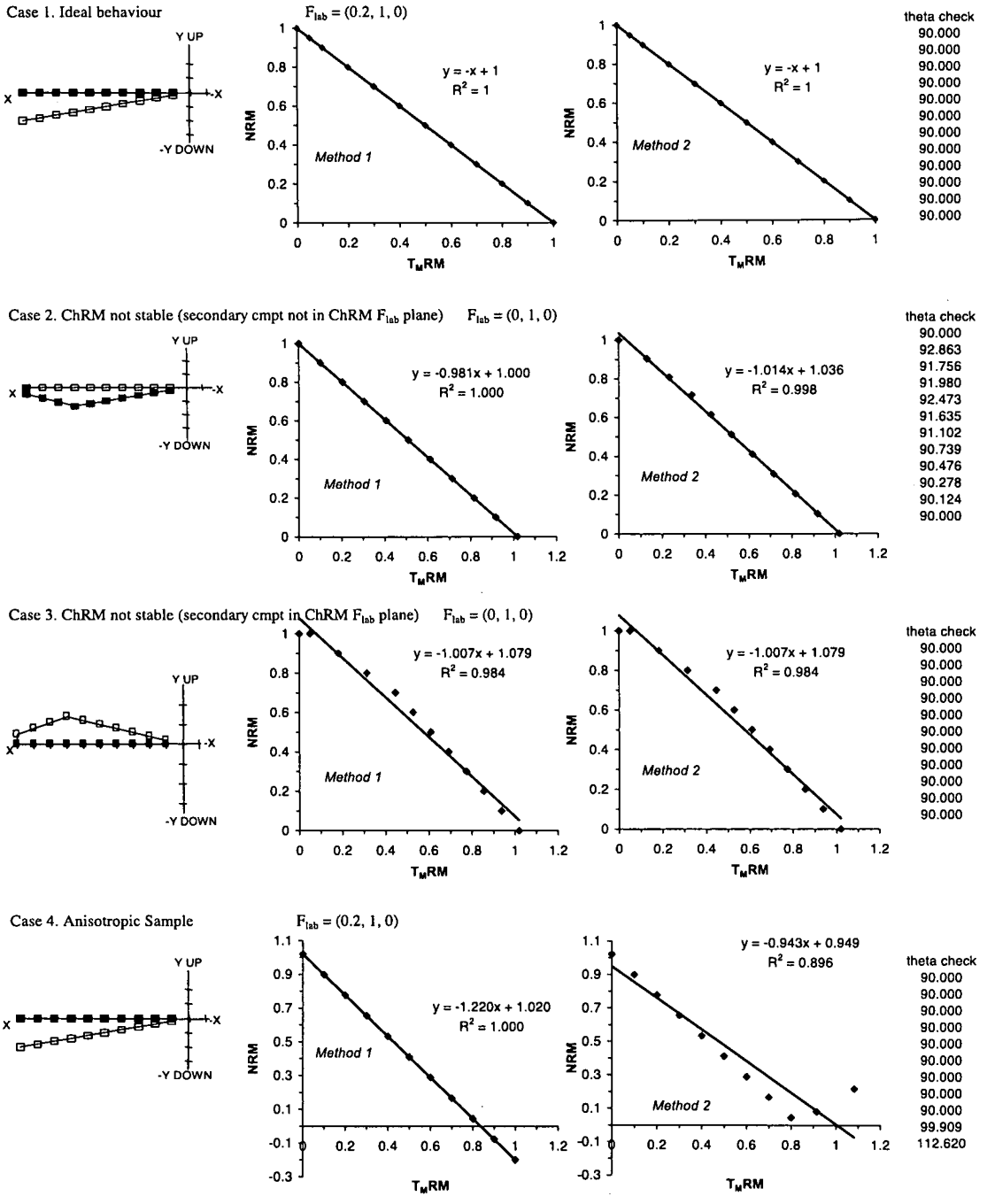


Figure 3.8: From Hill & Shaw (2007). Synthetically generated scenarios that can affect the outcome of perpendicular applied field experiments. The left hand plot is an orthogonal vector plot with solid (open) symbols representing the vertical (horizontal) projections of the NRM vector. Both methods of determining NRM and $T_M$RM are shown.

$pT_MRM$ checks and $pT_MRM$ tail checks are generally applied after the third remagnetisation and subsequently after every two remagnetisation steps (Fig. 3.9). Consistency checks are explained in Section 3.4.6.

### Quasi-perpendicular method

The majority of volcanic samples contain multi-domain particles, which can cause erroneous palaeointensity determinations (e.g. Coe (1967b); Levi (1977); Riisager & Riisager (2001); Biggin & Böhnel (2006); Yu & Dunlop (2006)). Biggin & Böhnel (2006) predicted that a protocol which uses a single remagnetisation step for every power step (as in the perpendicular method) would improve the accuracy of palaeointensity experiments on samples containing MD particles. Based on this result Biggin et al. (2007b) proposed the quasi-perpendicular single heating method for the microwave. This method has three essential differences to the perpendicular method:

1. After every remagnetisation step a microwave demagnetisation step at a lower power is included. This step is the power required to isolate the ChRM, and is the same for each demagnetisation step. These extra demagnetisation steps are applied to remove the MD contribution after every remagnetisation.

2. The applied field is applied along the z-axis. However, for the experiment to be successful the angle between the ChRM and the direction of $F_{lab}$ must be greater than 45°.

3. No consistency checks are applied, as this increases the number of steps and can result in less accurate palaeointensity determinations when the sample contains MD particles (Biggin & Böhnel, 2003).

The remanence after each demagnetisation step will be a combination of the ChRM and the $T_MRM$. The $T_MRM$ will be aligned with the z-axis so each measurement will be of $X_{nrm}$, $Y_{nrm}$ and $Z_{measured} = Z_{nrm} + Z_{lab}$. Two estimates of $Z_{nrm}$ are determined:

$$Z_{nrm1} = X_{nrm}\left(\frac{Z_0}{X_0}\right) \tag{3.15}$$

$$Z_{nrm2} = Y_{nrm}\left(\frac{Z_0}{X_0}\right) \tag{3.16}$$

$X_0$ and $Z_0$ are the values of $X$ and $Y$ after the initial characterisation demagnetisation step. If X or Y make up less than 15% of the full NRM vector, only the $Z_{nrm}$ with X or Y component greater than 15% of the full NRM vector is used as $Z_{nrm}$. If both X and Y are greater than 15% of the full NRM vector then the average of $Z_{nrm1}$ and $Z_{nrm2}$ is taken as $Z_{nrm}$ in the final NRM and $T_MRM$ calculations. The magnitude of the NRM is:

$$NRM = \sqrt{X_{nrm}^2 + Y_{nrm}^2 + Z_{nrm}^2} \tag{3.17}$$

and the magnitude of $T_M$RM is:

$$T_M RM = \sqrt{(Z_{measured} - Z_{nrm})^2} \tag{3.18}$$

### 3.4.6 Consistency checks

Consistency checks have been included in the microwave palaeointensity experiments to assess for thermochemical alteration and the effects of MD remanence carriers. Both $pT_M$RM-tail checks (Dunlop & Özdemir, 1997; Shcherbakova & Shcherbakova, 2000; Riisager & Riisager, 2001) and $pT_M$RM checks Thellier & Thellier (1959) have been incorporated into the double-heating and perpendicular experiments.

$pT_M$RM-tail checks are included to test for the presence of MD particles. Thellier's laws (Thellier, 1938) state that pTRMs must be independent and additive and this is only true for non-interacting SD particles (Néel, 1955). For MD particles, individual pTRMs may not be independent due to differences in blocking and unblocking temperatures (Fabian, 2001). Thellier palaeointensity experiments on samples with a significant proportion of MD particles may therefore lead to erroneous palaeofield estimates. Thermomagnetic experiments (Bolshakov & Shcherbakova, 1979; Shcherbakova & Shcherbakova, 2000) and theoretical models (Dunlop & Xu, 1994; Xu & Dunlop, 1994; Fabian, 2001) have shown that independence of pTRMs is not obeyed for pseudo-single domain (PSD) and multi-domain (MD) particles; however, additivity is still generally valid (Fabian, 2003; Yu & Dunlop, 2006). Failure of Thellier's laws for PSD and MD particles can lead, at low temperatures, to pTRM demagnetisation being greater than pTRM acquisition (Dunlop & Özdemir, 2000). This results in concave-up curvature of the Arai-Nagata plot.

$pT_M$RM-tail checks are performed by demagnetising the sample in a zero field at the same microwave power and for the same time as the previous remagnetisation step. In the double-heating method the tail check was calculated by calculating the magnitude of the vector difference between the NRM vector ($X_{nrm}$, $Y_{nrm}$, $Z_{nrm}$) and the $pT_M$RM-tail check vector ($X_{tail}$, $Y_{tail}$, $Z_{tail}$), where

$$pT_M RM{-}tail = \sqrt{(X_{nrm} - X_{tail})^2 + (Y_{nrm} - Y_{tail})^2 + (Z_{nrm} - Z_{tail})^2} \tag{3.19}$$

For the perpendicular method an orthogonal projection is made between the NRM vector and $pT_M$RM-tail check vector.

pTRM checks were initially suggested by Thellier & Thellier (1959) to detect thermomagnetic alteration of the the magnetic particles carrying the TRM. If magnetic minerals are oxidised during heating the composition and structure of the magnetic minerals can be altered and this results in a change in the samples ability to acquire a

TRM (or $T_M$RM). A p$T_M$RM check is performed after a p$T_M$RM-tail check by applying the same power for the same time as that of a previous applied field step. If there is no alteration, the p$T_M$RM check vector will be the same as $T_M$RM vector.

The DRAT criterion of Selkin & Tauxe (2000) is used to assess the accuracy of the p$T_M$RM check. The magnitude of the difference between the $T_M$RM vector and the p$T_M$RM check vector, at the same power and time step, is normalised by the magnitude of the selected NRM-$T_M$RM segment. This value is expressed as a percentage. This method reduces the bias introduced by using the absolute difference when the NRM lost and $T_M$RM gained are small.

### 3.4.7 Palaeointensity data analysis and representation

All NRM and $T_M$RM values are normalised to the NRM and plotted on an Arai-Nagata plot (Nagata et al., 1963) (Fig. 3.9). Analysis of NRM-$T_M$RM curves follows the calculations of Coe et al. (1978). Palaeointensity is determined by using a least-squared best fit to the data based on the method of York (1966, 1967). A least squares best fit slope is defined as:

$$b = -\left[\sum_i (NRM_i - N\bar{R}M)^2 / \sum_i (T_M RM_i - T_M \bar{R}M)^2\right]^{1/2} \tag{3.20}$$

and the standard error of the slope

$$\sigma_b = -\left[\frac{2\sum_i (NRM_i - N\bar{R}M)^2 - 2b\sum_i (T_M RM_i - T_M \bar{R}M)(NRM_i - N\bar{R}M)}{(N-2)\sum_i (T_M RM_i - T_M \bar{R}M)^2}\right]^{1/2} \tag{3.21}$$

where $N\bar{R}M$ and $T_M\bar{R}M$ are unweighted arithmetic means. The intercept on the y-axis ($NRM_t$) is simply

$$NRM_t = N\bar{R}M - bT_M\bar{R}M \tag{3.22}$$

and the intensity estimate is just

$$F_{anc} = |b|F_{lab} \tag{3.23}$$

The slope calculated using 3.20 is accurate enough for the usual sets of data in palaeointensity work, but the standard error of the slope, given by 3.21, cannot be attributed strict statistical meaning and must instead be regarded as an *ad hoc* measure of uncertainty (Coe et al., 1978).

To assess the quality of the palaeointensity determination Coe et al. (1978) introduced some statistical descriptions of NRM-$T_M$RM data:

1. The uncertainty in slope caused by the scatter of points about the least squares fit, $\sigma_b/|b|$. This description is independent of $F_{lab}$ and a measure of the relative

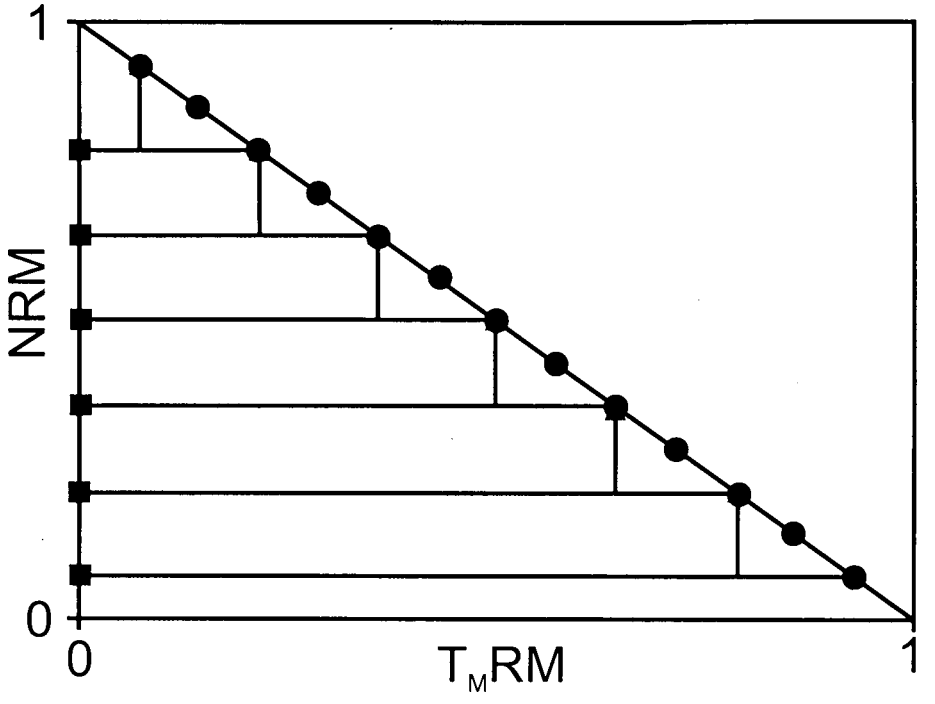


Figure 3.9: Ideal Arai-Nagata plot (Nagata et al., 1963). {NRM, $T_M$RM} points are circles. In this perfect example NRM-$T_M$RM points are all equally spaced and the majority of the NRM has been demagnetised. Triangles are $T_M$RM checks (vertical lines are extended from the check to meet the NRM value of the previous $T_M$RM step). Squares are $T_M$RM tail checks (horizontal lines have been extended back from the check to the result of the previous $T_M$RM step).

uncertainty in $F_{anc}$. The error in each palaeointensity determination is $\sigma_f = F_{lab}\sigma_b$, and the relative uncertainty in $F_{anc}$ is $\sigma_f/F_{anc} = (F_{lab}/F_{anc})\sigma_b = \sigma_b/|b|$.

2. The fraction of total extrapolated NRM spanned by the chosen segment of the NRM-$T_M$RM curve, $f$. $f$ is a measure between 0 and 1 and is

$$f = \frac{\Delta NRM_t}{NRM_t} \tag{3.24}$$

where $\Delta NRM_t$ is the total length of the NRM fraction.

3. A measure of the gaps between the NRM-$T_M$RM points called the gap factor, $g$, where

$$g = 1 - \frac{\Delta \bar{N}RM}{\Delta NRM_t} \tag{3.25}$$

and where

$$\Delta \bar{N}RM = \frac{1}{\Delta NRM_t} \sum_{i=1}^{N-1} \Delta NRM_i^2 \tag{3.26}$$

is a weighted mean of the gaps, $\Delta NRM_i$, between the $N$ points along the selected segment.

4. A quality factor, $q$, which is a combination of $\sigma_b/b$, $f$ and $g$, where

$$q = \frac{|b| f g}{\sigma_b} \tag{3.27}$$

with associated error on the palaeointensity estimate being

$$F_{error} = \frac{1}{q} F_{anc} \tag{3.28}$$

The linear regression coefficient, $r^2$ has also been calculated, where

$$r^2 = \left( \frac{COV(T_M RM, NRM)}{(VAR(T_M RM) VAR(NRM)^{1/2})} \right)^2 \tag{3.29}$$

The calculated statistics have been used to formulate a selection criteria for acceptable palaeointensity results.

### 3.4.8 Palaeointensity acceptability criteria

Palaeointensity estimates have been accessed using the criteria of Brown et al. (2006) and are split in to three categories: class 1, class 2, and class 3 . Three classes were chosen as they more successfully represent the variation in the quality of the data in this study. A class 1 result must have the following:

1. A stable primary natural remanent magnetisation (NRM) direction.

2. Greater than or equal to four data points in a single straight line on an NRM-$T_M$RM plot. No point is eliminated in the selected NRM segment, unless it can be proved to be caused by experimental error (these results are shown in open circles).

3. At least 30 per cent of the NRM is used ($f$ factor).

4. A quality factor, $q \geq 5$.

5. A gap factor, $g > 0.5$.

6. A regression coefficient, $r^2$ of the best-fitting line $\geq 0.98$.

7. For determinations made using the perpendicular method, $\theta 1 + \theta 2$ must be between 90° and 91° (the sum of the angles between the NRM and the ($T_M$RM) vector and the applied field vector and the ($T_M$RM) vector (Hill & Shaw, 2007)).

8. p$T_M$RM checks differing from the original value by $\leq$ 10% (using the DRAT criteria of Selkin & Tauxe (2000)).

9. p$T_M$RM-tail checks $\leq$ 10 % difference between two zero field power steps.

A class 2 result must pass all the criteria listed; however, it may fail p$T_M$RM checks or p$T_M$RM tail checks if there is little or no distortion to the straight line trend. This suggests that the sample failed tha check because of problems with the reproducibility of the reflected power in the microwave cavity during the microwave experiment rather than by alteration or non-ideal behaviour. This category has been included as many of the results have high $f$, $q$ and $r^2$ values but display this kind of behaviour. Results from the quasi-perpendicular method are class 2. Although this protocol has been successful in determining the historical geomagnetic field from lavas with a range of magnetic domain states where other protocols failed (Biggin et al., 2007a,b), it requires further validation. Class 3 results produce a linear relationship between NRM and $T_M$RM ($r^2 \geq 0.9$) but fail some of the selection criteria and checks, and represent data that are unreliable.

## 3.5 Summary

In this chapter all field and laboratory methods have been described. Experimental details of rock magnetic methods and palaeodirection determinations have been described along with details of the methods used to analyse the data. A large proportion of this chapter has been dedicated to explaining the microwave technique, different micowave protocols and the selection criteria used to assess whether palaeointensity determinations are accurate.

# Chapter 4

# Exploring the influence of the non-dipole field on magnetic records for reversals and excursions

This chapter describes a simple reversal model based upon CALS7K.2 (Korte & Constable, 2005a). The aim of the model is to test the possible level of complexity generated at the Earth's surface when only the most simple reversal or excursion scenarios are considered. Duration, reversal onset time, virtual geomagnetic pole paths, directional and intensity variations are all investigated and compared with published palaeomagnetic observations. This chapter is based on the paper entitled 'Exploring the influence of the non-dipole field on magnetic records for reversals and excursions', Brown et al. (2007) (a reprint is enclosed in the back cover).

## 4.1 Introduction

The behaviour of the geomagnetic field during reversals and excursions is unclear. Many palaeomagnetic studies from both lava sequences and sedimentary cores have sought to uncover details of these two processes. However, these records often only show the behaviour of the field at one location on the Earth's surface, and where multiple records exist it is extremely difficult to correlate them temporally and establish features globally (Constable, 1990; Gubbins, 1999). It is thought that reversals are complex (Constable, 1990; Coe & Glen, 2004), with many possible features being recorded at the Earth's surface; however, a paucity of data has hindered any robust conclusions concerning reversal behaviour.

Reversals have been reported from numerical dynamo models and their output has been analysed for insight into the reversal process (Coe et al., 2000; Kutzner & Christensen, 2004; Narteau & Le Mouël, 2005; Wicht, 2005). However, it is unclear how much direct relevance the results have for the Earth system as the fundamental magnetohydrodynamic parameters of these models are far from the Earth's true regime.

Here, an alternative, much simpler, approach has been adopted, based on a time-dependent observational model of the geomagnetic field for the last 7000 years, CALS7K.2 of Korte & Constable (2005a). CALS7K.2 is a continuous global model determined by a regularised least squares fit to archaeomagnetic and palaeomagnetic data using spherical harmonics in space and cubic B-splines in time. The field structure of this CALSK.2 is used and the effects on surface field morphology by varying the magnitude of the axial dipole component are examined. This apparently arbitrary approach is motivated by observations from the palaeomagnetic record, that suggest that statistical characteristics of the non-dipole field during a reversal are indistinguishable from those during stable periods of field behaviour (Valet et al., 1992). This perhaps surprising observation can be understood in terms of our understanding of the dynamics of magnetic secular variation at the top of the Earth's core. The evolution of the magnetic field is governed by the induction equation, of which the radial component is:

$$\frac{\partial B_r}{\partial t} = \frac{\eta}{r}\nabla^2(rB_r) - \nabla_H \cdot (\mathbf{u}B_r) \tag{4.1}$$

where $B_r$ is the radial field, $\mathbf{u}$ is the surface flow velocity, $\eta$ is the magnetic diffusivity, $r$ is the radius, $\theta$ is the colatitude, and $\nabla_H \cdot$ is the horizontal divergence operator. The terms on the right hand side represent secular variation generated by diffusion of the field and advection respectively. However, it is thought that on at least decadal time scales, advective processes at top of the core may be in the tangentially geostrophic regime (Le Mouël, 1984), in which the principal force balance is between pressure gradients and Coriolis force. In this regime, the horizontal flow at the core-mantle boundary obeys:

$$\nabla_H \cdot (\mathbf{u}\cos\theta) = 0 \tag{4.2}$$

Le Mouël (1984) realised that this condition has implications for the interpretation of equation (4.1). Specifically, any magnetic field of the form $\cos\theta$ will not contribute to secular variation by advection: this is precisely the form of the axial dipole component of the field. Further, the diffusion operator separates in spherical harmonics and so diffusional processes of different spherical harmonic field components can be considered as independent. Hence, to first order, the strength of the axial dipole field does not influence the secular variation of the non-dipole field. Therefore, it is at least kinematically consistent to consider an unchanged non-dipole field while imposing changes on the axial dipole component.

It is not claimed that the time-varying non-dipole field over the last 7000 years would have been the same without a strong axial dipole field. However, statistically the variation of the non-dipole field may not depend strongly on the dipole, and therefore the CALS7K.2 model may be a good source for a proxy for possible non-dipole variation during a reversal. It is also not unreasonable to use a model for the recent field as it is likely not to be grossly atypical of the palaeofield (Heller et al., 2003). Time averaged

models of the stable palaeomagnetic field for the last 5 Myr (Johnson & Constable, 1995; Kelly & Gubbins, 1997) show similar features to the time-averaged historical field, particularly high-latitude flux patches (Bloxham & Jackson, 1992; Jackson et al., 2000). Even without this justification, this approach provides a geometric model to examine how the slowly-varying changes in the field at the Core Mantle Boundary might be observed in Earth surface observations, complementary to those available from dynamo simulations.

A similar approach to the one used here, but with a constant non-dipole field from the IGRF, has been used to look at reversals (Constable, 1992; Quidelleur & Valet, 1996; Heller et al., 2003; Clement, 2004) and excursions (Heller et al., 2003; Quidelleur et al., 1999). Unlike these studies, the possible influence that a time-varying non-dipole field may have on field structure during reversals and excursions is explored. Possible changes and global variations in the direction and intensity of the field, both temporally and spatially, have been investigated.

## 4.2 Method

The geometrically simplest model for a geomagnetic field reversal is to decrease the axial dipole to zero and then increase it to the opposite polarity (Courtillot et al., 1992; Quidelleur & Valet, 1996). The axial dipole term ($g_1^0$) in CALS7K.2 was scaled linearly with time:

$$g_1^{0\prime} = g_1^0(t)\left(1 - 2\left(\frac{t - t_0}{t_1 - t_0}\right)\right) \tag{4.3}$$

where $t$ is varying time, $t_0$ is the starting time, and $t_1$ is the end time of the model. In this study the total reversal process is defined to last the whole 7000 year period of CALS7K.2. The time variation of the non-dipole field was unaltered. Although magnetic energy could be transferred from the dipole field into e.g., the axial quadrupole or octupole terms (Williams & Fuller, 1981; Clement, 2004; Merrill, 2004) there is no physical requirement for the magnetic energy of the geodynamo to be conserved (Constable, 1990).

Surface observations that could emerge from this simplistic reversal model are examined. To compare directional and intensity changes globally the standard palaeomagnetic convention of the virtual geomagnetic pole (VGP) and virtual dipole moment (VDM) is used. This characterisation assumes a simple geocentric dipole for the time-averaged field, an assumption unlikely to be physically appropriate for a reversal, but useful as a way of comparing measurements.

From observations, the duration of a directional reversal is often defined as the period in which the VGP lies between $+45°$ and $-45°$ latitude. A directional reversal's duration is defined based on the time of the last crossing of $+45°$ before the VGP crosses the equator and the first crossing of $-45°$ afterwards (Fig. 4.1).

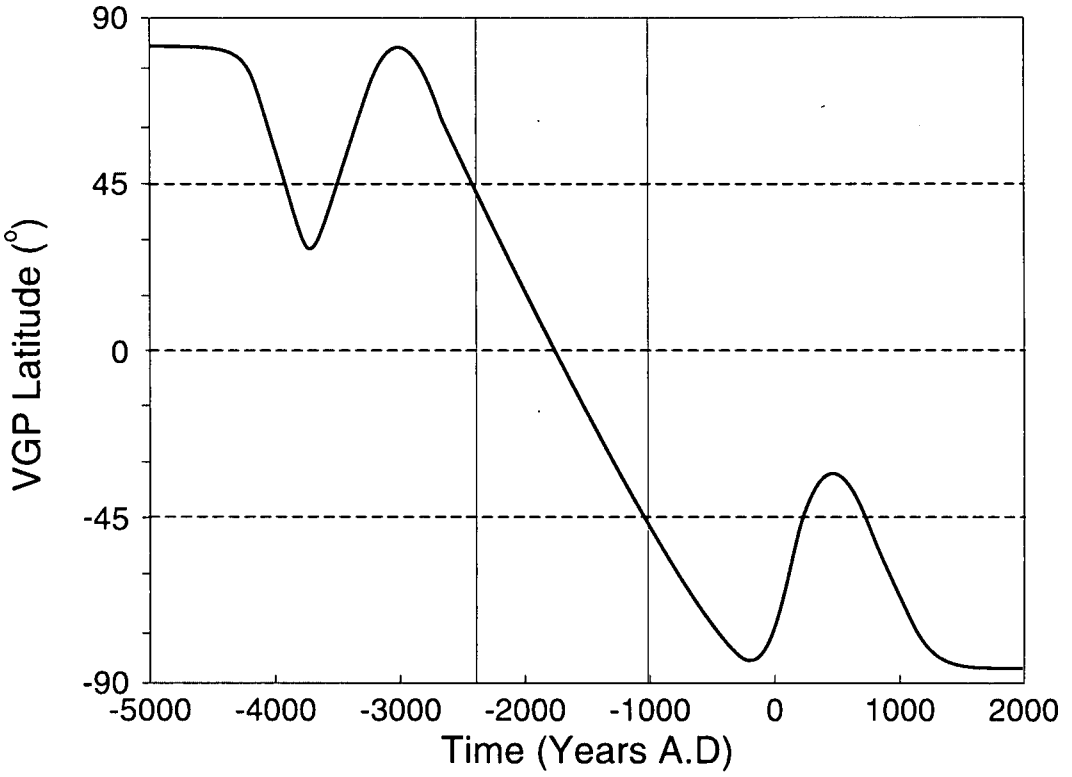


Figure 4.1: A schematic reversal path illustrating the duration of the directional reversal (grey shading) defined for this study.

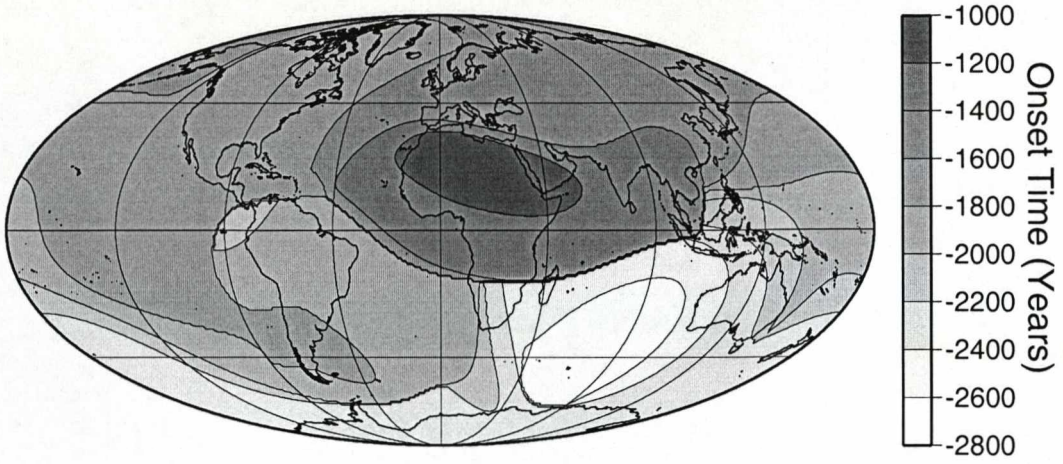


Figure 4.2: Time of onset for directional reversals for all global locations.

As a possible model of excursions the axial dipole is scaled to a reduced value for a set time period.

$$g_1^{0\prime} = \alpha g_1^0(t) \tag{4.4}$$

Varying the magnitude of the axial dipole field allows us to see at what point the non-dipole field becomes dominant and excursions are produced. An excursion is defined to have occurred whenever the VGP latitude is $< +45°$and then returns to a normal field latitude ($> +45°$).

## 4.3 Reversal features

The model exhibits both temporal and spatial variations in the behaviour of the field during the total reversal process. A global variation in the onset time of the directional reversal is observed (Fig. 4.2), of about 1800 years, approximately 25 of the total reversal process time. When specific locations are investigated (Fig. 4.3a) directional reversals are completed in some locations (e.g., New Zealand) before they have started elsewhere (e.g., Tenerife and UK). For all locations, the directional behaviour appears complex, and features are not globally uniform. Fig. 4.3a, also shows a fluctuation in VGP latitude around -2000 A.D for Iceland, UK and Tenerife which is not seen for Hawaii or New Zealand. Moreover, the magnitude of the fluctuation varies.

Variability in VDM is seen throughout the total reversal process for all locations. For example, Fig. 4.3b shows the VDM fluctuating over time periods of approximately

(a)

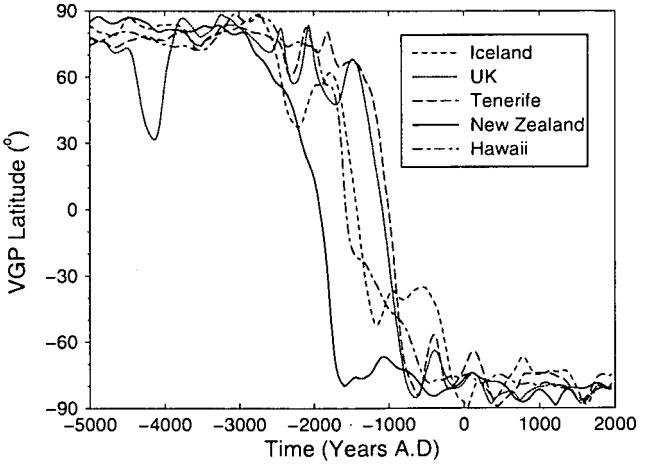


(b)

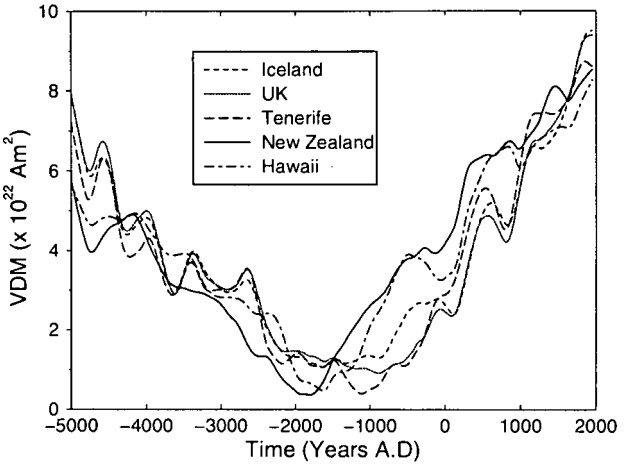


(c)

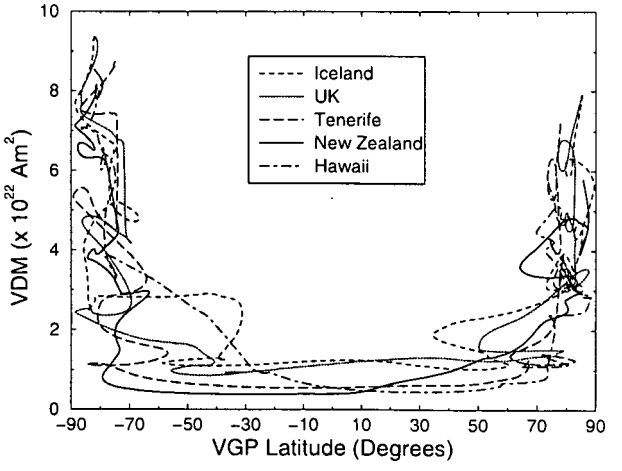


Figure 4.3: (a) Directional changes, (b) VDM changes, (c) VGP vs VDM, for five global locations during the simulated 7000 year reversal.

500 to 1000 years superimposed on the trend produced by scaling the axial dipole. In comparison to the directional reversal there is more global coherence in the VDM variations. The directional changes are also seen to be contained within the time that the VDM is significantly reduced (Fig. 4.3c).

A great variation in the duration of the directional reversal is observed (Fig. 4.4a). What is particularly notable is that from a total reversal time of 7000 years, some of the directional changes happen on sub-decadal time-scales (Fig. 4.4b), while others occur over a period of approximately 1500 years (Fig. 4.4c). Globally, the model has produced sharp boundaries distinguishing short and long directional reversals (Fig. 4.4a). These are most prominent running through the Indian Ocean, Southern Africa and the Southern Atlantic Ocean as well as through central North America and through the Pacific Ocean. These are the product of subtly changing directional variations across the globe and also the definition of a directional reversal. In Fig. 4.4c there is a small fluctuation in direction between -2000 A.D. and -1000 A.D for South Africa. Moving north from this location, the peak of the fluctuation increases in VGP latitude and at a specific point (the boundary) the peak exceeds $+45°$ and the start of the directional reversal is shifted to a later time (seen in Fig. 4.2), reducing the duration. Another sharp boundary in Fig. 4.4a is in the area of the Caspian Sea. Here the definition of a directional reversal is relaxed, as a large excursion re-crossing the equator was observed after the defined directional reversal (Fig. 4.4c). It was included in Fig. 4.4a to illustrate the variability in directional changes observed in this model. The Caspian Sea was the only area where such a large excursion was observed, post-directional reversal.

One of the more controversial features of the reversing field is preferred VGP paths (Laj et al., 1991). The model generates VGP paths with varying geometries (Fig. 4.5); however, plots such as in Fig. 4.5 give no analysis of the longitudinal distribution of the paths. To determine whether the model produced any longitudinal preference globally, an equal area distribution of site latitudes and longitudes was used. Initially, the percentage of VGP paths passing through ten-degree longitudinal intervals when crossing the equator was assessed. Two bands of longitudinal preference have been generated (Fig. 4.6). The dominant preference is between $+20°$ and $+80°$ and a lesser preference between $-90°$and $-130°$. To determine if these preferences are spatially coherent, the percentage of VGP paths passing through ten-degree longitudinal intervals crossing $+45°$, $+30°$, $-30°$ and $-45°$ latitude were assessed (Fig. 4.7). A similar preference in the results from the equator and the southern hemisphere crossings is seen. The northern hemisphere crossings show broader peaks with a much lower incidence of crossings between $+60°$ and $+180°$. Preferences for preferred paths are investigated when the reversal occurred over different time periods, to assess whether similar VGP paths would be seen for different reversals and therefore relate to a longer time-averaged feature of the non-dipole field. To determine this, the starting time of the reversal was changed,

(a)

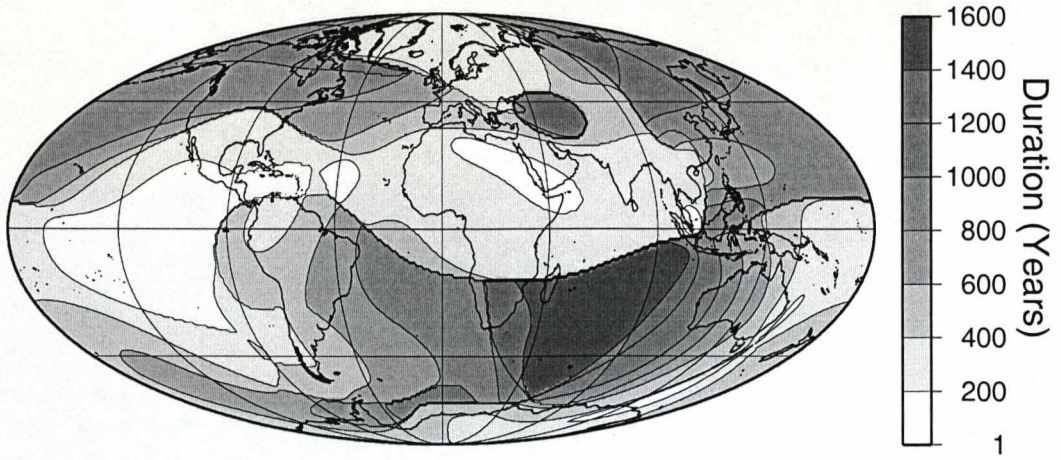


(b)

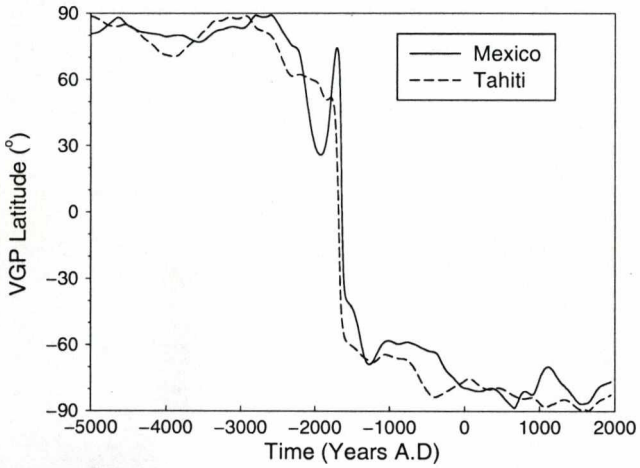


(c)

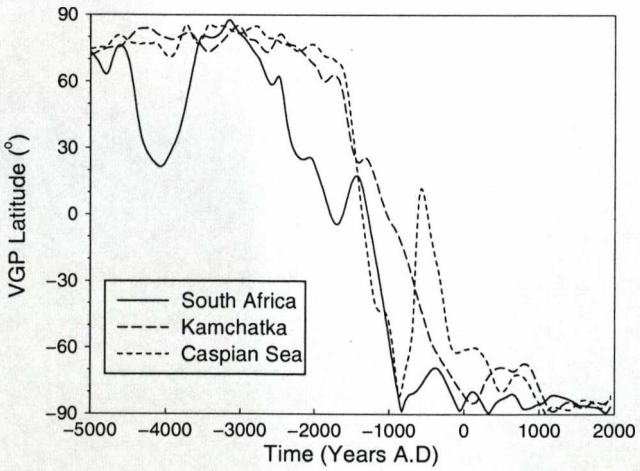


Figure 4.4: (a) Duration of directional reversals for all global locations. (b) Examples of rapid directional reversals. (c) Examples of slow directional reversals.

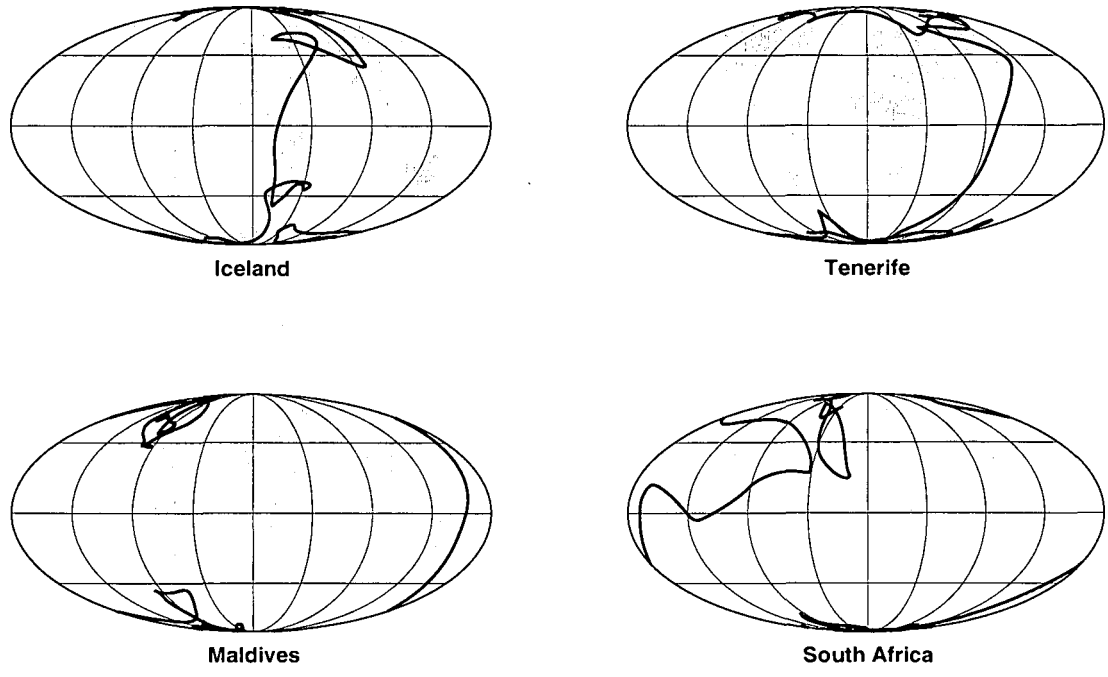


Figure 4.5: Examples of four locations with varying VGP paths.

but the rate of change of the axial dipole kept constant. This reduced the interval of CALS7K.2 used in calculating the percentage of paths, but it maintained the same temporal relationship between the non-dipole field and the changing axial dipole field for all time periods. The start of the total reversal process was set at -4000, -3000, and -2000 A.D. Longitudinal preferences were seen for all time periods (Fig. 4.8); however, the location of the preferences show only a weak correlation with those seen in Fig. 4.6, between each time period. When the results from all the time periods are averaged (Fig. 4.8d), preferred paths are still seen, but the pattern is less marked than for a single time, not inconsistent with the analysis of Love (2000).

## 4.4 Excursion features

With a scaled axial dipole over a set time period the reduction in dipole field strength at which major directional changes start to occur can be assessed. In this case the time period is set from -3000 A.D. to present day. Before -3000 A.D the South Atlantic anomaly appears to bias the behaviour of the field, which could be due to poor data coverage at this time (Korte & Constable, 2005b). Excursions are seen to appear naturally in the model and that large excursions appear between 25% $g_1^0$and 20% $g_1^0$ (Fig. 4.9). At 25% $g_1^0$ the most southerly latitude reached is approximately $-10°$, but at 20% $g_1^0$, full polarity reversals are observed for some locations before the VGP returns to a nor-

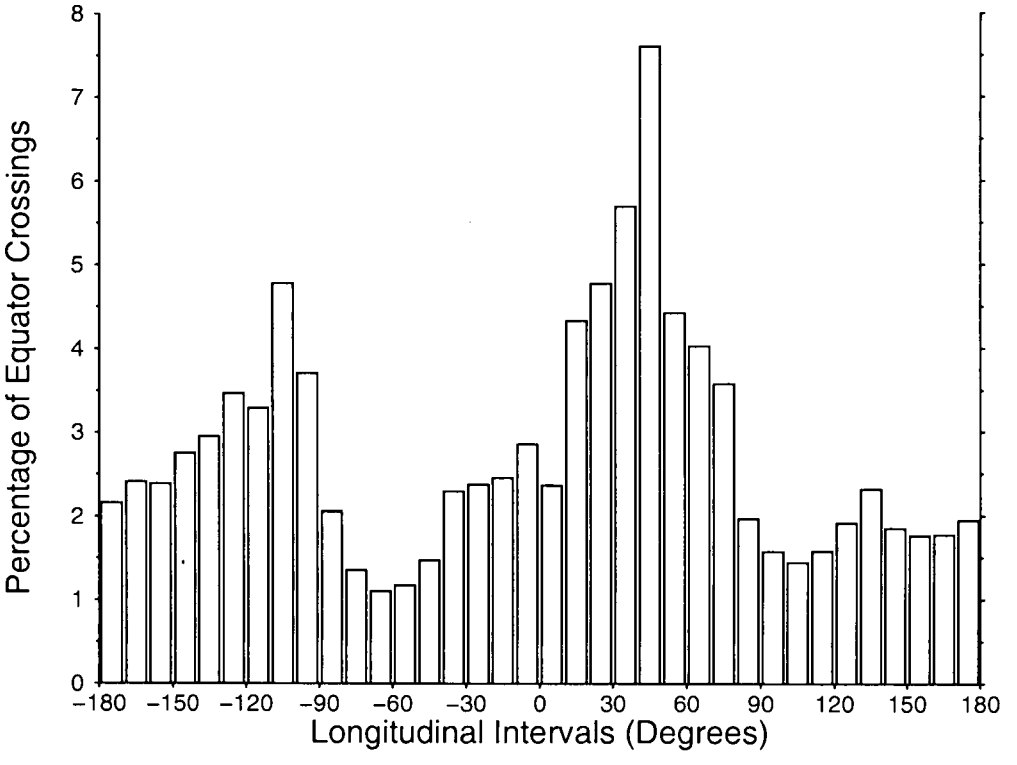


Figure 4.6: Percentage of VGP reversal paths crossing the equator from all global locations in 10° longitudinal intervals for the total time

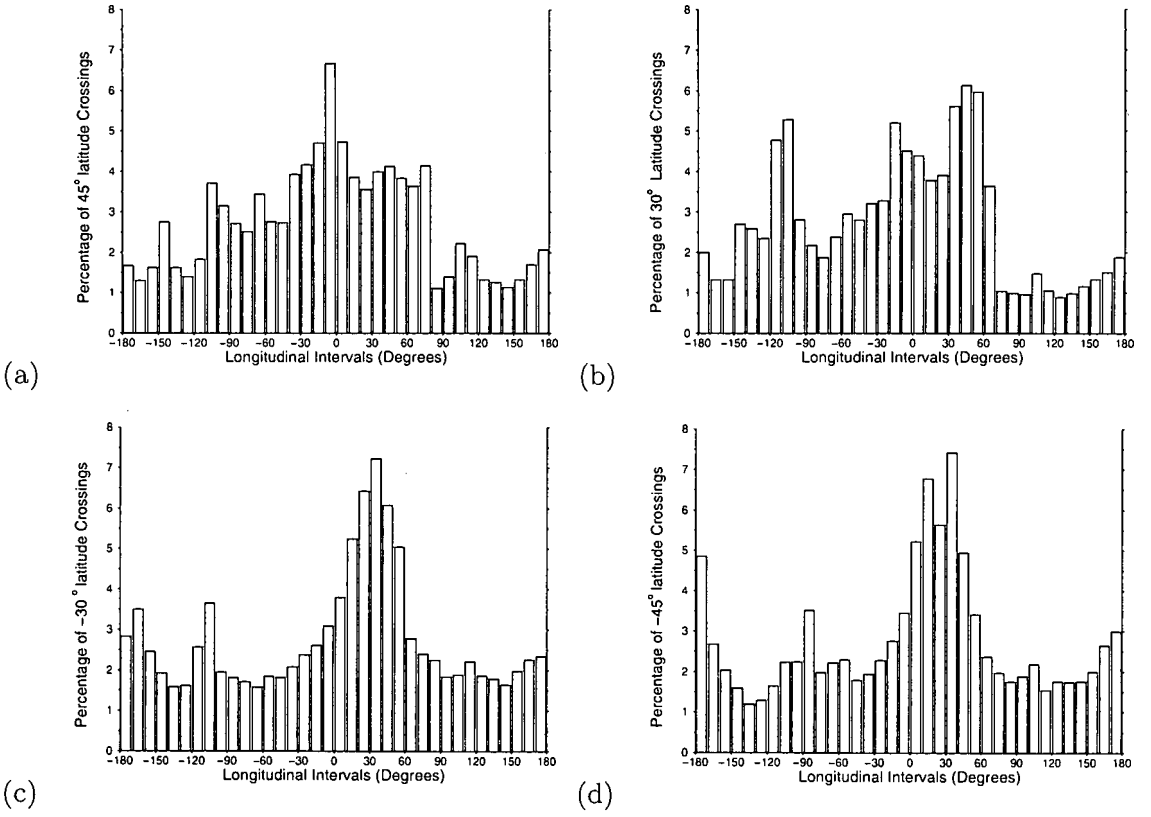


Figure 4.7: Percentage of VGP reversal paths crossing lines of latitude at (a) 45° (b) +30° (c) -30° (d) -45°, from all global locations in 10° longitudinal intervals.

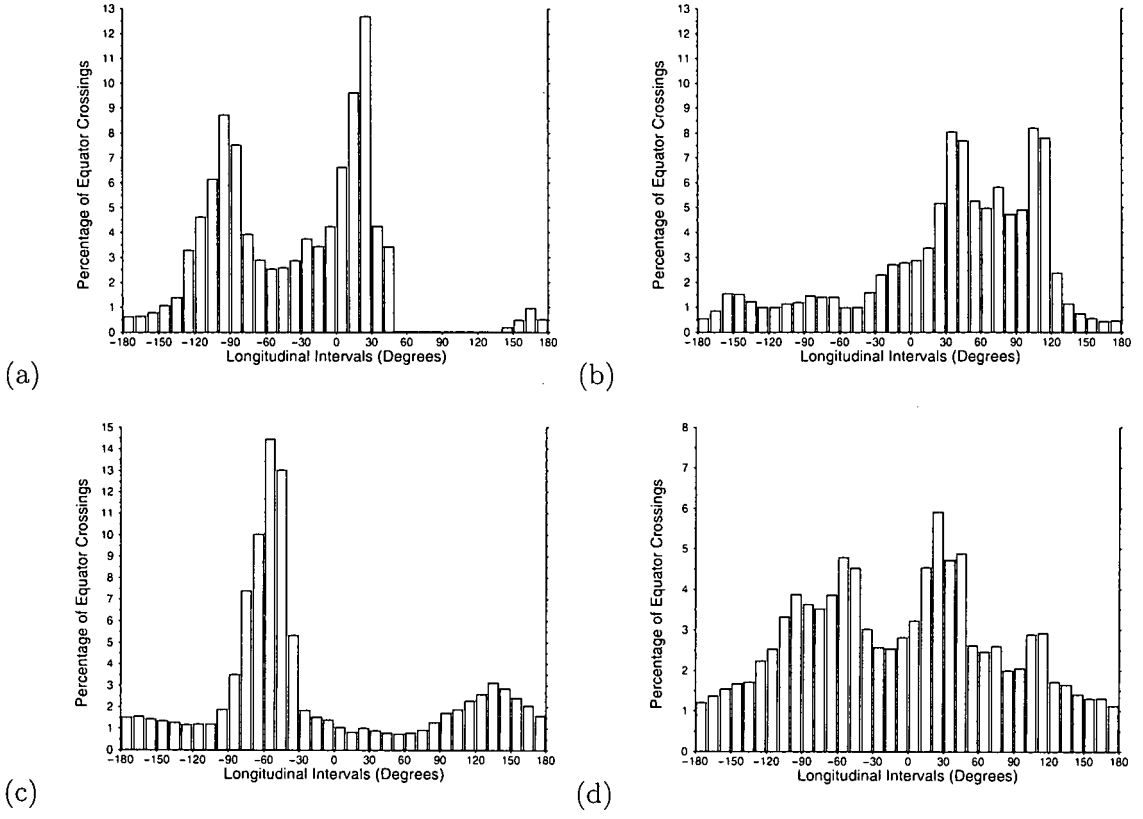


Figure 4.8: Percentage of VGP reversal paths crossing the equator from all global locations in 10°) longitudinal intervals when total reversal process starts at (a) -4000 A.D. (b) -3000 A.D. (c) -2000 A.D.. (d) Average percentage of VGP paths from time periods shown in (a), (b), (c) and Fig. 4.6.

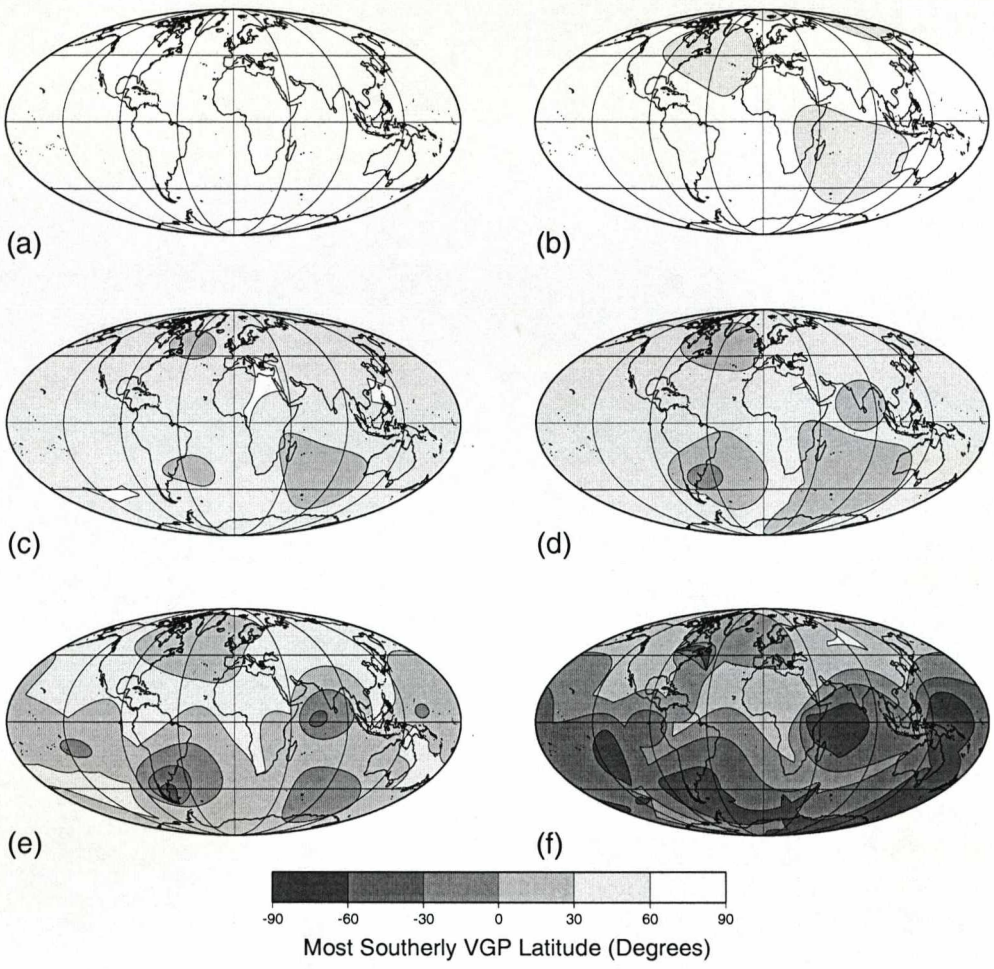


Figure 4.9: Global variation in most southerly VGP latitude reached when $g_1^0$ is set to (a) 100%, (b) 50%, (c) 30%, (d) 25%, (e) 20%, (f) 0%, over the last 5000 years.

mal field latitude. This behaviour, however, is not globally uniform, with some areas, for example Central America, observing directional changes of approximately 40-50° in latitude, while changes of almost 180° are observed in South America (Fig. 4.9e).

Importantly, the excursions generated by the model are neither global in extent or synchronous in occurrence. Fig. 4.10 shows an example of large excursions (Maldives and South Argentina) that are offset by approximately 1000 years. Both of these events coincide with minima in intensity. Although there appear to be excursions elsewhere around the time of the Maldives event, they are smaller in magnitude and emphasise the non-uniformity of the field globally.

Even for the extreme case of $g_1^0$ reduced to zero, (Fig. 4.9f) there is still a great variation in the maximum directional changes seen. The majority of locations show large VGP changes, but in some locations the VGP has only moved no further than 30-40° latitude (e.g., North Africa and North America).

(a)

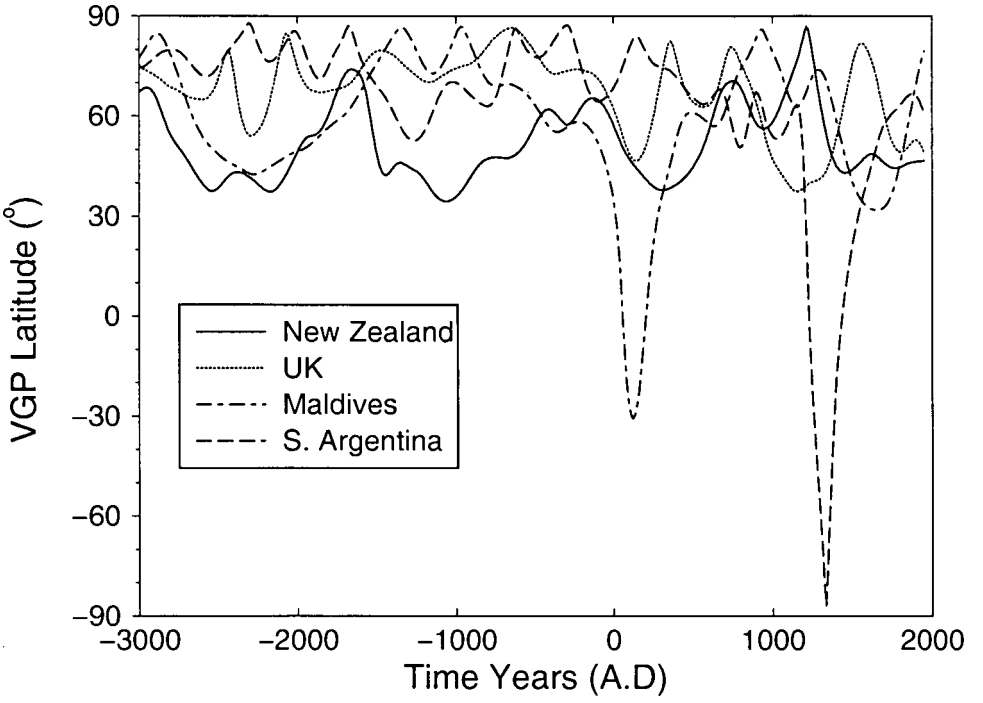


(b)

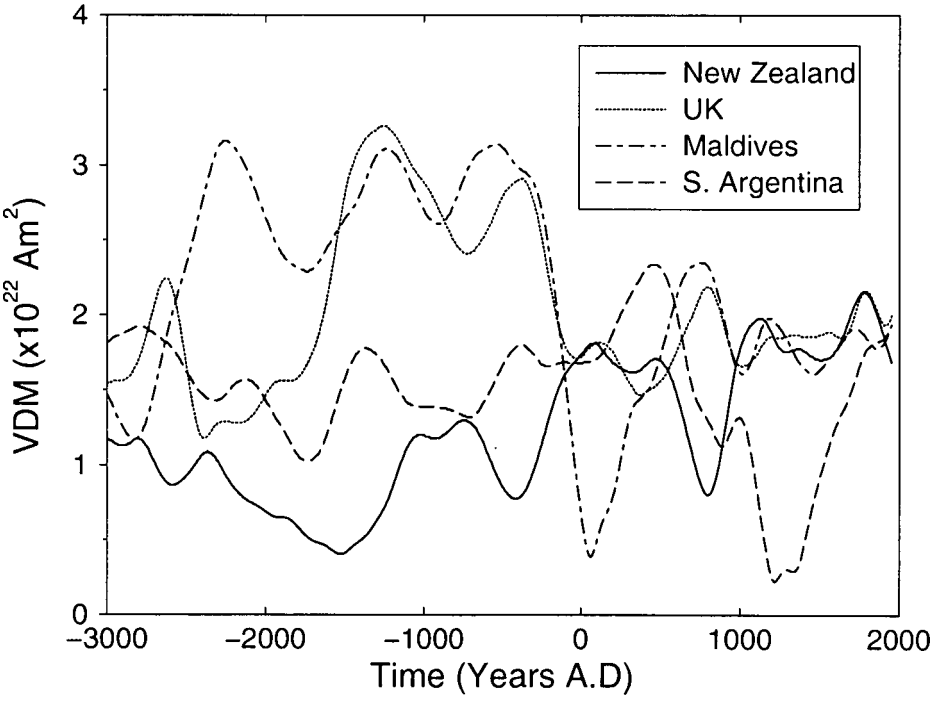


Figure 4.10: Variation in (a) VGP latitude and (b) VDM for four global locations when $g_1^0$ reduced to 20% over the last 5000 years.

## 4.5 Implications for palaeomagnetic observations

Many of the characteristics of the directional changes seen in this study have been noted in palaeomagnetic reversal studies. In Fig. 4.3c directional changes are seen to precede and follow the directional reversal. Precursor events have been well documented for the Brunhes-Matuyama field reversal (Chauvin et al., 1990; Hartl & Tauxe, 1996; Singer et al., 2002; Quidelleur et al., 2002; Brown et al., 2004; Coe et al., 2004a) and events following the main directional reversal have been recorded by Mankinen et al. (1985) and Roberts & Fuller (1990).

Directional variations are not seen globally and are not synchronous. This variation is a natural product of the combination of the non-dipole field with a reduction in axial dipole strength and does not need another specific physical mechanism. Variations in VDM through reversals have also been seen in the palaeomagnetic record. Recently, Valet et al. (1999) and Riisager & Abrahamsen (2000) have presented palaeointensity results showing large fluctuations in palaeointensity around the time of the directional reversal. These features could be attributed to the non-dipole field becoming relatively more prominent at the Earth's surface as the overall field is no longer dominated by the axial dipole component: this is observed in Fig. 4.3b.

The significant reduction in intensity observed in this model prior to the onset of the directional reversal (Fig. 4.3c) suggests that the axial dipole field needs to be substantially reduced in strength to allow the initiation of the directional reversal. This confines the directional reversal to a maximum of approximately 20% of the total reversal time in this model. Similar behaviour has been observed in the palaeomagnetic record (Quidelleur & Valet, 1996; Lin et al., 1994). Lava flows emplaced before or after flows that record the directional reversal may record a reduction in field intensity even when the VGP lies at normal or reversed latitudes (normally suggesting that the reversal had not started or had finished). These results suggest it may be important to record both intensity (including relative intensity for sedimentary records) and directional data in order to define the total length of a reversal (as noted by Williams & Fuller (1981); Prévot et al. (1985); Mary & Courtillot (1993)).

The variability in duration of the directional reversals produced using this model is of particular interest. Fig. 4.4a shows a concentration of faster directional reversals towards the equator. On average, directional reversals recorded at mid to high latitudes are over twice as long as those recorded at the equator. This result is broadly consistent with Clement (2004), who using palaeomagnetic data from the Jarmillo and Brunhes-Matuyama reversals observed that the duration of the directional reversal was shorter at equatorial latitudes.

The model generates some localised very rapid directional reversals, taking less than 10 years. The Steens Mountain lava flow studies of Mankinen et al. (1985), Coe & Prévot (1989), Coe et al. (1995) and Camps et al. (1999), all see an in-flow variation of remanent

magnetisation directions that is hard to explain with our present understanding of rock magnetic processes. Coe et al. (1995) suggest the possibility of a rapidly changing field at the time of flow emplacement. However, it was thought rapid processes within the core would be needed to produce rapid changes in the field at the Earth's surface and that this signal would be filtered out by the electrically conducting mantle (Fuller, 1989; Merrill, 1995). The rapid directional changes seen in this model are a product of only reducing the axial dipole, implying that no new core process is needed to generate this kind of feature, at least for geographically restricted locations. In effect, the rapid reversals result from a geometric rather than a physical process.

VGP paths have been the subject of much palaeomagnetic analysis. Both lava and sediment data (Valet & Laj, 1984; Tric et al., 1991; Laj et al., 1991; Clement, 1991) support the idea of preferred longitudinal paths through Eastern Asia and the Americas. Conversely, a number of studies have found no evidence for VGP paths (Valet et al., 1992; Prévot & Camps, 1993). Love (2000) carried out a statistical assessment of palaeomagnetic lava data recording reversals and excursions over the last 20 Myr. He concluded that American and Asian longitudes are preferred, with a statistical significance at about the 95% confidence level. The model of Constable (1992), applying the same method as used in this study but with with the static non-dipole field of the 1980 field, produced strongly preferred VGP paths, with two well defined longitudinal bands of preference through the Americas and Australia/Eastern Asia. In comparison, the model shows much greater complexity and variability in the geometry of the paths taken (Fig. 4.5). This can be attributed to influence of the time-varying non-dipole field.

In the model, there is evidence of a spatial preference of VGP paths from the same reversal and also a weak coherence of preferred paths between reversals occurring over different time periods. This trend is perhaps associated with a background time-averaged non-dipole field (Johnson & Constable, 1995); however, the preferred longitudes do not coincide with the longitudes of the magnetic flux patches described by Jackson et al. (2000).

The possible correlation with the location of flux patches at the core-mantle boundary and the location of the preferred VGP paths for the different time periods shown in Fig. 4.8 is investigated. For the reversal occurring between -4000 and 1950 A.D, there is a flux patch that persists through the central 1000 years of this reversal between approximately 40° to 135° longitude in the northern hemisphere in the CALS7K.2 model, but there is a lack of VGP crossings at the equator for this range of longitudes (Fig. 4.8a). This suggests that the presence of long-lived flux patches may not influence the the preference of VGP paths observed in this model; however, at least some of the confined paths result from a concentration of flux at the equator.

## 4.6 Discussion and conclusions

### 4.6.1 Reversals

A simple reduction of the axial dipole component of the field while leaving the time-varying non-dipole component of the field unaltered has yielded many interesting patterns. The emergence of the non-dipole field during the reversal has strongly influenced the features seen in this model. Surprisingly, for some locations, very rapid directional reversals have been seen, suggesting that rapid core processes are not necessary to produce rapid changes at the Earth's surface. The possible preference of VGP paths also suggests that new physical mechanisms are not needed to produce such features. Directional reversals occur in this model when the axial dipole component of the field has been reduced to approximately 25-20% (Fig. 4.3c).

As well as being variable in duration the directional reversal is not globally synchronous or uniform. The directional changes finished for some locations before starting elsewhere. This has important implications for possible global modelling of a reversal using palaeomagnetic data. Present age dating constraints from K/Ar or $^{40}Ar/^{39}Ar$ are on the same order of magnitude as possible reversal durations; it will therefore be difficult to resolve the possible complexity of a reversal globally, especially when so few global palaeomagnetic locations for the same reversal are available. However, at least in the model, the greater coherence in intensity between locations suggests that variations in intensity may be more useful in correlating reversal records temporally.

From palaeomagnetic data, the time it takes for the directional reversal is uncertain, with estimates ranging from a few thousand up to 28,000 years (based upon $^{40}Ar/^{39}Ar$ dating, for the Brunhes-Matuyama reversal) (Clement, 2004), suggesting the time period used in the model is at the lower limit of reversal durations. If so, then it be may expected that the true field to show greater complexity and variability in both direction and intensity than that generated by this model.

### 4.6.2 Excursions

Excursions occur naturally in the model and can be interpreted in terms of the emergence of the time-varying non-dipole components that are favoured when the axial dipole has been sufficiently reduced. In the terminology of Lund et al. (2005), these are Class I excursions, in that they are not associated with any field reversal. However, only a relatively weaker axial dipole field is required for this type of excursion, not the physical mechanisms suggested by Lund et al. (2005). A large reduction in the axial dipole to between 25-20% of the original field strength enabled large directional changes resulting in excursions. Importantly, large excursions were not global, with some areas only showing small deviations from their normal time-averaged position. This result is in good agreement with the model of Heller et al. (2003) who used the static non-dipole

field from the 1995 IGRF field model, with a reduced axial dipole. Excursions are also not synchronous, but are coupled with minima in intensity (Fig. 4.10). Therefore it is possible that excursions recorded in the palaeomagnetic record, such as the Laschamp excursion (see Merrill et al. (1996) and Lund et al. (2005) for detailed reviews) may be global to some extent, but may not be uniform in intensity or directional variations.

Quidelleur et al. (1999) also noted a similar correlation with intensity and directional variations when reducing the axial dipole component of the IGRF85 field model to 50% of its value. In addition, the spherical harmonic model of Quidelleur et al. (1999), using palaeomagnetic data from an excursion on La Palma and 30 sites from Carlut & Courtillot (1998), also produced excursions that are not global in extent; however, the axial dipole component was only reduced to 50%. As emphasised to us by C. Constable (*pers comm.*), CALS7K.2 underestimates the likely strength of the non-dipole field as the model has very little resolution above spherical harmonic degree 4. To test the influence of this effect, a similar experiment was performed with the model GUFM (Jackson et al., 2000), based on historical data, and reduced the magnitude of the axial dipole coefficient to 50%. While the time interval of that model is insufficient to generate a suite of clearly defined excursions, there is nonetheless a strongly reduced VGP latitude (approaching 0°) at some locations, and in comparison with CALS7K for the same interval, an average underestimate of the minimum latitude of about 30°. It is suggested that the excursion effects shown in Fig. 4.10 are likely to be even more significant in the real Earth than in these experiments, and could occur for an axial dipole magnitude only half of the current value, in agreement with Quidelleur et al. (1999).

### 4.6.3 Synthesis

The simple models for reversals and excursions that have been investigated have demonstrated many features seen in the palaeomagnetic record, but are by no means consistent with all the available data. In particular, some excursions are thought to be global, a feature that this model reproduces; however, they are not uniform in character, which is not observed in the palaeomagnetic record. The model does not include many physical effects which may be present; the study of suitable dynamo simulations is clearly the appropriate way of investigating such effects (e.g Coe et al., 2000). However, it does demonstrate that some observed features in the palaeomagnetic record may result from the geometric effect of the upward continuation of the geomagnetic field from the core-mantle boundary to the Earth's surface, and not require specific physical mechanisms. Perhaps most importantly, the results suggest that measurements of intensity (even relative intensity) may be of primary importance in considering the structure and development of reversals and excursions.

# Chapter 5

# The Matuyama-Brunhes geomagnetic field reversal recorded in lavas from La Palma (Canary Islands) and Guadeloupe (West Indies)

In the previous chapter a range of geomagnetic field behaviour was generated at the Earth's surface using a simple mathematical reversal model. The next step in developing our understanding of reversal behaviour is to analyse natural samples that have recorded past reversals. In this chapter the most recent field reversal, the Matuyama-Brunhes (MB), has been investigated. Lava samples that record the MB reversal have been collected from the islands of La Palma in the Canary Islands and Guadeloupe in the West Indies. Microwave absolute palaeointensity analysis, thermal palaeodirectional analysis and detailed rock magnetic experiments have all been performed. The majority of this chapter focuses on these results and their interpretation. The chapter ends with a discussion, in which results from this study are compared with previous MB studies, the simple mathematical reversal model presented in Chapter 4 and a model of the MB reversal by Leonhardt & Fabian (2007).

## 5.1 Introduction

Understanding the global temporal evolution of the geomagnetic field during reversals can provide important constraints on conditions at the core-mantle boundary and on geodynamo processes (Olson & Amit, 2006). Many palaeomagnetic studies from both sedimentary and lava sequences have sought to uncover details of the reversal process. To fully characterise the behaviour of the geomagnetic field the full magnetic vector must be calculated, requiring both directional and intensity data. Sedimentary sequences provide a quasi-continuous record of directional changes (Coe & Glen, 2004), but lack

absolute palaeointensity data. Volcanic records can provide both palaeodirection and absolute palaeointensity; however, they only record fragmentary behaviour of the field at one location on the Earth's surface and where geographically dispersed multiple records exist it is extremely difficult to correlate them temporally and establish features globally (Constable, 1990; Gubbins, 1999; Brown et al., 2007; Leonhardt & Fabian, 2007).

The fidelity of both sedimentary and volcanic records is of concern. Problems affecting sedimentary records include: secondary magnetic overprints that can be difficult to remove (Valet et al., 1988); smoothing of the geomagnetic signal caused by low sedimentation rates (Channell & Lehman, 1997; Channell et al., 2004) or to delayed NRM acquisition related to diagenesis and grain growth chemical-remanence mechanisms (Langereis et al., 1992; van Hoof et al., 1993); shallowing of inclination (Celaya & Clement, 1988; Barton & McFadden, 1996; Tauxe & Kent, 2004; Tan et al., 2007).

Determining absolute palaeointensity from volcanic rocks is also problematic, the accuracy of determinations being affected by the natural state of the samples and by laboratory experiments. The majority of volcanic samples contain a mixture of magnetic remanence carriers, which can cause non-ideal behaviour during palaeointensity experiments. Samples may have been oxidised at high or low temperatures in nature, possibly resulting in considerably inaccurate determinations (Tanaka & Kono, 1991; Yamamoto et al., 2003; Tarduno & Smirnov, 2004; Smirnov & Tarduno, 2005; Yamamoto, 2006; Biggin et al., 2007a). In the laboratory, methods that use bulk heating (Thellier & Thellier, 1959; Shaw, 1974a) can cause alteration of magnetic minerals, changing the changing the relationship between applied magnetic field and thermoremanent magnetisation (TRM): a common reason for the failure of palaeointensity experiments. Cooling rate differences between nature and the laboratory can also cause over or underestimation of palaeointensity depending upon the dominant remanence carrier (Fox & Aitken, 1980; Halgedahl et al., 1980; Leonhardt et al., 2006). The best method to obtain accurate absolute palaeointensity determinations without ambiguity from non-ideal recorders is still disputed; however, new techniques (Hill & Shaw, 1999; Cottrell & Tarduno, 1999; Yamamoto et al., 2003; Dekkers & Böhnel, 2006) and new protocols for the Thellier method (Riisager & Riisager, 2001; Fabian, 2001; Yu et al., 2004; Biggin et al., 2007b) have made significant improvements in obtaining accurate data and in detecting data affected by non-ideal remanence carriers.

In addition to having reliable magnetic measurements, accurate dating of both sedimentary and volcanic reversal sequences is required to correlate geomagnetic field variations globally and to constrain the core processes that generate the magnetic field (Singer et al., 2005; Leonhardt & Fabian, 2007). The need for accurate dating is highlighted when the possible complexity and global non-uniformity of the field during a reversal is considered (Coe & Glen, 2004; Brown et al., 2007).

In this chapter four sections from the island of La Palma, Canary Islands, and one

section from the island of Guadeloupe, West Indies have been revisited. Sections from La Palma were previously studied by Quidelleur & Valet (1996) and Valet et al. (1999) and the section from Guadeloupe was studied by Carlut et al. (2000) and Carlut & Quidelleur (2000). A recent study of the MB reversal by Gratton et al. (2007) using the microwave palaeointensity technique was able to determine palaeointensity from a series of lava flows from Chile recording the transitional field. This motivated a re-examine of these sections with the hope of improving the palaeointensity record.

## 5.2 Background

### 5.2.1 La Palma

The island of La Palma in the Canary Archipelago (Fig. 5.1a and b) is positioned on the slow moving African plate approximately 100 km north of the possible emergence of a mantle plume beneath the island of El Hierro (Prægel & Holm, 2006). Apart from the Hawaiian Islands, the Canary Islands are the most studied group of islands in the world (Carracedo et al., 1998). They are built on oceanic crust of Jurrasic age (Roest et al., 1992), with the crust underlying La Palma and El Hierro being 150-156 Ma (Watts, 1994). Unlike the Hawaiian-Emperor chain, there is not an age progression of volcanism related to a possible mantle plume. However, the origin and evolution of the islands is far from being well explained and modelled, especially when compared to the Hawaiian Islands (Carracedo et al., 1998).

La Palma rises 6500 m above the sea floor and 2400 m above sea level (Valet et al., 1999). It is divided into three main geological units (Singer et al., 2002): (1) Basement intrusive rocks exposed in the Caldera de Taburiente, which are part of the exhumed Pliocene sea mount; (2) Older subaerial lavas which form the Taburiente and Bejenado volcano's; (3) the younger Cumbre Vieja volcano (Staudigel et al., 1986; Guillou et al., 1998; Carracedo et al., 1999). The Taburiente Volcano formed the north part of the island during the Matuyama and Brunhes Chrons, with $^{40}K/^{40}Ar$ and $^{40}Ar/^{39}Ar$ ages dating lavas between 1.6 Ma to 0.5 Ma (Carracedo et al., 1999; Quidelleur et al., 1999; Tauxe et al., 2000; Valet et al., 1999; Guillou et al., 2001; Quidelleur et al., 2002, 2003).

ME and ET sections previously studied by Valet et al. (1998, 1999) are located at El Time in the western part of La Palma (Fig. 5.1a and c) and are part of the northwestern flank of the Caldera de Taburiente, which was formed by large landslides (Ancochea et al., 1994). This section either belongs to the the Upper Old Series (Ancochea et al., 1994) or the Cumbre Nueva Series (Navarro & Coello, 1993) and therefore could have originated from two different eruptive centres. The dominant lava type is Pahoehoe basalt, which is often topped with a layer of scoria. Palaeosol and cindercone layers are common throughout both sections. The ET section is especially complicated, with flows pinching in and out and intersected by dykes.

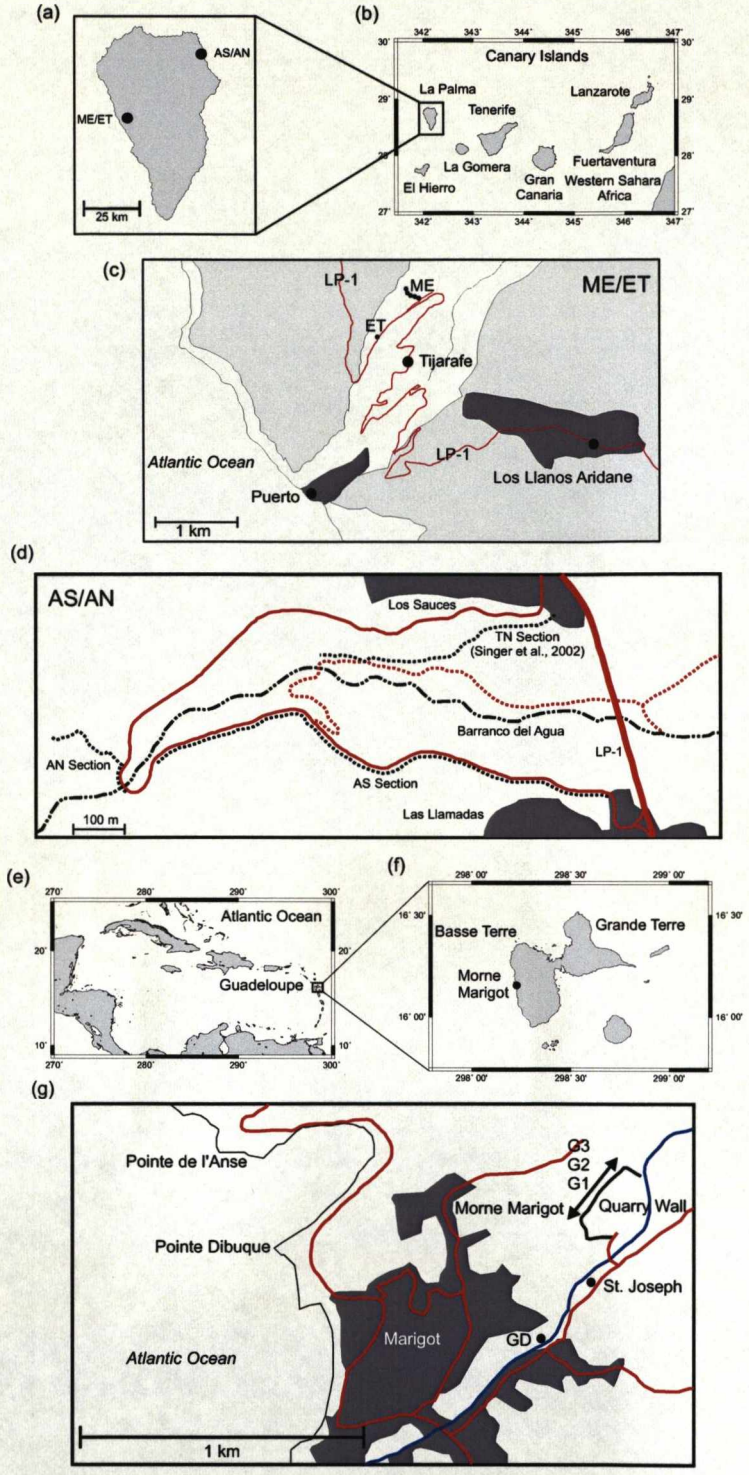


Figure 5.1: (a) Map of La Palma with studied sections labelled. (b) La Palma in relation to the other Canary Islands. (c) Detailed map of area around ME/ET sections. (d) Detailed map of area around AS/AN sections. (e) Guadeloupe's position in the Caribbean island chain. (f) Location of the Morne Marigot quarry sections on the island of Basse Terre, Guadeloupe. (g) Detailed map of the area around Morne Marigot. (c, d, g) Light grey blocks are areas of higher relief; dark grey blocks are urban areas; red lines are roads; dashed red lines are tracks; blue lines are rivers; Dash-dot-dot-dash lines are the trace of the base of valleys; dashed black lines are section lines.

Palaeomagnetic sampling was conducted in March 2006. Using previous field notes (VS) and markers left by Valet et al. (1998, 1999) the same sections and flows as Valet et al. (1999) were sampled. The ME and ET sections are located at 28.67°N, 17.94°W, approximately 700m apart along the road LP-1 (Fig. 5.1c and Fig. B.1). All flows are horizontal; however, given their thin nature and the distance between the sections, it was not possible to correlate the two sections in the field. Five flows from the ET section and the top 20 flows of the ME section were sampled. 11 25 mm cores were taken from the ET flows and 100 from the ME flows. The centres of the flows were sampled to avoid problems with remagnetisation by overlying flows (Valet et al., 1998) (e.g. Fig. 5.2a). $^{40}K/^{40}Ar$ dates place from the ME section two flows either side of the polarity reversal at 788 $\pm$ 12 ka and 784 $\pm$ 13 ka (Quidelleur et al., 2003).

The study of Valet et al. (1999) provides one of the most detailed records on palaeointensity variations around a geomagnetic field reversal. Although no transitional directions were obtained from these sections, palaeointensity was determined from 45 volcanic units. Results varied from 15 $\mu$T to 60 $\mu$T for a number of flows with stable directions before reducing to $\sim$ 7 $\mu$T prior to the polarity change. Palaeointensity after the reversal was also variable, recovering to $\sim$ 60 $\mu$T. Compared with other intensity data from the PINT03 database (Perrin & Schnepp, 2004) for the last 5 Myr these results seem anomalously high. The palaeointensity records from the ME and ET sections were used to calibrate the relative intensity data from the sedimentary records used in a model for the MB reversal (IMMAB4) (Leonhardt & Fabian, 2007).

The AS and AN sections are located in the Barranco del Agua, in the north east of the island (Fig. 5.1a and d) (28.80°N, 17.77°W). The lava flows are basaltic and part of the Upper Old Series of the Taburiente Stratovolcano (Navarro & Coello, 1993). It is unclear whether these flows are from the same eruptive centre that produced the flows at El Time. Scoria layers (in one case 5 metres thick) and palaeosols are again seen.

The sampling of Quidelleur & Valet (1996) and Singer et al. (2002) on the southern side of the gorge was roughly followed(Fig. B.2); the AS section (LL in Quidelleur & Valet (1996) and TS in Singer et al. (2002)). For the northern side of the gorge (AN section) the vertical section chosen by Quidelleur & Valet (1996) was followed (LS section) (Fig. B.3). The TN section from Singer et al. (2002) was difficult to trace and an accurate stratigraphy was not confidently resolved. The large number of flows and ambiguity in the delimitation of some of the flows means that the results from this chapter and the Quidelleur & Valet (1996) and Singer et al. (2002) studies can not be directly compared. 77 25 mm cores were taken from 20 flows from the AS section that sample the time around the reversal (107 cores from 29 flows were sampled in total; the youngest flows contain an excursion around 600 ka (Quidelleur et al., 1999) or 580 ka (Singer et al., 2002)). 57 25 mm cores were taken from 16 flows from the AN section.

Quidelleur & Valet (1996) obtained both palaeodirection and palaeointensity results

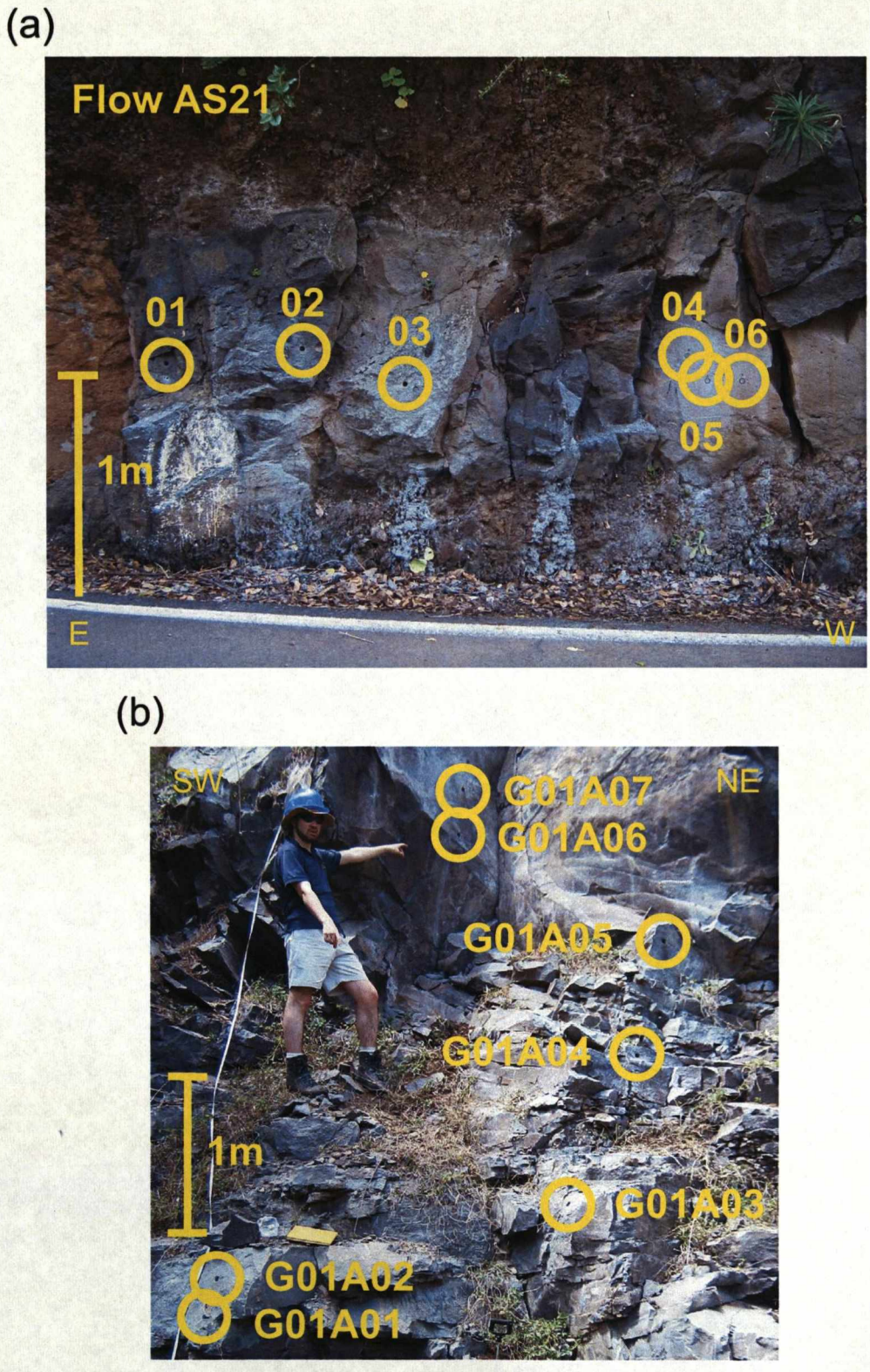


Figure 5.2: Field photographs of (a) flow 21 AS section, La Palma. Samples are taken approximately along a horizontal profile along the centre of the flow. (b) Flow G01 section A. Samples taken approximately along a vertical profile through the flow. Author is in shot. Yellow circles ring sample holes.

from flows on both sides of the gorge. Palaeointensity was obtained from 17 flows; however, results from 9 flows were corrected using the method of Valet et al. (1996). Palaeointensity prior to the polarity change is low with a minimum value of 4 $\mu$T. One $^{40}K/^{40}Ar$ date of 797 $\pm$ 12 ka was obtained from the northern side of the gorge from a reversed polarity flow (Quidelleur et al., 2002). No transitional directions were obtained in the Quidelleur & Valet (1996) study; however, Singer et al. (2002) sampling a different section on the northern side of the gorge found two flows that recorded transitionally reversed directions. These flows were dated by $^{40}Ar/^{39}Ar$ to be 780 $\pm$ 10 ka and 803 $\pm$ 10 ka. Two flows lower in the stratigraphy were dated at 791 $\pm$ 19 ka and 796 $\pm$ 10 ka and Singer et al. (2002, 2005) suggest these flows record a precursor event to the main polarity change of the MB (Hartl & Tauxe, 1996; Brown et al., 2004; Gratton et al., 2007).

### 5.2.2 Guadeloupe

The volcanic island of Guadeloupe is situated in the West Indies in the Atlantic Ocean (Fig. 5.1a) and is part of an island arc resulting from the subduction of the Atlantic plate under the Caribbean plate (Komorowski et al., 2005). The island is divided into two distinct parts; the older Grande-Terre in the east and Basse-Terre to the west. Grande-Terre comprises older volcanics of pre-Miocene age overlain by Pleistocene limestone, while Basse-Terre is entirely volcanic; the oldest parts of the island thought to be no older than 2.79 Ma from $^{40}K/^{40}Ar$ dating methods (Samper et al., 2007).

Palaeomagnetic sampling took place in March 2005 and was concentrated on the southern part of the west coast of Basse Terre (Fig. 5.1b), where the age of volcanism was determined to be less than 1 Ma by $^{40}K/^{40}Ar$ dating (Blanc (1983); Carlut et al. (2000), further $^{40}K/^{40}Ar$ dating by Samper et al. (2007) subsequent to this field trip is in agreement with this conclusion). The sampling sites for this study are: 1) Morne Marigot quarry (16.1°N, 298.2°E), at a rare exposure of superposed andesitic lavas (heavy vegetation on the island prevents good rock exposure)(Fig. 5.1g and Fig. B.4); 2) a river cut section $\sim$ 500 m to the south west of the quarry and $\sim$ 20 m below the base of the quarry (Fig. 5.1g).

The same Morne Marigot quarry flows studied in Carlut et al. (2000) and Carlut & Quidelleur (2000) was re-sampled. Carlut & Quidelleur (2000) first identified field variations related to the MB reversal in sections at Morne Marigot in three flows. Following alternating field and thermal demagnetisation experiments, a change in polarity up the sequence, from transitional to reversed to normal from bottom to top, was observed. $^{40}K/^{40}Ar$ dating of the lava flows yielded dates of 777 $\pm$ 14 ka for the stratigraphically lowest (transitional) flow (GU09) and 785 $\pm$ 19 ka for the stratigraphically highest (normal) flow (GU11), respectively. These ages identified the sequence as partially recording the MB reversal. Carlut et al. (2000) carried out palaeointensity experiments

on these three flows, using the double-heating variant of the Thellier method (Coe, 1967a). Some experiments were conducted in an Argon atmosphere, and some heated in air. Four samples yielded a mean flow value of 5.5 ± 1.0 $\mu$T for the reversed flow (GU09) and 2 samples yielded a mean flow value of 11.0 ± 2.7 $\mu$T for the normal flow (GU11), with one value corrected for non-linearity in the Arai-Nagata plot, using the correction method of (Valet et al., 1996). The transitional polarity flow (GU10) did not yield any palaeointensities because of thermochemical alteration observed during the Thellier experiments (Carlut et al., 2000). It is the failure of the Thermal palaeointensity experiments that prompted us to try microwave palaeointensity analysis to obtain transitional palaeointensity data from this section.

In this study flows GU09, GU10 and GU11 from Carlut et al. (2000) and Carlut & Quidelleur (2000) are called G01, G02 and G03 and divided the quarry into three vertical sections (e.g. Fig. 5.2b): A, B and C. Vertical sections were approximately 55 m apart. The A section included all three flows; B included G01 and G02; C only sampled G01. The quarry was heavily vegetated so exposure was limited. G01 is the lowest stratigraphic unit and is 160 m in lateral extent, with an average flow thickness of 7 m with 4 m of scoria on top (Fig. B.4); G02 is 10 m thick on average with 3 m of scoria above that; G03 is the highest stratigraphic unit and is on average 3 m thick with 3 m of scoria above that. 20 cores were sampled from G01, 14 were sampled from G02 and 8 were sampled from G03. Cores were taken in vertical sections throughout the thickness of the flows, with sample 01 being near to base of the exposed flow. Care was taken not to sample the Scoria.

The river cut section is labelled GD and has not been sampled before. No radiometric dates exist; however, the height of the flow and the roughly horizontal dip of the flows in this area suggests that GD is older than the sequence at Morne Marigot. It was sampled to provide directional and palaeointensity information prior to the transitional sequence. 8 cores were sampled.

For all La Palma and Guadeloupe flows the names assigned in the field are retained, but they have also been given a flow number (FN). Conversions from the field names to the flow numbers are shown in the tables in Section D. All graphs showing results from individual flows are plotted as flow number.

## 5.3 Results

### 5.3.1 Rock magnetism

The results of individual rock magnetic experiments and a summary table of these results are shown in Appendix C.

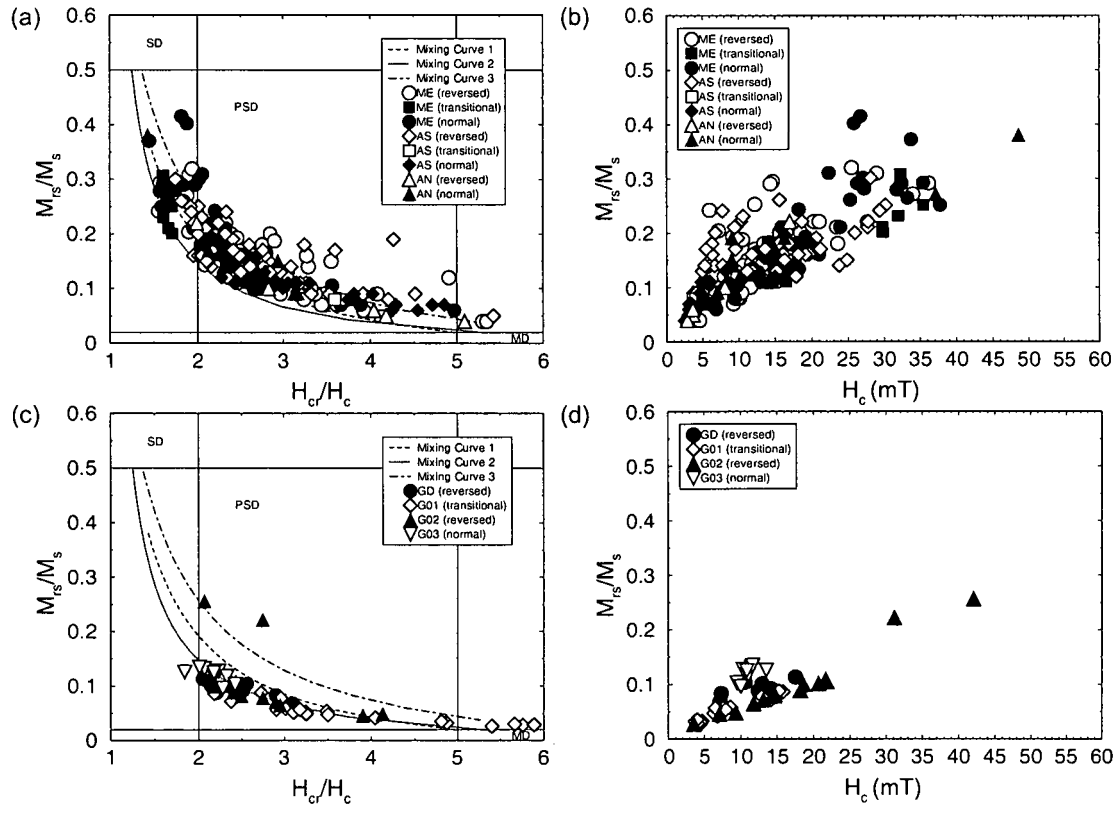


Figure 5.3: Day et al. (1977) plots (a and c) and squareness against coercivity plots (Tauxe et al., 2002) (b and d) for La Palma (a and b) and Guadeloupe (c and d) lava flows. Samples split between reversed, transitional and normal field directions. Transitional flows are ME45, ME46 and AS17 (FN18). Day et al. (1977) plots modified using results from (Dunlop, 2002). Curves 1 to 3 are theoretical mixing curves of SD and MD particles for TM0 from Dunlop (2002).

### La Palma

Hysteresis parameters are plotted in Fig. 5.3a and b and are listed in Table C.1, Table C.2, Table C.6 and Table C.9. The majority of samples plot in the pseudo-single domain (PSD) area of the Day et al. (1977) plot and along the theoretical mixing curves of single domain (SD) and multi-domain (MD) particles for TM0 from Dunlop (2002). All La Palma flows have similar characteristics on the Day et al. (1977) plot and squareness against coercivity plots (Tauxe et al., 2002). All flows show a spread in $M_{rs}/M_s$, $H_c$ and $H_{cr}/H_c$ to some degree. Some flows show a spread in $H_{cr}/H_c$ up to 4 and in $M_{rs}/M_s$ up to 0.3 (e.g. ME49). In these cases there is a range of magnetic particle types and behaviour (such as dipolar magnetostatic interactions between SD particles). The magnetic properties of ME47, ME48 and ME49 are discussed in Chapter 6.

Three broad types of thermomagnetic behaviour have been identified for the La Palma samples: Type 1, 3 and 5 (Fig. 5.4). All thermomagnetic results are listed in Table C.1, Table C.6 and Table C.9. 171 samples from all La Palma sections were

measured. 63 samples from 33 flows show type 1 behaviour. Type 1 curves show a single magnetic phase with Curie temperatures between 446°C and 540°C, corresponding to possible titanomagnetite compositions between TM19 and TM07. Magnetisation is reduced on cooling and there is range of irreversibility. At 100°C the difference in induced magnetisation between the two curves ranges from 3% to 45%. The magnetic phase producing type 1 behaviour could either be a low Ti-titanomagnetite or may result from high temperature deuteric oxidation of primary high titanium titanomagnetite producing a low titanium titanomagnetite phase (Carmichael & Nicolls, 1967; Mankinen et al., 1985). No microscopy was carried during this study so oxidation cannot be confirmed.

Type 3 curves (Fig. 5.4b-d) (70 samples from 45 flows) have a low titanium titanomagnetite phase (Curie temperatures between 398°C and 580°C, corresponding to compositions between TM29 and TM0) and another higher titanium titanomagnetite phase (Curie temperatures between 131°C and 333°C, corresponding to compositions between TM67 and TM38). The three divisions of type 3 show the variations in the titanomagnetite compositions. Such heating curves have been previously been observed for samples where high temperature deuteric oxidation has converted only part of the high titanium titanomagnetite phase to a low titanium titanomagnetite phase or the low Curie temperature phase results from the presence of titanomaghemite (Moskowitz, 1981; Mankinen et al., 1985; Yamamoto & Tsunakawa, 2005). All type 3 cooling curves show an increase in induced magnetisation (at least for some of the temperature range (type 2a)). Type 3c curves show the largest increase in induced magnetisation (up to 66% at 100°C). Some cooling curves show complete oxidation of the high titanium titanomagnetite phase to a single lower titanium phase (Fig. 5.4b). Other cooling curves show less oxidation of the higher titanium phase (Fig. 5.4c and d).

Type 5a and 5b curves (Fig. 5.4e and f) (39 samples from 18 flows) show a range of low Curie temperatures from between 94°C and 143°C. On heating, Curie temperatures rise to between approximately 450°C and 550°C and the curves show pronounced irreversibility. In some examples there is an increase in induced magnetisation on cooling (measured at 100°C) up to 14 times the original magnetisation. The oxidation product at the higher Curie temperature could either be titanomaghemite or a low titanium titanomagnetite formed from a primary high titanium titanomagnetite (between TM71 and TM65) (Grommé et al., 1969). In Type 5a curves there is a very slight increase in induced magnetisation between 400°C and 500°C which could suggest inversion of titanomaghemite to titanomagnetite; however, without performing thermomagnetic experiments in a vacuum it is not possible to determine whether this bump and the large increase in induced magnetisation on cooling are a product of oxidation during the laboratory heating or to the inversion of titanomaghemite to titanomagnetite. Type 5b curves do not show an increase in induced magnetisation on heating between 400°C

and 500°C. On cooling, type 5a curves show a mixture of secondary magnetic phases, whereas type 5b curves show a single secondary magnetic phase. An example of a microwave palaeointensity experiment performed on a sample with type 5b behaviour is shown in Fig. 5.13c.

Type 1 curves were dominant for the ME section (41 samples from 25 flows) and there were no examples of type 5 curves. The AS section was approximately equally divided between type 1, type 3 and type 5 curves. Type 3 curves were dominant for the AN section (11 samples from 11 flows). For a number of flows the thermomagnetic behaviour within a type is variable (see also Chapter 6) and for a number of flows two types of curve have been observed. For example, AS20 (FN22) shows both type 1 and type 5 curves. This variation could result from inhomogeneous starting compositions or to inhomogeneous oxidation of the titanomagnetite particles during initial cooling at high temperature or by low temperature oxidation during weathering.

Examples of low-temperature susceptibility curves are shown in Fig. 5.5 and Fig. 5.6. All results are listed in Table C.4, Table C.7 and Table C.10. 210 samples were tested and a range of low-temperature behaviour was determined. They are broadly categorised into eight types (Fig. 5.6). Considering titanomagnetite as the dominant magnetic phase in this sample set, low-temperature behaviour is influenced by a number factors including composition (titanium content in titanomagnetite) and oxidation (either partial maghemitization of magnetite at low temperatures ((Özdemir et al., 1993)) or to possible homogenisation of ilmenite intergrowths to titanomagnetite at high temperatures (c.f. Smirnov & Tarduno (2005)). Fig. 5.5a shows a susceptibility maximum at around 85 K. This is probably caused by partial suppression of the Verwey transition of a low titanium titanomagnetite phase containing MD particles (Moskowitz et al., 1998) and could be caused by a degree of partial oxidation. In some examples the transition is very suppressed with the ratio of initial susceptibility to room temperature susceptibility exceeding 1 (Type I, II and III (Fig. 5.6a, b, c)) and in some examples the isotropic point disappears.

In Fig. 5.5b there is an inflection at around 50 K and a susceptibility peak between 100 K and 120 K. The former could be caused the presence of an illmenite phase (Yamamoto, 2006). The latter could be caused by the presence of titanium poor titanomagnetite of varying compositions. These observations are consistent with the results of the thermomagnetic experiments: Fig. 5.5a and b are both from samples which show type 1 thermomagnetic heating and cooling curves (they suggest the existence of low-Ti titanomagnetite without any indications of low-temperature oxidation). In Fig. 5.5b and c there are inflection points around 110 K, although they are not as pronounced compared with those shown in Fig. 5.5a and d. These curves were observed from samples showing both type 1 and type 3 thermomagnetic heating and cooling curves suggesting that no low-temperature oxidation is present. Therefore, the inflection points probably

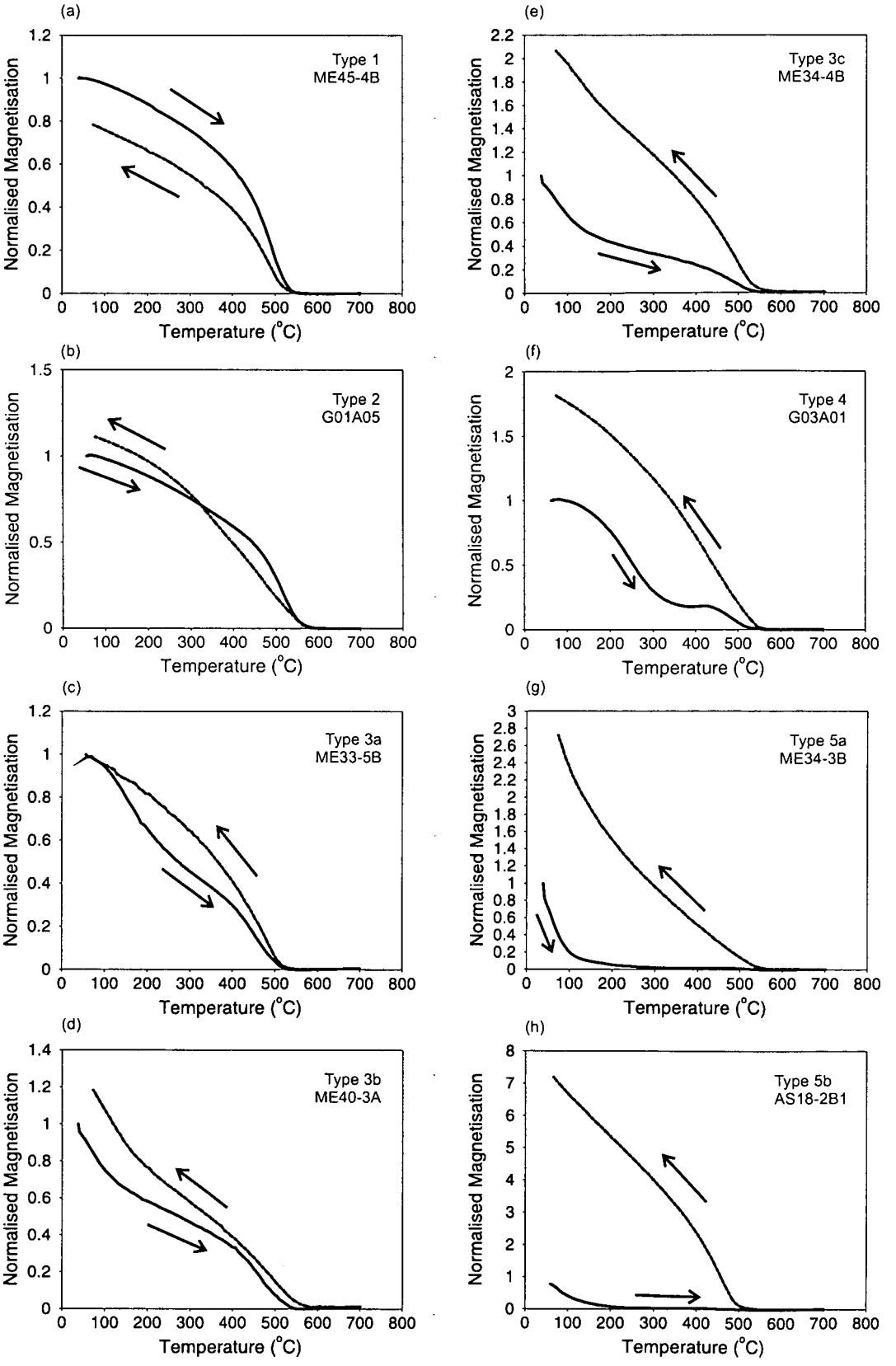


Figure 5.4: Examples of the 5 broad types of thermomagnetic curves from samples from La Palma and Guadeloupe. Arrows indicate heating (solid lines) and cooling (dashed lines).

originate from the Verwey transition of low-Ti titanomagnetite. Many flows show an internal variation of low temperature susceptibility characteristics and this in agreement with the high temperature heating and cooling curves. Such variation could possibly represent inhomogeneous deuteric oxidation of the flows.

Types III, IV and V could relate to composition (Senanayake & McElhinny, 1981; Moskowitz et al., 1998) or particle size (Thomas, 1993). Type I to V could show an increase in titanium content or a decrease an apparent decrease in particle size (or lack of MD contributions (SD magnetite particles are more readily oxidised than MD particles and easily become non-stoichiometric, and therefore no Verwey transition exists (Özdemir et al., 1993)); however, it is unclear which factor is dominant as thermomagnetic curves from sister samples indicate a range of compositions and the Day et al. (1977) plot also shows variations in particle sizes for samples from the same flows. Type VIII shows an RS value of 1.85 indicating a larger paramagnetic contribution (only two examples from ME49 show this behaviour). Type VII curves show a Hopkinson peak between -25°C and -50°C. 12 samples show this behaviour; however, it was not the only low temperature behaviour displayed form these flows (where multiple samples were measured).

Examples of frequency dependence of susceptibility results are shown in Table C.3. Fig 5.5a and c show a noticeable frequency dependence, with $\chi_{fd} = 14.6\%$ for (a) and 13.2% for (c). The frequency dependence of susceptibility may indicate superparamagnetic (SP) contributions (Mullins & Tite, 1973; Dearing et al., 1996; Worm & Jackson, 1999) or can show possible particle size variations, which could be related to the degree of high-temperature oxidation (from the partial breakdown of MD particles to SD particles) (Yamamoto, 2006).

### Guadeloupe

Hysteresis parameters are shown in Fig. 5.3c and d and are listed in Table C.12. Each flow has a distinctive distribution. The Day et al. (1977) plot shows that G01 (the transitional flow) has a range of particle types, but many samples are dominated by MD particles. G02 shows the biggest spread in hysteresis parameters, whereas G03 shows a tight cluster on both the Day et al. (1977) plot and the squareness against coercivity plots.

Four types of thermomagnetic curves are observed for the four Guadeloupe flows: Type 1, 2, 3 and 4 (Fig. 5.4). Type 1 curves (Fig. 5.4a) were determined from 29 samples from GD, G01 and G02. Curie temperatures range from 522°C to 580°C corresponding to compositions from TM09 to TM0. Induced magnetisation was reduced on cooling and the curves showed a range of irreversibility from 0% to 92% difference in induced magnetisation at 100°C. Seven type 1 curves show a small contribution from a second higher titanium titanomagnetite phase on heating above 500°C. In some examples this

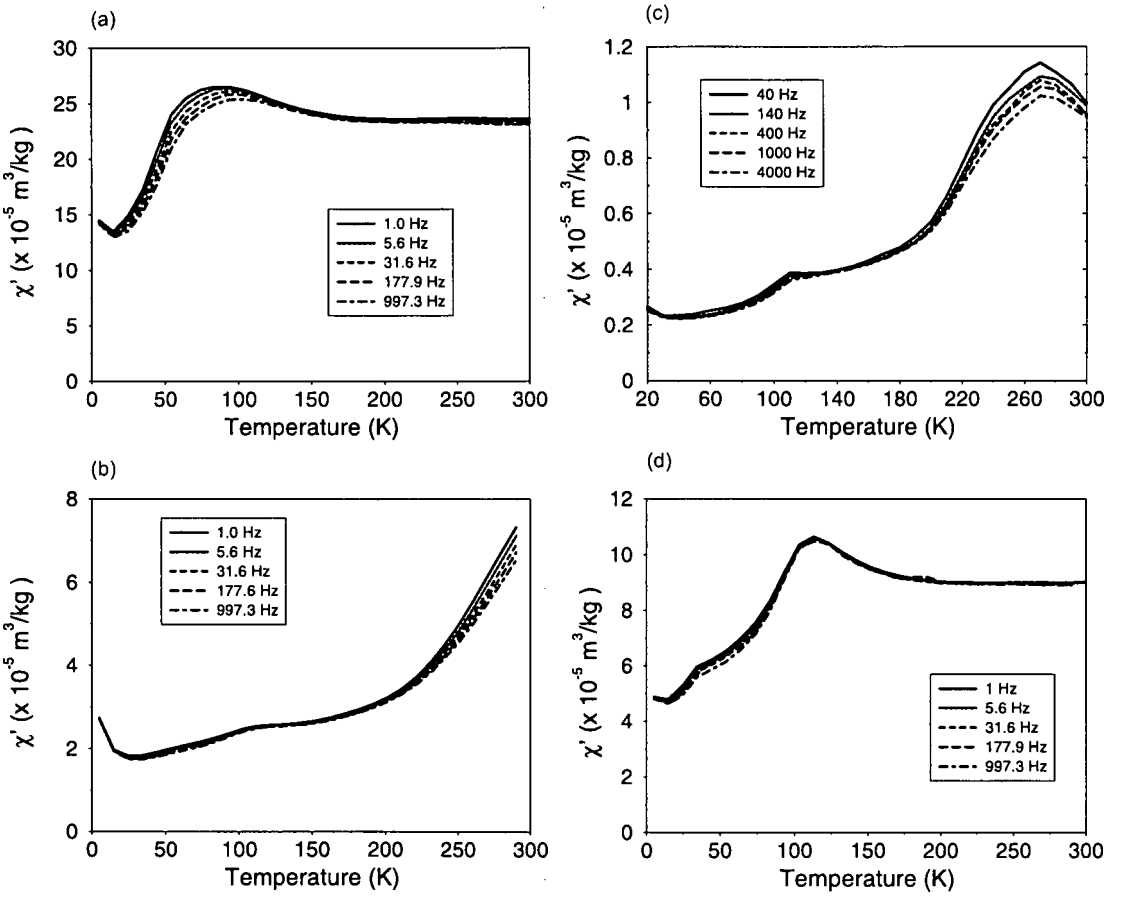


Figure 5.5: Examples of frequency dependence of low temperature susceptibility measurements for the ME section, La Palma. Samples shown are: (a) ME32-1A1; (b) ME36-1A1; (c) ME41-3B; (d) ME47-2A . (a, b, d) measured on MPMS, (c) measured on Lakeshore.

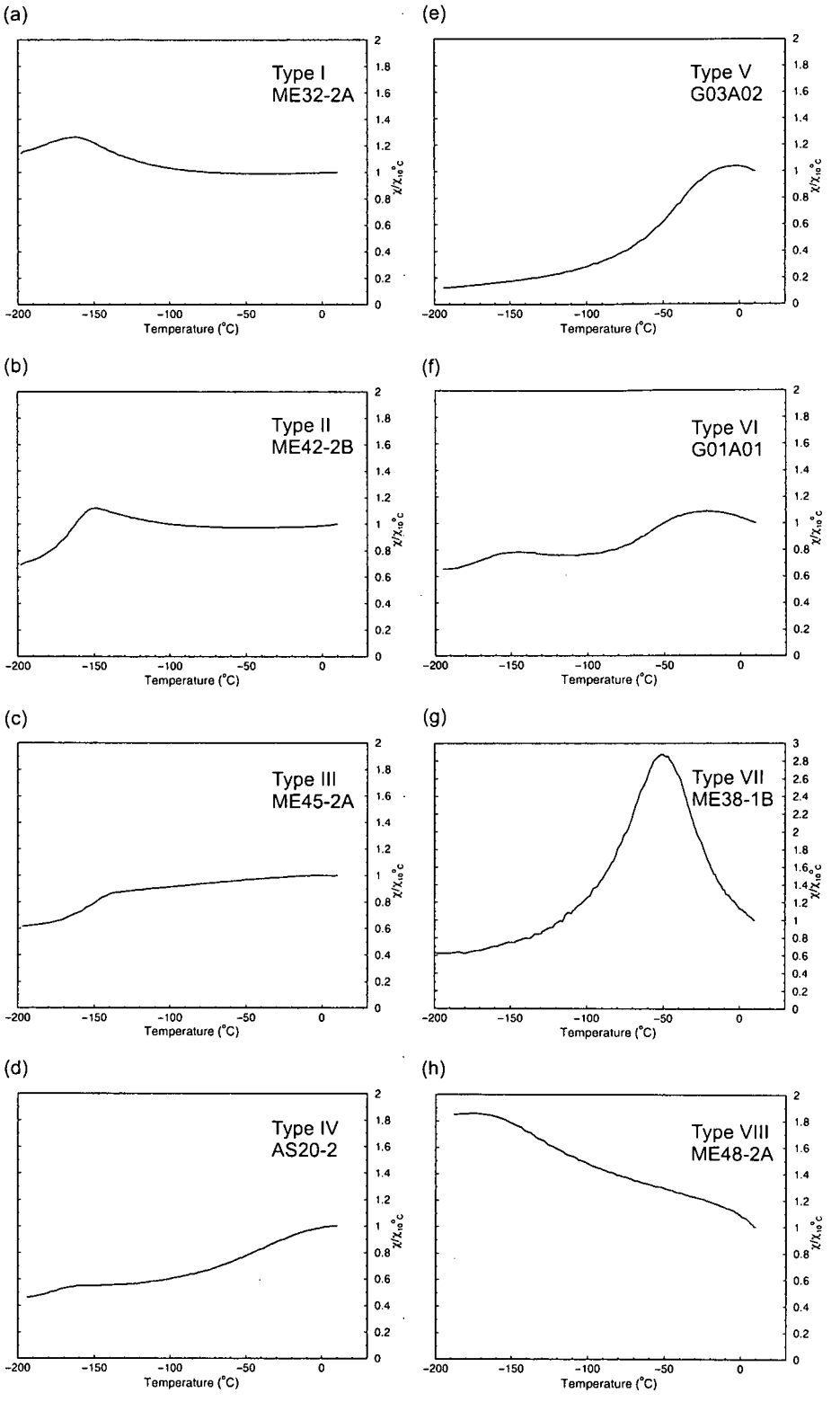


Figure 5.6: Examples of the eight types of low-temperature susceptibility graphs from La Palma and Guadeloupe. All experiments measured on Bartington MS2 susceptibility meter.

phase has a Curie temperature close to the primary phase. On cooling, a single phase was formed, with a lower Curie temperature and a reduction in induced magnetisation across the whole temperature range.

Type 2 curves (Fig. 5.4b) show a single phase, a small secondary phase or a mixture of phases on heating. On cooling the heating and cooling curves cross. 11 samples from all four flows show this behaviour. Some examples have a reduced Curie temperature on cooling and some have the same or slightly higher Curie temperature as the primary phase. This behaviour could result from a combination of oxidation of the low titanium titanomagnetite and alteration of the higher titanium magnetite to a lower titanium phase on heating (Moskowitz, 1981; Mankinen et al., 1985; Yamamoto & Tsunakawa, 2005). Type 3 curves were only observed for 10 samples from G01 and G03.

Type 4 curves (Fig. 5.4f) show a distinctive inflection point at around 420°C. Before this inflection there is a small increase induced magnetisation between 400°C and 420°C. This behaviour indicates un-mixing and inversion of titanomaghemite to titanomagnetite (Moskowitz, 1981). In these examples the amount of low-temperature oxidation of the the primary titanomagnetite to titanomaghemite is thought to be low (Yamamoto & Tsunakawa, 2005). Only four samples from G03 showed this behaviour; however, it could suggest that type 3 samples from G03 contain a mixture of titanomaghemite and titanomagnetite phases. Samples showing evidence of maghemitisation will be unsuitable for accurate palaeointensity determinations as their NRM will be a mixture of a TRM, and a chemical remanent magnetisation (CRM) carried by titanomaghemite (Tarduno & Smirnov, 2004). There are variations in thermomagnetic properties within the flows which could again suggest inhomogeneous oxidation of the lava flows and the magnetic minerals.

47 samples from the four flows underwent low-temperature susceptibility measurements. All results are listed in Table C.13. Like the samples from La Palma, Guadeloupe samples show large internal variations in low temperature types, with the exception of G03, which shows very consistent temperature dependence of susceptibility and RS values. The variability in G01, G02 and GD may be linked to different degrees of deuteric oxidation.

### 5.3.2 Directional results

Multiple 25 mm samples per flow were used to determine the directional changes recorded in the AS, AN and Guadeloupe sections (see tables in D). Only one sample per flow was used for the ME section as the initial results were in agreement with those obtained by Valet et al. (1999). Flows from the ET section appeared very weathered when sampled in the field and pilot microwave demagnetisation experiments revealed multiple components of magnetisation (Fig. 5.7). These samples are not suitable for directional or palaeointensity analysis and no further experiments were performed on

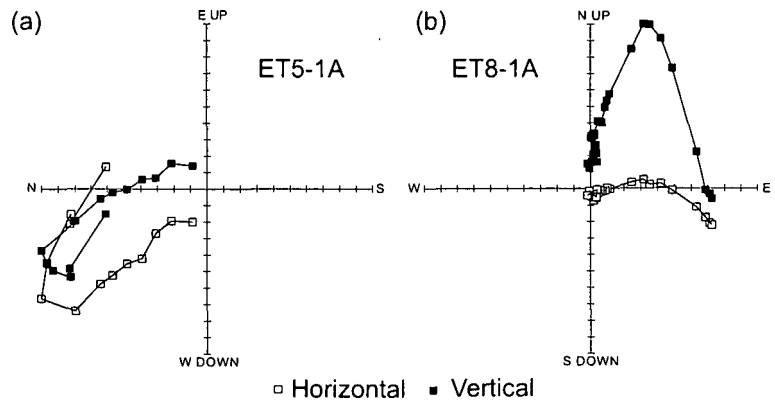


Figure 5.7: Examples of microwave demagnetisation OVPs for ET section, La Palma. Samples are unoriented.

samples from this section.

From the ME section, La Palma, one core from each of the 17 flows sampled was thermally demagnetised. The results are shown in Table D.1 and Fig. 5.9. 15 cores gave reliable directions that are in good agreement with the results from Valet et al. (1999) (Fig. 5.8). Examples of OVPs for samples recording the reversed, transitional and normal field are shown in Fig. 5.10. All samples record a secondary component of magnetisation, which was removed between 350°C and 400°C and remanent magnetisation was typically lost around 540°C. (The secondary component was also removed before applying the field in the perpendicular microwave palaeointensity experiment.) All samples that are accepted record vectors with maximum angular deviation (M.A.D.) (Kirschvink, 1980) less than 10°. 12 samples have M.A.D. less than 5°. The two flows that give no results are ME45 and ME46. These flows were emplaced between two flows recording reversed and normal directions and show overlapping components of magnetisation with high un-blocking temperatures, without a clear high temperature characteristic remanence component (Fig. 5.10). These flows were studied in detail by Valet et al. (1998) and they concluded that the complexity of the vector is caused by partial reheating by the overlying flows recording the post-transitional field and by progressive oxidation of titanomagnetite, which raised the Curie temperature of the magnetic grains carrying the remagnetisation (an observation consistent with the thermomagnetic analysis). It has therefore not been possible to obtain either palaeodirections or palaeointensity during the polarity transition.

75 samples from 20 flows from the AS section, La Palma, were thermally demagnetised. A primary component of magnetisation was obtained for 16 flows; however, only 13 flow means were determined from three or more samples per flow. Examples of OVPs for samples recording the reversed, transitional and normal field are shown in Fig. 5.10. All flows record secondary components of magnetisation, which were removed between

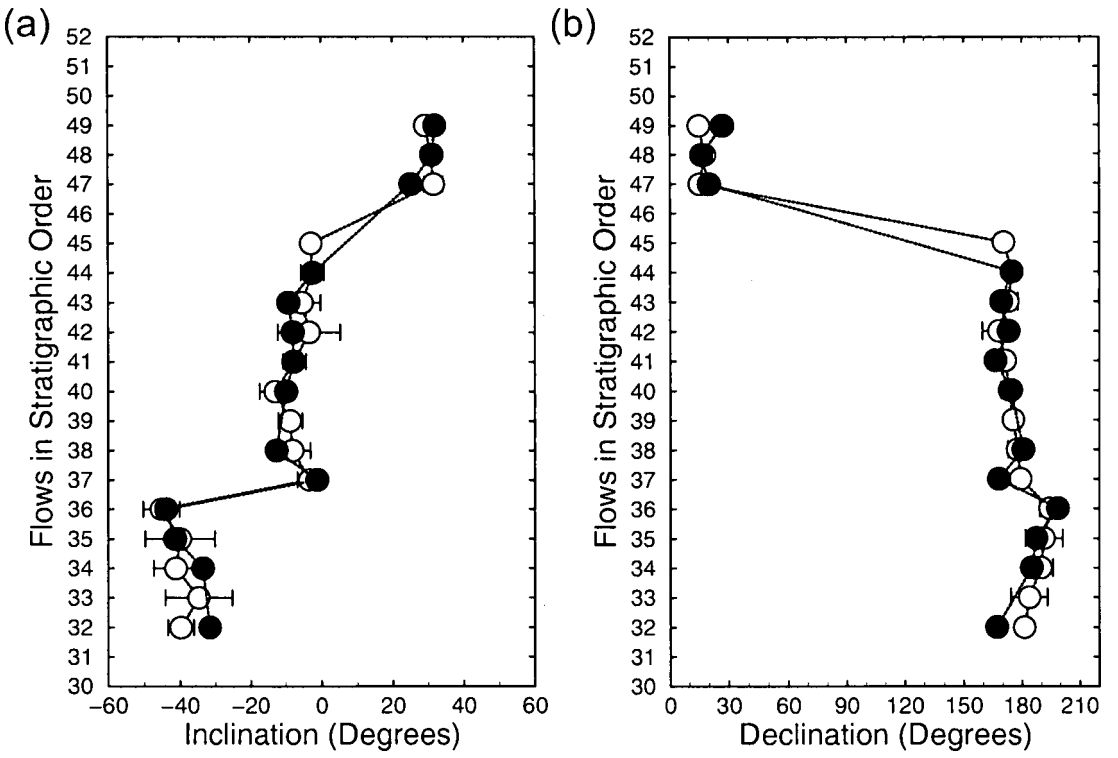


Figure 5.8: Inclination and declination results for the ME section from this study (filled circles) and Valet et al. (1999) (open circles).

250°C and 400°C. All 16 flows are included in the subsequent analysis, but advise great caution when interpreting results from the three flow means determined from less than three directions. All results are shown in Table D.2 and Fig. 5.9. There is a range of precision in the flow mean directions; from $\alpha_{95}$=1.3 to $\alpha_{95}$=14.8. Two flows (AS20 (FN22) and AS21 (FN23)) have $\alpha_{95}$ <5 and one flow (AS15 (FN15)) has $\alpha_{95}$ >10, the other 10 flows have 5> $\alpha_{95}$ <10. 10 flows record the reversed field, four flows record the normal field and two flows record the transitional field. The precision of the first transitional direction (AS23 (FN25)) is fair (Butler, 1992) (n=4, $\alpha_{95}$=9.4); however, the second transitional direction (AS17 (FN18)) is only determined from one sample. The transitional direction determined from AS23 records a large fluctuation (or excursion) in the geomagnetic field before the main polarity change. The timing of this event and how it relates to the evolution of the geomagnetic field is discussed in 5.4.1. Flow AS17 is between a normally and reversely magnetised flow and could record a transitional direction from the main directional reversal.

From the AN section, La Palma, 55 samples from 16 flows were thermally demagnetised. Palaeodirections are obtained for all the flows; however, only eight flow means are determined from three or more samples. 6 flows record large secondary components of magnetisation that were removed between 350°C to 400°C. The other flows record a

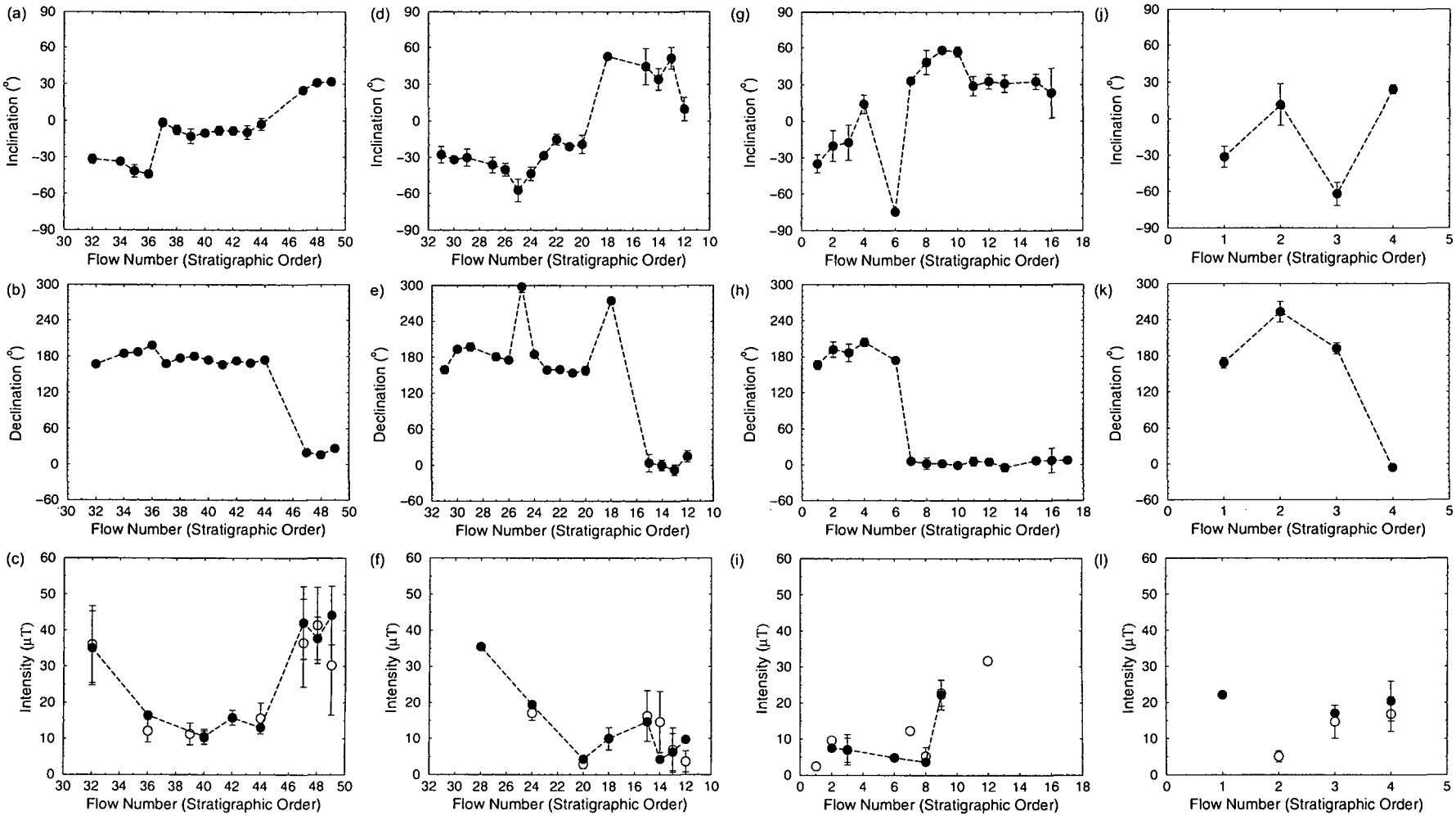


Figure 5.9: Inclination, declination and palaeointensity for the ME (a, b, c), AS (d, e, f), AN (g, h, i) and Guadeloupe (j, k, l) sections. Error bars on ME inclination and declination data are M.A.D. (Kirschvink, 1980) as only one measurement made per flow (see text for details); error bars on AS and AN inclination and declination data are $\alpha_{95}$ (Fisher, 1953). Open circles are flow mean palaeointensities determined using all estimates presented in Table E.1, Table E.2 and Table E.3; solid circles are more robust determinations and are calculated from 1st and 2nd class data (discussed in Section 3.4.8). The dashed lines join flow means calculated using 1st and 2nd class data.

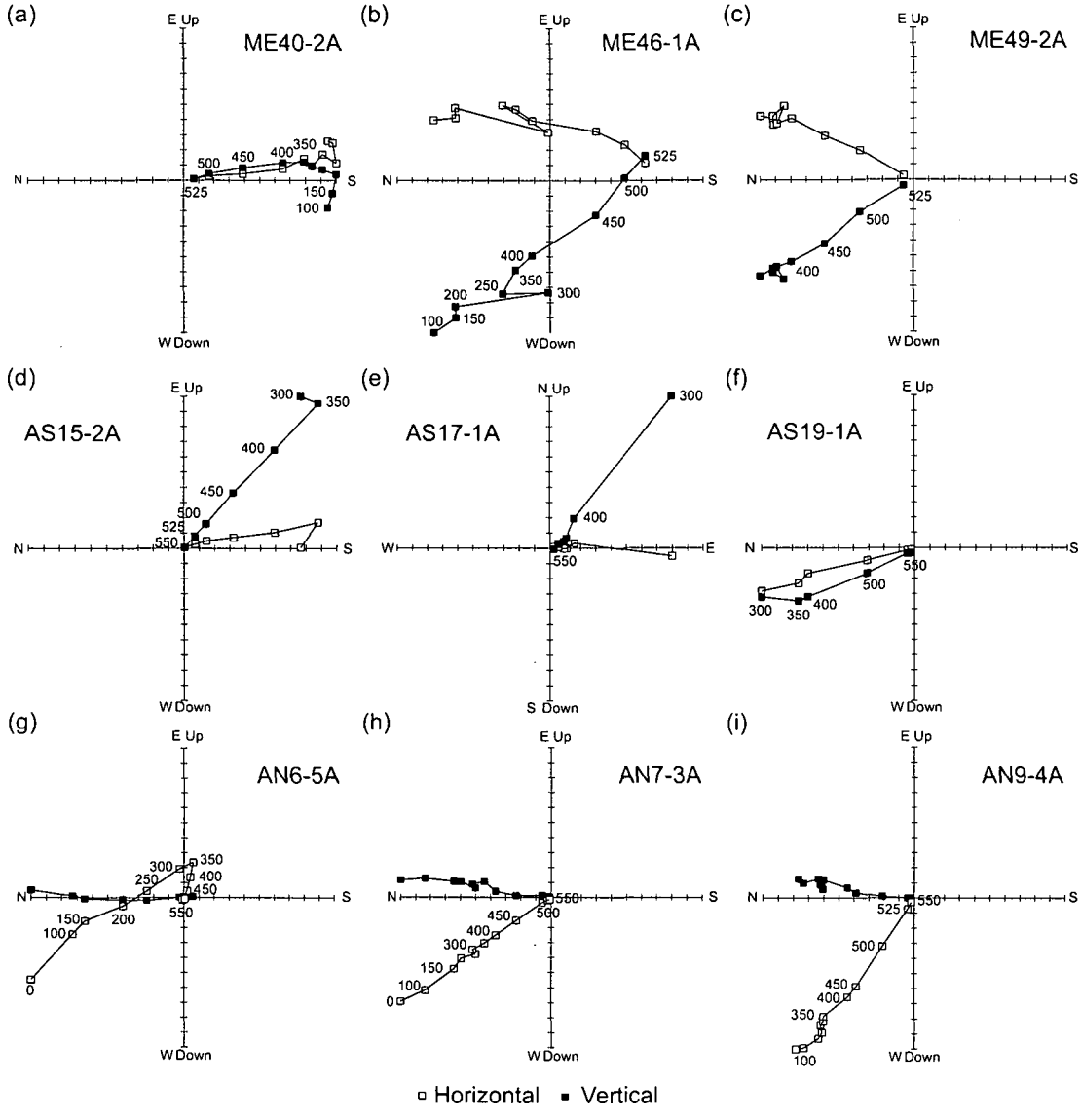


Figure 5.10: Examples of OVPs for the ME section (a, b, c), AS section (d, e, f) and AN section (g, h, i). (a, d, g) show results from samples that record the reversed field close to the directional reversal. (b and e) show results from samples that record directions that could relate to the directional reversal. (c, f, g, i) show results from samples that record the normal field close to the directional reversal. (b) Shows and example where no primary component is resolvable due to remagnetisation by the overlying flow (Valet et al., 1998). (g) Shows an example with a large secondary component that is removed at 350°C.

small viscous component of magnetisation. AN6 (FN6) (Fig. 5.10g) records palaeodirections just prior to the directional reversal; however, a very large secondary overprint is recorded to between 350°C to 400°C. In all samples except AN6-5A the directions recorded above this temperature are not stable and a primary component of magnetisation is not determined. Care was taken during subsequent palaeointensity experiments to identify and remove this secondary component. Only three flow mean directions have $\alpha_{95}$ <5, the remaining five flows have 5< $\alpha_{95}$ <10. All results are shown in Table D.3 and Fig. 5.9. All 16 determinations are again included in the analysis. No transitional directions were recorded: 5 flows record reversed directions and 11 flows record normal directions. As the normal flows are not dated it is not possible to relate these flows to the reversal process or to more stable field behaviour in the Brunhes Chron.

From the Guadeloupe section 26 samples from four flows were thermally demagnetised and 22 samples give reliable directions with an isolated primary component of magnetisation (Table D.4). Examples of OVPs for the four flows are shown in Fig. 5.11. Four samples are rejected because no stable component of magnetisation was recorded or the samples gave significantly different directional results from the majority of other samples in the flow. Samples from G01 (FN2) and G02 (FN3) record large secondary components of magnetisation; however, they were removed between 250°C and 300°C (Fig. 5.11b and c). As expected with lavas extruded during a transitional geomagnetic field, NRM (natural remanent magnetisation) intensity values varied from flow to flow. The NRM intensity ranged from 6 to 43 x $10^{-5}$ $Am^2/kg$ and from 3 to 8 x $10^{-5}$ $Am^2/kg$ for flows G01 and G02, respectively (transitional and reversed polarity field). For flow G03 (normal polarity), the NRM intensity was much higher, ranging from 46 to 85 x $10^{-5}$ $Am^2/kg$ and for GD the NRM intensity ranged from . All mean directional results are shown in Table D.4 and Fig. 5.9. For the stratigraphically lowest flow (GD (FN1)) all seven samples tested record stable primary components of magnetisation, with a mean reversed direction of 169° in declination and -31° in inclination. For flow G01 (FN2), four out of six samples give stable directions, with a mean intermediate polarity direction of 253° in declination and 12° in inclination; however, $\alpha_{95}$=17°. Seven out of eight samples from flow G02 (FN3) again record a reversed stable NRM direction, with a mean value of 192° in declination and -62° in inclination. Flow G03 recorded the most consistent directions ($\alpha_{95}$=3.8), with four out of five samples giving a stable normal polarity direction: mean declination of 354° and mean inclination of 24°.

### 5.3.3 Palaeointensity results

Individual palaeointensity results from the La Palma sections are listed in Table E.1, Table E.2 and Table E.3. Representative Arai-Nagata plots (Nagata et al., 1963) for class 1 and class 2 data are shown in Fig. 6.2a-f). 186 palaeointensity experiments were performed on samples from the ME, AS and AN sections. 119 (64%) experiments

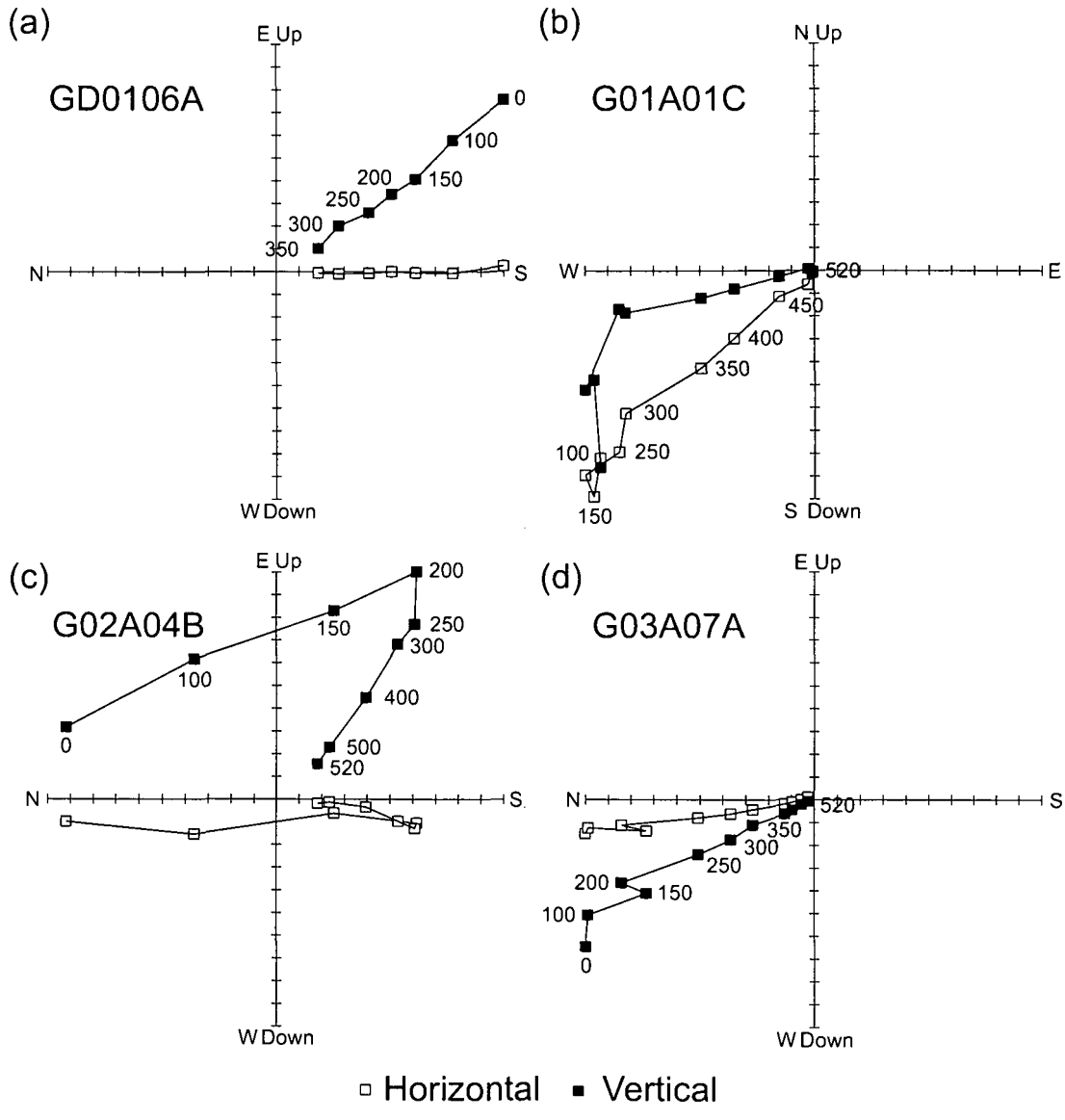


Figure 5.11: Examples of OVPs from all four Guadeloupe flows.

produced results that could be classified (class 1 to 3); 67 (36%) results are class 1 or 2; 7 (4%) are class 1. Palaeointensity results from Guadeloupe are of a lower quality. From 42 experiments, 19 palaeointensities were determined. Individual palaeointensity results are shown in Table E.4 and in Fig. 5.9. None passed the class 1 selection criteria, and only seven were classified as class 2. The remaining eleven are class 2 results and are likely to be unreliable. Individual Arai-Nagata plots from example class 3 results are shown in Fig. 6.2g and h).

Failure of experiments can be classified into three types:

1. Apparent instability in the NRM direction. Using the perpendicular method this is detectable by measuring the angle between the characteristic remanence (ChRM) and the resultant vector $\theta_1$, and the angle between the resultant vector and the applied field $\theta_2$ (if the instability is outside the ChRM applied field plane). Variations in $\theta_1 + \theta_2$ can also be generated if the sample is anisotropic, if there is an error in the direction of the applied field, or if the magnetometer is not measuring correctly (Hill & Shaw, 2007). If the NRM directional instability is in the ChRM applied field plane then the relationship between the NRM and $T_M$RM will be non-linear.

2. Concave-down NRM $T_M$RM slopes (Fig. 5.13a). 23 samples failed because of this behaviour and it was only seen in experiments using the perpendicular method. In all but two examples $\theta_1 + \theta_2$ is between 90° and 91°. There is no apparent relationship between this behaviour and the behaviour of either the $pT_M$RM checks or $T_M$RM tail checks; for some points the sample will pass the checks and for others the sample will fail. A more subtle variant of this behaviour is observed in the quasi-perpendicular experiments. For large fractions of the NRM the relationship between NRM and $T_M$RM is linear; however, at higher microwave powers a concave-down decreasing slope begins (Fig. 5.13b). A palaeointensity estimate has been taken for the straight line segment, but this behaviour needs further consideration.

3. Concave-up NRM $T_M$RM slopes (Fig. 5.13c). This behaviour is seen in 11 samples using the double heating or quasi-perpendicular protocol. Four experiments fail $pT_M$RM checks at maximum microwave power for times greater than 5 s, which would suggest magnetomineralogical alteration. (In theory a small sample in the centre of the cavity will not be subject to high electric fields but in practice this is not true. Magnetic and electric field distribution inside the cavity is influenced by the coupling slot, the sample rod, and the sample. Applying power to a pure quartz sample at 14.2 GHz will eventually heat it, clearly demonstrating the effect of dielectric heating and the presence of alternating electric fields in the sample.) Other examples pass both $pT_M$RM checks and $pT_M$RM tail checks, though as in

the example shown in Fig. 5.13c there is failure of some checks.

Flow mean palaeointensities have been calculated in three ways and are shown in Table 5.1 and plotted in Fig. 5.9. Using all the data that could be classified, 29 flow means were calculated. The second approach was just only include individual palaeointensity estimates that are class 1 and 2. 25 flow means were calculated from these determinations; however, only ten of these flows had three or more determinations.

Applying the in-flow variation criterion of Selkin & Tauxe (2000) (the ratio of the standard deviation of the palaeointensity estimates to the mean should be less than 25%) to the flow means calculated from class 1 and 2 data would cause rejection of a large amount of data with low flow means. For flows with palaeointensity estimates below 10 $\mu$T small variations in the estimates can greatly affect the in-flow variation value; this criterion has not been applied to these flows and these results are reliable (Hill et al., 2005). Four flows from the ME section (ME32, ME47, ME48 and ME49) show a large range of palaeointensity determinations. ME32 has an in-flow variation value of 29% and fails the criterion. The three other flows pass the criterion; however, they show non-ideal characteristics for acquisition of thermal remanent magnetisation and for Thellier type palaeointensity determinations. These flows are discussed further in Chapter 6. These four flows are included in the further analysis, but caution is expressed over their reliability.

## 5.4 Discussion

The temporal and global evolution of the field during the MB reversal is discussed and results determined in this study are compared previously published data. Results from this study are also compared with the output generated by model IMMAB4 by Leonhardt & Fabian (2007) and the simple mathematical reversal model described in Chapter 4 based upon CALS7K.2 (Korte & Constable, 2005a). Even though the data set is small, it is possible to make direct comparisons to IMMAB4; however, only a statistical comparison can be made to the model based on CALS7K.2.

IMMAB4 is global geomagnetic field model of the MB reversal and uses an iterative Bayesian inversion method to construct a spherical harmonic expansion of the transitional field from palaeomagnetic data. The initial model is based on the Atlantic ODP core of Valet et al. (1989) with the second iteration including a calibration for absolute palaeointensity from the volcanic section ME-ET, La Palma, from Valet et al. (1999). Subsequent iterations include the Atlantic sedimentary records of Clement & Kent (1986, 1991).

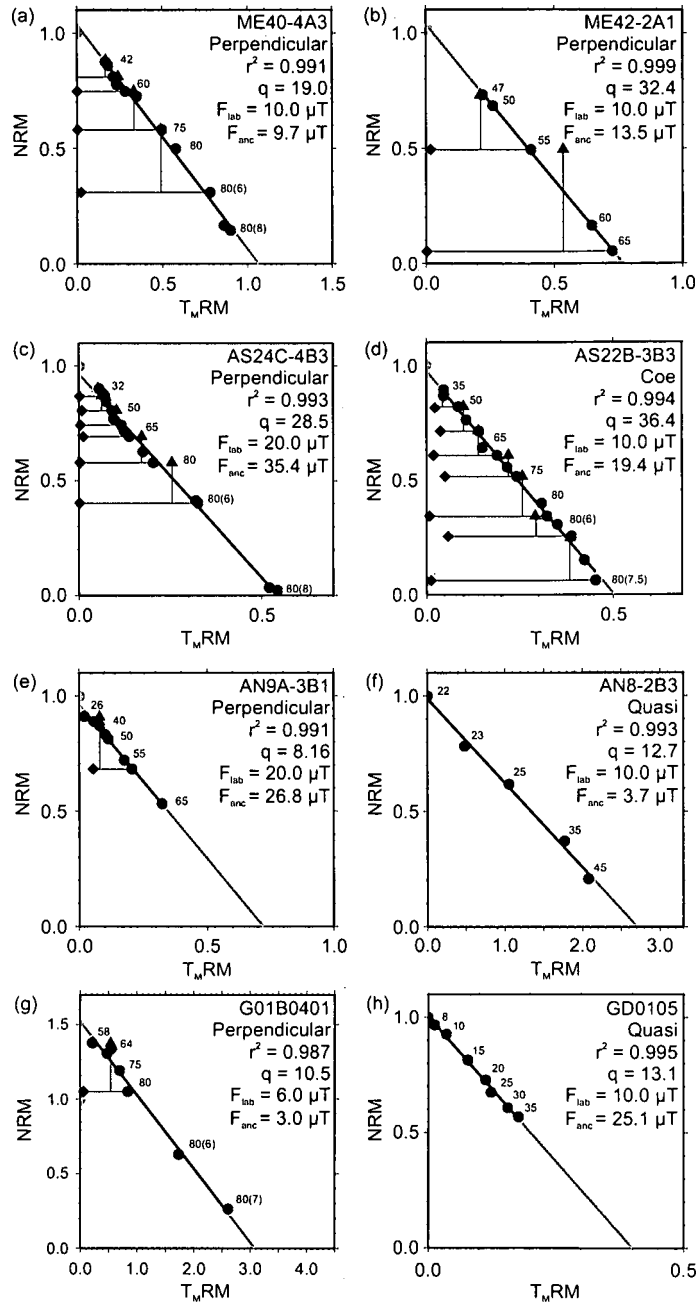


Figure 5.12: Examples of Arai-Nagata plots (Nagata et al., 1963) for the La Palma (a-f) and Guadeloupe (g and h) sections. (a) and (c) show 1st class results, (b, d-h) show 2nd class results. $r^2$ and $q$ are defined in Section 3.4.8. $F_{lab}$ is the applied field during the palaeointensity experiment and $F_{anc}$ is the palaeointensity estimate. Numbers accompanying the data points are the microwave power steps in watts. The numbers in brackets are time in seconds; where no bracketed numbers are shown, the time of application was 5 s. Perpendicular denotes that the perpendicular applied method was used; Coe, the double-heating method (Coe, 1967a); Quasi, the quasi-perpendicular applied field method (Biggin et al., 2007b). Examples (f) and (h) were determined using the quasi-perpendicular method, so no $pT_MRM$ checks or tail checks were used. Quasi-perpendicular experiments were performed on the Tristan 14 GHz system, which has a more efficient cavity, so the amount of power needed to de(re)magnetise the sample was much less.

| | *All estimates* | | | | *Class 1 and 2 estimates* | | | |
|---|---|---|---|---|---|---|---|---|
| Flow Number | Mean $F$ ($\mu T$) | $\sigma_F$ ($\mu T$) | VDM x $10^{22}$ ($Am^2$) | $\sigma_V$ x $10^{22}$ ($Am^2$) | Mean $F$ ($\mu T$) | $\sigma_F$ ($\mu T$) | VDM x $10^{22}$ ($Am^2$) | $\sigma_V$ x $10^{22}$ ($Am^2$) |
| *ME section, La Palma* | | | | | | | | |
| 32 | 36.1 | 10.7 | 8.3 | 2.4 | 35.0 | 10.2 | 8.1 | 2.4 |
| 36 | 12.1 | 3.1 | 2.5 | 0.8 | 16.4 | | 3.4 | |
| 39 | 11.3 | 3.1 | 2.9 | 0.8 | | | | |
| 40 | 10.3 | 1.8 | 2.6 | 0.5 | 10.5 | 2.1 | 2.7 | 0.5 |
| 42 | 15.8 | 2.1 | 4.0 | 0.5 | 15.8 | 2.1 | 4.0 | 0.5 |
| 44 | 15.7 | 4.3 | 4.0 | 1.1 | 13.1 | | 3.4 | |
| 47 | 36.6 | 12.2 | 8.8 | 2.9 | 42.1 | 10.0 | 10.1 | 2.4 |
| 48 | 41.4 | 10.5 | 9.5 | 2.4 | 37.7 | 5.9 | 8.7 | 1.4 |
| 49 | 30.3 | 13.8 | 6.9 | 3.2 | 44.2 | 8.1 | 10.1 | 1.9 |
| *AS section, La Palma* | | | | | | | | |
| 27 | 35.4 | | 7.9 | | 35.4 | | 7.9 | |
| 24 | 17.1 | 2.0 | 4.0 | 0.5 | 19.4 | | 4.6 | |
| 20 | 3.0 | 1.3 | 0.7 | 0.3 | 4.3 | | 1.1 | |
| 18 | 10.0 | 3.1 | 1.9 | 0.6 | 10.0 | 3.1 | 1.9 | 0.6 |
| 15 | 16.3 | 7.0 | 3.3 | 1.4 | 14.7 | | 3.0 | |
| 14 | 14.6 | 8.5 | 3.3 | 1.9 | 4.3 | | 1.0 | |
| 13 | 6.9 | 6.1 | 1.3 | 1.2 | 6.3 | 5.1 | 1.2 | 1.0 |
| 12 | 3.6 | 2.9 | 0.9 | 0.7 | 9.7 | | 0.6 | |
| *AN section, La Palma* | | | | | | | | |
| 1 | 2.4 | 0.8 | 0.5 | 0.2 | | | | |
| 2 | 9.6 | | 2.4 | | 7.5 | | 1.8 | |
| 3 | 6.9 | 3.3 | 1.7 | 0.8 | 7.1 | 4.2 | 1.8 | 1.0 |
| 6 | 4.8 | | 0.7 | | 4.8 | | 0.7 | |
| 7 | 12.3 | | 2.8 | | | | | |
| 8 | 5.3 | 2.5 | 1.0 | 0.5 | 3.7 | | 0.7 | |
| 9 | 22.8 | 3.5 | 4.0 | 0.6 | 22.3 | 4.2 | 3.9 | 0.7 |
| 12 | 31.7 | | 7.2 | | | | | |
| *Guadeloupe section, French West Indies* | | | | | | | | |
| 1 | 22.1 | | 5.1 | | 22.1 | | 5.1 | |
| 2 | 5.1 | 1.6 | 1.3 | 0.4 | 3.0 | | 0.8 | |
| 3 | 14.7 | 4.6 | 2.4 | 0.8 | 17.0 | | 2.8 | |
| 4 | 16.8 | 4.9 | 4.0 | 1.2 | 20.4 | 5.5 | 4.9 | 1.3 |

Table 5.1: Mean microwave palaeointensity results per flow for the AN section, La Palma. *All estimates* takes all class, 2 and 3 results; *Class 1 and 2 estimates* takes all estimates that pass the class 1 and 2 selection criteria (Section 3.4.8). Mean $F$ is the mean palaeointensity; $\sigma_F$ is one standard deviation of the flow mean intensity; VDM is the flow mean virtual dipole moment; $\sigma_V$ is the standard deviation of the flow mean VDM.

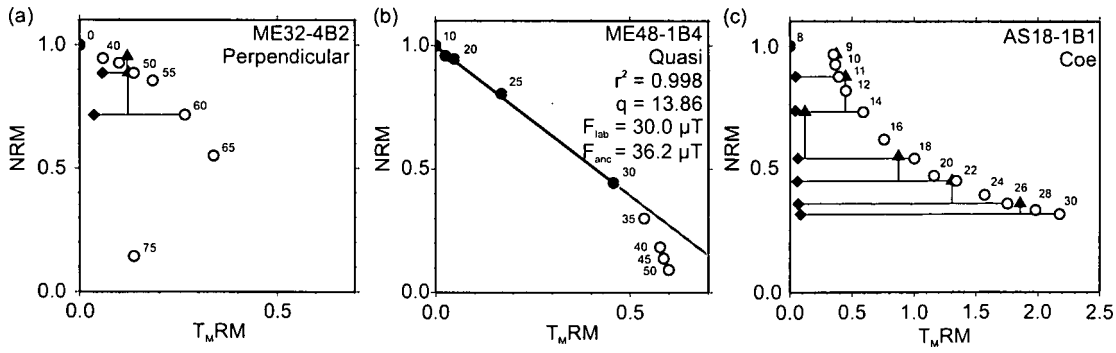


Figure 5.13: Examples of Arai-Nagata plots which fail the palaeointensity experiments (a and c) or have unusual non-ideal characteristics. Graph labels are explained in Fig. 6.2.

### 5.4.1 Palaeodirectional and palaeointensity variations

All three sections from La Palma sample the reversed and normal field either side of the main polarity change. Unfortunately, only one flow from the AS section (FN18) records the transitional field during the main polarity change; however, another flow from (FN23) records an equatorial virtual geomagnetic pole (VGP) at a time before the main polarity change (Fig. 5.14). Without $^{40}Ar/^{39}Ar$ dates for these two flows it is not possible to determine which stage of the reversal these transitional directions belong to. FN23 could record part of the precursor event relating to the MB reversal (Singer et al., 2002, 2005) or an earlier excursion at 821±13 ka (Quidelleur et al., 2003). The date of the excursion also corresponds with the dated flows from the TS section prior to the main polarity change (Singer et al., 2002) (Fig. 5.14) and also with a transitional direction from western Mexico (dated at 819 ± 2 ka (Petronille et al., 2005). It is also not clear whether this excursion is also part of the MB reversal (Gratton et al., 2007). FN18 could record the precursor, as determined for flows 17 and 18 from the TN section of Singer et al. (2002), or the main polarity change. Although Quidelleur et al. (2002), Quidelleur et al. (2003) and Singer et al. (2002) dated many flows from both the AS and AN sections, they did not record either of the transitional directions determined in this study (Fig 5.14). All three studies show differences in the number of flows sampled and the directional results obtained. This discrepancy is attributed to difficulties in re-identifying flows from previous studies in the field and also to the large number of flows which were often hard to delimit.

The inferred VGP paths from the three La Palma sections are quite different (Fig. 5.15a-c); however, these differences result from the discrete nature of the flows in each sequence and do not represent the behaviour of the field between VGPs. It is clear that many of the VGPs are similar in their location. Each volcanic sequence records part of a transitional field that is more complex than indicated by any of the three records. The

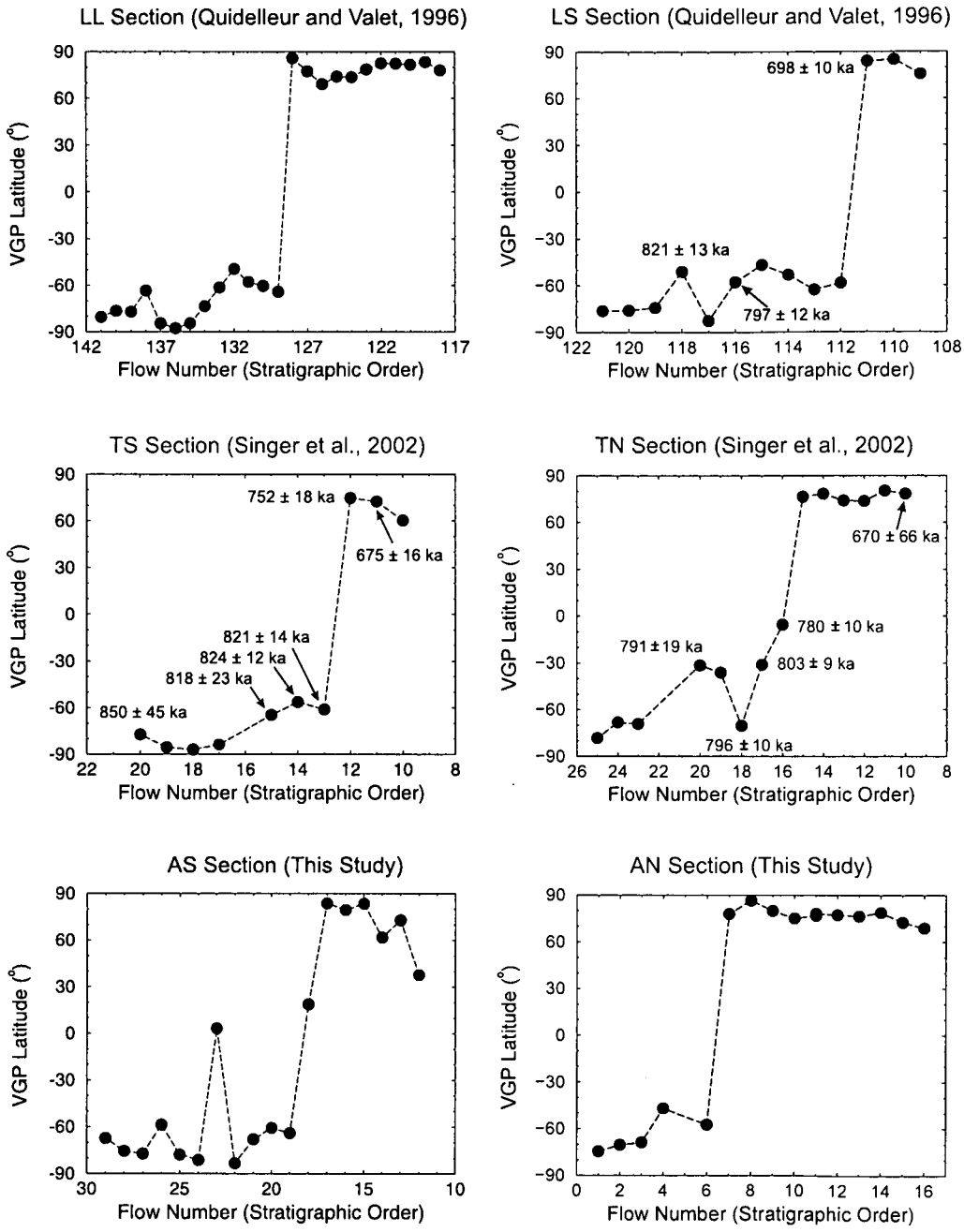


Figure 5.14: Comparison of VGP latitude against flow number for the Barranco del Agua sections, La Palma. Errors on VGP latitude can be found in Quidelleur & Valet (1996) and Singer et al. (2002) and in Table D.2. Dates on the LS section are $^{40}K/^{40}Ar$; TS and TN dates are $^{40}Ar/^{39}Ar$.

problem of assessing VGP paths (and the complexity of all directional changes) from volcanic sequences is highlighted when compared with the results generated for La Palma by IMMAB4 (Leonhardt & Fabian, 2007) (Fig. 5.15f). The new directional results do not match the results from IMMAB4 in detail (Fig. 5.15a, (b), (c) and (f)); however, the incorporation of sedimentary records in this model has greatly increased the detail that can be resolved for the reversal recorded on La Palma. Without analysis of sedimentary records in accompaniment to volcanic records the recorded transitional field behaviour can be simplified and misinterpreted. Such possible complexity in directional changes for the MB reversal is seen in the sedimentary records of Channell & Lehman (1997) and Yamazaki & Oda (2001), which both show multiple polarity changes and other large directional variations before the final polarity change. This behaviour has also been seen for a number of other reversals recorded in sedimentary sequences (see Coe & Glen (2004) and references therein). However, problems in the sedimentary recording mechanism and the fidelity of sedimentary records must always be considered. In addition, both volcanic and sedimentary records will always be incomplete and can only give a lower bound on the amount of directional and intensity variation for any particular reversal (Coe & Glen, 2004).

The palaeointensity results determined from the ME section using the microwave technique are in broad agreement with those determined by Valet et al. (1999) using the thermal Thellier method (Fig. 5.16). When no selection criteria is used the results from all flows agree (to within $2\sigma$) with the exceptions of ME36, ME38 and ME39 (Fig. 5.16a). For two flows only one thermal Thellier or microwave determination was possible. For the third flow (ME39) the thermal Thellier result is 2.5 times greater. The individual microwave results from this flow were all class 3 and only one thermal Thellier result passed the class 1 selection criteria. Results from this flow are deemed unreliable. When the microwave flow mean palaeointensities are compared with the flow means determined using the thermal Thellier method for the three normal flows (ME47, ME48 and ME49), the means are comparable; however there is a larger range of individual palaeointensity results determined using the microwave technique. Only the comparisons to ME48 and ME47 are statistically significant, as only two determinations were made using the thermal Thellier method for ME49. For ME48 the range of determinations using the microwave technique is 36.9 $\mu$T compared with 5.8 $\mu$T for the thermal Thellier technique; for ME47 the range of determinations using the microwave technique is 35.5 $\mu$T compared with 8.3 $\mu$T for the thermal Thellier technique. These three flows are investigated further in Chapter 6 and an explanation is proposed for the variation in individual palaeointensity determinations obtained using different sized samples. When the class 1 and 2 selection criteria is applied to both data sets the mean palaeointensities from the three normal polarity flows are no longer in good agreement (Fig 5.16b).

Palaeointensity was only obtained for one transitional flow on La Palma (FN18, AS

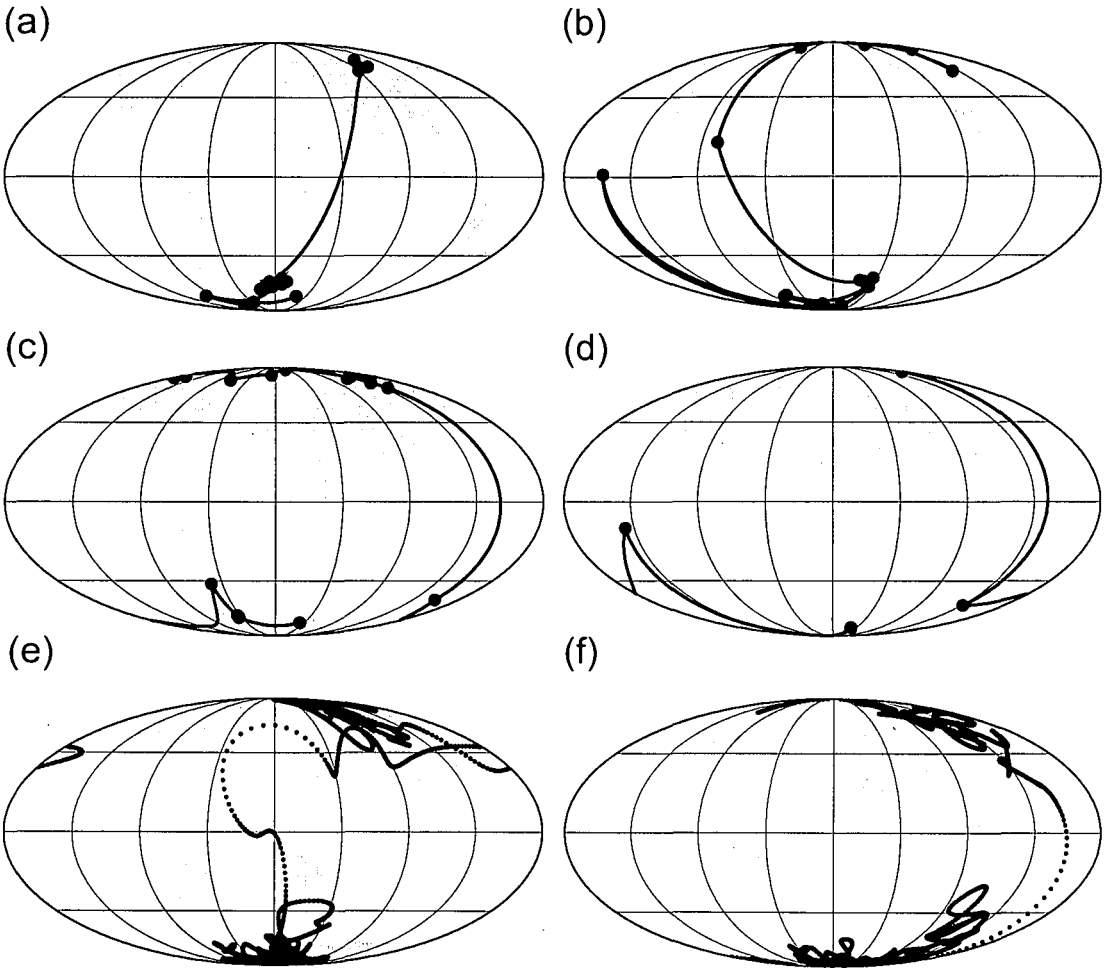


Figure 5.15: Calculated VGP paths for (a) ME, (b) AS, (c) AN sections from La Palma, (d) Guadeloupe. (e) VGP path for La Palma and (f) Guadeloupe, generated by IMMAB4 (Leonhardt & Fabian, 2007), with each dot at 100 year intervals.

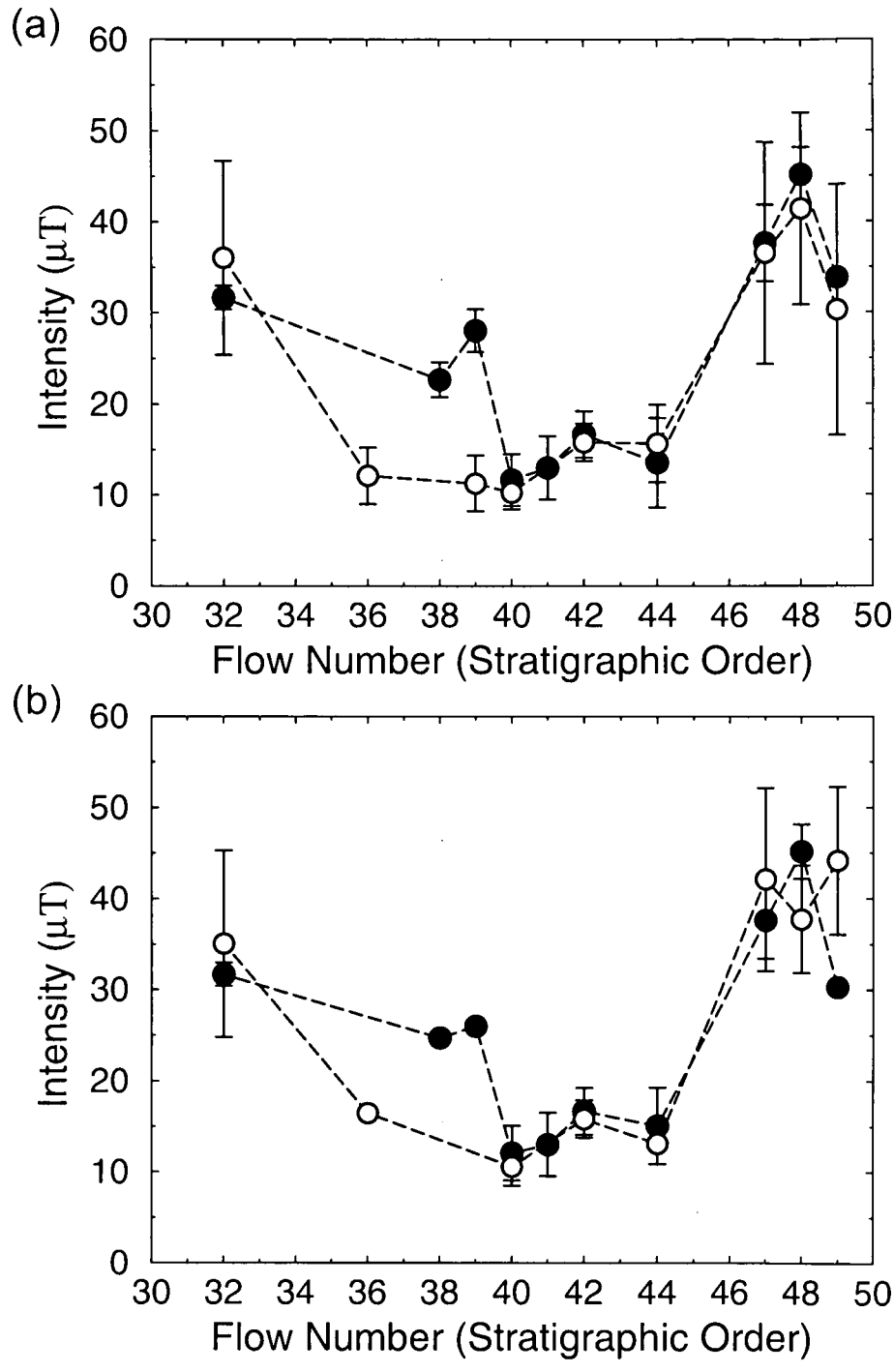


Figure 5.16: Comparison of microwave flow mean palaeointensity results from this study (open circles) and thermal Thellier results from Valet et al. (1999) (closed circles). (a) All estimates of palaeointensity. (b) Palaeointensity results that pass the class 1 and class 2 selection criteria. Error bars are $\pm\sigma$.

section) giving a value of 10 ± 3.1 $\mu$T (n=4,), corresponding to a virtual dipole moment (VDM) of 1.9 ± 0.6 x $10^{22}$Am$^2$. Before the main polarity change the ME section gives a mean VDM of 3.4 ± 0.53 x $10^{22}$Am$^2$ and the AS/AN sections give a mean VDM of 1.48 ± 0.52 x $10^{22}$Am$^2$ (determined using all class 1 and class 2 data). This result is 2.3 times lower than the results from the ME section. It has already been noted in Section 5.2.1 that the palaeointensity results from the ME section (Valet et al., 1999) appear anomalously high when compared to the PINT03 database (Perrin & Schnepp, 2004) and this is again seen in this study. One possibility for this discrepancy is that the ME section and AS/AN sections were erupted at different times and capture different parts of the reversal; the AS/AN sections recording times when the field was at a minimum and the ME section recording times, possibly earlier in the reversal's history, when the palaeointensity was higher. Another possibility is that these palaeointensities are erroneous and this is related to the samples' oxidation state. Yamamoto et al. (2003) determined overestimated palaeointensities from samples from the 1960 Hawaii lava flow. They observed that these samples had undergone intermediate oxidation on initial cooling below their Curie temperature and that they could have acquired a thermochemical remanent magnetisation (TCRM). No microscopy was done in this study so such bold conclusions can not be drawn; however, variations in the composition and the low-temperature properties of samples from the same flows and the same 25 mm cores suggest that some oxidation of these samples has occurred and that it was not homogeneous. Nevertheless, all La Palma sections show a decrease in palaeointensity during the directional changes (Fig. 5.17) and low palaeointensities have been recorded in flows that record both normal and reversed directions.

The directional record from Guadeloupe shows a reversed-transitional-reversed-normal progression with time (Fig. 5.15d). The transitional-reversed-normal progression was also recorded by Carlut et al. (2000); however, the directional results differ. For the transitional and reversed flows the two sets of results are comparable (within the 95% cone of confidence); however, for the normal flow there is a discrepancy. The mean direction for this flow from this study is D = 353.8°, I = 24.2° (N=4) compared with the equivalent result of flow GU11 (Carlut et al., 2000) of D = 340.7°; I = 31.4° (N=9). This discrepancy could be caused by not using enough samples to calculate the flow mean in this study.

The paleointensity results from the two flows of Carlut & Quidelleur (2000) determined by the thermal Thellier method are significantly different to the microwave results determined in this study. Both the flows gave higher palaeointensities when determined using the microwave technique. For G02 (FN3) (G10 (Carlut & Quidelleur, 2000)) there is a difference of 12.8 $\mu$T and for G03 (FN4) (GU1) there is a difference of 11.1 $\mu$T. Only one sample from all the Carlut & Quidelleur (2000) flows passes the class 1 and 2 selection criteria, and although the quality of the microwave results is generally

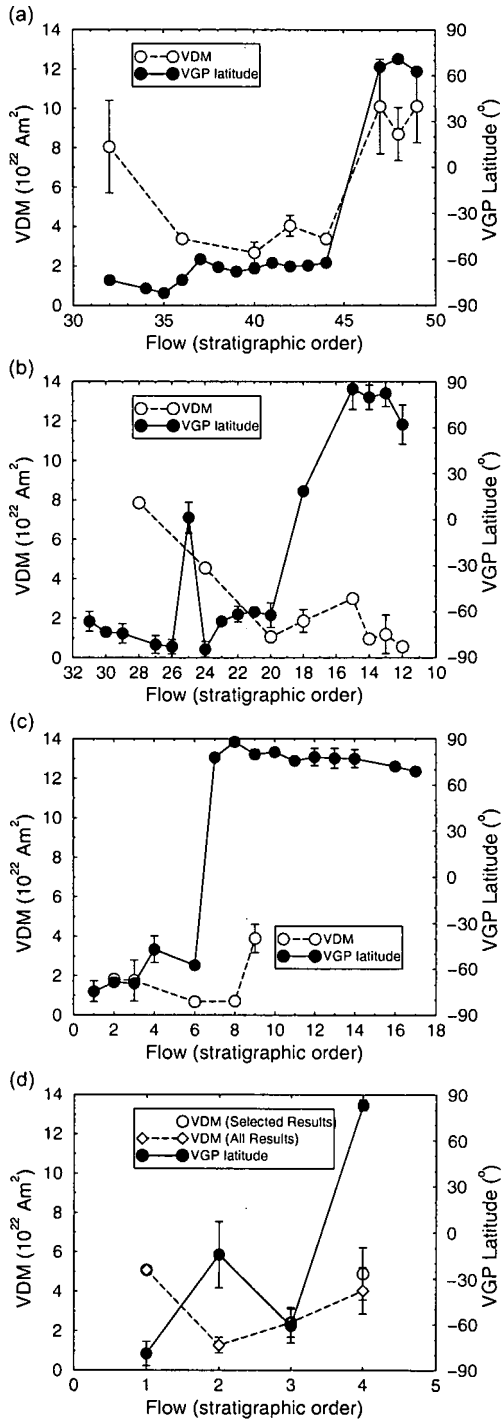


Figure 5.17: VGP latitude and VDM plots for (a) ME, (b) AS, (c) AN and (d) Guadeloupe sections. VDM determinations for ME, AS, AN sections are from class 1 and 2 determinations; VDM determinations for the Guadeloupe section show both VDM determinations from all classified data (open diamonds) and class 1 and 2 data (open circles). VDM error bars are $\sigma_v$ and are shown in Table 5.1. VGP latitude errors are *dm* (Butler, 1992). Where no error bars are present the palaeomagnetic result was determined from less than three samples.

low, it has improved upon the results from the original study.

$^{40}K/^{40}Ar$ dating of the flows studied in Carlut et al. (2000) and Carlut & Quidelleur (2000) ranges from 777 ± 14 ka (±$\sigma$) to 785 ± 22 (±$\sigma$) ka. The VGP calculated from the transitional flow is very similar to that recorded in FN23 from the AS section from La Palma. The errors on the dating, the agreement of VGPs and the reversed-transitional-reversed trend could suggest that the transitional flow records the precursor to the main polarity change at 793 ± 3 ka (Singer et al., 2005) or possibly an earlier excursion. Although the quality of the palaeointensity data determined for the transitional-reversed part of the Guadeloupe sequence is poor, the VDM remains low (below 3 x $10^{22}$ $Am^2$) during this time (Fig. 5.17d). This result is consistent with VDM values determined from the precursor event recorded in the Tatara-San Pedro lavas, Chile (Brown et al., 2004; Gratton et al., 2007). The Tatara-San Pedro section consists of a series of lavas that record very similar directions, with VGPs that cluster over Australia. $^{40}Ar/^{39}Ar$ dates place this VGP cluster at 791.7 ± 3 ka. It has been suggested that during the reversal there is sustained field behaviour related to mantle-controlled magnetic flux patches (Hoffman & Singer, 2004), which leads to clustering of VGPs. Such clusters have also been determined for a number of other reversal records (Mankinen et al., 1985; Hoffman, 1992, 1996; Glen et al., 1994, 2003). Consistent directions could have been recorded by rapidly erupted lavas with no requirement for another physical mechanism; however, debate about the meaning of the geochemical analysis (Dungan et al., 2001), rock magnetic results (Brown et al., 2004; Gratton et al., 2007), and our understanding of long-lived geochemical systems means that both hypotheses remain for this section.

Error in dating the normal flow from Guadeloupe means that it is not clear if this flow records the post-reversal normal field or part of the precursor event. Although VDM is seen to increase (4.9 ± 1.3 (±$\sigma$) x $10^{22}Am^2$) (Fig. 5.17a), this could be associated with the precursor, as seen in sedimentary records (Hartl & Tauxe, 1996) and possibly in the Tatara-San Pedro volcanic sequence (Gratton et al., 2007). The temporal evolution of the Guadeloupe and Tatara San Pedro sections is very difficult to interpret due to the discrete nature of the sampling. The interpretation is further complicated by the possible speed of directional changes. Leonhardt & Fabian (2007) determined from IMMAB4 that local field directions can rotate very quickly (up to 2.2°), a feature that has been generated in dynamo simulations (Coe et al., 2000) and simple mathematical models of reversals (Brown et al., 2007) and has been suggested to explain the palaeomagnetic record of Steens Mountain (Mankinen et al., 1985). This behaviour is thought to be significantly site dependent (Clement, 2004; Wicht, 2005; Brown et al., 2007; Leonhardt & Fabian, 2007)

IMMAB4 does not resolve the precursor in direction before the main polarity change (Fig. 5.15e and f); however, a broad decrease in intensity is seen between 790 ka and 780 ka before a peak in intensity prior to low field values during the main polarity change

(Leonhardt & Fabian (2007) do note the model is less reliable for dates > 782 ka). This intensity variation, but not a polarity change, is (unsurprisingly) seen in the sedimentary and volcanic records of Valet et al. (1989) and Valet et al. (1999). The difference between the records could be caused by non-uniformity in the timing and the size of the global reduction in the field during this time; however, low intensity approximately 16 kyr before the main polarity change has been observed globally (Schneider et al., 1992; Meynadier et al., 1994; Hartl & Tauxe, 1996; Dinarès-Turell et al., 1999).

The precursor event recorded in lavas at 793 ± 3 ka could relate to the initial onset of geodynamo instability (Singer et al., 2005), resulting in a reduction in the relative strength of the large-scale dipole contributions and an emergence of non-dipole contributions at the Earth's surface. Geodynamo instability could result from an emergence of magnetic upwellings (generated within buoyancy driven upwellings in the outer core, but with little or no dramatic change in fluid flow (Wicht & Olson, 2004)), which amplify and transport a generally multipolar magnetic field from the inner boundary to the core-mantle boundary (Aubert et al., 2008).

### 5.4.2 Comparison with other Matuyama-Brunhes data

To compare palaeodirection and palaeointensity results from multiple global locations data are characterised as VGPs and VDMs. The limitations of this approach are recognised. The assumption that the field is a geocentric dipole during the reversal (Merrill & McFadden, 1999) is certainly flawed due to the observation of various VGP paths for the MB reversal. Results from this study and all published MB data are shown in Fig 5.18a and b. A clear feature is the rather simple relationship between variations in VGP and VDM. There are two broad groups: data that lie between ± 90° to ± 60° VGP latitude and data that lie between -60° to 60° VGP latitude. Within the two high latitude bands VDM varies greatly, with VDMs at high VGP latitude both higher and lower than the present day dipole moment (7.9 x $10^{22}$ $Am^2$ calculated from the CHAOS geomagnetic field model (Olsen et al., 2006)) . Low values relate to times before and after the main polarity transition, where the dipole field is reduced in its strength but major directional changes have not occurred. This supports the idea that major directional changes have a shorter duration than intensity variations related to the reversal (Lin et al., 1994; Merrill & McFadden, 1999). All major directional changes (-60° to 60° VGP latitude) are coincident with VDMs less than 3 x $10^{22}Am^2$ (approximately 35% of the present day globally averaged dipole moment). This suggests that the dipole moment needs to be reduced to at least this value before major directional instability occurs due to the emergence of dominant non-dipolar fields. Interpretation of the MB transitional field is severely limited by the lack of data, especially if only flows with three or more palaeointensity determinations are included (Fig. 5.18b).

The MB dataset is compared with the IMMAB4 transitional field structure, which is

dominated by the quadrupole with a reduced dipole contribution (Leonhardt & Fabian, 2007) (Fig. 5.18c). For all locations except China, the general banding of VGPs and VDMs is observed. The generation of high VDM at equatorial VGP latitudes is inconsistent with the data. This analysis is clearly restricted by the characterisation of the data as VGPs and VDMs, which does not allow an assessment of the dominant non-dipolar terms. In addition, the data for a number of locations is considered from areas not included in the original model. In this case the model needs to be refined with additional data.

The same analysis using the simple reversing axial dipole model of Brown et al. (2007) based on CALS7K.2 (Korte & Constable, 2005a) as been carried out. The banding of VGPs and VDMs in the simulated reversal is again seen; however, generated VDMs are lower at transitional VGP latitudes. This is because CALS7K.2 underestimates the likely strength of the non-dipole field as the model has very little resolution above spherical harmonic degree four (C. Constable, *pers comm.*).

## 5.5 Conclusions

The microwave technique has been used to determine a fragmentary record of the evolution of geomagnetic field intensity through the Matuyama-Brunhes geomagnetic field reversal recorded in three sections on La Palma, and one section on Guadeloupe. These sections record the main polarity transition, possible precursors, and fluctuations in the magnetic field prior to the main polarity reversal; however, it has proved difficult to obtain robust palaeointensity determinations. Only ten flows from the twenty-nine flows studied gave reliable mean palaeointensities with three or more determinations per flow. Of these ten flows, only one records a transitional direction. The VDM determined from this flow is $1.9 \pm 0.6$ ($\pm\sigma$) x $10^{22}$ Am$^2$. Analysing both thermal Thellier and microwave palaeointensity results from all Matuyama-Brunhes studies suggests that the main directional changes occurred once the VDM was reduced below 3 x $10^{22}$ Am$^2$. However, the lack of transitional data prevents us from making any robust statements about the transitional field behaviour. To understand the reversal process and how this links to geodynamo behaviour, more accurate transitional palaeointensity determinations are required. In addition detailed $^{40}$K/$^{40}$Ar dating is needed to clearly determine the temporal variation and complexity of reversal features recorded in volcanic sections and, where more than one record exists for a particular reversal, correlate them globally.

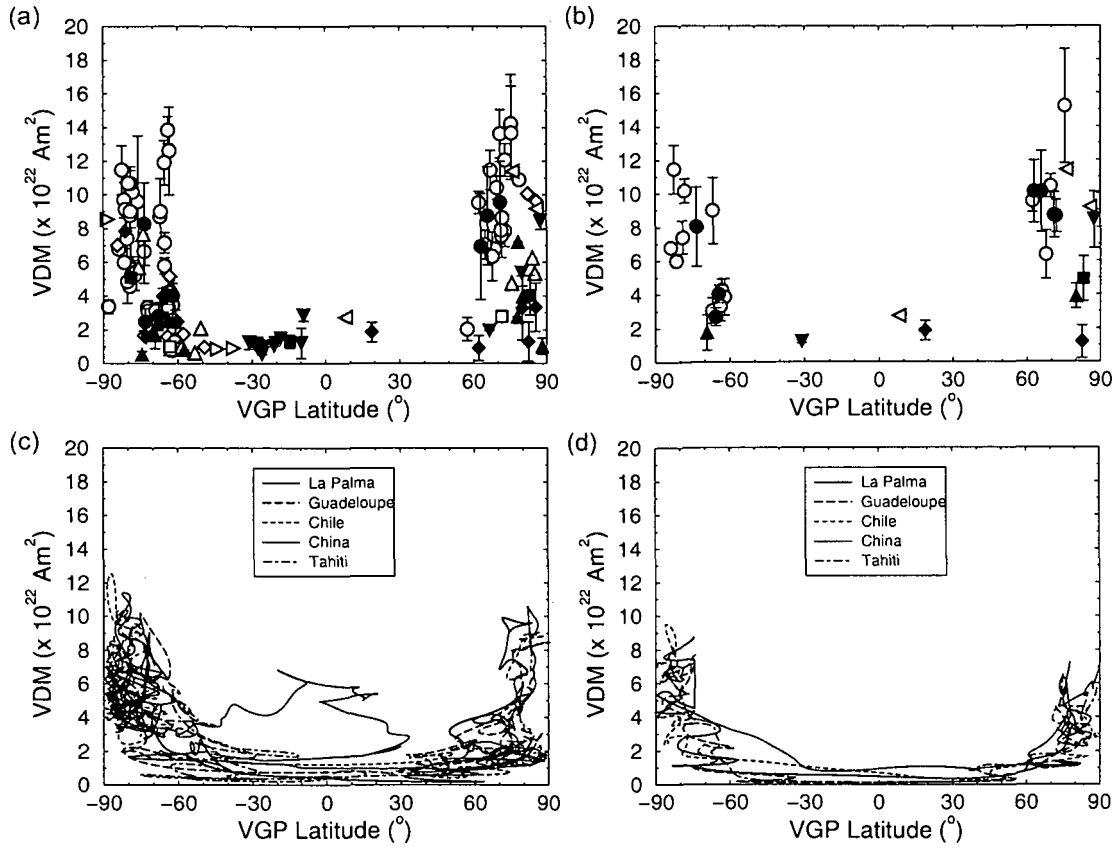


Figure 5.18: (a) VDM versus VGP for all Matuyama-Brunhes data (number of determined means=121). All estimates from this study and all other published data. No selection criteria was applied and many flow means were determined from less than three results. (b) VDM versus VGP for selected Matuyama-Brunhes data with three or more determinations per flow (n=31). The class 1 and 2 selection criteria was imposed on data from this study. Previously published data were assessed on the published statistical parameters and where possible the class 1 selection criteria from this study was applied. This includes the removal of any data that used the Valet et al. (1996) palaeointensity correction. (a-b) Solid circles are microwave data and open circles are thermal Thellier data; solid circles: ME section (this study); open circles: ME and ET section (Valet et al., 1999); solid diamonds: AS section (this study); open diamonds: LL section (Quidelleur & Valet, 1996); solid upwards triangles: AN section (this study); open upwards triangles: LS section (Quidelleur & Valet, 1996); solid squares: Guadeloupe section (this study); open squares: Guadeloupe section (Carlut et al., 2000; Carlut & Quidelleur, 2000); solid downward triangles: Tatara San Pedro sections, Chile (Brown et al., 2004; Gratton et al., 2007); left pointing triangles: Tongjing basalts, China (Zhu et al., 1991); right pointing triangles: Punaruu Valley, Tahiti (Chauvin et al., 1990). (c) VDMs and VGPs generated by IMMAB4 (Leonhardt & Fabian, 2007) for locations shown in (a) and (b). (d) VDMs and VGPs generated by a simple reversal model based on CALS7K.2 (Korte & Constable, 2005a; Brown et al., 2007) for the location shown in (a) and (b).

# Chapter 6

# Using first-order reversal curves to assess palaeointensity variations in samples recording the Matuyama-Brunhes geomagnetic field reversal

In Chapter 5 it was shown that a number of flows recorded significant variations in palaeointensity. In this chapter the palaeointensity determinations from three of these flows are investigated in more detail. Further rock magnetic experiments have been performed in addition to those presented in Chapter 5, with the aim assessing whether the rock magnetic properties of these samples have affected the palaeointensity determinations. This chapter is an adaptation of *Using first-order reversal curves to assess palaeointensity variations in samples recording the Matuyama-Brunhes geomagnetic field reversal* by Brown & Chen (2008), submitted to *Physics of the Earth and Planetary Interiors* (reprint enclosed in back cover).

## 6.1 Introduction

In recent years, absolute palaeointensity data have been incorporated into global models of the past geomagnetic field, such as CALS7K.2 (Korte & Constable, 2005a) and IMMAB4 (Leonhardt & Fabian, 2007); however, the reliability of the data is not always clear. A fundamental reason for ambiguous absolute palaeointensity determination is that the thermal remanent magnetisation (TRM) of volcanic rocks is not only carried by non-interacting single-domain ferromagnetic particles; however, the Thellier-Thellier family of absolute palaeointensity methods is based on the so-called Thellier's laws of reciprocity, independence, and additivity (Thellier, 1938), which are only valid for strictly non-interacting single domain (SD) particles (Néel, 1949).

In this study first-order reversal curve (FORC) diagrams have been used to char-

acterise possible TRM carriers in the chosen samples and to determine whether there is a variation in these carriers on a centimetre and metre scale. FORCs (Mayergoyz, 1986) were chosen as their two-dimensional representation, as a FORC diagram (Pike et al., 1999), allows analysis of the statistical distribution of both coercivity, $H_c$, and bias field, $H_u$.

Two previous studies (Wehland et al., 2005; Carvallo et al., 2006) have attempted use FORC diagrams as a tool for pre-selection of samples for palaeointensity analysis. Both studies investigated correlations between features on Arai-Nagata plots (Nagata et al., 1963) and FORC diagrams. Carvallo et al. (2006) provided some evidence for concave-up increasing plots with more multi-domain (MD)-like FORC diagrams. The results shown in this chapter will not be used in this way, but merely to investigate if small scale variations in rock magnetic properties can be observed, which may link to variations in palaeointensity.

The samples chosen for this study are from three lava flows from the island of La Palma and belong to the volcanic section ME (Valet et al., 1998, 1999) and described in Chapter 5. These flows record the geomagnetic field after the main polarity switch of the Matuyama-Brunhes reversal. Palaeointensity experiments were originally carried out by (Valet et al., 1999) using the thermal Thellier method (Table 6.1), and were incorporated into the iterative Bayesian model IMMAB4 of the Matuyama-Brunhes reversal (Leonhardt & Fabian, 2007).

## 6.2 Samples and methods

Flows ME47, ME48, and ME49, originally sampled by (Valet et al., 1999), were re-sampled in 2006 (the original flow names have been retained). Five cores of 25 mm in diameter were collected from each of the of the lava flows. Samples were taken from the centres of the flows to avoid problems of remagnetisation by the under or overlying flows (Valet et al., 1998). These cores were sampled approximately 2 m to 3 m apart.

The microwave system requires small cylindrical samples, which are 5 mm in diameter and typically 1 mm to 3 mm in length. They are drilled from 25 mm cores (Fig. 6.1), so allow multiple palaeointensity estimates per core (see Table 6.1 for number of determinations). The same size samples for the rock magnetic measurements and the palaeointensity experiments have been used and this allowed us to assess the rock magnetic variations on the same spatial scale as the palaeointensity variation.

Palaeointensity results were made on multiple 5 mm samples per flow using both microwave systems (see Chapter 3) To address whether variations in palaeointensity were linked to the particular experimental method, three different protocols were used: the perpendicular method (Kono & Ueno, 1977; Hill & Shaw, 2007), the double-heating method (Coe, 1967a) and the quasi-perpendicular method (Biggin et al., 2007b).

FORC measurements were performed on 3 samples per 25 mm core from up to 5

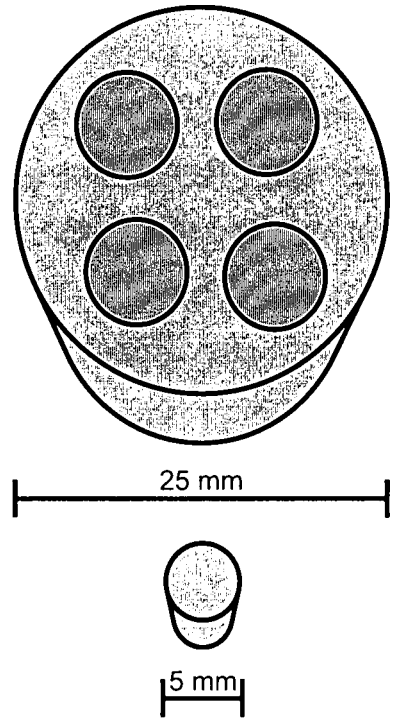


Figure 6.1: Schematic of a 25 mm rock core and 5 mm sub-sample. Circles in 25 mm core schematic represent hole sizes after drilling and removal of subsample

cores per flow. Hysteresis and back field coercivity measurements were made on the same samples which FORC measurements were performed (see Fig. 6.3 for number of samples). All hysteresis based measurements shown in this chapter were made with a MicroMag 2900 VSM at the Institute for Rock Magnetism, University of Minnesota. Thermomagnetic measurements were performed on five samples from ME47, 6 samples from ME48 and 5 samples from ME49.

## 6.3 Results

### 6.3.1 Microwave palaeointensity results

The initial palaeointensity analysis only uses one selection criterion: the straight line segment used must have a squared linear regression coefficient ($r^2$) greater than 0.98 A lenient starting criterion was chosen following the experimental results of (Biggin et al., 2007a). Their results suggest samples that have accurately recorded the recent field are not necessarily of high quality (large linear segments, with positive pTRM checks in thermal Thellier experiments), and those that are of high quality could be significantly inaccurate. Using this criterion all three flows in this study show a large variation in the palaeointensity estimates from single 25 mm cores and between cores (up to 38.3 $\mu$T for ME49) (Table 6.1); however, the flow means determined using the different methods

are similar.

Imposing the 1st and 2nd class selection criteria described in Section 3.4.8 has a large effect on the palaeointensity variations of all three flows (Table 6.1). The range of results is decreased by 22.4 $\mu$T for ME49 and 16.2 $\mu$T for ME48; however, the range still exceeds 15 $\mu$T for both flows. The range of ME47 is least affected. The most noticeable effect of applying the selection criteria is to change the mean palaeointensity estimates of the flows and to reduce their standard deviations; however, the standard deviations remain significant. The standard deviation is 18.4% of the flow-mean for ME49, 15.6% for ME48 and 24% for ME47 (Selkin & Tauxe, 2000). Applying the criteria reduced the range of estimates from a statistical approach; however, the range of palaeointensity results is still large.

All points on Arai-Nagata plots show straight line segments covering large NRM fractions. There is no evidence for concave-up increasing behaviour (Fig. 6.2), which is indicative of multidomain grains in thermal Thellier experiments (Carvallo et al., 2006). The most notable deviations from a straight line (despite having $r^2$ greater than 0.98) are concave-down increasing slopes (Fig. 6.2a, d, f). When experiments have failed, the Arai-Nagata plots show an exaggeration of this concave-down increasing slope. There is no biasing of estimates due to the determination protocol, with all protocols producing a variation in palaeointensity estimates.

### 6.3.2 Bulk rock-magnetic properties

Estimation of domain state can be obtained using a Day et al. (1977) plot. ME47 and ME49 show a significant spread in both $M_{rs}/M_s$ and $H_{cr}/H_c$ ratios, while ME48 shows a clustering of $0.1 < M_{rs}/M_s < 0.2$ and $2 < H_{cr}/H_c < 3$ (Fig. 6.3). These ratios indicate that particles present are pseudo-single domain (PSD) (Day et al., 1977) or a mixture of SD and MD (Dunlop, 2002).

Samples from ME49 show a range of Curie temperatures ($T_c$) on heating (Fig. 6.4a), from ~466°C to ~522°C, relating to a range of titanomagnetite compositions. Using the polynomial fit to experimental data for synthetic titanomagnetites (Bleil & Petersen, 1982), compositions between ~TM18 and ~TM09 are calculated. On cooling induced magnetisation was reduced by between 2% and 9% at 100°C compared with the heating curve (Fig. 6.4b).

Samples from ME48 show two groups of $T_c$: one group having a $T_c$ of ~525°C and the other ~540 °C (Fig. 6.4c), relating to compositions between ~TM07 and ~TM09. Cooling curves show a large range in the reduction of induced magnetism when compared with the heating curves (Fig. 6.4d): between 5% and 45% at 100°C. s.

Samples from ME47 have the narrowest range of thermomagnetic behaviour and $T_c$ of all three flows (Fig. 6.4e). $T_c$ range from ~507°C to 517°C), relating to compositions between ~TM12 and ~TM10. All samples show a reduction of induced magnetism on

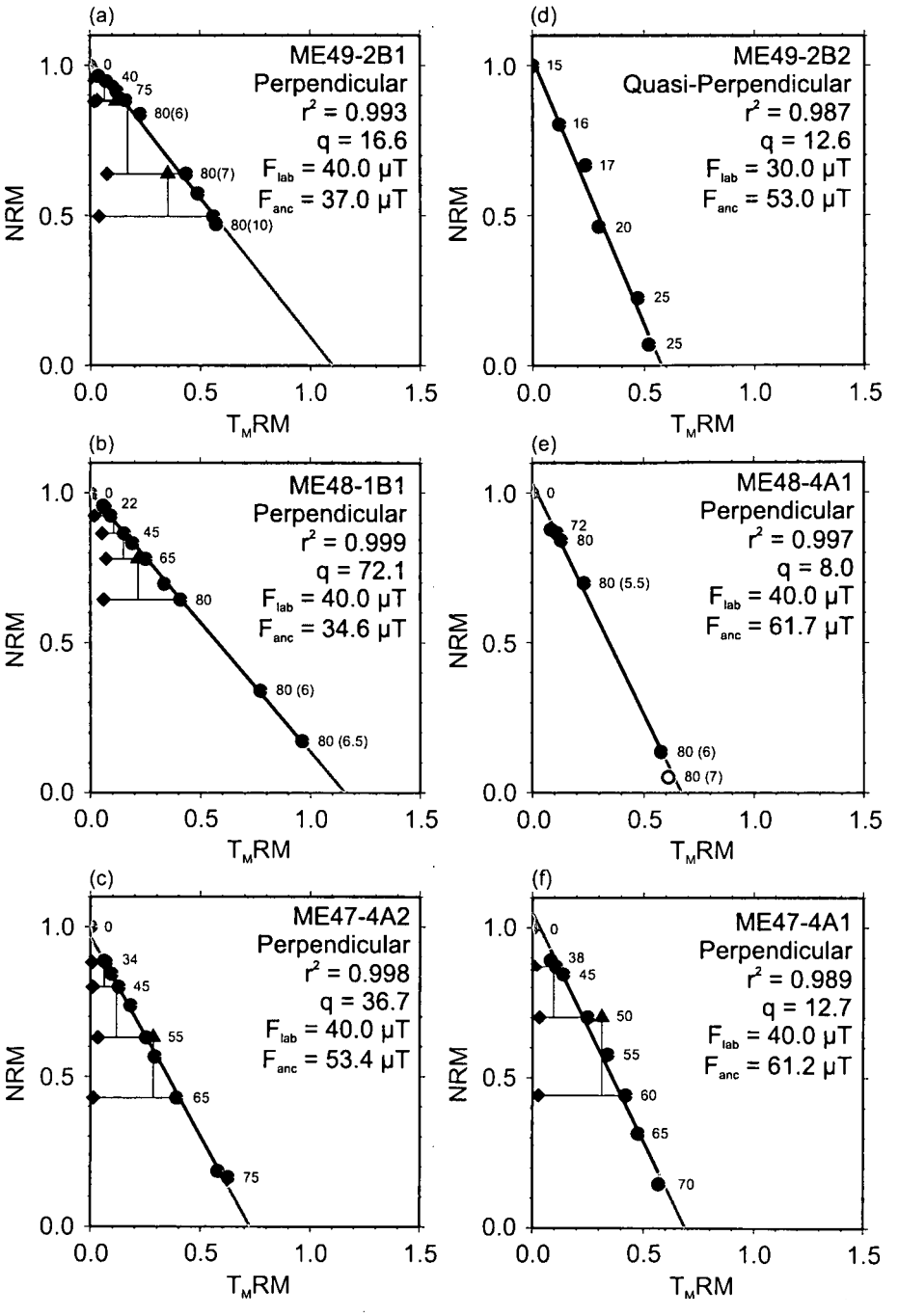


Figure 6.2: Examples of Arai-Nagata plots. (a), (b), and (c), are the best quality results from each flow. (d), (e), and (f), are examples of estimates that show a large deviation from the mean palaeointensity of each flow. $r^2$ is the squared linear regression coefficient, $q$ is the quality factor as defined by (Coe et al., 1978), $F_{lab}$ is the applied field during the palaeointensity experiment, $F_{anc}$ is the palaeointensity estimate. Numbers accompanying the data points are the microwave power steps in watts. The numbers in brackets are time in seconds; where no bracketed numbers are shown, the time of application was 5 s. Example (b) uses the quasi-perpendicular method, so no $pT_MRM$ checks or tail checks were used. This experiment was performed on the Tristan 14 GHz system, which has a more efficient cavity, so the amount of power needed to de(re)magnetise the sample was much less. No pTRM checks or tail checks were performed in example (d). $T_MRM$ denotes microwave TRM.

| *Flow* | *Microwave ($\mu T$)* | *n* | *Mean ± s.d ($\mu T$)* | *Thermal-Thellier ($\mu T$)* | *n* | *Mean ± s.d ($\mu T$)* |
|---|---|---|---|---|---|---|
| | *All Estimates* | | | | | |
| ME49 | 14.7 to 53.0 (38.3) | 8 | 30.3 ± 13.8 | 30.3 to 37.4 (7.1) | 2 | 33.9 |
| ME48 | 24.8 to 61.7 (36.9) | 14 | 41.4 ± 10.5 | 42.7 to 48.5 (5.8) | 3 | 45.2 ± 3.0 |
| ME47 | 17.9 to 53.4 (35.5) | 10 | 36.6 ± 12.2 | 33.2 to 41.5 (8.3) | 3 | 37.6 ± 4.2 |
| | *Class 1 and 2 Selection Criteria* | | | | | |
| ME49 | 37.1 to 53.0 (15.9) | 3 | 44.2 ± 8.1 | 30.3 (0) | 1 | |
| ME48 | 31.2 to 47.4 (16.2) | 8 | 37.7 ± 5.9 | 42.7 to 48.5 (5.8) | 3 | 45.2 ± 3.0 |
| ME47 | 28.8 to 53.4 (24.6) | 5 | 42.1 ± 10.0 | 33.2 to 41.5 (8.3) | 3 | 37.6 ± 4.2 |

Table 6.1: Microwave and Thermal-Thellier (Valet et al., 1999) palaeointensity results. *All Estimates* takes all results with a straight line portion on the Arai-Nagata plot, Class 1 and 2 Selection Criteria takes all estimates that pass the selection criteria (Section 3.4.8), $n$ is the number of palaeointensity estimates, $s.d$ is standard deviation of the palaeointensity estimates, numbers in brackets are the ranges of the palaeointensity estimates.

(a)

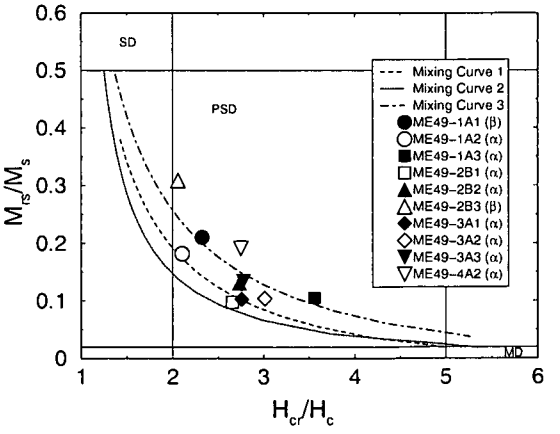


(b)

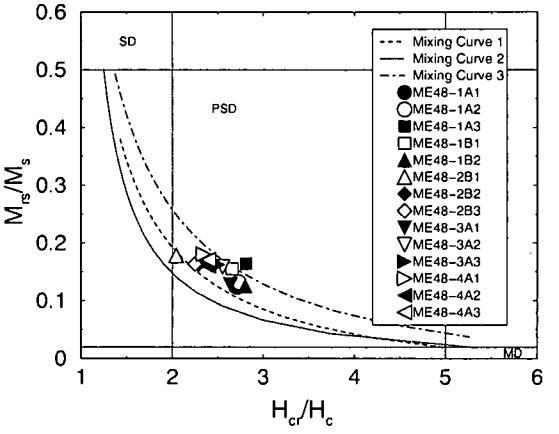


(c)

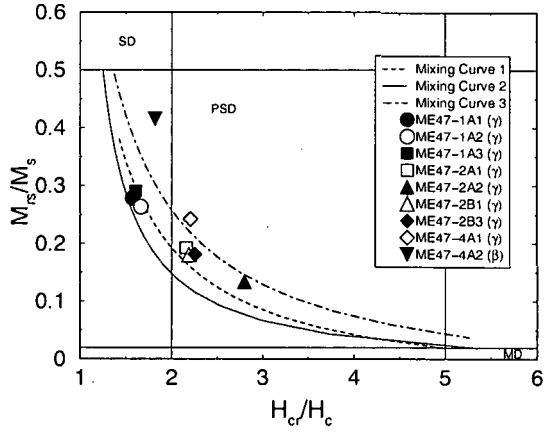


Figure 6.3: Day et al. (1977) plots with modifications from (Dunlop, 2002) for flows (a) ME49, (b) ME48, (c) ME47. Curves 1 to 3 are theoretical mixing curves of SD and MD particles for TM0 from (Dunlop, 2002). Bracketed numbers after sample names relate to FORC diagram types discussed in section 6.3.3. All ME48 FORC diagram are type $\gamma$.

cooling when compared with the heating curves (Fig. 6.4f): between 18% and 46% at 100°C.

The range of $T_c$ for ME49 is large and may result from heterogeneous deuteric oxidation. The reduction in magnetisation on cooling could result from the formation of a hematite phase due to oxidation on heating above the $T_c$ of the titanomagntite phase and towards 700°C (Böhnel et al., 2002). A small amount of hematite production could result in a reduction in induced magnetisation due to its low spontaneous magnetisation (Dunlop & Özdemir, 1997). There is no evidence for maghemitisation.

### 6.3.3 FORC diagrams

FORC distributions were calculated using the FORCLAB MATLAB code (Winklhofer & Zamanyi, 2006). Different smoothing factors were used during FORC measurement processing and are shown on Fig. 6.5, Fig. 6.6 and Fig. 6.7. FORC diagrams from each flow have varying dependency of $\rho(H_c, H_u)$ on $H_c$ and $H_u$ that is manifested in a wide range of $H_c$ and $H_u$ as well as in the shape of the FORC contours. Variations of $\rho(H_c, H_u)$ are not only observed between 25 mm cores from the same flows (Fig. 6.7), they are also seen within 25 mm cores (Fig. 6.5). FORC diagrams are broadly classified into three types:

$\alpha$. The outermost five $\rho(H_c, H_u)$ contours meet the $H_u$ axis at a high angle (e.g. Fig. 6.5a and b).

$\beta$. All contours have approximately the same width in the $H_u$ direction for all values of $H_c$ (e.g. Fig. 6.5c and Fig. 6.7).

$\gamma$. In the $H_u$ direction all contours are wider at lower $H_c$ and narrower at higher $H_c$, with the widest contours occurring at $H_c \geq 10$ mT (e.g. Fig. 6.6 and Fig. 6.7a and b).

The differences between the three types of FORC diagram result largely from variations in domain states. Type $\alpha$ FORC diagrams have previously been observed for synthetic and natural MD samples (Pike et al., 2001; Muxworthy & Dunlop, 2002). Type $\beta$ FORC diagrams are characteristic of interacting SD particles (Egli, 2006). Type $\gamma$ has been observed for synthetic magnetite at the SD/pseudo single domain (PSD) boundary (Smirnov, 2006).

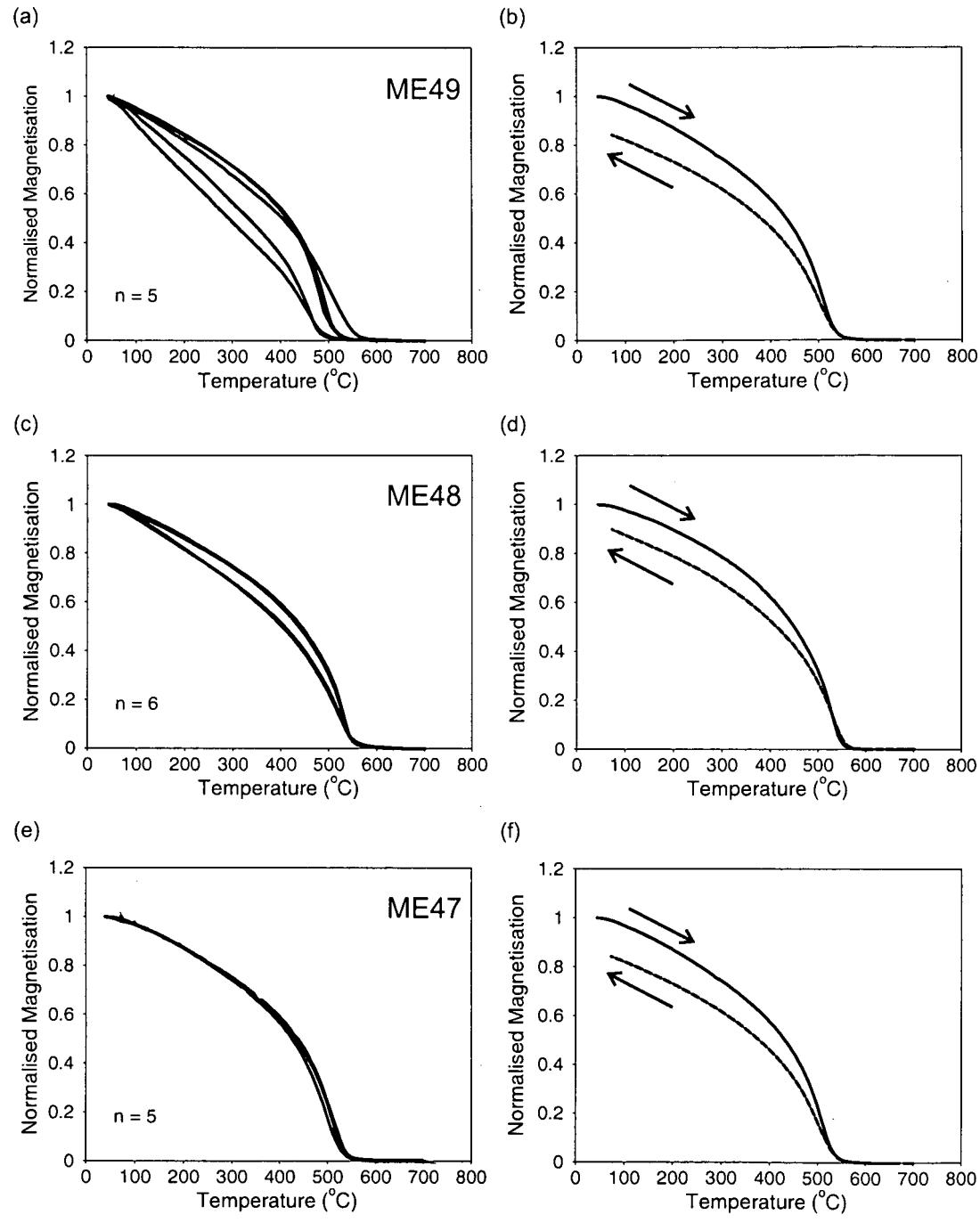


Figure 6.4: Thermomagnetic heating curves for different samples from (a) ME49, (c) ME48, (e) ME47. $n$ is number of samples from each flow. An example of heating (solid line) and cooling curves (dashed line) from one sample from (b) ME49, (d) ME48, (f) ME47. Arrows indicate the direction of the temperature change. All thermomagnetic curves are type 1, as defined in Section 5.3.1

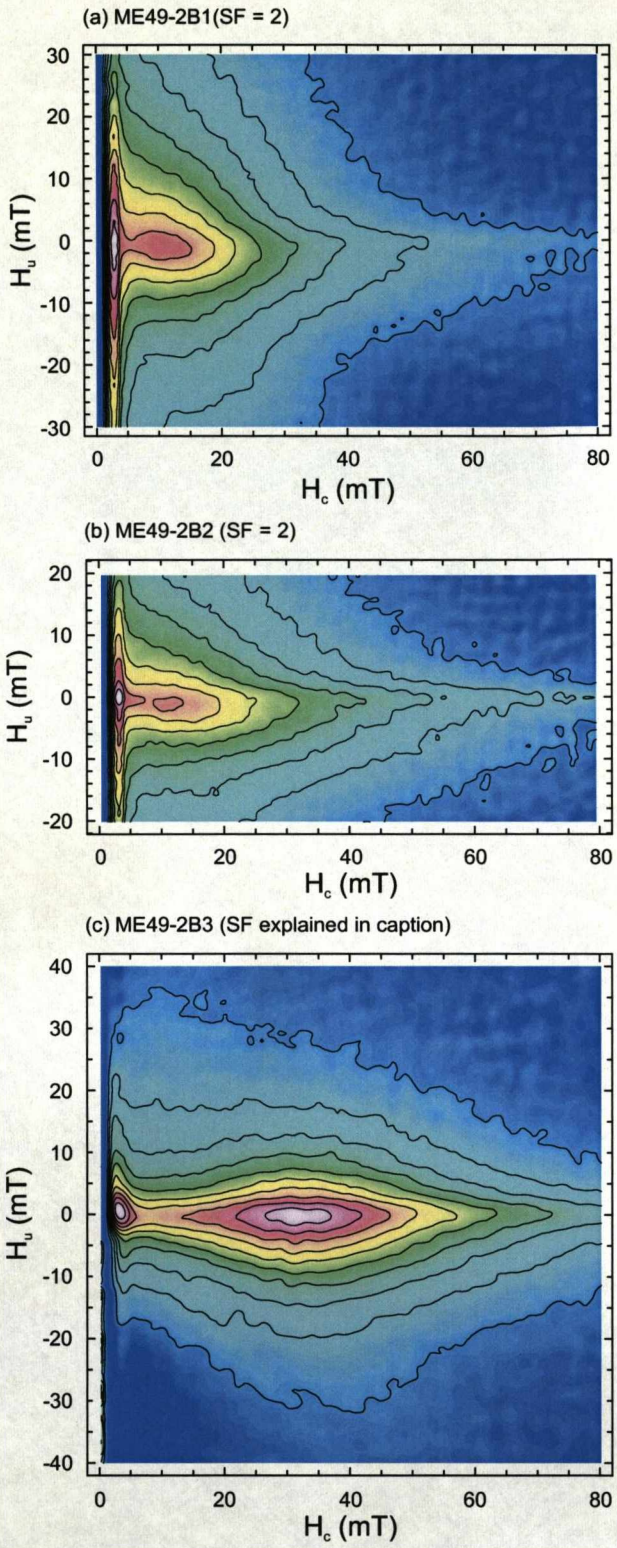


Figure 6.5: FORC diagrams for three samples from the same 25 mm core from flow ME49. All $\rho(H_c, H_u)$ values are normalised to the maximum value. Ten contours are at intervals of 10% of maximum $\rho(H_c, H_u)$. (c) is a composite of four FORC diagrams covering different regions, with SF = 2 and SF = 3 for different sections.

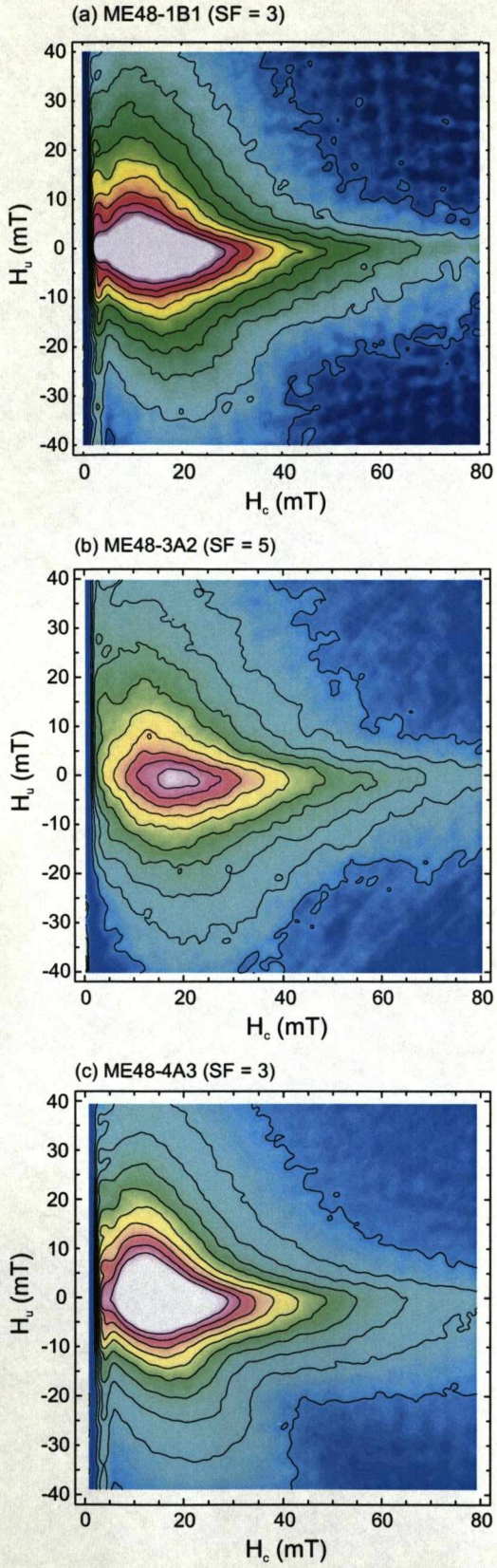


Figure 6.6: FORC diagrams for three samples from different 25 mm cores from ME48. Normalisation and contouring explained in Fig. 6.6.

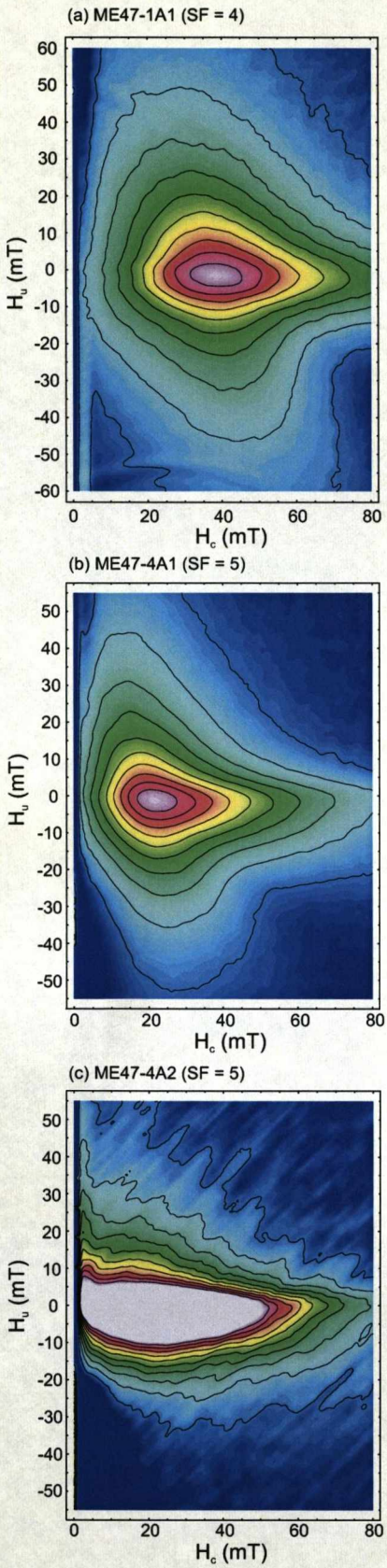


Figure 6.7: FORC diagrams for three samples from different 25 mm cores from ME47. Normalisation and contouring explained in Fig. 6.5.

## 6.4 Discussion and implications

### 6.4.1 FORC Diagrams and their relationship to rock magnetic parameters

From the FORC analysis samples that contain interacting SD particles have been identified. When the same samples are plotted on the Day plot (Fig. 6.3) none of them plot in the SD range. and they all show reduced $M_{rs}/M_s$ ratios from those predicted for SD particles. All examples plot along the mixing curves for MD and SD TM0 particles of (Dunlop, 2002) (with the exceptions of ME49-2B3 and ME47-4A2, which show a slight shift to the right). Samples characterised by type $\alpha$ FORC diagrams do not plot in the MD region of the Day plot; one interesting example is ME49-4A2 (Fig. 6.3a), which plots close to an example of an interacting SD sample characterised by the type $\beta$ FORC diagram.

### 6.4.2 Relationship between palaeointensity results and particle assemblages determined from FORC analyses

Large variations in microwave palaeointensity estimates and magnetic particle assemblages have been determined for all three flows. Importantly, both sets of variations are within 25 mm cores (see Fig. 6.2 and Fig. 6.5). Unfortunately, it is not possible to use the same samples for the FORC analyses and then for the microwave palaeointensity experiments without destroying the NRM of the samples. This means that a particular type of magnetic particle assemblage cannot be empirically linked to a particular outcome of an individual Thellier type palaeointensity experiment; however, if within a sample set rock magnetic variations are present, then random sampling would result in palaeointensity experiments being performed on samples with a range of characteristics. It is a non-trivial task to relate the contribution to the FORC distribution to the contribution to the TRM. This is due to the unequal response of remanence carrying ferro-magnetic particles to the TRM process compared with the hysteresis process. Even non-remanence carrying particles can contribute to the FORC distribution.

Although the data set presented in Table 6.1 is small, all palaeointensity estimates from the microwave and thermal Thllier techniques for ME47 and ME48 are compared. For this discussion data from ME49 is neglected as only two palaeointensity determinations were published in Valet et al. (1999). Both flows show very comparable flow mean palaeointensities when all estimates are considered; however, the range of microwave results is greater for both flows (see Table 6.1).

Using 25 mm cores for the thermal Thellier experiments may yield a weighted average of the samples intensity (weighted by the intensities recorded by different magnetic particles). Since 25 mm cores have been shown to have inhomogeneous distrubtion of magnetic particle assemblages, using smaller samples that better represent the scale of this variation will produce a larger variation in palaeointensity within a given 25 mm

core. It is inferred that the scale of variation in the magnetic partice assemblages is at least on the order of 5 mm spatially. This is a reflection of intrinsic differences in the samples and is not related to differences between the thermal and microwave excitation process. In other studies it has been demonstrated that thermal and microwave methods give comparable palaeointensity results and a low variation in palaeointensity (Hill & Shaw, 2000; Thomas et al., 2004; Gratton et al., 2005).

For this sample set the microwave palaeointensity technique produces results of two kinds: either Arai-Nagata plots show a straight line trend with large NRM fractions or they exhibit a concave-down increasing trend (failing when $r^2$ is too low to pass the selection criterion). The FORC diagrams show clear examples of MD dominated particle assemblages: however, the microwave technique has not produced concave-up increasing Arai-Nagata plots typical of MD contributions. Carvallo et al. (2006) found a different relationship between the MD contribution and the trend on the Arai-Nagata plot for a series of thermal Thellier experiments: the larger the MD contribution the greater the curvature in concave-up increasing trend. A possible explanation for the lack of curvature in the microwave experiments is that the microwaves may demagnetise the remanence held by the MD component at much low powers than is required to demagnetise the remanence held by the SD component. In the microwave experiment the cavity where the sample is held is tuned to a frequency at which there is minimum loss of microwave energy. This frequency is different for every experiment as the sample strongly effects the tuning frequency. During the experiment this frequency can also vary slightly and needs to be monitored, so a frequency sweep is performed before each microwave power application. To determine this optimum frequency a low amount of microwave power (1 W) is fed into the cavity, the microwave frequency is changed and the reflected power is monitored. This process takes approximately 10 s (10 joules of energy in total). The frequency at which the reflected power is a minimum is then chosen as the frequency at which the experiment will be performed at. It has been noted that the NRM for certain samples (and some samples from this study) often decreases after the very first tuning step (up to $\sim$ 10 %); however, it then requires a much greater amount of energy (microwave power and application time) to cause any further decrease in the remanence. This could relate to the coercivity distribution or, more likely, to the physical size of the grains and their relationship to ferromagnetic resonance.

For particles that are large (such as large PSD and MD magnetite particles in the $\mu$m range) microwave radiation will only penetrate to a certain depth. The skin depth (depth to 37% reduction of microwave radiation intensity) is frequency dependent and for magnetite is about 5 $\mu$m (Griscom, 1974). For titanomagnetites, increasing Ti substitution will reduce electrical conductivity and increase skin depth (Fischer et al., 2007). If a magnetic particle is larger than the skin depth then the radio frequency

field across the particle is not constant (Sparks, 1964). In this case nonzero wave-vector magnons are excited directly by the radio frequency field (Ament & Rado, 1955) and will cause the particle to demagnetise. The samples studied here are all low Ti titanomagnetites so could have sufficiently low skin depth to be affected by this process. The way that the MD particles behave could be the same for each power step, retaining the linearity between NRM and $pT_MRM$. This is very different to how the MD component responds to thermal processes (Fabian, 2003) and highlights that our understanding of the microwave process needs considerable attention.

The results shown in this chapter suggest that large variations in rock magnetic properties can occur on the scale of a few mm. This is not only important for palaeointensity techniques that use single samples, but has implications for the multi-specimen parallel differential pTRM method (Dekkers & Böhnel, 2006). This method requires samples (usually 25 mm) that are as similar in their rock magnetic properties as possible and contain SD and large MD particle sizes over intermediate particle sizes (PSD or small MD particles) (Fabian & Leonhardt, 2007). Great care must be taken to ensure that both these conditions are fulfilled before palaeointensity estimates from non-historical flows using this method can be determined to be robust.

## 6.5 Conclusions

1. All three flows have different magnetic particle assemblages and all show in-flow palaeointensity variation; they all have particles other than non-interacting single domain TRM carriers.

2. Both MD and interacting SD particles have been identified by FORC analyses within single 25 mm cores and in different 25 mm cores.

3. As it is not possible to use the same 5 mm samples for the palaeointensity experiment and FORC measurement, it is not possible to empirically link a particular type of magnetic particle assemblage to a particular outcome of an individual palaeointensity experiment.

4. Nevertheless, FORC diagrams have successfully detected a range of small-scale variations and features that are not possible to determine using more standard rock magnetic analyses.

# Chapter 7

# Statistical assessment of reversal behaviour based on palaeomagnetic lava data

In Chapter 5, new palaeodirectional and palaeointensity results from the Brunhes-Matuyama reversal recorded in lava flows from La Palma and Guadeloupe were presented and compared with data from previous studies of the MB. In this chapter the comparison will be extended to data from all reversals younger than 20 Ma. The relationship between intensity and directional changes during the reversal and the behaviour of transitional virtual geomagnetic poles are both considered.

## 7.1 Introduction

In the preceding chapters it was shown that the Brunhes-Matuyama geomagnetic field reversal has many interesting characteristics, but how do these compare with the behaviour of other geomagnetic field reversals? Many studies have aimed to uncover similarities in different reversals from palaeomagnetic data obtained from both sediments and volcanics, and have discussed possible implications for conditions at the core-mantle boundary (Laj et al., 1991; Hoffman & Singer, 2004) and for geodynamo behaviour (Valet, 2003).

Several compilations of sedimentary data appear to show a geometrical regularity between reversals, with virtual geomagnetic poles (VGPs) following preferred longitudinal paths (Valet & Laj, 1984; Tric et al., 1991; Clement, 1991; Laj et al., 1991), most prominently through the Americas and Asia (Clement, 1991; Laj et al., 1991). However, questions have been raised over the adequacy of the geographic distribution of sites (Egbert, 1992; Valet et al., 1992) and the reliability of the sedimentary records (Barton & McFadden, 1996; Langereis et al., 1992). To test the validity of preferred VGP paths Prévot & Camps (1993) assessed a compilation of transitional VGPs determined from volcanic sequences. As well as providing an independent (though discontinuous)

record of transitional behaviour, volcanic records are less contentious in their reliability compared with sedimentary records. In their analysis Prévot & Camps (1993) found an absence of preferred VGP longitudes from transitions recorded over the last 16 Myr. Love (1998) and Love (2000) compiled an expanded set of transitional VGPs from volcanic records for the last 20 Ma and applying a range of statistical analyses determined that there was a preference of transitional VGPs to fall along American and Asian longitudes. It has been postulated that preferred paths suggest the core and mantle are dynamically coupled. Changes in the mantle are slow compared with the rate of change of the geomagnetic field during reversals and it thought that the relatively steady conditions at the core-mantle boundary may influence the geometry of the transitional field (Laj et al., 1991; Hoffman & Singer, 2004; Costin & Buffett, 2004; Kutzner & Christensen, 2004). However, the need for a physical mechanism to generate such preferred reversal paths has been questioned in Chapter 4, as they may result from the geometric effect of the upward continuation of the geomagnetic field from the core-mantle boundary to the Earth's surface.

Relative palaeointensity for the last 4 Myr from sedimentary records suggest that there is a saw tooth pattern in palaeointenisty across reversals (Valet & Meynadier, 1993; Meynadier et al., 1994, 1995; Valet et al., 1994; Thibal et al., 1995), with an increase in intensity immediately after the reversal. Not all sedimentary relative palaeointensity records across reversals see such a pattern (Tauxe & Shackleton, 1994; Tauxe & Hartl, 1997; Yamazaki & Oda, 2001) and again the fidelity of the sedimentary records are often questioned (Guyodo et al., 2000). High post-transitional absolute palaeointensities have also been recorded in a number of volcanic sequences (Prévot et al., 1985; Bogue & Paul, 1993; Valet et al., 1999; Bogue, 2001; Riisager & Riisager, 2001; Goguitchaichvili et al., 2001; Glen et al., 2003; Hill et al., 2005). Tanaka et al. (1995) complied absolute palaeointensity data from several volcanic sections emplaced during the Cenozoic and determined that the transitional virtual dipole moment (VDM) was ~25% of today's. A difference in VDMs for normal and reversed states was not observed; however, no correction for the starting polarity of the reversals was made, so any asymmetry in the data may be disguised.

The studies of Love & Mazaud (1997), Love (1998), Love (2000) and Tanaka et al. (1995) are based on volcanic data that are at least ten years old. In this study the data base of transitional palaeodirections and palaeointensities determined from volcanic rocks has been updated and aspects of the transitional field proposed in these studies have been re-examined.

## 7.2 Data and methods

### 7.2.1 Palaeodirection data

All data considered in this analysis are shown in Table 7.1. To compare palaeodirections from multiple global locations, data are characterised as VGPs. In previous studies (Valet et al., 1992; Prévot & Camps, 1993; Johnson & Constable, 1996; Love & Mazaud, 1997; Love, 1998, 2000) transitional VGP latitudes have been considered to be between $\pm 60°$ or $\pm 55°$. This is often arbitrarily chosen. In Section 5.4.2 it was noted that VGP latitudes between $\pm 60°$ during the main MB polarity transition or precursor occurred when the VDM was low. This suggests that VGP latitudes that relate to the transitional field alone, and not to secular variation, occur between $\pm 60°$ and are chosen as the transitional VGP limits in this study. In a model of the modern field (Bloxham & Jackson, 1992) VGP latitudes as low as $\sim 55°$ resulted from secular variation. This again suggests that limits around $\pm 55°$ are appropriate to assess transitional VGP behaviour.

Deciding what data to include in the analysis presents three main problems: 1) deciding what data are reliable; 2) duplication of data from overlapping volcanic sequences; 3) determining what data relate to reversals or excursions. Only palaeodirectional flow mean inclinations and declinations determined from $\geq 3$ directions and with $\alpha_{95} \leq 10°$ have been accepted for analysis. This criteria is stricter than that used by Quidelleur et al. (1994), Johnson & Constable (1996) and Love (1998), but more lenient than using $\alpha_{95} < \approx 5°$ for fresh volcanic rocks noted by Butler (1992). Because of the varied approaches taken by different authors, reliability of the data can not be assessed using samples' rock magnetic properties.

Duplication of data from overlapping volcanic sections can overestimate the number VGPs and bias any statistical analysis. It is therefore important to choose volcanic sections carefully; however, this can be difficult. Stratigraphic sections often appear to vary across the same mountain side or from one side of a valley to another, making it very difficult to correlate multiple sections and determine an ideal stratigraphy with no overlap. This scenario is true for many Iceland sections and was explicitly shown for the Barranco del Agua sections in Chapter 5. In such cases the most continuous and detailed sequence has been included in the analysis, with the exception of the Steens Mountain section (Mankinen et al., 1985) where all sections were used, as different transitional data were recorded by the different sections. However, it is therefore likely that some duplication of VGPs has occurred. The disadvantage of only taking the most continuous section is that some transitional data are not included as all flows are contained in a chosen continuous section. This can result in an underestimation in the number of transitional VGPs.

An alternative approach would be to form VGP groups from the multiple sections;

however, this again is problematic, as it relies on the assumption that the field during the reversal is constantly changing direction, which may not be the case (Hoffman & Singer, 2004). It has been observed that multiple lava flows record similar transitional directions (Mankinen et al., 1985; Kristjánsson & Sigurgeirsson, 1993; Brown et al., 2004), which could be explained by rapid emplacement of multiple lava flows, recording similar directions, or to a longer period of time when the field becomes stable. If this stability is is influenced by conditions at the core-mantle boundary and only seen at certain locations, then using VGP groups is unsatisfactory as it will homogenise the data set (Love, 1998). In Chapter 4 it was suggested that preferred VGP paths may be generated by the geometric effect caused by the reduction of the axial dipole field and the relative emergence of the non-dipole field at the Earth's surface. In volcanic data this could be seen in VGPs as clusters in longitude and perhaps (but not necessarily) in latitude also. If similar VGPs are combined into a directional group then combining clusters as a few or one VGP would not distinguish a preference generated by this process. No directional groups have been used in this study.

In addition accurate $^{40}Ar/^{39}Ar$ dates are required to resolve the temporal variation of the field, however, in many cases the uncertainties in the dating are on the same magnitude as the possible length of the reversal process. In some studies where only partial records exist, palaeomagnetic vectors have been placed in order based on the smoothest change in direction and intensity (Roperch & Duncan, 1990). This approach is unsatisfactory as requires that the field behaves in a predictable way; however, large gaps in stratigraphy and rapid changes in the field may result in a direction and intensity of any value. Results from Roperch & Duncan (1990) that have used this method have not been included in the analysis.

The third issue is determining whether a transitional VGP relates to an excursion or a reversal. This task is simple for the Brunhes period as no reversals have taken place during this time, so no transitional data younger than $\approx$ 0.78 Ma have been included in the analysis. For other excursions such as the Santa Rosa event (Singer & Brown, 2002) $^{40}Ar/^{39}Ar$ dates are accurate enough to determine that this is an excursion. This is not as easy for long continuous volcanic sequences that may span millions of years, such as the Iceland sequences, where there are often one or two transitional VGPs within a sequence of normal and reversed lavas. Many of these Icelandic lavas are not radiometrically dated and where there are dates they are often inaccurate (B. Singer and L. Kristjánsson, *pers. comm.*). It is therefore not possible to know whether these directions are part of a known reversal from the geomagnetic polarity timescale or from an excursion. Broader questions relating to the origin of excursions also influence what data are to be selected. In some reversal records excursions of the field have been seen both before (the MB) and after the main polarity change (Steens Mountain (Mankinen et al., 1985)). This behaviour may be part of the reversal process and therefore should be

included in the analysis. Because of the sporadic nature of volcanic eruptions, variations before and after the main polarity change may be recorded, but not always the main polarity change. Unless the data unequivocally relate to an excursion (such as the Santa Rosa Event) the transitional data have been included in the analysis.

Some reversals from the same sites have been studied by many authors (e.g., Esja, Iceland (Shaw, 1974a; Kristjánsson & Sigurgeirsson, 1993; Goguitchaichvili et al., 1999a,b)). In this case the most detailed record is taken. This may again result in a loss of data; different authors will have sampled slightly different flows; however, inclusion of all data from the repeat studies is unsatisfactory.

All volcanic sequences are less than 20 Ma. Plate tectonic movements can be neglected relative to the 180° change in direction during reversals for the last 20 Myr and it is thought that conditions at the CMB are relatively stable through this time (McFadden et al., 1995; Biggin & Thomas, 2003a).

The number of VGPs accepted from each study are shown in column "I VGPs (2)" in Table 7.1. In total, 1681 transitional VGPs have been analysed. The data set is disproportionately composed of data derived from Iceland lava flows: 1140 VGPs. 64 VGPs are from the MB reversal. The remaining 456 VGPs are transitional data from all other times. Throughout the analysis the data from these different sources will be compared. Data are derived from only 27 localities, excluding those from Iceland (Fig. 7.1a), and are dominated by sites in the northern hemisphere, with only six locations from the southern hemisphere.

Initially only the raw data will be analysed and simply represented by binning VGPs in 10° longitude and latitude intervals (Fig. 7.2b, Fig. 7.4, Fig. 7.3). Although this analysis is simple, the results depend on both the choice of bin size and the bin boundaries. This is an obvious problem if clusters of directional data span a bin boundary. The data in a cluster may be equally split into two bins; however, if the same number of points from a different cluster at a different location with the same directional spread all lie within one bin then it would appear that the second location was twice as preferable as the first, when they are equally preferable.

It is possible to represent VGP data in two different ways. In this study only the so-called palaeomagnetic convention has been used. Using this convention, the sign of all magnetic south poles are retained. One problem of using this convention is that if the field is dominantly dipolar then two antipodal preferred VGP paths are produced. If the field is influenced more strongly by the non-dipole field, then additional preferred paths may exist and for each additional path there is an antipodal equivalent. This can make interpretation difficult. A different convention, called the geomagnetic convention, has been proposed to eliminate this problem (Hoffman, 1984). As the sign of the magnetic field is irrelevant in the theory of magnetohydrodynamics (Merrill et al., 1995; Stevenson, 1983), data can be plotted as a pole relative to the geographic north

or south pole regardless of its sign. Using this convention, it is much easier to identify geometric regularities, as a dipolar field will only produce one VGP path rather than two antipodal paths when using the palaeomagnetic convention. However, this convention requires the initial polarity of the reversal to be known. This is can be problematic and requires assumptions about the reversal process. As volcanic records are fragmentary two problems arise: 1) The volcanic sequence must record an initial polarity, therefore, records that have intermediate to normal/reversed directions can not be used; 2) all major directional changes may not be recorded by a volcanic sequence (Coe & Glen, 2004), which can lead to misidentification of the start and end polarities (especially when radiometric dating is inaccurate).

Only taking sites of known initial polarity seems unsatisfactory as it removes a large number of transitional data: for example, from Lousetown, Nevada (Heinrichs, 1967) and Necker Island, Hawaii (Doell, 1972). In addition, if the reversal is complex and displays large variations in direction as seen in, for example, Yamazaki & Oda (2001), then volcanic records may only record limited parts of a reversal that frequently fluctuates between normal and reversed polarities frequently. As the volcanic process is not influenced by field reversals, it is conceivable that a reversed-normal reversal could be recorded as a normal-reversed reversal. To allow any possible behaviour of the field, only the palaeomagnetic convention has been used.

### 7.2.2 Palaeointensity data

All studies where both palaeointensity and palaeodirection have been determined are shown in Table 7.2. To compare palaeointensity results from multiple global locations data are characterised as VDMs. Unlike the VGP analysis, data have not been restricted by VGP latitude limits as many studies observe fluctuations in palaeointensity around the main polarity reversal when directions are relatively stable and of normal or reversed polarity (Valet et al., 1999; Riisager & Abrahamsen, 2000; Brown et al., 2006). This makes delimitation of the total reversal process recorded in the volcanic sequences difficult. If both palaeodirection and palaeointensity are stable for a number of flows then all data between and including the last stable palaeodirection and palaeointensity before fluctuations in palaeointensity begin, and the first stable palaeodirection and palaeointensity after fluctuations in palaeointensity end, are included in the analysis. In many sequences this ideal situation is not observed and records are much more fragmentary.

Data from thermal Thellier, microwave and Shaw methods are all included. Where multiple palaeointensity studies have been performed on sister samples from the same flows, the data have been combined and new flow means calculated. In addition to the the La Palma and Guadeloupe sections (discussed in Chapter 5), there are four other studies that provide a direct comparison of palaeointensity methods. Three compare

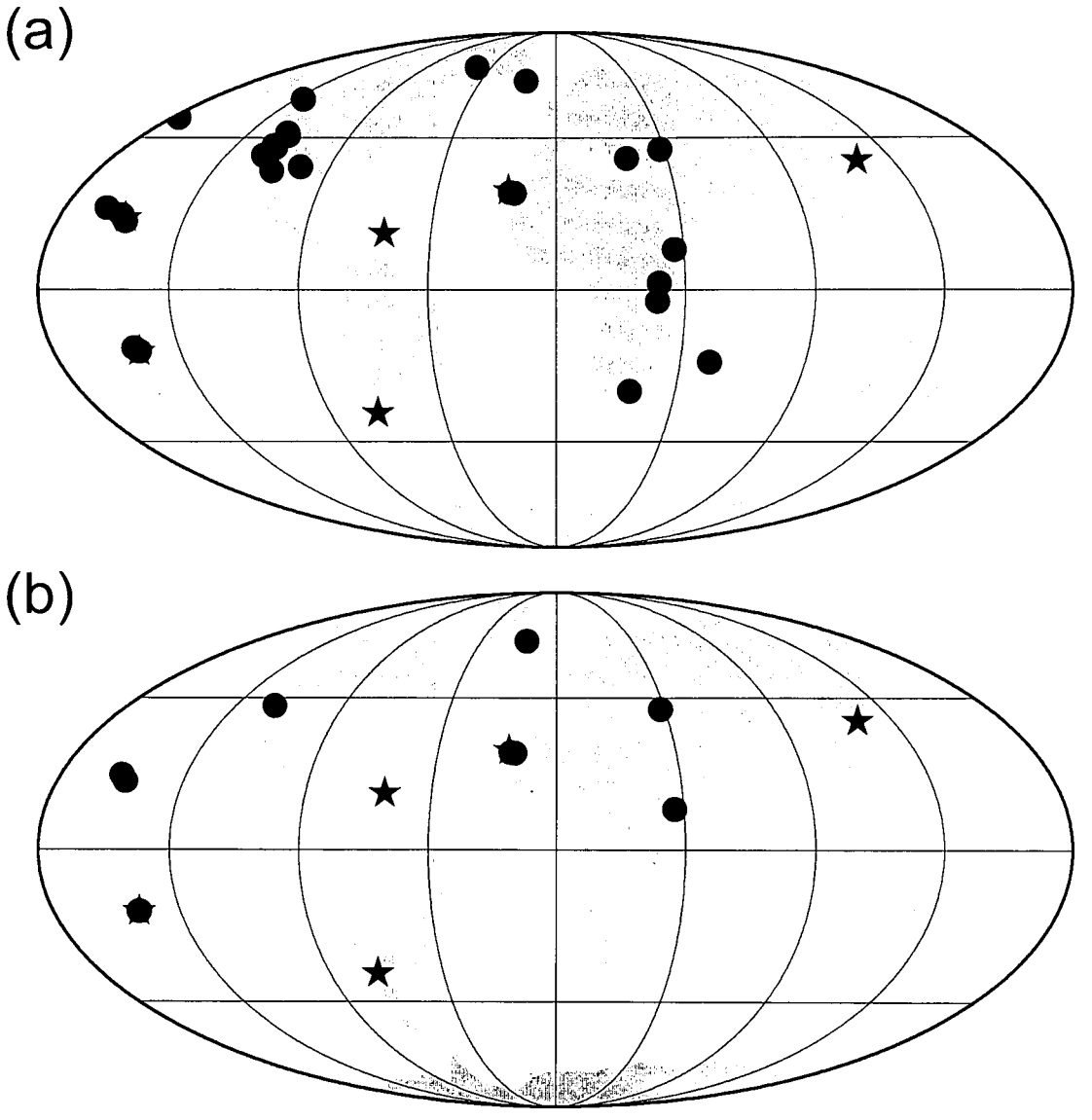


Figure 7.1: (a) Global distribution of volcanic sites recording directional changes between ±60° VGP latitude. (b) Global distribution of volcanic sites recording direction and intensity. Stars are locations recording the MB reversal, circles record other reversals.

| Location | Name | Lat °N | Long °E | Age Ma | Demag Method | I VGPs (1) | I VGPs (2) | Source |
|---|---|---|---|---|---|---|---|---|
| Aleutian Islands (USA) | Ashishik | 53.3 | 192.0 | 1.7-2.1 | AF | 10 | 7 | Bingham & Stone (1972) |
| Canada (British Columbia) | Level Mountain | 58.5 | 228.7 | 1.0-6.6 | AF | 19 | 16 | Hamilton & Evans (1983) |
| Canary Islands (Spain) | Gran Canaria | 27.9 | 344.3 | ≈14.1 | AF,T | 39 | 34 | Leonhardt et al. (2002) |
| Canary Islands (Spain) | Gomera | 28.1 | 342.9 | 9.7 | AF,T | 9 | 9 | Glen et al. (2003) |
| Canary Islands (Spain) | La Palma (ET-ME) | 28.7 | 342.1 | 0.78 | AF,T | 1 | 1 | Valet et al. (1999) |
| Canary Islands (Spain) | La Palma (LL-LS) | 28.8 | 342.3 | 0.79 | AF,T | 7 | 0 | Quidelleur & Valet (1996) |
| Canary Islands (Spain) | La Palma (TN) | 28.8 | 342.3 | 0.79 | AF | 5 | 5 | Singer et al. (2002) |
| Canary Islands (Spain) | La Palma (AS) | 28.8 | 342.3 | 0.79 | AF | 2 | 1 | This Study |
| Canary Islands (Spain) | La Palma (BS) | 28.8 | 342.0 | 0.80 | AF,T | 1 | 1 | Quidelleur et al. (2003) |
| Chile | Tatara-San Pedro | -36.0 | 289.0 | 0.79 | AF,T | 26 | 25 | Brown et al. (1994, 2004) |
| China | Tongjing | 37.8 | 120.8 | 0.73 | T | 1 | 1 | Zhu et al. (1991) |
| Ethiopia | Gamarri | 11.6 | 41.6 | 2.1 | AF,T | 3 | 1 | Kidane et al. (1999) |
| French Polynesia | Huahine | -16.0 | 209.0 | 2.9-3.1 | AF,T | 72 | 31 | Roperch & Duncan (1990) |
| French Polynesia | Tahiti | -17.7 | 210.3 | 0.79-1.2 | AF,T | 41 | 34 | Chauvin et al. (1990) |
| Georgia | Akhalkalaki | 41.5 | 43.3 | 3.6 | T | 25 | 14 | Camps et al. (1996) |
| Greenland | Vaigat Formation | 40.4 | 305.1 | ≈60 | AF,T | 65 | 63 | Riisager et al. (2003) |
| Guadeloupe (French West Indies) | Morne Marigot | 16.1 | 298.3 | 0.78 | AF,T | 1 | 0 | Carlut et al. (2000), This Study |
| Hawaii (USA) | Kauai | 22.0 | 199.5 | 3.8-5.1 | AF,T | 22 | 22 | Bogue & Coe (1984) |
| Hawaii (USA) | Kauai | 22.0 | 199.5 | 3.8-5.1 | AF | 1 | 1 | Bogue (2001) |
| Hawaii (USA) | Maui | 20.8 | 203.8 | 0.77-0.96 | AF,T | 28 | 22 | Coe et al. (2004a) |
| Hawaii (USA) | Necker | 23.6 | 195.3 | 10.0 | AF | 7 | 6 | Doell (1972) |
| Hawaii (USA) | Oahu | 21.4 | 201.9 | 3.3-3.6 | AF,T | 23 | 20 | Herrero-Bervera & Coe (1999) |
| Hawaii (USA) | Oahu | 21.4 | 201.9 | 2.1-3.9 | AF | 2 | 2 | Laj et al. (2000) |
| Hawaii (USA) | Oahu | 21.4 | 201.9 | 3.2 | T | 8 | 7 | Herrero-Bervera & Valet (2005) |
| Iceland | East Iceland | 65.2 | 346.3 | 12.1-16.3 | AF | 37 | 13 | Dagley & Lawley (1974) |
| Iceland | Esja | 64.3 | 338.4 | 2.1 | AF | 17 | 0 | Shaw (1974b) |
| Iceland | Jökuldalur | 65.2 | 346.3 | 12.1-16.3 | AF | 7 | 0 | Watkins et al. (1975) |
| Iceland | Bessastadaa | 65.0 | 345.0 | 4.8-6.5 | AF | 22 | 0 | McDougall et al. (1976) |
| Iceland | East Iceland | 65.0 | 345.0 | - | AF | 400 | 0 | Watkins & Walker (1977) |
| Iceland | Borgarfjördur | 64.5 | 337.5 | 1.6-6.7 | AF | 117 | 72 | Watkins et al. (1977)* |
| Iceland | Esja, Eyrarfjall and Akrafjall | 64.3 | 338.4 | 1.8-4.2 | AF | 103 | 69 | Kristjánsson et al. (1980) |
| Iceland | Tröllaskagi | 66.0 | 341.0 | 8.2-11.2 | AF | 174 | 128 | Sæmundsson et al. (1980) |
| Iceland | North West | 66.0 | 338.0 | 8-14 | AF | 541 | 352 | McDougall et al. (1984) |
| Iceland | Langidalur | 65.6 | 339.7 | 7.3-8.2 | AF | 68 | 54 | Kristjánsson et al. (1992) |
| Iceland | Esja and Skarðsheiði | 64.3 | 338.4 | 2.1-3.4 | AF | 51 | 50 | Kristjánsson & Sigurgeirsson (1993) |
| Iceland | Mt. Reynivallaháls | 64.4 | 338.5 | 2.5 | AF,T | 3 | 3 | Tanaka et al. (1995) |
| Iceland | Skorradalur Valley | 64.5 | 338.8 | 2.5 | AF | 16 | 16 | Kristjánsson (1995) |
| Iceland | Mjoifjördur | 65.3 | 346.5 | 10.0-13.0 | AF | 69 | 60 | Kristjánsson et al. (1995) |
| Iceland | Ísafjarðardjúp | 65.4 | 337.5 | 12.0-13.7 | AF | 114 | 95 | Kristjánsson & Jóhannesson (1996) |
| Iceland | Esja | 64.3 | 338.4 | 2.1 | AF,T | 44 | 40 | 0Goguitchaichvili et al. (1999a) |
| Iceland | Mt. Reynivallaháls | 64.4 | 338.5 | 2.5 | AF,T | 11 | 0 | Goguitchaichvili et al. (1999b) |
| Iceland | Snæfellsnes Peninsula | 64.8 | 337.7 | ≈6.9 | AF | 117 | 85 | Kristjánsson & Jóhannesson (1999) |
| Iceland | Jökuldalur | 65.2 | 344.8 | 0.78-1.8 | AF | 6 | 6 | Udagawa et al. (1999) |
| Iceland | North West | 66.1 | 336.7 | ≈15 | AF | 188 | 51 | Kristjánsson et al. (2003) |
| Iceland | Skarðsheiði and Akrafjall | 64.4 | 338.4 | 1.5-3.12 | AF | 38 | 9 | Kristjánsson & Guðmundsson (2004) |
| Iceland | Eyjafjördur | 65.7 | 341.3 | 5-9 | AF | 101 | 73 | Kristjánsson et al. (2004) |
| Iceland | Fljótsdalur | 64.9 | 344.8 | - | AF | 18 | 17 | Kristjánsson & Guðmundsson (2005) |
| Iceland | Skagafjörður | 65.5 | 341.8 | ≈9 | AF | 74 | 15 | Kristjánsson et al. (2006) |
| Kenya | Narosura and Magadi Volcanics | -1.5 | 37.4 | 6.9 | AF | 7 | 1 | Patel & Raja (1979) |
| Lesotho | Bushmen's and Sani Passes | -29.4 | 27.8 | 183 | AF,T | 34 | 34 | Prévot et al. (2003) |
| Réunion (France) | Rivière St. Denis | -20.9 | 55.4 | 2.0 | AF | 4 | 0 | McDougall & Watkins (1973) |
| Tanzania | Ngorongora | -3.3 | 35.6 | 2.5 | AF | 7 | 4 | Grommé et al. (1971) |
| Turkey | Gürün | 38.7 | 37.4 | Quaternary | AF | 4 | 4 | Sanver (1968) |

| Location | Name | Lat °N | Long °E | Age Ma | Demag Method | I VGPs (1) | I VGPs (2) | Source |
|---|---|---|---|---|---|---|---|---|
| USA (Arizona) | Hackberry Lavas | 34.4 | 248.2 | 7.9-11.5 | AF | 20 | 7 | Mckee & Elston (1980) |
| USA (Idaho) | Rocky Canyon | 46.0 | 243.0 | 16.0 | AF | 2 | 0 | Hooper et al. (1979) |
| USA (Nevada) | Lousetown | 39.4 | 240.2 | 1.1-6.8 | AF | 37 | 24 | Heinrichs (1967) |
| USA (Nevada) | Santa Rosa | 41.9 | 342.6 | 15.0 | AF | 10 | 7 | Roberts & Fuller (1990) |
| USA (Oregon) | Steens Mountain | 42.6 | 241.4 | 16.2 | AF,T | 75 | 70 | Mankinen et al. (1985) |
| USA (Oregon) | Steens Mountain | 42.6 | 241.4 | 16.2 | AF,T | 22 | 22 | Camps et al. (1999) |
| USA (Oregon) | Dug Bar and Fall Creek | 46.0 | 243.0 | 16.0 | AF | 3 | 0 | Hooper et al. (1979) |
| USA (Oregon) | Cape Foulweather and Depoe Bay | 44.8 | 236.6 | - | AF | 10 | 8 | Choiniere & Swanson (1979) |
| USA (Washington) | Columbia Plateau | 46.3 | 243.8 | 6.0-16.0 | AF | 12 | 9 | Choiniere & Swanson (1979) |
| USA (Washington) | Grande Ronde and Joseph Creek | 46.0 | 243.0 | 16.0 | AF | 6 | 0 | Hooper et al. (1979) |

Table 7.1: Table of all records that record transitional directions used in this study. Demag is the demagnetisation method used to determine the palaeodirection, AF is alternating field, T is thermal. I VGPs (1) is the number of VGPs between ±60° published, I VGPs (2) is the number chosen for analysis in this study. * re-sampled by Leó Kristjánsson; inconsistent flow means from Watkins et al. (1977) recalculated with new data and new tectonic corrections. Data provided by Leó Kristjánsson *pers. comm.*

thermal Thellier and microwave methods and one study compares the Shaw technique with the microwave method (see Table. 7.2). A special case has been made for the Shaw (1975) data. High palaeointensities were determined for a small number of flows with equatorial VGPs during the R3-N3 transition recorded in Iceland. On re-examination using the microwave technique (Brown et al., 2006), these flows gave low palaeointensities in accordance with the results of Goguitchaichvili et al. (1999a). This data is still included at this stage. In the case of the AS and AN sections from La Palma, shown in in Chapter 5, it is uncertain which flows are comparable with those of Quidelleur & Valet (1996), so both data sets have been included. Unfortunately, the detailed record of Riisager & Abrahamsen (2000) from Greenland could not be included in this analysis as it was not possible to correlate the palaeodirection and palaeointensity data.

In the initial assessment of the data no selection criteria have been applied (except to exclude palaeointensity results corrected using the method of Valet et al. (1996)) (Fig. 7.7a and Fig 7.8a and d). This lenient starting point was chosen following the experimental results of Biggin et al. (2007b). Their results suggest samples that have accurately recorded the recent field are not necessarily of high quality (large linear segments, with positive pTRM checks in thermal Thellier experiments), and those that are of high quality could be significantly inaccurate. In total 431 flow mean VDMs from 25 studies from 11 global regions are initially included (Fig. 7.1b).

The seconds stage of analysis only includes individual palaeointensity data that pass the class 1 and 2 selection criteria (Section 3.4.8). All flow means are recalculated. 317 flow means are calculated from data which pass this criteria (Fig. 7.7b and Fig. 7.8b and e). The final analysis only includes individual palaeointensity data that passed the selection criteria and where flow means were calculated from three or more determinations (Fig. 7.7c and Fig. 7.8c and f). Only 123 flow means meet this criteria.

VGP colatitude has been calculated and adjusted depending on the starting polarity of the reversal: the start of the directional changes will lie close to 0° adjusted VGP colatitude. We have taken this approach as many studies have determined high palaeointensities immediately after the main polarity change (Prévot et al., 1985; Bogue & Paul, 1993; Valet et al., 1999; Bogue, 2001; Riisager & Riisager, 2001; Goguitchaichvili et al., 2001; Glen et al., 2003; Hill et al., 2005). As the field can reverse in either direction, post-transitional values would be indistinguishable from those before the transition if the colatitude was not adjusted. In the studies used in this analysis, it was possible to determine the starting polarity; however, the theoretical caveats discussed in the previous section are recognised and must considered when making conclusions about the nature of the reversing field.

VDM-adjusted VGP colatitude data are first plotted as individual datum to assess datum of particular interest and address whether apparently outlying data are reliable (Fig. 7.7). VDM data are then binned by 5° adjusted VGP colatitude intervals and

mean VDMs and standard deviations are calculated for each bin (Fig. 7.8). The transitional field is defined between 30° to 150° adjusted VGP colatitude. Mean VDMs and standard deviations are calculated for adjusted VGP colatitudes between 0° and 30°, 30° and 150°, and 150° and 180°, to assess if the pre- and post-transitional field show a systematic difference and how this compares with the VDM of the transitional field.

## 7.3 Discussion

### 7.3.1 Virtual Geomagnetic Pole positions

In Fig. 7.2 all transitional VGPs are plotted along with their longitudinal preference. Visually, VGPs are not uniformally distributed in either latitude (Fig. 7.3) or longitude (Fig. 7.2b and Fig. 7.4). No uniformity tests have been performed in this analysis (e.g., Kuiper or Watson's (Prévot & Camps, 1993; Love, 1998)), so only a visual assessment can be made. Clearly preferred VGP longitudes are not obvious when all VGP data are considered, although there appears to be a possible preference for longitudes between 0° and 40°. A preference between -90° and -120° is also seen, but is dominated by the Iceland data set. Other longitudinal preferences are unclear. The MB data set is very sparse and is dominated by the Chile and Hawaii data sets, producing VGP clusters between 120° and 150° VGP longitude, and -40° to −60° VGP longitude, respectively. The data set that only considers VGPs that are not determined from Icelandic sequences or from the MB reversal shows a much greater relative range of VGPs between bins and a more distinctive relationship with VGP longitude. There are three blocks of VGP longitude that have a greater number of VGPs: 0° to 40°, 90° to 140° and 150° to 180°. There are quite different relationships depending on what data are selected.

Fig. 7.2a and Fig. 7.4 show that a key feature of the data set are clusters of VGPs. In the total data set, when only VGPs between ±40° VGP latitude are considered, there are four 10° VGP latitude by 10° VGP longitude bins that contain 10 or more VGPs (Fig. 7.4a). These bins have similar locations to the preferred VGP longitudes shown in Fig. 7.2b and may strongly influence the VGP longitude preference. The effect of the clustering on the data set can be seen in Fig. 7.5. When the VGP latitudes with which the data are accepted are varied, there is not a substantial change in the proportion of VGPs in each bin. This is due to the dominance of the equatorial VGP clusters.

In Section 5.4 hypotheses were proposed to explain the origin of the VGP cluster seen above Australia recorded in the Tatara-san Pedro lavas, Chile. Two possibilities exist, either lavas are extruded at a rate greater than the field changes or the field remains directionally stable and eruption rates are similar to those for the other flows recording the rest of the reversal. With the exception of one flow, palaeointensities determined from the Tatara-San Pedro lavas recording the directional cluster were low and consistant (Gratton et al., 2007). However, Love (1998) assessed records recording both

| Reversal | Location | Studies | Method | All flows | Selected flows 1 | Selected flows 2 |
|---|---|---|---|---|---|---|
| Brunhes-Matuyama | ME and ET Sections, La Palma | This study; Valet et al. (1999)* | T,M | 48 | 37 | 16 |
| Brunhes-Matuyama | AS Section, La Palma | This study | M | 8 | 8 | 2 |
| Brunhes-Matuyama | LL Section, La Palma | Quidelleur & Valet (1996)* | T | 9 | 8 | 0 |
| Brunhes-Matuyama | AN Section, La Palma | This study | M | 8 | 5 | 2 |
| Brunhes-Matuyama | LL Section, La Palma | Quidelleur & Valet (1996)* | T | 4 | 4 | 0 |
| Brunhes-Matuyama | Guadeloupe, West Indies | This study; Carlut et al. (2000); Carlut & Quidelleur (2000)* | T,M | 4 | 4 | 1 |
| Brunhes-Matuyama | Tatara San Pedro, Chile | Brown et al. (2004); Gratton et al. (2007) | M | 16 | 15 | 2 |
| Brunhes-Matuyama | Tongjing, China | Zhu et al. (1991) | T | 3 | 3 | 3 |
| Brunhes-Matuyama | Tahiti, Polynesia | Chauvin et al. (1990) | T | 3 | 3 | 0 |
| Lower Jaramillo | Tahiti, Polynesia | Chauvin et al. (1990) | T | 2 | 2 | 0 |
| Between 2.1 Ma and 3.9 Ma | Oahu, Hawaii | Laj et al. (2000) | T | 27 | 26 | 8 |
| Réunion | Ethiopia | Carlut & Courtillot (1999)* | T | 17 | 8 | 0 |
| Matuyama-Réunion (R3-N3) | SW Iceland | Goguitchaichvili et al. (1999a); Brown et al. (2006) | T,M | 23 | 10 | 8 |
| Matuyama-Réunion (R3-N3) | SW Iceland | Shaw (1975); Brown et al. (2006) | S,M | 23 | 0 | 0 |
| Gauss-Matuyama (N4-R3) | SW Iceland | Goguitchaichvili et al. (1999b) | T | 5 | 4 | 2 |
| Gauss-Matuyama (N4-R3) | SW Iceland | Tanaka et al. (1995) | T | 10 | 8 | 4 |
| Upper Mammoth | Oahu, Hawaii | Herrero-Bervera & Valet (2005) | T | 10 | 10 | 6 |
| Lower Mammoth | Oahu, Hawaii | Herrero-Bervera & Coe (1999); Herrero-Bervera & Valet (2005); Hill et al. (2005) | T,M | 24 | 18 | 18 |
| Gilbert-Gauss | Oahu, Hawaii | Herrero-Bervera & Coe (1999); Herrero-Bervera & Valet (2005); Hill et al. (2006) | T,M | 17 | 15 | 7 |
| 3.6 Ma | Georgia | Camps et al. (1996); Goguitchaichvili et al. (2001) | T | 30 | 19 | 12 |
| 3.95 Ma | Kauai, Hawaii | Bogue & Coe (1984); Bogue & Paul (1993) | T | 25 | 17 | 13 |
| 3.95 Ma | Kauai, Hawaii | Bogue (2001) | T | 18 | 10 | 1 |
| 9.7 Ma | Gomera, Canary Islands | Glen et al. (2003) | T | 13 | 3 | 0 |
| 14.1 Ma | Gran Canaria, Canary Islands | Leonhardt et al. (2002); Leonhardt & Soffel (2002) | T | 32 | 25 | 8 |
| 16.2 Ma (Baksi et al., 1991) | Steens Mtn., Oregon, USA | Prévot et al. (1985) | T | 51 | 24 | 8 |
| Total | | | | 431 | 293 | 123 |

Table 7.2: All reversal studies from volcanic sequences where both palaeodirection and palaeointensity have been determined (except Riisager & Abrahamsen (2000)). Where more than one study has been conducted on the same reversal the mean palaeodirection and palaeointensity for each flow has been calculated. All flows shows the number of flow units from all studies; no palaeointensity selection criteria are applied. Select flows 1 shows the number of flows that are accepted after applying the criteria in Section 3.4.8 to the individual palaeointensity results. Select flows 2 shows the number of flows that pass the selection criteria and have means that are determined from three or more palaeointensity results. The total number of flows in each category is shown in the row. * denotes studies where the correction of Valet et al. (1996) was used; these results have not been included in this analysis. T indicates thermal Thellier palaeointensity experiments; M, microwave; S, Shaw.

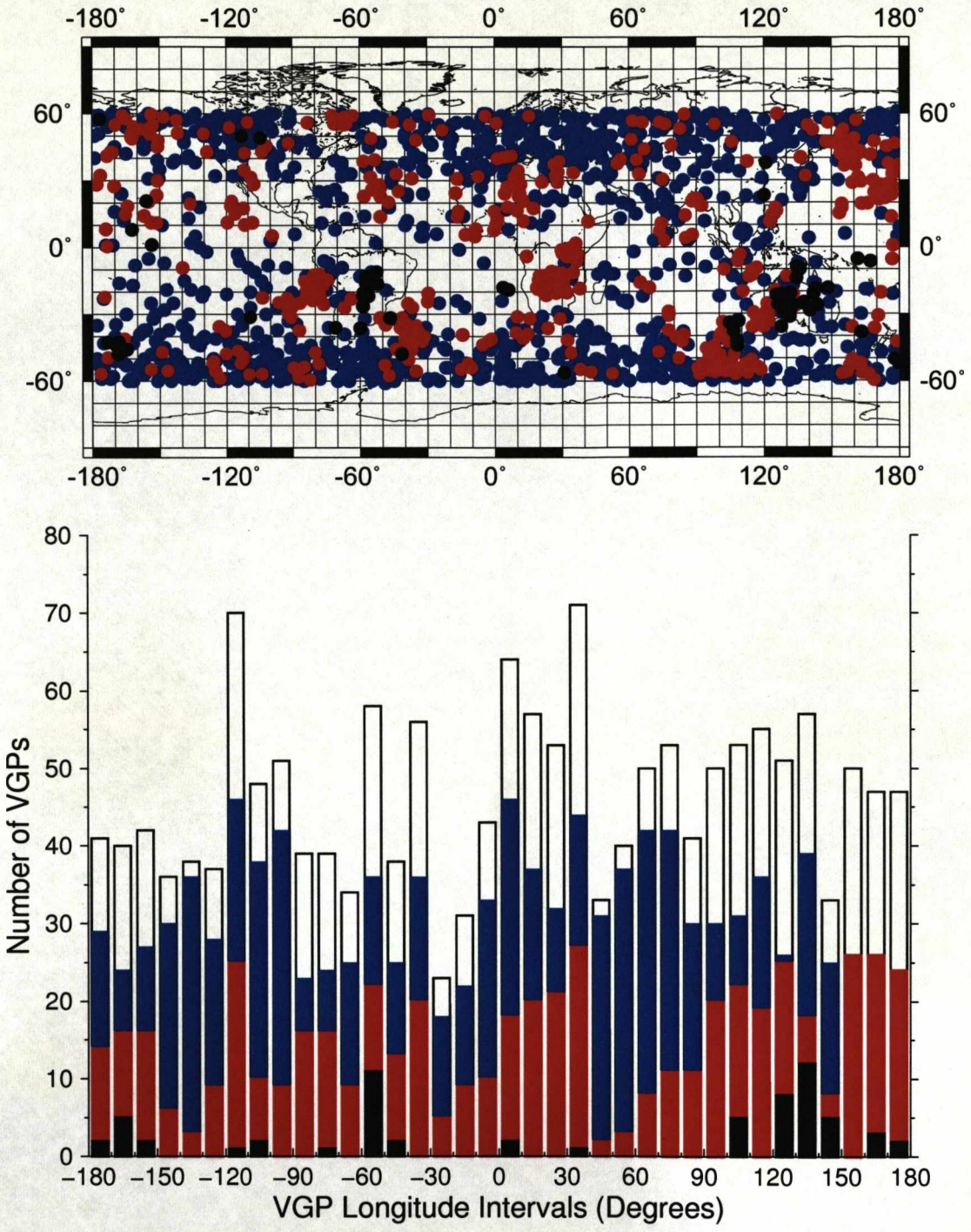


Figure 7.2: (a) All transitional VGP positions. Blue VGPs are derived from Icelandic volcanic sequences, black are VGPs from the Matuyama-Brunhes reversal, red are VGPs from all other reversals. (b) 10° VGP longitudinal bins for all transitional VGP data. Open bars are the total number of VGPs in each longitude bin, other colours are the same as for (a).

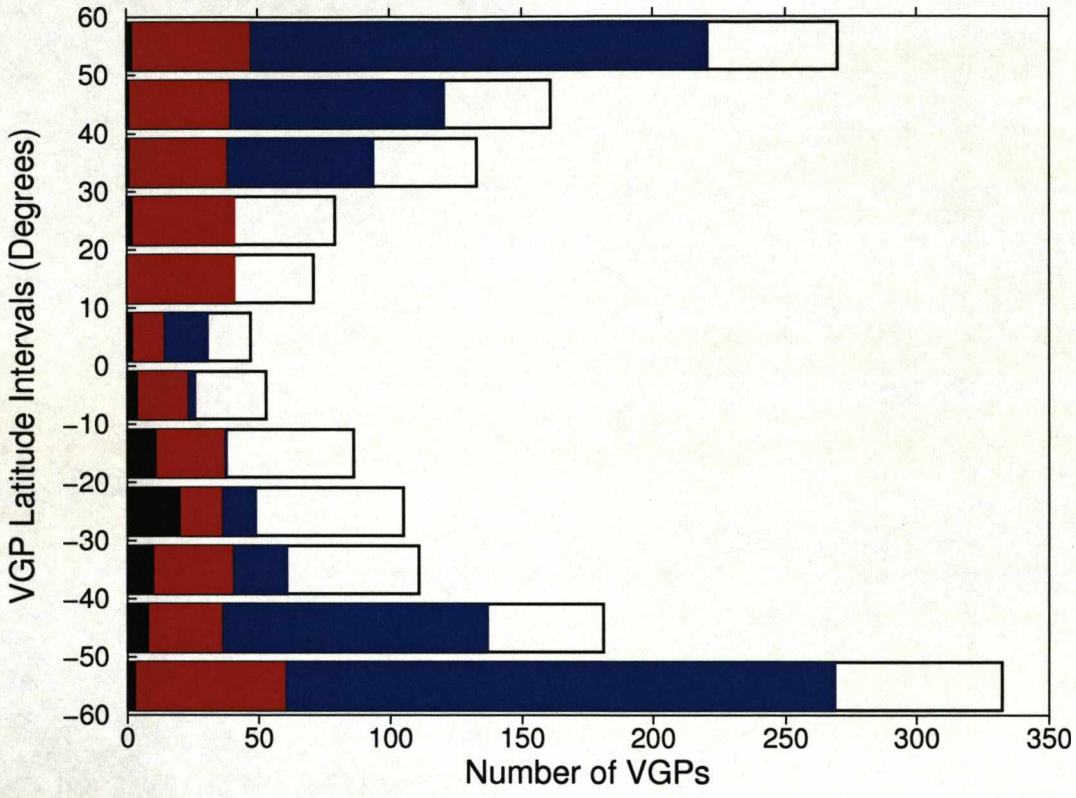


Figure 7.3: 10° VGP latitude bins for all transitional VGP data. Colours are the same as in Fig. 7.2.

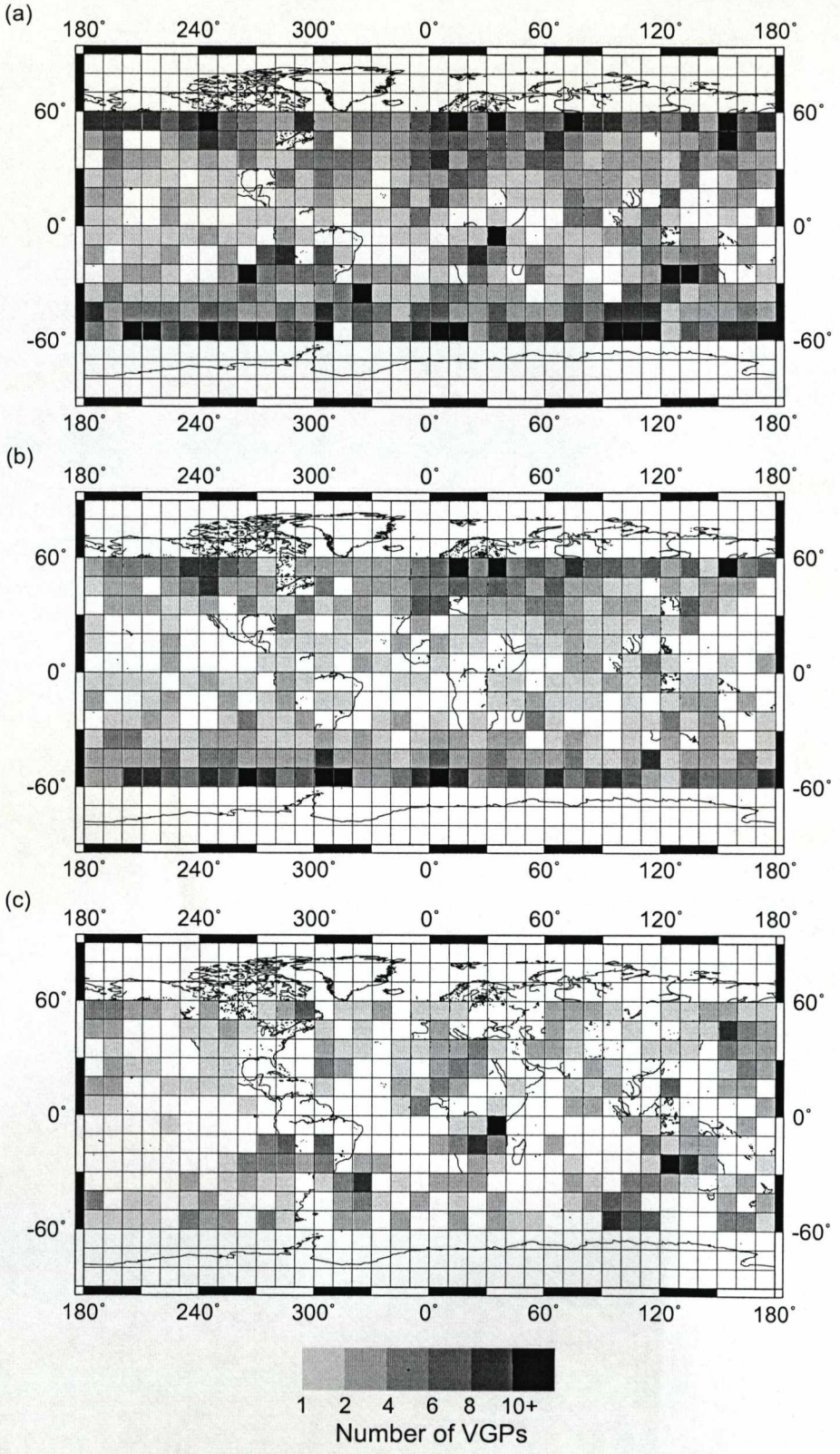


Figure 7.4: Maps of the number of VGPs in 10° VGP latitude and VGP longitude bins. (a) All transitional VGPs. (b) VGPs derived from Icelandic volcanic sequences. (c) All other transitional VGPs.

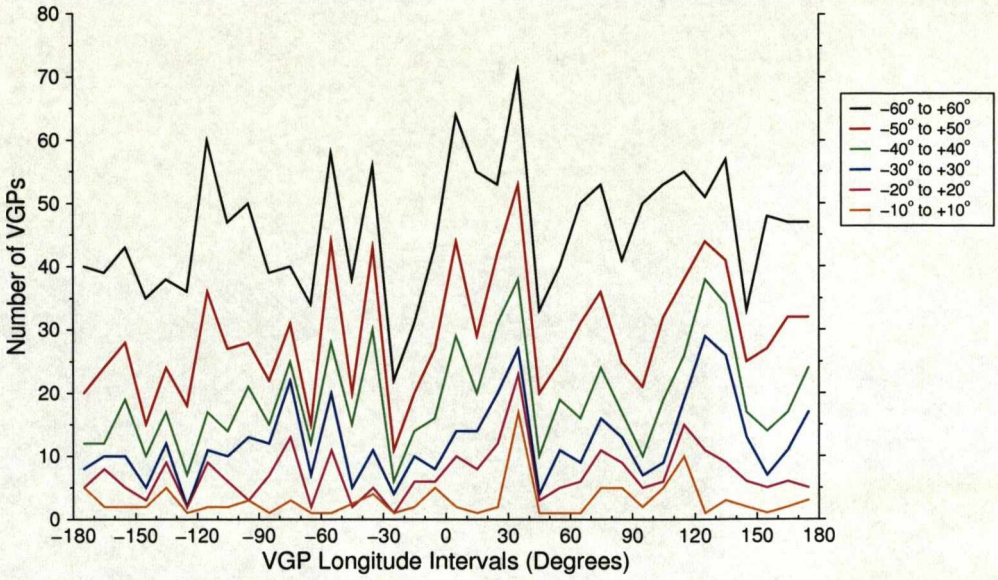


Figure 7.5: Variations in the number of VGPs in each 10° VGP longitude bin for different VGP latitude limits.

palaeodirectional and palaeointensity changes and determined that although the direction of the field may change only a few degrees (within the errors of the determination) the palaeointensity can change by tens of microtesla. Assessing the rate of free decay of the dipole ($\sim 15\mu$T/kyr), Love (1998) proposed that in such cases the VGP clusters can result from geomagnetic variations over a range of times, and do not exclusively relate to rapid eruptions. This highlights the need for both directional and intensity data for such clusters as well as a better understanding of the time scales of the volcanological processes that generate lavas with similar geochemical signatures and the variations in these geochemical signatures.

To account for eruptive variability that may cause the clustering of VGPs during each transitional event, the approach of Love (1998) has been taken. Clustered data are not combined or rejected as this would necessarily homogenise the distribution of VGP longitudes (Love, 1998, 2000). The data is weighted to account for the fact that the total duration of the reversal is recorded at different sites by different numbers of intermediate directions. The approach taken by Love (1998) is based on the Valet et al. (1992) method of calculating the mean VGP longitude for each transition at each site and assessing the distribution of means, instead of the total number of VGPs. This method weights all VGPs in a consistent manner and addresses, to some extent, the biasing caused by some transitions at some sites being represented by only a few VGPs, whereas others (such as Steens Mountain (Mankinen et al., 1985)) have a larger number of data that are often clustered. Fig. 7.3 shows a clear dependence of the number VGPs on the VGP latitude. To remove some of the sensitivity to the VGP latitude, each VGP is also weighted by $(cos\lambda)$, where $\lambda$ is VGP latitude. This gives a greater

to weighting to VGPs at equatorial latitudes and suppresses the influence of VGPs at higher latitudes. The total weighting of each VGP is $(cos\lambda)/N_i$, where $N_i$ is the total number of transitional directions for a particular reversal at a particular site. For the weighting to be meaningful a minimum of three transitional flows must exist per transition.

This analysis has only been made on results from sections that are not from Iceland or do not record the MB reversal, as it is seen in Fig. 7.2 and Fig. 7.4 that this data set contains a large amount of clustered VGPs. It is also difficult to distinguish individual reversal events in the Iceland data when such long sequences of poorly dated flows exists, making it difficult associate single transitional VGPs with one reversal or another. Therefore, it does not seem to be appropriate to use the $N_i$ weighting when such ambiguities exist. For some Icelandic sequences it is easier to determine individual reversals (e.g., the R3-N3 reversal Kristjánsson & Sigurgeirsson (1993)); however, to keep a constant segregation of data from different sources, no Icelandic data or MB data is included. This limits the analysis as the Iceland data set comprises 68% of all data, it would therefore be preferable to include this data in a further more robust analysis than is presented here. Only including transitional sequences containing a minimum of three VGPs eliminates data from Patel & Raja (1979), Choiniere & Swanson (1979), Kidane et al. (1999), Laj et al. (2000) and Bogue (2001).

Results of the $(cos\lambda)/N_i$ weighting are shown in Fig. 7.6a. A non-uniform distribution of VGPs with VGP longitude bin is again seen. The mean $(cos\lambda)/N_i$ is 0.59 and 11 bins have $(cos\lambda)/N_i > 1.5$ x mean and can be broadly split into 5 VGP longitude groups: (-120,-110), (-30,-60), (10,40), (90,130), and (170,180). The two clearest preferred longitudes relate to areas over Africa and eastern Asia. With the exception two bins between -100° and -120° all $(cos\lambda)/N_i$ between -160° and -80° are less than half the mean $(cos\lambda)/N_i$ (Fig. 7.6a). These two bins relate to areas over the eastern Pacific and western North America. It could also be suggested that there is a preference between -30° and -60° VGP longitude (note the -40° to -50° bin only has $(cos\lambda)/N_i = 0.52$). This band corresponds to a preference over eastern South America and Greenland. The four possible peaks in preference are seen more clearly in Fig. 7.6b. With the exception of the -110° to -120° maximum the three other peaks have very similar $(cos\lambda)/N_i$ maximums, suggesting an equal preference for VGPs in these areas. The preferred VGP longitudes near the Americas and Asia broadly agrees with the results of Laj et al. (1991) and Love (1998, 2000); however, the bands through Africa and eastern South America are as strong as the Asian band.

The results of the $(cos\lambda)/N_i$ VGP weighting are compared with the number of VGPs in each bin, to assess the effect of the weighting on the longitudinal preference (Fig. 7.6b). For VGP longitudes between -30° and 150° the two data sets are comparable, which suggests that although there are prominent clusters in this region (which

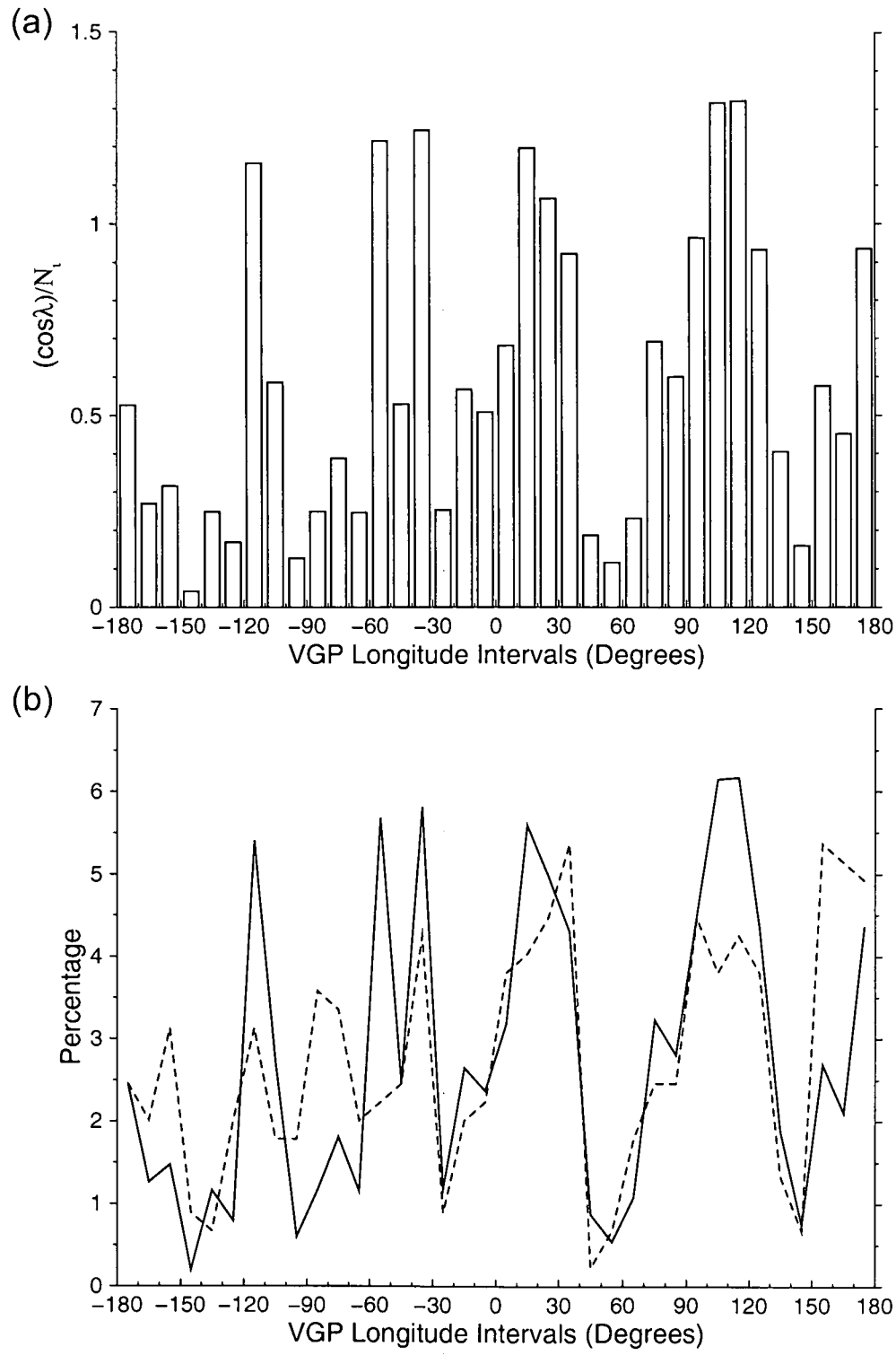


Figure 7.6: (a) Binned $\sum_{N_i}(cos\lambda)/N_i$ data. All data from studies not from Iceland locations or part of the MB data set. (b) Percentage of total $\sum_{N_i}(cos\lambda)/N_i$ (solid line) and percentage of total number of flows used to determine $\sum_{N_i}(cos\lambda)/N_i$ (dashed line).

is clear), they do not dominant the analysis. For other VGP longitudes the peaks and troughs are at the same VGP longitudes; however, there is a disparity in the relative significance of a particular bin compared with the data set as a whole. Between -150° and -30° only considering the number of VGPs per bin suppresses the influence of the peaks between -100° and -120°, and -30° and -90°. This means that small clusters of data at mid-latitudes were dominant and that there is no longitudinal preference over the whole VGP latitude range. This suggests that there may be a true preference for the 4 global locations and that the distribution of longitudinal data is non-uniform, at least within this data set. Such analysis would need to include both Iceland and MB data if such preferences are to be determined to be robust.

The provenance of the VGP data in 10° VGP latitude by 10° VGP longitude bins has been investigated to assess further the influence of VGP clusters (Fig. 7.4). The 10° VGP latitude by 10° VGP longitude bin that contains the most VGPs (18) is between -50° and -60° VGP latitude and 90° and 100° VGP longitude, and is derived from multiple records (Watkins et al., 1977; Sæmundsson et al., 1980; Kristjánsson et al., 1980; Hamilton & Evans, 1983; McDougall et al., 1984; Kristjánsson & Jóhannesson, 1999; Camps et al., 1996; Prévot et al., 2003). The study of Camps et al. (1996) provides a cluster of six VGPs; however, the other studies show individual VGPs separated by flows recording different directions. The most interesting VGP latitude and longitude bins are those from the non-iceland data set (Fig. 7.4c. Two areas with between ±40° VGP latitude containing at least one bin of ten or more VGPs are of particular interest (Fig. 7.4c). These areas are over Australasia and east central Africa. The VGP bins from all three areas are each composed of VGP clusters from two different reversals (as well as some additional VGPs from other reversals that are not part of a directional cluster).

The Australasia bins are composed of two large VGP clusters: one from the MB reversal recorded in Chile (Brown et al., 2004) and the other from the C27n-C26r reversal recorded in Greenland (Riisager et al., 2003). In addition there are smaller clusters from a number of reversals recorded in French Polynesia that span a range of bins that also plot in this area (Chauvin et al., 1990; Roperch & Duncan, 1990). Hoffman & Singer (2004) also determined a cluster of VGPs over Australasia for the Big Lost excursion during the Brunhes chron recorded in lavas from French Polynesia. In addition, the more diffuse R3-N3 VGP cluster is located over Indonesia.

It is highly improbable that rapid eruption rates occurred during all these geomagnetic events recorded at multiple global locations, resulting in a clustering of poles. As Hoffman & Singer (2004) points out, Australasia lies over a non-dipole field flux patch, which has been identified in surface field models for the modern day field (Johnson et al., 2003), the historic field Bloxham & Jackson (1992); Jackson et al. (2000), and the palaeomagnetic and archaeomagnetic fields (Kelly & Gubbins, 1997; Korte & Con-

stable, 2005a). This patch does vary in position and also in its polarity (a positive flux patch is necessarily accompanied by a negative flux patch). This non-dipole field flux patch may influence the geometric structure of the field at various points during the reversal. It may become more prominent at sometimes rather than others as the dipole field and other non-dipole features (possibly) vary through the reversal. In a hypothetical case where only the flux patch beneath Australasia is present during the reversal then a global of VGPs over Australasia would occur. Hoffman & Singer (2004) suggest that geomagnetic flux may be controlled by heterogeneous conditions at the core mantle boundary. The bins for the area over Africa are composed of clusters of VGPs from lavas from Greenland (Riisager et al., 2003) and lavas from Lousetown, Nevada, USA (Heinrichs, 1967). Central Africa is also above flux patches that have been seen to move through this area, although this has not been observed at this locations for all times (Jackson et al., 2000; Korte & Constable, 2005a).

These results suggest that clustering of VGPs may be a product of the non-dipole field structure and relate to conditions at the core-mantle boundary. Further investigation of the influence of flux patches is necessary and detailed studies of Brunhes age excursions recorded in long lava sequences may provide such an opportunity. If more transitional studies from different locations and from different transitional events show clustering over the same geographic areas then it would suggest that this a geomagnetic phenomena and not related to episodes of rapid volcanism.

### 7.3.2 Relationship between directional and intensity changes

Individual VDM-adjusted VGP colatitude data are shown in Fig. 7.7. The MB data set is broadly similar to the data from all other reversals, but the number of MB data are low (Fig. 7.8d-f). It is, therefore, not possible to make any significant comparisons, as for many transitional adjusted VGP colatitudes there are no data for the MB (see Chapter 5); however, some of the main features of the total data set will be highlighted.

In Fig. 7.7a there are two VDMs between 75° and 105° adjusted VGP colatitude that are higher than today's global VDM. These results are from Shaw (1975) and Camps et al. (1996). The samples from Shaw (1975) were re-examined by Brown et al. (2006) using the microwave technique and a mean VDM of 2.0 $\pm$ 0.7 x $10^{22}$ $Am^2$ was determined . By applying the selection criteria, the high values of Camps et al. (1996) are removed (Fig. 7.7b). Other high VDM values between 30° and 150° adjusted VGP colatitude, come from two reversals from the Canary Islands (Leonhardt et al., 2002; Leonhardt & Soffel, 2002). Only three other studies have reported high VDMs during a transitional field and these were from excursions (Coe et al., 1984; Leonhardt et al., 2000; Riisager et al., 2004); however, excursions and reversals could be related to different core processes (Gubbins, 1999).

Fig. 7.7 and Fig. 7.8 show an apparent increase in VDM between 75° and 105°

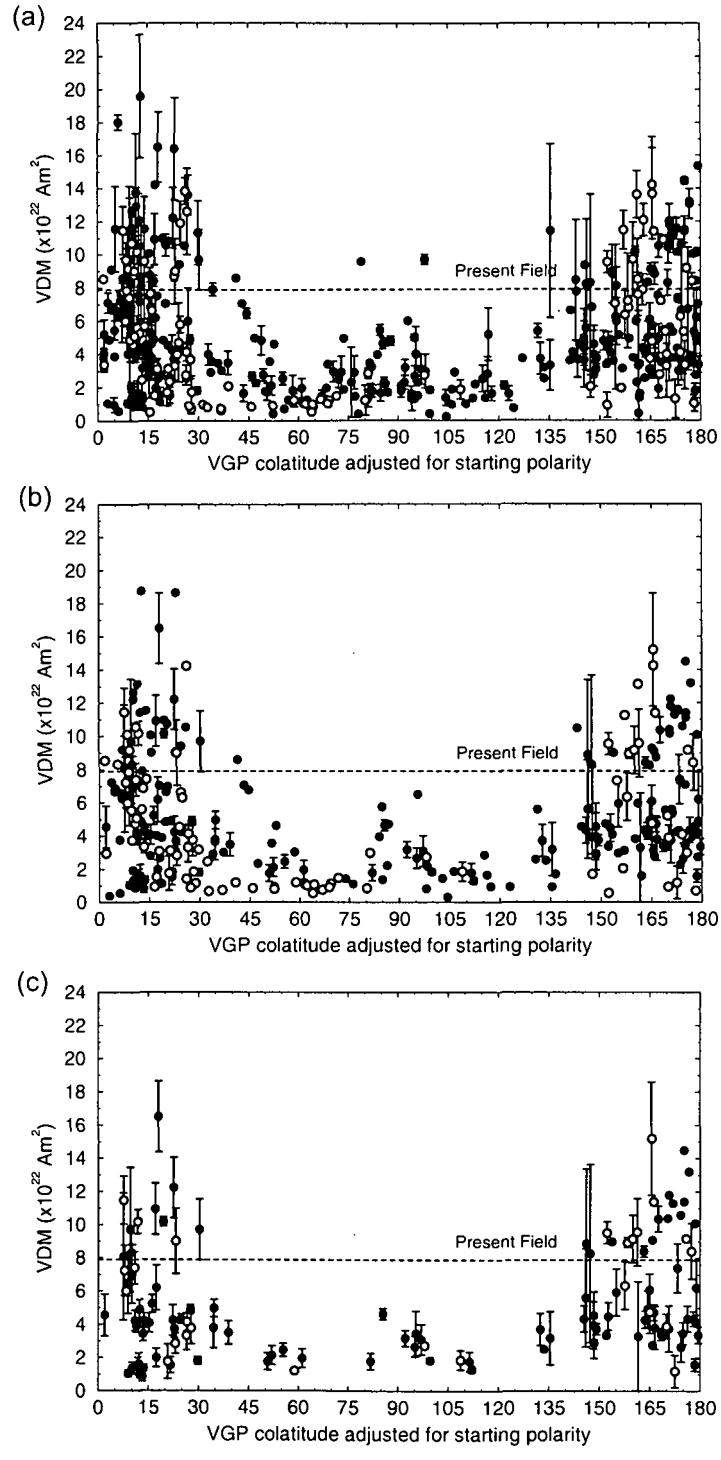


Figure 7.7: VDM versus the VGP angle away from ± 90° VGP determined from the starting polarity of the reversal. (a) All published VDMs and VGPs from reversals (excluding results determined using the correction method of Valet et al. (1996) and results from Riisager & Abrahamsen (2000)). (b) Flow means determined from class 1 and class 2 data using the individual sample selection criteria described in Section 3.4.8. Many flow means are determined from only one or two determinations. (c) Flow means determined from class 1 and 2 data and from more than three palaeointensity results per flow. See Table 7.2 for the studies used in this analysis.

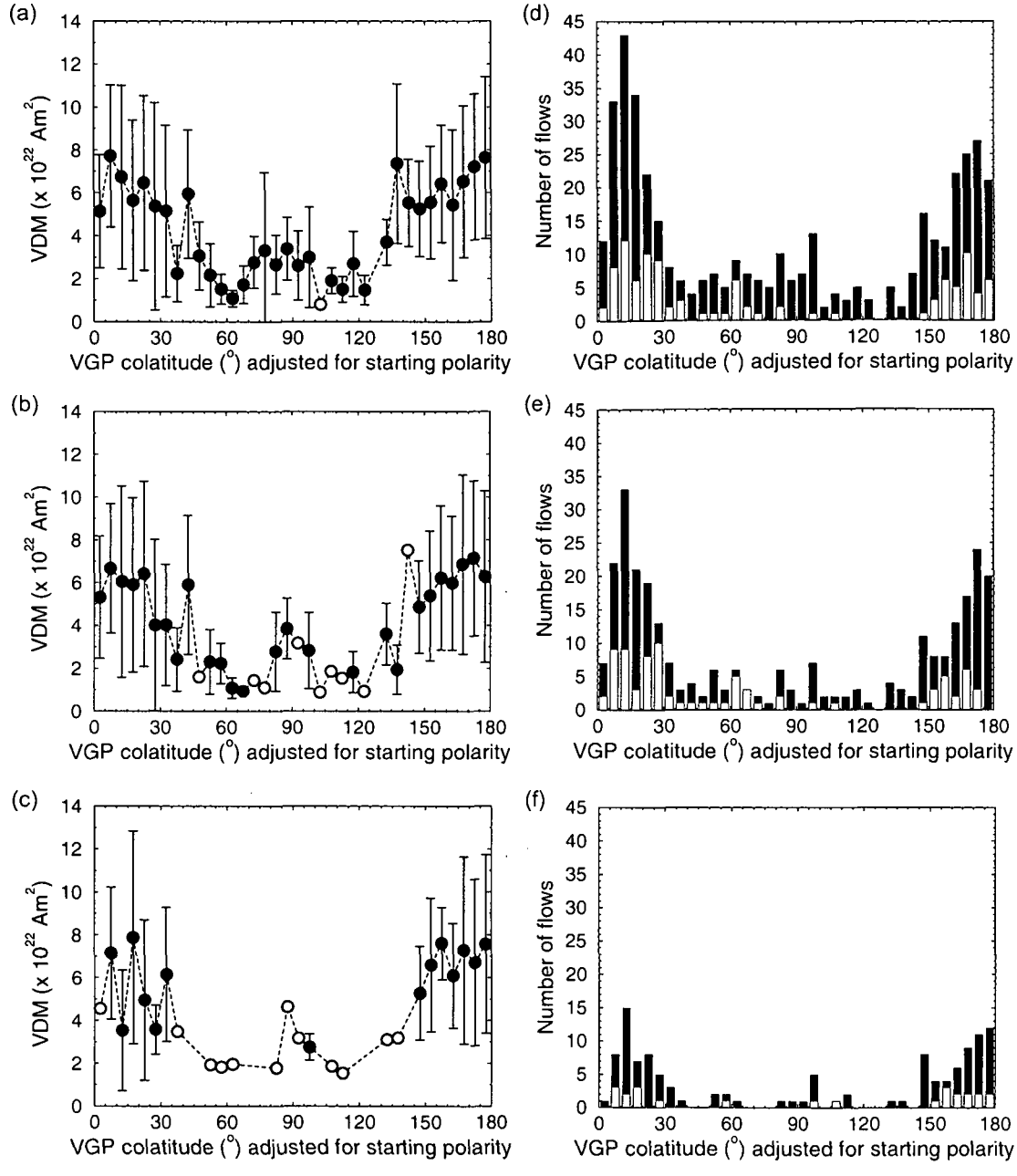


Figure 7.8: (a-c), mean VDM versus the VGP angle away from ± 90° VGP determined from the starting polarity of the reversal. Bins are VGP intervals of 5°. Closed circles are means determined from three or more VDMs per bin; open circles are means determined from 1 or 2 VDMs per bin. Error bars are $2\sigma$. (d-f), number of flows used to determine the mean VDMs for each VGP bin. (a) and (d), flow results determined from all published VDMs and VGPs from reversals (excluding results determined using the correction method of Valet et al. (1996) and results from Riisager & Abrahamsen (2000). (b) and (e), flow results determined from class 1 and class 2 data using the individual sample selection criteria described in Section 3.4.8. (c) and (f), flow results determined from class 1 and 2 data and from more than three palaeointensity results per flow. Filled bins are the total number of flows; white bins are the number of data from flows recording the MB reversal.

| Adjusted VGP colatitude bin | All data Mean VDM $\pm\sigma$ ($\times 10^{22}$ Am$^2$) | Number | Select 1 Mean VDM $\pm\sigma$ ($\times 10^{22}$ Am$^2$) | Number | Select 2 Mean VDM $\pm\sigma$ ($\times 10^{22}$ Am$^2$) | Number |
|---|---|---|---|---|---|---|
| 0° to 30° | 6.43±3.93 | 159 | 5.93±3.98 | 115 | 5.22±3.63 | 44 |
| 30° to 150° | 3.04±2.23 | 146 | 3.00±2.25 | 84 | 3.57±1.92 | 22 |
| 150° to 180° | 6.64±3.56 | 125 | 6.45±3.63 | 90 | 7.04±3.58 | 46 |

Table 7.3: Mean VDM results from all flows recording both palaeodirection and palaeointensity. Select 1 Mean VDMs are determined from all flows that pass the class 1 and 2 selection criteria (Section 3.4.8). Select 2 Mean VDMs are determined from flows with three or more palaeointensities that pass the selection criteria. Number are the total number of flows used to calculate the mean VDM of each adjusted VGP colatitude group.

adjusted VGP colatitude, which remains when the selection criteria are enforced. This could be a real feature, or could be biased by a small number of flows with erroneously high VDMs. It could also relate to a problem with the characterisation of the data based upon the geocentric axial dipole assumption. If the magnitude of the field remains constant during the transition, but there is a directional change (in inclination) then this will result in variations in the calculated VDM. This will depend on the observation site and the recorded inclination. This could result in a misleading representation of the transitional field; however, once the selection criteria have been applied there are no longer enough data to determine whether this feature is robust (Fig. 7.8c and f).

The mean of all transitional VDMs (between 30° and 150° adjusted VGP colatitude) is 3.0 ± 2.2 x $10^{22}$ Am$^2$, which is ~38% of the present day VDM (Table 7.3). The mean transitional VDM increases slightly to 3.6 ± 1.9 x $10^{22}$ Am$^2$ if only results from flows that pass the selection criteria and are calculated from three or more determinations are considered; however, this average is only calculated from 22 flow means from 12 bins and is statistically indistinguishable from the VDM calculated from all estimates of the transitional field. In addition, it is not strictly appropriate to take VDM values as absolute values of dipole moment strength when the field is clearly non-dipolar, but only as a guide to the general global behaviour of the intensity variations (Merrill & McFadden, 1999). When compared to the MB the mean transitional VDMs are indistinguishable.

A statistically significant difference in mean VDM between pre- and post-transitional adjusted VGP colatitude is not observed; however, the means are dependent on the different selection criteria applied (Table 7.3). Means of *all* VDM data that lie between 0° and 30° adjusted VGP colatitude, and between 120° and 180° adjusted VGP colatitude, are very similar and statistically indistinguishable (6.4 ± 3.9 x $10^{22}$ Am$^2$ compared with 6.6 ± 3.6 x $10^{22}$ Am$^2$). Applying an increasingly stringent selection criteria causes an increasing disparity in the mean pre- and post-transitional VDM, with the mean post-transitional field being ~34% greater than the mean pre-transitional field, when only accepting flow means determined from three or more individual palaeointensity results

that pass the selection. However, the standard deviations of these flow means are large: 60.5% of the pre-transition mean and 50.9% of the post-transitional mean. Therefore, the pre- and post-transitional means are statistically indistinguishable.

Such a large standard deviation between 0° and 30°, and 120° and 180°, is possibly caused by different stages of the reversal process. As the total reversal process is initiated a decrease in intensity will occur; however, directions may remain stable and the main directional changes may not occur until the field has weekend significantly (the lowest recorded VDM at these adjusted VGP colatitudes is 0.87 x $10^{22}$ $Am^2$). In addition, a large amount of directional complexity may occur once the field becomes significantly reduced (Yamazaki & Oda, 2001; Coe & Glen, 2004) and VGPs may return to normal or reversed positions (Hartl & Tauxe, 1996). This will result in the possibility of at least three phases of the reversal being recorded by a flows with a small range of VGPs. Because of the fragmentary nature of volcanic records it is not clear what phase is being recorded.

Another interesting aspect of the pre- and post-transitional data set are very high VDMs, with a maximum value of 16.5 ± 2.1 x $10^{22}$ $Am^2$ (if only accepting flow means determined from three or more individual palaeointensity results that pass the selection). This is approximately twice the present day field. 30 flows from the 123 that have flow means determined from three or more individual palaeointensity results that pass the selection, are greater than 7.9 x $10^{22}$ $Am^2$. This result is contrary to the global mean VDM determined from thermal Thellier data for the last 5 Ma from non-transitional data from the PINT03 database (Perrin & Schnepp, 2004), which gave a mean of 7.46 ± 3.10 (n=458). Yamamoto & Tsunakawa (2005) determined 24 site means using the LTD-DHT Shaw technique from lavas from French Polynesia, resulting in a mean of 3.64 ± 2.10 x $10^{22}$ $Am^2$. This value is ~4.5 times less than the maximum VDM found in this study. It has been suggested that the Thellier technique may, in some cases, overestimate palaeointensity determinations, sometimes by as much as two times (Yamamoto et al., 2003). Thermal Thellier experiments have also failed to give accurate determinations from historical lava flows. Biggin & Thomas (2003b) and Biggin et al. (2007a) demonstrated that the usual selection criteria of the Thellier method (Coe et al., 1978) was not effective at discriminating between accurate and inaccurate palaeointensity determinations. In many thermal Thellier studies, two sloped Arai-Nagata plot behaviour has been observed and it is not clear which slope (if either) should be taken. This choice is often subjective and may well have biased the results of the analysis. Such behaviour should be investigated further before any robust conclusions about the nature of the long term geomagnetic field are to be made.

In general, if only results from flows that pass the selection criteria and are determined from three or more determinations are considered, then there are two broad groups of data (Fig. 7.7c and Fig. 7.8c): data that lie between 0° and 30° and 150°

and 180° adjusted VGP colatitude, and data that lie between 30° and 150° adjusted VGP colatitude. This is very similar to the relationship observed for the MB reversal (Fig. 5.18). However, as Fig. 7.8c and Fig. 7.8f highlight, there is very sparse reliable data, with only two bins within the transitional field containing three or more flow means.

There are many problems in the approach present here. It is severely limited by the low number of transitional data, especially if any selection criteria is applied. This is further compounded by poor global coverage and for many reversals only one record may exist. The averages which we show are strictly valid only if the magnetic field is dipolar (Merrill & McFadden, 1999). The data are of different quality and the selection criteria used to assess the quality of data is based only on the statistics of Coe et al. (1978). It is also not clear what significance these statistics have for non-ideal recorders of palaeointensity Biggin et al. (2007a). It has also been difficult to apply a consistent analysis based upon the data available, as different studies have used different techniques and have applied different approaches to analysing the palaeointensity data. No assessment has been made (in this analysis) of the influence of rock magnetic properties, oxidation state and whether the NRM is a true TRM or a combination of a TRM, CRM or TCRM. If a secondary remanent magnetisation was acquired at non-transitional times, this could contribute relatively much more to the total magnetisation when the primary remanent magnetisation is weaker, such as during a polarity transition. This may cause a systematic biasing towards higher palaeointensity estimates during the transition (Merrill & McFadden, 1999). Fig. 7.8c and Fig. 7.8f highlight the need for more high quality transitional data for all reversals as at present no robust statements can be made about the nature of transitional reversal behaviour.

## 7.4 Conclusions

A global compilation of palaeodirections and palaeointensities from reversals recorded in volcanic sections during the last 20 Myr has been made and statistically assessed to determine whether there are any recurrent features from different reversals. The last compilation was made by Love (1998) and since its publication a number of new reversal studies containing palaeodirections and palaeointensities have been made. In this analysis, palaeodirections were not combined simply on the basis of their similarity, but assessed as individual VGPs or weighted by their VGP latitude and the number of VGPs per transition. The first approach allows clusters of VGPs to be recognised; if similar VGPs were grouped then the clusters would disappear. The second approach removes some of the sensitivity of the analysis caused by the relatively high number of VGPs at high VGP latitudes compared with those at low VGP latitudes and also takes into account that the durations of different reversals are recorded at different sites by different numbers of intermediate directions.

A possible longitudinal bias for VGPs is seen, with preferred longitudes over Africa, Australasia, western North America and eastern South America. A number of studies show clustering of VGPs and for areas over Australasia and Central Africa there are VGP clusters from multiple reversals. This suggests that the clustering of VGPs is not due to rapid eruption rates, but to a geomagnetic phenomena, possibly related to the location of magnetic flux patches. The assessment of VGPs described in this chapter is a rather crude attempt at determining the behaviour of transitional directions during reversals. It would be ideal to treat all data in a similar manner to Prévot & Camps (1993), Love (1998) and Love (2000) so that direct comparisons can be made between the three studies.

The relationship between VDM and VGP variations has also been assessed. When only VDM data derived from flows with three or more palaeointensity determinations that pass the selection criteria (described in Section 3.4.8) are analysed, there appears to be a rather simple relationship between variations in VGP and VDM. There are two broad groups: data that lie between 0° and 30°, and 150° and 180° adjusted VGP colatitude, and data that lie between 30° and 150° adjusted VGP colatitude. This features is also seen for the MB data set. The transitional adjusted VGP colatitude band (30° to 150°) shows low VDM values throughout, compared a large range of VDM values for the pre- and post-transitional bands. The mean VDM for the 30° to 150° adjusted VGP colatitude band is $3.0 \pm 2.3 \times 10^{22}$ $Am^2$, which is approximately 40% of today's field. This suggests that the field must reduce to at least this value before the larger directional changes associated with transitional phase of the reversal can occur.

The conclusions of this study are only tentative as the number of transitional data available is low; especially high quality palaeointensity data. It is therefore difficult to justify making robust statements about the nature of transitional reversal behaviour and the need for more high quality transitional data for all reversals is highlighted.

# Chapter 8

# Conclusions

Understanding the global temporal evolution of the geomagnetic field during reversals can provide important constraints on conditions at the core-mantle boundary and on geodynamo processes; however, the behaviour of the geomagnetic field during reversals is unclear. Many palaeomagnetic studies from both volcanic and sedimentary sequences have aimed to uncover details of the reversal processes; however, there is still controversy over a number of reversal characteristics, in part caused by a lack of reliable palaeodirectional and palaeointensity data. The aim of this thesis was to further our understanding of the reversal process by providing new palaeodirectional and palaeointensity data, and by conducting careful rock magnetic experiments, simple mathematical modelling, and basic statistical analyses of reversal data.

To assess the possible morphology of the surface field during reversals, a simple mathematical model was constructed. The field structure of a time-dependent global observational model of the geomagnetic field for the last 7000 years, CALS7K.2 (Korte & Constable, 2005a), was taken and the axial dipole component was scaled to simulate a simple reversal. The results suggest that non-dipole components could add significant structure to the field during the reversal processes. The model generates many features seen in the palaeomagnetic record, but there are also results that are no means consistent with all the available data. Variable reversal paths have been seen; however, there is a preference for certain longitudes, both spatially and, more weakly, temporally. Importantly, directional reversal features are not globally synchronous: some polarity changes finish before they start elsewhere; however, global intensity variations appear more coherent. The results of the model also support the idea that field intensity changes occur some time before and after the major directional changes of the reversal.

The model does not include many physical effects which may be present; the study of suitable dynamo simulations would be the appropriate way of investigating such effects. However, it does demonstrate that some observed features in the palaeomagnetic record may result from the geometric effect of the upward continuation of the geomagnetic field from the core-mantle boundary to the Earth's surface, and not require specific physical

mechanisms.

Many interesting reversal features have been generated by the above model; however, it is only through the investigation of the palaeomagnetic field through analysis of natural samples that real observations of the geomagnetic field during reversals can be made. Volcanic sequences from La Palma and Guadeloupe record the Matuyama-Brunhes boundary, possible precursors, and fluctuations in the magnetic field prior to the main polarity reversal. Absolute palaeointensity was determined using the microwave technique and palaeodirectional results were obtained from thermal demagnetisation. Ten flows from the twenty-nine flows studied gave reliable mean palaeointensities; however, only one of the ten flows records a transitional direction. The VDM determined from this flow is 1.9 $\pm$ 0.6 ($\pm\sigma$) x $10^{22}$ $Am^2$. Analysis of all Matuyama-Brunhes data suggests that the main directional changes occurred once the VDM was reduced below 3 x $10^{22}$ $Am^2$ ($\sim$40% of the present field value). Further comparisons with palaeointensity data compiled from all reversals younger than 20 Ma supports this conclusion; however, the lack of transitional data does not allow us to make any truly robust statements about the transitional field behaviour.

One particularly interesting outcome of the palaeointensity analysis performed on the samples from La Palma is that significant variations in palaeointensity were determined between 5 mm samples from the same 25 mm cores. Four flows showed this variation and three flows were investigated further in order to determine the source of this variation. Detailed rock magnetic analysis was carried out with the emphasis on FORC measurements. Samples from all three flows have particles other than non-interacting single domain TRM carriers: both MD and interacting SD particles have been identified in different 5 mm samples from the same 25 mm core. As it is not possible to use the same 5 mm samples for the palaeointensity experiment and FORC measurement, it was not possible to empirically link a particular type of magnetic particle assemblage to a particular outcome of an individual palaeointensity experiment. Nevertheless, FORC diagrams have successfully detected a range of small-scale variations and features that are not possible to determine using more standard rock magnetic analyses, and which can significantly affect a samples ability to provide reliable palaeointensity determinations.

To compare the palaeodirectional results from this study of the MB reversal with other reversals a new global compilation of palaeodirections from reversals recorded in volcanic sections during the last 20 Myr has been made. Data from this compilation have been carefully chosen and statistically assessed to determine whether there are any recurrent features from different reversals. A possible longitudinal bias for VGPs is observed, with preferred longitudes over Africa, Australasia, western North America and Eastern South America; however, there are many caveats that must remembered concerning the accuracy and number of the palaeomagnetic data, the methods of data selection and the data analysis . A number of the studies included in the analysis show

clustering of VGPs and for areas over Australasia and Central Africa there are VGP clusters from multiple reversals. This suggests that the clustering of VGPs may have a geomagnetic origin and may not be the result of rapidly erupted lava sequences.

The conclusions of this study are only tentative as the number of transitional data available is low; especially high quality palaeointensity data. It is therefore difficult to justify making robust statements about the nature of transitional reversal behaviour. The need for more high quality transitional data for all reversals is clear. Detailed and accurate $^{40}K/^{40}Ar$ dating is also needed to determine the temporal variation and complexity of reversal features recorded in volcanic sections and, where more than one record exists for a particular reversal, correlate them globally. More volcanic sequences that have recorded reversals need to be identified and examined for both palaeodirection and absolute palaeointensity. Further studying the behaviour of excursions can also help in our understanding of the transitional field and at the present time there are only 10 studies reporting absolute palaeointensities and palaeodirections from volcanic sequences. The differences and/or similarities between excursions will be key to understanding the long term evolution of the geomagnetic field.

Due to the fragmentary nature of volcanic records future studies must include palaeomagnetic data from sedimentary records, so that the possible complexity of the field is not underestimated. This approach may, where numerous sequences exist for the same period, allow the construction of time-varying global field models for reversals and excursions, as demonstrated by the model for the MB reversal by Leonhardt & Fabian (2007) based on an iterative Bayesian technique.

As discussed in Chapter 5, there are many factors that can affect the accuracy of absolute palaeointensity determinations. In any future studies such issues must be addressed so that conclusions about reversal behaviour are not based on erroneous data. One current area that is growing rapidly is the development of new palaeointensity techniques (Hill & Shaw, 1999; Cottrell & Tarduno, 1999; Yamamoto et al., 2003; Dekkers & Böhnel, 2006) and new protocols for the Thellier method (Riisager & Riisager, 2001; Fabian, 2001; Yu et al., 2004; Biggin et al., 2007b). These steps have made significant improvements in obtaining accurate data and in detecting data affected by non-ideal remanence carriers. This work needs to continue and develop if we are to get truly reliable estimates of palaeointensity during reversals.

# Appendix A

# All Matuyama-Brunhes Studies

| Volcanic Sequences | | | | | | |
|---|---|---|---|---|---|---|
| *Locality* | *Section* | *Lat.N* | *Long.E* | *Data* | *Dating* | *Author* |
| Tahiti | Punaruu | -17.7 | 210.3 | I,D,F | K(RC) | Chauvin et al. (1990) |
| Tahiti | Punaruu | -17.7 | 210.3 | I,D,F | | Mochizuki et al. (2005) |
| China | Tongjing | 37.8 | 120.8 | I,D,F | TL | Zhu et al. (1991) |
| Hawaii | Haleakala | 20.7 | 203.7 | I,D,N | Ar | Baksi et al. (1992) |
| Hawaii | Haleakala | 20.7 | 203.7 | I,D | Ar | Coe et al. (2004a) |
| Chile | Tatara San Pedro | -36.0 | 289.0 | I,D,N | Ar | Brown et al. (1994) |
| Chile | Tatara San Pedro | -36.0 | 289.0 | I,D | Ar | Brown et al. (2004) |
| Chile | Tatara San Pedro | -36.0 | 289.0 | F | | Gratton et al. (2007) |
| La Palma | LL | 28.6 | 342.2 | I,D,F | | Quidelleur & Valet (1996) |
| La Palma | LS | 28.6 | 342.2 | I,D,F | | Quidelleur & Valet (1996) |
| La Palma | LS | 28.6 | 342.2 | | Ar | Quidelleur et al. (2003) |
| La Palma | BA | 28.8 | 342.2 | I,D | Ar | Quidelleur et al. (2003) |
| La Palma | BN | 28.8 | 342.0 | I,D | Ar | Quidelleur et al. (2003) |
| La Palma | BS | 28.8 | 342.0 | I,D | Ar | Quidelleur et al. (2003) |
| La Palma | MO | 28.8 | 342.2 | I,D | Ar | Quidelleur et al. (2003) |
| La Palma | TR | 28.8 | 342.0 | I,D | Ar | Quidelleur et al. (2003) |
| La Palma | ME | 28.7 | 342.0 | | Ar | Quidelleur et al. (2003) |
| La Palma | ME | 28.7 | 342.0 | I,D,F | K | Valet et al. (1999) |
| La Palma | TN,TS | 28.6 | 342.2 | I,D | Ar | Singer et al. (2002) |
| Guadeloupe | Morne Marigot | 16.1 | 298.3 | I,D | Ar | Carlut et al. (2000) |
| Guadeloupe | Morne Marigot | 16.1 | 298.3 | F | Ar | Carlut & Quidelleur (2000) |
| Mexico | Ceboruco-San Pedro | 21.1 | 255.2 | I,D | Ar | Petronille et al. (2005) |

Table A.1: Complilation of all volcanic sections that record the Matuyama-Brunhes reversal and field variations close to this time. The column *Data* shows the type of data available; I is inclination, D is declination, N is NRM intensity, F is absolute palaeointensity. The column *Dating* shows the method used to date the sections; K is K/Ar, Ar is $^{40}Ar/^{39}Ar$, TL is thermal luminescence.

| Lake Sediments/Terrestrial Sediments | | | | | | |
|---|---|---|---|---|---|---|
| *Locality* | *Section* | *Lat.N* | *Long.E* | *Data* | *Dating* | *Author* |
| California | Tecopa 1 | 36.0 | 243.7 | I,D,J | | Hillhouse & Cox (1976) |
| California | Tecopa 2 | 36.0 | 243.7 | I,D,J | | Valet et al. (1988) |
| California | Tecopa 3 | 36.0 | 243.7 | I,D,J | | Larson & Patterson (1993) |
| California | Bishop A1 | 37.4 | 241.0 | I,D,J | | Liddicoat (1993) |
| California | Bishop A2 | 37.4 | 241.0 | I,D,J | | Liddicoat (1993) |
| California | Bishop A3 | 37.4 | 241.0 | I,D,J | | Liddicoat (1993) |
| Isreal | Geshor Benot Ya'aqov | 33.0 | 35.6 | I | | Goren-Inbar et al. (2000) |
| Australia | Robe-Naracoorte | -37.2 | 139.8 | I,D | TL | Idnurm & Cook (1980) for dates Huntley et al. (1993, 1994) |
| Australia | Lake Lefroy | -31.2 | 139.8 | I,D | | Zheng et al. (1998) |
| China | Xujiayao | 40.1 | 114.0 | I,D | | Løvlie et al. (2001) |
| China | Dongguo | 40.2 | 114.7 | I,D | | Zhu et al. (2001) |
| China | Xiaochangliang | 40.2 | 114.7 | I,D | | Zhu et al. (2001) |
| China | Xihoudu | 34.7 | 110.7 | I,D | | Zhu et al. (2003) |
| China | Tai'ergou | 40.2 | 114.6 | I,D | | Wang et al. (2004) |
| China | Donggutuo and Maliang | 40.2 | 114.6 | I,D | | Wang et al. (2005) |

Table A.2: Complilation of all lake sediment and terrestrial sediment records of the Matuyama-Brunhes reversal and field variations close to this time. The column *Data* shows the type of data available; I is inclination, D is declination, J is relative palaeointensity. The column *Dating* shows the method used to date the sections; TL is thermal luminescence.

| Loess/Palaeosols | | | | | | |
|---|---|---|---|---|---|---|
| *Locality* | *Section* | *Lat.N* | *Long.E* | *Data* | *Dating* | *Author* |
| Czech R. | Červený Kopec 1 | 49.3 | 16.5 | I,D | | Bucha (1970) |
| Czech R. | Červený Kopec 2 | 49.3 | 16.5 | I,D | | Kočí et al. (1974) |
| Czech R. | Suchdol | 50.2 | 14.2 | I,D | | Kočí et al. (1974) |
| Germany | Briiggen | 51.3 | 6.3 | I,D | | Kočí & Šibrava (1996) |
| Germany | Regansburg | 49.0 | 21.1 | I,D | | Kočí & Šibrava (1996) |
| Austria | Krems | 48.5 | 15.6 | I,D | | Kočí & Šibrava (1996) |
| China | Xifeng 1 | 36.0 | 108.0 | I,D,J | | Sun et al. (1993) |
| China | Xifeng 2 | 36.0 | 108.0 | I,D,J | | Zhu et al. (1993) |
| China | Weinan | 34.2 | 109.2 | I,D,J | | Zhu et al. (1994) |
| China | Lingtai | 34.9 | 107.5 | I,D | | Spassov et al. (2001) |
| China | Baoji | 34.4 | 107.1 | I,D | | Spassov et al. (2001) |
| China | Baoji | 34.4 | 107.1 | I,D,J | | Yang et al. (2004) |
| China | Dunajiapo | 34.2 | 109.2 | I,D | | Guo et al. (2001) |
| China | Gongwangling | | | I,D | | Zhu et al. (2003) |
| Ukraine | Zahvizdja | 48.9 | 24.6 | I,D, | | Nawrocki et al. (2002) |
| Ukraine | Roksolany | 45.8 | 30.4 | I,D | | Dodonov et al. (2006) |
| Ukraine | Roksolany | 45.8 | 30.4 | I,D | | Gendler et al. (2006) |
| Moldova | Khadzhimus | | | I,D | | Dodonov et al. (2006) |
| Moldova | Novoya Etuliya | 45.5 | 28.4 | I,D | | Gendler et al. (2006) |
| Russia | Strelitsa | 51.5 | 39.2 | I,D,J | | Velichko et al. (2006) |
| | | | | | | Bolshakov (2005) |

Table A.3: Complilation of all loess and palaeosol records of the Matuyama-Brunhes reversal and field variations close to this time. The column *Data* shows the type of data available; I is inclination, D is declination, J is relative palaeointensity. The column *Dating* shows the method used to date the sections.

| **Marine** | | | | | | |
|---|---|---|---|---|---|---|
| *Locality* | *Section* | *Lat.N* | *Long.E* | *Data* | *Dating* | *Author* |
| Japan | Boso Y | 35.2 | 140.2 | I,D,J | | Niitsuma (1971) see also Tsunakawa et al. (1995, 1996, 1999) |
| Japan | Boso H | 35.2 | 140.2 | I,D,J | | Okada & Niitsuma (1989) see also Tsunakawa et al. (1995, 1996, 1999) |
| Japan | Boso C | 35.2 | 140.2 | I,D,J | | Okada & Niitsuma (1989) see also Tsunakawa et al. (1995, 1996, 1999) |
| Japan | Osaka Bay | 34.7 | 135.3 | I | | Biswas et al. (1999) |
| Japan | Osaka Bay | 34.7 | 135.3 | I,D,J | | Hyodo et al. (2006) |
| New Zealand | Castlecliff, Wanganui Basin | -39.9 | 175.0 | I,D | FT | Turner & Kamp (1990) see also Pillans (2003) |
| New Zealand | Whangaehu, Wanganui Basin | -40.0 | 175.0 | I,D | FT | Pillans et al. (1994) see also Pillans (2003) |
| New Zealand | Turakina, Wanganui Basin | -40.1 | 175.3 | I,D | FT | Pillans et al. (1994) see also Pillans (2003) |
| New Zealand | Rangitikei, Wanganui Basin | -40.2 | 175.4 | I,D | FT | Pillans et al. (1994) see also Pillans (2003) |
| New Zealand | Cape Kidnappers | -39.6 | 177.1 | I,D | FT and Ar | Black (1992) see also Pillans (2003) |
| Mediterranean | KC-01B | 36.2 | 17.4 | I,D,J | | Langereis et al. (1997) |
| Mediterranean | LC07 | 38.1 | 10.1 | I,D,J | | Dinarès-Turell et al. (1999) |
| Mediterranean | LC10 | 35.2 | 16.6 | I | | Dinarès-Turell et al. (2003) |

Table A.4: Complilation of all marine records of the Matuyama-Brunhes reversal and field variations close to this time. The column *Data* shows the type of data available; I is inclination, D is declination, J is relative palaeointensity. The column *Dating* shows the method used to date the sections; FT is fission track, Ar is Ar-Ar.

| Ocean | | | | | | |
|---|---|---|---|---|---|---|
| *Locality* | *Section* | *Lat.N* | *Long.E* | *Data* | *Dating* | *Author* |
| Pacific | Papagayo | 14.8 | 240.1 | I,D,J | | Harrison & Somayajulu (1966) |
| Pacific | KH70-2-5 | 38.4 | 189.9 | I,D,J | | Kawai et al. (1973) |
| Pacific | KH73-4-7 | 2.7 | 164.8 | I,D,J | | Kawai et al. (1975, 1977) |
| Pacific | KH73-4-8 | -1.5 | 167.6 | I,D,J | | Kawai et al. (1975, 1977) |
| Pacific | RC10-167 | 33.4 | 150.4 | I,J | | Kent & Opdyke (1977) |
| Pacific | RC9-114 | -33.4 | 195.0 | I,D | | Clement & Kent (1984) |
| Pacific | RC9-119 | -23.2 | 188.4 | I,D | | Clement & Kent (1984) |
| Pacific | RC10-182 | 45.4 | 177.5 | I,D | | Clement & Kent (1984) |
| Pacific | RC15-21 | 1.5 | 227.0 | I,D | | Clement & Kent (1984) |
| Pacific | V20-104 | 37.2 | 181.1 | I,D | | Clement & Kent (1984) |
| Pacific | V20-107 | 43.4 | 181.1 | I,D | | Clement & Kent (1984) |
| Pacific | V20-108 | 45.4 | 180.8 | I,D | | Clement & Kent (1984) |
| Pacific | K78-10-19 | 9.0 | 189.8 | I,D,J | | Theyer et al. (1985) |
| Pacific | K78-10-30 | 18.9 | 199.6 | I,D,J | | Theyer et al. (1985) |
| Pacific | ODP767B | 4.8 | 123.5 | I,D,J | | Schneider et al. (1992) |
| Pacific | ODP769A | 8.8 | 121.3 | I,D,J | | Schneider et al. (1992) |
| Pacific | ODP792A | 30.4 | 140.4 | I,D,J | | Cisowski & Koyama (1992) |
| Pacific | ODP851D | 2.8 | 249.4 | I,D,J | | Valet & Meynadier (1993) |
| Pacific | ODP803B | 2.3 | 160.3 | I,D,J | | Hartl & Tauxe (1996) |
| Pacific | ODP804C | 1.0 | 161.4 | I,D,J | | Hartl & Tauxe (1996) |
| Pacific | ODP805B | 1.1 | 160.3 | I,D,J | | Hartl & Tauxe (1996) |
| Pacific | KK78030 | 18.9 | 160.3 | I,D,J | | Laj et al. (1996) |
| Pacific | K78030 | 18.9 | 160.3 | J | | Verosub et al. (1996) |
| Pacific | KII 73-4-7 | 2.7 | 164.8 | J | | Sato et al. (1998) |
| Pacific | KH 73-4-8 | 1.6 | 167.7 | J | | Sato et al. (1998) |
| Pacific | KH 90-3-5 | 4.0 | 160 | J | | Sato et al. (1998) |
| Pacific | ODP1010 | 30.0 | 241.9 | I,D,J | | Hayashida et al. (1999) |
| Pacific | ODP1021 | 39.1 | 232.5 | I,D,J | | Guyodo et al. (1999) |
| Pacific | ODP1014 | 32.8 | 240.0 | I,D,J | | Heider et al. (2000) |
| Pacific | ODP1020 | 41.0 | 233.6 | I,D,J | | Heider et al. (2000) |
| Pacific | ODP767 | 4.8 | 123.5 | I,D,J | | Oda et al. (2000) |
| Pacific | ODP769 | 8.8 | 121.3 | I,D,J | | Oda et al. (2000) |
| Pacific | MD982185 | 3.1 | 135.0 | I,D,J | | Yamazaki & Oda (2003) |
| Pacific | MD974123 | 15.9 | 124.7 | I,D,J | | Horng et al. (2003) |
| Pacific | ODP1146 | 19.5 | 116.3 | ,I,D,J | | Kissel et al. (2003) |
| Pacific | K94P31 | 10.8 | 131.5 | I,D,J | | Park et al. (2004) |
| Pacific | K95P02 | 10.0 | 131.9 | I,D,J | | Park et al. (2004) |
| Pacific | K95P09 | 10.5 | 132.1 | I,D,J | | Park et al. (2004) |

| Ocean | | | | | | |
|---|---|---|---|---|---|---|
| *Locality* | *Section* | *Lat.N* | *Long.E* | *Data* | *Dating* | *Author* |
| Atlantic | V30-45 | 6.2 | 340.4 | I,D | | Clement & Kent (1984) |
| Atlantic | ODP606A | 37.3 | 324.5 | I,D,J | | Clement & Kent (1986) |
| Atlantic | ODP607A | 41.0 | 327.0 | I,D,J | | Clement & Kent (1986) |
| Atlantic | ODP609B | 49.9 | 335.8 | I,D,J | | Clement & Kent (1986) |
| Atlantic | ODP610B | 53.2 | 341.1 | I,D,J | | Clement & Kent (1986) |
| Atlantic | ODP610C | 53.2 | 341.1 | I,D,J | | Clement & Kent (1986) |
| Atlantic | ODP642B | 67.2 | 2.9 | I,D | | Schönharting et al. (1989) |
| Atlantic | ODP642C | 67.2 | 2.9 | I,D | | Schönharting et al. (1989) |
| Atlantic | ODP643A | 67.7 | 1.0 | I,D | | Schönharting et al. (1989) |
| Atlantic | ODP644A | 67.0 | 4.5 | I,D | | Schönharting et al. (1989) |
| Atlantic | ODP659C | 18.1 | 339.0 | I,D,J | | Valet et al. (1989) |
| Atlantic | ODP664D | 0.1 | 336.7 | I,D,J | | Valet et al. (1989) |
| Atlantic | ODP665B | 0.0 | 336.7 | I,D,J | | Valet et al. (1989) |
| Atlantic | ODP981B | 55.5 | 345.3 | I,D | | Channell & Lehman (1997) |
| Atlantic | ODP983B | 60.4 | 336.4 | I,D,J | | Channell & Lehman (1997); Channell & Kleiven (2000) |
| Atlantic | ODP983C | 60.4 | 336.4 | I,D,J | | Channell & Lehman (1997); Channell & Kleiven (2000) |
| Atlantic | ODP984A | 61.4 | 335.9 | I,D | | Channell & Lehman (1997) |
| Atlantic | ODP984B | 61.4 | 335.9 | I,D | | Channell & Lehman (1997) |
| Atlantic | ODP984C | 61.4 | 335.9 | I,D | | Channell & Lehman (1997) |
| Atlantic | ODP897 | 41.2 | 347.5 | I | | Zhao et al. (2001) |
| Atlantic | ODP898 | 40.5 | 347.9 | I | | Zhao et al. (2001) |
| Atlantic | ODP1089 | -40.9 | 9.5 | I,J | | Channell & Stoner (2002) |
| Atlantic | ODP1091 | -47.1 | 5.9 | I,J | | Channell & Stoner (2002) |
| Atlantic | ODP1093 | -50.0 | 5.9 | I,J | | Channell & Stoner (2002) |
| Atlantic | ODP1094 | -53.2 | 5.1 | I,J | | Channell & Stoner (2002) |
| Atlantic | ODP980/981 | 55.49 | 345.3 | I,D,J | | Channell & Raymo (2003) |
| Atlantic | ODP983 | 60.4 | 336.4 | I,D,J | | Channell et al. (2004) |
| Atlantic | ODP984 | 61.4 | 335.9 | I,D,J | | Channell et al. (2004) |
| Indian | V16-58 | -46.0 | 30.0 | I,D,J | | Clement (1991) |
| Indian | MD90-0904 | -5.3 | 41.4 | I,D,J | | Meynadier et al. (1994) |

Table A.5: Complilation of all oceanic records of the Matuyama-Brunhes reversal and field variations close to this time. The column *Data* shows the type of data available; I is inclination, D is declination, J is relative palaeointensity. The column *Dating* shows the method used to date the sections; no dating was possible.

# Appendix B

# Location photos

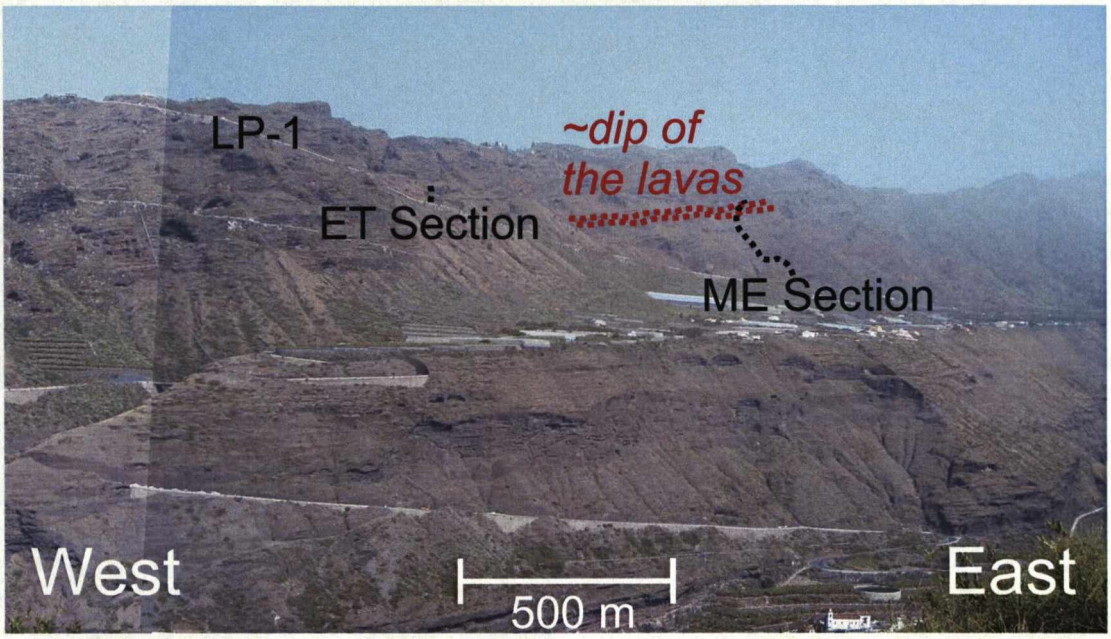


Figure B.1: Location photo of the ET and ME sections.

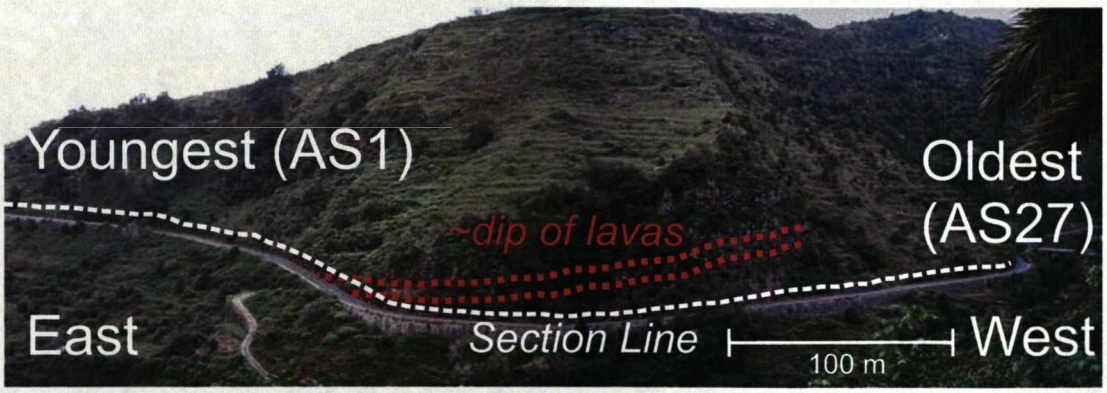


Figure B.2: Location photo of the AS section.

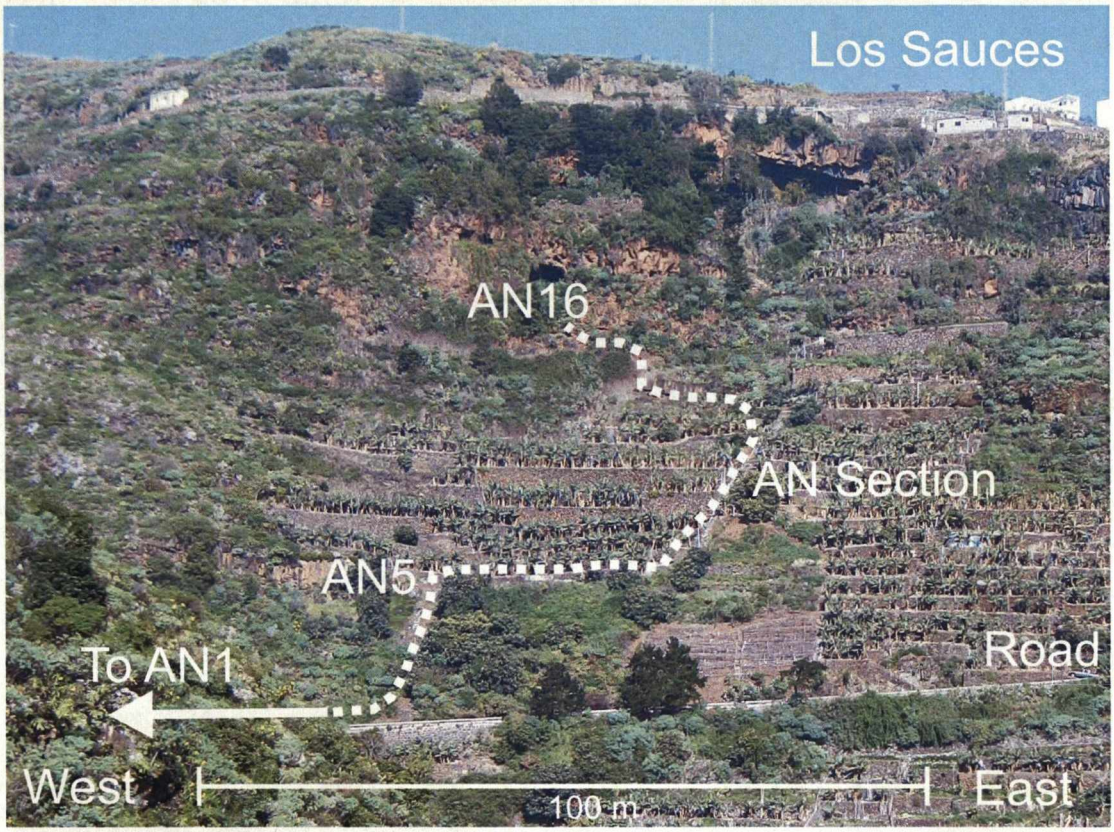


Figure B.3: Location photo of the AN section.


Figure B.4: Location photo of the Morne Marigot quarry section.

# Appendix C

# Rock Magnetic Results

| Sample | Hysteresis Properties | | | | | | Thermomagnetic Properties | | | | | |
|---|---|---|---|---|---|---|---|---|---|---|---|---|
| | $M_s$ (x $10^{-3}$ $Am^2/kg$) | $M_{rs}$ (x $10^{-3}$ $Am^2/kg$) | $H_c$ (mT) | $H_{cr}$ (mT) | $M_{rs}/M_s$ | $H_{cr}/H_c$ | $T_{c1}$ (°C) | $T_{c2}$ (°C) | $TMX_1$ | $TMX_2$ | % diff at 100°C | Type |
| ME32-1B | 6.555 | 0.542 | 9.26 | 33.76 | 0.08 | 3.65 | 466 | | 18 | | -9.4 | 1 |
| ME32-2B | 5.193 | 0.385 | 9.30 | 32.17 | 0.07 | 3.46 | 467 | | 18 | | -9.4 | 1 |
| ME32-3B | 3.072 | 0.256 | 9.51 | 36.49 | 0.08 | 3.84 | 471 | | 18 | | -13.9 | 1 |
| ME32-4A | 5.260 | 0.447 | 10.14 | 36.80 | 0.08 | 3.63 | 495 | | 14 | | -16.0 | 1 |
| ME33-1A | 9.437 | 0.419 | 4.65 | 24.64 | 0.04 | 5.30 | 469 | | 18 | | -10.1 | 1 |
| ME33-3B | 7.391 | 0.774 | 10.39 | 28.42 | 0.10 | 2.74 | 475 | | 17 | | -12.1 | 3a |
| ME33-4A | 7.948 | 0.688 | 9.97 | 34.56 | 0.09 | 3.47 | 492 | | 14 | | 10.3 | 1 |
| ME33-5B | 4.535 | 0.838 | 18.04 | 36.88 | 0.18 | 2.04 | 345 | 473 | 37 | 17 | -6.1 | 2 |
| ME34-2BOT | 1.722 | 0.153 | 5.62 | 17.83 | 0.09 | 3.17 | 126 | | 67 | | 80.4 | 5a |
| ME34-3B | 1.204 | 0.08 | 4.07 | 14.02 | 0.07 | 3.44 | 84 | | 72 | | 80.4 | 5a |
| ME34-3BOT | 1.360 | 0.094 | 4.32 | 15.67 | 0.07 | 3.62 | 120 | | 67 | | 91.5 | 5b |
| ME34-4B | 2.718 | 0.449 | 12.56 | 30.13 | 0.17 | 2.40 | 131 | 507 | 66 | 12 | 54.0 | 3c |
| ME35-1A | 3.761 | 0.573 | 11.30 | 26.73 | 0.15 | 2.37 | 267 | 472 | 48 | 17 | 53.2 | 3c |
| ME35-3A | 2.756 | 0.392 | 10.67 | 26.22 | 0.14 | 2.46 | 123 | 510 | 67 | 11 | 67.2 | 3c |
| ME35-3BOT | 4.404 | 0.776 | 23.57 | 52.05 | 0.18 | 2.21 | 505 | | 12 | | -19.7 | 1 |
| ME35-4BOT | 3.475 | 0.586 | 12.28 | 30.48 | 0.17 | 2.48 | 131 | 514 | 66 | 11 | 59.5 | 3c |
| ME35-5A | 1.921 | 0.122 | 3.79 | 14.86 | 0.06 | 3.92 | 96 | | 70 | | 76.9 | 3b |
| ME36-2A | 2.433 | 0.432 | 13.46 | 31.02 | 0.18 | 2.30 | 142 | 504 | 65 | 12 | 42.4 | 3b |
| ME36-2BOT | 6.375 | 1.245 | 15.63 | 36.23 | 0.20 | 2.32 | 181 | 494 | 59 | 14 | 49.9 | 3c |
| ME36-4A | 8.612 | 0.706 | 9.83 | 31.80 | 0.08 | 3.24 | 493 | | 14 | | -9.3 | 1 |
| ME36-5A | 3.529 | 0.467 | 9.58 | 24.05 | 0.13 | 2.51 | 222 | 492 | 54 | 14 | 32.9 | 3c |
| ME37-1A | 2.864 | 0.602 | 23.42 | 47.50 | 0.21 | 2.03 | 282 | 504 | 46 | 12 | 32.9 | 3b |
| ME37-2A2 | 2.096 | 0.574 | 33.93 | 63.93 | 0.27 | 1.88 | 378 | 528 | 32 | 8 | 26.4 | 3b |
| ME37-2A | 2.855 | 0.816 | 36.07 | 66.22 | 0.29 | 1.84 | 419 | 523 | 26 | 9 | 25.3 | 3b |
| ME37-3U | 0.669 | 0.069 | 7.45 | 22.10 | 0.10 | 2.97 | 528 | | 8 | | 74.8 | 5a |
| ME38-1B | 1.688 | 0.278 | 15.08 | 39.80 | 0.16 | 2.64 | 235 | 484 | 52 | 16 | 56.9 | 3c |
| ME38-2A | 2.982 | 0.642 | 20.30 | 45.74 | 0.22 | 2.25 | 249 | 513 | 50 | 11 | 29.3 | 3b |
| ME38-3BOT | 5.372 | 0.531 | 7.38 | 21.34 | 0.10 | 2.89 | 244 | 465 | 51 | 19 | 39.3 | 3b |
| ME38-4A | 6.238 | 0.717 | 12.21 | 33.29 | 0.11 | 2.73 | 487 | | 15 | | -0.3 | 1 |
| ME39-1A | 4.882 | 0.595 | 9.06 | 24.04 | 0.12 | 2.65 | 454 | | 20 | | 37.1 | 3b |
| ME39-4B | 8.558 | 0.739 | 9.56 | 32.18 | 0.09 | 3.37 | 487 | | 15 | | 0.5 | 1 |
| ME39-5A | 5.868 | 0.664 | 12.90 | 31.78 | 0.11 | 2.46 | 492 | | 14 | | -2.6 | 1 |
| ME39-6B | 5.591 | 0.564 | 11.63 | 31.41 | 0.10 | 2.70 | 486 | | 15 | | -4.9 | 1 |
| ME39-6C | 6.413 | 0.581 | 10.43 | 30.98 | 0.09 | 2.97 | 498 | | 13 | | -5.2 | 1 |

| Sample | Hysteresis Properties | | | | | | Thermomagnetic Properties | | | | | |
|---|---|---|---|---|---|---|---|---|---|---|---|---|
| | $M_s$ (x $10^{-3}$ $Am^2/kg$) | $M_{rs}$ (x $10^{-3}$ $Am^2/kg$) | $H_c$ (mT) | $H_{cr}$ (mT) | $M_{rs}/M_s$ | $H_{cr}/H_c$ | $T_{c1}$ (°C) | $T_{c2}$ (°C) | $TMX_1$ | $TMX_2$ | % diff at 100°C | Type |
| ME40-1A | 4.062 | 0.683 | 15.52 | 34.00 | 0.17 | 2.19 | 462 | | 19 | | 9.4 | 1 |
| ME40-2A | 2.179 | 0.442 | 16.48 | 39.39 | 0.20 | 2.39 | 157 | 503 | 63 | 13 | 66.2 | 3c |
| ME40-3A | 1.310 | 0.239 | 16.15 | 44.35 | 0.18 | 2.75 | 184 | 487 | 59 | 15 | 30.3 | 3b |
| ME40-4B | 1.607 | 0.466 | 32.36 | 57.97 | 0.29 | 1.79 | 227 | 513 | 53 | 11 | 21.7 | 3b |
| ME40-5A | 1.828 | 0.246 | 11.48 | 34.99 | 0.13 | 3.05 | 168 | 492 | 61 | 14 | 47.8 | 3b |
| ME41-1A | 1.337 | 0.202 | 13.00 | 46.13 | 0.15 | 3.55 | 168 | 502 | 61 | 13 | 24.9 | 3b |
| ME41-1B | 1.251 | 0.247 | 18.50 | 52.76 | 0.20 | 2.85 | 162 | 509 | 62 | 12 | 31.2 | 3b |
| ME41-2B | 1.672 | 0.364 | 21.04 | 49.00 | 0.22 | 2.33 | 204 | 500 | 56 | 13 | 24.6 | 3b |
| ME41-3B | 1.448 | 0.172 | 9.93 | 30.19 | 0.12 | 3.04 | 173 | 487 | 60 | 15 | 45.2 | 3b |
| ME41-4A | 2.379 | 0.283 | 8.05 | 39.51 | 0.12 | 4.91 | 164 | 502 | 62 | 13 | 24.3 | 3b |
| ME41-5A | 1.263 | 0.205 | 14.29 | 38.98 | 0.16 | 2.73 | 179 | 490 | 60 | 15 | 35.4 | 3b |
| ME42-2B | 4.978 | 0.727 | 15.97 | 38.03 | 0.15 | 2.38 | 467 | | 18 | | -12.6 | 1 |
| ME42-3A | 8.347 | 1.013 | 12.83 | 36.58 | 0.12 | 2.85 | 459 | | 20 | | -15.0 | 2 |
| ME42-5B | 4.490 | 0.701 | 16.89 | 39.98 | 0.16 | 2.37 | 463 | | 19 | | -9.8 | 1 |
| ME43-1A | 6.358 | 0.935 | 16.55 | 40.17 | 0.15 | 2.43 | 472 | | 17 | | -14.3 | 1 |
| ME43-2A | 3.082 | 0.133 | 2.95 | 15.77 | 0.04 | 5.35 | 360 | | 34 | | 13.5 | - |
| ME43-3A | 5.859 | 0.834 | 13.18 | 43.36 | 0.14 | 3.29 | 417 | 490 | 26 | 15 | -18.8 | 3b |
| ME43-4B | 4.479 | 0.728 | 15.63 | 51.17 | 0.16 | 3.27 | 426 | 499 | 25 | 13 | -20.0 | 3b |
| ME43-5B | 7.707 | 0.74 | 9.08 | 30.10 | 0.10 | 3.32 | 449 | 500 | 21 | 13 | -17.5 | 3b |
| ME44-1B | 4.592 | 0.42 | 6.75 | 27.56 | 0.09 | 4.08 | 491 | | 14 | | -15.9 | - |
| ME44-2A | 5.276 | 0.592 | 13.97 | 39.18 | 0.11 | 2.80 | 476 | | 17 | | -16.4 | 1 |
| ME44-3B | 5.742 | 0.649 | 14.54 | 39.89 | 0.11 | 2.74 | 486 | | 15 | | -15.2 | 1 |
| ME44-4A | 5.879 | 0.635 | 13.77 | 38.42 | 0.11 | 2.79 | 481 | | 16 | | -29.4 | 1 |
| ME45-2A | 6.227 | 0.903 | 16.13 | 42.72 | 0.14 | 2.65 | 476 | | 17 | | -27.9 | 1 |
| ME45-3A | 9.949 | 1.341 | 14.85 | 40.47 | 0.13 | 2.72 | 480 | | 16 | | -27.9 | 1 |
| ME45-4A | 10.864 | 1.197 | 16.46 | 42.38 | 0.11 | 2.57 | 506 | | 12 | | -23.4 | 1 |
| ME45-4B | 8.264 | 1.145 | 17.77 | 43.29 | 0.14 | 2.44 | 507 | | 12 | | -28.3 | 1 |
| ME46-1A | 14.128 | 2.944 | 29.72 | 49.52 | 0.21 | 1.67 | 527 | | 9 | | -36.5 | 1 |
| ME46-2BOT | 10.324 | 2.613 | 35.37 | 60.21 | 0.25 | 1.70 | 520 | | 10 | | -37.7 | 1 |
| ME46-4A | 13.061 | 2.979 | 31.93 | 51.53 | 0.23 | 1.61 | 529 | | 8 | | -32.5 | 1 |
| ME46-5BOT | 8.099 | 1.584 | 29.76 | 50.82 | 0.20 | 1.71 | 520 | | 10 | | -32.5 | 1 |
| ME47-1A | 13.745 | 3.406 | 37.65 | 59.95 | 0.25 | 1.59 | 517 | | 10 | | -46.3 | 1 |
| ME47-2B1 | 7.499 | 1.198 | 20.97 | 47.96 | 0.16 | 2.29 | 517 | | 10 | | -21.0 | 1 |
| ME47-2B2 | 2.540 | 0.524 | 23.92 | 46.68 | 0.21 | 1.95 | 507 | | 12 | | -17.8 | 1 |
| ME47-3A3 | 0.552 | 0.16 | 26.25 | 52.06 | 0.29 | 1.98 | 549 | | 5 | | 23.1 | - |
| ME47-3B | 1.003 | 0.218 | 27.61 | 60.42 | 0.22 | 2.19 | 455 | | 20 | | 28.8 | - |

| Sample | Hysteresis Properties | | | | | | Thermomagnetic Properties | | | | | |
|---|---|---|---|---|---|---|---|---|---|---|---|---|
| | $M_s$ (x $10^{-3}$ $Am^2/kg$) | $M_{rs}$ (x $10^{-3}$ $Am^2/kg$) | $H_c$ (mT) | $H_{cr}$ (mT) | $M_{rs}/M_s$ | $H_{cr}/H_c$ | $T_{c1}$ (°C) | $T_{c2}$ (°C) | $TMX_1$ | $TMX_2$ | % diff at 100°C | Type |
| ME47-3B2 | 0.277 | 0.084 | 27.04 | 54.70 | 0.30 | 2.02 | 548 | | 5 | | 3.3 | - |
| ME47-4A1 | 0.580 | 0.163 | 27.23 | 47.36 | 0.28 | 1.74 | 483 | | 16 | | -17.8 | 3b |
| ME47-4A2 | 0.361 | 0.095 | 25.30 | 46.64 | 0.26 | 1.84 | 517 | | 10 | | 29.8 | - |
| ME48-1A | 1.583 | 0.18 | 13.10 | 38.50 | 0.11 | 2.94 | 523 | | 9 | | -45.4 | 1 |
| ME48-1B | 1.408 | 0.181 | 15.25 | 43.95 | 0.13 | 2.88 | 526 | | 9 | | -6.7 | 1 |
| ME48-2A | 5.397 | 0.661 | 16.33 | 40.77 | 0.12 | 2.50 | 535 | | 7 | | -13.5 | 1 |
| ME48-2B | 6.277 | 0.852 | 17.28 | 41.18 | 0.14 | 2.38 | 535 | | 7 | | -9.5 | 1 |
| ME48-3A | 7.822 | 0.898 | 14.49 | 41.83 | 0.11 | 2.89 | 540 | | 6 | | -4.5 | 1 |
| ME49-1A | 2.389 | 0.88 | 33.70 | 48.75 | 0.37 | 1.45 | 491 | | 14 | | -8.7 | 1 |
| ME49-2A | 10.542 | 0.827 | 9.48 | 35.82 | 0.08 | 3.78 | 493 | | 14 | | -8.8 | 1 |
| ME49-3A | 12.617 | 0.762 | 6.93 | 34.40 | 0.06 | 4.97 | 500 | | 13 | | -2.1 | 1 |
| ME49-4A | 1.591 | 0.458 | 32.36 | 59.00 | 0.29 | 1.82 | 522 | | 9 | | 2.4 | 1 |
| ME49-5A2 | 8.046 | 0.57 | 5.65 | 20.70 | 0.07 | 3.66 | 334 | 463 | 38 | 19 | 7.8 | 2 |
| ME49-5A1 | 9.150 | 0.684 | 6.66 | 25.92 | 0.07 | 3.89 | 466 | | 18 | | 8.5 | 1 |
| ME50-1A | 0.544 | 0.172 | 27.30 | 45.56 | 0.32 | 1.67 | 495 | | 14 | | 16.5 | 1 |
| ME50-1B | 2.495 | 0.625 | 22.39 | 39.04 | 0.25 | 1.74 | 508 | | 12 | | -5.4 | 1 |
| ME50-2A | 6.368 | 1.312 | 20.22 | 42.58 | 0.21 | 2.11 | 509 | | 12 | | 11.1 | 1 |
| ME50-2BOT | 11.872 | 1.084 | 11.66 | 38.11 | 0.09 | 3.27 | 489 | | 15 | | -14.5 | 1 |

Table C.1: Summary of hysteresis and thermomagnetic properties of individual samples from the ME section, La Palma. Hysteresis parameters are explained in Chapter 3. $T_{c1}$ and $T_{c2}$ are Curie temperatures determined using the extrapolation method (Moskowitz, 1981); $TMX_1$ and $TMX_2$ are the corresponding titanomagnetite compositions calculated using the polynomial fit to experimental data of Bleil & Petersen (1982); % diff at 100°C is the difference between the heating and cooling curves at 100°C, a negative value indicates a decrease in magnetisation; Type is the classification of the thermomagnetic curves and is discussed in Section 5.3.1 and shown in Fig. 5.4.

| Sample | $M_s$ (Am/kg) | $M_{rs}$ (Am/kg) | $H_c$ (mT) | $H_{cr}$ (mT) | $M_{rs}/M_s$ | $H_{cr}/H_c$ |
|---|---|---|---|---|---|---|
| ME32-1A1 | 3.103 | 0.329 | 8.11 | 22.71 | 0.106 | 2.80 |
| ME33-5A1 | 2.016 | 0.592 | 14.68 | 23.09 | 0.294 | 1.57 |
| ME34-3B1 | 0.641 | 0.155 | 6.04 | 9.39 | 0.242 | 1.56 |
| ME35-1A1 | 1.719 | 0.433 | 12.25 | 20.19 | 0.252 | 1.65 |
| ME36-1B1 | 1.815 | 0.526 | 14.38 | 25.40 | 0.290 | 1.77 |
| ME37-2A1 | 1.294 | 0.399 | 28.92 | 55.07 | 0.308 | 1.90 |
| ME38-2A1 | 0.631 | 0.128 | 7.25 | 13.79 | 0.204 | 1.90 |
| ME39-6C1 | 2.643 | 0.379 | 11.81 | 24.64 | 0.143 | 2.09 |
| ME40-4A1 | 0.909 | 0.290 | 25.49 | 49.40 | 0.319 | 1.94 |
| ME41-3B1 | 1.363 | 0.263 | 9.22 | 22.65 | 0.193 | 2.46 |
| ME42-3A1 | 2.499 | 0.494 | 15.68 | 32.09 | 0.198 | 2.05 |
| ME43-3A1 | 2.475 | 0.463 | 10.57 | 30.67 | 0.187 | 2.90 |
| ME44-2B1 | 2.907 | 0.441 | 14.24 | 33.35 | 0.152 | 2.34 |
| ME45-2A1 | 3.125 | 0.562 | 14.09 | 32.56 | 0.180 | 2.31 |
| ME46-5A1 | 3.420 | 1.049 | 32.23 | 51.82 | 0.307 | 1.61 |
| ME47-1A1$^A$ | 4.504 | 1.254 | 31.71 | 49.76 | 0.278 | 1.57 |
| ME47-1A2$^A$ | 3.643 | 0.960 | 33.18 | 55.15 | 0.263 | 1.66 |
| ME47-1A3$^A$ | 4.466 | 1.300 | 35.34 | 56.77 | 0.291 | 1.61 |
| ME47-2A1 | 1.910 | 0.367 | 19.15 | 41.32 | 0.192 | 2.16 |
| ME47-2A2 | 1.973 | 0.264 | 18.23 | 51.02 | 0.134 | 2.80 |
| ME47-2B1$^A$ | 2.175 | 0.392 | 18.95 | 41.45 | 0.180 | 2.19 |
| ME47-2B3 | 1.930 | 0.350 | 18.23 | 41.08 | 0.181 | 2.25 |
| ME47-4A1 | 0.838 | 0.203 | 18.22 | 40.15 | 0.242 | 2.20 |
| ME47-4A2$^A$ | 0.121 | 0.050 | 26.74 | 48.58 | 0.415 | 1.82 |
| ME47-4A2$^A$ | 0.123 | 0.050 | 25.86 | 48.58 | 0.402 | 1.88 |
| ME48-1A1 | 1.428 | 0.176 | 11.46 | 31.06 | 0.123 | 2.71 |
| ME48-1A2 | 1.180 | 0.156 | 11.58 | 31.61 | 0.132 | 2.73 |
| ME48-1A32 | 0.442 | 0.073 | 12.51 | 35.14 | 0.164 | 2.81 |
| ME48-1B1$^A$ | 0.617 | 0.096 | 13.73 | 36.46 | 0.155 | 2.66 |
| ME48-1B2 | 1.545 | 0.194 | 11.29 | 31.61 | 0.125 | 2.80 |
| ME48-2B1 | 2.816 | 0.501 | 17.32 | 35.36 | 0.178 | 2.04 |
| ME48-2B2 | 2.072 | 0.339 | 15.61 | 35.74 | 0.164 | 2.29 |
| ME48-2B3 | 2.184 | 0.357 | 15.83 | 35.57 | 0.163 | 2.25 |
| ME48-3A1 | 0.171 | 0.022 | 12.67 | 33.43 | 0.128 | 2.64 |
| ME48-3A1$^A$ | 1.959 | 0.250 | 12.67 | 33.43 | 0.128 | 2.64 |
| ME48-3A2$^A$ | 1.106 | 0.175 | 15.12 | 38.58 | 0.158 | 2.55 |
| ME48-3A3$^A$ | 1.002 | 0.163 | 14.22 | 35.58 | 0.162 | 2.50 |
| ME48-4A1 | 1.266 | 0.229 | 15.32 | 35.86 | 0.180 | 2.34 |
| ME48-4A2 | 1.590 | 0.253 | 14.26 | 34.22 | 0.159 | 2.40 |
| ME48-4A3 | 1.121 | 0.192 | 14.71 | 35.24 | 0.171 | 2.40 |
| ME49-1A1 | 0.988 | 0.208 | 15.91 | 36.99 | 0.211 | 2.32 |
| ME49-1A2 | 1.470 | 0.268 | 14.16 | 29.80 | 0.182 | 2.10 |
| ME49-1A3 | 3.258 | 0.344 | 8.80 | 31.33 | 0.106 | 3.56 |
| ME49-2B1 | 3.740 | 0.366 | 9.32 | 24.75 | 0.098 | 2.66 |
| ME49-2B2 | 1.850 | 0.243 | 11.95 | 32.70 | 0.131 | 2.74 |
| ME49-2B3 | 0.637 | 0.197 | 22.33 | 45.96 | 0.309 | 2.06 |
| ME49-3A1 | 3.075 | 0.317 | 9.79 | 27.00 | 0.103 | 2.76 |
| ME49-3A2 | 2.803 | 0.293 | 8.60 | 25.92 | 0.104 | 3.01 |
| ME49-3A3 | 1.981 | 0.267 | 11.99 | 33.30 | 0.135 | 2.78 |
| ME49-4A2$^A$ | 0.990 | 0.190 | 16.31 | 44.87 | 0.191 | 2.75 |
| ME50-2A1 | 1.478 | 0.299 | 15.45 | 32.58 | 0.202 | 2.11 |

Table C.2: Hysteresis data determined using a VSM or AGFM (denoted $^A$) at the Institute for Rock Magnetism, University of Minnesota. Parameters are discussed in Chapter 3.

| *Sample* | *Machine* | *Frequency* (Hz) | *max* $\chi'$ (x $10^{-5}$ $m^3$/kg) | *max* $\chi'$ *temperature* (K) | $\chi'$ *inflection temperature 1* (K) | $\chi'$ *inflection temperature 2* (K) | % $\chi'_{fd}$ | % $\chi'_{fd}$ *temperature* (K) | *Type* |
|---|---|---|---|---|---|---|---|---|---|
| ME321A1 | Blue | 1.0 | 26.54 | 84.0 | 9.1 | | 14.6 | 44.3 | I |
| | | 5.6 | 26.35 | 86.8 | 9.7 | | | | |
| | | 31.6 | 26.07 | 90.1 | 10.3 | | | | |
| | | 177.9 | 25.81 | 92.5 | 11.0 | | | | |
| | | 997.3 | 25.38 | 95.5 | 11.8 | | | | |
| ME335A1 | Lakeshore | 40.0 | 1.23 | 300.0 | 25.3 | | 5.3 | 300.0 | II |
| | | 140.0 | 1.20 | 300.0 | 26.6 | | | | |
| | | 400.0 | 1.15 | 300.0 | 27.2 | | | | |
| | | 1000.0 | 1.16 | 300.0 | 27.6 | | | | |
| | | 4000.0 | 1.14 | 300.0 | 27.3 | | | | |
| ME343B1 | Lakeshore | 40.0 | 0.81 | 276.5 | 79.6 | | 15.2 | 260.0 | III |
| | | 140.0 | 0.76 | 277.0 | 79.6 | | | | |
| | | 400.0 | 0.74 | 276.8 | 79.6 | | | | |
| | | 1000.0 | 0.72 | 280.1 | 79.6 | | | | |
| | | 4000.0 | 0.69 | 276.3 | 79.6 | | | | |
| ME351A1 | Lakeshore | 40.0 | 1.03 | 300.0 | 23.0 | | 7.9 | 290.0 | II |
| | | 140.0 | 1.00 | 300.0 | 24.2 | | | | |
| | | 400.0 | 0.99 | 300.0 | 24.8 | | | | |
| | | 1000.0 | 0.97 | 300.0 | 24.7 | | | | |
| | | 4000.0 | 0.96 | 300.0 | 24.9 | | | | |
| ME361B1 | Red | 1.0 | 7.33 | 290.2 | 23.8 | 116.9 | 10.8 | 280.3 | II |
| | | 5.6 | 7.12 | 290.2 | 24.2 | 117.4 | | | |
| | | 31.6 | 6.91 | 290.2 | 24.6 | 117.3 | | | |
| | | 177.9 | 6.73 | 290.2 | 25.8 | 118.1 | | | |
| | | 997.3 | 6.54 | 290.2 | 25.6 | 118.5 | | | |
| ME404A1 | Lakeshore | 40.0 | 1.01 | 245.3 | 24.0 | 121.9 | 15.1 | 240.0 | III |
| | | 140.0 | 0.97 | 246.6 | 25.6 | 117.0 | | | |
| | | 400.0 | 0.93 | 246.6 | 28.2 | 117.1 | | | |
| | | 1000.0 | 0.92 | 246.8 | 27.1 | 118.3 | | | |
| | | 4000.0 | 0.88 | 247.3 | 25.4 | 119.6 | | | |
| ME413B1 | Lakeshore | 40.0 | 1.13 | 264.8 | 29.9 | 109.9 | 12.3 | 240.0 | VII |
| | | 140.0 | 1.08 | 268.0 | 35.8 | 110.5 | | | |
| | | 400.0 | 1.07 | 267.0 | 36.3 | 114.4 | | | |
| | | 1000.0 | 1.05 | 268.2 | 37.0 | 116.0 | | | |
| | | 4000.0 | 1.02 | 268.4 | 36.7 | 117.2 | | | |

| *Sample* | *Machine* | *Frequency* (Hz) | *max* $\chi'$ (x $10^{-5}$ $m^3$/kg) | *max* $\chi'$ *temperature* (K) | $\chi'$ *inflection temperature 1* (K) | $\chi'$ *inflection temperature 2* (K) | % $\chi'_{fd}$ | % $\chi'_{fd}$ *temperature* (K) | *Type* |
|---|---|---|---|---|---|---|---|---|---|
| ME433A1 | Lakeshore | 40.0 | 1.97 | 300.0 | 21.6 | | 7.5 | 300.0 | II |
| | | 140.0 | 1.91 | 300.0 | 22.1 | | | | |
| | | 400.0 | 1.86 | 300.0 | 22.7 | | | | |
| | | 1000.0 | 1.87 | 300.0 | 23.3 | | | | |
| | | 4000.0 | 1.82 | 300.0 | 23.0 | | | | |
| ME471A1 | Lakeshore | 40.0 | 2.50 | 107.3 | | | 7.7 | 90.0 | I |
| | | 140.0 | 2.47 | 106.5 | | | | | |
| | | 400.0 | 2.46 | 106.8 | | | | | |
| | | 1000.0 | 2.47 | 107.0 | | | | | |
| | | 4000.0 | 2.46 | 107.2 | | | | | |
| ME472A1 | Red | 1.0 | 10.52 | 108.9 | 6.5 | 34.3 | 17.3 | 24.7 | I |
| | | 5.6 | 10.50 | 109.1 | 7.1 | 43.5 | | | |
| | | 31.6 | 10.47 | 109.3 | 7.6 | 33.7 | | | |
| | | 177.9 | 10.43 | 111.1 | 8.0 | 33.5 | | | |
| | | 997.3 | 10.44 | 109.5 | 8.7 | 33.2 | | | |
| ME484A1 | Blue | 1.0 | 6.89 | 100.3 | 13.7 | | 12.2 | 44.3 | I |
| | | 5.6 | 6.86 | 100.6 | 14.3 | | | | |
| | | 31.6 | 6.82 | 100.9 | 14.8 | | | | |
| | | 177.9 | 6.79 | 100.1 | 15.5 | | | | |
| | | 997.3 | 6.74 | 100.7 | 15.9 | | | | |
| ME491A1 | Red | 1.0 | 7.57 | 91.5 | 12.8 | | 13.3 | 44.3 | I |
| | | 5.6 | 7.52 | 92.3 | 13.5 | | | | |
| | | 31.6 | 7.45 | 95.4 | 14.3 | | | | |
| | | 177.9 | 7.40 | 101.2 | 15.5 | | | | |
| | | 997.3 | 7.30 | 107.3 | 16.7 | | 16.7 | 44.3 | I |
| ME491A2 | Red | 1.0 | 10.07 | 85.2 | 10.8 | | | | |
| | | 5.6 | 9.99 | 88.0 | 11.6 | | | | |
| | | 31.6 | 9.90 | 91.5 | 12.4 | | | | |
| | | 177.9 | 9.80 | 96.4 | 13.2 | | | | |
| | | 997.3 | 9.64 | 100.5 | 14.1 | | | | |

Table C.3: Low temperature frequency dependence of susceptibility data from ME section, La Palma. *Machine* refers to the machine used at the Institute for Rock Magnetism, University of Minnesota, and are discussed in the text; *Frequency* is the frequency of the alternating current; *max* $\chi'$ is the maximum susceptibility and *max* $\chi'$ *temperature* is the temperature at which this occurs; $\chi'$ *inflection temperature 1 and 2* are temperatures where there are disinct changes in susceptibility as discussed in the text; % $\chi'_{fd}$ is the maximum percentage difference in susceptibility between the highest and lowest frequency used in the experiment and % $\chi'_{fd}$ *temperature* is the temperature at which this maximum difference occurs; *Type* is the classifcation of the curve types as discussed in the text.

| Sample | RS | Inflexion point temperatures (°C) | Type |
|---|---|---|---|
| ME30-2BOT | 0.33 | -120 | IV |
| ME30-3BOT | 0.43 | -148 | IV |
| ME30-4BOT | 0.48 | -150 | IV |
| ME31-2BOT | 0.40 | -150 | IV |
| ME31-3BOT | 0.97 | -163 | I |
| ME31-4BOT | 0.74 | -160 | II |
| ME31-5BOT | 0.41 | | IV |
| ME32-2A | 1.16 | -180 | I |
| ME32-3B | 1.11 | -180 | I |
| ME32-4A | 1.18 | -180 | I |
| ME33-1A | 1.17 | -170 | I |
| ME33-5A | 0.42 | | IV |
| ME34-3B | 0.18 | 5 | V |
| ME34-4B | 0.29 | 8 | V |
| ME34-4BOT | 0.13 | -3 | V |
| ME35-3A | 0.46 | | IV |
| ME35-4BOT | 0.27 | | IV |
| ME35-5A | 0.13 | | V |
| ME35-5BOT | 0.11 | | V |
| ME36-2A | 0.37 | | IV |
| ME36-5A | 0.32 | | IV |
| ME37-1A | 0.59 | -155 and -15 | VI |
| ME37-1BOT | 0.67 | -147 and -35 | VI |
| ME37-2A | 0.65 | -145 and -22 | VI |
| ME37-2BOT | 0.62 | -158 and -50 | VI |
| ME37-3U | 0.33 | -35 | V |
| ME37-4BOT | 0.60 | -163 and -37 | VI |
| ME38-1B | 0.67 | -50 | VII |
| ME38-1BOT | 0.62 | -50 | VII |
| ME38-2A | 0.46 | -160 | IV |
| ME38-2BOT | 0.43 | -42 | VII |
| ME38-4A | 1.35 | | I |
| ME39-1A | 0.55 | | II |
| ME39-4B | 1.32 | -164 | I |
| ME39-4BOT | 1.35 | -183 | I |
| ME39-5B | 1.20 | -170 | I |
| ME39-5BOT | 1.27 | -163 | I |
| ME39-6B | 1.17 | -177 | I |
| ME40-1BOT | 0.37 | | II |
| ME40-2A | 0.51 | -28 | VI |
| ME40-3A | 0.45 | -38 | VI |
| ME40-4B | 0.54 | -148 and -23 | VI |
| ME40-4BOT | 0.48 | -149 and -24 | VI |
| ME40-5A | 0.46 | -18 | VI |
| ME40-5BOT | 0.41 | -26 | VI |
| ME41-1B | 0.37 | -9 | V |
| ME41-1BOT | 0.44 | -29 | V |
| ME41-2A | 0.40 | -159 and -10 | VI |
| ME41-3BOT | 0.30 | -5 | V |
| ME41-4A | 0.35 | -154 and -5 | VI |
| ME41-4BOT | 0.28 | -30 | V |
| ME41-5B | 0.28 | | V |
| ME41-5BOT | 0.35 | -158 and -6 | VI |
| ME42-2B | 0.77 | -154 | II |
| ME42-3A | 0.77 | -150 | II |
| ME42-3BOT | 0.81 | -160 | II |

| Sample | RS | Inflexion point temperatures | Type |
|---|---|---|---|
| ME43-1A | 0.83 | -170 | II |
| ME43-2A | 0.19 | | IV |
| ME43-3A | 0.17 | | IV |
| ME43-3B | 0.54 | -158 | II |
| ME43-4B | 0.46 | | IV |
| ME43-4BOT | 0.69 | -150 | II |
| ME43-5A | 0.51 | -156 | II |
| ME43-5BOT | 0.40 | | IV |
| ME44-1B | 0.31 | | IV |
| ME44-1BOT | 0.23 | | IV |
| ME44-2A | 0.85 | -163 | II |
| ME44-3A | 0.76 | -150 | II |
| ME44-4A | 0.86 | -156 | II |
| ME44-4BOT | 0.83 | -150 | II |
| ME45-1A | 0.50 | -122 | III |
| ME45-1BOT | 0.67 | -115 | III |
| ME45-2A | 0.62 | -136 | III |
| ME45-2BOT | 0.65 | -153 | III |
| ME45-3A | 0.84 | -146 | II |
| ME45-4A | 0.78 | -143 | II |
| ME45-5A | 0.73 | -153 | II |
| ME45-5BOT | 0.76 | -154 | II |
| ME46-1A | 1.02 | -150 | II |
| ME46-1BOT | 0.95 | -133 | II |
| ME46-2BOT | 0.91 | -153 | II |
| ME46-4BOT | 1.12 | -154 | I |
| ME46-5A | 1.01 | -150 | I |
| ME46-5BOT | 1.16 | -142 | I |
| ME47-1BOT | 1.14 | -166 | I |
| ME47-2A | 1.25 | -175 | I |
| ME47-2BOT | 1.30 | | I |
| ME47-3A | 0.94 | | I |
| ME47-3B | 0.90 | | I |
| ME47-4B | 1.25 | | I |
| ME47-4BOT | 1.30 | | I |
| ME48-1A | 1.29 | | I |
| ME48-1BOT | 1.31 | -177 | I |
| ME48-2A | 1.85 | -175 | VIII |
| ME48-2BOT | 1.34 | -180 | I |
| ME49-2A | 1.25 | -159 | I |
| ME49-2BOT | 1.27 | -153 | VIII |
| ME49-3A | 1.47 | | I |
| ME49-4BOT | 1.30 | -176 | I |
| ME49-5BOT | 0.69 | | IV |
| ME50-1A | 1.01 | | I |
| ME50-1B | 1.13 | | I |
| ME50-1BOT | 1.17 | | I |
| ME50-2A | 1.16 | -154 | I |

Table C.4: Low temperature susceptibility data from the ME section, La Palma. Experiments measured on a Bartington Instruments MS2 susceptibility meter. RS is the ratio of susceptibility at -195 (°C) to 10 (°C). Inflexion point temperatures and Type are discussed in Section 5.3.1.

| | *Thermomagnetic Curve Types* | | | | | | | | *χ Curve Types* | | | | | | | | *FORC Types* | | |
|---|---|---|---|---|---|---|---|---|---|---|---|---|---|---|---|---|---|---|---|
| Flow | 1 | 2 | 3a | 3b | 3c | 4 | 5a | 5b | i | ii | iii | iv | v | vi | vii | viii | $\alpha$ | $\beta$ | $\gamma$ |
| ME32 | 4 | | | | | | | | 4 | | | | | | | | | | |
| ME33 | 2 | 1 | 1 | | | | | | 1 | 1 | | 1 | | | | | | | |
| ME34 | | | | | 1 | | 2 | 1 | | | 1 | | 3 | | | | | | |
| ME35 | 1 | | | 1 | 2 | | | | | 1 | | 2 | 2 | | | | | | |
| ME36 | 1 | | | 1 | 2 | | | | | 1 | | 2 | | | | | | | |
| ME37 | | | | 3 | | | 1 | | | | | | 1 | 5 | | | | | |
| ME38 | 1 | | | 2 | 1 | | | | 1 | | | 1 | | | 3 | | | | |
| ME39 | 4 | | | 1 | | | | | 5 | 1 | | | | | | | | | |
| ME40 | 1 | | | 3 | 1 | | | | | 1 | 1 | | | 6 | | | | | |
| ME41 | | | | 6 | | | | | | | | | 5 | 3 | 1 | | | | |
| ME42 | 2 | 1 | | | | | | | | 3 | | | | | | | | | |
| ME43 | 1 | | | 3 | | | | | | 5 | | 4 | | | | | | | |
| ME44 | 3 | | | | | | | | | 4 | | 2 | | | | | | | |
| ME45 | 4 | | | | | | | | | 4 | 4 | | | | | | | | |
| ME46 | 4 | | | | | | | | 3 | 3 | | | | | | | | | |
| ME47 | 5 | | | | | | | | 8 | | | | | | | | | 1 | 8 |
| ME48 | 5 | | | | | | | | 4 | | | | | | | 3 | | | 14 |
| ME49 | 5 | 1 | | | | | | | 5 | | | 1 | | | | 1 | 8 | 2 | |

Table C.5: Summary table of all ME rock magnetic experiment types. Numbers are the number of individual experiments that were classified as a certain type. See Section 5.3.1 for details of thermomagnetic and $\chi$ curve types; see Chapter 6 for details of FORC types.

| Sample | Hysteresis Properties | | | | | | Thermomagnetic Properties | | | | | |
|---|---|---|---|---|---|---|---|---|---|---|---|---|
| | $M_s$ (x $10^{-3}$ $Am^2/kg$) | $M_{rs}$ (x $10^{-3}$ $Am^2/kg$) | $H_c$ (mT) | $H_{cr}$ (mT) | $M_{rs}/M_s$ | $H_{cr}/H_c$ | $T_{c1}$ (°C) | $T_{c2}$ (°C) | $TMX_1$ | $TMX_2$ | % diff at 100°C | Type |
| AS1-2A1* | 4.691 | 0.406 | 5.82 | 20.64 | 0.09 | 3.55 | 132 | | 66 | | 82.9 | 5a |
| AS2-1A1* | 9.260 | 0.781 | 6.61 | 30.02 | 0.08 | 4.54 | 455 | | 20 | | -48.0 | 2 |
| AS3-1A1* | 17.024 | 4.894 | 43.71 | 72.22 | 0.29 | 1.65 | 516 | | 10 | | -63.8 | 1 |
| AS4-1A1* | 16.486 | 4.052 | 36.66 | 62.75 | 0.25 | 1.71 | 508 | | 12 | | -32.4 | 1 |
| AS5-2B1 | 5.359 | 1.658 | 31.41 | 60.04 | 0.31 | 1.91 | 495 | | 14 | | 96.4 | 1 |
| AS5-3A1* | 20.909 | 4.704 | 34.91 | 61.64 | 0.23 | 1.77 | 516 | | 10 | | -39.4 | 1 |
| AS6-2A1* | 12.116 | 2.132 | 15.23 | 48.63 | 0.18 | 3.19 | 315 | 538 | 41 | 7 | -6.2 | 2 |
| AS6-4BOT1 | 4.390 | 0.792 | 14.20 | 43.60 | 0.18 | 3.07 | 360 | 541 | 34 | 6 | -6.5 | 2 |
| AS7-1B1 | 1.427 | 0.361 | 24.93 | 56.84 | 0.25 | 2.28 | 529 | | 8 | | -19.6 | 1 |
| AS7-2A1* | 12.055 | 2.061 | 13.69 | 48.38 | 0.17 | 3.53 | 208 | 545 | 56 | 6 | 11.3 | 2 |
| AS7-2C1 | 4.868 | 1.109 | 18.33 | 51.64 | 0.23 | 2.82 | 261 | 501 | 49 | 13 | -11.9 | 2 |
| AS8-1A1* | 2.342 | 0.166 | 4.49 | 16.73 | 0.07 | 3.73 | 144 | | 64 | | 87.3 | 5b |
| AS8-1C1 | 1.155 | 0.144 | 6.33 | 16.87 | 0.13 | 2.67 | 156 | | 63 | | 92.5 | 5b |
| AS8-1C2 | 2.973 | 0.253 | 4.10 | 15.29 | 0.09 | 3.73 | 347 | | 36 | | 73.4 | 5a |
| AS8-2BOT1 | 1.390 | 0.156 | 4.67 | 16.42 | 0.11 | 3.52 | 421 | 545 | 25 | 6 | 89.6 | 3c |
| AS9-UA1 | 1.756 | 0.139 | 3.80 | 14.07 | 0.08 | 3.71 | 164 | | 62 | | 79.3 | 5b |
| AS9-UA2 | 3.266 | 0.271 | 3.66 | 14.13 | 0.08 | 3.86 | 162 | | 62 | | 71.7 | 5a |
| AS9-UA3 | 1.325 | 0.128 | 4.29 | 13.87 | 0.10 | 3.23 | 128 | | 66 | | | 5a |
| AS9-2A1 | 9.227 | 0.601 | 5.01 | 20.02 | 0.07 | 3.99 | 223 | 478 | 54 | 17 | 40.2 | 3c |
| AS10-1A1* | 11.748 | 2.055 | 22.97 | 48.96 | 0.17 | 2.13 | 507 | | 12 | | -27.9 | 1 |
| AS10-1C1 | 6.735 | 1.210 | 24.00 | 47.12 | 0.18 | 1.96 | | | | | | 1 |
| AS10-3C1 | 5.992 | 1.189 | 25.52 | 50.86 | 0.20 | 1.99 | 505 | | 12 | | -27.7 | 1 |
| AS10-4B1 | 5.498 | 1.104 | 23.33 | 44.21 | 0.20 | 1.89 | 506 | | 12 | | -22.3 | 1 |
| AS10-UA1 | 2.885 | 0.609 | 24.38 | 46.27 | 0.21 | 1.90 | 509 | | 12 | | -22.3 | 1 |
| AS11-2A1* | 16.331 | 1.701 | 10.63 | 31.42 | 0.10 | 2.96 | 460 | | 19 | | -15.0 | 1 |
| AS11-3BOT1 | 2.008 | 0.294 | 11.91 | 43.36 | 0.15 | 3.64 | 497 | | 14 | | 12.5 | 3a |
| AS11-4BOT1 | 1.565 | 0.229 | 9.64 | 37.71 | 0.15 | 3.91 | 329 | 476 | 39 | 17 | 11.7 | 3a |
| AS12-2A1* | 8.543 | 0.858 | 7.87 | 22.60 | 0.10 | 2.87 | 261 | 470 | 49 | 18 | 35.8 | 3a |
| AS13-1A1* | 11.534 | 1.438 | 12.50 | 32.87 | 0.12 | 2.63 | 327 | 475 | 39 | 17 | 16.0 | 3a |
| AS13-2BOT1 | 8.409 | 0.949 | 14.67 | 35.97 | 0.11 | 2.45 | 461 | | 19 | | 11.2 | 1 |
| AS13-3B1 | 8.189 | 0.576 | 4.72 | 20.28 | 0.07 | 4.30 | 210 | 379 | 55 | 32 | 38.4 | 3c |
| AS13-3B2 | 1.315 | 0.053 | 2.57 | 20.37 | 0.04 | 7.94 | 327 | 420 | 39 | 26 | 9.1 | 3a |
| AS13-4BOT1 | 5.513 | 0.357 | 4.28 | 18.21 | 0.06 | 4.25 | 169 | 339 | 61 | 38 | 42.5 | 5a |
| AS13-5B1 | 8.954 | 1.576 | 19.93 | 41.03 | 0.18 | 2.06 | 464 | | 19 | | -3.3 | 1 |
| AS13-5BOT1 | 6.915 | 0.794 | 8.51 | 26.03 | 0.11 | 3.06 | 251 | 460 | 50 | 19 | 36.4 | 3c |

| Sample | Hysteresis Properties | | | | | | Thermomagnetic Properties | | | | | |
|---|---|---|---|---|---|---|---|---|---|---|---|---|
| | $M_s$ (x $10^{-3}$ $Am^2/kg$) | $M_{rs}$ (x $10^{-3}$ $Am^2/kg$) | $H_c$ (mT) | $H_{cr}$ (mT) | $M_{rs}/M_s$ | $H_{cr}/H_c$ | $T_{c1}$ (°C) | $T_{c2}$ (°C) | $TMX_1$ | $TMX_2$ | % diff at 100°C | Type |
| AS14-1B1 | 2.847 | 0.309 | 5.39 | 17.81 | 0.11 | 3.31 | 103 | | 69 | | 91.1 | 5a |
| AS14-2B1 | 3.078 | 0.341 | 5.36 | 17.72 | 0.11 | 3.30 | 106 | | 69 | | 93.1 | 5a |
| AS14-2B2 | 3.185 | 0.359 | 5.80 | 18.15 | 0.11 | 3.13 | 107 | | 69 | | 96.4 | 5a |
| AS14-3A1* | 7.087 | 0.729 | 7.90 | 23.70 | 0.10 | 3.00 | 171 | 477 | 61 | 17 | 62.3 | 3c |
| AS14-3B1 | 4.617 | 0.592 | 8.22 | 22.89 | 0.13 | 2.78 | 183 | 461 | 59 | 19 | 54.9 | 3c |
| AS15-1A1* | 9.003 | 0.518 | 3.97 | 18.05 | 0.06 | 4.54 | 372 | | 33 | | 17.8 | - |
| AS15-1B1 | 5.707 | 0.494 | 4.68 | 18.85 | 0.09 | 4.03 | 273 | | 47 | | 54.9 | - |
| AS15-3BOT1 | 25.457 | 3.174 | 15.03 | 34.30 | 0.12 | 2.28 | | | | | | - |
| AS16-1A1* | 7.899 | 0.593 | 5.11 | 19.13 | 0.08 | 3.74 | 165 | 473 | 61 | 17 | 59.4 | 3c |
| AS16-1C1 | 4.783 | 0.411 | 4.84 | 18.46 | 0.09 | 3.81 | 146 | 462 | 64 | 19 | 63.7 | 3c |
| AS16-2B1 | 2.008 | 0.142 | 3.54 | 17.19 | 0.07 | 4.85 | 111 | | 68 | | 83.2 | 5a |
| AS16-3B1 | 2.362 | 0.165 | 3.16 | 305.18 | 0.07 | 96.53 | 102 | | 70 | | 92.7 | 5a |
| AS16-4C1 | 4.907 | 0.294 | 3.16 | 305.18 | 0.06 | 96.60 | 114 | | 68 | | 79.3 | 5a |
| AS16-5D1 | 3.490 | 0.254 | 3.34 | 15.75 | 0.07 | 4.71 | 114 | | 68 | | 70.2 | 5a |
| AS16B1-A1 | 4.315 | 0.400 | 4.71 | 18.62 | 0.09 | 3.95 | 118 | 311 | 68 | 42 | 77.6 | 5a |
| AS17-UA1* | 5.727 | 0.296 | 3.27 | 13.46 | 0.05 | 4.12 | 133 | 418 | 66 | 26 | 75.5 | 3c |
| AS17-UA2 | 2.571 | 0.200 | 3.76 | 13.88 | 0.08 | 3.69 | 137 | 398 | 65 | 29 | 75.9 | 3c |
| AS17-UA3 | 3.750 | 0.313 | 4.06 | 14.57 | 0.08 | 3.59 | 142 | 413 | 64 | 27 | 69.9 | 3c |
| AS18-1A1* | 9.102 | 0.468 | 3.17 | 17.20 | 0.05 | 5.42 | 140 | | 65 | | 52.0 | 5a |
| AS18-1B1 | 3.644 | 0.303 | 4.42 | 18.59 | 0.08 | 4.21 | 140 | | 65 | | 64.9 | 5a |
| AS18-1BOT1 | 3.763 | 0.330 | 5.18 | 18.28 | 0.09 | 3.53 | 144 | | 64 | | 54.1 | 5a |
| AS18-2B1 | 1.426 | 0.155 | 4.99 | 16.29 | 0.11 | 3.26 | 107 | | 69 | | 96.4 | 5b |
| AS18-3B1 | 1.064 | 0.163 | 6.13 | 17.40 | 0.15 | 2.84 | 94 | | 71 | | 95.9 | 5b |
| AS18-4BOT1 | 1.087 | 0.155 | 6.09 | 18.83 | 0.14 | 3.09 | 99 | | 70 | | 97.1 | 5b |
| AS18-UBOT1 | 1.489 | 0.169 | 5.13 | 16.40 | 0.11 | 3.19 | 98 | | 70 | | 93.3 | 5b |
| AS19-1A1 | 6.770 | 0.815 | 17.87 | 41.88 | 0.12 | 2.34 | 508 | | 12 | | -34.2 | 1 |
| AS19-2B1 | 3.565 | 0.324 | 6.84 | 22.74 | 0.09 | 3.32 | 260 | 446 | 49 | 22 | 31.9 | 3b |
| AS19-3B1 | 4.756 | 0.915 | 20.62 | 49.78 | 0.19 | 2.41 | 333 | 467 | 38 | 18 | 7.9 | 3a |
| AS19-5B1 | 3.747 | 0.938 | 30.14 | 60.68 | 0.25 | 2.01 | 483 | | 16 | | -23.2 | 1 |
| AS19B-2A1 | 10.635 | 2.627 | 30.15 | 57.91 | 0.25 | 1.92 | 491 | | 14 | | 17.7 | 3a |
| AS19B-2B1* | 6.538 | 1.375 | 27.69 | 56.96 | 0.21 | 2.06 | 406 | 483 | 28 | 16 | -29.4 | 1 |
| AS19B-3BOT1 | 31.491 | 4.456 | 23.76 | 51.29 | 0.14 | 2.16 | | | | | | |
| AS19B-4BOT1 | 6.713 | 1.607 | 29.36 | 56.66 | 0.24 | 1.93 | 482 | | 16 | | -30.0 | 1 |
| AS20-1BOT1 | 2.624 | 0.369 | 6.73 | 18.66 | 0.14 | 2.77 | 125 | | 67 | | 79.4 | 5a |
| AS20-2BOT1 | 5.397 | 0.706 | 11.91 | 33.26 | 0.13 | 2.79 | 329 | 460 | 39 | 19 | 14.9 | 3a |
| AS20-3A1 | 9.310 | 1.666 | 16.86 | 43.87 | 0.18 | 2.60 | 481 | | 16 | | 10.8 | 1 |

| Sample | Hysteresis Properties | | | | | | Thermomagnetic Properties | | | | | |
|---|---|---|---|---|---|---|---|---|---|---|---|---|
| | $M_s$ (x $10^{-3}$ $Am^2/kg$) | $M_{rs}$ (x $10^{-3}$ $Am^2/kg$) | $H_c$ (mT) | $H_{cr}$ (mT) | $M_{rs}/M_s$ | $H_{cr}/H_c$ | $T_{c1}$ (°C) | $T_{c2}$ (°C) | $TMX_1$ | $TMX_2$ | % diff at 100°C | Type |
| AS20-3B1 | 3.393 | 0.733 | 27.77 | 55.30 | 0.22 | 1.99 | 495 | | 14 | | -11.5 | 1 |
| AS20-UA1 | 6.529 | 1.297 | 25.93 | 52.03 | 0.20 | 2.01 | 488 | | 15 | | -8.9 | 1 |
| AS20-UA2 | 7.116 | 1.078 | 24.83 | 52.76 | 0.15 | 2.13 | 481 | | 16 | | -37.2 | 1 |
| AS21-1B1 | 4.248 | 0.699 | 19.62 | 38.29 | 0.16 | 1.95 | 476 | | 17 | | -34.1 | 1 |
| AS21-1BOT1 | 3.872 | 0.639 | 19.14 | 38.51 | 0.16 | 2.01 | 471 | | 18 | | -38.3 | 1 |
| AS21-2BOT1 | 4.662 | 0.746 | 18.19 | 37.30 | 0.16 | 2.05 | 467 | | 18 | | -25.4 | 1 |
| AS21-3B1 | 5.182 | 0.905 | 21.19 | 45.89 | 0.17 | 2.17 | 472 | | 17 | | -40.8 | 1 |
| AS21-4B1 | 4.155 | 0.663 | 16.11 | 40.46 | 0.16 | 2.51 | 446 | | 22 | | -22.1 | 1 |
| AS21-5A1 | 6.347 | 0.830 | 15.21 | 38.04 | 0.13 | 2.50 | 472 | | 17 | | -15.2 | 1 |
| AS22B-2B1 | 0.390 | 0.055 | 7.83 | 20.44 | 0.14 | 2.61 | 413 | | 27 | | 73.5 | 3c |
| AS22B-3B1 | 0.921 | 0.150 | 11.81 | 29.39 | 0.16 | 2.49 | 235 | 474 | 52 | 17 | 47.8 | 3c |
| AS22B-5A1 | 0.326 | 0.073 | 10.29 | 23.13 | 0.22 | 2.25 | 143 | | 64 | | 86.9 | - |
| AS22B-5A2 | 0.286 | 0.059 | 9.65 | 20.50 | 0.21 | 2.12 | 232 | | 53 | | 78.5 | 5a |
| AS22B-5BOT1 | 0.198 | 0.045 | 10.64 | 21.82 | 0.23 | 2.05 | 249 | | 50 | | 86.8 | 5a |
| AS22B-5C1 | 0.318 | 0.067 | 9.47 | 19.86 | 0.21 | 2.10 | 234 | | 52 | | 80.2 | 5a |
| AS23-2A1* | 4.309 | 0.770 | 15.57 | 32.53 | 0.18 | 2.09 | 184 | 496 | 59 | 14 | 32.3 | 3b |
| AS23-2A2 | 1.878 | 0.419 | 18.67 | 36.67 | 0.22 | 1.96 | 182 | 468 | 59 | 18 | 39.5 | 3b |
| AS23-3B1 | 0.364 | 0.060 | 9.59 | 23.18 | 0.17 | 2.42 | 349 | | 36 | | 87.7 | 5b |
| AS23-4B1 | 0.139 | 0.036 | 15.61 | 28.38 | 0.26 | 1.82 | 310 | | 42 | | 94.8 | 5b |
| AS23-5B1 | 1.295 | 0.117 | 3.82 | 15.00 | 0.09 | 3.92 | 99 | | 70 | | 93.3 | 5a |
| AS24-1A1* | 1.211 | 0.110 | 4.67 | 21.09 | 0.09 | 4.52 | 128 | 430 | 66 | 24 | 65.1 | 3c |
| AS24-3B1 | 0.103 | 0.024 | 7.80 | 18.23 | 0.24 | 2.34 | | | | | | - |
| AS24-6BOT1 | 0.482 | 0.086 | 6.38 | 20.71 | 0.18 | 3.25 | | | | | | - |
| AS24B-3A1* | 9.466 | 1.467 | 16.29 | 34.29 | 0.15 | 2.10 | 487 | | 15 | | -3.1 | 1 |
| AS24C-3A1* | 1.639 | 0.497 | 28.14 | 49.20 | 0.30 | 1.75 | 229 | 505 | 53 | 12 | 64.4 | 3c |
| AS25-1A1* | 3.847 | 0.429 | 6.06 | 19.13 | 0.11 | 3.16 | 124 | 417 | 67 | 26 | 71.7 | 3c |
| AS25-2B1 | 0.534 | 0.106 | 6.82 | 15.87 | 0.20 | 2.33 | 119 | 563 | 67 | 3 | 70.8 | 5a |
| AS25-3B1 | 0.749 | 0.122 | 6.39 | 17.85 | 0.16 | 2.79 | 156 | 552 | 63 | 4 | 52.3 | 3c |
| AS25-5B1 | 0.863 | 0.143 | 5.57 | 15.39 | 0.17 | 2.76 | 115 | | 68 | | 73.1 | 5a |
| AS26-3A1* | 2.125 | 0.268 | 11.19 | 33.23 | 0.13 | 2.97 | 490 | | 15 | | -26.5 | 1 |
| AS27-2B1 | 0.690 | 0.093 | 5.15 | 14.59 | 0.13 | 2.83 | 136 | 580 | 65 | 0 | 58.5 | 5a |
| AS27-3A1* | 6.324 | 1.071 | 13.66 | 49.13 | 0.17 | 3.60 | | | | | | 3c |
| AS27-4B1 | 0.752 | 0.070 | 4.19 | 16.40 | 0.09 | 3.92 | | | | | | - |
| AS27-4B2 | 0.775 | 0.104 | 5.03 | 14.33 | 0.13 | 2.85 | 127 | 576 | 66 | 0 | 42.8 | 3c |
| AS27-4B3 | 0.889 | 0.170 | 9.91 | 42.30 | 0.19 | 4.27 | 201 | 527 | 57 | 9 | 34.7 | 3c |
| AS27-4BOT1 | 1.285 | 0.180 | 5.40 | 15.89 | 0.14 | 2.95 | 137 | 560 | 65 | 3 | 66.5 | 3c |

Table C.6: Summary of hysteresis and thermomagnetic properties of individual samples from the AS section, La Palma. See Table C.1 for explanation of column headings and abbreviations. * indicates sample measured by Martin Gratton, analysis by the author.

| Sample | RS | Inflexion point temperatures (°C) | Type |
|---|---|---|---|
| AS1-2* | 0.46 | | IV |
| AS2-1* | 0.22 | | IV |
| AS3-1* | 0.89 | -155 | I |
| AS3-1(2) | 0.97 | -161 | I |
| AS3-2 | 0.91 | -161 | I |
| AS3-4 | 0.89 | -152 | I |
| AS3-5 | 0.54 | -141 | III |
| AS4-1* | 0.93 | -161 | I |
| AS4-2 | 0.87 | -143 | I |
| AS4-3 | 0.93 | -143 | I |
| AS4-4 | 1.07 | -128 | I |
| AS5-2 | 0.98 | -156 | I |
| AS5-3* | 0.82 | -158 | II |
| AS5-3(2) | 0.85 | -122 | II |
| AS5-U | 0.24 | | IV |
| AS6-1 | 0.42 | | IV |
| AS6-2 | 0.35 | | IV |
| AS6-3* | 0.58 | -159 | III |
| AS6-4 | 0.31 | | IV |
| AS6-5 | 0.33 | | IV |
| AS7-1 | 1.22 | -147 | I |
| AS7-2* | 0.36 | | IV |
| AS8-1* | 0.16 | -28 | VII |
| AS8-1(2) | 0.17 | -27 | VII |
| AS9-1 | 0.09 | -2 | V |
| AS9-1(2) | 0.16 | -9 | V |
| AS9-2 | 0.09 | | IV |
| AS9-2(2) | 0.66 | -147 | II |
| AS9-3* | 0.66 | -162 | II |
| AS9-U | 0.58 | -161 | II |
| AS9-U(2) | 0.13 | -21 | VII |
| AS10-1* | 1.21 | -145 | I |
| AS10-1(2) | 1.07 | -153 | I |
| AS10-2 | 1.14 | -147 | I |
| AS10-3 | 1.11 | -124 | I |
| AS10-4 | 1.15 | -173 | I |
| AS11-2* | 0.54 | -147 | II |
| AS11-2(2) | 0.53 | -147 | II |
| AS11-3 | 0.33 | | IV |
| AS11-4 | 0.30 | | IV |
| AS11-5 | 0.17 | | IV |
| AS12-1 | 0.97 | -167 | I |
| AS12-2* | 0.31 | | IV |
| AS12-4 | 0.12 | | IV |
| AS13-1* | 0.63 | -156 | II |
| AS13-2 | 0.97 | -149 | I |
| AS13-4 | 0.16 | | IV |
| AS13-5 | 0.47 | -176 | III |
| AS13-5(2) | 0.78 | -158 | II |
| AS14-1 | 0.02 | | IV |
| AS14-2(2) | 0.15 | | IV |
| AS14-2B | 0.15 | | IV |
| AS14-3* | 0.93 | -168 | I |
| AS14-3(2) | 0.24 | | IV |
| AS14-3(3) | 0.19 | | IV |
| AS15-1* | 0.14 | | IV |
| AS15-1(2) | 0.67 | -161 | II |

| Sample | RS | Inflexion point temperatures (°C) | Type |
|---|---|---|---|
| AS16-1* | 0.22 | | IV |
| AS16-1(2) | 0.15 | | IV |
| AS16-2 | 0.09 | | IV |
| AS16-3 | 0.08 | | IV |
| AS16-4 | 0.09 | | IV |
| AS16-5 | 0.10 | | IV |
| AS17-U* | 0.21 | | IV |
| AS17-U(2) | 0.15 | | IV |
| AS17-U(3) | 0.17 | | IV |
| AS18-1* | 0.12 | | IV |
| AS18-1(2) | 0.14 | | IV |
| AS18-1(3) | 0.15 | | IV |
| AS18-3 | 0.17 | -15 | V |
| AS18-4 | 0.14 | -12 | V |
| AS19-1* | 0.62 | -158 | II |
| AS19-1(2) | 0.42 | | III |
| AS19-2 | 0.41 | | III |
| AS19-3 | 0.59 | -157 | II |
| AS19-5 | 0.66 | -158 | II |
| AS19B-1* | 0.42 | | III |
| AS19B-3 | 1.10 | | I |
| AS20-1 | 0.15 | | V |
| AS20-2 | 0.61 | -154 | II |
| AS20-3* | 0.55 | -154 | II |
| AS20-3(2) | 0.51 | -139 | II |
| AS20-U | 0.76 | -147 | II |
| AS20-U(2) | 1.09 | -134 | I |
| AS20-U(3) | 0.13 | -3 | V |
| AS21-1 | 0.81 | -167 | II |
| AS21-1(2) | 2.09 | -140 | VIII |
| AS21-2 | 0.71 | -154 | II |
| AS21-4 | 0.50 | | III |
| AS21-5* | 0.69 | -135 | II |
| AS22B-2 | 0.69 | -35 | VII |
| AS22B-3 | 0.46 | -27 | VI |
| AS22B-4 | 0.72 | -30 | VII |
| AS22B-5* | 0.48 | -37 | VII |
| AS22B-5(2) | 0.66 | -25 | VII |
| AS23-1 | 0.56 | -168 | III |
| AS23-2* | 0.60 | -163 | III |
| AS23-2(2) | 0.61 | -162 | III |
| AS23-2(3) | 0.58 | -170 | III |
| AS23-3 | 0.44 | -48 | VII |
| AS23-3(2) | 0.54 | -45 | VII |
| AS23-4 | 0.77 | -48 | VII |

| Sample | RS | Inflexion point temperatures (°C) | Type |
|---|---|---|---|
| AS24-1* | 0.16 | | IV |
| AS24-1(2) | 0.16 | | IV |
| AS24-2 | 0.25 | | IV |
| AS24-3 | 0.44 | -46 | VII |
| AS24-4 | 0.27 | | IV |
| AS24-5 | 0.39 | | III |
| AS24-6 | 0.37 | | III |
| AS24B-1* | 0.62 | -130 | II |
| AS24B-2 | 0.68 | -147 | II |
| AS24B-4 | 0.77 | -161 | II |
| AS24B-4(2) | 0.68 | -112 | III |
| AS24C-3* | 0.55 | -13 | V |
| AS24C-3(2) | 0.55 | -19 | V |
| AS25-1* | 0.20 | | IV |
| AS25-1(2) | 0.14 | | IV |
| AS25-1(3) | 0.15 | | IV |
| AS25-4 | 0.33 | | IV |
| AS25-5B | 0.14 | | IV |
| AS25-5(2) | 0.00 | | IV |
| AS26-1* | 0.99 | -172 | I |
| AS27-2 | 0.09 | 5 | IV |
| AS27-2(2) | 0.09 | 3 | IV |
| AS27-3* | 0.41 | | III |
| AS27-3(2) | 0.38 | | III |
| AS27-3(3) | 0.31 | | III |

Table C.7: Low temperature susceptibility data from AS section, La Palma. Experiments measured on a Bartington Instruments susceptibility meter. RS is the ratio of susceptibility at -195 (°C) to 10 (°C). Inflexion point temperatures and Type are discussed in Section 5.3.1. * indicates measurements by Martin Gratton, data analysis by author.

| | *Thermomagnetic Curve Types* | | | | | | | | *χ Curve Types* | | | | | | | |
|---|---|---|---|---|---|---|---|---|---|---|---|---|---|---|---|---|
| Flow | 1 | 2 | 3a | 3b | 3c | 4 | 5a | 5b | i | ii | iii | iv | v | vi | vii | viii |
| AS1 | | | | | | | 1 | | | | | 1 | | | | |
| AS2 | | 1 | | | | | | | | | | 1 | | | | |
| AS3 | 1 | | | | | | | | 4 | | 1 | | | | | |
| AS4 | 1 | | | | | | | | 4 | | | | | | | |
| AS5 | | 2 | | | | | | | 1 | 2 | | 1 | | | | |
| AS6 | | 2 | | | | | | | | | 1 | 4 | | | | |
| AS7 | 1 | 2 | | | | | | | 1 | | | 1 | | | | |
| AS8 | | | | | 1 | | 1 | 2 | | | | | | | 2 | |
| AS9 | | | | | 1 | | 2 | 1 | | 3 | | 1 | 2 | | 1 | |
| AS10 | 5 | | | | | | | | 5 | | | | | | | |
| AS11 | 1 | | 2 | | | | | | | 2 | | 3 | | | | |
| AS12 | | | 1 | | | | | | 1 | | | 2 | | | | |
| AS13 | 2 | | 2 | | 2 | | 1 | | 1 | 2 | 1 | 1 | | | | |
| AS14 | | | | | 2 | | 3 | | 1 | | | 5 | | | | |
| AS15 | | | | | | | | | | 1 | | 1 | | | | |
| AS16 | | | | | 2 | | 5 | | | | | 6 | | | | |
| AS17 | | | | | 3 | | | | | | | 3 | | | | |
| AS18 | | | | | | | 3 | 4 | | | | 3 | 2 | | | |
| AS19 | 2 | | 1 | 1 | | | | | | 3 | 2 | | | | | |
| AS19B | 2 | | 1 | | | | | | 1 | | 1 | | | | | |
| AS20 | 4 | | 1 | | | | 1 | | 1 | 4 | | | 2 | | | |
| AS21 | 6 | | | | | | | | | 3 | 1 | | | | | 1 |
| AS22B | | | | | 2 | | 3 | | | | | | | 1 | 4 | |
| AS23 | | | | 2 | | | 1 | 2 | | | 4 | | | | 3 | |
| AS24 | | | | | 1 | | | | | | 2 | 4 | | | 1 | |
| AS24B | 1 | | | | | | | | | 3 | 1 | | | | | |
| AS24C | | | | | 1 | | | | | | | | 2 | | | |
| AS25 | | | | | 2 | | 2 | | | | | 6 | | | | |
| AS26 | 1 | | | | | | | | 1 | | | | | | | |
| AS27 | | | | | 4 | | 1 | | | | 3 | 2 | | | | |

Table C.8: Summary table of all Guadeloupe rock magnetic experiment types. Numbers are the number of individual experiments that were classified as a certain type. See Section 5.3.1 for details of thermomagnetic and $\chi$ curve types.

| Sample | Hysteresis Properties | | | | | | Thermomagnetic Properties | | | | | |
|---|---|---|---|---|---|---|---|---|---|---|---|---|
| | $M_s$ (x $10^{-3}$ $Am^2/kg$) | $M_{rs}$ (x $10^{-3}$ $Am^2/kg$) | $H_c$ (mT) | $H_{cr}$ (mT) | $M_{rs}/M_s$ | $H_{cr}/H_c$ | $T_{c1}$ (°C) | $T_{c2}$ (°C) | $TMX_1$ | $TMX_2$ | % diff at 100°C | Type |
| AN1-5 | 0.152 | 0.077 | 3.78 | 15.80 | 0.05 | 4.18 | 183 | 408 | 59 | 27 | 66.3 | 3c |
| AN2-2 | 0.711 | 0.746 | 8.13 | 23.05 | 0.10 | 2.83 | 234 | 461 | 52 | 19 | 32.9 | 3b |
| AN3-3 | 0.939 | 2.069 | 17.00 | 33.83 | 0.22 | 1.99 | 485 | | 15 | | 19.6 | 3a |
| AN4-2 | 0.230 | 0.102 | 2.94 | 14.97 | 0.04 | 5.09 | 148 | 352 | 64 | 36 | 69.3 | 3c |
| AN6-3 | 0.414 | 0.231 | 3.70 | 14.98 | 0.06 | 4.04 | 177 | 445 | 60 | 22 | 22.3 | 3b |
| AN7-3 | 0.907 | 0.823 | 7.19 | 22.48 | 0.09 | 3.13 | 210 | 431 | 55 | 24 | 35.9 | 3b |
| AN8-1 | 1.298 | 1.118 | 7.06 | 22.40 | 0.09 | 3.17 | 280 | 454 | 46 | 20 | 21.4 | 3b |
| AN9a-1 | 0.929 | 1.037 | 14.63 | 38.78 | 0.11 | 2.65 | 519 | | 10 | | -29.3 | 1 |
| AN9b-2 | 0.433 | 0.829 | 16.29 | 34.23 | 0.19 | 2.10 | 179 | 490 | 60 | 15 | 53.0 | 3c |
| AN10-2 | 0.606 | 0.888 | 9.07 | 26.64 | 0.15 | 2.94 | 154 | 480 | 63 | 16 | 55.3 | 3c |
| AN11-1 | 0.983 | 1.641 | 15.02 | 32.00 | 0.17 | 2.13 | 294 | 487 | 44 | 15 | 35.7 | 3b |
| AN12-2 | 1.162 | 3.179 | 37.06 | 61.31 | 0.27 | 1.65 | 521 | | 10 | | -45.9 | 1 |
| AN13-4 | 0.424 | 0.579 | 9.26 | 21.34 | 0.14 | 2.30 | 149 | 459 | 64 | 19 | 72.9 | 5a |
| AN14-1 | 0.218 | 0.415 | 9.11 | 18.93 | 0.19 | 2.08 | 104 | | 69 | | 91.9 | 5a |
| AN15-1 | 0.907 | 3.411 | 48.62 | 69.52 | 0.38 | 1.43 | 452 | | 21 | | -4.2 | 1 |
| AN16-3 | 1.188 | 1.373 | 10.20 | 29.29 | 0.12 | 2.87 | 470 | | 18 | | 3.8 | 1 |

Table C.9: Summary of hysteresis and thermomagnetic properties of individual samples from the AN section, La Palma. See Table C.1 for explanation of column headings and abbreviations. All samples measured by Martin Gratton, analysis by the author.

| Sample | RS | Inflexion point temperatures (°C) | Type |
|---|---|---|---|
| AN1-5 | 0.24 | -10 | V |
| AN2-2 | 0.46 | | IV |
| AN3-3 | 0.39 | -151 | III |
| AN4-2 | 0.17 | | IV |
| AN6-3 | 0.19 | | IV |
| AN7-3 | 0.32 | | IV |
| AN8-1 | 0.52 | | IV |
| AN9a-1 | 1.25 | | I |
| AN9b-1 | 0.40 | | III |
| AN10-2 | 0.23 | | IV |
| AN11-1 | 0.50 | | III |
| AN12-3 | 1.02 | -167 | I |
| AN13-4 | 0.21 | | IV |
| AN14-1 | 0.18 | | IV |
| AN15-2 | 0.77 | -159 | II |

Table C.10: Low temperature susceptibility data from AN section, La Palma. Experiments measured on a Bartington Instruments susceptibility meter. RS is the ratio of susceptibility at -195 (°C) to 10 (°C). Inflexion point temperatures and Type are discussed in Section 5.3.1. All measurements by Martin Gratton, data analysis by author.

| | *Thermomagnetic Curve Types* | | | | | | | | *χ Curve Types* | | | | | | | |
|---|---|---|---|---|---|---|---|---|---|---|---|---|---|---|---|---|
| Flow | 1 | 2 | 3a | 3b | 3c | 4 | 5a | 5b | i | ii | iii | iv | v | vi | vii | viii |
| AN1 | | | | | 1 | | | | | | | | 1 | | | |
| AN2 | | | | 1 | | | | | | | | 1 | | | | |
| AN3 | | | 1 | | | | | | | | 1 | | | | | |
| AN4 | | | | | 1 | | | | | | | 1 | | | | |
| AN6 | | | | 1 | | | | | | | | 1 | | | | |
| AN7 | | | | 1 | | | | | | | | 1 | | | | |
| AN8 | | | | 1 | | | | | | | | 1 | | | | |
| AN9a | 1 | | | | | | | | 1 | | | | | | | |
| AN9b | | | | | 1 | | | | | | 1 | | | | | |
| AN10 | | | | | 1 | | | | | | | 1 | | | | |
| AN11 | | | | 1 | | | | | | | 1 | | | | | |
| AN12 | 1 | | | | | | | | 1 | | | | | | | |
| AN13 | | | | | | | 1 | | | | | 1 | | | | |
| AN14 | | | | | | | 1 | | | | | 1 | | | | |
| AN15 | 1 | | | | | | | | | 1 | | | | | | |
| AN16 | 1 | | | | | | | | | | | | | | | |

Table C.11: Summary table of all AN rock magnetic experiment types. Numbers are the number of individual experiments that were classified as a certain type. See Section 5.3.1 for details of thermomagnetic and $\chi$ curve types.

| Sample | Hysteresis Properties | | | | | | Thermomagnetic Properties | | | | | |
|---|---|---|---|---|---|---|---|---|---|---|---|---|
| | $M_s$ (x $10^{-3}$ $Am^2/kg$) | $M_{rs}$ (x $10^{-3}$ $Am^2/kg$) | $H_c$ (mT) | $H_{cr}$ (mT) | $M_{rs}/M_s$ | $H_{cr}/H_c$ | $T_{c1}$ (°C) | $T_{c2}$ (°C) | $TMX_1$ | $TMX_2$ | % diff at 100°C | Type |
| G01A01 | 7.02 | 22.84 | 0.325 | 6.157 | 0.05 | 3.25 | 481 | | 16 | | 15.4 | 2 |
| G01A02 | 7.71 | 22.42 | 0.316 | 5.564 | 0.06 | 2.91 | 476 | | 17 | | 21.1 | 2 |
| G01A03 | 15.84 | 34.56 | 0.489 | 5.647 | 0.09 | 2.18 | 547 | | 5 | | -16.3 | 1 |
| G01A04 | 7.33 | 23.86 | 0.305 | 6.232 | 0.05 | 3.26 | 500 | | 13 | | -1.1 | 1 |
| G01A05 | 8.59 | 25.89 | 0.497 | 8.508 | 0.06 | 3.01 | 530 | | 8 | | 9.0 | 2 |
| G01A06 | 7.78 | 24.17 | 0.413 | 8.005 | 0.05 | 3.11 | 535 | | 7 | | 5.1 | 2 |
| G01A07 | 14.23 | 33.88 | 0.623 | 8.599 | 0.07 | 2.38 | 521 | | 10 | | -7.6 | 1 |
| G01B01 | 4.72 | 22.95 | 0.171 | 5.227 | 0.03 | 4.87 | 540 | | 6 | | 1.1 | 2 |
| G01B02 | 7.99 | 27.87 | 0.294 | 5.466 | 0.05 | 3.49 | 537 | | 7 | | -5.3 | 1 |
| G01B03 | 6.83 | 27.62 | 0.295 | 7.055 | 0.04 | 4.04 | 512 | | 11 | | -6.8 | 1 |
| G01B04 | 15.26 | 41.59 | 0.885 | 10.041 | 0.09 | 2.73 | 564 | | 2 | | -37.9 | 1 |
| G01B05 | 12.94 | 38.30 | 0.432 | 5.568 | 0.08 | 2.96 | 560 | | 3 | | -33.5 | 1 |
| G01C01 | 6.36 | 22.28 | 0.172 | 3.623 | 0.05 | 3.50 | 578 | | 0 | | 8.2 | 2 |
| G01C02 | 4.42 | 23.85 | 0.180 | 6.759 | 0.03 | 5.40 | 504 | | 12 | | 3.2 | 2 |
| G01C03 | 4.07 | 23.44 | 0.257 | 9.010 | 0.03 | 5.75 | 543 | | 6 | | -2.9 | 1 |
| G01C04 | 4.48 | 25.38 | 0.331 | 10.777 | 0.03 | 5.66 | 549 | | 5 | | -15.6 | 1 |
| G01C05 | 3.70 | 18.05 | 0.135 | 4.155 | 0.03 | 4.87 | 557 | | 4 | | 8.9 | 2 |
| G01C06 | 4.08 | 24.05 | 0.289 | 9.974 | 0.03 | 5.89 | 543 | | 6 | | -14.5 | 1 |
| G01C07 | 4.01 | 19.31 | 0.142 | 4.009 | 0.04 | 4.81 | 396 | 536 | 29 | 7 | 29.1 | 3b |
| G01C08 | 6.51 | 20.70 | 0.249 | 4.382 | 0.06 | 3.18 | 466 | 547 | 18 | 5 | 28.8 | 3b |
| G02A01 | 18.61 | 40.99 | 0.453 | 4.569 | 0.10 | 2.20 | 578 | | 0 | | -65.0 | 1 |
| G02A02 | 11.79 | 34.80 | 0.364 | 5.626 | 0.06 | 2.95 | 576 | | 0 | | -58.0 | 1 |
| G0203A | 18.18 | 43.65 | 0.505 | 5.743 | 0.09 | 2.40 | 580 | | 0 | | -56.2 | 1 |
| G02A04 | 3.55 | 26.59 | 0.095 | 3.473 | 0.03 | 7.49 | 557 | | 4 | | -92.1 | 1 |
| G02A05 | 13.12 | 37.97 | 0.371 | 5.216 | 0.07 | 2.89 | 573 | | 1 | | -27.9 | 1 |
| G02A06 | 14.68 | 36.69 | 0.412 | 5.072 | 0.08 | 2.50 | 566 | | 2 | | -39.2 | 1 |
| G02A07 | 7.10 | 27.72 | 0.433 | 9.531 | 0.05 | 3.90 | 539 | | 7 | | 4.4 | 2 |
| G02A08 | 21.81 | 52.26 | 0.507 | 4.837 | 0.10 | 2.40 | 563 | | 3 | | -10.4 | 1 |
| G02A09 | 9.37 | 38.72 | 0.297 | 6.155 | 0.05 | 4.13 | 546 | | 6 | | -27.5 | 1 |
| G02B01 | 42.08 | 87.00 | 0.126 | 0.492 | 0.26 | 2.07 | 579 | | 0 | | -8.7 | 1 |
| G02B02 | 31.14 | 85.50 | 0.071 | 0.322 | 0.22 | 2.75 | 580 | | 0 | | -10.8 | 1 |
| G02B03 | 20.65 | 48.75 | 0.378 | 3.754 | 0.10 | 2.36 | 565 | | 2 | | -47.7 | 1 |
| G02B04 | 14.53 | 39.90 | 0.303 | 3.877 | 0.08 | 2.75 | 578 | | 0 | | -41.5 | 1 |
| G02B05 | 21.62 | 52.61 | 0.537 | 4.961 | 0.11 | 2.43 | 542 | | 6 | | -47.8 | 1 |

| Sample | Hysteresis Properties | | | | | | Thermomagnetic Properties | | | | | |
|---|---|---|---|---|---|---|---|---|---|---|---|---|
| | $M_s$ (x $10^{-3}$ $Am^2/kg$) | $M_{rs}$ (x $10^{-3}$ $Am^2/kg$) | $H_c$ (mT) | $H_{cr}$ (mT) | $M_{rs}/M_s$ | $H_{cr}/H_c$ | $T_{c1}$ (°C) | $T_{c2}$ (°C) | $TMX_1$ | $TMX_2$ | % diff at 100°C | Type |
| G03A01 | 13.54 | 24.91 | 0.271 | 2.144 | 0.13 | 1.84 | 293 | 500 | 44 | 13 | 76.9 | 4 |
| G03A01B | 10.33 | 23.10 | 0.294 | 2.297 | 0.13 | 2.24 | 323 | 531 | 40 | 8 | 66.2 | 4 |
| G03A02 | 10.73 | 25.02 | 0.315 | 2.679 | 0.12 | 2.33 | 322 | 528 | 40 | 9 | 36.5 | 3b |
| G03A03 | 9.52 | 23.11 | 0.301 | 2.925 | 0.10 | 2.43 | 333 | 540 | 38 | 6 | 44.2 | 3b |
| G03A04 | 11.04 | 24.02 | 0.316 | 2.694 | 0.12 | 2.18 | 332 | 536 | 39 | 7 | 45.0 | 3c/4 |
| G03A05 | 11.52 | 23.79 | 0.316 | 2.389 | 0.13 | 2.07 | 337 | 532 | 38 | 8 | 68.7 | 4 |
| G03A06 | 11.66 | 23.44 | 0.325 | 2.407 | 0.14 | 2.01 | 344 | 532 | 37 | 8 | 60.2 | 3c/4 |
| G03A07 | 10.05 | 22.95 | 0.373 | 3.880 | 0.10 | 2.28 | 527 | | 9 | | 27.2 | 2 |
| G03A08 | 10.87 | 23.65 | 0.265 | 2.119 | 0.13 | 2.18 | 407 | 541 | 28 | 6 | 54.2 | 3c/4 |
| GD0100 | 10.58 | 27.08 | 0.346 | 3.326 | 0.10 | 2.56 | 578 | | 0 | | -11.2 | 1 |
| GD0101 | 17.52 | 35.85 | 0.521 | 4.602 | 0.11 | 2.05 | 563 | | 3 | | -19.6 | 1 |
| GD0102 | 14.18 | 35.69 | 0.409 | 4.438 | 0.09 | 2.52 | 581 | | -1 | | -33.3 | 1 |
| GD0103 | 12.96 | 27.71 | 0.317 | 3.145 | 0.10 | 2.14 | 576 | | 0 | | -16.7 | 1 |
| GD0104 | 7.15 | 22.15 | 0.171 | 2.516 | 0.07 | 3.10 | 571 | | 1 | | -8.9 | 1 |
| GD0105 | 12.45 | 27.47 | 0.288 | 3.278 | 0.09 | 2.21 | 522 | | 9 | | -28.6 | 1 |
| GD0106 | 7.35 | 21.29 | 0.186 | 2.233 | 0.08 | 2.90 | 492 | 563 | 14 | 3 | -9.4 | 1 |

Table C.12: Summary of hysteresis and thermomagnetic properties of individual samples from Guadeloupe. See Table C.1 for explanation of column headings and abbreviations. All measurements by Martin Gratton, analysis by the author.

| Sample | RS | Inflexion point temperatures (°C) | Type |
|---|---|---|---|
| G01A01 | 0.36 | | VI |
| G01A02 | 0.35 | | VI |
| G01A03 | 0.66 | | III |
| G01A04 | 0.69 | | III |
| G01A05 | 0.55 | | III |
| G01A06 | 0.61 | | III |
| G01A07 | 0.98 | | I |
| G01B01 | 0.72 | | III |
| G01B02 | 0.96 | -168 | I |
| G01B03 | 0.52 | | III |
| G01B04 | 0.80 | -155 | II |
| G01B05 | 0.83 | -165 | I |
| G01C01 | 0.86 | -50 | VII |
| G01C02 | 0.55 | | III |
| G01C03 | 0.65 | | VII |
| G01C04 | 0.73 | | VII |
| G01C05 | 0.60 | -40 | VII |
| G01C06 | 0.71 | -11 | II |
| G01C07 | 0.46 | | V |
| G01C08 | 0.60 | -39 | VII |
| G02A02 | 0.77 | | IV |
| G02A03 | 0.86 | | IV |
| G02A04 | 0.88 | | IV |
| G02A05 | 0.97 | -179 | II |
| G02A06 | 0.87 | -170 | IV |
| G02A07 | 0.73 | | IV |
| G02A08 | 1.08 | -176 | I |
| G02A09 | 0.99 | | I |
| G02B01 | 1.17 | -165 | I |
| G02B02 | 1.02 | -153 | I |
| G02B03 | 1.08 | | I |
| G02B04 | 0.82 | | IV |
| G02B05 | 1.06 | -175 | I |
| G03A01 | 0.37 | | V |
| G03A02 | 0.36 | | V |
| G03A03 | 0.35 | | V |
| G03A04 | 0.35 | | V |
| G03A05 | 0.40 | | V |
| G03A06 | 0.37 | | V |
| G03A07 | 0.34 | | V |
| G03A08 | 0.38 | | V |
| GD0100 | 0.62 | | V |
| GD0101 | 0.77 | | V |
| GD0102 | 1.03 | -180 | I |
| GD0103 | 0.58 | | IV |
| GD0104 | 0.50 | | V |
| GD0105 | 0.74 | | III |
| GD0106 | 0.51 | | V |

Table C.13: Low temperature susceptibility data from Guadeloupe, French West Indies. Experiments measured on a Bartington Instruments susceptibility meter. RS is the ratio of susceptibility at -195 (°C) to 10 (°C). Inflexion point temperatures and Type are discussed in Section 5.3.1. All measurements by Martin Gratton, data analysis by author.

| | *Thermomagnetic Curve Types* | | | | | | | | *χ Curve Types* | | | | | | | |
|---|---|---|---|---|---|---|---|---|---|---|---|---|---|---|---|---|
| Flow | 1 | 2 | 3a | 3b | 3c | 4 | 5a | 5b | i | ii | iii | iv | v | vi | vii | viii |
| G01 | 10 | 8 | | 2 | | | | | 3 | 2 | 7 | | 1 | 2 | 5 | |
| G02 | 13 | 1 | | | | | | | 6 | 1 | | 6 | | | | |
| G03 | | 1 | | 2 | 3 | 3 | | | | | | | 8 | | | |
| GD | 7 | | | | | | | | 1 | | 1 | 1 | 3 | | | |

Table C.14: Summary table of all Guadeloupe rock magnetic experiment types. Numbers are the number of individual experiments that were classified as a certain type. See Section 5.3.1 for details of thermomagnetic and $\chi$ curve types.

# Appendix D

# Palaeodirectional Results

| Sample | Flow Number | I (°) | D (°) | M.A.D (°) | Temp range (°C) | VGP Lat. (°) | VGP Long. (°) |
|---|---|---|---|---|---|---|---|
| ME30-3B | 30 | | | | | | |
| ME31-4B | 31 | | | | | | |
| ME32-4B | 32 | -31.6 | 167.0 | 3.8 | 350-525 | -73.4 | 30.8 |
| ME34-3A | 34 | -33.6 | 184.9 | 1.9 | 350-525 | -78.8 | 317.5 |
| ME35-5B | 35 | -41.4 | 187.3 | 5.1 | 450-525 | -81.8 | 287.1 |
| ME36-2A | 36 | -43.9 | 198.6 | 3.1 | 450-525 | -73.2 | 257.9 |
| ME37-1A | 37 | -1.3 | 168.0 | 3.4 | 350-525 | -59.7 | 6.4 |
| ME38-5A | 38 | -7.4 | 177.3 | 4.0 | 300-525 | -64.9 | 348.4 |
| ME39-5A | 39 | -12.7 | 180.5 | 6.1 | 400-525 | -67.8 | 340.7 |
| ME40-2A | 40 | -9.9 | 174.2 | 2.1 | 400-525 | -65.7 | 356.2 |
| ME41-1B | 41 | -7.9 | 166.3 | 3.8 | 400-525 | -62.1 | 12.4 |
| ME42-2B | 42 | -8.1 | 173.0 | 3.5 | 350-525 | -64.5 | 358.5 |
| ME43-4B | 43 | -9.3 | 169.2 | 5.7 | 450-525 | -63.9 | 7.2 |
| ME44-5B | 44 | -2.5 | 174.7 | 4.8 | 350-525 | -62.1 | 353.4 |
| ME45-1B | 45 | | | | | | |
| ME46-1A | 46 | | | | | | |
| ME47-4B | 47 | 25.1 | 20.0 | 2.5 | 350-525 | 65.8 | 107.7 |
| ME48-2A | 48 | 31.2 | 16.1 | 2.7 | 350-525 | 71.1 | 107.2 |
| ME49-2A | 49 | 32.0 | 26.8 | 2.9 | 400-525 | 62.9 | 90.9 |

Table D.1: Palaeodirection results for the MB reversal from the ME section, La Palma. Flow Number labels individual lava flows and is the number shown in any figure relating to palaeodirection or palaeointensity results. I is inclination; D is declination; M.A.D is maximum angular deviation (Kirschvink, 1980); Temp range is the temperature interval taken for the directional analysis of the primary component of magnetisation; End T is the final temperature step used for the analysis; Accept is whether the individual sample was included in the flow analysis; Flow I is the mean inclination; Flow D is the mean declination; $\alpha_{95}$ is the angular standard deviation (Fisher, 1953; Butler, 1992); $\kappa$ is the precision parameter (Butler, 1992); VGP Lat. is the virtual geomagnetic pole latitude and VGP Long. is the virtual geomagnetic pole longitude (Butler, 1992).

| Sample | Flow Number | I (°) | D (°) | M.A.D (°) | Temp range (°C) | Accept | Flow I (°) | Flow D (°) | $\alpha_{95}$ (°) | $\kappa$ | VGP Lat. (°) | VGP Long. (°) | $dm$ (°) | $dp$ (°) |
|---|---|---|---|---|---|---|---|---|---|---|---|---|---|---|
| AS27-1 | 31 | -19.8 | 157.8 | 4.2 | 200-525 | Y | | | | | | | | |
| AS27-2 | | -21.7 | 156.2 | 9.8 | 150-525 | Y | | | | | | | | |
| AS27-3 | | -33.6 | 157.8 | 4.4 | 450-525 | Y | | | | | | | | |
| AS27-4 | | -34.5 | 163.3 | 3.6 | 200-525 | Y | | | | | | | | |
| AS27-5 | | -29.4 | 161.9 | 8.4 | 150-525 | Y | -27.8 | 159.3 | 6.9 | 124.8 | -66.3 | 40.4 | 6.5 | 7.5 |
| AS26-1 | 30 | -32 | 193.5 | 4.1 | 400-525 | Y | -32 | 193.5 | | | -73.1 | 292.1 | | |
| AS25-1 | 29 | -4.7 | 205.3 | 5.4 | 250-525 | N | | | | | | | | |
| AS25-3 | | -33.3 | 161.6 | 4.5 | 0-525 | N | | | | | | | | |
| AS25-4 | | -28.9 | 198.3 | 2.0 | 150-525 | Y | | | | | | | | |
| AS25-5 | | -29.4 | 167.8 | 1.6 | 250-525 | N | | | | | | | | |
| AS25-6 | | -31.7 | 196.5 | 7.0 | 150-525 | Y | -30.3 | 197.4 | 7.0 | 1280.5 | -74.1 | 286.5 | 6.4 | 7.8 |
| AS24c-1 | 28 | -14 | 224.6 | 1.7 | 100-525 | N | | | | | | | | |
| AS24c-2 | | -44.6 | 170.8 | 7.4 | 350-525 | N | | | | | | | | |
| AS24c-3 | | -45.9 | 114 | 1.3 | 400-525 | N | | | | | | | | |
| AS24b-1 | 27 | -39.9 | 173.4 | 3.9 | 250-525 | Y | | | | | | | | |
| AS24b-2 | | -33.2 | 188.3 | 3.7 | 150-525 | Y | | | | | | | | |
| AS24b-3 | | -35.8 | 178.9 | 2.9 | 400-525 | Y | | | | | | | | |
| AS24b-4 | | -35.5 | 182.6 | 3.0 | 350-525 | Y | -36.2 | 181 | 6.5 | 197.9 | -81.3 | 336.3 | 5.8 | 7.6 |
| AS24-1 | 26 | | | | | | | | | | | | | |
| AS24-3 | | -38.9 | 179 | 5.5 | 350-525 | Y | | | | | | | | |
| AS24-4 | | -37.1 | 173.6 | 0.3 | 400-525 | Y | | | | | | | | |
| AS24-5 | | -39.5 | 170.1 | 17.3 | 350-525 | Y | | | | | | | | |
| AS24-6 | | -44.9 | 178.7 | 1.2 | 400-525 | Y | -40.2 | 175.3 | 5.3 | 298.8 | -82.7 | 19 | 4.8 | 6.4 |
| AS23-1 | 25 | -49.5 | 304.5 | 2.7 | 250-525 | Y | | | | | | | | |
| AS23-3 | | -59.6 | 292.7 | 5.4 | 400-525 | Y | | | | | | | | |
| AS23-4 | | -53.5 | 296.8 | 7.0 | 150-525 | Y | | | | | | | | |
| AS23-5 | | -67.2 | 294.3 | 3.1 | 250-525 | Y | -57.3 | 297.7 | 9.4 | 96.7 | 1.3 | 206.4 | 10.0 | 13.7 |
| AS22b-1 | 24 | -44.6 | 188.4 | 4.1 | 400-525 | Y | | | | | | | | |
| AS22b-2 | | -48.7 | 188.4 | 2.9 | 250-525 | Y | | | | | | | | |
| AS22b-3 | | -46.5 | 188.3 | 4.2 | 100-525 | Y | | | | | | | | |
| AS22b-4 | | -35.8 | 178.9 | 2.9 | 400-525 | Y | | | | | | | | |
| AS22b-5 | | -41.9 | 182.3 | 8.5 | 150-525 | Y | -43.6 | 185 | 5.6 | 185.3 | -84.4 | 288.1 | 5.1 | 7.0 |
| AS21-1 | 23 | -28.7 | 159.8 | 8.2 | 350-525 | Y | | | | | | | | |
| AS21-2 | | -29.5 | 158.3 | 9.5 | 250-525 | Y | | | | | | | | |
| AS21-3 | | -28 | 159.3 | 2.9 | 250-525 | Y | -28.7 | 158.8 | 1.3 | 8692.2 | -66.2 | 42.2 | 1.2 | 1.4 |
| AS21-4 | | | | | | | | | | | | | | |
| AS21-5 | | | | | | | | | | | | | | |
| AS20-1 | 22 | | | | | | | | | | | | | |
| AS20-2 | | -13.1 | 161 | 2.5 | 450-525 | Y | | | | | | | | |
| AS20-3 | | -17.3 | 157.3 | 4.3 | 300-525 | Y | | | | | | | | |
| AS20-4 | | -15.5 | 161 | 4.0 | 400-525 | Y | -15.3 | 159.8 | 4.5 | 758 | -61.6 | 28.4 | 5.2 | 4.6 |

| Sample | Flow Number | I (°) | D (°) | M.A.D (°) | Temp range (°C) | Accept | Flow I (°) | Flow D (°) | $\alpha_{95}$ (°) | $\kappa$ | VGP Lat. (°) | VGP Long. (°) | $dm$ (°) | $dp$ (°) |
|---|---|---|---|---|---|---|---|---|---|---|---|---|---|---|
| AS19b-1 | 21 | | | | | | | | | | | | | |
| AS19b-2 | | -21.2 | 153.9 | 4.3 | 400-525 | Y | -21.2 | 153.9 | | | -59.9 | 41.3 | | |
| AS19b-4 | | | | | | | | | | | | | | |
| AS19-1 | 20 | -22.7 | 166.2 | 5.1 | 350-500 | Y | | | | | | | | |
| AS19-3 | | -18.3 | 150.4 | 7.8 | 400-525 | Y | | | | | | | | |
| AS19-4 | | -16.2 | 157.3 | 6.7 | 400-525 | Y | | | | | | | | |
| AS19-5 | | -19.2 | 159.2 | 8.1 | 450-525 | Y | -19.2 | 158.2 | 7.6 | 147.2 | -62.2 | 33.8 | 8.0 | 7.9 |
| AS18-1 | 19 | | | | | | | | | | | | | |
| AS18-2 | | | | | | | | | | | | | | |
| AS18-3 | | | | | | | | | | | | | | |
| AS18-4 | | | | | | | | | | | | | | |
| AS17-1 | 18 | 52.7 | 274.5 | 2.5 | 300-500 | Y | 52.7 | 274.5 | | | 18.7 | 280.6 | | |
| AS16b-1 | 17 | | | | | | | | | | | | | |
| AS16-1 | 16 | | | | | | | | | | | | | |
| AS16-2 | | | | | | | | | | | | | | |
| AS16-3 | | | | | | | | | | | | | | |
| AS16-4 | | | | | | | | | | | | | | |
| AS16-5 | | | | | | | | | | | | | | |
| AS15-1 | 15 | 42 | 17 | 7.4 | 350-500 | Y | | | | | | | | |
| AS15-2 | | 46.9 | 351.1 | 2.6 | 350-550 | Y | | | | | | | | |
| AS15-3 | | 43 | 3.4 | 5.3 | 350-550 | Y | 44.5 | 4.2 | 14.8 | 70.7 | 85.4 | 107.1 | 13.5 | 18.6 |
| AS14-1 | 14 | 32.7 | 358.7 | 6.6 | 350-550 | Y | | | | | | | | |
| AS14-2 | | 32.6 | 41.7 | 5.9 | 350-550 | N | | | | | | | | |
| AS14-3 | | 35.6 | 2.1 | 2.1 | 350-550 | Y | 34.2 | 0.4 | 8.8 | 804.6 | 79.9 | 160.2 | 7.9 | 10.1 |
| AS13-1 | 13 | 48.7 | 344.1 | 1.3 | 400-550 | Y | | | | | | | | |
| AS13-2 | | 52.3 | 351.8 | 2.3 | 400-550 | Y | | | | | | | | |
| AS13-3 | | 43.6 | 18.3 | 5.3 | 350-500 | N | | | | | | | | |
| AS13-4 | | 35 | 350 | 15.7 | 350-550 | N | | | | | | | | |
| AS13-5 | | 52.6 | 52.6 | 2.4 | 350-550 | Y | 51.4 | 352.5 | 8.9 | 193.4 | 82.5 | 280 | 8.7 | 12.1 |
| AS12-1 | 12 | 12.3 | 6.9 | 3.0 | 350-550 | Y | | | | | | | | |
| AS12-2 | | 8.2 | 20.2 | 4.3 | 350-550 | Y | | | | | | | | |
| AS12-3 | | 13.2 | 10.4 | 11.1 | 400-550 | Y | | | | | | | | |
| AS12-4 | | 5 | 22.6 | 11.2 | 400-550 | Y | 9.7 | 15.1 | 9.5 | 93.9 | 62.2 | 128.5 | 12.7 | 9.6 |

Table D.2: Palaeodirection results from the AS section, La Palma. Flow Number 31 is the lowest strigraphic unit. Where no result is shown it was not possible to determine a primary component of magnetisation. Flow I is the mean inclination; Flow D is the mean declination; $\alpha_{95}$ is the angular standard deviation (Fisher, 1953; Butler, 1992); $\kappa$ is the precision parameter (Butler, 1992); VGP Lat. is the virtual geomagnetic pole latitude and VGP Long. is the virtual geomagnetic pole longitude (Butler, 1992); $dm$ is the confidence limit for VGP latitude and$dp$ is the confidence limit for VGP longitude (Butler, 1992). See Table D.1 for explanation of other column headings. All measurements Martin Gratton, analysis the author.

| Sample | Flow Number | I (°) | D (°) | M.A.D (°) | Temp range (°C) | Accept | Flow I (°) | Flow D (°) | $\alpha_{95}$ (°) | $\kappa$ | VGP Lat. (°) | VGP Long. (°) | $dm$ (°) | $dp$ (°) |
|---|---|---|---|---|---|---|---|---|---|---|---|---|---|---|
| AN1-1 | 1 | | | | | | | | | | | | | |
| AN1-2 | | -30.3 | 162.4 | 3.6 | 100-525 | Y | | | | | | | | |
| AN1-3 | | -31 | 169.1 | 2.6 | 100-525 | Y | | | | | | | | |
| AN1-4 | | -37.9 | 172.5 | 3.2 | 100-525 | Y | | | | | | | | |
| AN1-5 | | -41 | 162.0 | 2.4 | 250-525 | Y | -35.1 | 167 | 7.6 | 146 | -74.5 | 37.8 | 6.8 | 8.8 |
| AN2-1 | 2 | -23.3 | 191.9 | 0.7 | 450-525 | Y | | | | | | | | |
| AN2-2 | | -17.4 | 192.2 | 2.9 | 400-525 | Y | -20.3 | 192 | | | -68.5 | 308.2 | | |
| AN3-1 | 3 | -20.8 | 186.0 | 2.8 | 350-525 | Y | | | | | | | | |
| AN3-3 | | -14.2 | 187.4 | 2.4 | 350-525 | Y | -17.5 | 187 | | | -69.2 | 322.3 | | |
| AN4-1 | 4 | | | | | | | | | | | | | |
| AN4-2 | | | | | | | | | | | | | | |
| AN4-3 | | 18.4 | 202.3 | 3.7 | 450-550 | Y | | | | | | | | |
| AN4-4 | | 14.3 | 207.1 | 3.5 | 450-550 | Y | | | | | | | | |
| AN4-5 | | 10 | 203.5 | 2 | 450-550 | Y | 14.2 | 204 | 7.4 | 280 | -47 | 305.4 | 8.7 | 7.6 |
| AN6-1 | 6 | | | | | | | | | | | | | |
| AN6-2 | | | | | | | | | | | | | | |
| AN6-3 | | | | | | | | | | | | | | |
| AN6-4 | | | | | | | | | | | | | | |
| AN6-5 | | -74.6 | 174.1 | 3.6 | 350-500 | Y | -74.6 | 174 | | | -57.4 | 156.9 | | |
| AN7-1 | 7 | 31.2 | 9.0 | 2.4 | 400-525 | Y | | | | | | | | |
| AN7-2 | | 33.2 | 3.4 | 3.1 | 400-525 | Y | | | | | | | | |
| AN7-3 | | 34.3 | 4.8 | 2.5 | 400-525 | Y | | | | | | | | |
| AN7-4 | | 34.3 | 7.5 | 3.2 | 0-525 | Y | 33.3 | 6 | 2.9 | 984 | 77.9 | 132.8 | 2.6 | 3.3 |
| AN8-1 | 8 | 46 | 2.3 | 2.7 | 0-525 | Y | | | | | | | | |
| AN8-2 | | 50.5 | 1.8 | 3.4 | 0-525 | Y | | | | | | | | |
| AN8-3 | | -17.7 | 187.4 | 4.9 | 0-525 | N | 49.7 | 3 | | | 86.6 | 42.1 | | |
| AN9a-1 | 9 | 57.4 | 2.6 | 5 | 150-525 | Y | | | | | | | | |
| AN9a-2 | | 59.9 | 3.2 | 2.9 | 350-525 | Y | | | | | | | | |
| AN9a-3 | | 58.3 | 356.1 | 5 | 150-525 | Y | | | | | | | | |
| AN9a-4 | | 56.1 | 5.8 | 0.6 | 450-525 | Y | 58 | 2 | 3.1 | 891 | 80 | 351.2 | 3.3 | 4.6 |
| AN9b-1 | 10 | 54.9 | 2.2 | 3.1 | 100-525 | Y | | | | | | | | |
| AN9b-2 | | 59.2 | 359.6 | 4.1 | 100-525 | Y | | | | | | | | |
| AN9b-3 | | 56.2 | 355.9 | 6 | 100-525 | Y | | | | | | | | |
| AN9b-4 | | 51.8 | 314.5 | 4.4 | 400-525 | N | 56.8 | 359 | 4.3 | 825 | 81.4 | 338.3 | 4.5 | 6.2 |

| Sample | Flow Number | I (°) | D (°) | M.A.D (°) | Temp range(°C) | Accept | Flow I (°) | Flow D (°) | $\alpha_{95}$ (°) | $\kappa$ | VGP Lat. (°) | VGP Long. (°) | $dm$ (°) | $dp$ (°) |
|---|---|---|---|---|---|---|---|---|---|---|---|---|---|---|
| AN10-1 | 11 | | | | | | | | | | | | | |
| AN10-2 | | 30.9 | 5.6 | 3.9 | 100-550 | Y | | | | | | | | |
| AN10-3 | | 27.3 | 6.1 | 6.8 | 200-550 | Y | 29.1 | 6 | | | 75.7 | 138.8 | 7.3 | 8.7 |
| AN11-1 | 12 | 31.6 | 1.7 | 3 | 0-525 | Y | | | | | | | | |
| AN11-2 | | 29.6 | 2.3 | 3.4 | 100-525 | Y | | | | | | | | |
| AN11-3 | | 31.1 | 6.1 | 3 | 100-525 | Y | | | | | | | | |
| AN11-4 | | 39.2 | 10.6 | 1.6 | 200-400 | Y | 32.9 | 5 | 6.2 | 219 | 78.2 | 138.1 | 5.6 | 7.0 |
| AN12-1 | 13 | 29.3 | 354.7 | 2.1 | 350-550 | Y | | | | | | | | |
| AN12-2 | | 27.5 | 355.6 | 1.3 | 450-550 | Y | | | | | | | | |
| AN12-3 | | 36.4 | 356.3 | 2.4 | 450-550 | Y | 31.1 | 356 | 7.2 | 291 | 77.3 | 182.1 | 6.6 | 8.1 |
| AN12-4 | | | | | | | | | | | | | | |
| AN13-1 | 14 | 27.2 | 6.4 | 5 | 350-550 | Y | | | | | | | | |
| AN13-2 | | 29.7 | 9.4 | 4.1 | 150-550 | Y | | | | | | | | |
| AN13-3 | | 39.7 | 5.8 | 3.5 | 250-550 | Y | | | | | | | | |
| AN13-4 | | 34.1 | 6.7 | 3.2 | 350-550 | Y | 32.7 | 7 | 6.4 | 206 | 77.1 | 130.1 | | |
| AN14-1 | 15 | 23.5 | 4.2 | 2.2 | 350-550 | Y | | | | | | | | |
| AN14-2 | | 43.8 | 342.7 | 3.7 | 300-550 | Y | 34.1 | 355 | | | 78.8 | 188.8 | | |
| AN15-1 | 16 | 27.4 | 9.3 | 1.3 | 350-550 | Y | | | | | | | | |
| AN15-2 | | 18.9 | 5.3 | 1.5 | 300-550 | Y | 23.2 | 7 | | | 72 | 138.0 | | |
| AN16-2 | 17 | | | | | | | | | | | | | |
| AN16-3 | | 17 | 7.3 | 0.3 | 500-550 | Y | 17 | 7 | | | 68.8 | 142.2 | | |

Table D.3: Palaeodirection results for the MB reversal from the AN section, La Palma. Where no result is shown it was not possible to determine a primary component of magnetisation. See Table D.2 for explanation of column headings. All measurements by Martin Gratton, analysis by the author.

| Sample | Flow Number | I (°) | D (°) | M.A.D (°) | Temp range (°C) | Accept | Flow I (°) | Flow D (°) | $\alpha_{95}$ (°) | $\kappa$ | VGP Lat. (°) | VGP Long. (°) | $dm$ (°) | $dp$ (°) |
|---|---|---|---|---|---|---|---|---|---|---|---|---|---|---|
| GD0100* | 1 | -27.6 | 144.2 | 2.7 | 0-350 | Y | | | | | | | | |
| GD0101* | | -26.9 | 161.3 | 4.3 | 100-350 | Y | | | | | | | | |
| GD0102* | | -33.4 | 181.3 | 5.2 | 100-350 | Y | | | | | | | | |
| GD0103* | | -31.8 | 168.8 | 5.1 | 100-350 | Y | | | | | | | | |
| GD0104* | | -29.1 | 170.4 | 5.7 | 150-350 | Y | | | | | | | | |
| GD0105* | | -28.4 | 177.4 | 4.1 | 150-350 | Y | | | | | | | | |
| GD0106* | | -38.5 | 178.2 | 2.9 | 0-350 | Y | -31.4 | 168.6 | 8.8 | 47.8 | -79 | 35.1 | 8.0 | 9.9 |
| G01A01 | 2 | 10.1 | 233.5 | 3.5 | 300-540 | Y | | | | | | | | |
| G01A04 | | 19.7 | 266.5 | 5.2 | 250-520 | Y | | | | | | | | |
| G01A06 | | 12.9 | 90.8 | 2.6 | 300-520 | N | | | | | | | | |
| G01B02 | | -15.8 | 222.5 | 6.5 | 200-520 | N | | | | | | | | |
| G01C02 | | 9.2 | 257.7 | 3.8 | 300-450 | Y | | | | | | | | |
| G01C07 | | 6.3 | 255.4 | 4.8 | 200-520 | Y | 11.6 | 253.2 | 17.1 | 29.9 | -14.4 | 218.8 | 21.6 | 17.4 |
| G02A01 | 3 | -47.7 | 174.8 | 16.7 | 400-540 | N | | | | | | | | |
| G02A03 | | -67.4 | 188 | 4.9 | 300-520 | Y | | | | | | | | |
| G02A04 | | -53.5 | 193.2 | 8.3 | 250-520 | Y | | | | | | | | |
| G02A06 | | -76.9 | 249.2 | 8.2 | 250-520 | Y | | | | | | | | |
| G02A07 | | -55.4 | 186.4 | 3.6 | 250-520 | Y | | | | | | | | |
| G02A08 | | -50.8 | 175.8 | 2.7 | 200-520 | Y | | | | | | | | |
| G02B04 | | -66.2 | 200.4 | 7.1 | 250-520 | Y | | | | | | | | |
| G02B05 | | -56.4 | 193.4 | 4.8 | 250-520 | Y | -61.9 | 192.3 | 9.5 | 40.9 | -61 | 136.9 | 11.1 | 14.7 |
| G03A01 | 4 | -8.9 | 0.2 | 2.4 | 200-520 | N | | | | | | | | |
| G03A03 | | 22.3 | 351.3 | 4 | 100-540 | Y | | | | | | | | |
| G03A05 | | 23.2 | 356.6 | 3.1 | 200-520 | Y | | | | | | | | |
| G03A07 | | 24 | 351.4 | 2.2 | 200-520 | Y | | | | | | | | |
| G03A08 | | 27.1 | 356.1 | 2.5 | 200-520 | Y | 24.2 | 353.8 | 3.8 | 579.5 | 83.1 | 179.1 | 3.7 | 4.1 |

Table D.4: Palaeodirection results for the MB reversal from Guadeloupe, French West Indies. See Table D.2 for explanation of column headings. $*$ indicates experiments performes by Martin Gratton. All analysis by the author.

# Appendix E

# Palaeointensity Results

| Sample | Flow Number | Demag | Protocol | $F_{lab}$ | $n/N$ | $f$ | $g$ | $\beta$ | $q$ | $r^2$ | $pT_{M}RM$ Check | Tail Check | $F$ ($\mu T$) | uncert ($\mu T$) | Class |
|---|---|---|---|---|---|---|---|---|---|---|---|---|---|---|---|
| ME32-1B1 | 32 | Y | Perp | 40 | 7/7 | 0.47 | 0.64 | 0.06 | 5.18 | 0.983 | 1/1 | 1/1 | 37.5 | 7.2 | 2 |
| ME32-2B1 | | Y | Perp | 20 | 7/9 | 0.54 | 0.74 | 0.08 | 5.16 | 0.971 | 2/3 | 2/3 | 43.9 | 8.5 | 3 |
| ME32-4B1 | | Y | Perp | 10 | 6/6 | 0.60 | 0.49 | 0.03 | 10.22 | 0.997 | 2/2 | 0/2 | 47.7 | 4.7 | 2 |
| ME32-4B2 | | Y | Perp | 20 | 0/7 | | | | | | | | | | |
| ME32-4B3 | | Y | Perp | 20 | 0/8 | | | | | | | | | | |
| ME32-4B4 | | Y | Perp | 40 | 5/5 | 0.25 | 0.52 | 0.04 | 3.01 | 0.994 | 1/1 | 1/1 | 46.3 | 15.4 | 3 |
| ME32-5B1 | | Y | Perp | 40 | 6/6 | 0.58 | 0.33 | 0.01 | 19.72 | 1.000 | 2/2 | 2/2 | 23.3 | 1.2 | 1 |
| ME32-5B2 | | Y | Perp | 40 | 7/9 | 0.73 | 0.62 | 0.03 | 14.00 | 0.995 | 1/3 | 2/3 | 31.7 | 2.3 | 2 |
| ME32-5B3 | | Y | Perp | 40 | 4/4 | 0.35 | 0.29 | 0.04 | 2.46 | 0.997 | 0/0 | 0/0 | 22.0 | 8.9 | 3 |
| ME33-2A1 | 33 | Y | Perp | 10 | 0/5 | | | | | | | | | | |
| ME33-5B1 | | Y | Perp | 20 | 0/5 | | | | | | | | | | |
| ME34-4B1 | 34 | N | | | | | | | | | | | | | |
| ME35-5B1 | 35 | N | | | | | | | | | | | | | |
| ME36-1B1 | 36 | Y | Perp | 10 | 4/7 | 0.44 | 0.59 | 0.03 | 8.43 | 0.998 | 0/1 | 0/1 | 16.4 | 1.9 | 2 |
| ME36-2B1 | | N | Coe | | | | | | | | | | | | |
| ME36-3B1 | | Y | Perp | 10 | 8/11 | 0.28 | 0.81 | 0.07 | 3.25 | 0.970 | 2/3 | 3/3 | 9.5 | 2.7 | 3 |
| ME36-4B1 | | Y | Perp | 40 | 8/11 | 0.13 | 0.78 | 0.07 | 1.32 | 0.967 | 4/4 | 4/4 | 10.4 | 7.9 | 3 |
| ME36-5B1 | | N | Coe | | | | | | | | | | | | |
| ME37-1B1 | 37 | N | | | | | | | | | | | | | |
| ME38-1B1 | 38 | Y | Perp | 40 | 0/10 | | | | | | | | | | |
| ME39-4A1 | 39 | Y | Perp | 15 | 3/5 | 0.04 | 0.40 | 0.11 | 0.17 | 0.989 | 0/1 | 1/1 | 10.6 | 63.2 | 3 |
| ME39-6C1 | | Y | Perp | 40 | 6/7 | 0.73 | 0.45 | 0.03 | 11.76 | 0.997 | 2/2 | 2/2 | 15.8 | 1.3 | 3 |
| ME39-6C2 | | N | Coe | | | | | | | | | | | | |
| ME39-6C3 | | Y | Perp | 40 | 5/5 | 0.43 | 0.01 | 0.07 | 0.08 | 0.987 | 1/1 | 1/1 | 9.7 | 123.0 | 3 |
| ME39-6C4 | | Y | Perp | 10 | 4/4 | 0.15 | 0.57 | 0.03 | 2.78 | 0.998 | 0/0 | 0/0 | 9.0 | 3.2 | 3 |
| ME40-1A1 | 40 | Y | Perp | 10 | 9/9 | 0.59 | 0.72 | 0.03 | 14.09 | 0.993 | 2/3 | 3/3 | 13.0 | 0.9 | 2 |
| ME40-2B1 | | Y | Perp | 10 | 12/12 | 0.59 | 0.80 | 0.06 | 7.94 | 0.964 | 4/5 | 5/5 | 8.5 | 1.1 | 3 |
| ME40-3A1 | | Y | Perp | 10 | 11/11 | 0.68 | 0.86 | 0.02 | 31.27 | 0.997 | 5/5 | 4/5 | 8.2 | 0.3 | 2 |
| ME40-3A2 | | Y | Perp | 10 | 8/11 | 0.29 | 0.77 | 0.07 | 3.12 | 0.969 | 3/4 | 3/4 | 10.9 | 3.5 | 3 |
| ME40-4A1 | | Y | Perp | 40 | 0/11 | | | | | | | | | | |
| ME40-4A2 | | N | Coe | | | | | | | | | | | | |
| ME40-4A3 | | Y | Perp | 10 | 11/11 | 0.70 | 0.82 | 0.03 | 18.98 | 0.991 | 4/4 | 4/4 | 9.7 | 0.5 | 1 |
| ME40-5A1 | | N | Coe | | | | | | | | | | | | |
| ME40-5B1 | | Y | Perp | 15 | 9/10 | 0.50 | 0.68 | 0.03 | 13.43 | 0.996 | 3/4 | 3/4 | 11.3 | 0.8 | 2 |
| ME41-4A1 | 41 | Y | Perp | 10 | 0/4 | | | | | | | | | | |

| Sample | Flow Number | Demag | Protocol | $F_{lab}$ | $n/N$ | $f$ | $g$ | $\beta$ | $q$ | $r^2$ | $pT_M RM$ Check | Tail Check | $F$ ($\mu T$) | uncert ($\mu T$) | Class |
|---|---|---|---|---|---|---|---|---|---|---|---|---|---|---|---|
| ME42-2A1 | 42 | Y | Perp | 10 | 5/5 | 0.66 | 0.65 | 0.01 | 32.43 | 0.999 | 1/2 | 2/2 | 13.5 | 0.4 | 2 |
| ME42-3A1 | | Y | Perp | 10 | 7/7 | 0.84 | 0.77 | 0.04 | 17.02 | 0.993 | 0/2 | 2/2 | 14.6 | 0.9 | 2 |
| ME42-3A2 | | Y | Perp | 10 | 5/5 | 0.76 | 0.74 | 0.02 | 24.15 | 0.998 | 0/2 | 2/2 | 17.1 | 0.7 | 2 |
| ME42-5B1 | | Y | Perp | 40 | 0/11 | | | | | | | | | | |
| ME42-5B2 | | N | Coe | | | | | | | | | | | | |
| ME42-5B3 | | Y | Perp | 40 | 7/7 | 0.50 | 0.77 | 0.04 | 10.77 | 0.994 | 3/4 | 4/4 | 17.9 | 1.7 | 2 |
| ME43-5B1 | 43 | N | | | | | | | | | | | | | |
| ME44-2B1 | 44 | Y | Perp | 40 | 5/5 | 0.38 | 0.71 | 0.14 | 1.94 | 0.944 | 0/2 | 2/2 | 20.6 | 10.6 | 3 |
| ME44-2B2 | | Y | Perp | 40 | 4/4 | 0.48 | 0.53 | 0.00 | 59.56 | 1.000 | 0/1 | 1/1 | 13.1 | 0.2 | 2 |
| ME44-2B3 | | Y | Perp | 40 | 5/7 | 0.15 | 0.59 | 0.08 | 1.09 | 0.980 | 0/3 | 3/3 | 13.3 | 12.2 | 3 |
| ME45-1B1 | 45 | N | | | | | | | | | | | | | |
| ME46-4B1 | 46 | N | | | | | | | | | | | | | |
| ME47-1A1 | 47 | Y | Perp | 40 | 0/4 | | | | | | | | | | |
| ME47-1A2 | | Y | Quasi | 30 | 0/3 | | | | | | | | | | |
| ME47-2A1 | | Y | Perp | 40 | 8/8 | 0.59 | 0.59 | 0.01 | 55.05 | 1.000 | 2/2 | 2/2 | 40.3 | 0.7 | 1 |
| ME47-2A2 | | Y | Perp | 40 | 3/3 | 0.22 | 0.03 | 0.01 | 0.10 | 0.997 | 0/0 | 0/1 | 32.9 | 313.2 | 3 |
| ME47-2A3 | | Y | Coe | 40 | 5/6 | 0.77 | 0.50 | 0.02 | 15.76 | 0.998 | 1/2 | 1/2 | 50.7 | 3.2 | 2 |
| ME47-2A4 | | Y | Coe | 20 | 6/7 | 0.62 | 0.66 | 0.06 | 7.04 | 0.986 | 2/2 | 0/2 | 37.5 | 5.3 | 2 |
| ME47-2B1 | | Y | Perp | 40 | 5/5 | 0.70 | 0.58 | 0.05 | 8.11 | 0.994 | 2/2 | 2/2 | 28.8 | 3.5 | 1 |
| ME47-3A1 | | Y | Perp | 40 | 9/9 | 0.43 | 0.74 | 0.04 | 8.01 | 0.989 | 0/3 | 0/3 | 17.9 | 2.2 | 3 |
| ME47-4A1 | | Y | Perp | 40 | 5/8 | 0.31 | 0.62 | 0.05 | 4.81 | 0.995 | 1/1 | 1/1 | 50.2 | 10.4 | 3 |
| ME47-4A2 | | Y | Perp | 40 | 11/11 | 0.75 | 0.80 | 0.02 | 36.72 | 0.998 | 4/4 | 4/4 | 53.4 | 1.6 | 1 |
| ME47-4A3 | | Y | Perp | 30 | 7/7 | 0.28 | 0.69 | 0.01 | 13.23 | 0.988 | 1/2 | 1/2 | 31.6 | 2.4 | 3 |
| ME47-4A4 | | Y | Coe | 20 | 5/5 | 0.21 | 0.64 | 0.01 | 1.91 | 0.985 | 0/2 | 0/2 | 22.4 | 11.7 | 3 |
| ME48-1B1 | 48 | Y | Perp | 40 | 11/11 | 0.79 | 0.78 | 0.01 | 72.07 | 0.994 | 4/4 | 1/4 | 34.6 | 0.5 | 2 |
| ME48-1B2 | | Y | Perp | 40 | 6/6 | 0.41 | 0.56 | 0.02 | 13.83 | 0.999 | 2/2 | 2/2 | 31.2 | 2.3 | 1 |
| ME48-1B3 | | Y | Quasi | 30 | 6/11 | 0.56 | 0.50 | 0.02 | 13.86 | 0.998 | N/A | N/A | 36.2 | 2.6 | 2 |
| ME48-1B4 | | Y | Quasi | 30 | 6/9 | 0.82 | 0.68 | 0.02 | 31.99 | 0.999 | N/A | N/A | 41.5 | 1.3 | 2 |
| ME48-2A1 | | Y | Perp | 40 | 13/14 | 0.84 | 0.77 | 0.01 | 41.20 | 0.999 | 4/5 | 1/5 | 35.4 | 0.9 | 2 |
| ME48-2A2 | | Y | Perp | 40 | 7/7 | 0.21 | 0.76 | 0.06 | 2.86 | 0.985 | 1/1 | 1/1 | 46.9 | 16.9 | 3 |
| ME48-2A3 | | Y | Coe | 40 | 7/7 | 0.39 | 0.59 | 0.03 | 7.00 | 0.995 | 3/3 | 1/3 | 24.8 | 3.5 | 3 |
| ME48-2A4 | | Y | Perp | 40 | 6/6 | 0.71 | 0.71 | 0.03 | 19.23 | 0.997 | 1/2 | 0/2 | 43.9 | 2.3 | 2 |
| ME48-2A5 | | Y | Perp | 40 | 7/17 | 0.04 | 0.81 | 0.07 | 0.51 | 0.978 | 3/3 | 1/3 | 46.1 | 89.6 | 3 |
| ME48-3A1 | | Y | Perp | 40 | 13/13 | 0.20 | 0.86 | 0.41 | 4.22 | 0.981 | 0/1 | 0/1 | 38.5 | 9.1 | 3 |
| ME48-3A2 | | Y | Perp | 40 | 9/9 | 0.76 | 0.69 | 0.02 | 22.57 | 0.996 | 1/1 | 1/1 | 47.4 | 2.1 | 2 |
| ME48-3A3 | | Y | Perp | 30 | 11/11 | 0.69 | 0.58 | 0.04 | 10.75 | 0.988 | 5/6 | 0/5 | 31.7 | 2.9 | 2 |
| ME48-4A1 | | Y | Perp | 40 | 5/6 | 0.72 | 0.39 | 0.03 | 8.00 | 0.996 | 0/1 | 0/1 | 61.7 | 7.7 | 3 |
| ME48-4A2 | | Y | Perp | 40 | 11/11 | 0.10 | 0.81 | 0.04 | 2.29 | 0.988 | 2/2 | 0/2 | 60.0 | 26.2 | 3 |

| Sample | Flow Number | Demag | Protocol | $F_{lab}$ | $n/N$ | $f$ | $g$ | $\beta$ | $q$ | $r^2$ | $pT_MRM$ Check | Tail Check | $F$ ($\mu T$) | uncert ($\mu T$) | Class |
|---|---|---|---|---|---|---|---|---|---|---|---|---|---|---|---|
| ME49-1A1 | 49 | Y | Perp | 40 | 7/7 | 0.44 | 0.71 | 0.06 | 4.94 | 0.980 | 1/3 | 2/3 | 17.9 | 3.6 | 3 |
| ME49-2B1 | | Y | Perp | 40 | 14/14 | 0.48 | 0.78 | 0.02 | 16.58 | 0.994 | 5/6 | 2/6 | 37.1 | 2.2 | 2 |
| ME49-2B2 | | Y | Coe | 40 | 5/6 | 0.14 | 0.57 | 0.11 | 0.75 | 0.964 | 1/2 | 1/2 | 16.1 | 21.4 | 3 |
| ME49-2B3 | | Y | Quasi | 30 | 6/6 | 0.91 | 0.79 | 0.06 | 12.62 | 0.987 | N/A | N/A | 53.0 | 4.2 | 2 |
| ME49-2B4 | | Y | Quasi | 30 | 7/8 | 0.95 | 0.82 | 0.03 | 27.69 | 0.996 | N/A | N/A | 42.4 | 1.5 | 2 |
| ME49-3A1 | | Y | Perp | 40 | 7/7 | 0.81 | 0.33 | 0.05 | 5.75 | 0.992 | 2/2 | 0/2 | 33.6 | 5.8 | 3 |
| ME49-3A2 | | Y | Perp | 15 | 7/7 | 0.60 | 0.47 | 0.04 | 7.06 | 0.994 | 2/2 | 1/2 | 27.6 | 3.9 | 3 |
| ME49-4A1 | | Y | Perp | 30 | 0/6 | | | | | | | | | | |
| ME49-5A1 | | Y | Perp | 30 | 15/17 | 0.47 | 0.90 | 0.03 | 14.10 | 0.988 | 4/6 | 0/6 | 14.7 | 1.0 | 3 |

Table E.1: Individual microwave palaeointensity results from the ME section, La Palma. Flow Number labels individual lava flows and is the number shown in any figure relating to palaeodirection or palaeointensity results. Flows are in stratigraphic order in ascending number from oldest to youngest (32-49). Demag indicates whether it was possible to resolve a primary component of magnetisation large enough to perform a palaeointensity experiment. Protocol is the experimental design chosen (protocols are explaned in Section 3.4): Perp is the perpendicular applied field method (Kono & Ueno, 1977; Hill & Shaw, 2007); Coe is the double heating-method of Coe (1967a); Quasi is the quasi-perpendicular applied method (Biggin et al., 2007b). $F_{lab}$ is the laboratory applied field. $n/N$ is the number of accpeted NRM-$T_M$RM points against the total number of NRM-$T_M$RM points determined from the palaeointensity experiment. $f$, $g$, $\beta$ and $q$ are Coe et al. (1978) quality statistics (see Section 3.4.7 for explanation of individual statistics). $r^2$ is square of the correlation coefficent (discusssed in Section 3.4.8). $pT_MRM$ Check and Tail Check (explained in Section 3.4.6) columns show the number of checks that passed the selection criterion against the total number of checks relating to NRM-$T_M$RM points accepted for palaeointensity determination. $F$ is the palaeointensity determination; uncert is the uncertainty of the individual palaeointensity determination using $(1/q)F$ (Coe et al., 1978); Class is explained in Section 3.4.8. b

| Sample | Flow Number | Demag | Protocol | $F_{lab}$ | $n/N$ | $f$ | $g$ | $\beta$ | $q$ | $r^2$ | pTRM Check | Tail Check | $F$ ($\mu T$) | uncert ($\mu T$) | Class |
|---|---|---|---|---|---|---|---|---|---|---|---|---|---|---|---|
| AS25-5B1 | 29 | Y | Coe | 20 | 0/12 | | | | | | | | | | |
| AS24C-4B1 | 28 | Y | Coe | 20 | 0/17 | | | | | | | | | | |
| AS24C-4B2 | | Y | Perp | 20 | 0/4 | | | | | | | | | | |
| AS24C-4B3 | | Y | Perp | 20 | 15/15 | 0.90 | 0.47 | 0.02 | 28.45 | 0.993 | 5/5 | 5/5 | 35.4 | 0.9 | 1 |
| AS24C-4B4 | | Y | Perp | 20 | 0/24 | | | | | | | | | | |
| AS24B-1A1 | 27 | Y | Coe | 20 | 0/11 | | | | | | | | | | |
| AS23-5B1 | 25 | N | | | | | | | | | | | | | |
| AS22B-2B1 | 24 | Y | Perp | 20 | 11/18 | 0.32 | 0.87 | 0.03 | 7.90 | 0.989 | 3/4 | 1/4 | 16.0 | 2.0 | 3 |
| AS22B-3B1 | | Y | Coe | 20 | 7/7 | 0.39 | 0.78 | 0.07 | 4.50 | 0.977 | 1/3 | 3/3 | 15.8 | 3.5 | 3 |
| AS22B-3B2 | | Y | Coe | 10 | 15/15 | 0.85 | 0.91 | 0.02 | 36.37 | 0.994 | 7/7 | 2/7 | 19.4 | 0.5 | 2 |
| AS22B-3B3 | | Y | Perp | 20 | 0/10 | | | | | | | | | | |
| AS22B-5B1 | | Y | Quasi | 10 | 0/17 | | | | | | | | | | |
| AS21-1B1 | 23 | Y | | | | | | | | | | | | | |
| AS20-U1 | 22 | N | | | | | | | | | | | | | |
| AS20-U5 | | N | | | | | | | | | | | | | |
| AS19B-2B1 | 21 | Y | Quasi | 1 | 0/8 | | | | | | | | | | |
| AS19-1B1 | 20 | Y | Quasi | 10 | 9/9 | 0.42 | 0.65 | 0.09 | 2.88 | 0.939 | N/A | N/A | 1.77 | 0.614 | 3 |
| AS19-1B2 | | Y | Quasi | 1 | 7/7 | 0.43 | 0.77 | 0.09 | 3.62 | 0.959 | N/A | N/A | 2.85 | 0.7864889 | 3 |
| AS19-2B1 | | Y | Quasi | 5 | 0/9 | | | | | | | | | | |
| AS19-3B1 | | N | Coe | | | | | | | | | | | | |
| AS19-3B2 | | Y | Quasi | 5 | 0/8 | | | | | | | | | | |
| AS19-4B1 | | Y | Quasi | 5 | 5/9 | 0.69 | 0.73 | 0.04 | 13.90 | 0.996 | N/A | N/A | 4.3 | 0.3 | 2 |
| AS19-5B1 | | Y | Quasi | 1 | 0/8 | | | | | | | | | | |
| AS18-B1 | 19 | Y | Coe | 10 | 0/13 | | | | | | | | | | |
| AS17-U1 | 18 | Y | Coe | 20 | 7/14 | 0.46 | 0.80 | 0.06 | 6.45 | 0.984 | 3/3 | 3/3 | 10.38 | 1.60955 | 2 |
| AS17-U2 | | Y | Perp | 10 | 0/9 | | | | | | | | | | |
| AS17-U3 | | Y | Quasi | 10 | 14/15 | 0.97 | 0.87 | 0.03 | 31.53 | 0.991 | N/A | N/A | 13.2 | 0.4 | 2 |
| AS17-1B1 | | Y | Coe | 10 | 7/13 | 0.52 | 0.78 | 0.04 | 9.14 | 0.990 | 3/4 | 4/4 | 5.75 | 0.629 | 2 |
| AS17-2A1 | | Y | Perp | 20 | 12/12 | 0.48 | 0.83 | 0.04 | 9.49 | 0.982 | 3/4 | 1/5 | 10.7 | 1.1 | 2 |
| AS16-2B1 | 16 | N | | | | | | | | | | | | | |
| AS16-4B1 | | Y | | | | | | | | | | | | | |

| Sample | Flow Number | Demag | Protocol | $F_{lab}$ | $n/N$ | $f$ | $g$ | $\beta$ | $q$ | $r^2$ | pTRM Check | Tail Check | $F$ ($\mu T$) | uncert ($\mu T$) | Class |
|---|---|---|---|---|---|---|---|---|---|---|---|---|---|---|---|
| AS15-1B1 | 15 | Y | Coe | 20 | 0/15 | | | | | | | | | | |
| AS15-1B2 | | Y | Quasi | 10 | 13/13 | 0.74 | 0.84 | 0.06 | 9.69 | 0.955 | N/A | N/A | 7.9 | 0.8 | 3 |
| AS15-1B3 | | Y | Quasi | 5 | 7/17 | 0.66 | 0.78 | 0.04 | 12.02 | 0.990 | N/A | N/A | 14.7 | 1.2 | 2 |
| AS15-2B1 | | Y | Coe | 20 | 5/6 | 0.52 | 0.65 | 0.06 | 5.68 | 0.989 | 2/2 | 0/2 | 24.8 | 4.4 | 3 |
| AS15-3B1 | | Y | Perp | 20 | 5/6 | 0.08 | 0.66 | 0.04 | 1.14 | 0.994 | 0/2 | 0/2 | 17.9 | 15.6 | 3 |
| AS14-1B1 | 14 | Y | Coe | | 0/18 | | | | | | | | | | |
| AS14-1B2 | | Y | Coe | 20 | 10/12 | 0.45 | 0.88 | 0.08 | 5.17 | 0.953 | 5/5 | 4/5 | 11.7 | 2.3 | 3 |
| AS14-1B3 | | Y | Quasi | 10 | 6/16 | 0.26 | 0.73 | 0.08 | 2.38 | 0.975 | N/A | N/A | 14.1 | 5.9 | 3 |
| AS14-1B4 | | Y | Quasi | 10 | 7/11 | 0.28 | 0.68 | 0.08 | 2.35 | 0.967 | N/A | N/A | 15.3 | 6.5 | 3 |
| AS14-3B5 | | Y | Quasi | 5 | 9/14 | 0.58 | 0.73 | 0.02 | 19.21 | 0.997 | N/A | N/A | 4.3 | 0.2 | 2 |
| AS14-3B6 | | Y | Quasi | 5 | 5/9 | 0.23 | 0.73 | 0.08 | 2.18 | 0.982 | N/A | N/A | 27.7 | 12.7 | 3 |
| AS13-2B1 | 13 | Y | Perp | 20 | 11/11 | 0.60 | 0.81 | 0.02 | 22.72 | 0.996 | 4/4 | 2/4 | 18.1 | 0.8 | 2 |
| AS13-3B1 | | Y | Coe | 10 | 0/15 | | | | | | | | | | |
| AS13-3B2 | | Y | Coe | 20 | 0/8 | | | | | | | | | | |
| AS13-3B3 | | Y | Quasi | 10 | 6/6 | 0.23 | 0.74 | 0.03 | 5.05 | 0.994 | N/A | N/A | 3.3 | 0.6 | 3 |
| AS13-3B4 | | Y | Quasi | 10 | 9/9 | 0.73 | 0.82 | 0.02 | 31.46 | 0.997 | N/A | N/A | 2.4 | 0.1 | 2 |
| AS13-3B5 | | Y | Quasi | 10 | 9/9 | 0.87 | 0.79 | 0.04 | 15.46 | 0.986 | N/A | N/A | 2.6 | 0.2 | 2 |
| AS13-3B6 | | Y | Quasi | 10 | 11/21 | 0.45 | 0.83 | 0.08 | 4.94 | 0.949 | N/A | N/A | 21.0 | 4.3 | 3 |
| AS13-3B7 | | Y | Quasi | 10 | 7/15 | 0.54 | 0.78 | 0.04 | 10.25 | 0.992 | N/A | N/A | 4.5 | 0.4 | 2 |
| AS13-3B8 | | Y | Quasi | 10 | 14/14 | 0.75 | 0.85 | 0.04 | 15.06 | 0.979 | N/A | N/A | 4.1 | 0.3 | 3 |
| AS13-3B9 | | Y | Perp | 10 | 10/12 | 0.69 | 0.76 | 0.06 | 8.16 | 0.967 | 1/5 | 3/5 | 4.2 | 0.5 | 3 |
| AS13-3B10 | | Y | Perp | 10 | 12/20 | 0.53 | 0.79 | 0.01 | 39.61 | 0.999 | 0/0 | 0/0 | 4.6 | 0.1 | 2 |
| AS13-3B11 | | Y | Perp | 10 | 9/9 | 0.68 | 0.80 | 0.05 | 11.71 | 0.985 | 1/3 | 2/3 | 3.7 | 0.3 | 2 |
| AS13-4B1 | | Y | Coe | 20 | 12/26 | 0.48 | 0.88 | 0.03 | 14.74 | 0.991 | 4/5 | 5/5 | 6.5 | 0.4 | 2 |
| AS13-4B2 | | Y | Perp | 20 | 15/16 | 0.61 | 0.87 | 0.01 | 18.36 | 0.989 | 4/7 | 1/7 | 7.8 | 0.4 | 2 |
| AS12-2B1 | 12 | Y | Perp | 10 | 7/9 | 0.58 | 0.45 | 0.40 | 6.51 | 0.992 | 2/3 | 0/3 | 2.2 | 0.3 | 3 |
| AS12-2B2 | | Y | Perp | 5 | 10/10 | 0.53 | 0.83 | 0.02 | 19.88 | 0.996 | 2/4 | 4/4 | 2.2 | 0.1 | 2 |
| AS12-2B3 | | Y | Perp | 5 | 9/13 | 0.42 | 0.80 | 0.05 | 6.36 | 0.980 | 3/5 | 3/4 | 4.2 | 0.7 | 3 |
| AS12-2B4 | | Y | Perp | 5 | 15/15 | 0.39 | 0.85 | 0.05 | 7.27 | 0.973 | 3/7 | 2/7 | 1.1 | 0.2 | 3 |
| AS12-4B1 | | Y | Quasi | 5 | 6/10 | 0.65 | 0.77 | 0.08 | 6.44 | 0.975 | N/A | N/A | 8.5 | 1.3 | 3 |

Table E.2: Individual microwave palaeointensity results from the AS section, La Palma. Flows are in stratigraphic order in ascending number from oldest to youngest. All column headings are explained in the caption to Table E.1.

| Sample | Flow Number | Demag | Protocol | $F_{lab}$ | $n/N$ | $f$ | $g$ | $\beta$ | $q$ | $r^2$ | $pT_M$RM Check | Tail Check | $F$ ($\mu T$) | uncert ($\mu T$) | Class |
|---|---|---|---|---|---|---|---|---|---|---|---|---|---|---|---|
| AN1-1B1 | 1 | Y | Perp | 10 | 0/4 | | | | | | | | | | |
| AN1-1B2 | | Y | Perp | 15 | 10/10 | 0.54 | 0.56 | 0.11 | 2.88 | 0.912 | 1/2 | 1/2 | 2.5 | 0.9 | 3 |
| AN1-1B3 | | Y | Perp | 2 | 0/9 | | | | | | | | | | |
| AN1-2A1 | | Y | Perp | 15 | 0/3 | | | | | | | | | | |
| AN1-2A2 | | Y | Perp | 4 | 6/7 | 0.38 | 0.40 | 0.14 | 1.07 | 0.920 | 0/1 | 0/1 | 3.2 | 3.0 | 3 |
| AN1-4A1 | | Y | Perp | 5 | 0/3 | | | | | | | | | | |
| AN1-5A1 | | Y | Perp | 5 | 9/9 | 0.41 | 0.61 | 0.08 | 3.20 | 0.958 | 1/1 | 0/1 | 1.6 | 0.5 | 3 |
| AN2-1B1 | 2 | Y | Coe | 40 | 0/4 | | | | | | | | | | |
| AN2-1B2 | | Y | Perp | 10 | 6/6 | 0.63 | 0.71 | 0.02 | 20.86 | 0.998 | 1/1 | 1/2 | 7.5 | 0.4 | 2 |
| AN2-2B1 | | Y | Coe | 40 | 5/5 | 0.43 | 0.56 | 0.08 | 2.88 | 0.979 | 1/3 | 2/3 | 11.7 | 4.1 | 3 |
| AN3-1B1 | 3 | Y | Perp | 10 | 7/8 | 0.39 | 0.67 | 0.09 | 2.93 | 0.961 | 2/2 | 0/2 | 4.6 | 1.6 | 3 |
| AN3-1B2 | | Y | Perp | 10 | 13/13 | 0.60 | 0.85 | 0.03 | 19.91 | 0.993 | 3/3 | 0/3 | 3.2 | 0.2 | 2 |
| AN3-1B3 | | Y | Perp | 10 | 5/5 | 0.53 | 0.68 | 0.04 | 8.85 | 0.995 | 0/1 | 1/1 | 6.6 | 0.7 | 2 |
| AN3-2B1 | | Y | Coe | 20 | 0/4 | | | | | | | | | | |
| AN3-3B1 | | Y | Perp | 10 | 7/8 | 0.39 | 0.34 | 0.04 | 3.64 | 0.993 | 0/1 | 0/1 | 8.8 | 2.4 | 3 |
| AN3-3B2 | | Y | Perp | 10 | 8/8 | 0.38 | 0.70 | 0.04 | 6.50 | 0.990 | 1/2 | 2/2 | 11.5 | 1.8 | 2 |
| AN4-1B1 | 4 | Y | Coe | 10 | 0/6 | | | | | | | | | | |
| AN4-2B1 | | Y | Coe | 10 | 0/7 | | | | | | | | | | |
| AN4-3B1 | | Y | Perp | 10 | 0/7 | | | | | | | | | | |
| AN4-4B1 | | Y | Perp | 10 | 0/11 | | | | | | | | | | |
| AN6-1B1 | 6 | Y | Perp | 10 | 6/8 | 0.69 | 0.61 | 0.03 | 15.16 | 0.997 | 1/1 | 0/1 | 4.8 | 0.3 | 2 |
| AN7-2B1 | 7 | Y | Perp | 10 | 3/4 | 0.28 | 0.35 | 0.03 | 3.53 | 0.999 | 0/0 | 0/0 | 13.9 | 3.9 | 3 |
| AN7-3B1 | | Y | Perp | 10 | 6/6 | 0.27 | 0.45 | 0.05 | 2.57 | 0.991 | 1/1 | 0/1 | 10.7 | 4.2 | 3 |
| AN7-4B1 | | Y | Coe | 30 | 0/5 | | | | | | | | | | |
| AN7-4B2* | | Y | Quasi | 30 | 0/6 | | | | | | | | | | |
| AN8-2B1 | 8 | Y | Perp | 10 | 8/8 | 0.31 | 0.62 | 0.12 | 1.66 | 0.918 | 0/1 | 1/1 | 3.4 | 2.1 | 3 |
| AN8-2B2 | | Y | Perp | 10 | 10/10 | 0.53 | 0.56 | 0.07 | 4.13 | 0.958 | 1/2 | 0/2 | 5.1 | 1.2 | 3 |
| AN8-2B3* | | Y | Quasi | 10 | 5/5 | 0.80 | 0.74 | 0.05 | 12.66 | 0.993 | N/A | N/A | 3.7 | 0.3 | 2 |
| AN8-3B1 | | Y | Perp | 20 | 7/7 | 0.22 | 0.75 | 0.04 | 4.05 | 0.992 | 0/1 | 0/1 | 8.8 | 2.2 | 3 |
| AN9A-1B1 | 9 | Y | Perp | 10 | 10/10 | 0.77 | 0.59 | 0.02 | 22.07 | 0.997 | 0/0 | 0/0 | 21.6 | 1.0 | 2 |
| AN9A-2B1 | | Y | Perp | 10 | 9/10 | 0.19 | 0.84 | 0.04 | 4.34 | 0.990 | 0/0 | 0/0 | 24.2 | 5.6 | 3 |
| AN9A-3B1 | | Y | Perp | 20 | 9/9 | 0.39 | 0.75 | 0.04 | 8.16 | 0.991 | 0/1 | 0/1 | 26.8 | 3.3 | 2 |
| AN9A-4B1 | | Y | Perp | 20 | 15/15 | 0.40 | 0.64 | 0.02 | 10.10 | 0.992 | 0/0 | 0/0 | 18.5 | 1.8 | 2 |
| AN9B-4B1 | 10 | Y | Perp | 10 | 0/12 | | | | | | | | | | |
| AN10-1B1 | 11 | N | | | | | | | | | | | | | |
| AN10-2B1 | | N | | | | | | | | | | | | | |
| AN10-3B1 | | N | | | | | | | | | | | | | |

| Sample | Number Flow | Demag | Protocol | $F_{lab}$ | $n/N$ | $f$ | $g$ | $\beta$ | $q$ | $r^2$ | pTRM Check | Tail Check | $F$ ($\mu T$) | uncert ($\mu T$) | Class |
|---|---|---|---|---|---|---|---|---|---|---|---|---|---|---|---|
| AN11-1B1 | 12 | Y | Perp | 10 | 3/3 | 0.73 | 0.50 | 0.09 | 4.13 | 0.992 | 1/1 | 1/1 | 31.7 | 7.7 | 3 |
| AN14-1B1 | 15 | Y | Perp | 15 | 0/13 | | | | | | | | | | |
| AN14-1B2 | | Y | Perp | 10 | 0/7 | | | | | | | | | | |
| AN14-1B3* | | Y | Quasi | 10 | 0/6 | | | | | | | | | | |
| AN14-2B1 | | Y | Perp | 8 | 10/12 | 0.81 | 0.74 | 0.04 | 15.16 | 0.988 | 0/2 | 0/2 | 6.6 | 0.4 | 2 |
| AN14-3B1 | | Y | Perp | 8 | 0/14 | | | | | | | | | | |

Table E.3: Individual microwave palaeointensity results from the AN section, La Palma. Flows are in stratigraphic order in ascending number from oldest to youngest. All column headings are explained in the caption to Table E.1. All experiments performed by Martin Gratton except *, which were performed by the author. All analysis by the author.

| Sample | Flow Number | Demag | Protocol | $F_{lab}$ | $n/N$ | $f$ | $g$ | $\beta$ | $q$ | $r^2$ | $pTRM_M$ Check | Tail Check | $F$ ($\mu T$) | uncert ($\mu T$) | Class |
|---|---|---|---|---|---|---|---|---|---|---|---|---|---|---|---|
| GD0102 | 1 | Y | Perp | 10 | 0/12 | | | | | | | | | | |
| GD0103 | | Y | Perp | 20 | 0/8 | | | | | | | | | | |
| GD0104 | | Y | Coe | 20 | 0/9 | | | | | | | | | | |
| GD0105* | | Y | Quasi | 10 | 8/8 | 0.43 | 0.83 | 0.03 | 13.10 | 0.995 | N/A | N/A | 25.1 | 1.9 | 2 |
| GD0106* | | Y | Quasi | 20 | 11/12 | 0.51 | 0.89 | 0.02 | 19.15 | 0.995 | N/A | N/A | 19.1 | 1.0 | 2 |
| GD0201 | | Y | Perp | 30 | 0/8 | | | | | | | | | | |
| GD0301 | | Y | Perp | 10 | 0/12 | | | | | | | | | | |
| GD0601 | | Y | Perp | 10 | 0/9 | | | | | | | | | | |
| G01A0101 | 2 | Y | Perp | 6 | 0/9 | | | | | | | | | | |
| G01A0201 | | Y | Perp | 6 | 8/10 | 0.41 | 0.71 | 0.10 | 2.89 | 0.940 | 1/2 | 0/2 | 4.2 | 1.5 | 3 |
| G01A0401 | | Y | Perp | 6 | | | | | | | | | | | |
| G01A0402 | | Y | Perp | 6 | 0/16 | | | | | | | | | | |
| G01A0501 | | Y | Perp | 10 | 9/11 | 0.37 | 0.77 | 0.04 | 7.57 | 0.990 | 0/3 | 0/3 | 6.2 | 0.8 | 3 |
| G01A0601 | | Y | Perp | 6 | 7/9 | 0.31 | 0.75 | 0.16 | 1.42 | 0.870 | 0/1 | 0/1 | 5.2 | 3.6 | 3 |
| G01A0701 | | Y | Perp | 6 | 0/10 | | | | | | | | | | |
| G01B0102 | | Y | Perp | 6 | 0/4 | | | | | | | | | | |
| G01B0201 | | Y | Perp | 6 | 6/6 | 0.20 | 0.57 | 0.05 | 2.17 | 0.989 | 0/0 | 0/0 | 7.0 | 3.2 | 3 |
| G01B0301 | | Y | Perp | 6 | 0/9 | | | | | | | | | | |
| G01B0302 | | Y | Perp | 6 | 0/9 | | | | | | | | | | |
| G01B0401 | | Y | Perp | 6 | 7/7 | 0.73 | 0.72 | 0.05 | 10.48 | 0.987 | 0/1 | 1/1 | 3.0 | 0.3 | 2 |
| G01B0402 | | Y | Perp | 6 | 0/11 | | | | | | | | | | |
| G01B0501 | | Y | Perp | 6 | 0/3 | | | | | | | | | | |
| G02A0101 | 3 | Y | Perp | 10 | 0/10 | | | | | | | | | | |
| G02A0201 | | Y | Perp | 5 | 4/5 | 0.31 | 0.33 | 0.07 | 1.48 | 0.990 | 0/0 | 0/0 | 17.2 | 11.6 | 3 |
| G02A0501 | | Y | Perp | 10 | 0/5 | | | | | | | | | | |
| G02A0701 | | Y | Perp | 20 | 0/12 | | | | | | | | | | |
| G02A0801 | | Y | Perp | 10 | 0/4 | | | | | | | | | | |
| G02A0901 | | Y | Perp | 5 | 7/7 | 0.26 | 0.75 | 0.09 | 2.26 | 0.963 | 0/1 | 0/1 | 7.8 | 3.5 | 3 |
| G02A0902 | | Y | Perp | 10 | 0/15 | | | | | | | | | | |
| G02B0101 | | Y | Perp | 10 | 4/6 | 0.17 | 0.41 | 0.04 | 1.91 | 0.996 | 0/1 | 1/1 | 16.6 | 8.7 | 3 |
| G02B0102 | | Y | Perp | 10 | 5/5 | 0.46 | 0.72 | 0.04 | 8.95 | 0.996 | 1/1 | 1/1 | 17.0 | 1.9 | 2 |
| G03A0101 | 4 | Y | Perp | 10 | 15/15 | 0.66 | 0.90 | 0.02 | 23.86 | 0.992 | 3/4 | 0/4 | 14.0 | 0.6 | 3 |
| G03A0102 | | Y | Perp | 20 | 11/11 | 0.84 | 0.81 | 0.03 | 21.56 | 0.991 | 0/3 | 0/1 | 15.4 | 0.7 | 3 |
| G03A0201 | | Y | Perp | 10 | 13/13 | 0.70 | 0.87 | 0.02 | 34.58 | 0.997 | 4/4 | 0/4 | 18.9 | 0.5 | 2 |
| G03A0301 | | Y | Perp | 15 | 0/13 | | | | | | | | | | |
| G03A0401 | | Y | Perp | 15 | 10/10 | 0.71 | 0.61 | 0.04 | 9.90 | 0.985 | 0/2 | 0/2 | 19.7 | 2.0 | 3 |
| G03A0501 | | Y | Perp | 15 | 0/10 | | | | | | | | | | |
| G03A0502 | | Y | Perp | 20 | 11/11 | 0.51 | 0.74 | 0.03 | 13.33 | 0.993 | 1/2 | 1/2 | 26.5 | 2.0 | 2 |
| G03A0601 | | Y | Perp | 15 | 8/8 | 0.44 | 0.64 | 0.04 | 6.86 | 0.990 | 2/2 | 0/2 | 15.7 | 2.3 | 2 |
| G03A0701 | | Y | Perp | 15 | 0/6 | | | | | | | | | | |
| G03A0801 | | Y | Perp | 15 | 12/12 | 0.34 | 0.80 | 0.05 | 5.90 | 0.979 | 0/1 | 0/1 | 13.2 | 2.2 | 3 |
| G03A0802 | | Y | Perp | 20 | 5/17 | 0.13 | 0.51 | 0.16 | 1.26 | 0.992 | 1/2 | 0/2 | 10.8 | 8.6 | 3 |

Table E.4: Individual microwave palaeointensity results from Guadeloupe, French West Indies. Column headings are explained in Table E.1. All experiments performed by Martin Gratton except $*$, which were performed by the author. All analysis by the author.

# Bibliography


Ament, W. S. & Rado, G. T., 1955. Electromagnetic effects of spin wave resonance in ferromagnetic metals, *Phys. Rev.*, **97**, 1558.

Ancochea, E., Hernán, F., Cendrero, A., Cantagrel, J. M., Fúster, J. M., Ibarrola, E. & Coello, J., 1994. Constructive and destructive episodes in the building of a young Oceanic Island, La Palma, Canary Islands and genesis of the Caldera de Taburiente, *J. Volcanol. Geotherm. Res.*, **60**, 243–262.

Aubert, J., Aurnou, J. & Wicht, J., 2008. The magnetic structure of convection-driven numerical dynamos, *Geophys. J. Int.*, pp. doi: 10.1111/j.1365–246X.2007.03693.x.

Baksi, A. K., Hall, C. M. & York, D., 1991. Laser probe $^{40}Ar/^{39}Ar$ dating studies on sub-milligram whole-rock basalt samples: the age of the Steens Mountain geomagnetic polarity transition (revisited), *Earth Plant. Sci. Lett.*, **104**, 292–298.

Baksi, A. K., Hsu, V., Williams, M. O. & Farrar, E., 1992. $^{40}Ar/^{39}Ar$ dating of the Brunhes-Matuyama geomagnetic field reversal, *Science*, **256**, 356–357.

Balsley, J. R. & Buddington, A. F., 1954. Correlation of reverse remanent magnetism and negative anomalies with certain minerals, *J. Geomag. Geoelectr.*, **6**, 176–181.

Barton, C. E. & McFadden, P. L., 1996. Inclination shallowing and preferred transitional vgp paths, *Earth Plant. Sci. Lett.*, **140**, 147–157.

Biggin, A. J. & Böhnel, H. N., 2003. A method to reduce the curvature of Arai plots produced during Thellier palaeointensity experiments on mutlidomain grains, *Geophys. J. Int.*, **155**, F13–F19.

Biggin, A. J. & Böhnel, H. N., 2006. First-order symmetry of weak-field partial thermoremanence in multi-domain (MD) ferromagnetic grains: 2. implications for Thellier-type palaeointensity determination, *Earth Plant. Sci. Lett.*, **245**, 453–470.

Biggin, A. J. & Thomas, D. N., 2003a. Analysis of long-term variations in the geomagnetic poloidal field intensity and evaluation of their relationship with global geodynamics, *Geophys. J. Int.*, **152**, 392–415.

Biggin, A. J. & Thomas, D. N., 2003b. The application of acceptance criteria to results of Thellier palaeointensity experiments performed on samples with pseudo-single-domain-like characteristics, *Phys. Earth Plant. Inter.*, **138**, 279–287.

Biggin, A. J., Perrin, M. & Dekkers, M. J., 2007a. A reliable absolute palaeointensity determination obtained from a non-ideal recorder, *Earth Plant. Sci. Lett.*, **257**, 545–563.

Biggin, A. J., Perrin, M. & Shaw, J., 2007b. A comparison of a quasi-perpendicular method of palaeointensity determination with other thermal and microwave techniques, *Earth Plant. Sci. Lett.*, **257**, 564–581.

Bingham, D. K. & Stone, D. B., 1972. Palaeosecular variation of the geomagnetic field in the Aleutian Islands, Alaska, *Geophys. J. R. ast. Soc.*, **28**, 317–335.

Biswas, D. K., Hyodo, M., Taniguchi, Y., Kaneko, M., Katoh, S., Sato, H., Kinugasa, Y. & Mizuno, K., 1999. Magnetostratigraphy of Plio-Pleistocene sediments in a 1700-m core from Osaka Bay, southwestern Japan and short geomagnetic events in the middle Matuyama and early Brunhes chrons, *Palaeogeogr. Palaeoclimatol. Palaeoecol.*, **148**, 233–238.

Black, T. M., 1992. Chronology of the Middle Pleistocene Kidnappers Group, New Zealand and correlation to global oxygen isotope stratigraphy, *Earth Plant. Sci. Lett.*, **109**, 573–584.

Blanc, F., 1983. *Corrélations chronologiques et géochemique des formations volcanique du sud de la Basse-Terre, Guadeloupe (Petites Antilles)*, Début du cycle récent, 3e cycle thesis, Univ. Sci. Medic. Grenoble.

Bleil, U. & Petersen, N., 1982. *Magnetic properties of natural samples in Numerical data and functional relationships in science and technology, Group V: Geophysics and space research, edited by G. Angenheister*, Springer, New York.

Bloxham, J. & Gubbins, D., 1989. The evolution of the Earth's magnetic field, *Scientific American*, **261**, 30–37.

Bloxham, J. & Jackson, A., 1992. Time-dependant mapping of the magnetic field at the core-mantle boundary, *J. Geophys. Res.*, **97**, 19537–19563.

Bogue, S. W., 2001. Geomagnetic field behavior before and after the Kauai reverse-normal polarity transition, *J. Geophys. Res.*, **106 (B1)**, 447–461.

Bogue, S. W. & Coe, R. S., 1984. Transitional paleointensities from Kauai, Hawaii, and geomagnetic reversal models, *J. Geophys. Res.*, **89 (B12)**, 10341–10354.

Bogue, S. W. & Paul, H. A., 1993. Distinctive field behavior following geomagnetic reversals, *Geophys. Res. Lett.*, **20 (21)**, 2399–2402.

Böhnel, H., McIntosh, G. & Sherwood, G., 2002. A parameter characterising the irreversibility of thermomagnetic curves, *Phys. Chem. Earth*, **27**, 1305–1309.

Bolshakov, A. S. & Shcherbakova, V. V., 1979. A thermomagnetic criterion for determining the domain structure of ferrimagnetics (translated from russian), *Izvestiya Phys. Solid Earth*, **15**, 111–117.

Bolshakov, V. A., 2005. Determination of the climatostratographic position of the Matuyama/Brunhes reversalin loess formation deposits as a multidisciplinary problem of Earth sciences, *Izvestiya Phys. Solid Earth*, **40**, 1015–1030.

Brown, L. L., Pickens, J. & Singer, B., 1994. Matuyama-Brunhes transition recorded in lava flows of the Chilean Andes: Evidence for dipolar fields during reversals, *Geology*, **22**, 299–302.

Brown, L. L., Singer, B. S., Pickens, J. C. & Jicha, R., 2004. Paleomagnetic directions and $^{40}Ar/^{39}Ar$ ages from the Tatara-San Pedro volcanic complex, Chilean Andes: Lava record of a Matuyama-Brunhes precursor?, *J. Geophys. Res.*, **109**, B12101 doi:10.1029/2004JB003007.

Brown, M. C. & Chen, A. P., 2008. Using first-order reversal curves to assess palaeointensity variations in samples recording the Matuyama-Brunhes geomagnetic field reversal, *in prep.*.

Brown, M. C., Shaw, J. & Goguitchaichvili, A. T., 2006. Microwave palaeointensity from the R3-N3 geomagnetic field reversal, *Geophys. J. Int.*, **167**, 53–69.

Brown, M. C., Holme, R. & Bargary, A., 2007. Exploring the influence of the non-dipole field on magnetic records for reversals and excursions, *Geophys. J. Int.*, **168**, 541–550.

Bruckshaw, J. M. & Robertson, E. I., 1949. The magnetic properties of the tholeiite dykes of north england, *Roy. Astron. Soc. Geophys. Supp. Mon. Not.*, **5(8)**, 308–320.

Brunhes, B., 1906. Recherches dur la diection de l'aimantation des roches volcaniques, *J. de Phys*, **4**, 705–724.

Brynjolfsson, A., 1956. Ergebnisse bei partieller Entmagnetisierung des natürlichen Magnetismus isländischer Basalt, *Naturwissensch*, **43**, 153–155.

Brynjolfsson, A., 1957. Studies of remanent magnetism and viscous magnetism in the basalts of Iceland, *Adv. Phys.*, **6**, 247–254.

Bucha, V., 1970. Geomagnetic reversals in quaternary revealed from a paleomagnetic investigation of sedimentary rocks, *J. Geomag. Geoelectr.*, **22**, 253–271.

Butler, R. F., 1992. *Paleomagnetism: Magnetic domains to geologic terrains*, Blackwell Science.

Camps, P., Ruffet, G., Shcherbakov, V., Shcherbakova, V., Prévot, M., Moussine-Pouchkine, A., Sholpo, L., Goguitchaichvili, A. & Asanidzé, B., 1996. Paleomagnetic and geolchronological study of a geomagnetic field reversal or excursion recorded in pliocene vocanic rocks from Georgia(Lesser Caucasus, *Phys. Earth Plant. Inter.*, **96**, 41–59.

Camps, P., Coe, R. S. & Prévot, M., 1999. Transitional geomagnetic impulse hypothesis: Geomagnetic fact or rock-magnetic artefact?, *J. Geophys. Res.*, **104**, 17,747–17,758.

Carlut, J. & Courtillot, V., 1998. How complex is the time-averaged field over the past 5 million years, *Geophys. J. Int.*, **134**, 527–544.

Carlut, J. & Courtillot, V., 1999. Paleointensity across the Réunion event in Ethiopia, *Earth Plant. Sci. Lett.*, **170**, 17–34.

Carlut, J. & Quidelleur, X., 2000. Absolute paleointensities recorded during the Brunhes chron at La Gaudeloupe Island, *Phys. Earth Plant. Inter.*, **120**, 255–269.

Carlut, J., Quidelleur, X., Courtillot, V. & Boudon, G., 2000. Paleomagnetic directions and K/Ar dating of 0 to 1 Ma lava flows from La Gaudeloupe Island (French West Indies: Implications for time-averaged field models, *J. Geophys. Res.*, **105**, 835–849.

Carmichael, I. S. E. & Nicolls, J., 1967. Iron-titanium oxides and oxygen fugacities in volcanic rocks, *J. Geophys. Res.*, **72**, 4665–4687.

Carracedo, J. C., Day, S., Guillou, H., Badiola, E. R., Canas, J. A. & Torrado, F. J. P., 1998. Hot spot volcanism close to a passive continental margin: the Canary Islands, *Geol. Mag.*, **5**, 591–604.

Carracedo, J. C., Day, S. J., Guillou, H. & Gravestock, P., 1999. Later stages of volcanic evolution of La Palma, Canary Islands: Rift evolution, giant landslides, and the genesis of the Caldera de Taburiente, *Geol. Soc. Am. Bull*, **111**, 755–768.

Carter-Stiglitz, B., Moskowitz, B. & Jackson, M., 2001. Unmixing magnetic assemblages and the magnetic behavior of bimodal mixtures, *J. Geophys. Res.*, **106 (B11)**, 26397–2641.

Carter-Stiglitz, B., Moskowitz, B., Solheid, P., Berquó, T., Jackson, M. & Kosterov, A., 2006. Low-temperature magnetic behaviour of multidomain titanomagnetites: TM0, TM16 and TM35, *J. Geophys. Res.*, **111, B12S05**, doi:10.1029/2006JB004561.

Carvallo, C., Roberts, A. P., Leonhardt, R., Laj, C., Kissel, C., Perrin, M. & Camps, P., 2006. Increasing the efficiency of paleointensity analyses by selection of samples using first-order reversal curve diagrams, *J. Geophys. Res.*, **111, B12103**, doi:10.1029/2005JB004126.

Celaya, M. & Clement, B., 1988. Inclination shallowing in deep sea sediments from the north atlantic, *Geophys. Res. Lett.*, **15**, 52–55.

Channell, J. E. T. & Kleiven, H. F., 2000. Geomagnetic palaeointensities and astrochronological ages for the Matuyama-Brunhes boundary and the boundaries of the Jaramillo Subchron: palaeomagnetic and oxygen isotope records from ODP Site 983, *Phil. Trans. R. Soc. Lond.*, **358**, 1027–1047.

Channell, J. E. T. & Lehman, B., 1997. The last two geomagnetic polarity reversals recorded in high-deposition-rate sediment drifts, *Nature*, **389**, 712–715.

Channell, J. E. T. & Raymo, M. E., 2003. Paleomagnetic record at ODP Site 980 (Feni Drift, Rockallfor the past 1.2 Myrs, *Geochem. Geophys. Geosyst.*, **4**, 1033, doi:1029/2002GC000440.

Channell, J. E. T. & Stoner, J. S., 2002. Plio-Pleistocenemagnetic polarity stratigraphies and diagenetic magnetite dissolution at ODP Leg 177 Sites (1089, 1091, 1093, 1094), *Mar. Micropaleotol*, **45**, 269–290.

Channell, J. E. T., Curtis, J. H. & Flower, B. P., 2004. The Matuyama-Brunhes boundary interval (500-900 ka) in North Atlantic drift sediments, *Geophys. J. Int.*, **158**, 489–505.

Chauvin, A., Roperch, P. & Duncan, R. A., 1990. Records of geomagnetic reversals from volcanic islands of French Polynesia 2. paleomagnetic study of a flow sequence (1.2-0.6 ma) from the island of Tahiti and discussion of reversal models, *J. Geophys. Res.*, **95**, 2727–2752.

Choiniere, S. R. & Swanson, D. A., 1979. Magnetostratigraphy and correlation of Miocene basalts of the northern Oregon coast and Columbia Plateau, south east Washington, *Am. J. Sci*, **279**, 755–777.

Cisowski, S. M. & Koyama, M., 1992. Detailed record of the Brunhes-Matuyama polarity in high sedimentation rate marine sediments from the Izu-Bonin Arc, *Ocean Drill. Prog. Sci. Results*, **126**, 341–352.

Clement, B. M., 1991. Geographical distribution of transitional VGPs: evidence for nonzonal equatorial symmetry during the Brunhes-Matuyama geomagnetic reversal, *Earth Plant. Sci. Lett.*, **104**, 48–58.

Clement, B. M., 2004. Dependence of the duration of geomagnetic polarity reversals on site latitude, *Nature*, **428**, 637–640.

Clement, B. M. & Kent, D. V., 1984. Latitudinal dependency of geomagentic polarity transition durations, *Nature*, **310**, 488–491.

Clement, B. M. & Kent, D. V., 1986. Geomagnetic polarity transition records from from five hydraulic piston core sites in the north Atlantic, *Init. Rep. Deep Sea Drill. Proj.*, **94**, 831–852.

Clement, B. M. & Kent, D. V., 1991. A southern hemisphere record of the Matuyama-Brunhes polarity reversal, *Geophys. Res. Lett.*, **18**, 81–84.

Coe, R. S., 1967a. Paleo-intensities of the Earth's magnetic field determined from Tertiary and Quaternary rocks, *J. Geophys. Res.*, **72**, 3247–3262.

Coe, R. S., 1967b. The determination of palaeointensities of the Earth's magnetic field with an emphasis on mecnahisms which would cause non-ideal behaviour in Theliers method, *J. Geomag. Geoelectr.*, **19**, 157–179.

Coe, R. S. & Glen, J., 2004. The complexity of reversals, *Timescales of the paleomagnetic field, Geophysical Monograph Series*, **145**, 221–232 doi:10.29/145GM16.

Coe, R. S. & Prévot, M., 1989. Evidence suggesting extremely rapid field variation during a geomagnetic reversal, *Earth Plant. Sci. Lett.*, **92**, 292–298.

Coe, R. S., Grommé, S. & Mankinen, E. A., 1978. Geomagnetic paleointensities from radiocarbon-dated lava flows on Hawaii and the question of the Pacific nondiple low, *J. Geophys. Res.*, **83**, 1740–1756.

Coe, R. S., Grommé, S. & Mankinen, E. A., 1984. Geomagnetic palaeointensities from excursion sequences in lava on Oahu, Hawaii, *J. Geophys. Res.*, **89 (B12)**, 1059–1069.

Coe, R. S., Prévot, M. & Camps, P., 1995. New evidence for extraordinary rapid change of the geomagnetic field during a reversal, *Nature*, **374**, 687–692.

Coe, R. S., Hongre, L. & Glatzmaier, G. A., 2000. An examination of simulated geomagnetic reversals from a palaeomagnetic perspective, *Phil. Trans. R. Soc. Lond.*, **358**, 1141–1170.

Coe, R. S., Singer, B. S., Pringle, M. S. & Zhao, X., 2004a. Matuyama-Brunhes reversal and Kaikatsura event on Maui: palaomagnetic directions, $^{40}Ar/^{39}Ar$ ages and implications, *Earth Plant. Sci. Lett.*, **222**, 667–684.

Constable, C., 1990. A simple statistical model for geomagnetic reversals, *J. Geophys. Res.*, **95**, 4587–4596.

Constable, C., 1992. Link between geomagnetic reversal paths and secular variation of the field over the last 5 Myr, *Nature*, **358**, 230–233.

Costin, S. O. & Buffett, B. A., 2004. Preferred reversal paths caused by a hetrogeneous conducting layer at the base of the mantle, *J. Geophys. Res.*, **109**, B06101, doi:10.1029/2003JB002853.

Cottrell, R. D. & Tarduno, J. A., 1999. Geomagnetic paleointensity derived from single plagioclase crystals, *Earth Plant. Sci. Lett.*, **169**, 1–5.

Courtillot, V., Valet, J.-P., Hulot, G. & Mouël, J.-L., 1992. The Earth's magnetic field: Which geometry?, *Eos Trans. AGU*, **73, 337**, 340–342.

Cox, A., Doell, D. R. & Dalrymple, G. B., 1963. Geomagnetic polarity epochs and Pleistocene geochronology, *Nature*, **198**, 1049.

Cui, Y., Verosub, K. L. & Roberts, A. P., 1994. The effect of low-temperature oxidation on large multi-domain magnetite, *Geophys. Res. Lett.*, **21 (9)**, 757–760.

Dagley, P. & Lawley, E., 1974. Palaeomagnetic evidence for the transitional behaviour of the geomagnetic field, *Geophys. J. R. astr. Soc.*, **36**, 577–598.

Day, R., Fuller, M. & Schmidt, V. A., 1977. Hysteresis properties of Titanomagnetites: grain size and compisitional dependence, *Phys. Earth Plant. Inter.*, **13**, 260–267.

Dearing, J. A., Dann, R. J. L., Hay, K., Lees, J. A., Loveland, P. J. & Maher, B. A., 1996. Frequency-dependent susceptibility measurements of environmental materials, *Geophys. J. Int.*, **124**, 228–240.

Deaver, B. & Goree, W. S., 1967. Some techniques for sensitive magnetic measurements using superconducting circuits and magnetic shields, *Rev. Sci. Inst.*, **38**, 311–318.

Dekkers, M. J. & Böhnel, H. N., 2006. Reliable absolute palaeointensities independent of magnetic domain state, *Earth Plant. Sci. Lett.*, **248**, 508–517.

Didier, J. & Roche, A., 1999. Vie et œuvre d'un physicien: Bernard Brunhes (1847 - 1910), pionnier du géomagnétisme, *C. R. Acad. Sci. Paris, Sciences de la Terre et des planètes*, **328**, 141–152.

Dinarès-Turell, J., Sagnotti, L. & Roberts, A. P., 1999. Realtive paleointensity from the Jaramillo Subchron to the Matuyama/Brunhes as recorded in a Mediterranean piston core, *Earth Plant. Sci. Lett.*, **194**, 327–341.

Dinarès-Turell, J., Roberts, B. A. A. H. A. P., Rohling, E. J. & Sagnotti, L., 2003. Quaternary climatic control of biogenic magnetite productionand eolin dust inputsin cores from the Mediterranean Sea, *Palaeogeogr. Palaeoclimat. Palaeoecol.*, **190**, 195–209.

Dodonov, A. E., Zhou, L. P., Markova, A. K., Tchepalyga, A. L., Trubikhin, V. M., Aleksandrovdki, A. L. & Simakova, A. N., 2006. Middle-upper Pleistocene bio-climatic and magnetic records of the northern Black Sea coastal area, *Quart. Int.*, **149**, 44–54.

Doell, R. R., 1972. Paleomagnetism of volcanic rocks from Niihau, Nihoa, and Necker Islands, Hawaii, *J. Geophys. Res.*, **77 (20)**, 3725–3730.

Dormy, E., Valet, J.-P. & Courtillot, V., 2000. Numerical models of the geodynamo and observational constraints, *Geochem. Geophys. Geosyst.*, **1**, 2000GC000062.

Dungan, M., Wulff, A. & Thompson, R., 2001. Eruptive stratigraphy of the tatara-san pedro complex, 36°, southern volcanic zone, chilean andes: reconstruction method and implications for magma evolution at long-lived arc volcanic centers, *J. Petrol.*, **42**, 555–626.

Dunlop, D., 2002. Theory and application of the Day plot (Mrs/Ms versus Hcr/Hc) 2. Application to data for rocks, sediments, soils, *J. Geophys. Res.*, **103**, doi:10.1029/2001JB000486.

Dunlop, D. J. & Özdemir, O., 1997. *Rock magnetism: Fundamentals and frontiers*, Cambridge Univeristy Press.

Dunlop, D. J. & Özdemir, O., 2000. Effect of grain size and domain state on thermal demagnetization tails, *Geophys. Res. Lett.*, **27**, 1311–1214.

Dunlop, D. J. & Xu, S., 1994. Theory of partial thermoremanent magnetization in multidomain grains. 1. Repeated identical barriers to wall motion (single microcoercivity), *J. Geophys. Res.*, **99**, 9005–9023.

Egbert, G. D., 1992. Sampling bias in vgp longitudes, *Geophys. Res. Lett.*, **19**, 2533–2356.

Egli, R., 2006. Theoretical aspects of dipolar interactions and their appearance in first-order reversal curves of thermally activated single-domain particles, *J. Geophys. Res.*, **111**, B12S17, doi:10.1029/2006JB004567.

Einarsson, T., 1957. Magneto-geological mapping in Iceland with the use of a compass, *Adv. Phys.*, **6**, 232–239.

Einarsson, T. & Sigurgeirsson, T., 1955. Rock magnetism in Iceland, *Nature*, **197**, 892.

Fabian, K., 2001. A theoretical treatment of palaeointensity determination experiments on rocks containing pseudo-single or multi domain magnetic particles, *Earth Plant. Sci. Lett.*, **188**, 45–58.

Fabian, K., 2003. Statistical theory of weak fieldthrmoremanenct magnetization in multidomain ensambles, *Geophys. J. Int.*, **155**, 479–488.

Fabian, K., 2006. Approach to saturation analysis of hysteresis measurements in rock magnetism and evidence for stress dominated magnetic anisotropy in young mid-ocean ridge basalt, *Phys. Earth Plant. Inter.*, **154**, 299–307.

Fabian, K. & Leonhardt, R., 2007. *Testing multi specimen absolute paleointensity determination: theory and experiments (abstract)*, XXIV IUGG General Assembly, Perugia.

Fischer, H., Luster, J. & Gehring, A. U., 2007. Epr evidence for maghemitization of magnetite in a tropical soil, *Geophys. J. Int.*, **169**, 909–916.

Fisher, R. A., 1953. Dispersion on a sphere, *Proceedings of the Royal Society of London, Series A*, **217**, 295–305.

Folgheraiter, G., 1894. Origine del magnetisimo nelle roccie vulcaniche del Lazio, *Rendiconti, R. Acad. Lincei*, **3**, 53–61.

Fox, J. M. W. & Aitken, M. J., 1980. Cooling-rate dependency of thermoremanent magnetisation, *Nature*, **283**, 462–463.

Fuller, M., 1989. Fast changes in geomagnetism, *Nature*, **339**, 582–583.

Gelletich, H., 1934. Über magnetitführende eruptive Gange und,Gangsysteme im mittleven Teil des südlichen Transvaals, *Beitr. Angew. Geophys.*, **6**, 337–406.

Gendler, T. S., Heller, F., Tsatskin, H., Spassov, S., Pasquier, J. D. & Faustov, S., 2006. Roxolany and Novaya etuliya - key sections in the western Black Sea loess area: Magnetostratigraphy, rock magnetism, and paleopedology, *Quatern. Int.*, **152-153**, 78–93.

Glatzmaier, G. & Olson, P., 2005. Probing the geodynamo, *Scientific American*, **292(4)**, 32–39.

Glatzmaier, G. & Roberts, P., 1995. A three-dimensional convective dynamo solution with rotating and finitely conducting inner core and mantle, *Phys. Earth Plant. Inter.*, **91**, 63–75.

Glatzmaier, G., Coe, R., Hongre, L. & Roberts, P., 1999. The role of the Earth's mantle in controlling the frequency of geomagnetic field reversals, *Nature*, **401**, 885–890.

Glen, J. M. G., Coe, R. & Liddicoat, J., 1994. Persistent features of polarity transition records from western North America, *Geophys. Res. Lett.*, **21**, 1165–1168.

Glen, J. M. G., Valet, J.-P., Soler, V., Renne, P. R. & Elmaleh, A., 2003. A Neogene geomagnetic polarity transition record from lavas of the Canary Islands, Spain: episodic volcanism and/or metatable transitional fields?, *Geophys. J. Int.*, **154**, 426–440.

Glen, W., 1982. *The Road to Jaramillo: Critical Years in the Revolution of Earth Sciences*, Stanford Univer. Press, Stanford, Calif.

Goguitchaichvili, A., Camps, P. & Urrutia-Fucugauchi, J., 2001. On the features of the geodynamo following reversals or excursions: by absolute geomagnetic palaeointensity data, *Phys. Earth Plant. Inter.*, **124**, 81–93.

Goguitchaichvili, A. T., Prévot, M. & Camps, P., 1999a. No evidence for strong fields during the R3-N3 Icelandic geomagnetic reversal, *Earth Plant. Sci. Lett.*, **167**, 15–34.

Goguitchaichvili, A. T., Prévot, M., Thompson, J. & Roberts, N., 1999b. An attempt to determine the absolute geomagnetic field intensity in Southwestern Iceland during the Gauss-Matuyama reversal, *Phys. Earth Plant. Inter.*, **115**, 53–66.

Goree, W. S., 2007. *Encyclopedia of geomagnetism and paleomagnetism*, Encyclopedia of Earth Sciences, Springer.

Goree, W. S. & Fuller, M. D., 1976. Magnetometers using RF-driven SQUIDs and their application in rock magnetism and paleomagnetism, *Rev. Geophys. Space Phys.*, **14**, 591–608.

Goren-Inbar, N., Feibel, C. S., Verosub, K. L., Melamed, Y., Kislev, M. E., Tchernov, E. & Saragusti, I., 2000. Pleistocene milestones on the Out-of-Africa corridor at Gescher Benot Ya'aqov, Israel, *Science*, **289**, 944–947.

Graham, J. W., 1953. Changes of ferromagneticminerals and their bearing on magnetic properties of rocks, *J. Geophys. Res.*, **58**, 243–260.

Gratton, M. N., 2004. Variation of geomagnetic field intensity over the last 45,000 years in Hawaii using the microwave palaeointensity technique, *Ph.D. Thesis, University of Liverpool*, **20441.GRA**.

Gratton, M. N., Shaw, J. & Herrero-Bervera, E., 2005. An absolute palaeointensity record from SOH1 lava core, Hawaii using the microwave technique, *Phys. Earth Plant. Inter.*, **148**, 193–214.

Gratton, M. N., Shaw, J. & Brown, L. L., 2007. Absolute palaeointensity variations during a precursor to the Matuyama-Brunhes transition recorded in Chilean lavas, *Phys. Earth Plant. Inter.*, **162**, 61–72.

Griscom, D. L., 1974. Ferromagnetic resonance spectra of lunar fines: some implications of line shape analysis, *Geochim. Cosmochim. Acta*, **38**, 1509–1519.

Grommé, C. S., Wright, T. L. & Peak, D. L., 1969. Magnetic properties and oxidation of iron-titanium oxide minerals in Alae and Makaopulhi lava lakes, *J. Geophys. Res.*, **74**, 5277–5293.

Grommé, C. S., Reilly, T. A., Mussett, A. E. & Hay, R. L., 1971. Palaeomagnetism and potassium-argon ages of volcanic rocks of Ngorongoro Caldera, Tanzania, *Geophys. J. R. astr. Soc.*, **22**, 105–115.

Gubbins, D., 1999. The distinction between geomagnetic excursions and reversals, *Geophys. J. Int.*, **137**, F1–F2.

Gubbins, D. & Coe, R. S., 1993. Longitudinally confined geomagnetic reversal paths from non-dipolar transition fields, *Nature*, **362**, 51–53.

Gubbins, D., Jones, A. & Finlay, C. C., 2006. Fall in the Earth's field is erratic, *Science*, **312**, 900–902.

Guillou, H., Carracedo, J. C. & Day, S. J., 1998. Dating of the upper Pleistocene Holocene volcanic activity of La Palma using the unspiked K-Ar technique, *J. Volcanol. Geotherm. Res.*, **86**, 137–149.

Guillou, H., Carracedo, J. C. & Duncan, R. A., 2001. K-Ar, $^{40}Ar/^{39}Ar$ ages and magnetostratigraphy of Brunhes and Matuyama lava sequences from La Palma Island, *J. Volcanol. Geotherm. Res.*, **106**, 175–194.

Guo, B., Zhu, R., Florindo, F., Pan, Y. & Yue, L., 2001. Pedogenesis affecting the Matuyama-Brunhes polarity transition recorded in Chinese loess?, *Chinese Sci. Bull.*, **46**, 975–980.

Guyodo, Y., Richter, C. & Valet, J.-P., 1999. Paleointensity record from Pleistocene sediments (1.4-0) Ma off the California margin, *J. Geophys. Res.*, **104**, 22953–22964.

Guyodo, Y., Gaillot, P. & Channell, J. E. T., 2000. Wavelet analysis of relative geomagnetic paleointensity at ODP site 983, *Earth Plant. Sci. Lett.*, **184**, 109–123.

Halgedahl, S. L., Day, R. & Fuller, M., 1980. The effect of cooling rate on the intensity of weak-field TRM in single-domain magnetite, *J. Geophys. Res.*, **85**, 3690–3698.

Hamilton, T. S. & Evans, M. E., 1983. A magnetostratigraphic and secular variation study of Level Mountain, northern British Columbia, *Geophys. J. R. astr. Soc.*, **73**, 39–49.

Harrison, C. G. A. & Somayajulu, B. L. K., 1966. Behavior of the earth's magnetic field during a reversal, *Nature*, **211**, 1193–1195.

Hartl, P. & Tauxe, L., 1996. A precursor to the Matuyama/Brunhes transition-field instability as recorded in pelagic sediments, *Earth Plant. Sci. Lett.*, **138**, 121–135.

Hayashida, A., Verosub, K. L., Heider, F. & Leonahardt, R., 1999. Magnetostratigraphy and relative palaeointensity of late Neogene sediments at ODP Leg 167 Site 1010 off Baja California, *Geophys. J. Int.*, **139**, 829–840.

Heider, F., Hufenbecher, F., Draeger, U. & Hayashida, A., 2000. The Brunhes-Matuyama and the upper Jaramillo transitions recorded in sediments from the California Margin (ODP Leg 167), *Proc. ODP. Sci. Res.*, **167**, 311–318.

Heinrichs, D. F., 1967. Paleomagnetism of the Plio-Pleistocene Lousetown Formation, Virginia City, Nevada, *J. Geophys. Res.*, **72(12)**, 3277–3294.

Heirtzler, J. R., Dickson, G. O., Herron, E. M., III, W. C. P. & Pichon, X. L., 1968. Marine magnetic anomalies, geomagnetic field reversals and motions of the ocean floor and continents, *J. Geophys. Res.*, **73**, 2119–2136.

Heller, R., Merrill, R. T. & McFadden, P. L., 2003. The two states of the paleomagnetic field intensities for the past 320 million years, *Phys. Earth Plant. Inter.*, **135**, 211–223.

Herrero-Bervera, E. & Coe, R. S., 1999. Transitional field behaviour during the Gilbert-Gauss and Lower Mammoth reversals recorded inlavas from the Wai'anae volcano, O'ahu, Hawaii, *J. Geophys. Res.*, **104 (B12)**, 29,157–29,173.

Herrero-Bervera, E. & Valet, J.-P., 2005. Absolue paleointensity and reversal records from the Waianae sequence (Oahu, Hawaii, USA), *Earth Plant. Sci. Lett.*, **234**, 279–296.

Hill, M. J., 2000. The microwave palaeointensity technique and its application to lava, *Ph.D. Thesis, University of Liverpool*, **20041.HIL**.

Hill, M. J. & Shaw, J., 1999. Palaeointensity results for historic lavas from Mt Etna using microwave demagnetization/remagnetization in a modified Thellier-type experiment, *Geophys. J. Int.*, **139**, 583–590.

Hill, M. J. & Shaw, J., 2000. Magnetic field intensity study of the 1960 Kilauea lava flow, Hawaii, using the microwave palaeointensity technique, *Geophys. J. Int.*, **142**, 487–504.

Hill, M. J. & Shaw, J., 2007. The use of the 'Kono perpendicular applied field method' in microwave palaeointensity experiments, *Earth Planets Space*, **59**, 711–716.

Hill, M. J., Gratton, M. N. & Shaw, J., 2002. A comparison of thermal and microwave palaeomagnetic techniques using lava containing laboratory induced remanence, *Geophys. J. Int.*, **151**, 157–163.

Hill, M. J., Shaw, J. & Herrero-Bervera, E., 2005. Palaeointensity record through the Lower Mammoth reversal from the Waianae volcano, Hawaii, *Earth Plant. Sci. Lett.*, **230**, 255–272.

Hill, M. J., Shaw, J. & Herrero-Bervera, E., 2006. Determining palaeointensity from the Gilbert Gauss Reversal recorded in the Pu'u Heleakala lava section, Wai'anae volcano, Oahu, Hawaii, *Earth Plant. Sci. Lett.*, **245**, 29–38.

Hillhouse, J. & Cox, A., 1976. Brunhes-Matuyama polarity transition, *Earth Plant. Sci. Lett.*, **29**, 51–64.

Hoffman, K. A., 1984. Geomagnetic reversals, *Nature*, **309**, 90–91.

Hoffman, K. A., 1992. Dipolar reversal states of the geomagnetic field and core-mantle dynamics, *Nature*, **359**, 789–794.

Hoffman, K. A., 1996. Transitional paleomagnetic field behavior: preferred paths or patches?, *Surv. Geophys.*, **17**, 207–211.

Hoffman, K. A., 2000. Temporal aspects of the last geomagnetic last reversal of the Earth's geomagnetic field, *Philos. Trans. R. Soc. Lond.*, **358**, 1181–1190.

Hoffman, K. A. & Singer, B. S., 2004. Reginonally recurrent paleomagnetic transitional field and mantle processes, *Timescales of the paleomagnetic field, Geophysical Monograph Series*, **145**, 233–243 doi:10.29/145GM16.

Hooper, P. R., Knowles, C. R. & Watkins, N. D., 1979. Magnetostratigraphy of the Imnaha and Grande Basalts in the south east part of the Columbia Plateau, *Am. J. Sci.*, **279**, 737–754.

Horng, C.-S., Roberts, A. P. & Liang, W.-T., 2003. A 2.14-Myr astronomically tuned record of relative geomagnetic paleointensity from the western Philippine Sea, *J. Geophys. Res.*, **108**, doi: 1029/2001JB001698.

Hospers, J., 1953. Reversals of the main geomagnetic field I, II, *Proc. Kon. Nederl. Akad. Wetensch*, **56**, 467–491.

Hospers, J., 1954. Reversals of the main geomagnetic field III, *Proc. Kon. Nederl. Akad. Wetensch*, **57**, 112–121.

Hulot, G., Eymin, C., Langlais, B., Mandea, M. & Olson, N., 2002. Small-scale structure from the geodynamo inferred from Oersted and Magsat satellite data, *Nature*, **416**, 620–623.

Huntley, D. J., Hutton, J. T. & Prescott, J. R., 1993. The stranded beach-dune sequence of south-east South Australia: a test of thermoluminescence dating, 0-800 ka, *Quatern. Sci. Rev.*, **12**, 1–20.

Huntley, D. J., Hutton, J. T. & Prescott, J. R., 1994. Further luminescence dates from the dune sequence of the south-east of South Australia, *Quatern. Sci. Rev.*, **13**, 201–207.

Hyodo, H., Diswas, D. K., Nado, T., Tomioka, N., Mishima, T., Itota, C. & Sato, H., 2006. Millennial- to submillenial-scale features of the Matuyama-Brunhes geomagnetic polarity transition from Osaka Bay, southwestern Japan, *J. Geophys. Res.*, **111**, doi: 1029/2004JB003584.

Idnurm, M. & Cook, P. J., 1980. Palaeomagnetism of beach ridges in South Australia and the Milankovitchtheory of ice ages, *Nature*, **286**, 699–702.

Jackson, A., Jonkers, A. R. T. & Walker, M. R., 2000. Four centuries of geomagnetic secular variation from historical records, *Phil. Trans. R. Soc. Lond.*, **358**, 957–990.

Johnson, C. L. & Constable, C. G., 1995. The time-averaged geomagnetic field as recoreded by lava flows over the past 5 Myr, *Geophys. J. Int.*, **122**, 489–519.

Johnson, C. L. & Constable, C. G., 1996. Palaeosecular varaition recorded by transitional lava flows over the past five million years, *Philos. Trans. R. Soc. London*, **354**, 89–141.

Johnson, C. L., Wijbrans, J. R., Constable, C. G., Gee, J., Staudigel, H., Tauxe, L., Forjaz, V.-H. & Salgueiro, M., 1998. $^{40}Ar/^{39}Ar$ ages and paleomagnetism of São Miguel lavas, Azores, *Earth Plant. Sci. Lett.*, **160**, 637–649.

Johnson, C. L., Constable, C. G. & Tauxe, L., 2003. Mapping long-term changes in Earth's magnetic field, *Science*, **300**, 2044–2045.

Jonkers, A. R. T., Jackson, A. & Murray, A., 2003. Four centuries of geomagnetic data from historical records, *Rev. Geophys.*, **41(2)**, 1006, doi:10.1029/2002RG000115.

Kawai, N., 1954. Instability of natural remanent magnetism of rocks, *J. Geomag. Geoelectr.*, **6**, 208–209.

Kawai, N., Nakajima, T., Hirooka, K. & Kobayashi, K., 1973. The transition of the field at the Brunhes and Jaramillo boundaries in the Matuyama epoch, *Proc. Jpn. Acad.*, **49**, 820–824.

Kawai, N., Otofuji, Y., Nakajima, T. & Kobayashi, K., 1975. Geomagnetic stage transition from the Matuyama to Brunhes epochs, *Proc. Jpn. Acad.*, **51**, 634–638.

Kawai, N., Sato, T., Sueishi, T. & Kobayashi, K., 1977. Paleomagnetic study of deep-sea sediments using thin sections, *J. Geomag. Geoelectr.*, **29**, 211–223.

Kelly, P. & Gubbins, D., 1997. The geomagnetic field over the last 5 million years, *Geophys. J. Int.*, **128**, 315–330.

Kent, D. V. & Opdyke, N. D., 1977. Paleomagnetic field intensity variation recorded in Brunhes epoch deep-sea sediment core, *Nature*, **266**, 156–159.

Khramov, A. N., 1955. Study of remanent magnetization and the problem of stratigraphic correlation and subdivision, *Akad. Nauk SSSR*, **100**, 551–554.

Khramov, A. N., 1957. Paleomagnetism as a basis for a new technique of sedimentary rock correlation and subdivision, *Akad. Nauk SSSR*, **112**, 849–852.

Khramov, A. N., 1958. *Paleomagnetism and Stratigraphic Correlation*, Gostoptechizdat, Leningrad.

Kida, S., Araki, K. & Kitauchi, H., 1997. Periodic reversals of magnetic fields generated by thermal convection in a rotating spherical shell, *J. Phys. Soc. Jpn.*, **66**, 2194–2201.

Kidane, T., X. Quidelleur, J. C., Courtillot, V., Gallet, Y., Gillot, P. Y. & Haile, T., 1999. Paleomagnetic and geochronological identification of the Réunion subchron in Ethiopian Afar, *J. Geophys. Res.*, **104**, 10,405–10,419.

Kirschvink, J. L., 1980. The least-squares line and the plane and the analysis of palaeomagnetic data, *Geophys. J. R. Astron. Soc*, **62**, 699–718.

Kissel, C., Laj, C., Clemens, S. & Solheid, P., 2003. Magnetic signature of environmental changes in the last 1.2 Myr at ODP Site 1146, South China Sea, *Mar. Geol.*, **201**, 119–132.

Komorowski, J.-C., Boudon, G., Semet, M., Beauducel, F., Antenor-Habazac, C., Bazin, S. & Hammouya, G., 2005. *Guadeloupe. In: Lindsay J M, Robertson R E A, Shepherd J B, Ali S (eds). Volcanic Hazard Atlas of the Lesser Antilles*, Seismic Res Unit, Univ West Indies.

Kono, M. & Tanaka, H., 1984. Analysis of the Thelliers' method of paleointensity determination 1: Estimation of statistical errors, *J. Geomag. Geoelectr.*, **36**, 267–284.

Kono, M. & Ueno, N., 1977. Paleointensity determination by a modified Thellier method, *Phys. Earth Plant. Inter.*, **13**, 305–314.

Korte, M. & Constable, C. G., 2005a. Continuous geomagnetic field models for the past 7 millenia: 2. CALS7K, *Geochem. Geophys. Geosyst.*, **6**, Q02H16, doi:10.1029/2004GC000801.

Korte, M. & Constable, C. G., 2005b. The geomagnetic dipole moment over the last 7000 years - new results from a global model, *Earth Plant. Sci. Lett.*, **236**, 348–358.

Korte, M. & Constable, C. G., 2006. Centennial to millennial geomagnetic secular variation, *Geophys. J. Int.*, **67**, 43–52.

Korte, M., Genevey, A., Constable, C. G., Frank, U. & Schnepp, E., 2005. Continuous geomagnetic field models for the past 7 millenia: 1. a new global data compliation, *Geochem. Geophys. Geosyst.*, **6**, Q02H15, doi:10.1029/2004GC000800.

Kočí, A. & Šibrava, 1996. The Brunhes-Matuyama at central European localities. glaciations in the Northern Hemisphere, *IUGS-UNESCO*, **0**, 135–160.

Kočí, A., Ložek, V. & Malkowski, Z., 1974. Paleomagnetic investigation of the Suchdol Terrace of the River Vltava, *Studia. Geophys. Geod.*, **18**, 259–265.

Krása, D. & Fabian, K., 2007. *Encyclopedia of geomagnetism and paleomagnetism*, Encyclopedia of Earth Sciences, Springer.

Kristjánsson, L., 1993. Investigations on geomagnetic reversals in Icelandic lavas, 1953-78, *Terra Nova*, **5**, 6–12.

Kristjánsson, L., 1995. New palaeomagnetic results from Icelandic Neogene lavas, *Geophys. J. Int.*, **121**, 435–443.

Kristjánsson, L. & Guðmundsson, A., 2004. Paleomagnetic studies in Skarðsheiði, South-Western Iceland, *Jökull*, **50**, 33–48.

Kristjánsson, L. & Guðmundsson, A., 2005. Stratigraphy and paleomagnetism study of lava pile sequences in the Suðurdalur area, fljótsdalur, Eastern Iceland, *Jökull*, **55**, 39–56.

Kristjánsson, L. & Jóhannesson, H., 1996. Stratigraphy and paleomagnetism of the lava pile south of Ísafjarðardjúp, NW-Iceland, *Jökull*, **44**, 3–16.

Kristjánsson, L. & Jóhannesson, H., 1999. Secular variation and reversals in composite 2.5 km thick lava section in central Western Iceland, *Earth Planets Space*, **51**, 261–276.

Kristjánsson, L. & Sigurgeirsson, M., 1993. The R3-N3 and R5-N5 palaeomagnetic transition zones in SW-Icelandic lavas revisited, *J. Geomag. Geoelectr.*, **45**, 275–288.

Kristjánsson, L., Fridleifsson, I. B. & Watkins, N. D., 1980. Stratigraphy and paleomagnetism of the Esja, Eyrarfjall and Akrfjall mountains, SW-Iceland, *J. Geophys*, **47**, 31–42.

Kristjánsson, L., Jóhannesson, H. & McDougall, I., 1992. Stratigraphy, age and paleomagnetism of Langidalur, northern Iceland, *Jökull*, **42**, 31–44.

Kristjánsson, L., Guðmundsson, A. & Haraldsson, H., 1995. Stratigraphy and paleomagnetism of a 3-km-thick Miocene lava pile in the Mjoifjördur area, eastern Iceland, *Geol. Rundsch*, **84**, 813–830.

Kristjánsson, L., Hardarsson, B. S. & Audunsson, H., 2003. A detailed palaeomagnetic study of the oldest (≈15 Myr) lava sequences in Northwest Iceland, *Geophys. J. Int.*, **155**, 991–1005.

Kristjánsson, L., Guðmundsson, A. & Hardarson, B., 2004. Stratigraphy and paleomagnetism of a 2.9-km composite lava section in Eyjafjördur, Northern Iceland: a reconnaissance study, *Int. J. Earth Sci. (Geol Rundsch)*, **93**, 582–595.

Kristjánsson, L., Guðmundsson, A., Hjartarson, A. & Hallsteinsson, H., 2006. A paleomagnetic study of the stratigraphic relations in the lava pile of Norðurárdalur and Austurdalur, Skagafjörður, North Iceland, *Jökull*, **56**, 17–32.

Kutzner, C. & Christensen, U. R., 2002. From stable dipolar to reversing numerical dynamos, *Phys. Earth Plant. Inter.*, **131**, 29–45.

Kutzner, C. & Christensen, U. R., 2004. Simulated geomagnetic reversals and preferred virtual geomagnetic pole paths, *Geophys. J. Int.*, **157**, 1105–1118.

Laj, C., Mazaud, A., Weeks, R., Fuller, M. & Herrero-Bervera, E., 1991. Geomagnetic reversal paths, *Nature*, **351**, 447.

Laj, C., Mazaud, A., Weeks, R., Fuller, M. & Herrero-Bervera, E., 1996. Relative geomagnetic field intensity and reversals for the last 1.8 My from central equatorial Pacific core, *Geophys. Res. Lett.*, **23**, 3393–3396.

Laj, C., Szermeta, N., Kissel, C. & Guillou, H., 2000. Geomagnetic paleointensities at Hawaii between 3.9 Ma and 2.1 Ma: preliminary results, *Earth Plant. Sci. Lett.*, **179**, 191–204.

Laj, C., Kissel, C. & Guillou, H., 2002. Brunhes' research revisited: Magnetization of volcanic flows and baked clays, *Eos Trans. AGU*, **83**, 381–384.

Langereis, C. G., van Hoof, A. A. M. & Rochette, P., 1992. Longitudinal confinement of geomagnetic reversal paths as a possible sedimentary artefact, *Nature*, **358**, 226–230.

Langereis, C. G., Dekkers, M. J., de Lange, G. J., Paterne, M. & van Santvoort, P. J. M., 1997. Magnetostratigraphy and astronomical calibration of the last 1.1 Myr from an eastern Mediterranean piston core and dating of short events in the Brunhes, *Geophys. J. Int.*, **129**, 75–94.

Larson, E. & Patterson, P., 1993. The Matuyama-Brunhes reversal at Tecopa basin, southeastern California, revisted again, *Earth Plant. Sci. Lett.*, **120**, 311–325.

Lattard, D., Engelmann, R., Kontny, A. & Sauerzapf, U., 2006. Curie tempertaures of synthetic titanomagnetites in the Fe-Ti-O system: Effects of composition, crystal chemistry, and thermomagnetic methods, *J. Geophys. Res.*, **111**, B12S28, doi:10.1029/2006JB004591.

Le Mouël, J.-L., 1984. Outer-core geostrophic flow and secular varaition of earth's geomagnetic-field, *Nature*, **311**, 734–735.

Leonhardt, R. & Fabian, K., 2007. Paleomagnetic reconstruction of the global geomagnetic field evolution during the Matuyama/Brunhes transition: iterative Bayesian inversion and independent verification, *Earth Plant. Sci. Lett.*, **253**, 172–195.

Leonhardt, R. & Soffel, H. C., 2002. A reversal of the Earth's magnetic field recorded in mid-Miocebe lava flows of Gran-Canaria: Paleointensities, *J. Geophys. Res.*, **107 (B11)**, 2299, doi: 10.1029/2001JB000322.

Leonhardt, R., Hufenbecher, F., Heider, F. & Soffel, H. C., 2000. High absolute palaeointensity during a mid mioene excursion of the Earth's magneticfield, *Earth Plant. Sci. Lett.*, **184**, 141–154.

Leonhardt, R., Matzka, J., Hufenbecher, F., Soffel, H. C. & Heider, F., 2002. A reversal of the Earth's magnetic field recorded in mid-Miocebe lava flows of Gran-Canaria: Paleodirections, *J. Geophys. Res.*, **107 (B11)**, doi: 10.1029/2001JB000322.

Leonhardt, R., Matzka, J., Nichols, A. R. L. & Dingwell, D. B., 2006. Cooling rate correction of paleointensity determination for volcanic glasses by relaxation geospeedometry, *Earth Plant. Sci. Lett.*, **243**, 282–292.

Levi, S., 1977. The effect of magnetite particle size on paleointensity determinations of the geomagnetic field, *Phys. Earth Plant. Inter.*, **13**, 245–259.

Liddicoat, J. C., 1993. Matuyama/Brunhes polarity transition near Bishop, California, *Geophys. J. Int.*, **112**, 497–506.

Lin, J. L., Verosub, K. L. & Roberts, A. P., 1994. Decay of the virtual dipole moment during polarity transitions and geomagnetic excursions, *Geophys. Res. Lett.*, **21**, 525–528.

Love, J. J., 1998. Paleomagnetic volcanic data and geometric regularity of reversals and excursions, *J. Geophys. Res.*, **103**, 12,435–12,452.

Love, J. J., 2000. Statistical assessment of preferred transitional VGP longitudes based on palaeomagnetic lava data, *Geophys. J. Int.*, **140**, 211–221.

Love, J. J. & Mazaud, A., 1997. A database for the Matuyama-Brunhes magnetic reversal, *Phys. Earth Plant. Inter.*, **103**, 204–245.

Løvlie, R., Su, P., Fan, X. Z., Zhao, Z. J. & Lui, C., 2001. A revised paleomagnetic age of the Nihewan Group at the Xujiayao Paleolithic site, China, *Quatern. Sci. Rev.*, **20**, 1341–1353.

Lund, S. P., Schwartz, M., Keigwin, L. & Johnson, T., 2005. Deep-sea sediment records of the Laschamp geomagnetic field excursion $\sim$ 41,000 calendar years before present, *J. Geophys. Res.*, **110 (B04101)**, 1–15.

Mankinen, E. A., Prévot, M., Grommé, C. S. & Coe, R. S., 1985. The Steens Mountain (Oregon) geomagnetic polarity transition 1. Directional history, duration of episodes, and rock magnetism, *J. Geophys. Res.*, **90(B12)**, 10,393–10,416.

Mary, C. & Courtillot, V., 1993. A three-dimensional representation of geomagnetic reversal records, *J. Geophys. Res.*, **98**, 22,461–22,475.

Matuyama, M., 1929. On the direction of magnetisation of basalt in Japan, Tyosen and Manchuria, *Proc. Imp. Acad. Japan*, **5**, 203–205.

Mayergoyz, I. D., 1986. Mathematical models of hysteresis, *Phys. Rev. Lett.*, **56**, 1518–1561.

McDougall, I. & Watkins, N. D., 1973. Age and duration of the Réunion geomagnetic polarity event, *Earth Plant. Sci. Lett.*, **19**, 443–452.

McDougall, I., Watkins, N. D. & Kristjánsson, L., 1976. Geochronology and paleomagnetism of a Miocene-Pliocene lava sequence at Bessastadaa, Eastern Iceland, *Am. J. Sci.*, **276**, 1078–1095.

McDougall, I., Kristjánsson, L. & Sæmundsson, K., 1984. Magnetostratigraphy and geochronology of Northwest Iceland, *J. Geophys. Res.*, **89**, 7029–7060.

McFadden, P. L., Barton, C. E. & Merrill, R. T., 1995. History of earth's magnetic field and possible connections to core-mantle processes, *J. Geophys. Res.*, **100**, 307–316.

Mckee, E. H. & Elston, D. P., 1980. Reversal chronology from a 7.9- to 11.5-M.Y.-old volcanic sequence in Central Arizona: Comparison with ocean floor polarity record, *J. Geophys. Res.*, **85**, 327–337.

Mercanton, P.-L., 1926a. Aimantation de basaltes groënlandais, *C. R. Acad. Sci. Paris*, **182**, 859.

Mercanton, P.-L., 1926b. Aimantation des roche volcaniques australiennes, *C. R. Acad. Sci. Paris*, **182**, 1231.

Merrill, R. T., 1995. Principle of least astonishment, *Nature*, **374**, 674–675.

Merrill, R. T., 2004. Time of reversal, *Nature*, **428**, 608–609.

Merrill, R. T. & McFadden, P. L., 1999. Geomagnetic polarity reversals, *Rev. Geophys.*, **37(2)**, 201–226.

Merrill, R. T., McElhinny, M. W. & Stevenson, D. J., 1995. Evidence for long term asymmetries in the Earth's magnetic field and possible implications for dynamo theories, *Phys. Earth Plant. Inter.*, **20**, 75–82.

Merrill, R. T., McElhinny, M. W. & McFadden, P. L., 1996. *The Magnetic Field of the Earth: Palaeomagnetism, the Core, and the Deep Mantle*, vol. 63 of *International geophysics series*, Academic Press.

Meynadier, L., Valet, J.-P., Bassinot, F. C., Shackleton, N. J. & Guyodo, N. J., 1994. Asymmetrical saw-tooth pattern of the geomagnetic field intensity from equatorial sediments in the Pacific and Indian Oceans, *Earth Plant. Sci. Lett.*, **126**, 109–127.

Meynadier, L., Valet, J.-P. & Shackleton, N. J., 1995. Relative geomagnetic intensity during the last 4 m.y. from the equatorial Pacific, *Proc. Ocean Drill. Program Sci. Results*, **138**, 779–795.

Mochizuki, N., Tsunakawa, H., Kurata, M., Yamazaki, T. & Oda, H., 2005. Palaeointensity study of the Brunhes-Matuyama polarity reversal recorded in the lava sequence in Punaruu valley, Tahiti Island, *10th Scientific Assembly of the IAGA*, pp. IAGA2005–A–01158.

Moskowitz, B. M., 1981. Methods for estimating Curie temperatures of titanomaghemites from experimental Js-T data, *Earth Plant. Sci. Lett.*, **52**, 84–88.

Moskowitz, B. M., Jackson, M. & Kissel, C., 1998. Low-temperature magnetic behavior of titanomagnetites, *Earth Plant. Sci. Lett.*, **157**, 141–149.

Mullins, C. E. & Tite, M. S., 1973. Magnetic viscosity, quadrature of susceptibility, and frequency dependence of susecptibility in single-domain assemblies of magnetite and maghemite, *J. Geophys. Res.*, **78**, 804–809.

Muxworthy, A. R. & Dunlop, D., 2002. First-order reversal curve (FORC)diagrams for psuedo-single-domain magnetites at high temperature, *Earth Plant. Sci. Lett.*, **203**, 369–382.

Nagata, T., 1953. *Rock Magnetism*, Tokyo: Maruzen.

Nagata, T., Akimoto, S. & Uyeda, S., 1951. Reverse thermoremanent magnetisation, *Japan Acad. Proc*, **27**, 643–645.

Nagata, T., Arai, Y. & Momose, K., 1963. Secular varaition of the geomagnetic force during the last 5000 years, *J. Geophys. Res.*, **68**, 5277–5281.

Narteau, C. & Le Mouël, J.-L., 2005. Transient evolution regimes in a multiscale dynamo model: Timescales of the reversal mechanism, *J. Geophys. Res.*, **110**, B01104 doi:1029/2004JB002983.

Navarro, J. M. & Coello, J., 1993. *Geological map of the national park of the Caldera de Taburiente*, vol. 1 of *1*, Instituto Nacional para la Conservacion de la Naturaleza, La Palma.

Nawrocki, J., Bogucki, A., Łanczont, M. & Nowaczyk, N. R., 2002. The Matuyama-Brunhes boundary and the nature of magnetic remanence acquisition in the loess-palaeosol sequence from the western part of the East European loess province, *Palaeogeogr. Palaeoclimatol. Palaeoecol.*, **188**, 39–50.

Néel, L., 1949. Théorie du traînage magnétique des ferromagnétiques en grains fins avec applications aux terre cuites, *Ann. Géophys.*, **5**, 99–136.

Néel, L. E. F., 1951. L'inversion de l'aimantation permanente des roches, *Ann. Géophys.*, **7**, 90–102.

Néel, L. E. F., 1955. Some theoretical aspects of rock magnetism, *Adv. Phys.*, **4**, 191–243.

Niitsuma, N., 1971. Detailed study of the sediments recording the Matuyama-Brunhes geomagnetic rever sal, *Tohoku Univ. Sci. Rep. 2nd Ser Geol.*, **43**, 1–39.

Oda, H., Shibuya, H. & Hsu, V., 2000. Paleomagnetic records of the Brunhes/Matuyama polarity transition from ODPLeg 124 (Celebs and and Sulu seas, *Geophys. J. Int.*, **142**, 319–338.

Okada, M. & Niitsuma, N., 1989. Detailed paleomagnetic records during the Brunhes-Matuyama geomagnetic rever sal, and a direct determination of depth lag for magnetization in marine sediments, *Phys. Earth Plant. Inter.*, **56**, 133–150.

Olsen, N., Lühr, H., Sabaka, T. J., Mandea, M., M.Rother, Tøffner-Clausen, L. & Choi, S., 2006. CHAOS - a model of the Earth's magnetic field derived from CHAMP, Ørsted, and SAC-C magnetic satellite data, *Geophys. J. Int.*, **166 (1)**, 65–75.

Olson, P. & Amit, H., 2006. Changes in earth's dipole, *Naturwissenschaften*, **93**, 519–542.

Özdemir, O., Dunlop, D. J. & Moskowitz, B. M., 1993. The effect of oxidation on the Verwey transition in magnetite, *Geophys. Res. Lett.*, **20**, 1671–1674.

Park, C.-K., Son, S.-K., Kim, K. H., Chi, S.-B. & Doh, S.-J., 2004. Paleomagnetic records from deep-sea sediment of the Korea Deep Ocean Study (KODOS) area (northern equatorial Pacific) and their paleodepositional implications, *Geo-Mar. Lett.*, **24**, 112–124.

Patel, J. P. & Raja, P. K. S., 1979. Paleomagnetic results from the narosura and magadivolcanics of kenya, *Earth Plant. Sci. Lett.*, **19**, 7–14.

Perrin, M. & Schnepp, E., 2004. Iaga paleointensity database: distribution and quality of the data set, *Phys. Earth Plant. Inter.*, **147**, 255–267.

Petronille, M., Goguitchaichvili, A., Henry, B., Alva-Valdivia, L. M., Rosas-Elguera, J., Urrutia-Fucugauchi, J., Cejá, M. R. & Calvo-Rathert, M., 2005. Paleomagnetism of Ar-Ar dated lava flows from the Caboruco-San Pedro vocanic field (western Mexico): Evidence for the Matuyama-Brunhes transition precursor and a fully reversed geomagnetic event in the Brunhes chron, *J. Geophys. Res.*, **110**, B08101, doi:10.1029/2004JB003321.

Pike, C. R., Roberts, A. P. & Verosub, K. L., 1999. Characterizing interactions in fine magnetic particl systems using first order reversal curves, *J. Appl. Phys.*, **85**, 6661–6667.

Pike, C. R., Roberts, A. P., Dekkers, M. J. & Verosub, K. L., 2001. An investigation of multi-domain hysteresis mechanisms using forc diagrams, *PEPI*, **126**, 11–25.

Pillans, B., 2003. Subdividing the Pleistocene using the Matuyama-Brunhes boundary (MBB): an Australian perspective, *Quatern. Sci. Rev*, **22**, 1569–1577.

Pillans, B. J., Roberts, A. P., Wilson, G. S., Abbott, S. T. & Alloway, B. V., 1994. Magnetostratographic, lithostratographic and tephrostratigraphic constraints on Lower and Middle Pleistocene sea-level changes, Wanganui Basin, New Zealand, *Earth Plant. Sci. Lett.*, **121**, 81–98.

Prægel, N. O. & Holm, P. M., 2006. Lithospheric contributions to high MgO basanites from the Cumbre Vieja volcano, La Palma, Canary Islands and evidence for temporal variation in plume influence, *J. Volcanol. Geotherm. Res.*, **149**, 213–239.

Prévot, M. & Camps, P., 1993. Absence of preferred longitudinal sectors for poles from volcanic records of geomagnetic reversals, *Nature*, **336**, 53–57.

Prévot, M., Mankinen, E. A., Coe, R. S. & Grommé, C. S., 1985. The Steens Mountain (Oregon) geomagnetic polarity transition; 2. Field intensity variation and discussion of reversal models, *J. Geophys. Res.*, **90**, 10,417–10,448.

Prévot, M., Roberts, N., Thompson, J., Faynot, L. & Perrin, M., 2003. Revisiting the Jurassic geomagnetic reversal recordedin the Lesotho Basalt, (Southern Africa), *Geophys. J. Int.*, **155**, 367–378.

Purucker, M. E., 2007. *Encyclopedia of geomagnetism and paleomagnetism*, Encyclopedia of Earth Sciences, Springer.

Quidelleur, X. & Valet, J.-P., 1996. Geomagnetic changes across the last reversal recorded in lava flows from La Palma, Canary Islands, *J. Geophys. Res.*, **101**, 13,755–13,773.

Quidelleur, X., Valet, J.-P., Courtillot, V. & Hulot, G., 1994. Long-term geometry of the geomagnetic field for the last five million years: An updated secular variation database, *Geophys. Res. Lett.*, **21 (15)**, 1639–1642.

Quidelleur, X., Gillot, P.-Y., Carlut, J. & Courtillot, V., 1999. Link between excursions and palaeointensity inferred from abnormal field directions recorded at La Palma around 600ka, *Earth Plant. Sci. Lett.*, **168**, 233–242.

Quidelleur, X., Carlut, J., Gillot, P.-Y. & Soler, V., 2002. Evolution of the geomagnetic field prior to the Matuyama-Brunhes transition: radiometric dating of a 820Ka excursion at La Palma, *Geophys. J. Int.*, **151**, F6–F10.

Quidelleur, X., Carlut, J., Soler, V., Valet, J.-P. & Gillot, P.-Y., 2003. The age and duration of the Matuyama-Brunhes transition from new K-Ar data from La Palma (Canary Islands) and revisted $^{40}Ar/^{39}Ar$, *Earth Plant. Sci. Lett.*, **208**, 149–163.

Radhakrishnamurty, C. & Likhite, S. D., 1993. Frequency dependence of low-temperature susceptibility peak in some titanomagnetites, *Phys. Earth Plant. Inter.*, **76**, 131–135.

Radhakrishnamurty, C., Likhite, S. D. & Sahasrabudhe, D. H., 1977. Nature of magnetic grains and their effect on the remanent magnetisation of basalts, *Phys. Earth Plant. Inter.*, **13**, 289–300.

Raisbeck, G. M., Yiou, F., Cattani, O. & Jouzel, J., 2006. $^{10}$be evidence for the Matuyama-Brunhes geomagnetic reversal in the EPICA Dome C ice core, *Nature*, **44**, 82–84.

Riisager, J., Riisager, P., & Pedersen, A. K., 2003. The C27n-C26r geomagnetic polarity reversal recorded in the west Greenland flood basalt province: How complex is the transitional field?, *J. Geophys. Res.*, **108**, 2155, doi:10.1029/2002JB002124.

Riisager, J., Riisager, P., Zhao, X., Coe, R. S. & Pedersen, A. K., 2004. Paleointensity during a chron C26r excursion recorded in west Greenland lava flows, *J. Geophys. Res.*, **109**, B04107, doi:10.1029/2003JB002887.

Riisager, P. & Abrahamsen, N., 2000. Palaeonintensity of West Greenland Palaeocene basalts: asymmetric intensity around the C27n-C26r transition, *Phys. Earth Plant. Inter.*, **118**, 53–64.

Riisager, P. & Riisager, J., 2001. Detecting multidomain magnetic grains in Thellier palaeointensity experiments, *Phys. Earth Plant. Inter.*, **125**, 111–117.

Roberts, A. P., Pike, C. R. & Verosub, K. L., 2000. First-order reversal curve diagrams: A new tool for characterizing the magnetite properties of natural samples, *J. Geophys. Res.*, **105**, 461–28,475.

Roberts, N. & Fuller, M., 1990. Similarity of new palaeomagnetic data from the Santa Rosa Mountains with those from Steens Mountain gives wide regional evidence for a two stage-reversal process of geomagnetic field reversal, *Geophys. J. Int.*, **100 (3)**, 521–526.

Roche, A., 1951. Sur les inversions de l'aimantation remanente des roche volcaniques dans les monts d'Auvergne, *C. R. Acad. Sci. Paris*, **233**, 1132–1134.

Roche, A., 1953. Sur l'origine des inversions de l'aimantation constantées dans les roche d'Auvergne, *C. R. Acad. Sci. Paris*, **236**, 107–109.

Roche, A., 1956. Sur le date de la dernière inversion du champ magnétique terrestre, *C. R. Acad. Sci. Paris*, **243**, 812–814.

Roche, A., 1958. Sur les variation de direction du champ magnétique terrestre, *C. R. Acad. Sci. Paris*, **246**, 3364–3366.

Rochette, P., 1990. Rationale of geomagnetic reversals versus remanence recording processes in rocks: a critical review, *Earth Plant. Sci. Lett.*, **98**, 33–39.

Roest, W. R., Danobeitia, J. J., Verhoef, J. & Collete, B. J., 1992. Magnetic anomalies in the Canary basin and the Mesozoic evolution of the central North Atlantic, *Mar. Geophys. Res.*, **14**, 1–24.

Rolph, T. C. & Shaw, J., 1985. A new method of paleofield magnitude correction for thermally altered samples and its application to Lower Carboniferous lavas, *Geophys. J. R. Astr. Soc.*, **80**, 773–781.

Roperch, P. & Duncan, R. A., 1990. Records of geomagnetic reversals from volcanic islands of French Polynesia1. paleomagnetic study of a polarity transition in a lava sequence from the island of Huahine, *J. Geophys. Res.*, **95**, 2713–2726.

Sæmundsson, K., Kristjánsson, L., McDougall, I. & Watkins, N. D., 1980. K-Ar dating, geological and paleomagnetic study of a 5-km lava succession in northern Iceland, *J. Geophys. Res.*, **85**, 3628–3646.

Samper, A., Quidelleur, X., Lahitte, P. & Mollex, D., 2007. Timng of effusive volcanism and collapse events within an oceanic arc island: Guadeloupe archipelago ( Lesser Antilles Arc, *Earth Plant. Sci. Lett.*, **258**, 175–191.

Sanver, M., 1968. A palaeomagnetic study of Quaternary volcanic rocks from Turkey, *Earth Plant. Sci. Lett.*, **1**, 403–421.

Sarson, G. & Jones, C., 1999. A convection driven geodynamo reversal model, *Phys. Earth Plant. Inter.*, **111**, 3–20.

Sarson, G. R., 2007. *Encyclopedia of geomagnetism and paleomagnetism*, Encyclopedia of Earth Sciences, Springer.

Sato, T., Kikuchi, H., Nakashizuka, M. & Okada, M., 1998. Quaternary geomagnetic field intensity: constant peridocity or varaible period?, *Geophys. Res. Lett.*, **25**, 2221–2224.

Schneider, D. A., Kent, D. V. & Mello, G. A., 1992. A detailed chronology of the Australian impact event, the Brunhes-Matuyama polarity reversal, and global climate change, *Earth Plant. Sci. Lett.*, **111**, 395–405.

Schönharting, G., Sharma, P. V. & Kentved, S., 1989. Magnetic polarity transition zomes at the Brunhes-Matuyama and upper Olduvai boundaries: preliminary results from ODP leg 104, *Proc. Ocean Drill. Prog. Sci. Results*, **104**, 903–910.

Selkin, P. A. & Tauxe, L., 2000. Long-term varations in palaeointensity, *Philos. Trans. R. Soc. Lond.*, **A, 358**, 1065–1088.

Senanayake, W. E. & McElhinny, M. W., 1981. Hysteresis and susceptibility characteristics of magnetite and titanomagnetite: interpretation of results from basaltic rocks, *Phys. Earth Plant. Inter.*, **26**, 47–55.

Shao, J. C., Fuller, M., Tanimoto, T., Dunn, J. R. & Stone, D., 1999. Spherical harmonic analyses of paleomagnetic data: The timeaveraged geomagnetic field for the past 5 Myr and the Brunhes-Matuyama reversal, *J. Geophys. Res.*, **104**, 5015–5030.

Shaw, J., 1974a. A new method of determining the magnitude of the palaeomagnetic field. Application to to five historic lavas and five archaeological samples, *Geophys. J. R. Astr. Soc.*, **39**, 133–141.

Shaw, J., 1974b. The magnitude of the palaeomagnetic field during a polarity transition. A new technique and its application., *Ph.D. Thesis, University of Liverpool*, **7441 SHA**.

Shaw, J., 1975. Strong geomagnetic fields during a single Icelandic polarity transition, *Geophys. J. R. Astr. Soc.*, **40**, 345–350.

Shaw, J. & Share, J. A., 2007. A new automated microwave demagnetiser/remagnetiser system for palaeointensity studies, *Eos Trans. AGU*, **Fall Meet. Suppl., Abstract**, GP53C–1371.

Shaw, J., Share, J. A. & Rogers, J., 1984. An automated superconducting magnetometer and demagnetizing system, *Geophys J. R. astr. Soc*, **78**, 209–218.

Shcherbakova, V. V. & Shcherbakova, V. P., 2000. Properties of partial thermoremanent magnetization in pseudosingle domain and multidomain magnetite grains, *J. Geophys. Res.*, **105**, 767–781.

Sigurgeirsson, T., 1957. Direction of magnetization in Icelandic baslats, *Adv. Phys.*, **6**, 240–246.

Singer, B. S. & Brown, L. L., 2002. The Santa Rosa Event: $^{40}Ar/^{39}Ar$ and paleomagnetic results from the Valles rhyolite near Jaramillo Creek, Jemez Mountains, New Mexico, *Earth Plant. Sci. Lett.*, **197**, 51–64.

Singer, B. S., Relle, M. K., Hoffman, K. A., Battle, A., Laj, C., Guillou, H. & Carracedo, J. C., 2002. Ar/Ar ages from transitionally magnetized lavas on La Palma, Canary Islands, and the geomagnetic instability timescale, *J. Geophys. Res.*, **107**, 2307 doi:10.1029/2001JB001613.

Singer, B. S., Hoffman, K. A., Coe, R. S., L. L. Brown, B. R. J., Pringle, M. S. & Chauvin, A., 2005. Structural and temporal requirements for geomagnetic field reversal deduced from lava flows, *Nature*, **434**, 633–636.

Smirnov, A. V., 2006. Low temperature magnetic properties of magnetite using first-order revresal curve analysis: Implications for the pseudo-single-domain state, *Geochem. Geophys. Geosyst.*, **7**, Q11011, doi:10.1029/2006GC001397.

Smirnov, A. V. & Tarduno, J. A., 2005. Thermochemical remanent magnetization in Precambrian rocks: Are we sure the geomagnetic field was weak?, *J. Geophys. Res.*, **110**, B06103, doi:10.1029/2004JB003445.

Sparks, M., 1964. *Ferromagnetic-relaxation theory*, Advanced Physics Monograph Series, McGraw-Hill Book Company.

Spassov, S., Heller, F., Evans, M. E., Yue, L. P. & Ding, Z. L., 2001. The Matuyama/Brunhes geomagnetic polarity transitions at Lingtai and Baoji, Chinese loess plateau, *Phys. Chem. Earth (A)*, **26**, 899–904.

Staudigel, H., Feraud, G. & Giannerini, G., 1986. The history of intrusive activity on the island of La Palma (Canary Islands), *J. Volcanol. Geotherm. Res.*, **27**, 299–322.

Stevenson, D. J., 1983. Planetary magnetic fields, *Rep. Prog. Phys*, **46**, 555–620.

Sun, D., Shaw, J., An, Z. & Rolph, T., 1993. Matuyama-Brunhes (M/B) transition recorded in Chinese loess, *J. Geomag. Geoelectr.*, **45**, 319–330.

Takahashi, F., Matsushima, M. & Honkura, Y., 2005. Simulations of a quasi-Taylor state geomagnetic field including polarity reversals on the Earth Simulator, *Science*, **27**, 299–322.

Tan, X., kodama, K. P., Gilder, S. & Courtillot, V., 2007. Rock magnetic evidence for inclination shallowing in the Passaic Formation red beds from the Newark basin and a systematic bias of the Late Triassic apparent polar wander path for North America, *Earth Plant. Sci. Lett.*, **254**, 345–357.

Tanaka, H. & Kono, M., 1991. Preliminary results and reliability of paleointensity studies on historical and 14C dated Hawaiian lavas, *J. Geomag. Geoelectr.*, **43**, 375–388.

Tanaka, H., Kono, M. & Kaneko, S., 1995. Secular variation of direction and intensity from two Pliocene-Pleistocene lava sections in Southwestern Iceland, *J. Geomag. Geoelectr.*, **47**, 89–102.

Tarduno, J. A. & Smirnov, A. V., 2004. The paradox of low field values and the long-term history of the geodynamo, *Timescales of the paleomagnetic field, Geophysical Monograph Series*, **145**, 75–84 doi:10.29/145GM08.

Tauxe, L., 1998. *Paleomagnetic Principles and Practice (Modern Approaches in Geophysics)*, Kluwer Academic Publishers.

Tauxe, L. & Hartl, P., 1997. 11 million years of Oligocene geomagnetic field behaviour, *Geophys. J. Int.*, **128**, 217–229.

Tauxe, L. & Kent, D. V., 2004. A simplified statistical model for the geomagnetic field and the detection of shallow bias in paleomagnetic inclinations: was the ancient magnetic field dipolar?, *Timescales of the paleomagnetic field, Geophysical Monograph Series*, **145**, 101–115 doi:10.29/145GM08.

Tauxe, L. & Shackleton, N. J., 1994. Relative paleointensity records from the Ontong-Java Plateau, *Geophys. J. Int.*, **117**, 769–782.

Tauxe, L., Herbert, T., Shackleton, N. J. & Kok, Y. S., 1996a. Astronomical calibration of the Matuyama-Brunhes boundary: Consequences for magnetic remanence acquisition in marine carbonates and the Asian loess sequences, *Earth Plant. Sci. Lett.*, **140**, 133–146.

Tauxe, L., Mullender, A. T. & Pick, T., 1996b. Potbellies, waspwaists, and superparamagnetism in magnetic hysteresis, *J. Geophys. Res.*, **101**, 571–583.

Tauxe, L., Staudigel, H. & Wijbrans, J. R., 2000. $^{40}Ar/^{39}Ar$ ages from La Palma in the Canary Islands), *Geochem. Geophys. Geosyst.*, **1**, 63.

Tauxe, L., Bertram, H. N. & Seberino, C., 2002. Physical interpretation of hysteresis loops: Micromagnetic modeling of fine particle magnetite, *Geochem. Geophys. Geosyst.*, **3(10)**, 1055, doi:10.1029/2001GC000241.

Thellier, E., 1938. Sur l'aimantation des terres cuites et ses applications geophysiques, *Ann. Inst. Globe Univ. Paris*, **16**, 157–302.

Thellier, E. & Thellier, O., 1959. Sur l'intensité du champ magnétique terrestre dans le passé historique et géologique, *Ann. Géophys.*, **15**, 285–376.

Theyer, F., Herrero-Bervera, E., Hsu, V. & Hammond, S. R., 1985. The zonal harmonic model of polarity transitions: a test using successive reversals, *J. Geophys. Res.*, **90**, 1963–1982.

Thibal, J., Pozzi, J. P., Bathès, V. & Dubuisson, G., 1995. Continuous record of geomagnetic field intensity between 4.7 and 2.7 Ma from downhole measurements, *Earth Plant. Sci. Lett.*, **136**, 541–550.

Thomas, D. N., Hill, M. J. & Garcia, A. S., 2004. Comparison of the Coe-Thellier-Thellier and microwave palaeointensity techniques using high-titanium titanomagnetites: results from a Tertiary basaltic intrusion from the Sydney Basin, New South Wales, *Earth Plant. Sci. Lett.*, **229**, 15–29.

Thomas, N., 1993. An integrated rock magnetic approach to the selection or rejection of ancient basalt samples for palaeointensity experiments, *Phys. Earth Plant. Inter.*, **75**, 329–342.

Tric, E., Laj, C., Jehanno, C., Valet, J.-P., Kissel, C., Mazaud, A. & Iaccarino, S., 1991. High-resolution of the upper Olduvai transition flow from Po Valley, (Italy) sediments; support for dipolar transition geometry?, *Phys. Earth Plant. Inter.*, **65**, 319–336.

Tsunakawa, H., Okada, M. & Niitsuma, N., 1995. About 100 year directional variations in the Matuyama-Brunhes transition field inferred from the sedimentary records in the Boso Peninsula, Japan, *J. Geomag. Geoelectr.*, **47**, 337–345.

Tsunakawa, H., Okada, M. & Niitsuma, N., 1996. Deconvolution of paleomagnetic directions from marine sediments in the Boso Peninsula, Japan, and implications for the Matuyama-Brunhes transitional field, *J. Geomag. Geoelectr.*, **48**, 1541–1552.

Tsunakawa, H., Okada, M. & Niitsuma, N., 1999. Further application of the deconvolution method of post-depositional DRM to the precise record of the Matuyama-Brunhes reversal in the sediments from the Boso Peninsula, Japan, *Earth Plants Space*, **51**, 169–173.

Turner, G. M. & Kamp, P. J. J., 1990. Palaeomagnetic location of the Jaramillo Subchron and Matuyama-Brunhes transition in the Castlecliff stratotype section, Wanganui Basin, New Zealand, *Earth Plant. Sci. Lett.*, **100**, 42–50.

Udagawa, S., Kitagawa, H., Guðmundsson, A., Hiroi, O., Koyaguchi, T., Tanaka, H., Kristjánsson, L. & Kono, M., 1999. Age and magnetism of lavas in Jökuldalur area, Eastern Iceland: Gilsá event revisited, *Phys. Earth Plant. Inter.*, **115**, 147–171.

Uyeda, S., 1957. Thermo-remanent magnetism and coercive force of the ilmenite-hematite series, *J. Geomag. Geoelectr.*, **9**, 61–78.

Uyeda, S., 1958. Thermoremanent magnetism as a medium of paleomagnetism, with special reference to reverse thermoremanent magnetism, *Jap. J. Geophys.*, **2**, 1–123.

Valet, J.-P., 2003. Time variations in geomagnetic intensity, *Rev. Geophys.*, **41(1)**, 1004 doi:10/2001RG000104.

Valet, J.-P. & Laj, C., 1984. Paleomagnetic record of two successive Miocene geomagnetic reversals in western Crete, *Earth Plant. Sci. Lett.*, **54**, 53–63.

Valet, J.-P. & Meynadier, L., 1993. Geomagnetic field intensity and reversals during the past four million years, *Nature*, **366**, 234–238.

Valet, J.-P., Tauxe, L. & Clark, D. R., 1988. The Matuyama-Brunhes transition recorded from Lake Tecopa sediments (California), *Nature*, **315**, 217–218.

Valet, J.-P., Tauxe, L. & Clement, B., 1989. Equatorial and mid-latitude records of the last geomagnetic field reversal from the Atlantic Ocean, *Earth Plant. Sci. Lett.*, **94**, 371–384.

Valet, J.-P., Tucholka, P., Courtillot, V. & Meynadier, L., 1992. Palaeomagnetic constraints on the geometry of the geomagnetic field during reversals, *Nature*, **356**, 400–407.

Valet, J.-P., Meynadier, L., Bassinot, F. & Garnier, F., 1994. Relative paleointensity across the last geomagnetic reversal from sediments of the Atlantic, Indian and Pacific Oceans, *Geophys. Res. Lett.*, **21**, 485–488.

Valet, J.-P., Brassart, J., LeMeur, I., Soler, V., Quidelleur, X., Tric, E. & Gillot, P.-Y., 1996. Absolute paleointensity and magnetomineralogical changes, *J. Geophys. Res.*, **101**, 25,029–25,044.

Valet, J.-P., Kidane, T., Soler, V., Brassart, J., Courtillot, V. & Meynadier, L., 1998. Remagnetization in lava flows recording pretransitional directions, *J. Geophys. Res.*, **103**, 9755–9775.

Valet, J.-P., Brassart, J., Quidelleur, X., Soler, V., Gillot, P.-Y. & Hongre, L., 1999. Paleointensity variations across the last geomagnetic reversal at La Palma, Canary Islands, Spain, *J. Geophys. Res.*, **104 (B4)**, 7577–7598.

van Hoof, A. A. M., Vanos, B. J. H., Rademakers, J. G., Langereis, C. G. & Delange, G. J., 1993. A paleomagnetic and geochemical record of the upper Cochiti reversal and two subsequent precessional cycles from southern Sicily (Italy), *Earth Plant. Sci. Lett.*, **117**, 235–250.

Velichko, A. A., Semenov, V. V., Pospelova, G. A., Morozova, T. D., Nechaev, V. P., Gribchenko, Y. N., Dlusskii, K. G., Rutter, N., Catto, N. & Little, E., 2006. Matuyama-Brunhes boundary in key sections of the loess-palaeosol-glacial formationson the East European Plain, *Quatern. Int.*, **152-153**, 94–102.

Verhoogen, J., 1956. Ionic ordering and self-reversal of magnetization in impure magnetites, *J. Geophys. Res.*, **61**, 201–209.

Verosub, K. L., Herrero-Bervera, E. & Roberts, A. P., 1996. Relative geomagnetic paleointensity across the Jaramillo and the Matuyama/Brunhes boundary, *Geophys. Res. Lett.*, **23**, 467–470.

Verwey, E. J. W., 1939. Electronic conduction of magnetite ($Fe_3O_4$) and its transition point at low temperatures, *Nature*, **144**, 327–328.

Vine, F. J., 1966. Spreading of the ocean floor: new evidence, *Science*, **154**, 1405.

Vine, F. J. & Matthews, D. H., 1963. Magnetic anomalies over oceanic ridges, *Nature*, **199**, 977–949.

Walton, D., 1988. The lack of reproducibility in experimentally determined intensities of the Earth's magnetic field, *Rev. Geophys.*, **26**, 15–22.

Walton, D., 2002. Conditions for ferromagnetic resonance in nanoparticles and microwave magnetization, *Geophys. Res. Lett.*, **29**, 2165, doi:10.1029/2002GL016049.

Walton, D., 2004a. Avoiding mineral alteration during microwave magnetization, *Geophys. Res. Lett.*, **31**, L03606, doi:10.1029/2003GL019011.

Walton, D., 2004b. Resetting the magnetization of assemblies of nanoparticles with microwaves, *J. Appl. Phys.*, **95**, 5247–5248, doi: 10.1063/1.1695605.

Walton, D., Böhnel, H. & Dunlop, D. J., 2004. 2d order ferromagnetic resonance in nanoparticles, *Phys. Stat. Sol.*, **201**, 3257–3262, doi: 10.1002/pssa.200405435.

Wang, H., Deng, C., Zhu, R., Wei, Q., Hou, Y. & Boëda, E., 2005. Magnetostratigraphic dating of the Donggutuo and Maliang Paleolithic sitesin the Nihewan Basin, northern China, *Quart. Res.*, **64**, 1–11.

Wang, X., Yang, Z., Løvlie, R. & Min, L., 2004. High-resolution magnetic stratigraphy fluvio-lucustrine successionin the Nihewan Basin, China, *Quart. Sci. Rev.*, **23**, 1187–1198.

Wasilewski, P., 1973. Magnetic hysteresis in natural materials, *Earth Plant. Sci. Lett.*, **20**, 67–72.

Watkins, N. D. & Walker, G. P. L., 1977. Magnetostratigraphy of Eastern Iceland, *Am. J. Sci.*, **277**, 513–584.

Watkins, N. D., Kristjánsson, L. & McDougall, I., 1975. A detailed paleomagnetic survey of the type location for the Gilsa geomagnetic polarity event, *Earth Plant. Sci. Lett.*, **27**, 436–444.

Watkins, N. D., McDougall, I. & Kristjánsson, L., 1977. Upper Miocene and Pliocene geomagnetic secular variation in the Borgarfjördur area of Western Iceland, *Geophys. J. R. astr. Soc.*, **49**, 603–632.

Watts, A. B., 1994. Crustal structure, gravity anomalies and flexure of lithopshere in the vicinity of the Canary Islands, *Geophys. J. Int.*, **119**, 648–666.

Wehland, F., Leonhardt, R., Vadeboin, F. & Appel, E., 2005. Magnetic interaction analysis of basaltic samples and pre-selection for absolute palaeointensity measurements, *Geophys. J. Int.*, **162**, 315–320.

Wicht, J., 2005. Palaeomagnetic interpretation of dynamo simulations, *Geophys. J. Int.*, **162**, 371–380.

Wicht, J. & Olson, P., 2004. A detailed study of the polarity reversal mechnaism in a numerical dynamo model, *Geochem. Geophys. Geosyst.*, **5(3)**, doi:10.1029/2003GC000602.

Williams, I. & Fuller, M., 1981. Zonal harmonic models of reversal transitional fields, *J. Geophys. Res.*, **86**, 11,657–11,665.

Winklhofer, M. & Zamanyi, G. T., 2006. Extracting the intrinsic switching field distribution in perpendicular media: a comparative analysis, *J. Appl. Phys.*, **99**, O8E710.

Worm, H.-U. & Jackson, M., 1999. The superparamagnetism of the Yucca Mountain Tuff, *J. Geophys. Res.*, **104**, 25,415–25,425.

Xu, S. & Dunlop, D. J., 1994. he theory of partial thermoremanent magnetization in multidomain grains. 2. Effect of microcoercivity distribution and comparison with experiment, *J. Geophys. Res.*, **99**, 9025–9033.

Yamamoto, Y., 2006. Possible TCRM acquisition of the Kilauea 1960 lava, Hawaii: failure of the Thellier paleointensity determination inferred from equilibrium temperature of the Fe-Ti oxide, *Earth Planets Space*, **58**, 1033–1044.

Yamamoto, Y. & Tsunakawa, H., 2005. Geomagnetic field intensity during the last 5Myr: LTD-DHT Shaw palaeointensities from volcanic rocks of the Society Islands, French Polynesia, *Geophys. J. Int.*, **162**, 79–114.

Yamamoto, Y., Tsunakawa, H. & Shibuya, H., 2003. Palaeointensity study of the Hawaiian 1960 lava: implications for possible causes of erroneously high intensities, *Geophys. J. Int.*, **153**, 263–276.

Yamazaki, T. & Oda, H., 2001. A Brunhes-Matuyama polarity transition record from anoxic sediments in the South Atlantic (Ocean Drilling Program Hole 1082C), *Earth Planets Space*, **53**, 817–827.

Yamazaki, T. & Oda, H., 2003. Orbital influence on Earth's magnetic field: 10,000-year periodicity and in inclination, *Science*, **295**, 2435–2438.

Yang, T., Hyodo, M., Yang, Z. & Fu, J., 2004. Evidence for the Kamikatsura and Santa Rosa excursion recorded in eolin and deposits from the southern Chinese Loess Plateau, *J. Geophys. Res.*, **109**, doi: 1029/2004JB002966.

York, D., 1966. Least-squares fitting of a straight line, *Can. J. Phys.*, **44**, 1079–1086.

York, D., 1967. The best isochron, *Earth Plant. Sci. Lett.*, **2**, 479–482.

Yu, Y. & Dunlop, D. J., 2006. Testing the independence of partial thermoremanent magnetizations of single-domain and multidomain grains: Implications for paleointensity determination, *J. Geophys. Res.*, **111**, B12S31, doi:10.1029/2006JB004434.

Yu, Y., Tauxe, L. & Genevey, A., 2004. Toward an optimal geomagnetic field intensity determination technique, *Geochem. Geophys. Geosyst.*, **5(2), Q02H07**, doi:10.1029/2003GC000630.

Zhao, X., Ladner, B. C., Roessig, K., Wise, S. W. & Urquhardt, E., 2001. Magnetostratigraphy and biostratigraphy of Cenozoic sediments recovered from the Iberia Abyssal Plain, *Proc. ODP Sci. Res.*, **173**, 1–73.

Zheng, H., Wyrwoll, K.-H., Li, Z. & Powell, C. M., 1998. Onset of the aridity in southern Western Australia - a preliminary palaeomagnetic appraisal, *Glob. and Planet. Change*, **18**, 117–130.

Zhu, R., Liu, C., Wu, H. & Zhu, G., 1991. Transitional field behaviour for the Matuyama-Brunhes, *Sci. China Ser B*, **34**, 1252–1257.

Zhu, R., Ding, Z., Wu, H., Huang, B. & Jiang, L., 1993. Details of magnetic polarity transition recorded in Chinese loess, *J. Geomag. Geoelectr.*, **45**, 289–299.

Zhu, R., Laj, C. & Mazaud, A., 1994. The Matuyama-Brunhes and Upper Jaramillo transitions recorded in a loess section at Weinan, north central China, *Earth Plant. Sci. Lett.*, **125**, 143–158.

Zhu, R. X., Hoffman, K. A., Potts, R., Deng, C. L., Pan, Y. X., Guo, B., Shi, C. D., Guo, Z. T., Yuan, B. Y., Hou, Y. M. & Huang, W. W., 2001. Earliest presence of humans in noertheast Asia, *Nature*, **413**, 413–417.

Zhu, R. X., An, Z. S., Potts, R. & Hoffman, K. A., 2003. Magnetostratigraphic dating of the early humans in China, *Earth Sci. Rev.*, **61**, 341–359.

Zijderveld, J. D. A., 1967. *A.C. demagnetisation of rocks: analysis of results. In Methods in Palaeomagnetism*, Eds. D. W. Collinson, K. M. Creer and S. K. Runcorn, Elsevier.

*Geophys. J. Int.* (2007) **168**, 541–550 doi: 10.1111/j.1365-246X.2006.03234.x



# Exploring the influence of the non-dipole field on magnetic records for field reversals and excursions

Maxwell C. Brown, Richard Holme and Alistair Bargery*

*Department of Earth and Ocean Sciences, Geomagnetism Laboratory, Oliver Lodge Building, Oxford Street, University of Liverpool, Liverpool* L69 7ZE, *UK. E-mail: m.c.brown@liv.ac.uk*

Accepted 2006 September 12. Received 2006 August 14; in original form 2006 May 9

## SUMMARY

We have used the model CALS7K.2 to explore the possible influence of the time-varying non-dipole components of the geomagnetic field during field reversals and excursions. Our findings suggest that non-dipole components could add significant structure to the field during the reversal and excursion processes. Globally, the main polarity reversal is variable in duration and rapid reversals on subdecadal timescales are seen for a small number of locations. The model generates variable reversal paths; however, there is a longitudinal preference both spatially and, more weakly, temporally. Directional reversal features are not globally synchronous: some polarity changes finish before they start elsewhere. Global intensity variations, however, appear more coherent. We also find support for the idea that field intensity changes occur some time before and after the major directional changes of the reversal. Large excursions appear naturally when the axial dipole has been reduced to 20 per cent for the whole time period; however, they are not globally synchronous or uniform.

**Key words:** CALS7K.2, excursions, field reversals, geomagnetism, palaeomagnetism.

## 1 INTRODUCTION

The behaviour of the geomagnetic field during reversals and excursions is unclear. Many palaeomagnetic studies from both lava sequences and sedimentary cores have sought to uncover details of these two processes. However, these records often only show the behaviour of the field at one location on the Earth's surface, and where multiple records exist it is extremely difficult to correlate them temporally and establish features globally (Constable 1990; Gubbins 1999). It is thought that reversals are complex (Constable 1990; Coe & Glen 2004), with many possible features being recorded at the Earth's surface; however, a paucity of data has hindered any robust conclusions concerning reversal behaviour.

Reversals have been reported from numerical dynamo models and their output has been analysed for insight into the reversal process (Coe *et al.* 2000; Kutzner & Christensen 2004; Narteau & Le Mouël 2005; Wicht 2005). However, it is unclear how much direct relevance the results have for the Earth system as the fundamental magnetohydrodynamic parameters of these models are far from the Earth's true regime.

Here, we have adopted an alternative, much simpler, approach, based on a time-dependent observational model of the geomagnetic field for the last 7000 yr, CALS7K.2 of Korte & Constable (2005). CALS7K.2 is a continuous global model determined by a regularized least squares fit to archaeomagnetic and palaeomagnetic data using spherical harmonics in space and cubic B-splines in time. We take the field structure of this model and examine the effects on the surface field morphology of varying the magnitude of the axial dipole component. This apparently arbitrary approach is motivated by observations from the palaeomagnetic record, that suggest that statistical characteristics of the non-dipole field during a reversal are indistinguishable from those during stable periods of field behaviour (Valet *et al.* 1992). This perhaps surprising observation can be understood in terms of our understanding of the dynamics of magnetic secular variation at the top of the Earth's core. The evolution of the magnetic field is governed by the induction equation, of which the radial component is:

$$\frac{\partial B_r}{\partial t} = \frac{\eta}{r}\nabla^2(r B_r) - \nabla_H \cdot (\mathbf{u} B_r) \tag{1}$$

where $B_r$ is the radial field, $\mathbf{u}$ is the surface flow velocity, $\eta$ is the magnetic diffusivity, $r$ is the radius, $\theta$ is the colatitude, and $\nabla_H \cdot$ is the horizontal divergence operator. The terms on the right hand side represent secular variation generated by diffusion of the field and advection respectively. However, it is thought that on at least decadal time scales, advective processes at top of the core may be in the tangentially geostrophic regime (Le Mouël 1984), in which the principal force balance is between pressure gradients and Coriolis force. In this regime, the horizontal flow at the core–mantle boundary obeys:

$$\nabla_H \cdot (\mathbf{u} \cos\theta) = 0 \tag{2}$$

*Now at: Planetary Science Research Group, Environmental Science Department, Lancaster University, Lancaster LA1 4YQ, UK

Le Mouël (1984) realized that this condition has implications for the interpretation of eq. (1). Specifically, any magnetic field of the form $\cos\theta$ will not contribute to secular variation by advection: this is precisely the form of the axial dipole component of the field. Further, the diffusion operator separates in spherical harmonics and so diffusional processes of different spherical harmonic field components can be considered as independent. Hence, to first order, the strength of the axial dipole field does not influence the secular variation of the non-dipole field. Therefore, it is at least kinematically consistent to consider an unchanged non-dipole field while imposing changes on the axial dipole component.

We do not claim that the time-varying non-dipole field over the last 7000 yr would have been the same without a strong axial dipole field. However, statistically the variation of the non-dipole field may not depend strongly on the dipole, and therefore the CALS7K.2 model may be a good source for a proxy for possible non-dipole variation during a reversal. It is also not unreasonable to use a model for the recent field as it is likely not to be grossly atypical of the palaeofield (Heller *et al.* 2003). Time averaged models of the stable palaeomagnetic field for the last 5 Myr (Johnson & Constable 1995; Kelly & Gubbins 1997) show similar features to the time-averaged historical field, particularly high-latitude flux patches (Bloxham & Jackson 1992; Jackson *et al.* 2000). Even without this justification, our approach provides a geometric model to examine how the slowly-varying changes in the field at the core–mantle boundary might be observed in the Earth surface observations, complementary to those available from dynamo simulations.

A similar approach to the one used here, but with a constant non-dipole field from the IGRF, has been used to look at reversals (Constable 1992; Quidelleur & Valet 1996; Heller *et al.* 2003; Clement 2004) and excursions (Heller *et al.* 2003; Quidelleur *et al.* 1999). Unlike these studies, we explore the possible influence that a time-varying non-dipole field may have on field structure during reversals and excursions. Possible changes and global variations in the direction and intensity of the field, both temporally and spatially, have been investigated.

## 2 METHOD

The geometrically simplest model for a geomagnetic field reversal is to decrease the axial dipole to zero and then increase it to the opposite polarity (Courtillot *et al.* 1992; Quidelleur & Valet 1996). The axial dipole term ($g_1^0$) in CALS7K.2 was scaled linearly with time:

$$g_1^{0'} = g_1^0(t)\left(1 - 2\left(\frac{t - t_0}{t_1 - t_0}\right)\right) \tag{3}$$

where $t$ is varying time, $t_0$ is the starting time, and $t_1$ is the end time of the model. In this study the total reversal process is defined to last the whole 7000 yr period of CALS7K.2. The time variation of the non-dipole field was unaltered. Although magnetic energy could be transferred from the dipole field into e.g., the axial quadrupole or octupole terms (Williams & Fuller 1981; Clement 2004; Merrill 2004) there is no physical requirement for the magnetic energy of the geodynamo to be conserved (Constable 1990).

We examine what surface observations could emerge from this simplistic reversal model. To compare directional and intensity changes globally we use the standard palaeomagnetic convention of the virtual geomagnetic pole (VGP) and virtual dipole moment (VDM). (Note that we encountered a systematic error in using the standard formula with data in the north, east, down coordinate system—see the Appendix.) This characterization assumes a simple geocentric dipole for the time-averaged field, an assumption unlikely to be physically appropriate for a reversal, but useful as a way of comparing measurements.

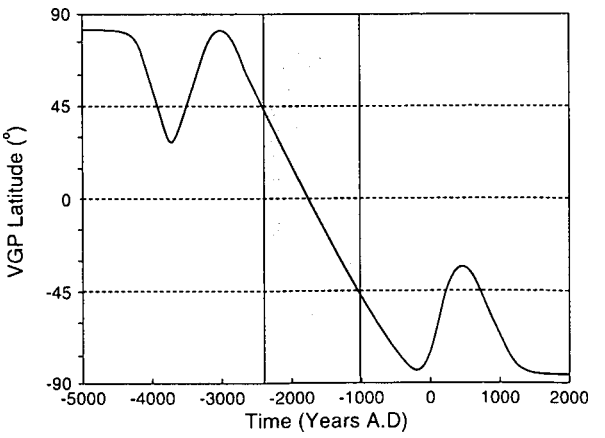


**Figure 1.** A schematic reversal path illustrating the duration of the directional reversal (grey shading) defined for this study.

From observations, the duration of a directional reversal is often defined as the period in which the VGP lies between $+45°$ and $-45°$ latitude. We define directional reversal duration based on the time of the last crossing of $+45°$ before the VGP crosses the equator and the first crossing of $-45°$ afterwards (Fig. 1).

As a possible model of excursions the axial dipole is scaled to a reduced value for a set time period.

$$g_1^{0'} = \alpha g_1^0(t) \tag{4}$$

Varying the magnitude of the axial dipole field allows us to see at what point the non-dipole field becomes dominant and excursions are produced. We define an excursion to have occurred whenever the VGP latitude is $<+45°$ and then returns to a normal field latitude ($>+45°$).

There is a risk that our results are influenced by the imperfections in the CALS7K.2 model. CALS7K.2 does not resolve the non-zonal structures noted by (Jackson *et al.* 2000) in the Southern Hemisphere and is more poorly constrained before $-1000$ AD (Korte & Constable 2005). In order to limit these effects, especially in assessing preferred paths and excursion behaviour, the model has been run over varying time periods, and our analysis focuses more strongly on the later part of the model.

## 3 REVERSAL FEATURES

Our model exhibits both temporal and spatial variations in the behaviour of the field during the total reversal process. A global variation in the onset time of the directional reversal is observed (Fig. 2), of about 1800 yr, approximately 25 per cent of the total reversal process time. When specific locations are investigated (Fig. 3a) we see the directional reversal completed in some locations (e.g. New Zealand) before it has started elsewhere (e.g. Tenerife and UK). For all locations, the directional behaviour appears complex, and features are not globally uniform. Fig. 3(a), also shows a fluctuation in VGP latitude around $-2000$ AD for Iceland, UK and Tenerife which is not seen for Hawaii or New Zealand. Moreover, the magnitude of the fluctuation varies.

Variability in VDM is seen throughout the total reversal process for all locations. For example, Fig. 3(b) shows the VDM fluctuating

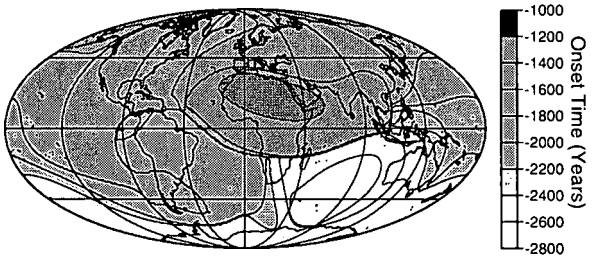


**Figure 2.** Time of onset for directional reversals for all global locations.

over time periods of approximately 500 to 1000 yr superimposed on the trend produced by scaling the axial dipole. In comparison to the directional reversal there is more global coherence in the VDM variations. The directional changes are also seen to be contained within the time that the VDM is significantly reduced (Fig. 3c).

We see great variation in the duration of the directional reversal (Fig. 4a). What is particularly notable is that from a total reversal time of 7000 yr, some of the directional changes happen on sub-decadal timescales (Fig. 4b), while others occur over a period of approximately 1500 yr (Fig. 4c). Globally, our model has produced sharp boundaries distinguishing short and long directional reversals (Fig. 4a). These are most prominent running through the Indian Ocean, Southern Africa and the Southern Atlantic Ocean as well as through central North America and through the Pacific Ocean. These are the product of subtly changing directional variations across the globe and also our definition of a directional reversal. In Fig. 4(c), we note a small fluctuation in direction between −2000 and −1000 AD for South Africa. Moving north from this location, the peak of the fluctuation increases in VGP latitude and at a specific point (the boundary) the peak exceeds +45° and the start of the directional reversal is shifted to a later time (seen in Fig. 2), reducing the duration. Another sharp boundary in Fig. 4(a) is in the area of the Caspian Sea. Here, we relaxed our definition of a directional reversal as a large excursion re-crossing the equator was observed after the defined directional reversal (Fig. 4c). It was included in Fig. 4(a) to illustrate the variability in directional changes observed in this model. The Caspian Sea was the only area where such a large excursion was observed, post-directional reversal.

One of the more controversial features of the reversing field is preferred VGP paths (Laj *et al.* 1991). Our model generates VGP paths with varying geometries (Fig. 5); however, plots such as in Fig. 5 give no analysis of the longitudinal distribution of the paths. To determine whether our model produced any longitudinal preference globally, an equal area distribution of site latitudes and longitudes was used. Initially we assessed the percentage of VGP paths passing through 10° longitudinal intervals when crossing the equator. Two bands of longitudinal preference have been generated (Fig. 6). The dominant preference is between +20° and +80° and a lesser preference between −90° and −130°. To determine if these preferences are spatially coherent, we assessed the percentage of VGP paths passing through 10° longitudinal intervals crossing +45°, +30°, −30° and −45° latitude (Fig. 7). We see a similar preference in the results from the equator and the Southern Hemisphere crossings. The Northern Hemisphere crossings show broader peaks with a much lower incidence of crossings between +60° and +180°. We also investigated if preferences are found when the reversal occurred over different time periods, to assess whether similar VGP paths would be seen for different reversals and therefore related to a longer time-averaged feature of the non-dipole field. To determine

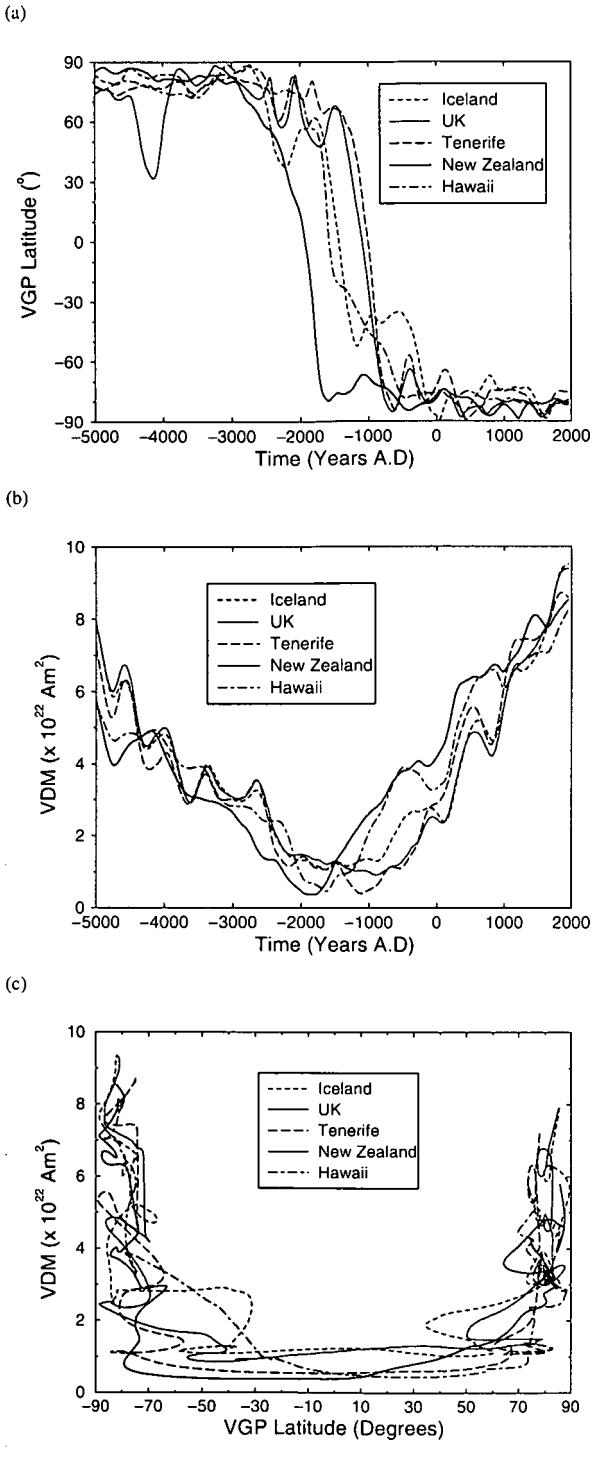


**Figure 3.** (a) Directional changes, (b) VDM changes, (c) VGP vs VDM, for five global locations during the simulated 7000 yr reversal.

this, the starting time of the reversal was changed, but the rate of change of the axial dipole kept constant. This reduced the interval of CALS7K.2 used in calculating the percentage of paths, but it maintained the same temporal relationship between the non-dipole

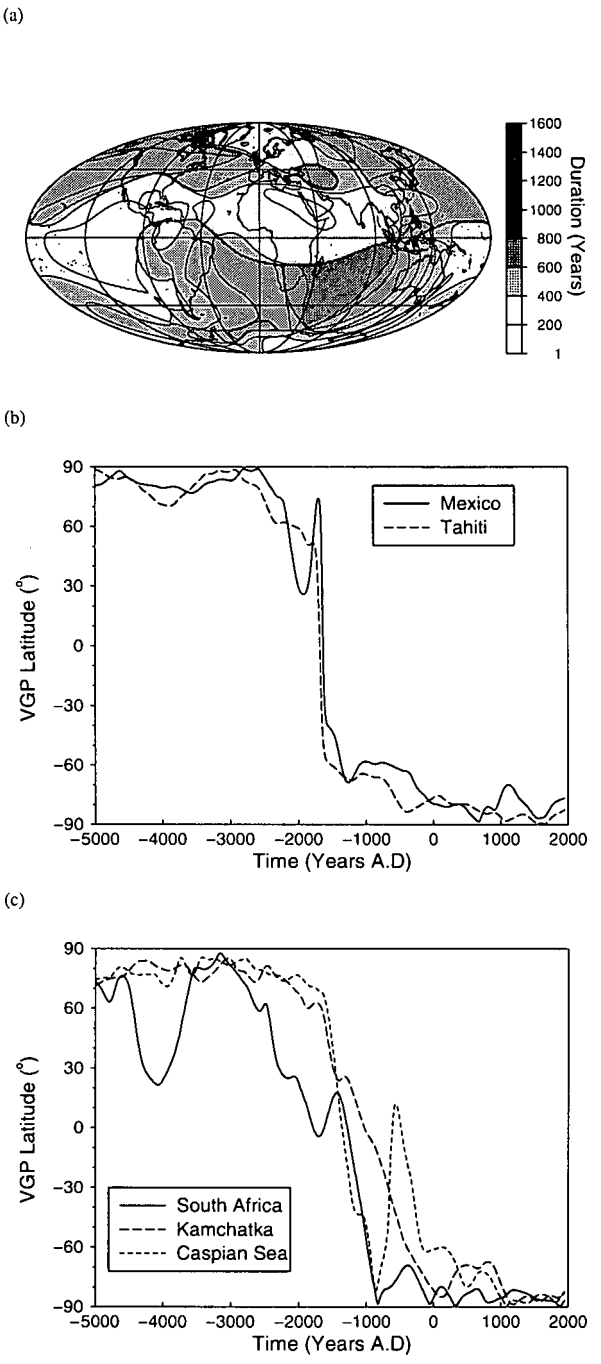


**Figure 4.** (a) Duration of directional reversals for all global locations. (b) Examples of rapid directional reversals. (c) Examples of slow directional reversals.

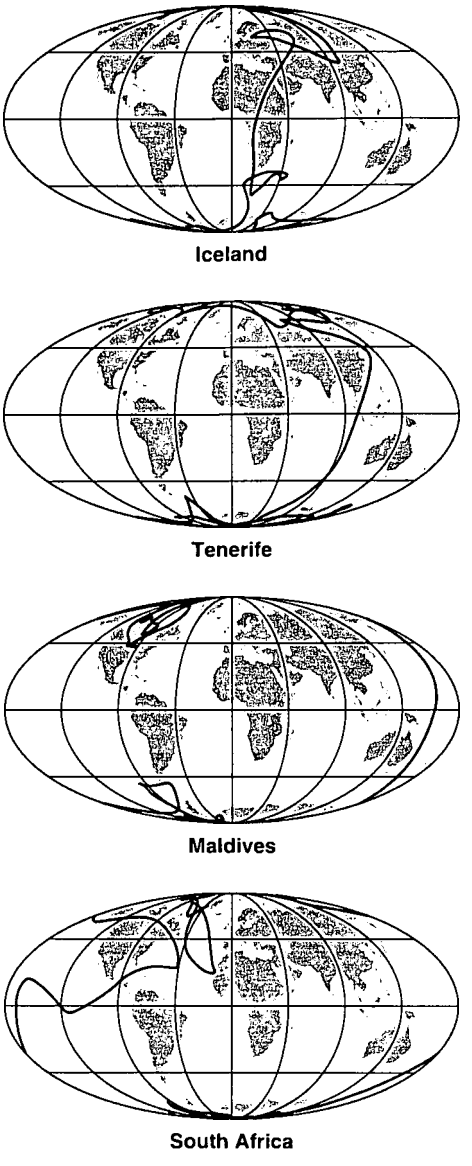


**Figure 5.** Examples of four locations with varying VGP paths.

field and the changing axial dipole field for all time periods. The start of the total reversal process was set at −4000, −3000, and −2000 A.D. Longitudinal preferences were seen for all time periods (Fig. 8); however, the location of the preferences show only a weak correlation with those seen in Fig. 6, between each time period. When the results from all the time periods are averaged (Fig. 8d), preferred paths are still seen, but the pattern is less marked than for a single time, not inconsistent with the analysis of Love (2000).

## 4 EXCURSION FEATURES

With a scaled axial dipole over a set time period we can see at what field strength major directional changes start to occur. In this case we have set the time period from −3000 A.D. to present day. Before −3000 A.D. the South Atlantic anomaly appears to bias the behaviour of the field, which could be due to poor data coverage at this time (Korte & Constable 2005).We have found that excursions appear naturally in the model and that large excursions appear between 25 per cent $g_1^0$ and 20 per cent $g_1^0$ (Fig. 9). At 25 per cent $g_1^0$ the most southerly latitude reached is approximately −10°, but at 20 per cent $g_1^0$, full polarity reversals are observed for some locations

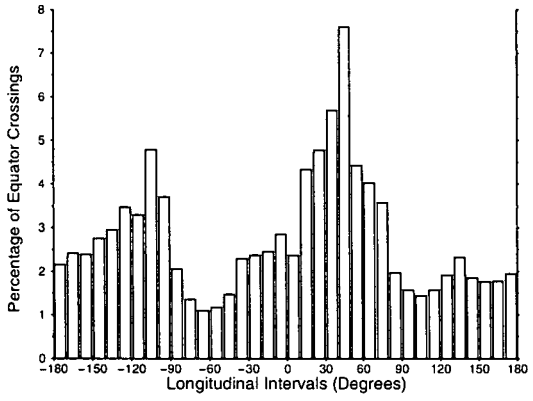


**Figure 6.** Percentage of VGP reversal paths crossing the equator from all global locations in 10° longitudinal intervals for the total time period.

before the VGP returns to a normal field latitude. This behaviour, however, is not globally uniform, with some areas, for example Central America, observing directional changes of approximately 40–50° in latitude, while changes of almost 180° are observed in South America (Fig. 9e).

Importantly, the excursions in our model are neither global in extent or synchronous in occurrence. Fig. 10 shows an example of large excursions (Maldives and South Argentina) that are offset by approximately 1000 yr. Both of these events coincide with minima in intensity. Although there appear to be excursions elsewhere around the time of the Maldives event, they are smaller in magnitude and emphasize the non-uniformity of the field globally.

Even for the extreme case of $g_1^0$ reduced to zero, (Fig. 9f) there is still a great variation in the maximum directional changes seen. The majority of locations show large VGP changes, but in some locations the VGP has only moved no further than 30–40° latitude (e.g. North Africa and North America).

## 5 IMPLICATIONS FOR PALAEOMAGNETIC OBSERVATIONS

Many of the characteristics of the directional changes seen in this study have been noted in palaeomagnetic reversal studies. In Fig. 3(c), we see directional changes that precede and follow the directional reversal. Precursor events have been well documented for the Brunhes–Matuyama field reversal (Chauvin *et al.* 1990; Hartl & Tauxe 1996; Singer *et al.* 2002; Quidelleur *et al.* 2002; Brown *et al.* 2004; Coe *et al.* 2004a) and events following the main directional reversal have been recorded by Mankinen *et al.* (1985) and Roberts & Fuller (1990).

Directional variations are not seen globally and are not synchronous. This variation is a natural product of the combination of the non-dipole field with a reduction in axial dipole strength and does not need another specific physical mechanism. Variations in VDM through reversals have also been seen in the palaeomagnetic record. Recently, Valet *et al.* (1999) and Riisager & Abrahamsen (2000) have presented palaeointensity results showing large fluctuations in palaeointensity around the time of the directional reversal. These features could be attributed to the non-dipole field becoming relatively more prominent at the Earth's surface as the overall field is no longer dominated by the axial dipole component: this is what we observe in Fig. 3(b).

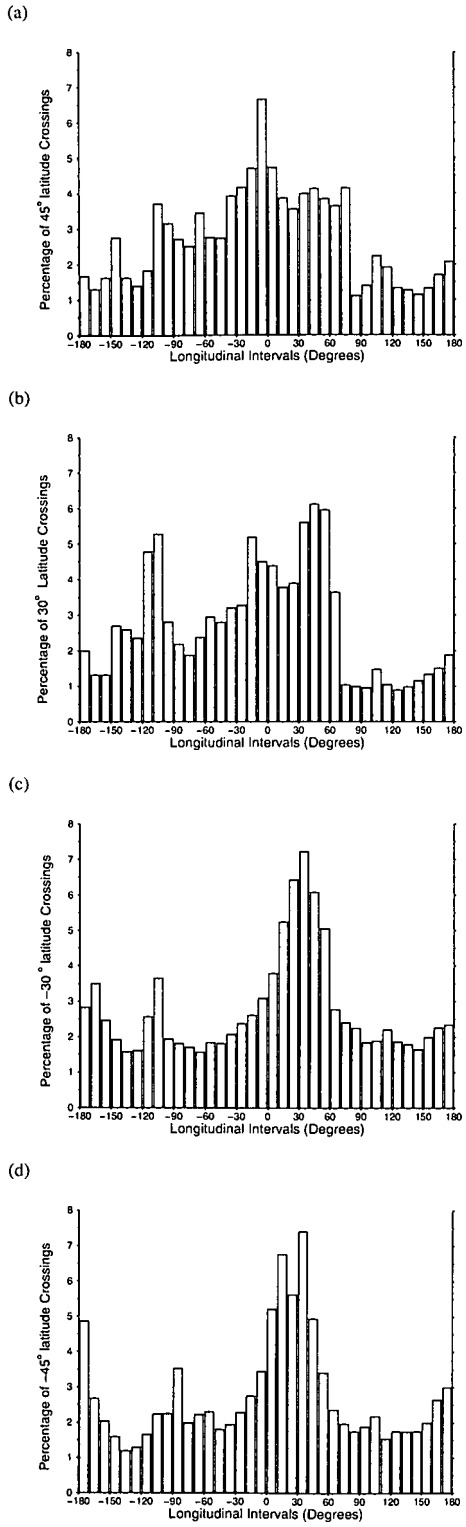


**Figure 7.** Percentage of VGP reversal paths crossing lines of latitude at (a) +45° (b) +30° (c) −30° (d) −45°, from all global locations in 10° longitudinal intervals.

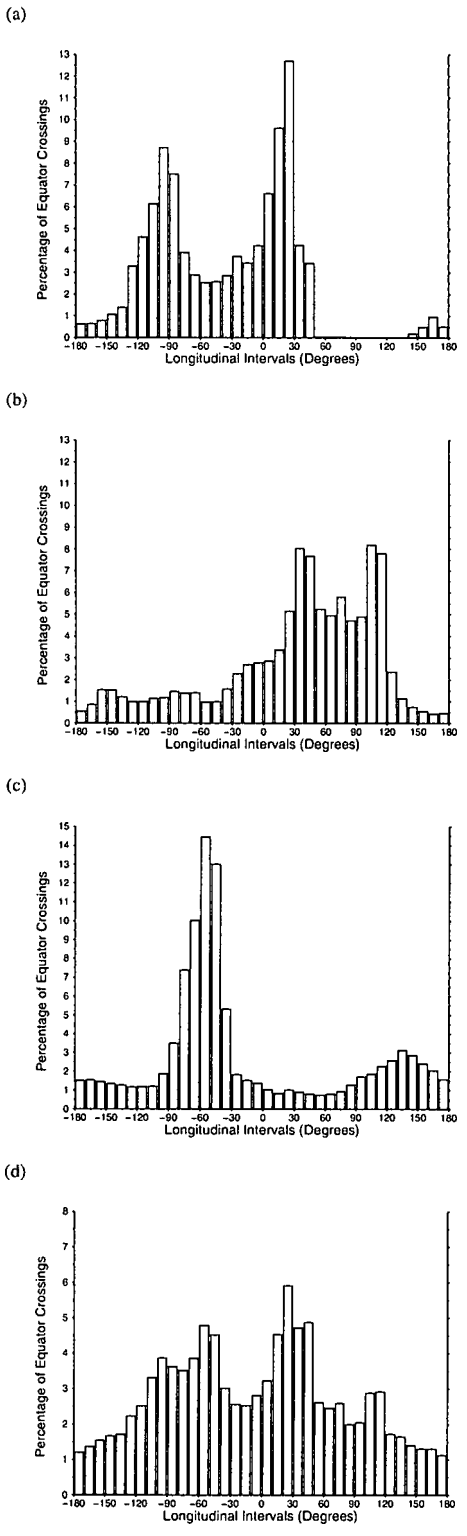


**Figure 8.** Percentage of VGP reversal paths crossing the equator from all global locations in 10° longitudinal intervals when total reversal process starts at (a) −4000 AD (b) −3000 AD (c) −2000 AD. (d) Average percentage of VGP paths from time periods shown in (a), (b), (c) and Fig. 6.

The significant reduction in intensity observed in this model prior to the onset of the directional reversal (Fig. 3c) suggests that the axial dipole field needs to be substantially reduced in strength to allow the initiation of the directional reversal. This confines the directional reversal to a maximum of approximately 20 per cent of the total reversal time in this model. Similar behaviour has been observed in the palaeomagnetic record (Quidelleur & Valet 1996; Lin *et al.* 1994). Lava flows emplaced before or after flows that record the directional reversal may record a reduction in field intensity even when the VGP lies at normal or reversed latitudes (normally suggesting that the reversal had not started or had finished). Our results suggest it may be important to record both intensity (including relative intensity for sedimentary records) and directional data in order to define the total length of a reversal (as noted by Williams & Fuller 1981; Prévot *et al.* 1985; Mary & Courtillot 1993).

The variability in duration of the directional reversals produced using this model is of particular interest. Fig. 4(a) shows a concentration of faster directional reversals towards the equator. On average, directional reversals recorded at mid to high latitudes are over twice as long as those recorded at the equator. This result is broadly consistent with Clement (2004), who using palaeomagnetic data from the Jarmillo and Brunhes–Matuyama reversals observed that the duration of the directional reversal was shorter at equatorial latitudes.

Our model generates some localized very rapid directional reversals, taking less than 10 yr. The Steens Mountain lava flow studies of Mankinen *et al.* (1985), Coe & Prévot (1989), Coe *et al.* (1995) and Camps *et al.* (1999), all see an in-flow variation of remanent magnetization directions that is hard to explain with our present understanding of rock magnetic processes. Coe *et al.* (1995) suggest the possibility of a rapidly changing field at the time of flow emplacement. However, it was thought rapid processes within the core would be needed to produce rapid changes in the field at the Earth's surface and that this signal would be filtered out by the electrically conducting mantle (Fuller 1989; Merrill 1995). The rapid directional changes seen in this model are a product of only reducing the axial dipole, implying that no new core process is needed to generate this kind of feature, at least for geographically restricted locations. In effect, our rapid reversals result from a geometric rather than a physical process.

VGP paths have been the subject of much palaeomagnetic analysis. Both lava and sediment data (Valet & Laj 1984; Tric *et al.* 1991; Laj *et al.* 1991; Clement 1991) support the idea of preferred longitudinal paths through Eastern Asia and the Americas. Conversely, a number of studies have found no evidence for VGP paths (Valet *et al.* 1992; Prévot & Camps 1993). Love (2000) carried out a statistical assessment of palaeomagnetic lava data recording reversals and excursions over the last 20 Myr. He concluded that American and Asian longitudes are preferred, with a statistical significance at about the 95 per cent confidence level. The model of Constable (1992), applying the same method as used in this study but with with the static non-dipole field of the 1980 field, produced strongly preferred VGP paths, with two well defined longitudinal bands of preference through the Americas and Australia/Eastern Asia. In comparison, our model shows much greater complexity and variability in the geometry of the paths taken (Fig. 5). This can be attributed to influence of the time-varying non-dipole field.

In our model, there is evidence of a spatial preference of VGP paths from the same reversal and also a weak coherence of preferred paths between reversals occurring over different time periods. This trend is perhaps associated with a background time-averaged non-dipole field (Johnson & Constable 1995); however, the preferred

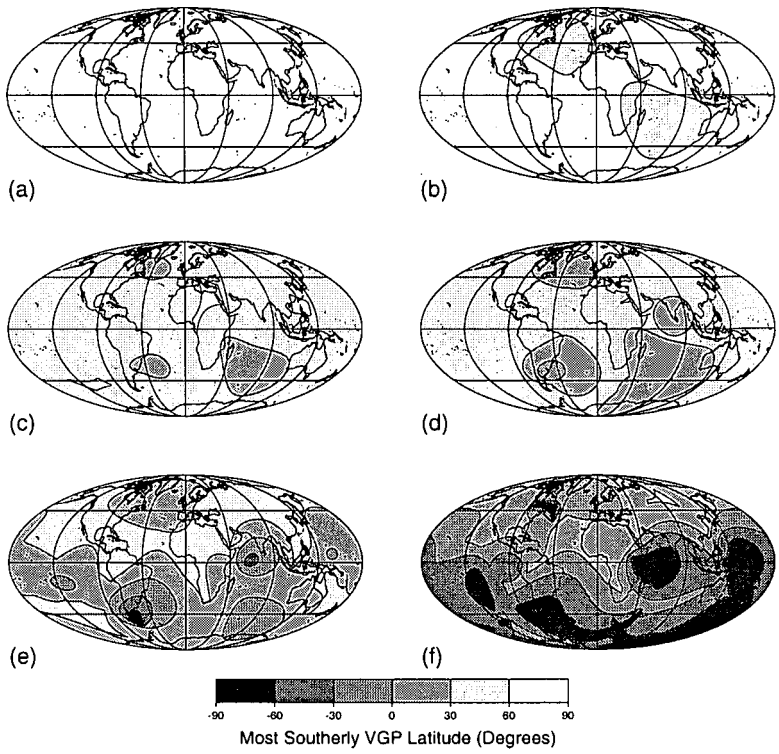


**Figure 9.** Global variation in most southerly VGP latitude reached when $g_1^0$ is set to (a) 100 per cent, (b) 50 per cent, (c) 30 per cent, (d) 25 per cent, (e) 20 per cent, (f) 0 per cent, over the last 5000 yr.

longitudes do not coincide with the longitudes of the magnetic flux patches described by Jackson *et al.* (2000). We investigated whether the location of flux patches observed at the core–mantle boundary in the CALS7K.2 model correlate with the location of the preferred VGP paths for the different time periods shown in Fig. 8. For the reversal occurring between −4000 and 1950 AD, there is a flux patch that persists through the central 1000 yr of this reversal between approximately 40° to 135° longitude in the Northern Hemisphere in the CALS7K.2 model, but there is a lack of VGP crossings at the equator for this range of longitudes (Fig. 8a). This suggests that the presence of long-lived flux patches may not influence the the preference of VGP paths observed in this model; however, at least some of our confined paths result from a concentration of flux at the equator.

## 6 DISCUSSION AND CONCLUSIONS

### 6.1 Reversals

A simple reduction of the axial dipole component of the field while leaving the time-varying non-dipole component of the field unaltered has yielded many interesting patterns. The emergence of the non-dipole field during the reversal has strongly influenced the features seen in this model. Surprisingly, for some locations, very rapid directional reversals have been seen, suggesting that rapid core processes are not necessary to produce rapid changes at the Earth's surface. The possible preference of VGP paths also suggests that new physical mechanisms are not needed to produce such features. Directional reversals occur in this model when the axial dipole component of the field has been reduced to approximately 25–20 per cent (Fig. 3c).

As well as being variable in duration the directional reversal is not globally synchronous or uniform. The directional changes finished for some locations before starting elsewhere. This has important implications for possible global modelling of a reversal using palaeomagnetic data. Present age dating constraints from K/Ar or $^{40}Ar/^{39}Ar$ are on the same order of magnitude as possible reversal durations; it will therefore be difficult to resolve the possible complexity of a reversal globally, especially when so few global palaeomagnetic locations for the same reversal are available. However, at least in our model, the greater coherence in intensity between locations suggests that variations in intensity may be more useful in correlating reversal records temporally.

From palaeomagnetic data, the time it takes for the directional reversal is uncertain, with estimates ranging from a few thousand up to 28 000 yr (based upon $^{40}Ar/^{39}Ar$ dating, for the Brunhes–Matuyama reversal) (Clement 2004), suggesting the time period used in our model is at the lower limit of reversal durations. If so, then we may expect the true field to show greater complexity and variability in both direction and intensity than that generated by this model.

### 6.2 Excursions

Excursions occur naturally in the model and can be interpreted in terms of the emergence of the time-varying non-dipole components that are favoured when the axial dipole has been sufficiently reduced. In the terminology of Lund *et al.* (2005), these are Class I excursions, in that they are not associated with any field reversal. However, we do not require the physical mechanisms sug-

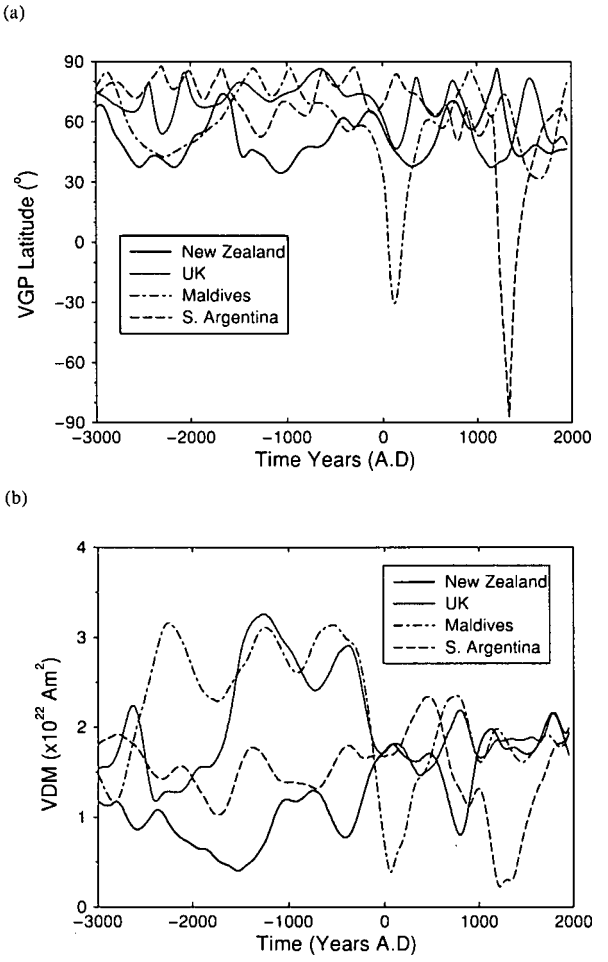


**Figure 10.** Variation in (a) VGP latitude and (b) VDM for four global locations when $g_1^0$ reduced to 20 per cent over the last 5000 yr.

gested by Lund *et al.* (2005) for this type of excursion, only a relatively weaker axial dipole field. We have observed that a large reduction in the axial dipole to between 25 and 20 per cent of the original field strength enabled large directional changes resulting in excursions. Importantly, large excursions were not global, with some areas only showing small deviations from their normal time-averaged position. This result is in good agreement with the model of Heller *et al.* (2003) who used the static non-dipole field from the 1995 IGRF field model, with a reduced axial dipole. Excursions are also not synchronous, but are coupled with minima in intensity (Fig. 10). Therefore it is possible that excursions recorded in the palaeomagnetic record, such as the Laschamp excursion (see Merrill *et al.* 1996; Lund *et al.* 2005, for detailed reviews) may be global to some extent, but may not be uniform in intensity or directional variations.

Quidelleur *et al.* (1999) also noted a similar correlation with intensity and directional variations when reducing the axial dipole component of the IGRF85 field model to 50 per cent of its value. In addition, the spherical harmonic model of Quidelleur *et al.* (1999), using palaeomagnetic data from an excursion on La Palma and 30 sites from Carlut & Courtillot (1998), also produced excursions that are not global in extent; however, the axial dipole component was only reduced to 50 per cent. As emphasized to us by C. Constable (*pers comm.*), CALS7K.2 underestimates the likely strength of the non-dipole field as the model has very little resolution above spherical harmonic degree 4. To test the influence of this effect, we performed a similar experiment with the model GUFM (Jackson *et al.* 2000), based on historical data, and reduced the magnitude of the axial dipole coefficient to 50 per cent. While the time interval of that model is insufficient to generate a suite of clearly defined excursions, we nonetheless see strongly reduced VGP latitude (approaching 0°) at some locations, and in comparison with CALS7K for the same interval, an average underestimate of the minimum latitude of about 30°. We therefore suggest that the excursion effects shown in Fig. 10 are likely to be even more significant in the real Earth than in our experiments, and could occur for an axial dipole magnitude only half of the current value, in agreement with Quidelleur *et al.* (1999).

### 6.3 Synthesis

The simple models for reversals and excursions that we have investigated have demonstrated many features seen in the palaeomagnetic record, but are by no means consistent with all the available data. In particular, some excursions are thought to be global, a feature which our model does not reproduce. Our model does not include many physical effects which may be present; the study of suitable dynamo simulations is clearly the appropriate way of investigating such effects (e.g Coe *et al.* 2000). However, it does demonstrate that some observed features in the palaeomagnetic record may result from the geometric effect of the upward continuation of the geomagnetic field from the core–mantle boundary to the Earth's surface, and not require specific physical mechanisms. Perhaps most importantly, our results suggest that measurements of intensity (even relative intensity) may be of primary importance in considering the structure and development of reversals and excursions.

## ACKNOWLEDGMENTS

This work was carried out under NERC grant NER/S/J/2004/13080. We thank J. Shaw, E. Horncastle and M. Gratton for useful discussions and help.

## REFERENCES

Bloxham, J. & Jackson, A., 1992. Time-dependant mapping of the magnetic field at the core-mantle boundary, *J. geophys. Res.*, **97**, 19 537–19 563.

Brown, L.L., Singer, B.S., Pickens, J.C. & Jicha, R., 2004. Paleomagnetic directions and $^{40}Ar/^{39}Ar$ ages from the Tatara-San Pedro volcanic complex, Chilean Andes: Lava record of a Matuyama-Brunhes precursor?, *J. geophys. Res.*, **109**, B12101 doi: 10.1029/2004JB003007.

Camps, P., Coe, R.S. & Prévot, M., 1999. Transitional geomagnetic impulse hypothesis: Geomagnetic fact or rock-magnetic artefact?, *J. geophys. Res.*, **104**, 17 747–17 758.

Carlut, J. & Courtillot, V., 1998. How complex is the time-averaged field over the past 5 million years, *Geophys. J. Int.*, **134**, 527–544.

Chauvin, A., Roperch, P. & Duncan, R.A., 1990. Records of geomagnetic reversals from volcanic islands of French Polynesia 2. paleomagnetic study of a flow sequence (1.2–0.6 ma) from the island of Tahiti and discussion of reversal models, *J. geophys. Res.*, **95**, 2727–2752.

Clement, B.M., 1991. Geographical distribution of transitional VGPs: evidence for nonzonal equatorial symmetry during the Brunhes-Matuyama geomagnetic reversal, *Earth planet. Sci. Lett.*, **104**, 48–58.

Clement, B.M., 2004. Dependence of the duration of geomagnetic polarity reversals on site latitude, *Nature*, **428**, 637–640.

Coe, R.S. & Glen, J., 2004. The complexity of reversals, *Timescales of the paleomagnetic field, Geophysical Monograph Series*, **145**, 221–232 doi: 10.29/145GM16.

Coe, R.S. & Prévot, M., 1989. Evidence suggesting extremely rapid field variation during a geomagnetic reversal, *Earth planet. Sci. Lett.*, **92**, 292–298.

Coe, R.S., Prévot, M. & Camps, P., 1995. New evidence for extraordinary rapid change of the geomagnetic field during a reversal, *Nature*, **374**, 687–692.

Coe, R.S., Hongre, L. & Glatzmaier, G.A., 2000. An examination of simulated geomagnetic reversals froma palaeomagnetic perspective, *Phil. Trans. R. Soc. Lond.*, **358**, 1141–1170.

Coe, R.S., Singer, B.S., Pringle, M.S. & Zhao, X., 2004a. Matuyama-Brunhes reversal and Kaikatsura event on Maui: palaomagnetic directions, $^{40}Ar/^{39}Ar$ ages and implications, *Earth planet. Sci. Lett.*, **222**, 667–684.

Constable, C., 1990. A simple statistical model for geomagnetic reversals, *J. geophys. Res.*, **95**, 4587–4596.

Constable, C., 1992. Link between geomagnetic reversal paths and secular variation of the field over the last 5 Myr, *Nature*, **358**, 230–233.

Courtillot, V., Valet, J.-P., Hulot, G. & Mouël, J.-L., 1992. The Earth's magnetic field: Which geometry?, *EOS, Trans. Am. geophys. Un.*, **73**, **337**, 340–342.

Fuller, M., 1989. Fast changes in geomagnetism, *Nature*, **339**, 582–583.

Gubbins, D., 1999. The distinction between geomagnetic excursions and reversals, *Geophys. J. Int.*, **137**, F1–F2.

Hartl, P. & Tauxe, L., 1996. A precursor to the Matuyama/Brunhes transition-field instability as recorded in pelagic sediments, *Earth planet. Sci. Lett.*, **138**, 121–135.

Heller, R., Merrill, R.T. & McFadden, P.L., 2003. The two states of the paleomagnetic field intensities for the past 320 million years, *Phys. Earth planet. Inter.*, **135**, 211–223.

Jackson, A., Jonkers, A.R.T. & Walker, M.R., 2000. Four centuries of geomagnetic secular variation from historical records, *Phil. Trans. R. Soc. Lond.*, **358**, 957–990.

Johnson, C.L. & Constable, C.G., 1995. The time-averaged geomagnetic field as recoreded by lava flows over the past 5Myr, *Geophys. J. Int.*, **122**, 489–519.

Kelly, P. & Gubbins, D., 1997. The geomagnetic field over the last 5 million years, *Geophys. J. Int.*, **128**, 315–330.

Korte, M. & Constable, C.G., 2005. Continous geomagnetic field models for the past 7 millenia: 2. CALS7K, *Geochem. Geophys. Geosyst.*, **6**, Q02H16 doi: 10.1029/2004GC000801.

Korte, M. & Constable, C.G., 2005. The geomagnetic dipole moment over the last 7000 years — new results from a global model, *Earth planet. Sci. Lett.*, **236**, 348–358.

Kutzner, C. & Christensen, U.R., 2004. Simulated geomagnetic reversals and preferred virtual geomagnetic pole paths, *Geophys. J. Int.*, **157**, 1105–1118.

Laj, C., Mazaud, A., Weeks, R., Fuller, M. & Herrero-Bervera, E., 1991. Geomagnetic reversal paths, *Nature*, **351**, 447.

LeMouël, J.-L., 1984. Outer-core geostrophic flow and secular varaition of earth's geomagnetic-field, *Nature*, **311**, 734–735.

Lin, J.L., Verosub, K.L. & Roberts, A.P., 1994. Decay of the virtual dipole moment during polarity transitions and geomagnetic excursions, *Geophys. Res. Lett.*, **21**, 525–528.

Love, J.J., 2000. Statistical assessment of preferred transitional VGP longitudes based on palaeomagnetic lava data, *Geophys. J. Int.*, **140**, 211–221.

Lund, S.P., Schwartz, M., Keigwin, L. & Johnson, T., 2005. Deep-sea sediment records of the Laschamp geomagnetic field excursion ~41 000 calendar years before present, *J. geophys. Res.*, **110**(B04101), 1–15.

Mankinen, E.A., Prévot, M., Grommé, C.S. & Coe, R.S., 1985. The Steens Mountain (Oregon) geomagnetic polarity transition 1. Directional history, duration of episodes, and rock magnetism, *J. geophys. Res.*, **90**(B12), 10 393–10 416.

Mary, C. & Courtillot, V., 1993. A three-dimensional representation of geomagnetic reversal records, *J. geophys. Res.*, **98**, 22 461–22 475.

Merrill, R.T., 1995. Principle of least astonishment, *Nature*, **374**, 674–675.

Merrill, R.T., 2004. Time of reversal, *Nature*, **428**, 608–609.

Merrill, R.T., McElhinny, M.W. & McFadden, P.L., 1996. *The magnetic field of the Earth: palaeomagnetism, the core, and the deep mantle*, Vol. 63 of International geophysics series, Academic Press.

Narteau, C. & Le Mouël, J.-L., 2005. Transient evolution regimes in a multiscale dynamo model: Timescales of the reversal mechanism, *J. geophys. Res.*, **110**, B01104 doi: 1029/2004JB002983.

Prévot, M. & Camps, P., 1993. Absence of preferred longitudinal sectors for poles from volcanic records of geomagnetic reversals, *Nature*, **336**, 53–57.

Prévot, M., Mankinen, E.A., Coe, R.S. & Grommé C.S., 1985. The Steens Mountain (Oregon) geomagnetic polarity transition; 2. Field intensity variation and discussion of reversal models, *J. geophys. Res.*, **90**, 10 417–10 448.

Quidelleur, X. & Valet, J.-P., 1996. Geomagnetic changes across the last reversal recorded in lava flows from La Palma, Canary Islands, *J. geophys. Res.*, **101**, 13 755–13 773.

Quidelleur, X., Gillot, P.-Y., Carlut, J. & Courtillot, V., 1999. Link between excursions and palaeointensity inferred from abnormal field directions recorded at La Palma around 600ka, *Earth planet. Sci. Lett.*, **168**, 233–242.

Quidelleur, X., Carlut, J., Gillot, P.-Y. & Soler, V., 2002. Evolution of the geomagnetic field prior to the Matuyama-Brunhes transition: radiometric dating of a 820Ka excursion at La Palma, *Geophys. J. Int.*, **151**, F6–F10.

Riisager, P. & Abrahamsen, N., 2000. Palaeonintensity of West Greenland Palaeocene basalts: asymmetric intensity around the C27n-C26r transition, *Phys. Earth planet. Inter.*, **118**, 53–64.

Roberts, N. & Fuller, M., 1990. Similarity of new palaeomagnetic data from the Santa Rosa Mountains with those from Steens Mountain gives wide regional evidence for a two stage-reversal process of geomagnetic field reversal, *Geophys. J. Int.*, **100**(3), 521–526.

Singer, B.S., Relle, M.K., Hoffman, K.A., Battle, A., Laj, C., Guillou, H., &Carracedo, J.C., 2002. Ar/Ar ages from transitionally magnetized lavas on La Palma, Canary Islands, and the geomagnetic instability timescale, *J. geophys. Res.*, **107**, 2307 doi: 10.1029/2001JB001613.

Tric, E., Laj, C., Jehanno, C., Valet, J.-P., Kissel, C., Mazaud, A. & Iaccarino, S., 1991. High-resolution of the upper Olduvai transition flow from Po Valley, (Italy) sediments; support for dipolar transition geometry?, *Phys. Earth planet. Inter.*, **65**, 319–336.

Valet, J.-P. & Laj, C., 1984. Paleomagnetic record of two successive Miocene geomagnetic reversals in western Crete, *Earth planet. Sci. Lett.*, **54**, 53–63.

Valet, J.-P., Tucholka, P., Courtillot, V. & Meynadier, L., 1992. Palaeomagnetic constraints on the geometry of the geomagnetic field during reversals, *Nature*, **356**, 400–407.

Valet, J.-P., Brassart, J., Quidelleur, X., Soler, V., Gillot, P.-Y. & Hongre, L., 1999. Paleointensity variations across the last geomagnetic reversal at La Palma, Canary Islands, Spain, *J. geophys. Res.*, **104**(B4), 7577–7598.

Wicht, J., 2005. Palaeomagnetic interpretation of dynamo simulations, *Geophys. J. Int.*, **162**, 371–380.

Williams, I. & Fuller, M., 1981. Zonal harmonic models of reversal transitional fields, *J. geophys. Res.*, **86**, 11 657–11 665.

## APPENDIX: THE EFFECT OF THE ELLIPTICITY OF THE EARTH ON THE CALCULATION OF VGP POSITION

The calculations presented in this paper of the positions of the VGP and the magnitude of the VDM were made with a consideration of

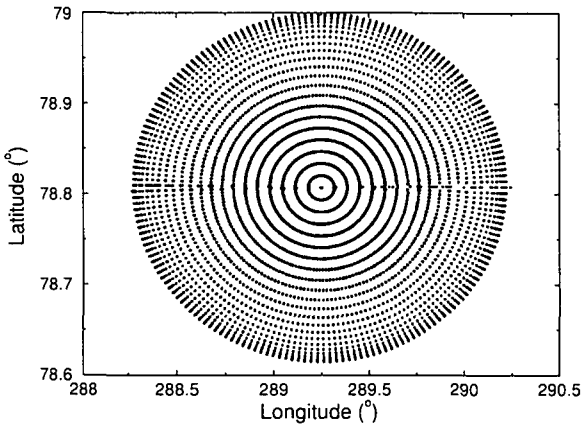


**Figure A1.** The effect of the ellipticity of the Earth on the calculation of VGP position. VGPs are calculated for a simple centred tilted dipole field, but without converting from geodetic (for the field measurement) to geocentric coordinates (for the VGP formula).

the geometrical shape of the Earth: in other words, the field components (such as declination and inclination) were calculated in the appropriate geodetic coordinate system, rather than in geocentric coordinates. This exposed the possibility of a small systematic error in the determination of both VGP and VDM by standard methods. The usual formulae used for this purpose (e.g. Merrill *et al.* 1996) assume a spherical Earth. Fig. A1 presents calculated VGP positions for synthetic locations all over the Earth, assuming a simple tilted dipole field. As can be seen, the calculated direction of the VGP varies by almost half a degree in latitude, and about 2° in longitude. This is clearly a small effect, but it is systematic (as a function of the location of the observation site) and is largest in mid-latitudes, where most of the available observations are taken. A similar effect is seen in calculations of VDM using the standard formulae, with a variation with position of up to 1 per cent. Such small errors are unlikely to be of great significance, but the fact that they are systematic suggests that it may be worth considering correcting for them (for example, by locally re-orienting observations into a geocentric coordinate system before calculating VGP and VDM).

# Microwave palaeointensity results from the Matuyama-Brunhes geomagnetic field reversal

Maxwell C. Brown[a] *, Martin N. Gratton[a], John Shaw[a], Richard Holme[a], Vicente Soler[b]

[a] *Geomagnetism Laboratory, Department of Earth and Ocean Sciences, Oliver Lodge Building, Oxford Street, University of Liverpool, Liverpool, L69 7ZE, United Kingdom*

[b] *Estación Volcanológica, Instituto de Productos Naturales (CSIC), Avda. Astr. Fco. Sanchez 3. 38206, La Laguna, Tenerife, Spain*

**Abstract**

We present new palaeointensity and palaeodirectional results from the Matuyama-Brunhes geomagnetic field reversal. Volcanic sequences from La Palma and Guadeloupe record the Matuyama-Brunhes boundary, possible precursors, and fluctuations in the magnetic field prior to the main polarity reversal. Absolute palaeointensity was determined using the microwave technique and palaeodirectional results were obtained from thermal demagnetisation. Ten flows from the twenty-nine flows studied gave reliable mean palaeointensities; however, only one of the ten flows records a transitional direction. The VDM determined from this flow is 1.9 ± 0.6 ($\pm\sigma$) x $10^{22}$ $Am^2$. Analysis of all Matuyama-Brunhes data suggests that the main directional changes occurred once the VDM was reduced below 3 x $10^{22}$ $Am^2$ (~35% of the present field value).

*Key words:* Matuyama-Brunhes; reversals; microwave; palaeomagnetism; palaeointensity; La Palma; Guadeloupe

## 1 Introduction

The behaviour of the geomagnetic field during reversals is unclear. Understanding the global temporal evolution of the geomagnetic field dfuring reversals can provide important constraints on conditions at the core-mantle

* Corresponding author.
*Email address:* m.c.brown@liv.ac.uk (Maxwell C. Brown[a]).

boundary and on geodynamo processes (Olson and Amit, 2006). Many palaeomagnetic studies from both sedimentary and lava sequences have sought to uncover details of the reversal process. To fully characterise the behaviour of the geomagnetic field the full magnetic vector must be calculated, requiring both directional and intensity data. Sedimentary sequences provide a quasi-continuous record of directional changes (Coe and Glen, 2004), but lack absolute palaeointensity data. Volcanic records can provide both palaeodirection and absolute palaeointensity; however, they only record fragmentary behaviour of the field at one location on the Earth's surface and where multiple records exist it is extremely difficult to correlate them temporally and establish features globally (Constable, 1990; Gubbins, 1999; Brown et al., 2007; Leonhardt and Fabian, 2007).

The fidelity of both sedimentary and volcanic records is of concern. Problems affecting sedimentary records include: secondary magnetic overprints that can be difficult to remove (Valet et al., 1988); smoothing of the geomagnetic signal caused by low sedimentation rates (Channell and Lehman, 1997; Channell et al., 2004) or to delayed NRM acquisition related to diagenesis and grain growth chemical-remanence mechanisms (Langereis et al., 1992; van Hoof et al., 1993); shallowing of inclination (Celaya and Clement, 1988; Barton and McFadden, 1996; Tauxe and Kent, 2004; Tan et al., 2007).

Determining absolute palaeointensity from volcanic rocks is also problematic, the accuracy of determinations being affected by the natural state of the samples and by laboratory experiments. The majority of volcanic samples contain a mixture of magnetic remanence carriers, which can cause non-ideal behaviour during palaeointensity experiments. Samples may have been oxidised at high or low temperatures in nature, possibly resulting in considerably inaccurate determinations (Tanaka and Kono, 1991; Yamamoto et al., 2003; Tarduno and Smirnov, 2004; Smirnov and Tarduno, 2005; Yamamoto, 2006; Biggin et al., 2007a). In the laboratory, methods that use bulk heating (Thellier and Thellier, 1959; Shaw, 1974) can cause alteration of magnetic minerals, changing the changing the relationship between applied magnetic field and thermoremanent magnetisation (TRM): a common reason for the failure of palaeointensity experiments. Cooling rate differences between nature and the laboratory can also cause over or underestimation of palaeointensity depending upon the dominant remanence carrier (Fox and Aitken, 1980; Halgedahl et al., 1980; Leonhardt et al., 2006). The best method to obtain accurate absolute palaeointensity determinations without ambiguity from non-ideal recorders is still disputed; however, new techniques (Hill and Shaw, 1999; Cottrell and Tarduno, 1999; Yamamoto et al., 2003; Dekkers and Böhnel, 2006) and new protocols for the Thellier method (Riisager and Riisager, 2001; Fabian, 2001; Yu et al., 2004; Biggin et al., 2007b) have made significant improvements in obtaining accurate data and in detecting data affected by non-ideal remanence carriers.

In addition to having reliable magnetic measurements, accurate dating of both sedimentary and volcanic reversal sequences is required to correlate geomagnetic field variations globally and to constrain the core processes that generate the magnetic field (Singer et al., 2005; Leonhardt and Fabian, 2007). The need for accurate dating is highlighted when the possible complexity and global non-uniformity of the field during a reversal is considered (Coe and Glen, 2004; Brown et al., 2007).

The Matuyama-Brunhes (MB) reversal is the most recent geomagnetic field reversal and is recorded in numerous sedimentary sequences and by 16 volcanic sequences at seven locations globally (Fig. 1). It provides our best chance to characterise a reversal globally. Astronomical dating, using tuned oxygen isotopes from sediments, places the main polarity change at 781 $\pm$ 2 ka in the Atlantic and at 775 $\pm$ 2 ka from cores from the Indian-Pacific-Caribbean (Tauxe et al., 1996). A significant reduction in intensity approximately 15 kyr before the main polarity change is also recorded (Hartl and Tauxe, 1996). Astronomical dates from Yamazaki and Oda (2001) from South Atlantic anoxic sediments agree with the 781 ka estimate of Tauxe et al. (1996). They also date a number of large geomagnetic field fluctuations before the main polarity change to be between 788 ka and 795 ka. Channell et al. (2004) using Atlantic sediments south of Iceland have dated the mid-point of the reversal to be between approximately 772.5 ka and 773.5 ka, younger than the mean estimates of previous estimates; however, within the range of results obtained by Tauxe et al. (1996): 769.9 $\pm$ 3.8 ka to 784.2 $\pm$ 19.4 ka (from 18 sites). The variations in dating could be caused by problems with the sedimentary recording process and/or by real global offsets in the timing of directional changes (Coe et al., 2000; Brown et al., 2007; Leonhardt and Fabian, 2007). $^{40}Ar/^{39}Ar$ dating of lava flows has identified features relating to the reversal process at between 776 ka and 798 ka (Singer et al., 2002; Brown et al., 2004; Coe et al., 2004a; Singer et al., 2005). $^{40}K/^{40}Ar$ dating of lava flows has identified features that could belong to the MB reversal process at between approximately 777 ka and 825 ka (Valet et al., 1999; Carlut et al., 2000; Carlut and Quidelleur, 2000; Quidelleur et al., 2002, 2003). $^{10}Be$ records from Antarctic ice cores have also been used to calculate virtual axial dipole moment (VADM) variations at the time of the MB reversal. Raisbeck et al. (2006) calculated two intensity lows, one related to the main polarity change at approximately 780 ka and another at approximately 800 ka.

Global modelling of the MB reversal has been attempted by Shao et al. (1999) and Leonhardt and Fabian (2007) with the IMMAB4 model of Leonhardt and Fabian (2007) being particularly impressive in its approach and its reproducibility of some features of the MB transitional field; however, as the authors note, more detailed palaeomagnetic records of transitional fields are required to gain further insight into the reversal process. We aim to provide new reliable microwave palaeointensity and thermal palaeodirection data for

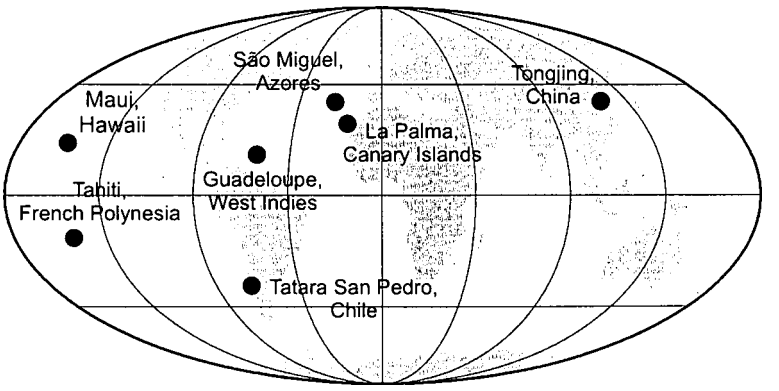


Fig. 1. Location map for lava flows that record the MB reversal. La Palma (Quidelleur and Valet, 1996; Valet et al., 1998, 1999; Quidelleur et al., 1999; Singer et al., 2002; Quidelleur et al., 2002, 2003), Guadeloupe (Carlut et al., 2000; Carlut and Quidelleur, 2000),Tahiti (Chauvin et al., 1990; Mochizuki et al., 2005), Tatara San Pedro(Brown et al., 1994, 2004; Gratton et al., 2007), Maui (Coe et al., 2004a), Tongjing (Zhu et al., 1991), São Miguel (Johnson et al., 1998).

the reversal. In this study we have revisited four sections from the island of La Palma, Canary Islands, and one section from the island of Guadeloupe, West Indies. A recent study of the MB reversal by Gratton et al. (2007) using the microwave palaeointensity technique was able to determine palaeointensity from a series of lava flows from Chile recording the transitional field. This motivated us to re-examine these sections with the hope of improving the palaeointensity record.

## 2 Background

### *2.1 La Palma*

The island of La Palma in the Canary Archipelago (Fig. 2a and b) is positioned on the slow moving African plate approximately 100 km north of the possible emergence of a mantle plume beneath the island of El Hierro (Prægel and Holm, 2006). Apart from the Hawaiian Islands, the Canary Islands are the most studied group of islands in the world (Carracedo et al., 1998). They are built on oceanic crust of Jurrasic age (Roest et al., 1992), with the crust underlying La Palma and El Hierro being 150-156 Ma (Watts, 1994). Unlike the Hawaiian-Emperor chain, there is not an age progression of volcanism related to a possible mantle plume. However, the origin and evolution of the islands is far from being well explained and modelled, especially when compared to the Hawaiian Islands (Carracedo et al., 1998).

La Palma rises 6500 m above the sea floor and 2400 m above sea level (Valet

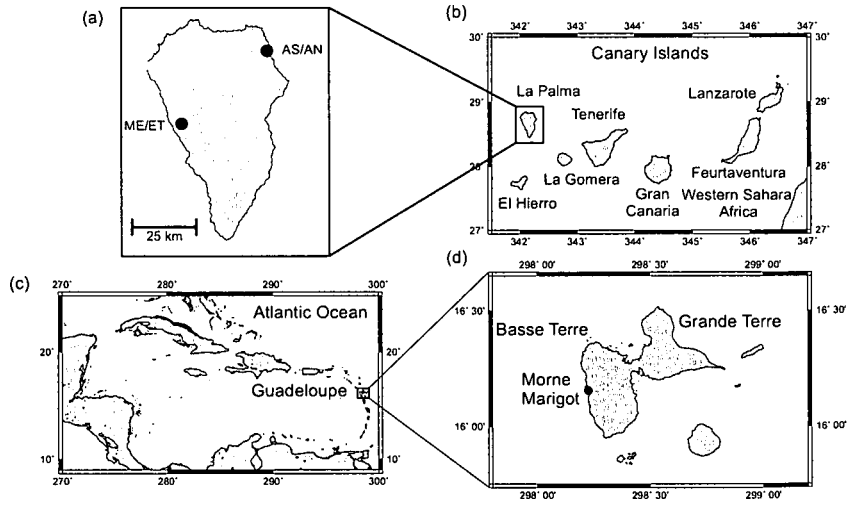


Fig. 2. (a) Map of La Palma with studied sections labelled. (b) La Palma in relation to the other Canary Islands. (c) Guadeloupe's position in the Caribbean island chain. (d) Location of the Morne Marigot quarry sections on the island of Basse Terre, Guadeloupe.

et al., 1999). It is divided into three main geological units (Singer et al., 2002): (1) Basement intrusive rocks exposed in the Caldera de Taburiente, which are part of the exhumed Pliocene sea mount; (2) Older subaerial lavas which form the Taburiente and Bejenado volcanoes; (3) the younger Cumbre Vieja volcano (Staudigel et al., 1986; Guillou et al., 1998; Carracedo et al., 1999). The Taburiente Volcano formed the north part of the island during the Matuyama and Brunhes Chrons, with $^{40}K/^{40}Ar$ and $^{40}Ar/^{39}Ar$ ages dating lavas between 1.6 Ma to 0.5 Ma (Carracedo et al., 1999; Quidelleur et al., 1999; Tauxe et al., 2000; Valet et al., 1999; Guillou et al., 2001; Quidelleur et al., 2002, 2003).

ME and ET sections previously studied by Valet et al. (1998, 1999) are located at El Time in the western part of La Palma (Fig. 2a) and are part of the northwestern flank of the Caldera de Taburiente, which was formed by large landslides (Ancochea et al., 1994). This section either belongs to the the Upper Old Series (Ancochea et al., 1994) or the Cumbre Nueva Series (Navarro and Coello, 1993) and therefore could have originated from two different eruptive centres. The dominant lava type is Pahoehoe basalt, which is often topped with a layer of scoria. Palaeosol and cindercone layers are common throughout both sections. The ET section is especially complicated, with flows pinching in and out and intersected by dykes.

Palaeomagnetic sampling was conducted in March 2006. Using previous field notes (VS) and markers left by Valet et al. (1998, 1999) we sampled the same sections and flows as Valet et al. (1999). The ME and ET sections are located at 28.67°N, 17.94°W, approximately 700m apart along the road LP-1. All flows very horizontal; however, given their thin nature and the distance between

the sections, it was not possible to correlate the two sections in the field. We sampled five flows from the ET section and the top 20 flows of the ME section. 11 25 mm cores were taken from the ET flows and 100 from the ME flows. We sampled the centres of the flows to avoid problems with remagnetisation by overlying flows (Valet et al., 1998). $^{40}K/^{40}Ar$ dates place from the ME section two flows either side of the polarity reversal at 788 $\pm$ 12 ka and 784 $\pm$ 13 ka (Quidelleur et al., 2003).

The study of Valet et al. (1999) provides one of the most detailed records on palaeointensity variations around a geomagnetic field reversal. Although no transitional directions were obtained from these sections, palaeointensity was determined from 45 volcanic units. Results varied from 15 $\mu$T to 60 $\mu$T for a number of flows with stable directions before reducing to $\sim$ 7 $\mu$T prior to the polarity change. Palaeointensity after the reversal was also variable, recovering to $\sim$ 60 $\mu$T. Compared with other intensity data from the PINT03 database (Perrin and Schnepp, 2004) for the last 5 Ma these results seem anomalously high. The palaeointensity records from the ME and ET sections were used to calibrate the relative intensity data from the sedimentary records used in IMMAB4 (Leonhardt and Fabian, 2007).

The AS and AN sections are located in the Barranco del Agua, in the north east of the island (Fig. 2a) (28.80°N, 17.77°W). The lava flows are basaltic and part of the Upper Old Series of the Taburiente Stratovolcano (Navarro and Coello, 1993). It is unclear whether these flows are from the same eruptive centre that produced the flows at El Time. Scoria layers (in one case 5 metres thick) and palaeosols are again seen.

We roughly followed the sampling of Quidelleur and Valet (1996) and Singer et al. (2002) on the southern side of the gorge; the AS section (LL in Quidelleur and Valet (1996) and TS in Singer et al. (2002)). For the northern side of the gorge (AN section) we followed the vertical section chosen by Quidelleur and Valet (1996) (LS section). The TN section from Singer et al. (2002) was difficult to trace and we were not confident that we could resolve an accurate stratigraphy. The large number of flows and ambiguity in the delimitation of some of the flows means that the results from our study and the Quidelleur and Valet (1996) and Singer et al. (2002) studies can not be directly compared. 77 25 mm cores were taken from 20 flows from the AS section that sample the time around the reversal (107 cores from 29 flows were sampled in total; the youngest flows contain an excursion around 600 ka (Quidelleur et al., 1999) or 580 ka (Singer et al., 2002)). 57 25 mm cores were taken from 16 flows from the AN section.

Quidelleur and Valet (1996) obtained both palaeodirection and palaeointensity results from flows on both sides of the gorge. Palaeointensity was obtained from 17 flows; however, results from 9 flows were corrected using the method

of Valet et al. (1996). Palaeointensity prior to the polarity change is low with a minimum value of 4 $\mu$T. One $^{40}K/^{40}Ar$ date of 797 $\pm$ 12 ka was obtained from the northern side of the gorge from a reversed polarity flow (Quidelleur et al., 2002). No transitional directions were obtained in the Quidelleur and Valet (1996) study; however, Singer et al. (2002) sampling a different section on the northern side of the gorge found two flows that recorded transitionally reversed directions. These flows were dated by $^{40}Ar/^{39}Ar$ to be 780 $\pm$ 10 ka and 803 $\pm$ 10 ka. Two flows lower in the stratigraphy were dated at 791 $\pm$ 19 ka and 796 $\pm$ 10 ka and Singer et al. (2002, 2005) suggest these flows record a precursor event to the main polarity change of the MB (Hartl and Tauxe, 1996; Brown et al., 2004; Gratton et al., 2007).

### *2.2 Guadeloupe*

The volcanic island of Guadeloupe is situated in the West Indies in the Atlantic Ocean (Fig. 2a) and is part of an island arc resulting from the subduction of the Atlantic plate under the Caribbean plate (Komorowski et al., 2005). The island is divided into two distinct parts; the older Grande-Terre in the east and Basse-Terre to the west. Grande-Terre comprises older volcanics of pre-Miocene age overlain with Pleistocene limestone, while Basse-Terre is entirely volcanic; the oldest parts of the island thought to be no older than 2.79 Ma from $^{40}K/^{40}Ar$ dating methods (Samper et al., 2007).

Palaeomagnetic sampling took place in March 2005 (MCB and MNG) and was concentrated on the southern part of the west coast of Basse Terre (Fig. 2b), where the age of volcanism was determined to be less than 1 Ma by $^{40}K/^{40}Ar$ dating (Blanc (1983); Carlut et al. (2000), further $^{40}K/^{40}Ar$ dating by Samper et al. (2007) subsequent to our field trip is in agreement with this conclusion). The sampling sites for this study are: 1) Morne Marigot quarry (16.1°N, 298.2°E), at a rare exposure of superposed andesitic lavas (heavy vegetation on the island prevents good rock exposure); 2) a river cut section $\sim$ 500 m to the south west of the quarry and $\sim$ 20 m below the base of the quarry.

We re-sampled the same Morne Marigot quarry flows studied in Carlut et al. (2000) and Carlut and Quidelleur (2000). Carlut and Quidelleur (2000) first identified field variations related to the MB reversal in sections at Morne Marigot in three flows. Following alternating field and thermal demagnetisation experiments, a change in polarity up the sequence, from transitional to reversed to normal from bottom to top, was observed. $^{40}K/^{40}Ar$ dating of the lava flows yielded dates of 777 $\pm$ 14 ka for the stratigraphically lowest (transitional) flow (GU09) and 785 $\pm$ 19 ka for the stratigraphically highest (normal) flow (GU11), respectively. These ages identified the sequence as partially recording the MB reversal. Carlut et al. (2000) carried out palaeoin-

tensity experiments on these three flows, using the double-heating variant of the Thellier method (Coe, 1967). Some experiments were conducted in an Argon atmosphere, and some heated in air. Four samples yielded a mean flow value of 5.5 $\pm$ 1.0 $\mu$T for the reversed flow (GU09) and 2 samples yielded a mean flow value of 11.0 $\pm$ 2.7 $\mu$T for the normal flow (GU11), with one value corrected for non-linearity in the Arai-Nagata plot, using the correction method of (Valet et al., 1996). The transitional polarity flow (GU10) did not yield any palaeointensities because of thermochemical alteration observed during the Thellier experiments (Carlut et al., 2000). It is the failure of the Thermal palaeointensity experiments that prompted us to try microwave palaeointensity analysis to obtain transitional palaeointensity data from this section.

In this study we have called flows GU09, GU10 and GU11 from Carlut et al. (2000) and Carlut and Quidelleur (2000) G01, G02 and G03 and divided the quarry into three vertical sections: A, B and C. Vertical sections were approximately 55 m apart. The A section included all three flows; B included G01 and G02; C only sampled G01. The quarry was heavily vegetated so exposure was limited. G01 is the lowest stratigraphic unit and is 160 m in lateral extent, with an average flow thickness of 7 m with 4 m of scoria on top; G02 is 10 m thick on average with 3 m of scoria above that; G03 is the highest stratigraphic unit and is on average 3 m thick with 3 m of scoria above that. 20 cores were sampled from G01, 14 were sampled from G02 and 8 were sampled from G03. Cores were taken in vertical sections throughout the thickness of the flows, with sample 01 being near to base of the exposed flow.

The river cut section is labelled GD and has not been sampled before. No radiometric dates exist; however, the height of the flow and the roughly horizontal dip of the flows in this area suggests that GD is older than the sequence at Morne Marigot. It was sampled to provide directional and palaeointensity information prior to the transitional sequence. 8 cores were sampled.

For all La Palma and Guadeloupe flows we have retained the names assigned in the field, but we have also given the flows a flow number (FN). Conversions from the field names to the flow numbers are shown in the tables in Section A. All graphs showing results from individual flows are plotted as flow number.

# 3 Methods

## *3.1 Rock magnetic methods*

A number of magnetic property measurements were made on samples from the La Palma and Guadeloupe sections to evaluate their suitability for palaeointensity experiments and to identify those samples which might be expected to give the most accurate results. Multiple measurements were made on 5 mm sub-samples from 25 mm cores and from multiple 25 mm cores per flows. Hysteresis and back field coercivity measurements were carried out on a Variable Field Translation Balance (MMVFTB) at the University of Liverpool and on a Princeton Measurement Corporation MicroMag 2900 vibrating sample magnetometer (VSM) at the Institute for Rock Magnetism, University of Minnesota. Hysteresis measurements allow the determination of saturation magnetisation, $M_s$, saturation of remanence, $M_{rs}$, and coercivity, $H_c$; back field remanence measurements give $H_{cr}$. These measurements have been used to calculate ratios of $M_{rs}/M_s$ and $H_{cr}/H_c$ and plotted as a Day plot (Day et al., 1977) or a squareness plot (Tauxe et al., 2002).

Thermomagnetic measurements were carried out in air using the MMVFTB. Magnetisation in an applied field of 0.75 T was measured as temperature was increased from room temperature to 700 °C and then allowed to cool back to room temperature. All thermomagnetic curves are corrected for their paramagnetic content, calculated from hysteresis measurements on the same sample prior to heating using the VFTB. Curie temperature is determined using the extrapolation method (Moskowitz, 1981). The titanium content of the titanomagnetite is estimated using a polynomial fit to experimental data for synthetic titanomagnetites (Bleil and Petersen, 1982). We recognise the limitations of this approach for determining the composition of natural titanomagnetites (see Lattard et al. (2006)).

Low temperature susceptibility was measured on a small number of samples from the ME section using a Quantum Design Magnetic Properties Measurement System at the Institute for Rock Magnetism, University of Minnesota. Temperature was increased from 5 K to 300 K and measured at 1 Hz. Multiple samples per flow were measured on a Bartington MS2 susceptibility meter at the Geomagnetism Laboratory, University of Liverpool. 1 mm x 5 mm discs of the cores were placed in liquid nitrogen for twenty minutes and then allowed to heat up in the ambient conditions of the laboratory while susceptibility was continuously measured.

### *3.2 Thermal demagnetisation*

Thermal demagnetisation was used to obtain palaeodirections from samples from La Palma and Guadeloupe. A Magnetic Measurements thermal demagnetiser was used to demagnetise the samples and magnetic measurements were made using a Molspin spinner magnetometer. Samples were demagnetised in 50°C steps up to 500°C and then in 20°C steps until the remanent magnetisation was lost (typically around 540°C). Multiple 25 mm samples per flow were used to determine the directional changes recorded in the AS, AN and Guadeloupe sections (see tables in A). Only one sample per flow was used for the ME section as our initial results were in agreement with those obtained by Valet et al. (1999). Flows from the ET section appeared very weathered when sampled in the field and pilot microwave demagnetisation experiments revealed multiple components of magnetisation. These samples are not suitable for directional or palaeointensity analysis and no further experiments were performed on samples from this section.

### *3.3 Microwave palaeointensity method*

The microwave method is an alternative to thermal techniques and can substantially limit thermochemical alteration of magnetic grains during experimentation; such alteration is the main reason for the failure of palaeointensity experiments with thermal techniques such as the Thellier (Thellier and Thellier, 1959; Coe, 1967) and Shaw techniques (Shaw, 1974; Rolph and Shaw, 1985). Thermal methods involve bulk heating samples, creating phonons (lattice vibrations) that then generate magnons (electron spin waves) causing the magnetic grains to demagnetise in a zero field. The microwave procedure does not use bulk heating of the sample matrix, but instead uses high-frequency microwaves that are resonant with the magnetic grains, exciting the magnons within those grains directly (Walton, 2002, 2004a,b; Walton et al., 2004). It has been shown by Hill et al. (2002a) and Biggin et al. (2007b) that in most cases were both methods are successful microwave-thermoremanent magnetisation ($T_M$RM) is equivalent to conventional thermoremanent magnetisation (TRM).

From January 2007, two 14 GHz microwave systems with 80 W amplifiers have been in operation at the Geomagnetism Laboratory, University of Liverpool: one with a liquid-nitrogen FIT SQUID magnetometer and another with a more sensitive three axis liquid-helium Tristan Technologies SQUID magnetometer (maximum sensitivity $\sim$ 1x10$^{-11}$ Am$^2$ (Shaw and Share, 2007)). The systems have different microwave resonant cavities. Both systems have programmable field coils (up to 100 $\mu$T) surrounding the microwave cavity and a microwave

TRM ($T_M$RM) can be induced in any specified direction. This allowed us to address whether there was any biasing of palaeointensity determinations caused by a particular experimental methodology. Three different protocols were used: the perpendicular method (Kono and Ueno, 1977; Hill and Shaw, 2007), the double-heating method (Coe, 1967) and the quasi-perpendicular method (Biggin et al., 2007b). The majority of experiments used the perpendicular method. The microwave system with the Tristan magnetometer was only used for the quasi-perpendicular experiments.

5mm samples were drilled from 25 mm cores and were attached by glue to the sample rod. During the experiments microwave power was applied for 5 s for each step. Microwave power was increased in steps at the discretion of the operator; the next step was determined based on the result of the previous step. Once the maximum power of 80 W was reached, the time of microwave power application was increased until a maximum of 20 s and the experiment stopped when the sample was fully demagnetised or became detached from the sample rod. Further experimental details and the development of the systems are well documented in Hill et al. (2002a,b, 2005), McArdle et al. (2004) and Gratton et al. (2005b,a, 2007).

### *3.4 Palaeointensity acceptability criteria*

Palaeointensity estimates have been accessed using the criteria of Brown et al. (2006) and are split in to three categories: class 1, class 2, and class 3 . Three classes were chosen as they more successfully represent the variation in the quality of the data in this study. A class 1 result must have the following:

(1) A stable primary natural remanent magnetisation (NRM) direction.
(2) Greater than or equal to four data points in a single straight line on an NRM/$T_M$RM plot. No point is eliminated in the selected NRM segment, unless it can be proved to be caused by experimental error (these results are shown in open circles).
(3) At least 30 per cent of the NRM is used ($f$ factor as defined by Coe et al. (1978)).
(4) A quality factor, $q$ (defined in Coe et al. (1978)) $\geq 5$.
(5) A gap factor, $g$ (defined in Coe et al. (1978)) $> 0.5$.
(6) A regression coefficient, $r^2$ of the best-fitting line $\geq 0.98$.
(7) For determinations made using the perpendicular method, $\theta 1 + \theta 2$ must be between 90° and 91° (the sum of the angles between the NRM and the ($T_M$RM) vector and the applied field vector and the ($T_M$RM) vector (Hill and Shaw, 2007)).
(8) p$T_M$RM checks differing from the original value by $\leq$ 10% (using the DRAT criteria of Selkin and Tauxe (2000)).

(9) $pT_MRM \leq 10$ % difference between two zero field applied power steps ($P_i - P_{i-1}$, where $P_i$ is a given applied microwave power (Riisager and Riisager, 2001)) for double-heating experiments.

A class 2 result must pass all the criteria listed; however, it may fail $pT_MRM$ checks or $pT_MRM$ tail checks if there is little or no distortion to the straight line trend. This suggests that the check failure is caused by problems with the reproducibility of the reflected power in the microwave cavity during the microwave experiment rather than by alteration or non-ideal behaviour. This category has been included as many of the results have high $f$, $q$ and $r^2$ values but display this kind of behaviour. Results from the quasi-perpendicular method are class 2. Although this protocol has been successful in determining the historical geomagnetic field from lavas with a range of magnetic domain states where other protocols failed (Biggin et al., 2007a,b), it requires further validation. Class 3 results produce a linear relationship between NRM and $T_MRM$ ($r^2 \geq 0.9$) but fail some of the selection criteria and checks, and represent data that are unreliable.

## 4 Results

### *4.1 Rock magnetism*

#### *4.1.1 La Palma*

Hysteresis parameters are plotted in Fig. 3a and b. The majority of samples plot in the pseudo-single domain (PSD) area of the Day et al. (1977) plot and along the theoretical mixing curves of single domain (SD) and multi-domain (MD) particles for TM0 from Dunlop (2002). All La Palma flows have similar characteristics on the Day et al. (1977) plot and squareness against coercivity plots (Tauxe et al., 2002). All flows show a spread in $M_{rs}/M_s$, $H_c$ and $H_{cr}/H_c$ to some degree. Some flows show a spread in $H_{cr}/H_c$ up to 4 and in $M_{rs}/M_s$ up to 0.3 (e.g. ME49). In these cases there is a range of magnetic particle types and behaviour (such as dipolar magnetostatic interactions between SD particles). The magnetic properties of ME47, ME48 and ME49 are discussed in Brown and Chen (2008). We find no relationship between the palaeomagnetic direction and the samples' hysteresis properties.

Three broad types of thermomagnetic behaviour have been identified for the La Palma samples: Type 1, 3 and 5 (Fig. 4). 171 samples from all La Palma sections were measured. 63 samples from 33 flows show type 1 behaviour. Type 1 curves show a single magnetic phase with Curie temperatures between 446°C and 540°C, corresponding to possible titanomagnetite compositions between

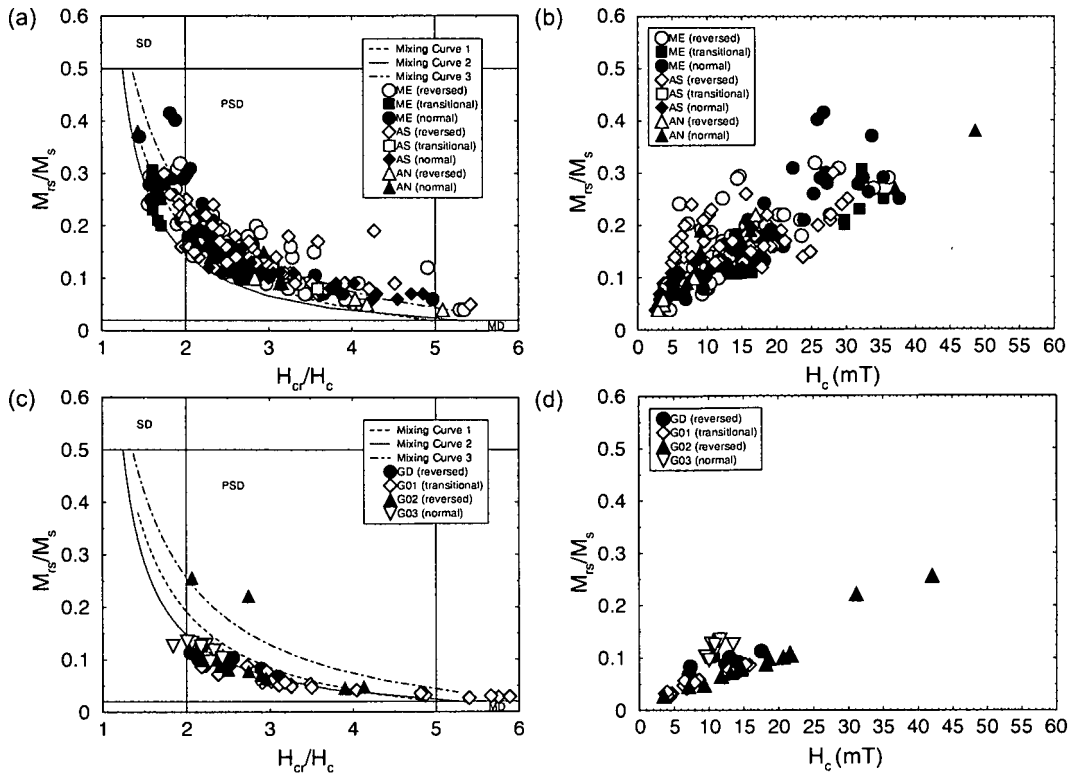


Fig. 3. Day et al. (1977) plots (a and c) and squareness against coercivity plots (Tauxe et al., 2002) (b and d) for La Palma (a and b) and Guadeloupe (c and d) lava flows. Samples split between reversed, transitional and normal field directions. Transitional flows are ME45, ME46 and AS17 (FN18). Day et al. (1977) plots modified using results from (Dunlop, 2002). Curves 1 to 3 are theoretical mixing curves of SD and MD particles for TM0 from Dunlop (2002).

TM19 and TM07. Magnetisation is reduced on cooling and there is range of irreversibility. At 100°C the difference in induced magnetisation between the two curves ranges from 3% to 45%. The magnetic phase producing type 1 behaviour could either be a low Ti-titanomagnetite or may result from high temperature deuteric oxidation of primary high titanium titanomagnetite producing a low titanium titanomagnetite phase (Carmichael and Nicolls, 1967; Mankinen et al., 1985). No microscopy was carried during this study so oxidation cannot be confirmed.

Type 3 curves (Fig. 4b-d) (70 samples from 45 flows) have a low titanium titanomagnetite phase (Curie temperatures between 398°C and 580°C, corresponding to compositions between TM29 and TM0) and another higher titanium titanomagnetite phase (Curie temperatures between 131°C and 333°C, corresponding to compositions between TM67 and TM38). The three divisions of type 3 show the variations in the titanomagnetite compositions. Such heating curves have been previously been observed for samples where high temperature deuteric oxidation has converted only part of the high titanium titanomagnetite phase to a low titanium titanomagnetite phase or the low

Curie temperature phase results from the presence of titanomaghemite. All type 3 cooling curves show an increase in induced magnetisation (at least for some of the temperature range (type 2a)). Type 3c curves show the largest increase in induced magnetisation (up to 66% at 100°C). Some cooling curves show complete oxidation of the high titanium titanomagnetite phase to a single lower titanium phase (Fig. 4b). Other cooling curves show less oxidation of the higher titanium phase (Fig. 4c and d).

Type 5a and 5b curves (Fig. 4e and f) (39 samples from 18 flows) show a range of low Curie temperatures from between 94°C and 143°C. On heating, Curie temperatures rise to between approximately 450°C and 550°C and the curves show pronounced irreversibility. In some examples there is an increase in induced magnetisation on cooling (measured at 100°C) up to 14 times the original magnetisation. The oxidation product at the higher Curie temperature could either be titanomaghemite or a low titanium titanomagnetite formed from a primary high titanium titanomagnetite (between TM71 and TM65). In Type 5a curves there is a very slight increase in induced magnetisation between 400°C and 500°C which could suggest inversion of titanomaghemite to titanomagnetite; however, without performing thermomagnetic experiments in a vacuum it is not possible to determine whether this bump and the large increase in induced magnetisation on cooling are a product of oxidation during the laboratory heating or to the inversion of titanomaghemite to titanomagnetite. Type 5b curves do not show an increase in induced magnetisation on heating between 400°C and 500°C. On cooling, type 5a curves show a mixture of secondary magnetic phases, whereas type 5b curves show a single secondary magnetic phase. An example of a microwave palaeointensity experiment performed on a sample with type 5b behaviour is shown in Fig. 8c.

Type 1 curves were dominant for the ME section (41 samples from 25 flows) and there were no examples of type 5 curves. The AS section was approximately equally divided between type 1, type 3 and type 5 curves. Type 3 curves were dominant for the AN section (11 samples from 11 flows). For a number of flows the thermomagnetic behaviour within a type is variable (see also Brown and Chen (2008)) and for a number of flows two types of curve have been observed. For example, AS20 (FN22) shows both type 1 and type 5 curves. This variation could result from inhomogeneous starting compositions or to inhomogeneous oxidation of the titanomagnetite particles during initial cooling at high temperature or by low temperature oxidation during weathering.

Examples of low-temperature susceptibility curves are shown in Fig. 5. 210 samples were tested and a range of low-temperature behaviour was determined. They are broadly categorized into four types (Fig. 5a-d). Considering titanomagnetite as the dominant magnetic phase in this sample set, low-temperature behaviour is influenced by a number factors including com-

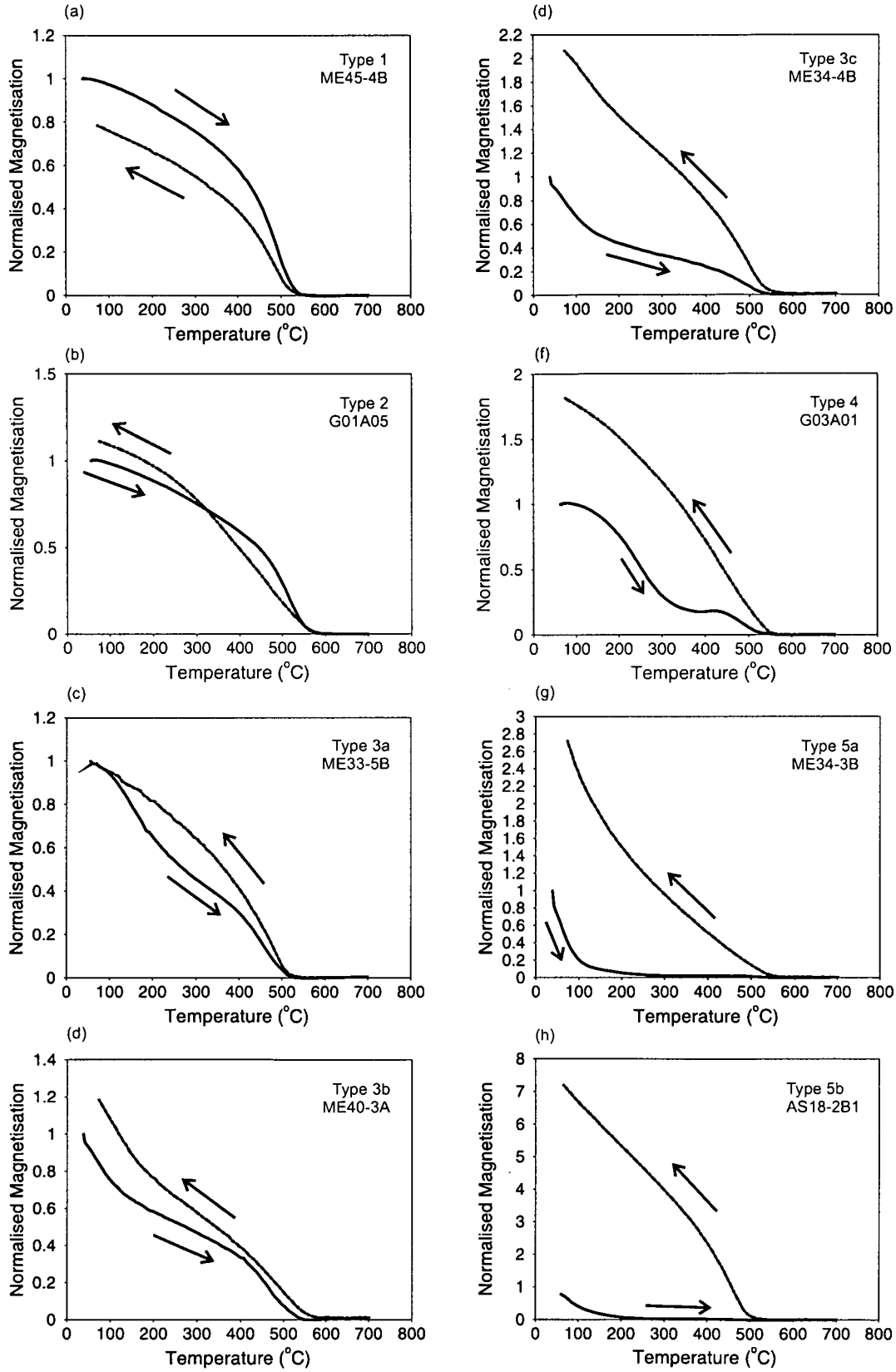


Fig. 4. Examples of the 5 broad types of thermomagnetic curves from samples from La Palma and Guadeloupe. Arrows indicate heating (solid lines) and cooling (dashed lines).

position (titanium content in titanomagnetite) and oxidation (either partial maghemitization of magnetite at low temperatures ((Özdemir et al., 1993)) or to possible homogenisation of ilmenite intergrowths to titanomagnetite at high temperatures (c.f. Smirnov and Tarduno (2005)). Fig. 5a shows a susceptibility maximum at around 85 K. This is probably caused by partial suppression of the Verwey transition of a low titanium titanomagnetite phase containing MD particles (Moskowitz et al., 1998) and could be caused by a degree of partial oxidation. In some examples the transition is very supressed with the ratio of initial susecptibility to room temperature susceptibility exceeding 1 and a disappearance of any isotropic point. In Fig. 4b there is an inflection at around 50 K and a susceptibility peak between 100 K and 120 K. The former could be caused the presence of an illmenite phase (Yamamoto, 2006). The latter could be caused by the presence of titanium poor titanomagnetite of varying compositions. These observations are consistent with the results of the thermomagnetic experiments: Fig. 4a and b are both from samples which show type 1 thermomagnetic heating and cooling curves (they suggest the existence of low-Ti titanomagnetite without any indications of low-temperature oxidation). In Fig. 4c and d there are inflection points around 110 K, although they are not as pronounced compared with those shown in Fig. 4a and b. These curves were observed from samples showing both type 1 and type 3 thermomagnetic heating and cooling curves suggesting that no low-temperature oxidation is present. Therefore, the inflection points probably originate from the Verwey transition of low-Ti titanomagnetite. Many flows show an internal variation of low temperature susceptibility characteristics and this in agreement with the high temperature heating and cooling curves. Such variation could possibly represent inhomogeneous deuteric oxidation of the flows.

### *4.1.2 Guadeloupe*

Hysteresis parameters are shown in Fig. 3c and d. Each flow has a distinctive distribution, but this does not relate to the palaeomagnetic direction recorded by the flow. The Day et al. (1977) plot shows that G01 (the transitional flow) has a range of particle types, but many samples are dominated by MD particles. G02 shows the biggest spread in hysteresis parameters, whereas G03 shows a tight cluster on both the Day et al. (1977) plot and the squareness against coercivity plots.

Four types of thermomagnetic curves are observed for the four Guadeloupe flows: Type 1, 2, 3 and 4 (Fig. 4). Type 1 curves (Fig. 4a) were determined from 29 samples from GD, G01 and G02. Curie temperatures range from 522°C to 580°C corresponding to compositions from TM09 to TM0. Induced magnetisation was reduced on cooling and the curves showed a range of irreversibility from 0% to 92% difference in induced magnetisation at 100°C. Seven type 1 curves show a small contribution from a second higher titanium

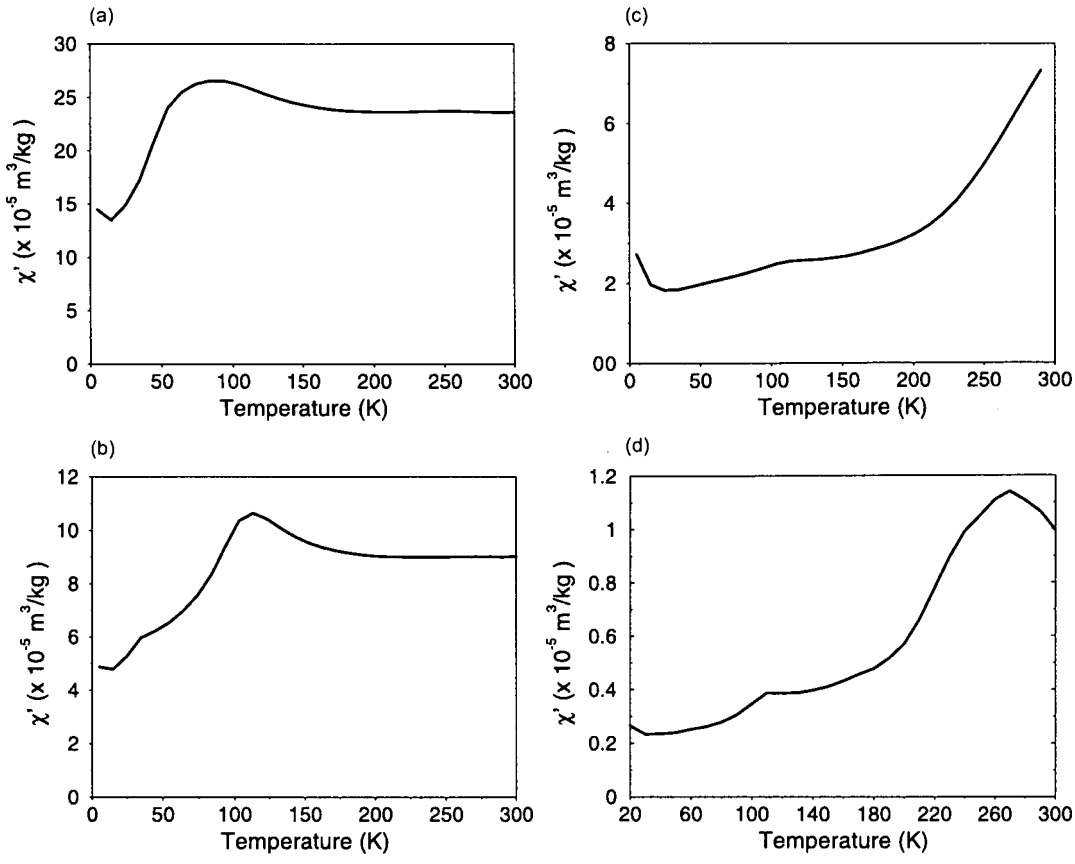


Fig. 5. Examples of low temperature frequency dependence of susceptibility measurements for the ME section, La Palma. Samples shown are: (a) ME32-1A1; (b) ME47-2A; (c) ME36-1A1; (d) ME41-3B

titanomagnetite phase on heating above 500°C. In some examples this phase has a Curie temperature close to the primary phase. On cooling, a single phase was formed, with a lower Curie temperature and a reduction in induced magnetisation across the whole temperature range.

Type 2 curves (Fig. 4b) show a single phase, a small secondary phase or a mixture of phases on heating. On cooling the heating and cooling curves cross. 11 samples from all four flows show this behaviour. Some examples have a reduced Curie temperature on cooling and some have the same or slightly higher Curie temperature as the primary phase. This behaviour could result from a combination of oxidation of the low titanium titanomagnetite and alteration of the higher titanium magnetite to a lower titanium phase on heating. Type 3 curves were only observed for 10 samples from G01 and G03.

Type 4 curves (Fig. 4f) show a distinctive inflection point at around 420°C. Before this inflection there is a small increase induced magnetisation between 400°C and 420°C. This behaviour indicates un-mixing and inversion of titanomaghemitite to titanomagnetite (Moskowitz, 1981). In these examples the amount of low-temperature oxidation of the the primary titanomagnetite

to titanomaghemite is thought to be low (Yamamoto and Tsunakawa, 2005). Only four samples from GA03 showed this behaviour; however, it could suggest that type 3 samples from GA03 contain a mixture of titanomaghemite and titanomagnetite phases. Samples showing evidence of maghemitisation will be unsuitable for accurate palaeointensity determinations as their NRM will be a mixture of a TRM, and a chemical remanent magnetisation (CRM) carried by titanomaghemite (Tarduno and Smirnov, 2004). There are variations in thermomagnetic properties within the flows which could again suggest inhomogeneous oxidation of the lava flows and the magnetic minerals.

47 samples from the four flows underwent low-tempearure susceptibility measurements. Like the samples from La Palma, Guadeloupe samples show a range of low-temperature curves, and also show large internal variations. This could again be interpreted as showing varying degrees of deuteric oxidation.

### *4.2 Directional results*

From the ME section, La Palma, one core from each of the 17 flows sampled was thermally demagnetised. The results are shown in Table A.1 and Fig. 6. 15 cores gave reliable directions that are in good agreement with the results from Valet et al. (1999). All samples record a secondary component of magnetisation, which was removed between 350°C and 400°C. (This component was also removed before applying the field in the perpendicular microwave palaeointensity experiment.) All samples that are accepted record vectors with maximum angular deviation (M.A.D.) (Kirschvink, 1980) less than 10°. 12 samples have M.A.D. less than 5°. The two flows that give no results are ME45 and ME46. These flows were emplaced between two flows recording reversed and normal directions and show overlapping components of magnetisation with high un-blocking temperatures, without a clear high temperature characteristic remanence component. These flows were studied in detail by Valet et al. (1998) and they concluded that the complexity of the vector is caused by partial reheating by the overlying flows recording the post-transitional field and by progressive oxidation of titanomagnetite, which raised the Curie temperature of the magnetic grains carrying the remagnetisation (an observation consistent with our thermomagnetic analysis). It has therefore not been possible to obtain either palaeodirections or palaeointensity during the polarity transition.

75 samples from 20 flows from the AS section, La Palma, were thermally demagnetised. A primary component of magnetisation was obtained for 16 flows; however, only 13 flow means were determined from three or more samples per flow. All flows record secondary components of magnetisation, which were removed between 250°C and 400°C. We include all 16 flows in our subsequent

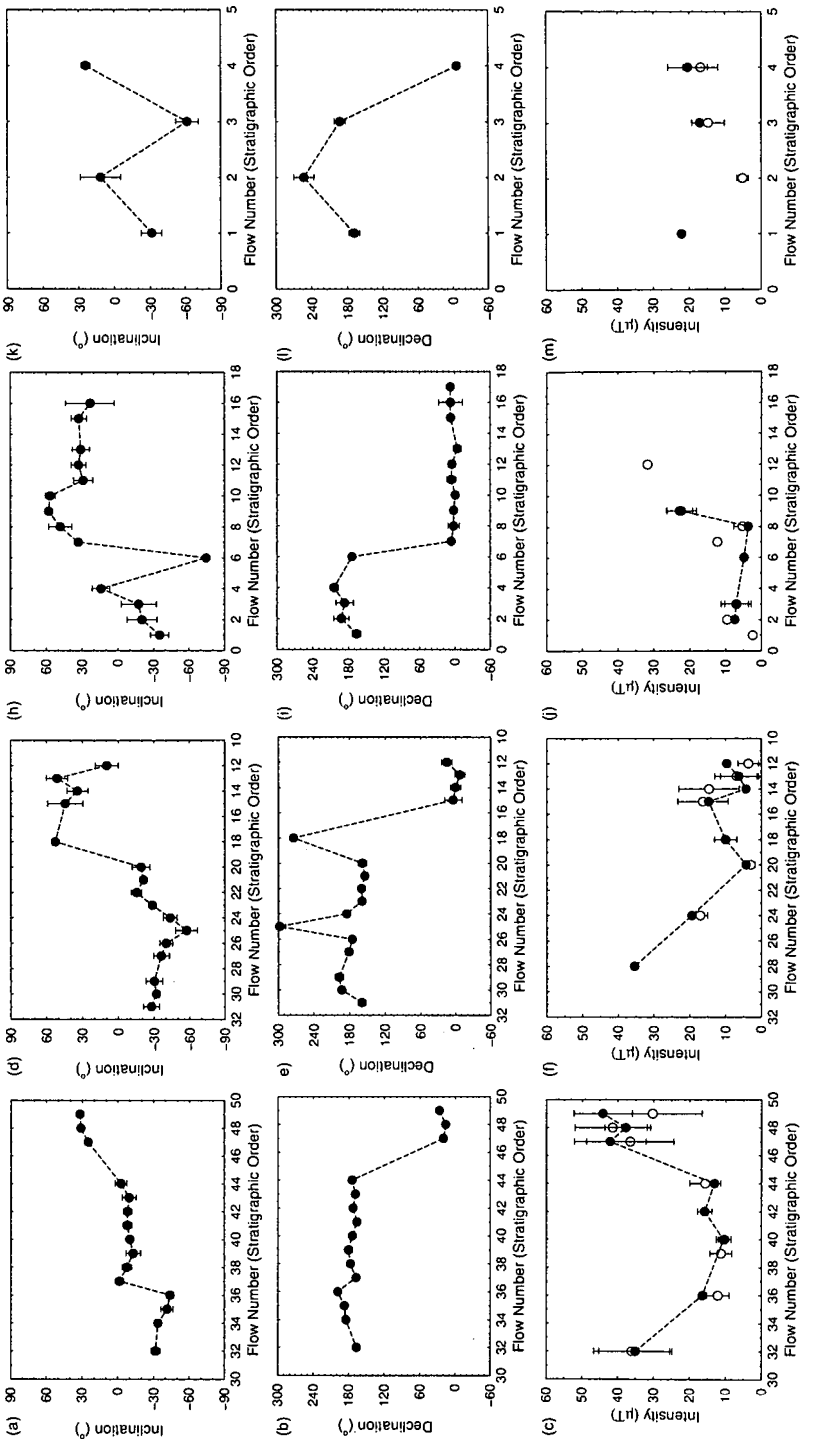


Fig. 6. Inclination, declination and palaeointensity for the ME (a, b, c), AS (d, e, f) and AN (h, i, j) sections. Error bars on ME inclination and declination data are M.A.D. (Kirschvink, 1980) as only one measurement made per flow (see text for details); error bars on AS and AN inclination and declination data are $\alpha_{95}$ (Fisher, 1953). Open circles are flow mean palaeointensities determined using all estimates presented in Table B.1, Table B.2 and Table B.3; solid circles are more robust determinations and are calculated from 1st and 2nd class data (discussed in Section 3.4). The dashed lines join flow means calculated using 1st and 2nd class data.

analysis, but advise great caution when interpreting results from the three flow means determined from less than three directions. All results are shown in Table A.2 and Fig. 6. There is a range of precision in the flow mean directions; from $\alpha_{95}$=1.3 to $\alpha_{95}$=14.8. Two flows (AS20 (FN22) and AS21 (FN23)) have $\alpha_{95}$ <5 and one flow (AS15 (FN15)) has $\alpha_{95}$ >10, the other 10 flows have 5> $\alpha_{95}$ <10. 10 flows record the reversed field, four flows record the normal field and two flows record the transitional field. The precision of the first transitional direction (AS23 (FN25)) is fair (Butler, 1992) (n=4, $\alpha_{95}$=9.4); however, the second transitional direction (AS17 (FN18)) is only determined from one sample. The transitional direction determined from AS23 records a large fluctuation (or excursion) in the geomagnetic field before the main polarity change. The timing of this event and how it relates to the evolution of the geomagnetic field is discussed in 5.1. Flow AS17 is between a normally and reversely magnetised flow and could record a transitional direction from the main directional reversal.

From the AN section, La Palma, 55 samples from 16 flows were thermally demagnetised. Palaeodirections are obtained for all the flows; however, only eight flow means are determined from three or more samples. 6 flows record large secondary components of magnetisation that were removed between 350°C to 400°C. The other flows record a small viscous component of magnetisation. Only three flow mean directions have $\alpha_{95}$ <5, the remaining five flows have 5> $\alpha_{95}$ <10. All results are shown in Table A.3 and Fig. 6. We again include all 16 determinations in our analysis. No transitional directions were recorded: 5 flows record reversed directions and 11 flows record normal directions. As the normal flows are not dated we do not know if they relate to the reversal process or to more stable field behaviour in the Brunhes Chron.

From the Guadeloupe section 26 samples from four flows were thermally demagnetised and 22 samples give reliable directions with an isolated primary component of magnetisation (Table A.4). Four samples are rejected because no stable component of magnetisation was recorded or the samples gave significantly different directional results from the majority of other samples in the flow. Samples from G01 (FN2) and G02 (FN3) record large secondary components of magnetisation; however, they were removed between 250°C and 300°C. All mean directional results are shown in Table A.4 and Fig. 6. For the stratigraphically lowest flow (GD (FN1)) all seven samples tested record stable primary components of magnetisation, with a mean reversed direction of 169° in declination and -31° in inclination. For flow G01 (FN2), four out of six samples give stable directions, with a mean intermediate polarity direction of 253° in declination and 12° in inclination; however, $\alpha_{95}$=17°. Seven out of eight samples from flow G02 (FN3) again record a reversed stable NRM direction, with a mean value of 192° in declination and -62° in inclination. Flow G03 recorded the most consistent directions ($\alpha_{95}$=3.8), with four out of five samples giving a stable normal polarity direction: mean declination of 354°

and mean inclination of 24°.

### *4.3 Palaeointensity results*

Individual palaeointensity results from the La Palma sections are listed in Table B.1, Table B.2 and Table B.3. Representative Arai-Nagata plots (Nagata et al., 1963) for class 1 and class 2 data are shown in Fig. 7a-f). 186 palaeointensity experiments were performed on samples from the ME, AS and AN sections. 119 (64%) experiments produced results that could be classified (class 1 to 3); 67 (36%) results are class 1 or 2; 7 (4%) are class 1. Palaeointensity results from Guadeloupe are of a lower quality. From 42 experiments, 19 palaeointensities were determined. Individual palaeointensity results are shown in Table B.4 and in Fig. 6. None passed the class 1 selection criteria, and only seven were classified as class 2. The remaining eleven are class 2 results and are likely to be unreliable. Individual Arai-Nagata plots from example class 3 results are shown in Fig. 7g and h).

Failure of experiments can be classified into three types:

(1) Apparent instability in the NRM direction. Using the perpendicular method this is detectable by measuring the angle between the characteristic remanence (ChRM) and the resultant vector $\theta_1$, and the angle between the resultant vector and the applied field $\theta_2$ (if the instability is outside the ChRM applied field plane). Variations in $\theta_1 + \theta_2$ can also be generated if the sample is anisotropic, if there is an error in the direction of the applied field, or if the magnetometer is not measuring correctly (Hill and Shaw, 2007). If the NRM directional instability is in the ChRM applied field plane then the relationship between the NRM and $T_M$RM will be non-linear.

(2) Concave-down NRM $T_M$RM slopes (Fig. 8a). 23 samples failed because of this behaviour and it was only seen in experiments using the perpendicular method. In all but two examples $\theta_1+\theta_2$ are between 90° and 91°. There is no apparent relationship between this behaviour and the behaviour of either the p$T_M$RM checks or $T_M$RM tail checks; for some points these checks will pass and for others they will fail. A more subtle variant of this behaviour is observed in the quasi-perpendicular experiments. For large fractions of the NRM the relationship between NRM and $T_M$RM is linear; however, at higher microwave powers a concave-down decreasing slope begins (Fig. 8b). A palaeointensity estimate has been taken for the straight line segment, but this behaviour needs further consideration.

(3) Concave-up NRM $T_M$RM slopes (Fig. 8c). This behaviour is seen in 11 samples using the double heating or quasi-perpendicular protocol. Four experiments fail p$T_M$RM checks at maximum microwave power for times

greater than 5 s, which would suggest magnetomineralogical alteration. (In theory a small sample in the centre of the cavity will not be subject to high electric fields but in practice this is not true. Magnetic and electric field distribution inside the cavity is influenced by the coupling slot, the sample rod, and the sample. Applying power to a pure quartz sample at 14.2 GHz will eventually heat it, clearly demonstrating the effect of dielectric heating and the presence of alternating electric fields in the sample.) Other examples pass both $pT_MRM$ checks and $pT_MRM$ tail checks, though as in the example shown in Fig. 8c there is failure of some checks.

Flow mean palaeointensities have been calculated in three ways and are shown in Table 1 and plotted in Fig. 6. Using all the data that could be classified, 29 flow means were calculated. The second approach was just only include individual palaeointensity estimates that are class 1 and 2. 25 flow means were calculated from these determinations; however, only ten of these flows had three or more determinations.

Applying the in-flow variation criterion of Selkin and Tauxe (2000) (the ratio of the standard deviation of the palaeointensity estimates to the mean should be less than 25%) to the flow means calculated from class 1 and 2 data would cause rejection of a large amount of data with low flow means. For flows with palaeointensity estimates below 10 $\mu$T small variations in the estimates can greatly affect the in-flow variation value; this criterion has not been applied to these flows and these results are reliable (Hill et al., 2005). Four flows from the ME section (ME32, ME47, ME48 and ME49) show a large range of palaeointensity determinations. ME32 has an in-flow variation value of 29% and fails the criterion. The three other flows pass the criterion; however, they show non-ideal characteristics for acquisition of thermal remanent magnetisation and for Thellier type palaeointensity determinations. These flows are discussed further in Brown and Chen (2008). We include these four flows in the further analysis, but express caution over their reliability.

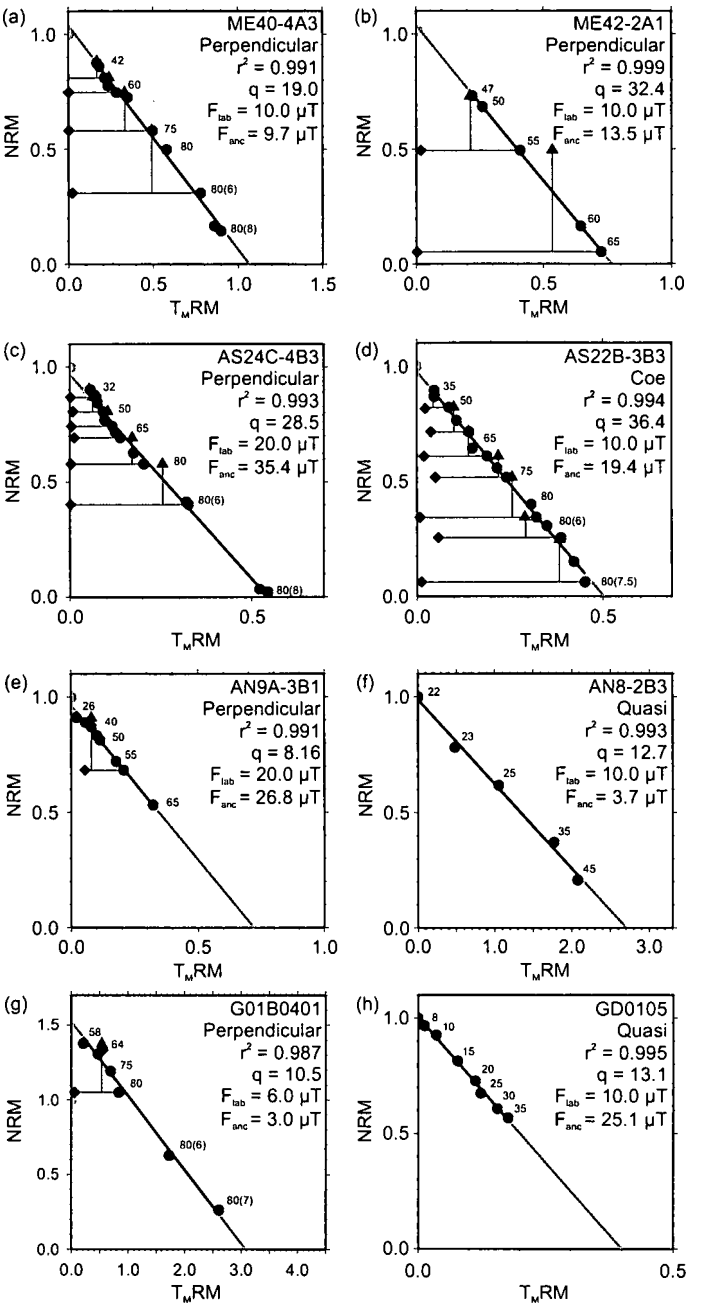


Fig. 7. Examples of Arai-Nagata plots (Nagata et al., 1963) for the La Palma (a-f) and Guadeloupe (g and h) sections. (a) and (c) show 1st class results, (b, d-h) show 2nd class results. $r^2$ and $q$ are defined in Section 3.4. $F_{lab}$ is the applied field during the palaeointensity experiment and $F_{anc}$ is the palaeointensity estimate. Numbers accompanying the data points are the microwave power steps in watts. The numbers in brackets are time in seconds; where no bracketed numbers are shown, the time of application was 5 s. Perpendicular denotes that the perpendicular applied method was used; Coe, the double-heating method (Coe, 1967); Quasi, the quasi-perpendicular applied field method (Biggin et al., 2007b). Examples (f) and (h) were determined using the quasi-perpendicular method, so no $pT_MRM$ checks or tail checks were used. Quasi-perpendicular experiments were performed on the Tristan 14 GHz system, which has a more efficient cavity, so the amount of power needed to de(re)magnetise the sample was much less.

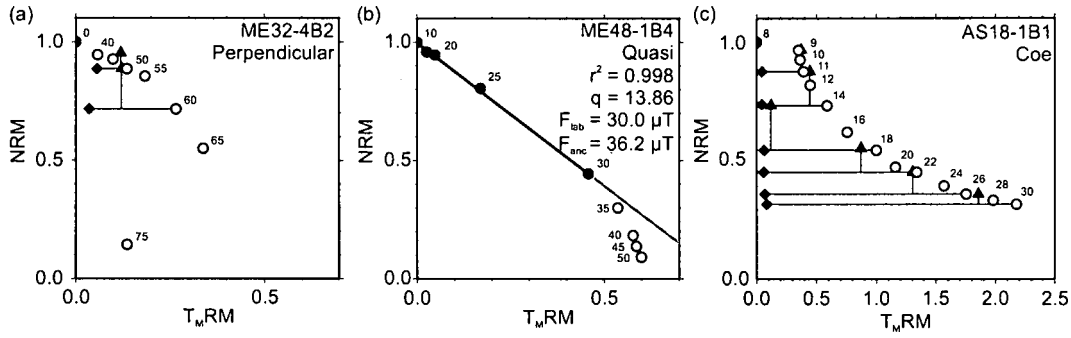


Fig. 8. Examples of Arai-Nagata plots which fail the palaeointensity experiments (a and c) or have unusual non-ideal characteristics. Graph labels are explained in Fig. 7.

| | *All estimates* | | | | *Class 1 and 2 estimates* | | | |
|---|---|---|---|---|---|---|---|---|
| Flow Number | Mean $F$ ($\mu T$) | $\sigma_F$ ($\mu T$) | VDM x $10^{22}$ ($Am^2$) | $\sigma_V$ x $10^{22}$ ($Am^2$) | Mean $F$ ($\mu T$) | $\sigma_F$ ($\mu T$) | VDM x $10^{22}$ ($Am^2$) | $\sigma_V$ x $10^{22}$ ($Am^2$) |
| *ME section, La Palma* | | | | | | | | |
| 32 | 36.1 | 10.7 | 8.3 | 2.4 | 35.0 | 10.2 | 8.1 | 2.4 |
| 36 | 12.1 | 3.1 | 2.5 | 0.8 | 16.4 | | 3.4 | |
| 39 | 11.3 | 3.1 | 2.9 | 0.8 | | | | |
| 40 | 10.3 | 1.8 | 2.6 | 0.5 | 10.5 | 2.1 | 2.7 | 0.5 |
| 42 | 15.8 | 2.1 | 4.0 | 0.5 | 15.8 | 2.1 | 4.0 | 0.5 |
| 44 | 15.7 | 4.3 | 4.0 | 1.1 | 13.1 | | 3.4 | |
| 47 | 36.6 | 12.2 | 8.8 | 2.9 | 42.1 | 10.0 | 10.1 | 2.4 |
| 48 | 41.4 | 10.5 | 9.5 | 2.4 | 37.7 | 5.9 | 8.7 | 1.4 |
| 49 | 30.3 | 13.8 | 6.9 | 3.2 | 44.2 | 8.1 | 10.1 | 1.9 |
| *AS section, La Palma* | | | | | | | | |
| 27 | 35.4 | | 7.9 | | 35.4 | | 7.9 | |
| 24 | 17.1 | 2.0 | 4.0 | 0.5 | 19.4 | | 4.6 | |
| 20 | 3.0 | 1.3 | 0.7 | 0.3 | 4.3 | | 1.1 | |
| 18 | 10.0 | 3.1 | 1.9 | 0.6 | 10.0 | 3.1 | 1.9 | 0.6 |
| 15 | 16.3 | 7.0 | 3.3 | 1.4 | 14.7 | | 3.0 | |
| 14 | 14.6 | 8.5 | 3.3 | 1.9 | 4.3 | | 1.0 | |
| 13 | 6.9 | 6.1 | 1.3 | 1.2 | 6.3 | 5.1 | 1.2 | 1.0 |
| 12 | 3.6 | 2.9 | 0.9 | 0.7 | 9.7 | | 0.6 | |
| *AN section, La Palma* | | | | | | | | |
| 1 | 2.4 | 0.8 | 0.5 | 0.2 | | | | |
| 2 | 9.6 | | 2.4 | | 7.5 | | 1.8 | |
| 3 | 6.9 | 3.3 | 1.7 | 0.8 | 7.1 | 4.2 | 1.8 | 1.0 |
| 6 | 4.8 | | 0.7 | | 4.8 | | 0.7 | |
| 7 | 12.3 | | 2.8 | | | | | |
| 8 | 5.3 | 2.5 | 1.0 | 0.5 | 3.7 | | 0.7 | |
| 9 | 22.8 | 3.5 | 4.0 | 0.6 | 22.3 | 4.2 | 3.9 | 0.7 |
| 12 | 31.7 | | 7.2 | | | | | |
| *Guadeloupe section, French West Indies* | | | | | | | | |
| 1 | 22.1 | | 5.1 | | 22.1 | | 5.1 | |
| 2 | 5.1 | 1.6 | 1.3 | 0.4 | 3.0 | | 0.8 | |
| 3 | 14.7 | 4.6 | 2.4 | 0.8 | 17.0 | | 2.8 | |
| 4 | 16.8 | 4.9 | 4.0 | 1.2 | 20.4 | 5.5 | 4.9 | 1.3 |

Table 1. Mean microwave palaeointensity results per flow for the AN section, La Palma. *All estimates* takes all class, 2 and 3 results; *Class 1 and 2 estimates* takes all estimates that pass the class 1 and 2 selection criteria (Section 3.4). Mean $F$ is the mean palaeointensity; $\sigma_F$ is one standard deviation of the flow mean intensity; VDM is the flow mean virtual dipole moment; $\sigma_V$ is the standard deviation of the flow mean VDM.

## 5 Discussion

We discuss the temporal and global evolution of the field during the MB reversal and compare our data with previously published data. We also compare our results with the output generated by model IMMAB4 by Leonhardt and Fabian (2007) and a simple mathematical reversal model (Brown et al., 2007) based upon CALS7K.2 (Korte and Constable, 2005). Even though our data set is small, it is possible to make direct comparisons to IMMAB4; however, only a statistical comparison can be made to the model based on CALS7K.2.

IMMAB4 is global geomagnetic field model of the MB reversal and uses an iterative Bayesian inversion method to construct a spherical harmonic expansion of the transitional field from paleomagnetic data. The initial model is based on the Atlantic ODP core of Valet et al. (1989) with the second iteration including a calibration for absolute palaeointensity from the volcanic section ME-ET, La Palma, from Valet et al. (1999). Subsequent iterations include the Atlantic sedimentary records of Clement and Kent (1986, 1991).

CALS7K.2 is a continuous global model for the last 7000 years determined by a regularized least squares fit to archaeomagnetic and palaeomagnetic data using spherical harmonics in space and cubic B-splines in time. We follow the approach of Brown et al. (2007) and take the field structure of CALS7K.2 and examine the effects on the surface field morphology by scaling the the magnitude of the axial dipole component linearly with time.

### *5.1 Palaeodirectional and palaeointensity variations*

All three sections from La Palma sample the reversed and normal field either side of the main polarity change. Unfortunately, only one flow from the AS section (FN18) records the transitional field during the main polarity change; however, another flow from (FN23) records an equatorial virtual geomagnetic pole (VGP) at a time before the main polarity change (Fig. 9). Without $^{40}Ar/^{39}Ar$ dates for these two flows it is not possible to determine which stage of the reversal these transitional directions belong to. FN23 could record part of the precursor event relating to the MB reversal (Singer et al., 2002, 2005) or an earlier excursion at 821±13 ka (Quidelleur et al., 2003). The date of the excursion also corresponds with the dated flows from the TS section prior to the main polarity change (Singer et al., 2002) (Fig. 9) and also with a transitional direction from western Mexico (dated at 819 ± 2 ka (Petronille et al., 2005). It is also not clear whether this excursion is also part of the MB reversal (Gratton et al., 2007). FN18 could record the precursor, as determined for flows 17 and 18 from the TN section of Singer et al. (2002), or the main po-

larity change. Although Quidelleur et al. (2002), Quidelleur et al. (2003) and Singer et al. (2002) dated many flows from both the AS and AN sections, they did not record either of the transitional directions determined in this study (Fig 9). All three studies show differences in the number of flows sampled and the directional results obtained. We attribute this discrepancy to difficulties in re-identifying flows from previous studies in the field and also to the large number of flows which were often hard to delimit.

VGP paths from the three La Palma sections are quite different (Fig. 10a-c); however, these differences result from the discrete nature of the flows in each sequence and do not represent the behaviour of the field between VGPs. Each volcanic sequence records part of a transitional field that is more complex than indicated by any of the three records. The problem of assessing VGP paths (and the complexity of all directional changes) from volcanic sequences is highlighted when compared with the results generated for La Palma by IMMAB4 (Leonhardt and Fabian, 2007) (Fig. 10f). Our new directional results do not match the results from IMMAB4 in detail (Fig. 10a, (b), (c) and (f)); however, the incorporation of sedimentary records in this model has greatly increased the detail that can be resolved for the reversal recorded on La Palma. Without analysis of sedimentary records in accompaniment to volcanic records the recorded transitional field behaviour can be simplified and misinterpreted. Such possible complexity in directional changes for the MB reversal is seen in the sedimentary records of Channell and Lehman (1997) and Yamazaki and Oda (2001), which both show multiple polarity changes and other large directional variations before the final polarity change. This behaviour has also been seen for a number of other reversals recorded in sedimentary sequences (see Coe and Glen (2004) and references therein). However, problems in the sedimentary recording mechanism and the fidelity of sedimentary records must always be considered. In addition, both volcanic and sedimentary records will always be incomplete and can only give a lower bound on the amount of directional and intensity variation for any particular reversal (Coe and Glen, 2004).

The palaeointensity results determined from the ME section using the microwave technique are in broad agreement with those determined by Valet et al. (1999) using the thermal Thellier method (Fig. 11). When no selection criteria is used the results from all flows agree (to within $2\sigma$) with the exceptions of ME36, ME38 and ME39 (Fig. 11a). For two flows only one thermal Thellier or microwave determination was possible. For the third flow (ME39) the thermal Thellier result is 2.5 times greater. The individual microwave results from this flow were all class 3 and only one thermal Thellier result passed the class 1 selection criteria. Results from this flow are deemed unreliable. When the microwave flow mean palaeointensities are compared with the flow means determined using the thermal Thellier method for the three mormal flows (ME47, ME48 and ME49), the means are comparable; however there is

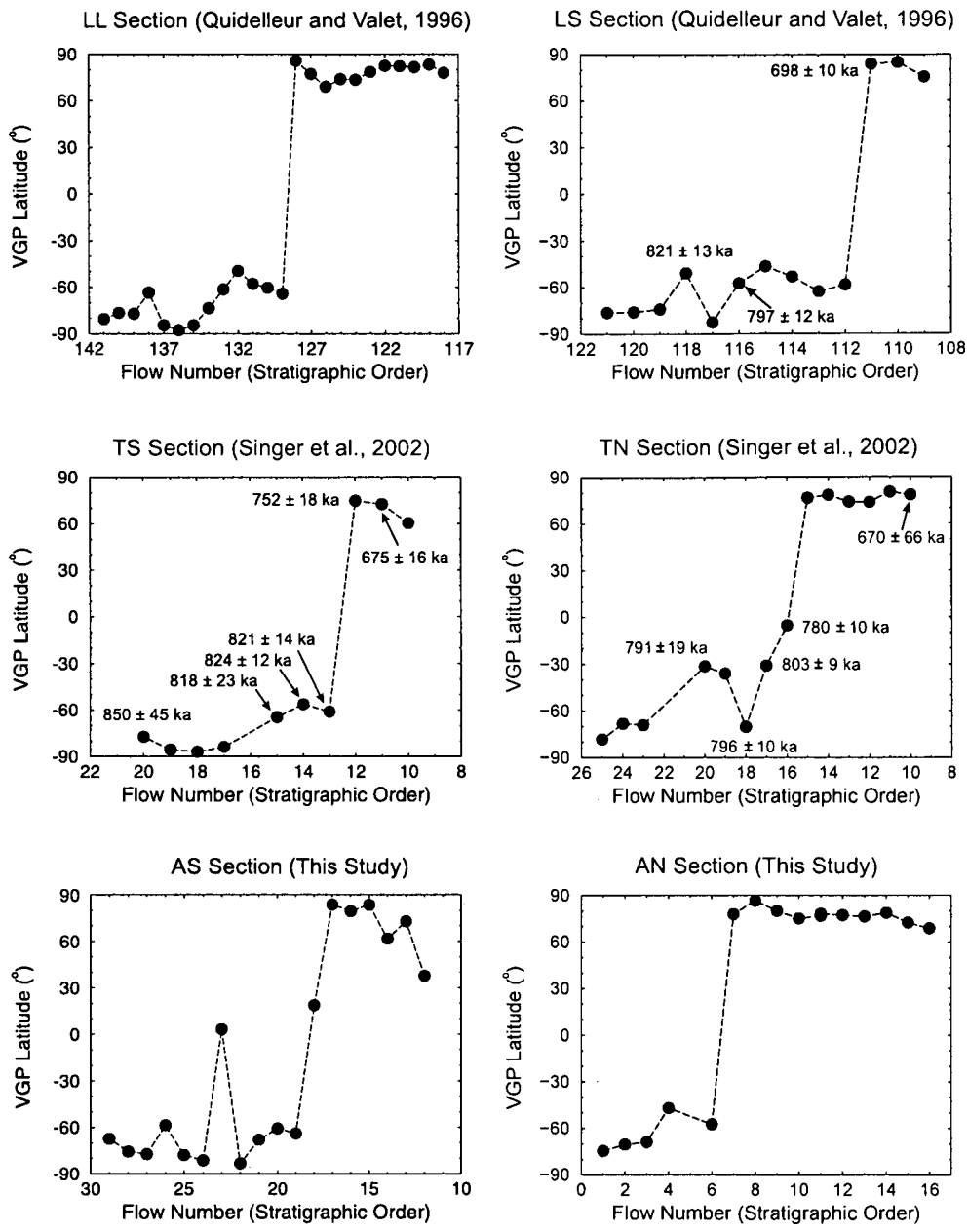


Fig. 9. Comparison of VGP latitude against flow number for the Barranco del Agua sections, La Palma. Errors on VGP latitude can be found in Quidelleur and Valet (1996) and Singer et al. (2002) and in Table A.2. Dates on the LS section are $^{40}K/^{40}Ar$; TS and TN dates are $^{40}Ar/^{39}Ar$.

a larger range of individual palaeointensity results determined using the microwave technique. Only the comparisons to ME48 and ME47 are statistically significant, as only two determinations were made using the thermal Thellier method for ME49. For ME48 the range of determinations using the microwave technique is 36.9 $\mu$T compared with 5.8 $\mu$T for the thermal Thellier technique; for ME47 the range of determinations using the microwave technique is 35.5

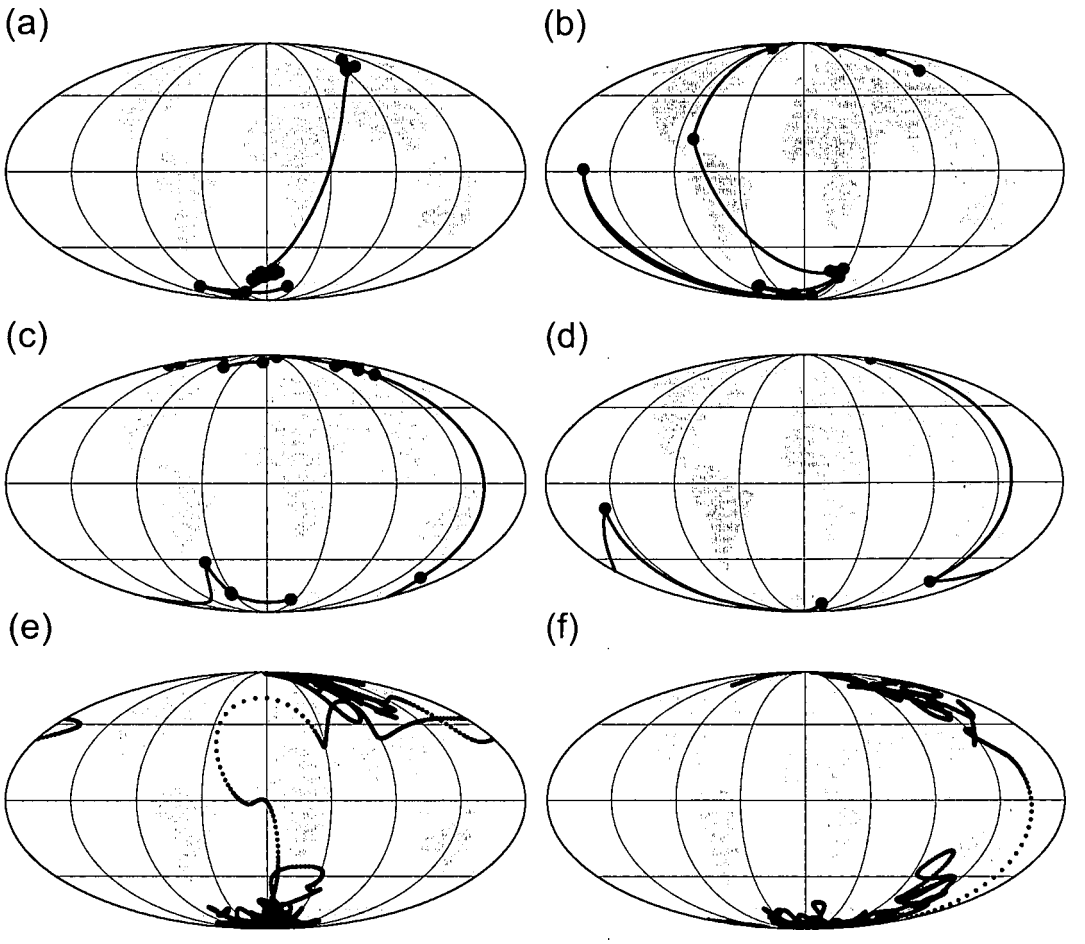


Fig. 10. Calculated VGP paths for (a) ME, (b) AS, (c) AN sections from La Palma, (d) Guadeloupe. (e) VGP path for La Palma and (f) Guadeloupe, generated by IMMAB4 (Leonhardt and Fabian, 2007), with each dot at 100 year intervals.

$\mu$T compared with 8.3 $\mu$T for the thermal Thellier technique. These three flows are investigated further in Brown and Chen (2008) and an explanation is proposed for the variation in individual palaeointensity determinations obtained using different sized samples. When the class 1 and 2 selection criteria is applied to both data sets the mean palaeointensities from the three normal polarity flows are no longer in good agreement (Fig 11b).

Palaeointensity was only obtained for one transitional flow on La Palma (FN18, AS section) giving a value of 10 $\pm$ 3.1 $\mu$T (n=4,), corresponding to a virtual dipole moment (VDM) of 1.9 $\pm$ 0.6 x $10^{22}$Am$^2$. Before the main polarity change the ME section gives a mean VDM of 3.4 $\pm$ 0.53 x $10^{22}$Am$^2$ and the AS/AN sections give a mean VDM of 1.48 $\pm$ 0.52 x $10^{22}$Am$^2$ (determined using all class 1 and class 2 data). This result is 2.3 times lower than the results from the ME section. It has already been noted in Section 2.1 that the palaeointensity results from the ME section (Valet et al., 1999) appear anomalously high when compared to the PINT03 database (Perrin and Schnepp, 2004) and this is again seen in our study. One possibility for this discrepancy is that the ME

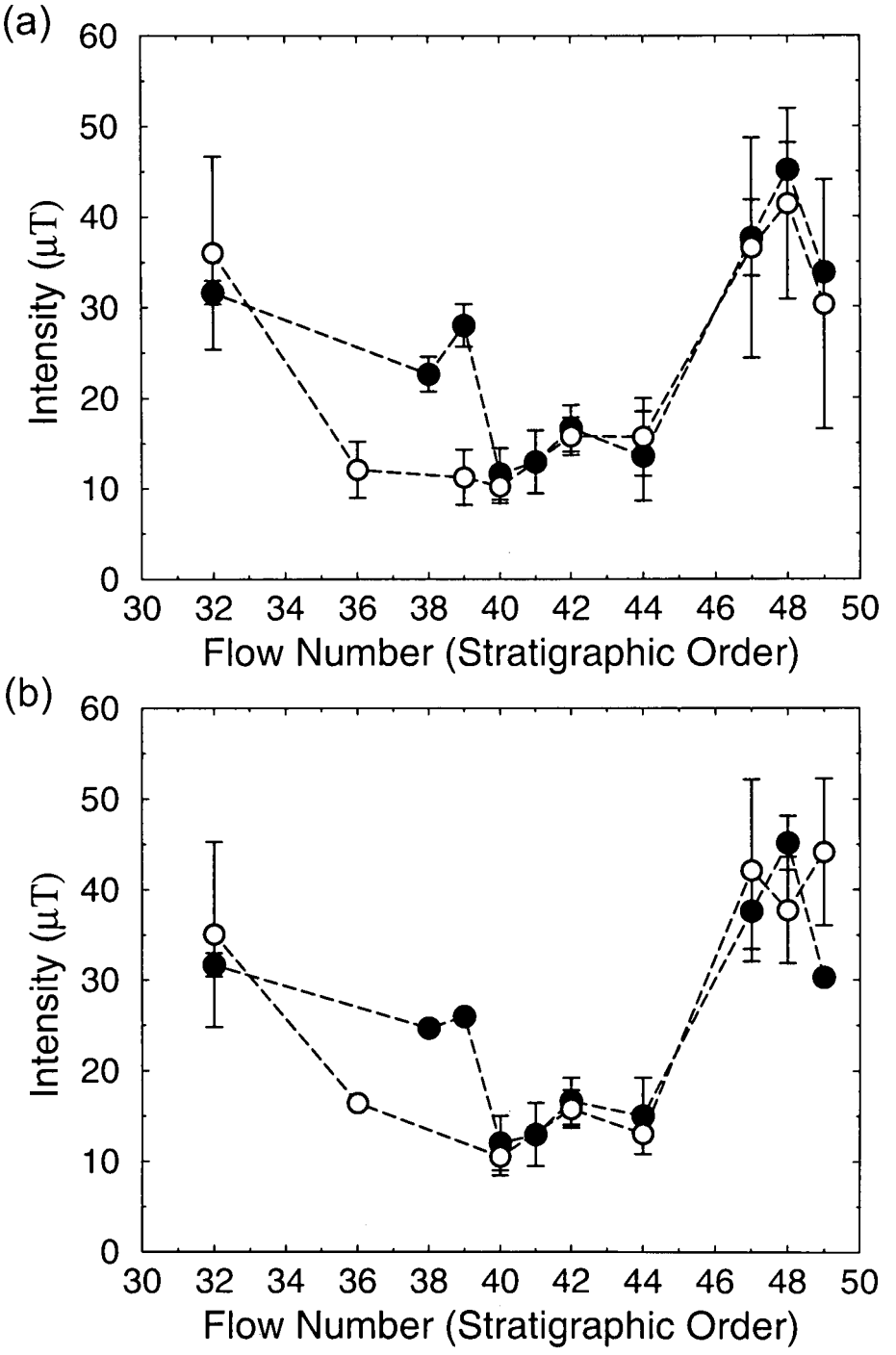


Fig. 11. Comparison of microwave flow mean palaeointensity results from this study (open circles) and thermal Thellier results from Valet et al. (1999) (closed circles). (a) All estimates of palaeointensity. (b) Palaeointensity results that pass the class 1 and class 2 selection criteria. Error bars are $\pm\sigma$.

section and AS/AN sections were erupted at different times and capture different parts of the reversal; the AS/AN sections recording times when the field was at a minimum and the ME section recording times, possibly earlier in the reversal's history, when the palaeointensity was higher. Another possibility is that these palaeointensities are erroneous and this is related to the samples' oxidation state. Yamamoto et al. (2003) determined overestimated palaeointensities from samples from the 1960 Hawaii lava flow. They observed that these samples had undergone intermediate oxidation on initial cooling below their Curie temperature and that they could have acquired a thermochemical remanent magnetisation (TCRM). No microscopy was done in this study so such bold conclusions can not be drawn; however, variations in the composition and the low-temperature properties of samples from the same flows and the same 25 mm cores suggest that some oxidation of these samples has occurred and that it was not homogeneous. Nevertheless, all La Palma sections show a decrease in palaeointensity during the directional changes (Fig. 12) and low palaeointensities have been recorded in flows that record both normal and reversed directions.

The directional record from Guadeloupe shows a reversed-transitional-reversed-normal progression with time (Fig. 10d). The transitional-reversed-normal progression was also recorded by Carlut et al. (2000); however, our directional results differ. For the transitional and reversed flows the two sets of results are comparable (within the 95% cone of confidence); however, for the normal flow there is a discrepancy. The mean direction for this flow from this study is D = 353.8°, I = 24.2° (N=4) compared with the equivalent result of flow GU11 (Carlut et al., 2000) of D = 340.7°; I = 31.4° (N=9). This discrepancy could be caused by not using enough samples to calculate the flow mean in this study.

The paleointensity results from the two flows of Carlut and Quidelleur (2000) determined by the thermal Thellier method are significantly different to the microwave results determined in this study. Both the flows gave higher palaeointensities when determined using the microwave technique. For G02 (FN3) (G10 (Carlut and Quidelleur, 2000)) there is a difference of 12.8 $\mu$T and for G03 (FN4) (GU1) there is a difference of 11.1 $\mu$T. Only one sample from all the Carlut and Quidelleur (2000) flows passes the class 1 and 2 selection criteria, and although the quality of the microwave results is generally low, it has improved upon the results from the original study.

$^{40}K/^{40}Ar$ dating of the flows studied in Carlut et al. (2000) and Carlut and Quidelleur (2000) ranges from 777 $\pm$ 14 Ka ($\pm\sigma$) to 785 $\pm$ 22 ($\pm\sigma$) ka. The VGP calculated from the transitional flow is very similar to that recorded in FN23 from the AS section from La Palma. The errors on the dating, the agreement of VGPs and the reversed-transitional-reversed trend could suggest that the transitional flow records the precursor to the main polarity change at

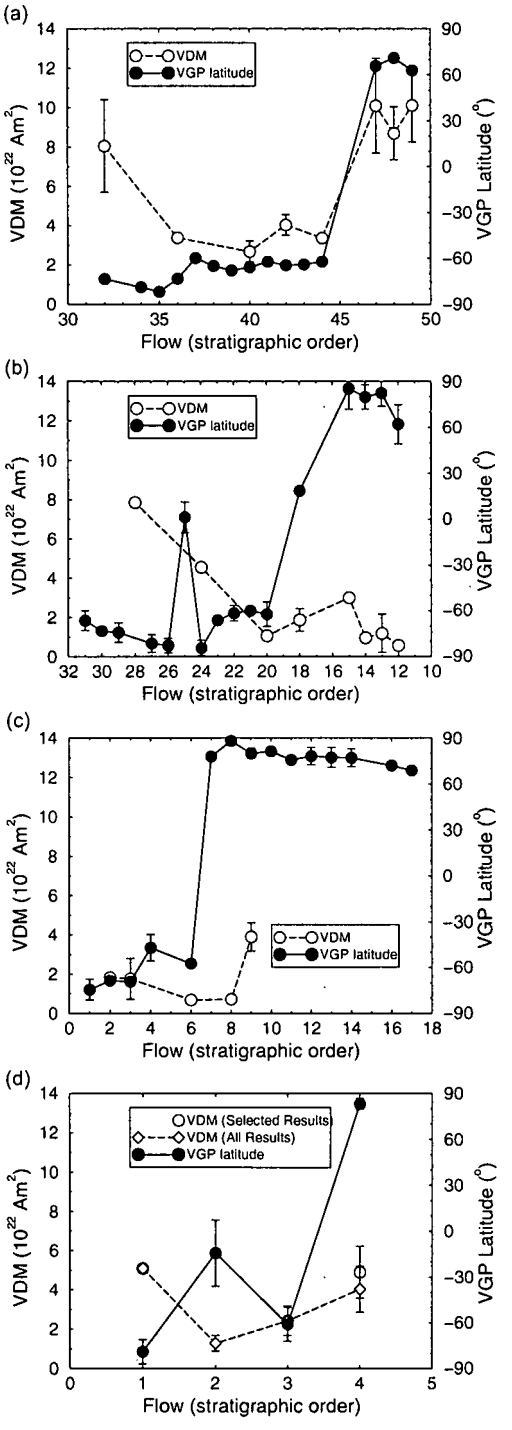


Fig. 12. VGP latitude and VDM plots for (a) ME, (b) AS, (c) AN and (d) Guadeloupe sections. VDM determinations for ME, AS, AN sections are from class 1 and 2 determinations; VDM determinations for the Guadeloupe section show both VDM determinations from all classified data (open diamonds) and class 1 and 2 data (open circles). VDM error bars are $\sigma_v$ and are shown in Table 1. VGP latitude errors are *dm* (Butler, 1992). Where no error bars are present the palaeomagnetic result was determined from less than three samples.

793 ± 3 ka (Singer et al., 2005) or possibly an earlier excursion. Although the quality of the palaeointensity data determined for the transitional-reversed part of the Guadeloupe sequence is poor, the VDM remains low (below 3 x $10^{22}$ $Am^2$) during this time (Fig. 12d). This result is consistent with VDM values determined from the precursor event recorded in the Tatara-San Pedro lavas, Chile (Brown et al., 2004; Gratton et al., 2007). The Tatara-San Pedro section consists of a series of lavas that record very similar directions, with VGPs that cluster over Australia. $^{40}Ar/^{39}Ar$ dates place this VGP cluster at 791.7 ± 3 ka. It has been suggested that during the reversal there is sustained field behaviour related to mantle-controlled magnetic flux patches (Hoffman and Singer, 2004), which leads to clustering of VGPs. Such clusters have also been determined for a number of other reversal records (Mankinen et al., 1985; Hoffman, 1992, 1996; Glen et al., 1994, 2003). Consistent directions could have been recorded by rapidly erupted lavas with no requirement for another physical mechanism; however, debate about the meaning of the geochemical analysis (Dungan et al., 2001), rock magnetic results (Brown et al., 2004; Gratton et al., 2007), and our understanding of long-lived geochemical systems means that both hypotheses remain for this section.

Error in dating the normal flow from Guadeloupe means that it is not clear if this flow records the post-reversal normal field or part of the precursor event. Although VDM is seen to increase (4.9 ± 1.3 ($\pm\sigma$) x $10^{22}Am^2$) (Fig. 12a), this could be associated with the precursor, as seen in sedimentary records (Hartl and Tauxe, 1996) and possibly in the Tatara-San Pedro volcanic sequence (Gratton et al., 2007). The temporal evolution of the Guadeloupe and Tatara San Pedro sections is very difficult to interpret due to the discrete nature of the sampling. The interpretation is further complicated by the possible speed of directional changes. Leonhardt and Fabian (2007) determined from IMMAB4 that local field directions can rotate very quickly (up to 2.2°), a feature that has been generated in dynamo simulations (Coe et al., 2000) and simple mathematical models of reversals (Brown et al., 2007) and has been suggested to explain the palaeomagnetic record of Steens Mountain (Mankinen et al., 1985). This behaviour is thought to be significantly site dependent (Clement, 2004; Wicht, 2005; Brown et al., 2007; Leonhardt and Fabian, 2007)

IMMAB4 does not resolve the precursor in direction before the main polarity change (Fig. 10e and f); however, a broad decrease in intensity is seen between 790 ka and 780 ka before a peak in intensity prior to low field values during the main polarity change (Leonhardt and Fabian (2007) do note the model is less reliable for dates > 782 ka). This intensity variation, but not a polarity change, is (unsurprisingly) seen in the sedimentary and volcanic records of Valet et al. (1989) and Valet et al. (1999). The difference between the records could be caused by non-uniformity in the timing and the size of the global reduction in the field during this time; however, low intensity approximately 16 ka before the main polarity change has been observed globally (Schneider

et al., 1992; Meynadier et al., 1994; Hartl and Tauxe, 1996; Dinarès-Turell et al., 1999).

The precursor event recorded in lavas at 793 ± 3 ka could relate to the initial onset of geodynamo instability (Singer et al., 2005), resulting in a reduction in the relative strength of the large-scale dipole contributions and an emergence of non-dipole contributions at the Earth's surface. Geodynamo instability could result from an emergence of magnetic upwellings (generated within buoyancy driven upwellings in the outer core, but with little or no dramatic change in fluid flow (Wicht and Olson, 2004)), which amplify and transport a generally multipolar magnetic field from the inner boundary to the core-mantle boundary (Aubert et al., 2008).

### *5.2 Comparison with other Matuyama-Brunhes data*

To compare palaeodirection and palaeointensity results from multiple global locations we characterise all results as VGPs and VDMs. We recognise the limitations of this approach. The assumption that the field is a geocentric dipole during the reversal (Merrill and McFadden, 1999) is certainly flawed due to the observation of various VGP paths for the MB reversal. Results from this study and all published MB data are shown in Fig 13a and b. A clear feature is the rather simple relationship between variations in VGP and VDM. There are two broad groups: data that lie between ± 90° to ± 60° VGP latitude and data that lie between -60° to 60° VGP latitude. Within the two high latitude bands VDM varies greatly, with VDMs at high VGP latitude both higher and lower than the present day dipole moment (7.9 x $10^{22}$ $Am^2$ calculated from the CHAOS geomagnetic field model (Olsen et al., 2006)) . Low values relate to times before and after the main polarity transition, where the dipole field is reduced in its strength but major directional changes have not occurred. This supports the idea that major directional changes have a shorter duration than intensity variations related to the reversal (Lin et al., 1994; Merrill and McFadden, 1999). All major directional changes (-60° to 60° VGP latitude) are coincident with VDMs less than 3 x $10^{22}Am^2$ (approximately 35% of the present day globally averaged dipole moment). This suggests that the dipole moment needs to be reduced to at least this value before major directional instability occurs due to the emergence of dominant non-dipolar fields. Our interpretation of the MB is severely limited by the lack of data, especially if only flows with three or more palaeointensity determinations are included (Fig. 13b).

We compare the MB dataset with IMMAB4 transitional field structure dominated by the quadrupole with a reduced dipole contribution (Leonhardt and Fabian, 2007) (Fig. 13c). For all locations except China, the general banding

of VGPs and VDMs is observed. The generation of high VDM at equatorial VGP latitudes is inconsistent with our data. Our analysis is clearly restricted by the characterisation of the data as VGPs and VDMs, which does not allow an assessment of the dominant non-dipolar terms. In addition, the data for a number of locations is considered from areas not included in the original model. In this case the model needs to be refined with additional data.

We have carried the same analysis using the simple reversing axial dipole model of Brown et al. (2007) based on CALS7K.2 (Korte and Constable, 2005). We again see the banding of VGPs and VDMs in the simulated reversal; however, generated VDMs are lower at transitional VGP latitudes. This is because CALS7K.2 underestimates the likely strength of the non-dipole field as the model has very little resolution above spherical harmonic degree four (C. Constable, *pers comm.*).

## 6 Conclusions

The microwave technique has been used to determine a fragmentary record of the evolution of geomagnetic field intensity through the Matuyama-Brunhes geomagnetic field reversal recorded in three sections on La Palma, and one section on Guadeloupe. These sections record the main polarity transition, possible precursors, and fluctuations in the magnetic field prior to the main polarity reversal; however, it has proved difficult to obtain robust palaeointensity determinations. Only ten flows from the twenty-nine flows studied gave reliable mean palaeointensities with three or more determinations per flow. Of these ten flows, only one records a transitional direction. The VDM determined from this flow is $1.9 \pm 0.6$ ($\pm\sigma$) x $10^{22}$ $Am^2$. Analysing both thermal Thellier and microwave palaeointensity results from all Matuyama-Brunhes studies suggests that the main directional changes occurred once the VDM was reduced below 3 x $10^{22}$ $Am^2$. However, the lack of transitional data does not allow us to make any robust statements about the transitional field behaviour. To understand the reversal process and how this links to geodynamo behaviour, more accurate transitional palaeointensity determinations are required. In addition detailed $^{40}K/^{40}Ar$ dating is needed to clearly determine the temporal variation and complexity of reversal features recorded in volcanic sections and, where more than one record exists for a particular reversal, correlate them globally.

Acknowledgements

This work was carried out under NERC grants NER/S/J/2004/13080 and NERC/A/S/2003/00330 and a visiting fellowship to the Institute for Rock Magnetism, University of Minnesota. The microwave instrumentation was

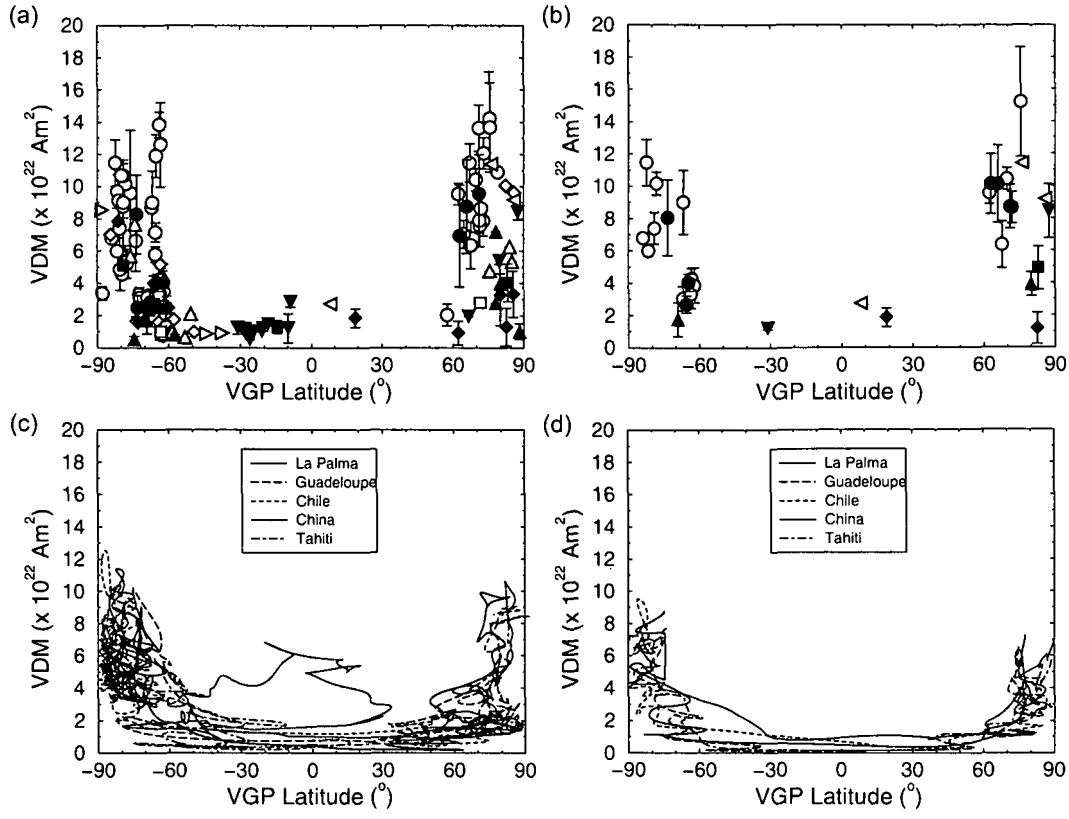


Fig. 13. (a) VDM versus VGP for all Matuyama-Brunhes data (number of determined means=121). All estimates from this study and all other published data. No selection criteria was applied and many flow means were determined from less than three results. (b) VDM versus VGP for selected Matuyama-Brunhes data with three or more determinations per flow (n=31). The class 1 and 2 selection criteria was imposed on data from this study. Previously published data were assessed on the published statistical parameters and where possible the class 1 selection criteria from this study was applied. This includes the removal of any data that used the Valet et al. (1996) palaeointensity correction. (a-b) Solid circles are microwave data and open circles are thermal Thellier data; solid circles: ME section (this study); open circles: ME and ET section (Valet et al., 1999); solid diamonds: AS section (this study); open diamonds: LL section (Quidelleur and Valet, 1996); solid upwards triangles: AN section (this study); open upwards triangles: LS section (Quidelleur and Valet, 1996); solid squares: Guadeloupe section (this study); open squares: Guadeloupe section (Carlut et al., 2000; Carlut and Quidelleur, 2000); solid downward triangles: Tartara San Pedro sections, Chile (Brown et al., 2004; Gratton et al., 2007); left pointing triangles: Tongjing basalts, China (Zhu et al., 1991); right pointing triangles: Punaruu Valley, Tahiti (Chauvin et al., 1990). (c) VDMs and VGPs generated by IMMAB4 (Leonhardt and Fabian, 2007) for locations shown in (a) and (b). (d) VDMs and VGPs generated by a simple reversal model based on CALS7K.2 (Korte and Constable, 2005; Brown et al., 2007) for the location shown in (a) and (b).

funded by NERC grant NE/B50572X/1. The Institute for Rock Magnetism is supported by a grant from the Instruments and Facilities program, Earth Science Division, the National Science Foundation. Roman Leonhardt and Karl Fabian are thanked for their time and for providing us with the code for the IMMAB4 model. Monika Korte is thanked for providing the CALS7K.2 model. Edward Horncastle, Amy Chen, Yuhji Yamamoto, Mimi Hill, Neil Suttie, Mike Jackson and John Share are thanked for scientific discussions and their experimental assistance. We would like to thank the Medio Ambiente of Santa Cruz de La Palma for providing us with sampling permits.

## References

Ancochea, E., Hernán, F., Cendrero, A., Cantagrel, J. M., Fúster, J. M., Ibarrola, E., Coello, J., 1994. Constructive and destructive episodes in the building of a young Oceanic Island, La Palma, Canary Islands and genesis of the Caldera de Taburiente. J. Volcanol. Geotherm. Res. 60, 243–262.

Aubert, J., Aurnou, J., Wicht, J., 2008. The magnetic structure of convection-driven numerical dynamos. Geophys. J. Int., doi: 10.1111/j.1365–246X.2007.03693.x.

Barton, C. E., McFadden, P. L., 1996. Inclination shallowing and preferred transitional vgp paths. Earth Plant. Sci. Lett. 140, 147–157.

Biggin, A. J., Perrin, M., Dekkers, M. J., 2007a. A reliable absolute palaeointensity determination obtained from a non-ideal recorder. Earth Plant. Sci. Lett. 257, 545–563.

Biggin, A. J., Perrin, M., Shaw, J., 2007b. A comparison of a quasi-perpendicular method of palaeointensity determination with other thermal and microwave techniques. Earth Plant. Sci. Lett. 257, 564–581.

Blanc, F., 1983. Corrélations chronologiques et géochemique des formations volcanique du sud de la Basse-Terre, Guadeloupe (Petites Antilles). Début du cycle récent, 3e cycle thesis, Univ. Sci. Medic. Grenoble.

Bleil, U., Petersen, N., 1982. Magnetic properties of natural samples in *Numerical data and functional relationships in science and technology, Group V: Geophysics and space research*, edited by G. Angenheister. Springer, New York.

Brown, L. L., Pickens, J., Singer, B., 1994. Matuyama-Brunhes transition recorded in lava flows of the Chilean Andes: Evidence for dipolar fields during reversals. Geology 22, 299–302.

Brown, L. L., Singer, B. S., Pickens, J. C., Jicha, R., 2004. Paleomagnetic directions and $^{40}Ar/^{39}Ar$ ages from the Tatara-San Pedro volcanic complex, Chilean Andes: Lava record of a Matuyama-Brunhes precursor? J. Geophys. Res. 109, B12101 doi:10.1029/2004JB003007.

Brown, M. C., Chen, A. P., 2008. Using first-order reversal curves to assess palaeointensity variations in samples recording the Matuyama-Brunhes ge-

omagnetic field reversal. *in prep.*

Brown, M. C., Holme, R., Bargary, A., 2007. Exploring the influence of the non-dipole field on magnetic records for reversals and excursions. Geophys. J. Int. 168, 541–550.

Brown, M. C., Shaw, J., Goguitchaichvili, A. T., 2006. Microwave palaeointensity from the R3-N3 geomagnetic field reversal. Geophys. J. Int. 167, 53–69.

Butler, R. F., 1992. Paleomagnetism: Magnetic domains to geologic terrains. Blackwell Science.

Carlut, J., Quidelleur, X., 2000. Absolute paleointensities recorded during the Brunhes chron at La Gaudeloupe Island. Phys. Earth Plant. Inter. 120, 255–269.

Carlut, J., Quidelleur, X., Courtillot, V., Boudon, G., 2000. Paleomagnetic directions and K/Ar dating of 0 to 1 Ma lava flows from La Gaudeloupe Island (French West Indies: Implications for time-averaged field models. J. Geophys. Res. 105, 835–849.

Carmichael, I. S. E., Nicolls, J., 1967. Iron-titanium oxides and oxygen fugacities in volcanic rocks. J. Geophys. Res. 72, 4665–4687.

Carracedo, J. C., Day, S., Guillou, H., Badiola, E. R., Canas, J. A., Torrado, F. J. P., 1998. Hot spot volcanism close to a passive continental margin: the Canary Islands. Geol. Mag. 5, 591–604.

Carracedo, J. C., Day, S. J., Guillou, H., Gravestock, P., 1999. Later stages of volcanic evolution of La Palma, Canary Islands: Rift evolution, giant landslides, and the genesis of the Caldera de Taburiente. Geol. Soc. Am. Bull 111, 755–768.

Celaya, M., Clement, B., 1988. Inclination shallowing in deep sea sediments from the north atlantic. Geophys. Res. Lett. 15, 52–55.

Channell, J. E. T., Curtis, J. H., Flower, B. P., 2004. The Matuyama-Brunhes boundary interval (500-900 ka) in North Atlantic drift sediments. Geophys. J. Int. 158, 489–505.

Channell, J. E. T., Lehman, B., 1997. The last two geomagnetic polarity reversals recorded in high-deposition-rate sediment drifts. Nature 389, 712–715.

Chauvin, A., Roperch, P., Duncan, R. A., 1990. Records of geomagnetic reversals from volcanic islands of French Polynesia 2. paleomagnetic study of a flow sequence (1.2-0.6 ma) from the island of Tahiti and discussion of reversal models. J. Geophys. Res. 95, 2727–2752.

Clement, B. M., 2004. Dependence of the duration of geomagnetic polarity reversals on site latitude. Nature 428, 637–640.

Clement, B. M., Kent, D. V., 1986. Geomagnetic polarity transition records from from five hydraulic piston core sites in the north Atlantic. Init. Rep. Deep Sea Drill. Proj. 94, 831–852.

Clement, B. M., Kent, D. V., 1991. A southern hemisphere record of the Matuyama-Brunhes polarity reversal. Geophys. Res. Lett. 18, 81–84.

Coe, R. S., 1967. Paleo-intensities of the Earth's magnetic field determined from Tertiary and Quaternary rocks. J. Geophys. Res. 72, 3247–3262.

Coe, R. S., Glen, J., 2004. The complexity of reversals. Timescales of the paleomagnetic field, Geophysical Monograph Series 145, 221–232 doi:10.29/145GM16.

Coe, R. S., Grommé, S., Mankinen, E. A., 1978. Geomagnetic paleointensities from radiocarbon-dated lava flows on Hawaii and the question of the Pacific nondiple low. J. Geophys. Res. 83, 1740–1756.

Coe, R. S., Hongre, L., Glatzmaier, G. A., 2000. An examination of simulated geomagnetic reversals from a palaeomagnetic perspective. Phil. Trans. R. Soc. Lond. 358, 1141–1170.

Coe, R. S., Singer, B. S., Pringle, M. S., Zhao, X., 2004a. Matuyama-Brunhes reversal and Kaikatsura event on Maui: palaomagnetic directions, $^{40}Ar/^{39}Ar$ ages and implications. Earth Plant. Sci. Lett. 222, 667–684.

Constable, C., 1990. A simple statistical model for geomagnetic reversals. J. Geophys. Res. 95, 4587–4596.

Cottrell, R. D., Tarduno, J. A., 1999. Geomagnetic paleointensity derived from single plagioclase crystals. Earth Plant. Sci. Lett. 169, 1–5.

Day, R., Fuller, M., Schmidt, V. A., 1977. Hysteresis properties of Titanomagnetites: grain size and compisitional dependence. Phys. Earth Plant. Inter. 13, 260–267.

Dekkers, M. J., Böhnel, H. N., 2006. Reliable absolute palaeointensities independent of magnetic domain state. Earth Plant. Sci. Lett. 248, 508–517.

Dinarès-Turell, J., Sagnotti, L., Roberts, A. P., 1999. Realtive paleointensity from the Jaramillo Subchron to the Matuyama/Brunhes as recorded in a Mediterranean piston core. Earth Plant. Sci. Lett. 194, 327–341.

Dungan, M., Wulff, A., Thompson, R., 2001. Eruptive stratigraphy of the tatara-san pedro complex, 36°, southern volcanic zone, chilean andes: reconstruction method and implications for magma evolution at long-lived arc volcanic centers. J. Petrol. 42, 555–626.

Dunlop, D., 2002. Theory and application of the Day plot(Mrs/Ms versus Hcr/Hc) 2. Application to data for rocks , sediments, soils. J. Geophys. Res. 103, doi:10.1029/2001JB000486.

Fabian, K., 2001. A theoretical treatment of palaeointensity determination experiments on rocks containing pseudo-single or multi domain magnetic particles. Earth Plant. Sci. Lett. 188, 45–58.

Fisher, R. A., 1953. Dispersion on a sphere. Proceedings of the Royal Society of London, Series A 217, 295–305.

Fox, J. M. W., Aitken, M. J., 1980. Cooling-rate dependency of thermoremanent magnetisation. Nature 283, 462–463.

Glen, J. M. G., Coe, R., Liddicoat, J., 1994. Persistent features of polarity transition records from western North America. Geophys. Res. Lett. 21, 1165–1168.

Glen, J. M. G., Valet, J.-P., Soler, V., Renne, P. R., Elmaleh, A., 2003. A Neogene geomagnetic polarity transition record from lavas of the Canary Islands, Spain: episodic volcanism and/or metatable transitional fields? Geophys. J. Int. 154, 426–440.

Gratton, M. N., Goguitchaichvili, A., Conte, G., Shaw, J., Urrutia-Fucugauchi, J., 2005a. Microwave palaeointensity study of the Jorullo volcano, (Central Mexico). Geophys. J. Int. 161, 627–634.

Gratton, M. N., Shaw, J., Brown, L. L., 2007. Absolute palaeointensity variations during a precursor to the Matuyama-Brunhes transition recorded in Chilean lavas. Phys. Earth Plant. Inter. 162, 61–72.

Gratton, M. N., Shaw, J., Herrero-Bervera, E., 2005b. An absolute palaeointensity record from SOH1 lava core, Hawaii using the microwave technique. Phys. Earth Plant. Inter. 148, 193–214.

Gubbins, D., 1999. The distinction between geomagnetic excursions and reversals. Geophys. J. Int. 137, F1–F2.

Guillou, H., Carracedo, J. C., Day, S. J., 1998. Dating of the upper Pleistocene Holocene volcanic activity of La Palma using the unspiked K-Ar technique. J. Volcanol. Geotherm. Res. 86, 137–149.

Guillou, H., Carracedo, J. C., Duncan, R. A., 2001. K-Ar, $^{40}Ar/^{39}Ar$ ages and magnetostratigraphy of Brunhes and Matuyama lava sequences from La Palma Island. J. Volcanol. Geotherm. Res. 106, 175–194.

Halgedahl, S. L., Day, R., Fuller, M., 1980. The effect of cooling rate on the intensity of weak-field TRM in single-domain magnetite. J. Geophys. Res. 85, 3690–3698.

Hartl, P., Tauxe, L., 1996. A precursor to the Matuyama/Brunhes transition-field instability as recorded in pelagic sediments. Earth Plant. Sci. Lett. 138, 121–135.

Hill, M. J., Gratton, M. N., Shaw, J., 2002a. A comparison of thermal and microwave palaeomagnetic techniques using lava containing laboratory induced remanence. Geophys. J. Int. 151, 157–163.

Hill, M. J., Gratton, M. N., Shaw, J., 2002b. Palaeomagnetic investigation of Tertiary lava from Barrington Tops, NSW, Australia, using thermal and microwave techniques. Earth Plant. Sci. Lett. 198, 245–256.

Hill, M. J., Shaw, J., 1999. Palaeointensity results for historic lavas from Mt Etna using microwave demagnetization/remagnetization in a modified Thellier-type experiment. Geophys. J. Int. 139, 583–590.

Hill, M. J., Shaw, J., 2007. The use of the 'Kono perpendicular applied field method' in microwave palaeointensity experiments. Earth Planets Space 59, 711–716.

Hill, M. J., Shaw, J., Herrero-Bervera, E., 2005. Palaeointensity record through the Lower Mammoth reversal from the Waianae volcano, Hawaii. Earth Plant. Sci. Lett. 230, 255–272.

Hoffman, K. A., 1992. Dipolar reversal states of the geomagnetic field and core-mantle dynamics. Nature 359, 789–794.

Hoffman, K. A., 1996. Transitional paleomagnetic field behavior: preferred paths or patches? Surv. Geophys. 17, 207–211.

Hoffman, K. A., Singer, B. S., 2004. Reginonally recurrent paleomagnetic transitional field and mantle processes. Timescales of the paleomagnetic field, Geophysical Monograph Series 145, 233–243 doi:10.29/145GM16.

Johnson, C. L., Wijbrans, J. R., Constable, C. G., Gee, J., Staudigel, H., Tauxe, L., Forjaz, V.-H., Salgueiro, M., 1998. $^{40}ar/^{39}ar$ ages and paleomagnetism of São Miguel lavas, Azores. Earth Plant. Sci. Lett. 160, 637–649.

Kirschvink, J. L., 1980. The least-squares line and the plane and the analysis of palaeomagnetic data. Geophys. J. R. Astron. Soc 62, 699–718.

Komorowski, J.-C., Boudon, G., Semet, M., Beauducel, F., Antenor-Habazac, C., Bazin, S., Hammouya, G., 2005. Guadeloupe. In: Lindsay J M, Robertson R E A, Shepherd J B, Ali S (eds). Volcanic Hazard Atlas of the Lesser Antilles. Seismic Res Unit, Univ West Indies.

Kono, M., Ueno, N., 1977. Paleointensity determination by a modified Thellier method. Phys. Earth Plant. Inter. 13, 305–314.

Korte, M., Constable, C. G., 2005. Continuous geomagnetic field models for the past 7 millenia: 2. CALS7K. Geochem. Geophys. Geosyst. 6, Q02H16, doi:10.1029/2004GC000801.

Langereis, C. G., van Hoof, A. A. M., Rochette, P., 1992. Longitudinal confinement of geomagnetic reversal paths as a possible sedimentary artefact. Nature 358, 226–230.

Lattard, D., Engelmann, R., Kontny, A., Sauerzapf, U., 2006. Curie tempertaures of synthetic titanomagnetites in the Fe-Ti-O system: Effects of composition, crystal chemistry, and thermomagnetic methods. J. Geophys. Res. 111, B12S28, doi:10.1029/2006JB004591.

Leonhardt, R., Fabian, K., 2007. Paleomagnetic reconstruction of the global geomagnetic field evolution during the Matuyama/Brunhes transition: iterative Bayesian inversion and independent verification. Earth Plant. Sci. Lett. 253, 172–195.

Leonhardt, R., Matzka, J., Nichols, A. R. L., Dingwell, D. B., 2006. Cooling rate correction of paleointensity determination for volcanic glasses by relaxation geospeedometry. Earth Plant. Sci. Lett. 243, 282–292.

Lin, J. L., Verosub, K. L., Roberts, A. P., 1994. Decay of the virtual dipole moment during polarity transitions and geomagnetic excursions. Geophys. Res. Lett. 21, 525–528.

Mankinen, E. A., Prévot, M., Grommé, C. S., Coe, R. S., 1985. The Steens Mountain (Oregon) geomagnetic polarity transition 1. Directional history, duration of episodes, and rock magnetism. J. Geophys. Res. 90(B12), 10,393–10,416.

McArdle, N. J., Halls, H. C., Shaw, J., 2004. Rock magnetic and a comparison between microwave and Thellier palaeointensities for Precambrian dykes. Phys. Earth Plant. Inter. 147, 247–254.

Merrill, R. T., McFadden, P. L., 1999. Geomagnetic polarity reversals. Rev. Geophys. 37(2), 201–226.

Meynadier, L., Valet, J.-P., Bassinot, F. C., Shackleton, N. J., Guyodo, N. J., 1994. Asymmetrical saw-tooth pattern of the geomagnetic field intensity from equatorial sediments in the Pacific and Indian Oceans. Earth Plant. Sci. Lett. 126, 109–127.

Mochizuki, N., Tsunakawa, H., Kurata, M., Yamazaki, T., Oda, H., 2005.

Palaeointensity study of the Brunhes-Matuyama polarity reversal recorded in the lava sequence in Punaruu valley, Tahiti Island. 10th Scientific Assembly of the IAGA, IAGA2005–A–01158.

Moskowitz, B. M., 1981. Methods for estimating Curie temperatures of titanomaghemites from experimental Js-T data. Earth Plant. Sci. Lett. 52, 84–88.

Nagata, T., Arai, Y., Momose, K., 1963. Secular varaition of the geomagnetic force during the last 5000 years. J. Geophys. Res. 68, 5277–5281.

Navarro, J. M., Coello, J., 1993. Geological map of the national park of the Caldera de Taburiente. Vol. 1 of 1. Instituto Nacional para la Conservacion de la Naturaleza, La Palma.

Olsen, N., Lühr, H., Sabaka, T. J., Mandea, M., M.Rother, Tøffner-Clausen, L., Choi, S., 2006. CHAOS - a model of the Earth's magnetic field derived from CHAMP, Ørsted, and SAC-C magnetic satellite data. Geophys. J. Int. 166 (1), 65–75.

Olson, P., Amit, H., 2006. Changes in earth's dipole. Naturwissenschaften 93, 519–542.

Özdemir, O., Dunlop, D. J., Moskowitz, B. M., 1993. The effect of oxidation on the Verwey transition in magnetite. Geophys. Res. Lett. 20, 1671–1674.

Perrin, M., Schnepp, E., 2004. Iaga paleointensity database: distribution and quality of the data set. Phys. Earth Plant. Inter. 147, 255–267.

Petronille, M., Goguitchaichvili, A., Henry, B., Alva-Valdivia, L. M., Rosas-Elguera, J., Urrutia-Fucugauchi, J., Cejá, M. R., Calvo-Rathert, M., 2005. Paleomagnetism of Ar-Ar dated lava flows from the Caboruco-San Pedro vocanic field (western Mexico): Evidence for the Matuyama-Brunhes transition precursor and a fully reversed geomagnetic event in the Brunhes chron. J. Geophys. Res. 110, B08101, doi:10.1029/2004JB003321.

Prægel, N. O., Holm, P. M., 2006. Lithospheric contributions to high MgO basanites from the Cumbre Vieja volcano, La Palma, Canary Islands and evidence for temporal variation in plume influence. J. Volcanol. Geotherm. Res. 149, 213–239.

Quidelleur, X., Carlut, J., Gillot, P.-Y., Soler, V., 2002. Evolution of the geomagnetic field prior to the Matuyama-Brunhes transition: radiometric dating of a 820Ka excursion at La Palma. Geophys. J. Int. 151, F6–F10.

Quidelleur, X., Carlut, J., Soler, V., Valet, J.-P., Gillot, P.-Y., 2003. The age and duration of the Matuyama-Brunhes transition from new K-Ar data from La Palma (Canary Islands) and revisted $^{40}Ar/^{39}Ar$. Earth Plant. Sci. Lett. 208, 149–163.

Quidelleur, X., Gillot, P.-Y., Carlut, J., Courtillot, V., 1999. Link between excursions and palaeointensity inferred from abnormal field directions recorded at La Palma around 600ka. Earth Plant. Sci. Lett. 168, 233–242.

Quidelleur, X., Valet, J.-P., 1996. Geomagnetic changes across the last reversal recorded in lava flows from La Palma, Canary Islands. J. Geophys. Res. 101, 13,755–13,773.

Raisbeck, G. M., Yiou, F., Cattani, O., Jouzel, J., 2006. $^{10}$be evidence for the

Matuyama-Brunhes geomagnetic reversal in the EPICA Dome C ice core. Nature 44, 82–84.

Riisager, P., Riisager, J., 2001. Detecting multidomain magnetic grains in Thellier palaeointensity experiments. Phys. Earth Plant. Inter. 125, 111–117.

Roest, W. R., Danobeitia, J. J., Verhoef, J., Collete, B. J., 1992. Magnetic anomalies in the Canary basin and the Mesozoic evolution of the central North Atlantic. Mar. Geophys. Res. 14, 1–24.

Rolph, T. C., Shaw, J., 1985. A new method of paleofield magnitude correction for thermally altered samples and its application to Lower Carboniferous lavas. Geophys. J. R. Astr. Soc. 80, 773–781.

Samper, A., Quidelleur, X., Lahitte, P., Mollex, D., 2007. Timng of effusive volcanism and collapse events within an oceanic arc island: Guadeloupe archipelago ( Lesser Antilles Arc. Earth Plant. Sci. Lett. 258, 175–191.

Schneider, D. A., Kent, D. V., Mello, G. A., 1992. A detailed chronology of the Australian impact event, the Brunhes-Matuyama polarity reversal, and global climate change. Earth Plant. Sci. Lett. 111, 395–405.

Selkin, P. A., Tauxe, L., 2000. Long-term varations in palaeointensity. Philos. Trans. R. Soc. Lond. A, 358, 1065–1088.

Shao, J. C., Fuller, M., Tanimoto, T., Dunn, J. R., Stone, D., 1999. Spherical harmonic analyses of paleomagnetic data: The timeaveraged geomagnetic field for the past 5 myr and the brunhes-matuyama reversal. J. Geophys. Res. 104, 5015–5030.

Shaw, J., 1974. A new method of determining the magnitude of the palaeomagnetic field. Application to to five historic lavas and five archaeological samples. Geophys. J. R. Astr. Soc. 39, 133–141.

Shaw, J., Share, J. A., 2007. A new automated microwave demagnetiser/remagnetiser system for palaeointensity studies. Eos Trans. AGU Fall Meet. Suppl., Abstract, GP53C–1371.

Singer, B. S., Hoffman, K. A., Coe, R. S., L. L. Brown, B. R. J., Pringle, M. S., Chauvin, A., 2005. Structural and temporal requirements for geomagnetic field reversal deduced from lava flows. Nature 434, 633–636.

Singer, B. S., Relle, M. K., Hoffman, K. A., Battle, A., Laj, C., Guillou, H., Carracedo, J. C., 2002. Ar/Ar ages from transitionally magnetized lavas on La Palma, Canary Islands, and the geomagnetic instability timescale. J. Geophys. Res. 107, 2307 doi:10.1029/2001JB001613.

Smirnov, A. V., Tarduno, J. A., 2005. Thermochemical remanent magnetization in Precambrian rocks: Are we sure the geomagnetic field was weak? J. Geophys. Res. 110, B06103, doi:10.1029/2004JB003445.

Staudigel, H., Feraud, G., Giannerini, G., 1986. The history of intrusive activity on the island of La Palma (Canary Islands). J. Volcanol. Geotherm. Res. 27, 299–322.

Tan, X., kodama, K. P., Gilder, S., Courtillot, V., 2007. Rock magnetic evidence for inclination shallowing in the Passaic Formation red beds from the Newark basin and a systematic bias of the Late Triassic apparent polar

wander path for North America. Earth Plant. Sci. Lett. 254, 345–357.
Tanaka, H., Kono, M., 1991. Preliminary results and reliability of paleointensity studies on historical and 14C dated Hawaiian lavas. J. Geomag. Geoelectr. 43, 375–388.
Tarduno, J. A., Smirnov, A. V., 2004. The paradox of low field values and the long-term history of the geodynamo. Timescales of the paleomagnetic field, Geophysical Monograph Series 145, 75–84 doi:10.29/145GM08.
Tauxe, L., Bertram, H. N., Seberino, C., 2002. Physical interpretation of hysteresis loops: Micromagnetic modeling of fine particle magnetite. Geochem. Geophys. Geosyst. 3(10), 1055, doi:10.1029/2001GC000241.
Tauxe, L., Herber, T., Shackleton, N. J., Kok, Y. S., 1996. Astronomical calibration of the Matuyama-Brunhes boundary: Consequences for magnetic remanence acquisition in marine carbonates and the Asian loess sequences. Earth Plant. Sci. Lett. 140, 133–146.
Tauxe, L., Kent, D. V., 2004. A simplified statistical model for the geomagnetic field and the detection of shallow bias in paleomagnetic inclinations: was the ancient magnetic field dipolar? Timescales of the paleomagnetic field, Geophysical Monograph Series 145, 101–115 doi:10.29/145GM08.
Tauxe, L., Staudigel, H., Wijbrans, J. R., 2000. $^{40}Ar/^{39}Ar$ ages from La Palma in the Canary Islands). Geochem. Geophys. Geosyst. 1, 63.
Thellier, E., Thellier, O., 1959. Sur l'intensité du champ magnétique terrestre dans le passé historique et géologique. Ann. Géophys. 15, 285–376.
Valet, J.-P., Brassart, J., LeMeur, I., Soler, V., Quidelleur, X., Tric, E., Gillot, P.-Y., 1996. Absolute paleointensity and magnetomineralogical changes. J. Geophys. Res. 101, 25,029–25,044.
Valet, J.-P., Brassart, J., Quidelleur, X., Soler, V., Gillot, P.-Y., Hongre, L., 1999. Paleointensity variations across the last geomagnetic reversal at La Palma, Canary Islands, Spain. J. Geophys. Res. 104 (B4), 7577–7598.
Valet, J.-P., Kidane, T., Soler, V., Brassart, J., Courtillot, V., Meynadier, L., 1998. Remagnetization in lava flows recording pretransitional directions. J. Geophys. Res. 103, 9755–9775.
Valet, J.-P., Tauxe, L., Clark, D. R., 1988. The Matuyama-Brunhes transition recorded from Lake Tecopa sediments (California). Nature 315, 217–218.
Valet, J.-P., Tauxe, L., Clement, B., 1989. Equatorial and mid-latitude records of the last geomagnetic field reversal from the Atlantic Ocean. Earth Plant. Sci. Lett. 94, 371–384.
van Hoof, A. A. M., Vanos, B. J. H., Rademakers, J. G., Langereis, C. G., Delange, G. J., 1993. A paleomagnetic and geochemical record of the upper Cochiti reversal and two subsequent precessional cycles from southern Sicily (Italy). Earth Plant. Sci. Lett. 117, 235–250.
Walton, D., 2002. Conditions for ferromagnetic resonance in nanoparticles and microwave magnetization. Geophys. Res. Lett. 29, 2165, doi:10.1029/2002GL016049.
Walton, D., 2004a. Avoiding mineral alteration during microwave magnetization. Geophys. Res. Lett. 31, L03606, doi:10.1029/2003GL019011.

Walton, D., 2004b. Resetting the magnetization of assemblies of nanoparticles with microwaves. J. Appl. Phys. 95, 5247–5248, doi: 10.1063/1.1695605.

Walton, D., Böhnel, H., Dunlop, D. J., 2004. 2d order ferromagnetic resonance in nanoparticles. Phys. Stat. Sol. 201, 3257–3262, doi: 10.1002/pssa.200405435.

Watts, A. B., 1994. Crustal structure, gravity anomalies and flexure of lithopshere in the vicinity of the Canary Islands. Geophys. J. Int. 119, 648–666.

Wicht, J., 2005. Palaeomagnetic interpretation of dynamo simulations. Geophys. J. Int. 162, 371–380.

Wicht, J., Olson, P., 2004. A detailed study of the polarity reversal mechnaism in a numerical dynamo model. Geochem. Geophys. Geosyst. 5(3), doi:10.1029/2003GC000602.

Yamamoto, Y., 2006. Possible TCRM acquisition of the Kilauea 1960 lava, Hawaii: failure of the Thellier paleointensity determination inferred from equilibrium temperature of the Fe-Ti oxide. Earth Planets Space 58, 1033–1044.

Yamamoto, Y., Tsunakawa, H., 2005. Geomagnetic field intensity during the last 5Myr: LTD-DHT Shaw palaeointensities from volcanic rocks of the Society Islands, French Polynesia. Geophys. J. Int. 162, 79–114.

Yamamoto, Y., Tsunakawa, H., Shibuya, H., 2003. Palaeointensity study of the Hawaiian 1960 lava: implications for possible causes of erroneously high intensities. Geophys. J. Int. 153, 263–276.

Yamazaki, T., Oda, H., 2001. A Brunhes-Matuyama polarity transition record from anoxic sediments in the South Atlantic (Ocean Drilling Program Hole 1082C). Earth Planets Space 53, 817–827.

Yu, Y., Tauxe, L., Genevey, A., 2004. Toward an optimal geomagnetic field intensity determination technique. Geochem. Geophys. Geosyst. 5(2), Q02H07, doi:10.1029/2003GC000630.

Zhu, R., Liu, C., Wu, H., Zhu, G., 1991. Transitional field behaviour for the Matuyama-Brunhes. Sci. China Ser B 34, 1252–1257.

## A Palaeodirection results

| Sample | Flow Number | I (°) | D (°) | M.A.D (°) | Temp range (°C) | VGP Lat. (°) | VGP Long. (°) |
|---|---|---|---|---|---|---|---|
| ME30-3B | 30 | | | | | | |
| ME31-4B | 31 | | | | | | |
| ME32-4B | 32 | -31.6 | 167.0 | 3.8 | 350-525 | -73.4 | 30.8 |
| ME34-3A | 34 | -33.6 | 184.9 | 1.9 | 350-525 | -78.8 | 317.5 |
| ME35-5B | 35 | -41.4 | 187.3 | 5.1 | 450-525 | -81.8 | 287.1 |
| ME36-2A | 36 | -43.9 | 198.6 | 3.1 | 450-525 | -73.2 | 257.9 |
| ME37-1A | 37 | -1.3 | 168.0 | 3.4 | 350-525 | -59.7 | 6.4 |
| ME38-5A | 38 | -7.4 | 177.3 | 4.0 | 300-525 | -64.9 | 348.4 |
| ME39-5A | 39 | -12.7 | 180.5 | 6.1 | 400-525 | -67.8 | 340.7 |
| ME40-2A | 40 | -9.9 | 174.2 | 2.1 | 400-525 | -65.7 | 356.2 |
| ME41-1B | 41 | -7.9 | 166.3 | 3.8 | 400-525 | -62.1 | 12.4 |
| ME42-2B | 42 | -8.1 | 173.0 | 3.5 | 350-525 | -64.5 | 358.5 |
| ME43-4B | 43 | -9.3 | 169.2 | 5.7 | 450-525 | -63.9 | 7.2 |
| ME44-5B | 44 | -2.5 | 174.7 | 4.8 | 350-525 | -62.1 | 353.4 |
| ME45-1B | 45 | | | | | | |
| ME46-1A | 46 | | | | | | |
| ME47-4B | 47 | 25.1 | 20.0 | 2.5 | 350-525 | 65.8 | 107.7 |
| ME48-2A | 48 | 31.2 | 16.1 | 2.7 | 350-525 | 71.1 | 107.2 |
| ME49-2A | 49 | 32.0 | 26.8 | 2.9 | 400-525 | 62.9 | 90.9 |

Table A.1. Palaeodirection results for the MB reversal from the ME section, La Palma. Flow Number labels individual lava flows and is the number shown in any figure relating to palaeodirection or palaeointensity results. I is inclination; D is declination; M.A.D is maximum angular deviation (Kirschvink, 1980); Temp range is the temperature interval taken for the directional analysis of the primary component of magnetisation; End T is the final temperature step used for the analysis; Accept is whether the individual sample was included in the flow analysis; Flow I is the mean inclination; Flow D is the mean declination; $\alpha_{95}$ is the angular standard deviation (Fisher, 1953; Butler, 1992); $\kappa$ is the precision parameter (Butler, 1992); VGP Lat. is the virtual geomagnetic pole latitude and VGP Long. is the virtual geomagnetic pole longitude (Butler, 1992).

| | | | | | | | | | | | | | |
|---|---|---|---|---|---|---|---|---|---|---|---|---|---|
| AS27-1 | 31 | -19.8 | 157.8 | 4.2 | 200-525 | Y | | | | | | | |
| AS27-2 | | -21.7 | 156.2 | 9.8 | 150-525 | Y | | | | | | | |
| AS27-3 | | -33.6 | 157.8 | 4.4 | 450-525 | Y | | | | | | | |
| AS27-4 | | -34.5 | 163.3 | 3.6 | 200-525 | Y | | | | | | | |
| AS27-5 | | -29.4 | 161.9 | 8.4 | 150-525 | Y | -27.8 | 159.3 | 6.9 | 124.8 | -66.3 | 40.4 | 6.5 | 7.5 |
| AS26-1 | 30 | -32 | 193.5 | 4.1 | 400-525 | Y | -32 | 193.5 | | | -73.1 | 292.1 | | |
| AS25-1 | 29 | -4.7 | 205.3 | 5.4 | 250-525 | N | | | | | | | | |
| AS25-3 | | -33.3 | 161.6 | 4.5 | 0-525 | N | | | | | | | | |
| AS25-4 | | -28.9 | 198.3 | 2.0 | 150-525 | Y | | | | | | | | |
| AS25-5 | | -29.4 | 167.8 | 1.6 | 250-525 | N | | | | | | | | |
| AS25-6 | | -31.7 | 196.5 | 7.0 | 150-525 | Y | -30.3 | 197.4 | 7.0 | 1280.5 | -74.1 | 286.5 | 6.4 | 7.8 |
| AS24c-1 | 28 | -14 | 224.6 | 1.7 | 100-525 | N | | | | | | | | |
| AS24c-2 | | -44.6 | 170.8 | 7.4 | 350-525 | N | | | | | | | | |
| AS24c-3 | | -45.9 | 114 | 1.3 | 400-525 | N | | | | | | | | |
| AS24b-1 | 27 | -39.9 | 173.4 | 3.9 | 250-525 | Y | | | | | | | | |
| AS24b-2 | | -33.2 | 188.3 | 3.7 | 150-525 | Y | | | | | | | | |
| AS24b-3 | | -35.8 | 178.9 | 2.9 | 400-525 | Y | | | | | | | | |
| AS24b-4 | | -35.5 | 182.6 | 3.0 | 350-525 | Y | -36.2 | 181 | 6.5 | 197.9 | -81.3 | 336.3 | 5.8 | 7.6 |
| AS24-1 | 26 | | | | | | | | | | | | | |
| AS24-3 | | -38.9 | 179 | 5.5 | 350-525 | Y | | | | | | | | |
| AS24-4 | | -37.1 | 173.6 | 0.3 | 400-525 | Y | | | | | | | | |
| AS24-5 | | -39.5 | 170.1 | 17.3 | 350-525 | Y | | | | | | | | |
| AS24-6 | | -44.9 | 178.7 | 1.2 | 400-525 | Y | -40.2 | 175.3 | 5.3 | 298.8 | -82.7 | 19 | 4.8 | 6.4 |
| AS23-1 | 25 | -49.5 | 304.5 | 2.7 | 250-525 | Y | | | | | | | | |
| AS23-3 | | -59.6 | 292.7 | 5.4 | 400-525 | Y | | | | | | | | |
| AS23-4 | | -53.5 | 296.8 | 7.0 | 150-525 | Y | | | | | | | | |
| AS23-5 | | -67.2 | 294.3 | 3.1 | 250-525 | Y | -57.3 | 297.7 | 9.4 | 96.7 | 1.3 | 206.4 | 10.0 | 13.7 |
| AS22b-1 | 24 | -44.6 | 188.4 | 4.1 | 400-525 | Y | | | | | | | | |
| AS22b-2 | | -48.7 | 188.4 | 2.9 | 250-525 | Y | | | | | | | | |
| AS22b-3 | | -46.5 | 188.3 | 4.2 | 100-525 | Y | | | | | | | | |
| AS22b-4 | | -35.8 | 178.9 | 2.9 | 400-525 | Y | | | | | | | | |
| AS22b-5 | | -41.9 | 182.3 | 8.5 | 150-525 | Y | -43.6 | 185 | 5.6 | 185.3 | -84.4 | 288.1 | 5.1 | 7.0 |
| AS21-1 | 23 | -28.7 | 159.8 | 8.2 | 350-525 | Y | | | | | | | | |
| AS21-2 | | -29.5 | 158.3 | 9.5 | 250-525 | Y | | | | | | | | |
| AS21-3 | | -28 | 159.3 | 2.9 | 250-525 | Y | -28.7 | 158.8 | 1.3 | 8692.2 | -66.2 | 42.2 | 1.2 | 1.4 |
| AS21-4 | | | | | | | | | | | | | | |
| AS21-5 | | | | | | | | | | | | | | |
| AS20-1 | 22 | | | | | | | | | | | | | |
| AS20-2 | | -13.1 | 161 | 2.5 | 450-525 | Y | | | | | | | | |
| AS20-3 | | -17.3 | 157.3 | 4.3 | 300-525 | Y | | | | | | | | |
| AS20-4 | | -15.5 | 161 | 4.0 | 400-525 | Y | -15.3 | 159.8 | 4.5 | 758 | -61.6 | 28.4 | 5.2 | 4.6 |

| | | | | | | | | | | | | | | |
|---|---|---|---|---|---|---|---|---|---|---|---|---|---|---|
| AS19b-1 | 21 | | | | | | | | | | | | | |
| AS19b-2 | | -21.2 | 153.9 | 4.3 | 400-525 | Y | -21.2 | 153.9 | | | -59.9 | 41.3 | | |
| AS19b-4 | | | | | | | | | | | | | | |
| AS19-1 | 20 | -22.7 | 166.2 | 5.1 | 350-500 | Y | | | | | | | | |
| AS19-3 | | -18.3 | 150.4 | 7.8 | 400-525 | Y | | | | | | | | |
| AS19-4 | | -16.2 | 157.3 | 6.7 | 400-525 | Y | | | | | | | | |
| AS19-5 | | -19.2 | 159.2 | 8.1 | 450-525 | Y | -19.2 | 158.2 | 7.6 | 147.2 | -62.2 | 33.8 | 8.0 | 7.9 |
| AS18-1 | 19 | | | | | | | | | | | | | |
| AS18-2 | | | | | | | | | | | | | | |
| AS18-3 | | | | | | | | | | | | | | |
| AS18-4 | | | | | | | | | | | | | | |
| AS17-1 | 18 | 52.7 | 274.5 | 2.5 | 300-500 | Y | 52.7 | 274.5 | | | 18.7 | 280.6 | | |
| AS16b-1 | 17 | | | | | | | | | | | | | |
| AS16-1 | 16 | | | | | | | | | | | | | |
| AS16-2 | | | | | | | | | | | | | | |
| AS16-3 | | | | | | | | | | | | | | |
| AS16-4 | | | | | | | | | | | | | | |
| AS16-5 | | | | | | | | | | | | | | |
| AS15-1 | 15 | 42 | 17 | 7.4 | 350-500 | Y | | | | | | | | |
| AS15-2 | | 46.9 | 351.1 | 2.6 | 350-550 | Y | | | | | | | | |
| AS15-3 | | 43 | 3.4 | 5.3 | 350-550 | Y | 44.5 | 4.2 | 14.8 | 70.7 | 85.4 | 107.1 | 13.5 | 18.6 |
| AS14-1 | 14 | 32.7 | 358.7 | 6.6 | 350-550 | Y | | | | | | | | |
| AS14-2 | | 32.6 | 41.7 | 5.9 | 350-550 | N | | | | | | | | |
| AS14-3 | | 35.6 | 2.1 | 2.1 | 350-550 | Y | 34.2 | 0.4 | 8.8 | 804.6 | 79.9 | 160.2 | 7.9 | 10.1 |
| AS13-1 | 13 | 48.7 | 344.1 | 1.3 | 400-550 | Y | | | | | | | | |
| AS13-2 | | 52.3 | 351.8 | 2.3 | 400-550 | Y | | | | | | | | |
| AS13-3 | | 43.6 | 18.3 | 5.3 | 350-500 | N | | | | | | | | |
| AS13-4 | | 35 | 350 | 15.7 | 350-550 | N | | | | | | | | |
| AS13-5 | | 52.6 | 52.6 | 2.4 | 350-550 | Y | 51.4 | 352.5 | 8.9 | 193.4 | 82.5 | 280 | 8.7 | 12.1 |
| AS12-1 | 12 | 12.3 | 6.9 | 3.0 | 350-550 | Y | | | | | | | | |
| AS12-2 | | 8.2 | 20.2 | 4.3 | 350-550 | Y | | | | | | | | |
| AS12-3 | | 13.2 | 10.4 | 11.1 | 400-550 | Y | | | | | | | | |
| AS12-4 | | 5 | 22.6 | 11.2 | 400-550 | Y | 9.7 | 15.1 | 9.5 | 93.9 | 62.2 | 128.5 | 12.7 | 9.6 |

Table A.2. Palaeodirection results from the AS section, La Palma. Flow Number 31 is the lowest strigraphic unit. Where no result is shown it was not possible to determine a primary component of magnetisation. Flow I is the mean inclination; Flow D is the mean declination; $\alpha_{95}$ is the angular standard deviation (Fisher, 1953; Butler, 1992); $\kappa$ is the precision parameter (Butler, 1992); VGP Lat. is the virtual geomagnetic pole latitude and VGP Long. is the virtual geomagnetic pole longitude (Butler, 1992); *dm* is the confidence limit for VGP latitude and*dp* is the confidence limit for VGP longitude (Butler, 1992). See Table A.1 for explanation of other column headings

| Sample | Flow Number | I (°) | D (°) | M.A.D (°) | Temp range (°C) | Accept | Flow I (°) | Flow D (°) | $\alpha_{95}$ (°) | $\kappa$ | VGP Lat. (°) | VGP Long. (°) | $dm$ (°) | $dp$ (°) |
|---|---|---|---|---|---|---|---|---|---|---|---|---|---|---|
| AN1-1 | 1 | | | | | | | | | | | | | |
| AN1-2 | | -30.3 | 162.4 | 3.6 | 100-525 | Y | | | | | | | | |
| AN1-3 | | -31 | 169.1 | 2.6 | 100-525 | Y | | | | | | | | |
| AN1-4 | | -37.9 | 172.5 | 3.2 | 100-525 | Y | | | | | | | | |
| AN1-5 | | -41 | 162.0 | 2.4 | 250-525 | Y | -35.1 | 167 | 7.6 | 146 | -74.5 | 37.8 | 6.8 | 8.8 |
| AN2-1 | 2 | -23.3 | 191.9 | 0.7 | 450-525 | Y | | | | | | | | |
| AN2-2 | | -17.4 | 192.2 | 2.9 | 400-525 | Y | -20.3 | 192 | | | -68.5 | 308.2 | | |
| AN3-1 | 3 | -20.8 | 186.0 | 2.8 | 350-525 | Y | | | | | | | | |
| AN3-3 | | -14.2 | 187.4 | 2.4 | 350-525 | Y | -17.5 | 187 | | | -69.2 | 322.3 | | |
| AN4-1 | 4 | | | | | | | | | | | | | |
| AN4-2 | | | | | | | | | | | | | | |
| AN4-3 | | 18.4 | 202.3 | 3.7 | 450-550 | Y | | | | | | | | |
| AN4-4 | | 14.3 | 207.1 | 3.5 | 450-550 | Y | | | | | | | | |
| AN4-5 | | 10 | 203.5 | 2 | 450-550 | Y | 14.2 | 204 | 7.4 | 280 | -47 | 305.4 | 8.7 | 7.6 |
| AN6-1 | 6 | | | | | | | | | | | | | |
| AN6-2 | | | | | | | | | | | | | | |
| AN6-3 | | | | | | | | | | | | | | |
| AN6-4 | | | | | | | | | | | | | | |
| AN6-5 | | -74.6 | 174.1 | 3.6 | 350-500 | Y | -74.6 | 174 | | | -57.4 | 156.9 | | |
| AN7-1 | 7 | 31.2 | 9.0 | 2.4 | 400-525 | Y | | | | | | | | |
| AN7-2 | | 33.2 | 3.4 | 3.1 | 400-525 | Y | | | | | | | | |
| AN7-3 | | 34.3 | 4.8 | 2.5 | 400-525 | Y | | | | | | | | |
| AN7-4 | | 34.3 | 7.5 | 3.2 | 0-525 | Y | 33.3 | 6 | 2.9 | 984 | 77.9 | 132.8 | 2.6 | 3.3 |
| AN8-1 | 8 | 46 | 2.3 | 2.7 | 0-525 | Y | | | | | | | | |
| AN8-2 | | 50.5 | 1.8 | 3.4 | 0-525 | Y | | | | | | | | |
| AN8-3 | | -17.7 | 187.4 | 4.9 | 0-525 | N | 49.7 | 3 | | | 86.6 | 42.1 | | |
| AN9a-1 | 9 | 57.4 | 2.6 | 5 | 150-525 | Y | | | | | | | | |
| AN9a-2 | | 59.9 | 3.2 | 2.9 | 350-525 | Y | | | | | | | | |
| AN9a-3 | | 58.3 | 356.1 | 5 | 150-525 | Y | | | | | | | | |
| AN9a-4 | | 56.1 | 5.8 | 0.6 | 450-525 | Y | 58 | 2 | 3.1 | 891 | 80 | 351.2 | 3.3 | 4.6 |
| AN9b-1 | 10 | 54.9 | 2.2 | 3.1 | 100-525 | Y | | | | | | | | |
| AN9b-2 | | 59.2 | 359.6 | 4.1 | 100-525 | Y | | | | | | | | |
| AN9b-3 | | 56.2 | 355.9 | 6 | 100-525 | Y | | | | | | | | |
| AN9b-4 | | 51.8 | 314.5 | 4.4 | 400-525 | N | 56.8 | 359 | 4.3 | 825 | 81.4 | 338.3 | 4.5 | 6.2 |

| Sample | Flow Number | I (°) | D (°) | M.A.D (°) | Temp range(°C) | Accept | Flow I (°) | Flow D (°) | $\alpha_{95}$ (°) | $\kappa$ | VGP Lat. (°) | VGP Long. (°) | $dm$ (°) | $dp$ (°) |
|---|---|---|---|---|---|---|---|---|---|---|---|---|---|---|
| AN10-1 | 11 | | | | | | | | | | | | | |
| AN10-2 | | 30.9 | 5.6 | 3.9 | 100-550 | Y | | | | | | | | |
| AN10-3 | | 27.3 | 6.1 | 6.8 | 200-550 | Y | 29.1 | 6 | | | 75.7 | 138.8 | 7.3 | 8.7 |
| AN11-1 | 12 | 31.6 | 1.7 | 3 | 0-525 | Y | | | | | | | | |
| AN11-2 | | 29.6 | 2.3 | 3.4 | 100-525 | Y | | | | | | | | |
| AN11-3 | | 31.1 | 6.1 | 3 | 100-525 | Y | | | | | | | | |
| AN11-4 | | 39.2 | 10.6 | 1.6 | 200-400 | Y | 32.9 | 5 | 6.2 | 219 | 78.2 | 138.1 | 5.6 | 7.0 |
| AN12-1 | 13 | 29.3 | 354.7 | 2.1 | 350-550 | Y | | | | | | | | |
| AN12-2 | | 27.5 | 355.6 | 1.3 | 450-550 | Y | | | | | | | | |
| AN12-3 | | 36.4 | 356.3 | 2.4 | 450-550 | Y | 31.1 | 356 | 7.2 | 291 | 77.3 | 182.1 | 6.6 | 8.1 |
| AN12-4 | | | | | | | | | | | | | | |
| AN13-1 | 14 | 27.2 | 6.4 | 5 | 350-550 | Y | | | | | | | | |
| AN13-2 | | 29.7 | 9.4 | 4.1 | 150-550 | Y | | | | | | | | |
| AN13-3 | | 39.7 | 5.8 | 3.5 | 250-550 | Y | | | | | | | | |
| AN13-4 | | 34.1 | 6.7 | 3.2 | 350-550 | Y | 32.7 | 7 | 6.4 | 206 | 77.1 | 130.1 | | |
| AN14-1 | 15 | 23.5 | 4.2 | 2.2 | 350-550 | Y | | | | | | | | |
| AN14-2 | | 43.8 | 342.7 | 3.7 | 300-550 | Y | 34.1 | 355 | | | 78.8 | 188.8 | | |
| AN15-1 | 16 | 27.4 | 9.3 | 1.3 | 350-550 | Y | | | | | | | | |
| AN15-2 | | 18.9 | 5.3 | 1.5 | 300-550 | Y | 23.2 | 7 | | | 72 | 138.0 | | |
| AN16-2 | 17 | | | | | | | | | | | | | |
| AN16-3 | | 17 | 7.3 | 0.3 | 500-550 | Y | 17 | 7 | | | 68.8 | 142.2 | | |

Table A.3. Palaeodirection results for the MB reversal from the AN section, La Palma. Where no result is shown it was not possible to determine a primary component of magnetisation. See Table A.2 for explanation of column headings.

| Sample | Flow Number | I (°) | D (°) | M.A.D (°) | Temp range (°C) | Accept | Flow I (°) | Flow D (°) | $\alpha_{95}$ (°) | $\kappa$ | VGP Lat. (°) | VGP Long. (°) | $dm$ (°) | $dp$ (°) |
|---|---|---|---|---|---|---|---|---|---|---|---|---|---|---|
| GD0100 | 1 | -27.6 | 144.2 | 2.7 | 0-350 | Y | | | | | | | | |
| GD0101 | | -26.9 | 161.3 | 4.3 | 100-350 | Y | | | | | | | | |
| GD0102 | | -33.4 | 181.3 | 5.2 | 100-350 | Y | | | | | | | | |
| GD0103 | | -31.8 | 168.8 | 5.1 | 100-350 | Y | | | | | | | | |
| GD0104 | | -29.1 | 170.4 | 5.7 | 150-350 | Y | | | | | | | | |
| GD0105 | | -28.4 | 177.4 | 4.1 | 150-350 | Y | | | | | | | | |
| GD0106 | | -38.5 | 178.2 | 2.9 | 0-350 | Y | -31.4 | 168.6 | 8.8 | 47.8 | -79 | 35.1 | 8.0 | 9.9 |
| G01A01 | 2 | 10.1 | 233.5 | 3.5 | 300-540 | Y | | | | | | | | |
| G01A04 | | 19.7 | 266.5 | 5.2 | 250-520 | Y | | | | | | | | |
| G01A06 | | 12.9 | 90.8 | 2.6 | 300-520 | N | | | | | | | | |
| G01B02 | | -15.8 | 222.5 | 6.5 | 200-520 | N | | | | | | | | |
| G01C02 | | 9.2 | 257.7 | 3.8 | 300-450 | Y | | | | | | | | |
| G01C07 | | 6.3 | 255.4 | 4.8 | 200-520 | Y | 11.6 | 253.2 | 17.1 | 29.9 | -14.4 | 218.8 | 21.6 | 17.4 |
| G02A01 | 3 | -47.7 | 174.8 | 16.7 | 400-540 | N | | | | | | | | |
| G02A03 | | -67.4 | 188 | 4.9 | 300-520 | Y | | | | | | | | |
| G02A04 | | -53.5 | 193.2 | 8.3 | 250-520 | Y | | | | | | | | |
| G02A06 | | -76.9 | 249.2 | 8.2 | 250-520 | Y | | | | | | | | |
| G02A07 | | -55.4 | 186.4 | 3.6 | 250-520 | Y | | | | | | | | |
| G02A08 | | -50.8 | 175.8 | 2.7 | 200-520 | Y | | | | | | | | |
| G02B04 | | -66.2 | 200.4 | 7.1 | 250-520 | Y | | | | | | | | |
| G02B05 | | -56.4 | 193.4 | 4.8 | 250-520 | Y | -61.9 | 192.3 | 9.5 | 40.9 | -61 | 136.9 | 11.1 | 14.7 |
| G03A01 | 4 | -8.9 | 0.2 | 2.4 | 200-520 | N | | | | | | | | |
| G03A03 | | 22.3 | 351.3 | 4 | 100-540 | Y | | | | | | | | |
| G03A05 | | 23.2 | 356.6 | 3.1 | 200-520 | Y | | | | | | | | |
| G03A07 | | 24 | 351.4 | 2.2 | 200-520 | Y | | | | | | | | |
| G03A08 | | 27.1 | 356.1 | 2.5 | 200-520 | Y | 24.2 | 353.8 | 3.8 | 579.5 | 83.1 | 179.1 | 3.7 | 4.1 |

Table A.4. Palaeodirection results for the MB reversal from Guadeloupe, French West Indies. See Table A.2 for explanation of column headings.

# B Palaeointensity results

| Sample | Flow Number | Demag | Protocol | $F_{lab}$ | $n/N$ | $f$ | $g$ | $\beta$ | $q$ | $r^2$ | $pT_MRM$ Check | Tail Check | $F$ ($\mu T$) | uncert ($\mu T$) | Class |
|---|---|---|---|---|---|---|---|---|---|---|---|---|---|---|---|
| ME32-1B1 | 32 | Y | Perp | 40 | 7/7 | 0.47 | 0.64 | 0.06 | 5.18 | 0.983 | 1/1 | 1/1 | 37.5 | 7.2 | 2 |
| ME32-2B1 | | Y | Perp | 20 | 7/9 | 0.54 | 0.74 | 0.08 | 5.16 | 0.971 | 2/3 | 2/3 | 43.9 | 8.5 | 3 |
| ME32-4B1 | | Y | Perp | 10 | 6/6 | 0.60 | 0.49 | 0.03 | 10.22 | 0.997 | 2/2 | 0/2 | 47.7 | 4.7 | 2 |
| ME32-4B2 | | Y | Perp | 20 | 0/7 | | | | | | | | | | |
| ME32-4B3 | | Y | Perp | 20 | 0/8 | | | | | | | | | | |
| ME32-4B4 | | Y | Perp | 40 | 5/5 | 0.25 | 0.52 | 0.04 | 3.01 | 0.994 | 1/1 | 1/1 | 46.3 | 15.4 | 3 |
| ME32-5B1 | | Y | Perp | 40 | 6/6 | 0.58 | 0.33 | 0.01 | 19.72 | 1.000 | 2/2 | 2/2 | 23.3 | 1.2 | 1 |
| ME32-5B2 | | Y | Perp | 40 | 7/9 | 0.73 | 0.62 | 0.03 | 14.00 | 0.995 | 1/3 | 2/3 | 31.7 | 2.3 | 2 |
| ME32-5B3 | | Y | Perp | 40 | 4/4 | 0.35 | 0.29 | 0.04 | 2.46 | 0.997 | 0/0 | 0/0 | 22.0 | 8.9 | 3 |
| ME33-2A1 | 33 | Y | Perp | 10 | 0/5 | | | | | | | | | | |
| ME33-5B1 | | Y | Perp | 20 | 0/5 | | | | | | | | | | |
| ME34-4B1 | 34 | N | | | | | | | | | | | | | |
| ME35-5B1 | 35 | N | | | | | | | | | | | | | |
| ME36-1B1 | 36 | Y | Perp | 10 | 4/7 | 0.44 | 0.59 | 0.03 | 8.43 | 0.998 | 0/1 | 0/1 | 16.4 | 1.9 | 2 |
| ME36-2B1 | | N | Coe | | | | | | | | | | | | |
| ME36-3B1 | | Y | Perp | 10 | 8/11 | 0.28 | 0.81 | 0.07 | 3.25 | 0.970 | 2/3 | 3/3 | 9.5 | 2.7 | 3 |
| ME36-4B1 | | Y | Perp | 40 | 8/11 | 0.13 | 0.78 | 0.07 | 1.32 | 0.967 | 4/4 | 4/4 | 10.4 | 7.9 | 3 |
| ME36-5B1 | | N | Coe | | | | | | | | | | | | |
| ME37-1B1 | 37 | N | | | | | | | | | | | | | |
| ME38-1B1 | 38 | Y | Perp | 40 | 0/10 | | | | | | | | | | |
| ME39-4A1 | 39 | Y | Perp | 15 | 3/5 | 0.04 | 0.40 | 0.11 | 0.17 | 0.989 | 0/1 | 1/1 | 10.6 | 63.2 | 3 |
| ME39-6C1 | | Y | Perp | 40 | 6/7 | 0.73 | 0.45 | 0.03 | 11.76 | 0.997 | 2/2 | 2/2 | 15.8 | 1.3 | 3 |
| ME39-6C2 | | N | Coe | | | | | | | | | | | | |
| ME39-6C3 | | Y | Perp | 40 | 5/5 | 0.43 | 0.01 | 0.07 | 0.08 | 0.987 | 1/1 | 1/1 | 9.7 | 123.0 | 3 |
| ME39-6C4 | | Y | Perp | 10 | 4/4 | 0.15 | 0.57 | 0.03 | 2.78 | 0.998 | 0/0 | 0/0 | 9.0 | 3.2 | 3 |
| ME40-1A1 | 40 | Y | Perp | 10 | 9/9 | 0.59 | 0.72 | 0.03 | 14.09 | 0.993 | 2/3 | 3/3 | 13.0 | 0.9 | 2 |
| ME40-2B1 | | Y | Perp | 10 | 12/12 | 0.59 | 0.80 | 0.06 | 7.94 | 0.964 | 4/5 | 5/5 | 8.5 | 1.1 | 3 |
| ME40-3A1 | | Y | Perp | 10 | 11/11 | 0.68 | 0.86 | 0.02 | 31.27 | 0.997 | 5/5 | 4/5 | 8.2 | 0.3 | 2 |
| ME40-3A2 | | Y | Perp | 10 | 8/11 | 0.29 | 0.77 | 0.07 | 3.12 | 0.969 | 3/4 | 3/4 | 10.9 | 3.5 | 3 |
| ME40-4A1 | | Y | Perp | 40 | 0/11 | | | | | | | | | | |
| ME40-4A2 | | N | Coe | | | | | | | | | | | | |
| ME40-4A3 | | Y | Perp | 10 | 11/11 | 0.70 | 0.82 | 0.03 | 18.98 | 0.991 | 4/4 | 4/4 | 9.7 | 0.5 | 1 |
| ME40-5A1 | | N | Coe | | | | | | | | | | | | |
| ME40-5B1 | | Y | Perp | 15 | 9/10 | 0.50 | 0.68 | 0.03 | 13.43 | 0.996 | 3/4 | 3/4 | 11.3 | 0.8 | 2 |
| ME41-4A1 | 41 | Y | Perp | 10 | 0/4 | | | | | | | | | | |

| Sample | Flow Number | Demag | Protocol | $F_{lab}$ | $n/N$ | $f$ | $g$ | $\beta$ | $q$ | $r^2$ | $pT_MRM$ Check | Tail Check | $F$ ($\mu T$) | uncert ($\mu T$) | Class |
|---|---|---|---|---|---|---|---|---|---|---|---|---|---|---|---|
| ME42-2A1 | 42 | Y | Perp | 10 | 5/5 | 0.66 | 0.65 | 0.01 | 32.43 | 0.999 | 1/2 | 2/2 | 13.5 | 0.4 | 2 |
| ME42-3A1 | | Y | Perp | 10 | 7/7 | 0.84 | 0.77 | 0.04 | 17.02 | 0.993 | 0/2 | 2/2 | 14.6 | 0.9 | 2 |
| ME42-3A2 | | Y | Perp | 10 | 5/5 | 0.76 | 0.74 | 0.02 | 24.15 | 0.998 | 0/2 | 2/2 | 17.1 | 0.7 | 2 |
| ME42-5B1 | | Y | Perp | 40 | 0/11 | | | | | | | | | | |
| ME42-5B2 | | N | Coe | | | | | | | | | | | | |
| ME42-5B3 | | Y | Perp | 40 | 7/7 | 0.50 | 0.77 | 0.04 | 10.77 | 0.994 | 3/4 | 4/4 | 17.9 | 1.7 | 2 |
| ME43-5B1 | 43 | N | | | | | | | | | | | | | |
| ME44-2B1 | 44 | Y | Perp | 40 | 5/5 | 0.38 | 0.71 | 0.14 | 1.94 | 0.944 | 0/2 | 2/2 | 20.6 | 10.6 | 3 |
| ME44-2B2 | | Y | Perp | 40 | 4/4 | 0.48 | 0.53 | 0.00 | 59.56 | 1.000 | 0/1 | 1/1 | 13.1 | 0.2 | 2 |
| ME44-2B3 | | Y | Perp | 40 | 5/7 | 0.15 | 0.59 | 0.08 | 1.09 | 0.980 | 0/3 | 3/3 | 13.3 | 12.2 | 3 |
| ME45-1B1 | 45 | N | | | | | | | | | | | | | |
| ME46-4B1 | 46 | N | | | | | | | | | | | | | |
| ME47-1A1 | 47 | Y | Perp | 40 | 0/4 | | | | | | | | | | |
| ME47-1A2 | | Y | Quasi | 30 | 0/3 | | | | | | | | | | |
| ME47-2A1 | | Y | Perp | 40 | 8/8 | 0.59 | 0.59 | 0.01 | 55.05 | 1.000 | 2/2 | 2/2 | 40.3 | 0.7 | 1 |
| ME47-2A2 | | Y | Perp | 40 | 3/3 | 0.22 | 0.03 | 0.01 | 0.10 | 0.997 | 0/0 | 0/1 | 32.9 | 313.2 | 3 |
| ME47-2A3 | | Y | Coe | 40 | 5/6 | 0.77 | 0.50 | 0.02 | 15.76 | 0.998 | 1/2 | 1/2 | 50.7 | 3.2 | 2 |
| ME47-2A4 | | Y | Coe | 20 | 6/7 | 0.62 | 0.66 | 0.06 | 7.04 | 0.986 | 2/2 | 0/2 | 37.5 | 5.3 | 2 |
| ME47-2B1 | | Y | Perp | 40 | 5/5 | 0.70 | 0.58 | 0.05 | 8.11 | 0.994 | 2/2 | 2/2 | 28.8 | 3.5 | 1 |
| ME47-3A1 | | Y | Perp | 40 | 9/9 | 0.43 | 0.74 | 0.04 | 8.01 | 0.989 | 0/3 | 0/3 | 17.9 | 2.2 | 3 |
| ME47-4A1 | | Y | Perp | 40 | 5/8 | 0.31 | 0.62 | 0.05 | 4.81 | 0.995 | 1/1 | 1/1 | 50.2 | 10.4 | 3 |
| ME47-4A2 | | Y | Perp | 40 | 11/11 | 0.75 | 0.80 | 0.02 | 36.72 | 0.998 | 4/4 | 4/4 | 53.4 | 1.6 | 1 |
| ME47-4A3 | | Y | Perp | 30 | 7/7 | 0.28 | 0.69 | 0.01 | 13.23 | 0.988 | 1/2 | 1/2 | 31.6 | 2.4 | 3 |
| ME47-4A4 | | Y | Coe | 20 | 5/5 | 0.21 | 0.64 | 0.01 | 1.91 | 0.985 | 0/2 | 0/2 | 22.4 | 11.7 | 3 |
| ME48-1B1 | 48 | Y | Perp | 40 | 11/11 | 0.79 | 0.78 | 0.01 | 72.07 | 0.994 | 4/4 | 1/4 | 34.6 | 0.5 | 2 |
| ME48-1B2 | | Y | Perp | 40 | 6/6 | 0.41 | 0.56 | 0.02 | 13.83 | 0.999 | 2/2 | 2/2 | 31.2 | 2.3 | 1 |
| ME48-1B3 | | Y | Quasi | 30 | 6/11 | 0.56 | 0.50 | 0.02 | 13.86 | 0.998 | N/A | N/A | 36.2 | 2.6 | 2 |
| ME48-1B4 | | Y | Quasi | 30 | 6/9 | 0.82 | 0.68 | 0.02 | 31.99 | 0.999 | N/A | N/A | 41.5 | 1.3 | 2 |
| ME48-2A1 | | Y | Perp | 40 | 13/14 | 0.84 | 0.77 | 0.01 | 41.20 | 0.999 | 4/5 | 1/5 | 35.4 | 0.9 | 2 |
| ME48-2A2 | | Y | Perp | 40 | 7/7 | 0.21 | 0.76 | 0.06 | 2.86 | 0.985 | 1/1 | 1/1 | 46.9 | 16.9 | 3 |
| ME48-2A3 | | Y | Coe | 40 | 7/7 | 0.39 | 0.59 | 0.03 | 7.00 | 0.995 | 3/3 | 1/3 | 24.8 | 3.5 | 3 |
| ME48-2A4 | | Y | Perp | 40 | 6/6 | 0.71 | 0.71 | 0.03 | 19.23 | 0.997 | 1/2 | 0/2 | 43.9 | 2.3 | 2 |
| ME48-2A5 | | Y | Perp | 40 | 7/17 | 0.04 | 0.81 | 0.07 | 0.51 | 0.978 | 3/3 | 1/3 | 46.1 | 89.6 | 3 |
| ME48-3A1 | | Y | Perp | 40 | 13/13 | 0.20 | 0.86 | 0.41 | 4.22 | 0.981 | 0/1 | 0/1 | 38.5 | 9.1 | 3 |
| ME48-3A2 | | Y | Perp | 40 | 9/9 | 0.76 | 0.69 | 0.02 | 22.57 | 0.996 | 1/1 | 1/1 | 47.4 | 2.1 | 2 |
| ME48-3A3 | | Y | Perp | 30 | 11/11 | 0.69 | 0.58 | 0.04 | 10.75 | 0.988 | 5/6 | 0/5 | 31.7 | 2.9 | 2 |
| ME48-4A1 | | Y | Perp | 40 | 5/6 | 0.72 | 0.39 | 0.03 | 8.00 | 0.996 | 0/1 | 0/1 | 61.7 | 7.7 | 3 |
| ME48-4A2 | | Y | Perp | 40 | 11/11 | 0.10 | 0.81 | 0.04 | 2.29 | 0.988 | 2/2 | 0/2 | 60.0 | 26.2 | 3 |

| Sample | Flow Number | Demag | Protocol | $F_{lab}$ | $n/N$ | $f$ | $g$ | $\beta$ | $q$ | $r^2$ | $pT_MRM$ Check | Tail Check | $F$ ($\mu T$) | uncert ($\mu T$) | Class |
|---|---|---|---|---|---|---|---|---|---|---|---|---|---|---|---|
| ME49-1A1 | 49 | Y | Perp | 40 | 7/7 | 0.44 | 0.71 | 0.06 | 4.94 | 0.980 | 1/3 | 2/3 | 17.9 | 3.6 | 3 |
| ME49-2B1 | | Y | Perp | 40 | 14/14 | 0.48 | 0.78 | 0.02 | 16.58 | 0.994 | 5/6 | 2/6 | 37.1 | 2.2 | 2 |
| ME49-2B2 | | Y | Coe | 40 | 5/6 | 0.14 | 0.57 | 0.11 | 0.75 | 0.964 | 1/2 | 1/2 | 16.1 | 21.4 | 3 |
| ME49-2B3 | | Y | Quasi | 30 | 6/6 | 0.91 | 0.79 | 0.06 | 12.62 | 0.987 | N/A | N/A | 53.0 | 4.2 | 2 |
| ME49-2B4 | | Y | Quasi | 30 | 7/8 | 0.95 | 0.82 | 0.03 | 27.69 | 0.996 | N/A | N/A | 42.4 | 1.5 | 2 |
| ME49-3A1 | | Y | Perp | 40 | 7/7 | 0.81 | 0.33 | 0.05 | 5.75 | 0.992 | 2/2 | 0/2 | 33.6 | 5.8 | 3 |
| ME49-3A2 | | Y | Perp | 15 | 7/7 | 0.60 | 0.47 | 0.04 | 7.06 | 0.994 | 2/2 | 1/2 | 27.6 | 3.9 | 3 |
| ME49-4A1 | | Y | Perp | 30 | 0/6 | | | | | | | | | | |
| ME49-5A1 | | Y | Perp | 30 | 15/17 | 0.47 | 0.90 | 0.03 | 14.10 | 0.988 | 4/6 | 0/6 | 14.7 | 1.0 | 3 |

Table B.1. Individual microwave palaeointensity results from the ME section, La Palma. Flow Number labels individual lava flows and is the number shown in any figure relating to palaeodirection or palaeointensity results. Flows are in stratigraphic order in ascending number from oldest to youngest (32-49). Demag indicates whether it was possible to resolve a primary component of magnetisation large enough to perform a palaeointensity experiment. Protocol is the experimental design chosen (protocols are explaned in Section 3.3): Perp is the perpendicular applied field method (Kono and Ueno, 1977; Hill and Shaw, 2007); Coe is the double heating-method of Coe (1967); Quasi is the quasi-perpendicular applied method (Biggin et al., 2007b). $F_{lab}$ is the laboratory applied field. $n/N$ is the number of accpeted NRM-$pT_MRM$ points against the total number of pNRM-$pT_MRM$ points determined from the palaeointensity experiment. $f$, $g$, $\beta$ and $q$ are Coe et al. (1978) quality statistics (see Section 3.4 for explanation of individual statistics and Section ?? for further discussion). $r^2$ is square of the correlation coefficent (discusssed in Section 3.4). $pT_MRM$ Check and Tail Check (explained in Section 3.4) columns show the number of checks that passed the selection criterion against the total number of checks relating to pNRM-$pT_MRM$ points accepted for palaeointensity determination. $F$ is the palaeointensity determination; uncert is the uncertainty of the individual palaeointensity determination using $(1/q)F$ (Coe et al., 1978); Class is explained in Section 3.4.

b

| Sample | Flow Number | Demag | Protocol | $F_{lab}$ | $n/N$ | $f$ | $g$ | $\beta$ | $q$ | $r^2$ | $pT_M RM$ Check | Tail Check | $F$ ($\mu T$) | uncert ($\mu T$) | Class |
|---|---|---|---|---|---|---|---|---|---|---|---|---|---|---|---|
| AS25-5B1 | 29 | Y | Coe | 20 | 0/12 | | | | | | | | | | |
| AS24C-4B1 | 28 | Y | Coe | 20 | 0/17 | | | | | | | | | | |
| AS24C-4B2 | | Y | Perp | 20 | 0/4 | | | | | | | | | | |
| AS24C-4B3 | | Y | Perp | 20 | 15/15 | 0.90 | 0.47 | 0.02 | 28.45 | 0.993 | 5/5 | 5/5 | 35.4 | 0.9 | 1 |
| AS24C-4B4 | | Y | Perp | 20 | 0/24 | | | | | | | | | | |
| AS24B-1A1 | 27 | Y | Coe | 20 | 0/11 | | | | | | | | | | |
| AS23-5B1 | 25 | N | | | | | | | | | | | | | |
| AS22B-2B1 | 24 | Y | Perp | 20 | 11/18 | 0.32 | 0.87 | 0.03 | 7.90 | 0.989 | 3/4 | 1/4 | 16.0 | 2.0 | 3 |
| AS22B-3B1 | | Y | Coe | 20 | 7/7 | 0.39 | 0.78 | 0.07 | 4.50 | 0.977 | 1/3 | 3/3 | 15.8 | 3.5 | 3 |
| AS22B-3B2 | | Y | Coe | 10 | 15/15 | 0.85 | 0.91 | 0.02 | 36.37 | 0.994 | 7/7 | 2/7 | 19.4 | 0.5 | 2 |
| AS22B-3B3 | | Y | Perp | 20 | 0/10 | | | | | | | | | | |
| AS22B-5B1 | | Y | Quasi | 10 | 0/17 | | | | | | | | | | |
| AS21-1B1 | 23 | Y | | | | | | | | | | | | | |
| AS20-U1 | 22 | N | | | | | | | | | | | | | |
| AS20-U5 | | N | | | | | | | | | | | | | |
| AS19B-2B1 | 21 | Y | Quasi | 1 | 0/8 | | | | | | | | | | |
| AS19-1B1 | 20 | Y | Quasi | 10 | 9/9 | 0.42 | 0.65 | 0.09 | 2.88 | 0.939 | N/A | N/A | 1.77 | 0.614 | 3 |
| AS19-1B2 | | Y | Quasi | 1 | 7/7 | 0.43 | 0.77 | 0.09 | 3.62 | 0.959 | N/A | N/A | 2.85 | 0.7864889 | 3 |
| AS19-2B1 | | Y | Quasi | 5 | 0/9 | | | | | | | | | | |
| AS19-3B1 | | N | Coe | | | | | | | | | | | | |
| AS19-3B2 | | Y | Quasi | 5 | 0/8 | | | | | | | | | | |
| AS19-4B1 | | Y | Quasi | 5 | 5/9 | 0.69 | 0.73 | 0.04 | 13.90 | 0.996 | N/A | N/A | 4.3 | 0.3 | 2 |
| AS19-5B1 | | Y | Quasi | 1 | 0/8 | | | | | | | | | | |
| AS18-B1 | 19 | Y | Coe | 10 | 0/13 | | | | | | | | | | |
| AS17-U1 | 18 | Y | Coe | 20 | 7/14 | 0.46 | 0.80 | 0.06 | 6.45 | 0.984 | 3/3 | 3/3 | 10.38 | 1.60955 | 2 |
| AS17-U2 | | Y | Perp | 10 | 0/9 | | | | | | | | | | |
| AS17-U3 | | Y | Quasi | 10 | 14/15 | 0.97 | 0.87 | 0.03 | 31.53 | 0.991 | N/A | N/A | 13.2 | 0.4 | 2 |
| AS17-1B1 | | Y | Coe | 10 | 7/13 | 0.52 | 0.78 | 0.04 | 9.14 | 0.990 | 3/4 | 4/4 | 5.75 | 0.629 | 2 |
| AS17-2A1 | | Y | Perp | 20 | 12/12 | 0.48 | 0.83 | 0.04 | 9.49 | 0.982 | 3/4 | 1/5 | 10.7 | 1.1 | 2 |
| AS16-2B1 | 16 | N | | | | | | | | | | | | | |
| AS16-4B1 | | Y | | | | | | | | | | | | | |

| Sample | Flow Number | Demag | Protocol | $F_{lab}$ | $n/N$ | $f$ | $g$ | $\beta$ | $q$ | $r^2$ | $pT_MRM$ Check | Tail Check | $F$ ($\mu T$) | uncert ($\mu T$) | Class |
|---|---|---|---|---|---|---|---|---|---|---|---|---|---|---|---|
| AS15-1B1 | 15 | Y | Coe | 20 | 0/15 | | | | | | | | | | |
| AS15-1B2 | | Y | Quasi | 10 | 13/13 | 0.74 | 0.84 | 0.06 | 9.69 | 0.955 | N/A | N/A | 7.9 | 0.8 | 3 |
| AS15-1B3 | | Y | Quasi | 5 | 7/17 | 0.66 | 0.78 | 0.04 | 12.02 | 0.990 | N/A | N/A | 14.7 | 1.2 | 2 |
| AS15-2B1 | | Y | Coe | 20 | 5/6 | 0.52 | 0.65 | 0.06 | 5.68 | 0.989 | 2/2 | 0/2 | 24.8 | 4.4 | 3 |
| AS15-3B1 | | Y | Perp | 20 | 5/6 | 0.08 | 0.66 | 0.04 | 1.14 | 0.994 | 0/2 | 0/2 | 17.9 | 15.6 | 3 |
| AS14-1B1 | 14 | Y | Coe | | 0/18 | | | | | | | | | | |
| AS14-1B2 | | Y | Coe | 20 | 10/12 | 0.45 | 0.88 | 0.08 | 5.17 | 0.953 | 5/5 | 4/5 | 11.7 | 2.3 | 3 |
| AS14-1B3 | | Y | Quasi | 10 | 6/16 | 0.26 | 0.73 | 0.08 | 2.38 | 0.975 | N/A | N/A | 14.1 | 5.9 | 3 |
| AS14-1B4 | | Y | Quasi | 10 | 7/11 | 0.28 | 0.68 | 0.08 | 2.35 | 0.967 | N/A | N/A | 15.3 | 6.5 | 3 |
| AS14-3B5 | | Y | Quasi | 5 | 9/14 | 0.58 | 0.73 | 0.02 | 19.21 | 0.997 | N/A | N/A | 4.3 | 0.2 | 2 |
| AS14-3B6 | | Y | Quasi | 5 | 5/9 | 0.23 | 0.73 | 0.08 | 2.18 | 0.982 | N/A | N/A | 27.7 | 12.7 | 3 |
| AS13-2B1 | 13 | Y | Perp | 20 | 11/11 | 0.60 | 0.81 | 0.02 | 22.72 | 0.996 | 4/4 | 2/4 | 18.1 | 0.8 | 2 |
| AS13-3B1 | | Y | Coe | 10 | 0/15 | | | | | | | | | | |
| AS13-3B2 | | Y | Coe | 20 | 0/8 | | | | | | | | | | |
| AS13-3B3 | | Y | Quasi | 10 | 6/6 | 0.23 | 0.74 | 0.03 | 5.05 | 0.994 | N/A | N/A | 3.3 | 0.6 | 3 |
| AS13-3B4 | | Y | Quasi | 10 | 9/9 | 0.73 | 0.82 | 0.02 | 31.46 | 0.997 | N/A | N/A | 2.4 | 0.1 | 2 |
| AS13-3B5 | | Y | Quasi | 10 | 9/9 | 0.87 | 0.79 | 0.04 | 15.46 | 0.986 | N/A | N/A | 2.6 | 0.2 | 2 |
| AS13-3B6 | | Y | Quasi | 10 | 11/21 | 0.45 | 0.83 | 0.08 | 4.94 | 0.949 | N/A | N/A | 21.0 | 4.3 | 3 |
| AS13-3B7 | | Y | Quasi | 10 | 7/15 | 0.54 | 0.78 | 0.04 | 10.25 | 0.992 | N/A | N/A | 4.5 | 0.4 | 2 |
| AS13-3B8 | | Y | Quasi | 10 | 14/14 | 0.75 | 0.85 | 0.04 | 15.06 | 0.979 | N/A | N/A | 4.1 | 0.3 | 3 |
| AS13-3B9 | | Y | Perp | 10 | 10/12 | 0.69 | 0.76 | 0.06 | 8.16 | 0.967 | 1/5 | 3/5 | 4.2 | 0.5 | 3 |
| AS13-3B10 | | Y | Perp | 10 | 12/20 | 0.53 | 0.79 | 0.01 | 39.61 | 0.999 | 0/0 | 0/0 | 4.6 | 0.1 | 2 |
| AS13-3B11 | | Y | Perp | 10 | 9/9 | 0.68 | 0.80 | 0.05 | 11.71 | 0.985 | 1/3 | 2/3 | 3.7 | 0.3 | 2 |
| AS13-4B1 | | Y | Coe | 20 | 12/26 | 0.48 | 0.88 | 0.03 | 14.74 | 0.991 | 4/5 | 5/5 | 6.5 | 0.4 | 2 |
| AS13-4B2 | | Y | Perp | 20 | 15/16 | 0.61 | 0.87 | 0.01 | 18.36 | 0.989 | 4/7 | 1/7 | 7.8 | 0.4 | 2 |
| AS12-2B1 | 12 | Y | Perp | 10 | 7/9 | 0.58 | 0.45 | 0.40 | 6.51 | 0.992 | 2/3 | 0/3 | 2.2 | 0.3 | 3 |
| AS12-2B2 | | Y | Perp | 5 | 10/10 | 0.53 | 0.83 | 0.02 | 19.88 | 0.996 | 2/4 | 4/4 | 2.2 | 0.1 | 2 |
| AS12-2B3 | | Y | Perp | 5 | 9/13 | 0.42 | 0.80 | 0.05 | 6.36 | 0.980 | 3/5 | 3/4 | 4.2 | 0.7 | 3 |
| AS12-2B4 | | Y | Perp | 5 | 15/15 | 0.39 | 0.85 | 0.05 | 7.27 | 0.973 | 3/7 | 2/7 | 1.1 | 0.2 | 3 |
| AS12-4B1 | | Y | Quasi | 5 | 6/10 | 0.65 | 0.77 | 0.08 | 6.44 | 0.975 | N/A | N/A | 8.5 | 1.3 | 3 |

Table B.2. Individual microwave palaeointensity results from the AS section, La Palma. Flows are in stratigraphic order in ascending number from oldest to youngest. All column headings are explained in the caption to Table B.1.

| Sample | Flow Number | Demag | Protocol | $F_{lab}$ | $n/N$ | $f$ | $g$ | $\beta$ | $q$ | $r^2$ | pTRM Check | Tail Check | $F$ ($\mu T$) | uncert ($\mu T$) | Class |
|---|---|---|---|---|---|---|---|---|---|---|---|---|---|---|---|
| AN1-1B1 | 1 | Y | Perp | 10 | 0/4 | | | | | | | | | | |
| AN1-1B2 | | Y | Perp | 15 | 10/10 | 0.54 | 0.56 | 0.11 | 2.88 | 0.912 | 1/2 | 1/2 | 2.5 | 0.9 | 3 |
| AN1-1B3 | | Y | Perp | 2 | 0/9 | | | | | | | | | | |
| AN1-2A1 | | Y | Perp | 15 | 0/3 | | | | | | | | | | |
| AN1-2A2 | | Y | Perp | 4 | 6/7 | 0.38 | 0.40 | 0.14 | 1.07 | 0.920 | 0/1 | 0/1 | 3.2 | 3.0 | 3 |
| AN1-4A1 | | Y | Perp | 5 | 0/3 | | | | | | | | | | |
| AN1-5A1 | | Y | Perp | 5 | 9/9 | 0.41 | 0.61 | 0.08 | 3.20 | 0.958 | 1/1 | 0/1 | 1.6 | 0.5 | 3 |
| AN2-1B1 | 2 | Y | Coe | 40 | 0/4 | | | | | | | | | | |
| AN2-1B2 | | Y | Perp | 10 | 6/6 | 0.63 | 0.71 | 0.02 | 20.86 | 0.998 | 1/1 | 1/2 | 7.5 | 0.4 | 2 |
| AN2-2B1 | | Y | Coe | 40 | 5/5 | 0.43 | 0.56 | 0.08 | 2.88 | 0.979 | 1/3 | 2/3 | 11.7 | 4.1 | 3 |
| AN3-1B1 | 3 | Y | Perp | 10 | 7/8 | 0.39 | 0.67 | 0.09 | 2.93 | 0.961 | 2/2 | 0/2 | 4.6 | 1.6 | 3 |
| AN3-1B2 | | Y | Perp | 10 | 13/13 | 0.60 | 0.85 | 0.03 | 19.91 | 0.993 | 3/3 | 0/3 | 3.2 | 0.2 | 2 |
| AN3-1B3 | | Y | Perp | 10 | 5/5 | 0.53 | 0.68 | 0.04 | 8.85 | 0.995 | 0/1 | 1/1 | 6.6 | 0.7 | 2 |
| AN3-2B1 | | Y | Coe | 20 | 0/4 | | | | | | | | | | |
| AN3-3B1 | | Y | Perp | 10 | 7/8 | 0.39 | 0.34 | 0.04 | 3.64 | 0.993 | 0/1 | 0/1 | 8.8 | 2.4 | 3 |
| AN3-3B2 | | Y | Perp | 10 | 8/8 | 0.38 | 0.70 | 0.04 | 6.50 | 0.990 | 1/2 | 2/2 | 11.5 | 1.8 | 2 |
| AN4-1B1 | 4 | Y | Coe | 10 | 0/6 | | | | | | | | | | |
| AN4-2B1 | | Y | Coe | 10 | 0/7 | | | | | | | | | | |
| AN4-3B1 | | Y | Perp | 10 | 0/7 | | | | | | | | | | |
| AN4-4B1 | | Y | Perp | 10 | 0/11 | | | | | | | | | | |
| AN6-1B1 | 6 | Y | Perp | 10 | 6/8 | 0.69 | 0.61 | 0.03 | 15.16 | 0.997 | 1/1 | 0/1 | 4.8 | 0.3 | 2 |
| AN7-2B1 | 7 | Y | Perp | 10 | 3/4 | 0.28 | 0.35 | 0.03 | 3.53 | 0.999 | 0/0 | 0/0 | 13.9 | 3.9 | 3 |
| AN7-3B1 | | Y | Perp | 10 | 6/6 | 0.27 | 0.45 | 0.05 | 2.57 | 0.991 | 1/1 | 0/1 | 10.7 | 4.2 | 3 |
| AN7-4B1 | | Y | Coe | 30 | 0/5 | | | | | | | | | | |
| AN7-4B2 | | Y | Quasi | 30 | 0/6 | | | | | | | | | | |
| AN8-2B1 | 8 | Y | Perp | 10 | 8/8 | 0.31 | 0.62 | 0.12 | 1.66 | 0.918 | 0/1 | 1/1 | 3.4 | 2.1 | 3 |
| AN8-2B2 | | Y | Perp | 10 | 10/10 | 0.53 | 0.56 | 0.07 | 4.13 | 0.958 | 1/2 | 0/2 | 5.1 | 1.2 | 3 |
| AN8-2B3 | | Y | Quasi | 10 | 5/5 | 0.80 | 0.74 | 0.05 | 12.66 | 0.993 | N/A | N/A | 3.7 | 0.3 | 2 |
| AN8-3B1 | | Y | Perp | 20 | 7/7 | 0.22 | 0.75 | 0.04 | 4.05 | 0.992 | 0/1 | 0/1 | 8.8 | 2.2 | 3 |
| AN9A-1B1 | 9 | Y | Perp | 10 | 10/10 | 0.77 | 0.59 | 0.02 | 22.07 | 0.997 | 0/0 | 0/0 | 21.6 | 1.0 | 2 |
| AN9A-2B1 | | Y | Perp | 10 | 9/10 | 0.19 | 0.84 | 0.04 | 4.34 | 0.990 | 0/0 | 0/0 | 24.2 | 5.6 | 3 |
| AN9A-3B1 | | Y | Perp | 20 | 9/9 | 0.39 | 0.75 | 0.04 | 8.16 | 0.991 | 0/1 | 0/1 | 26.8 | 3.3 | 2 |
| AN9A-4B1 | | Y | Perp | 20 | 15/15 | 0.40 | 0.64 | 0.02 | 10.10 | 0.992 | 0/0 | 0/0 | 18.5 | 1.8 | 2 |
| AN9B-4B1 | 10 | Y | Perp | 10 | 0/12 | | | | | | | | | | |
| AN10-1B1 | 11 | N | | | | | | | | | | | | | |
| AN10-2B1 | | N | | | | | | | | | | | | | |
| AN10-3B1 | | N | | | | | | | | | | | | | |

| Sample | Number Flow | Demag | Protocol | $F_{lab}$ | $n/N$ | $f$ | $g$ | $\beta$ | $q$ | $r^2$ | $pT_MRM$ Check | Tail Check | $F$ ($\mu T$) | uncert ($\mu T$) | Class |
|---|---|---|---|---|---|---|---|---|---|---|---|---|---|---|---|
| AN11-1B1 | 12 | Y | Perp | 10 | 3/3 | 0.73 | 0.50 | 0.09 | 4.13 | 0.992 | 1/1 | 1/1 | 31.7 | 7.7 | 3 |
| AN14-1B1 | 15 | Y | Perp | 15 | 0/13 | | | | | | | | | | |
| AN14-1B2 | | Y | Perp | 10 | 0/7 | | | | | | | | | | |
| AN14-1B3 | | Y | Quasi | 10 | 0/6 | | | | | | | | | | |
| AN14-2B1 | | Y | Perp | 8 | 10/12 | 0.81 | 0.74 | 0.04 | 15.16 | 0.988 | 0/2 | 0/2 | 6.6 | 0.4 | 2 |
| AN14-3B1 | | Y | Perp | 8 | 0/14 | | | | | | | | | | |

Table B.3. Individual microwave palaeointensity results from the AN section, La Palma. Flows are in stratigraphic order in ascending number from oldest to youngest. All column headings are explained in the caption to Table B.1

| Sample | Flow Number | Demag | Protocol | $F_{lab}$ | $n/N$ | $f$ | $g$ | $\beta$ | $q$ | $r^2$ | $pT_M RM$ Check | Tail Check | $F$ ($\mu T$) | uncert ($\mu T$) | Class |
|---|---|---|---|---|---|---|---|---|---|---|---|---|---|---|---|
| GD0102 | 1 | Y | Perp | 10 | 0/12 | | | | | | | | | | |
| GD0103 | | Y | Perp | 20 | 0/8 | | | | | | | | | | |
| GD0104 | | Y | Coe | 20 | 0/9 | | | | | | | | | | |
| GD0105 | | Y | Quasi | 10 | 8/8 | 0.43 | 0.83 | 0.03 | 13.10 | 0.995 | N/A | N/A | 25.1 | 1.9 | 2 |
| GD0106 | | Y | Quasi | 20 | 11/12 | 0.51 | 0.89 | 0.02 | 19.15 | 0.995 | N/A | N/A | 19.1 | 1.0 | 2 |
| GD0201 | | Y | Perp | 30 | 0/8 | | | | | | | | | | |
| GD0301 | | Y | Perp | 10 | 0/12 | | | | | | | | | | |
| GD0601 | | Y | Perp | 10 | 0/9 | | | | | | | | | | |
| G01A0101 | 2 | Y | Perp | 6 | 0/9 | | | | | | | | | | |
| G01A0201 | | Y | Perp | 6 | 8/10 | 0.41 | 0.71 | 0.10 | 2.89 | 0.940 | 1/2 | 0/2 | 4.2 | 1.5 | 3 |
| G01A0401 | | Y | Perp | 6 | | | | | | | | | | | |
| G01A0402 | | Y | Perp | 6 | 0/16 | | | | | | | | | | |
| G01A0501 | | Y | Perp | 10 | 9/11 | 0.37 | 0.77 | 0.04 | 7.57 | 0.990 | 0/3 | 0/3 | 6.2 | 0.8 | 3 |
| G01A0601 | | Y | Perp | 6 | 7/9 | 0.31 | 0.75 | 0.16 | 1.42 | 0.870 | 0/1 | 0/1 | 5.2 | 3.6 | 3 |
| G01A0701 | | Y | Perp | 6 | 0/10 | | | | | | | | | | |
| G01B0102 | | Y | Perp | 6 | 0/4 | | | | | | | | | | |
| G01B0201 | | Y | Perp | 6 | 6/6 | 0.20 | 0.57 | 0.05 | 2.17 | 0.989 | 0/0 | 0/0 | 7.0 | 3.2 | 3 |
| G01B0301 | | Y | Perp | 6 | 0/9 | | | | | | | | | | |
| G01B0302 | | Y | Perp | 6 | 0/9 | | | | | | | | | | |
| G01B0401 | | Y | Perp | 6 | 7/7 | 0.73 | 0.72 | 0.05 | 10.48 | 0.987 | 0/1 | 1/1 | 3.0 | 0.3 | 2 |
| G01B0402 | | Y | Perp | 6 | 0/11 | | | | | | | | | | |
| G01B0501 | | Y | Perp | 6 | 0/3 | | | | | | | | | | |
| G02A0101 | 3 | Y | Perp | 10 | 0/10 | | | | | | | | | | |
| G02A0201 | | Y | Perp | 5 | 4/5 | 0.31 | 0.33 | 0.07 | 1.48 | 0.990 | 0/0 | 0/0 | 17.2 | 11.6 | 3 |
| G02A0501 | | Y | Perp | 10 | 0/5 | | | | | | | | | | |
| G02A0701 | | Y | Perp | 20 | 0/12 | | | | | | | | | | |
| G02A0801 | | Y | Perp | 10 | 0/4 | | | | | | | | | | |
| G02A0901 | | Y | Perp | 5 | 7/7 | 0.26 | 0.75 | 0.09 | 2.26 | 0.963 | 0/1 | 0/1 | 7.8 | 3.5 | 3 |
| G02A0902 | | Y | Perp | 10 | 0/15 | | | | | | | | | | |
| G02B0101 | | Y | Perp | 10 | 4/6 | 0.17 | 0.41 | 0.04 | 1.91 | 0.996 | 0/1 | 1/1 | 16.6 | 8.7 | 3 |
| G02B0102 | | Y | Perp | 10 | 5/5 | 0.46 | 0.72 | 0.04 | 8.95 | 0.996 | 1/1 | 1/1 | 17.0 | 1.9 | 2 |
| G03A0101 | 4 | Y | Perp | 10 | 15/15 | 0.66 | 0.90 | 0.02 | 23.86 | 0.992 | 3/4 | 0/4 | 14.0 | 0.6 | 3 |
| G03A0102 | | Y | Perp | 20 | 11/11 | 0.84 | 0.81 | 0.03 | 21.56 | 0.991 | 0/3 | 0/1 | 15.4 | 0.7 | 3 |
| G03A0201 | | Y | Perp | 10 | 13/13 | 0.70 | 0.87 | 0.02 | 34.58 | 0.997 | 4/4 | 0/4 | 18.9 | 0.5 | 2 |
| G03A0301 | | Y | Perp | 15 | 0/13 | | | | | | | | | | |
| G03A0401 | | Y | Perp | 15 | 10/10 | 0.71 | 0.61 | 0.04 | 9.90 | 0.985 | 0/2 | 0/2 | 19.7 | 2.0 | 3 |
| G03A0501 | | Y | Perp | 15 | 0/10 | | | | | | | | | | |
| G03A0502 | | Y | Perp | 20 | 11/11 | 0.51 | 0.74 | 0.03 | 13.33 | 0.993 | 1/2 | 1/2 | 26.5 | 2.0 | 2 |
| G03A0601 | | Y | Perp | 15 | 8/8 | 0.44 | 0.64 | 0.04 | 6.86 | 0.990 | 2/2 | 0/2 | 15.7 | 2.3 | 2 |
| G03A0701 | | Y | Perp | 15 | 0/6 | | | | | | | | | | |
| G03A0801 | | Y | Perp | 15 | 12/12 | 0.34 | 0.80 | 0.05 | 5.90 | 0.979 | 0/1 | 0/1 | 13.2 | 2.2 | 3 |
| G03A0802 | | Y | Perp | 20 | 5/17 | 0.13 | 0.51 | 0.16 | 1.26 | 0.992 | 1/2 | 0/2 | 10.8 | 8.6 | 3 |

Table B.4. Individual microwave palaeointensity results from Guadeloupe, French West Indies. Column headings are explained in Table B.1.

# Using first-order reversal curves to assess palaeointensity variations in samples recording the Matuyama-Brunhes geomagnetic field reversal

Maxwell C. Brown [a,*], Amy P. Chen [b]

[a] *Department of Earth and Ocean Sciences, Geomagnetism Laboratory, Oliver Lodge Building, Oxford Street, University of Liverpool, Liverpool, L69 7ZE, United Kingdom*

[b] *Institute for Rock Magnetism and Department of Geology and Geophysics, University of Minnesota, Minneapolis, MN 55455, USA*

**Abstract**

First-order reversal curves have been used to investigate the magnetic properties of lava flows showing a large variation in palaeointensity. Three lava flows were studied from the island of La Palma that record the geomagnetic field immediately after the Matuyama-Brunhes reversal. All three flows have magnetic particle assemblages other than non-interacting single domain thermoremanent magnetisation carriers. Importantly, within standard 25 mm cores, both multidomain and interacting single domain particles are identified. As it is not possible to use the same piece of core for the paleointensity experiment and the first order reversal curve measurement we are unable to empirically link a particular type of magnetic particle assemblage to a particular outcome of an individual palaeointensity experiment. Nevertheless, first-order reversal curves have successfully detected a range of small scale variations and where interacting single domian particles are present, enabled us to calculate the interaction field distribution and packing fraction of the particles.

*Key words:* FORC, palaeointensity, Matuyama-Brunhes

* corresponding author
*Email address:* m.c.brown@liv.ac.uk (Maxwell C. Brown [a,]).

# 1 Introduction

Palaeointensity measurements of the Earth's magnetic field are crucial for our understanding of its behaviour through time and provide important constraints on processes within the core and at the core-mantle boundary (Kono and Roberts, 2002; Valet, 2003; Coe and Glatzmaier, 2006). In recent years, absolute palaeointensity data have been incorporated into global models of the past geomagnetic field, such as CALS7K.2 (Korte and Constable, 2005) and IMMAB4 (Leonhardt and Fabian, 2007); however, the reliability of the data is not always clear. A fundamental reason for ambiguous absolute paleointensity determination is that the thermal remanent magnetisation (TRM) of volcanic rocks is not only carried by non-interacting single-domain ferromagnetic particles; however, the Thellier-Thellier family of absolute palaeointensity methods is based on the so-called Thellier's laws of reciprocity, independence, and additivity (Thellier, 1938), which are only proven for strictly non-interacting single domain (SD) particles (Néel, 1949).

In this study we have used first-order reversal curve (FORC) diagrams to characterise possible TRM carriers in our samples and to determine whether there is a variation in these carriers on a centimetre and metre scale. FORCs (Mayergoyz, 1986) were chosen as their two-dimensional representation, as a FORC diagram (Pike et al., 1999), allows analysis of the statistical distribution of both coercivity, $H_c$, and bias field, $H_u$.

Two previous studies (Wehland et al., 2005; Carvallo et al., 2006) have attempted use FORC diagrams as a tool for pre-selection of samples for palaeointensity analysis. Both studies investigated correlations between features on Arai-Nagata plots (Nagata et al., 1963) and FORC diagrams. Carvallo et al. (2006) provided some evidence for concave-up increasing plots with more multi-domain (MD)-like FORC diagrams. We do not wish to use our results in this way, but merely to investigate if we can observe small scale variations in rock magnetic properties, which may link to variations in palaeointensity.

The samples chosen for this study are from three lava flows from the island of La Palma and belong to the volcanic section ME (Valet et al., 1998, 1999; Brown et al., 2008). These flows record the geomagnetic field after the main polarity switch of the Matuyama-Brunhes reversal. Palaeointensity experiments were originally carried out by (Valet et al., 1999) using the thermal Thellier method (Table 1), and were incorporated into the iterative Baysian model IMMAB4 of the Matuyama-Brunhes reversal (Leonhardt and Fabian, 2007).

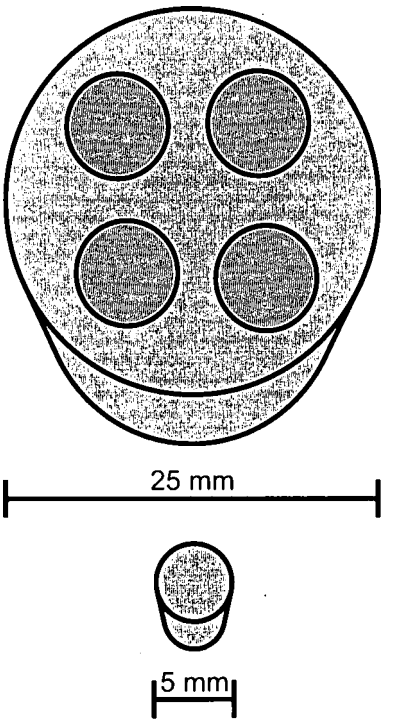


Fig. 1. Schematic of a 25 mm rock core and 5 mm subsample. Circles in 25 mm core schematic represent hole sizes after drilling and removal of subsample

## 2 Samples and Experimental Methods

### *2.1 Sample selection*

Flows ME47, ME48, and ME49, originally sampled by (Valet et al., 1999), were re-sampled in 2006 (we have retained the the original flow names). Five cores of 25 mm in diameter were collected from each of the of the lava flows. Samples were taken from the centres of the flows to avoid problems of remagnetisation by the under or overlying flows (Valet et al., 1998). These cores were sampled approximately 2 m to 3 m apart.

The microwave system requires small cylindrical samples, which are 5 mm in diameter and typically 1 mm to 3 mm in length. They are drilled from 25 mm cores (Fig. 1), so allow multiple palaeointensity estimates per core (see Table 1 for number of determinations). We used the same size samples for the rock magnetic measurements and the palaeointensity experiments and this allowed us to assess the rock magnetic variations on the same spatial scale as the palaeointensity variation.

### 2.2 *Microwave palaeointensity determination*

From January 2007, two 14 GHz microwave systems have been in operation at the Geomagnetism Laboratory, University of Liverpool: one with a liquid-nitrogen FIT SQUID magnetometer and another with a more sensitive three axis liquid-helium Tristan Technologies SQUID magnetometer (maximum sensitivity $\sim$ 1x10$^{-11}$ Am$^2$ (Shaw and Share, 2007)). Measurements were made with both systems. To address whether variations in palaeointensity were linked to the particular experimental method, three different protocols were used: the perpendicular method (Kono and Ueno, 1977; Hill and Shaw, 2007), the double-heating method (Coe, 1967) and the quasi-perpendicular method (Biggin et al., 2007b).

### 2.3 *FORC measurements*

FORC measurements were performed on 3 samples per 25 mm core from up to 5 cores per flow, and were measured using a Princeton Measurements Corporation MicroMag 2900 vibrating sample magnetometer (VSM) at the Institute for Rock Magnetism, University of Minnesota. FORC diagrams were obtained from partial hysteresis curves using a maximum field of 300 mT, with 1 mT incremental field step bewteen partial hysteresis curves and an averaging time of 100 ms. The range of $H_a$ and $H_b$ and the number of curves varied for each sample; however, as the field step used in each experiment was the same, the resolution of each diagram was also the same. This allowed a consistent comparison of FORC diagrams.

The FORC measurement starts by applying user-defined high positive field. The field is then decreased to a reversed field, $H_a$. The induced magnetisation is measured at defined fields, $H_b$, as the applied field is increased back to the user defined high positive field. A set of FORCs is obtained by repeating the process for increasing values of $H_a$. Each magnetisation measurement is denoted as $M(H_a, H_b)$, where $H_b > H_a$. The FORC distribution $\rho(H_a, H_b)$ is defined as the mixed second derivative:

$$\rho(H_a, H_b) = -\frac{1}{2}\frac{\partial^2 M(H_a, H_b)}{\partial H_a \partial H_b} \tag{1}$$

A FORC diagram is a contour plot of the FORC distribution on a transformed coordinate system: $H_c = (H_b - H_a)/2$ and $H_u = (H_b + H_a)/2$.

### *2.4 Other rock magnetic measurements*

Thermomagnetic measurements were carried out using a Magnetic Measurements variable field translation balance (VFTB) at the Geomagnetism Laboratory, University of Liverpool. Magnetisation in an applied field of 0.75 T was measured as temperature was increased from room temperature to 700°C and then allowed to cool back to room temperature. All thermomagnetic curves are corrected for their paramagnetic content, calculated from hysteresis measurements on the same sample prior to heating using the VFTB. Curie temperature is determined using the extrapolation method (Moskowitz, 1981). The titanium content of the titanomagnetite is estimated using a polynomial fit to experimental data for synthetic titanomagnetites (Bleil and Petersen, 1982). We recognise that this approach only allows rough estimates of the composition of natural titanomagnetites, with uncertainties of $\pm$ 0.1 for the mole fraction of the ülvospinel end-member. This uncertainty comes from variations in Curie temperature determined from synthetic titanomagnetites with the same apparent composition (Lattard et al., 2006).

## 3 Results

### *3.1 Microwave palaeointensity results*

Our initial palaeointensity analysis only uses one selection criterion: the straight line segment used must have a squared linear regression coefficient ($r^2$) greater than 0.98 A lenient starting criterion was chosen following the experimental results of (Biggin et al., 2007a). Their results suggest samples that have accurately recorded the recent field are not necessarily of high quality (large linear segments, with positive pTRM checks in thermal Thellier experiments), and those that are of high quality could be significantly inaccurate. Using this criterion all three flows in this study show a large variation in the palaeointensity estimates from single 25 mm cores and between cores (up to 38.3 $\mu$T for ME49) (Table 1); however, the flow means determined using the different methods are similar.

Imposing the 1st and 2nd class selection criteria of (Brown et al., 2008) has a large effect on the palaeointensity variations of all three flows (Table 1). The range of results is decreased by 22.4 $\mu$T for ME49 and 16.2 $\mu$T for ME48; however, the range still exceeds 15 $\mu$T for both flows. The range of ME47 is least affected. The most noticeable effect of applying the selection criteria is to change the mean palaeointensity estimates of the flows and to reduce their standard deviations; however, the standard deviations remain significant. The

standard deviation is 18.4% of the flow-mean for ME49, 15.6% for ME48 and 24% for ME47 (Selkin and Tauxe, 2000). Applying the criteria reduced the range of estimates from a statistical approach; however, the range of palaeointensity results is still large.

All points on Arai-Nagata plots show straight line segments covering large NRM fractions. There is no evidence for concave-up increasing behaviour (Fig. 2), which is indicative of multidomain grains in thermal Thellier experiments (Carvallo et al., 2006) . The most notable deviations from a straight line (despite having $r^2$ greater than 0.98) are concave-down increasing slopes (Fig. 2a, d, f). When experiments have failed, the Arai-Nagata plots show an exaggeration of this concave-down increasing slope. There is no biasing of estimates due to the determination protocol, with all protocols producing a variation in palaeointensity estimates.

### *3.2 Bulk rock-magnetic properties*

Samples from ME49 show a range of Curie temperatures ($T_c$) on heating (Fig. 3a), from ~466°C to ~522°C, relating to a range of titanomagnetite compositions. Using the polynomial fit to experimental data for synthetic titanomagnetites (Bleil and Petersen, 1982), compositions between ~TM18 and ~TM09 are calculated. On cooling induced magnetisation was reduced by between 2% and 9% at 100°C compared with the heating curve (Fig. 3b).

Samples from ME48 show two groups of $T_c$: one group having a $T_c$ of ~525°C and the other ~540 °C (Fig. 3c), relating to compositions between ~TM07 and ~TM09. Cooling curves show a large range in the reduction of induced magnetism when compared with the heating curves (Fig. 3d): between 5% and 45% at 100°C. s.

Samples from ME47 have the narrowest range of thermomagnetic behaviour and $T_c$ of all three flows (Fig. 3e). $T_c$ range from ~507°C to 517°C), relating to compositions between ~TM12 and ~TM10. All samples show a reduction of induced magnetism on cooling when compared with the heating curves (Fig. 3f): between 18% and 46% at 100°C.

The range of $T_c$ for ME49 is large and may result from heterogeneous deuteric oxidation. The reduction in magnetisation on cooling could result from the formation of a hematite phase due to oxidation on heating above the $T_c$ of the titanomagntite phase and towards 700°C (Böhnel et al., 2002). A small amount of hematite production could result in a reduction in induced magnetisation due to its low spontaneous magnetisation (Dunlop and Özdemir, 1997). There is no evidence for maghemitisation.

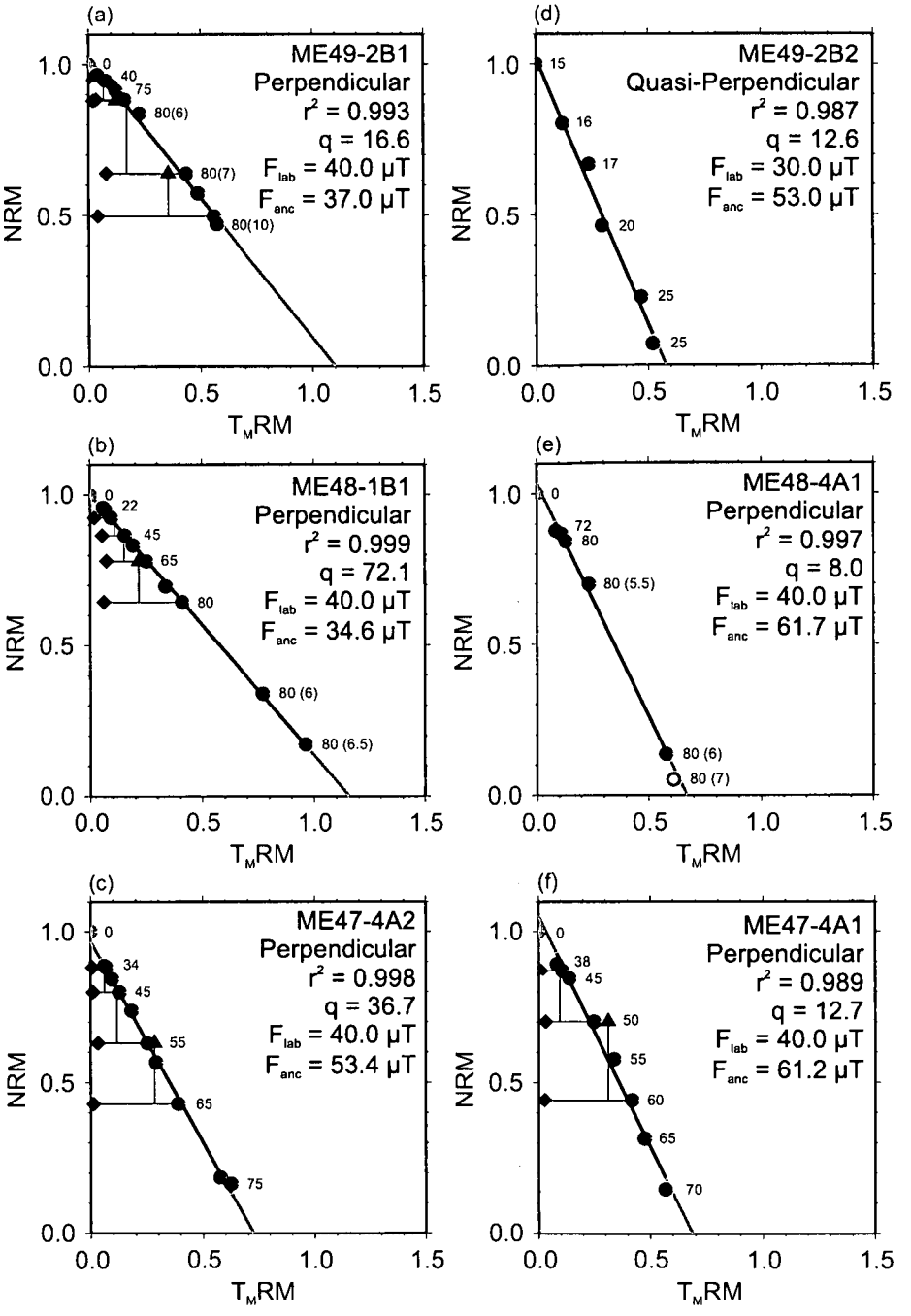


Fig. 2. Examples of Arai-Nagata plots. (a), (b), and (c), are the best quality results from each flow. (d), (e), and (f), are examples of estimates that show a large deviation from the mean palaeointensity of each flow. $r^2$ is the squared linear regression coefficient, $q$ is the quality factor as defined by (Coe et al., 1978), $F_{lab}$ is the applied field during the palaeointensity experiment, $F_{anc}$ is the palaeointensity estimate. Numbers accompanying the data points are the microwave power steps in watts. The numbers in brackets are time in seconds; where no bracketed numbers are shown, the time of application was 5 s. Example (b) uses the quasi-perpendicular method, so no $pT_MRM$ checks or tail checks were used. This experiment was performed on the Tristan 14 GHz system, which has a more efficient cavity, so the amount of power needed to de(re)magnetise the sample was much less. No pTRM checks or tail checks were performed in example (d). $T_MRM$ denotes microwave TRM.

| *Flow* | *Microwave ($\mu T$)* | *n* | *Mean ± s.d ($\mu T$)* | *Thermal-Thellier ($\mu T$)* | *n* | *Mean ± s.d ($\mu T$)* |
|---|---|---|---|---|---|---|
| | *All Estimates* | | | | | |
| ME49 | 14.7 to 53.0 (38.3) | 8 | 30.3 ± 13.8 | 30.3 to 37.4 (7.1) | 2 | 33.9 |
| ME48 | 24.8 to 61.7 (36.9) | 14 | 41.4 ± 10.5 | 42.7 to 48.5 (5.8) | 3 | 45.2 ± 3.0 |
| ME47 | 17.9 to 53.4 (35.5) | 10 | 36.6 ± 12.2 | 33.2 to 41.5 (8.3) | 3 | 37.6 ± 4.2 |
| | *Brown et al. (2008) Class 1 and 2 Selection* | | | | | |
| ME49 | 37.1 to 53.0 (15.9) | 3 | 44.2 ± 8.1 | 30.3 (0) | 1 | |
| ME48 | 31.2 to 47.4 (16.2) | 8 | 37.7 ± 5.9 | 42.7 to 48.5 (5.8) | 3 | 45.2 ± 3.0 |
| ME47 | 28.8 to 53.4 (24.6) | 5 | 42.1 ± 10.0 | 33.2 to 41.5 (8.3) | 3 | 37.6 ± 4.2 |

Table 1. Microwave (Brown et al., 2008) and Thermal-Thellier (Valet et al., 1999) palaeointensity results. *All Estimates* takes all results with a straight line portion on the Arai-Nagata plot, Brown et al. (2008) Class 1 and 2 Selection takes all estimates that pass the selection criteria of (Brown et al., 2008) (see text for explanation), $n$ is the number of palaeointensity estimates, $s.d$ is standard deviation of the palaeointensity estimates, numbers in brackets are the ranges of the palaeointensity estimates.

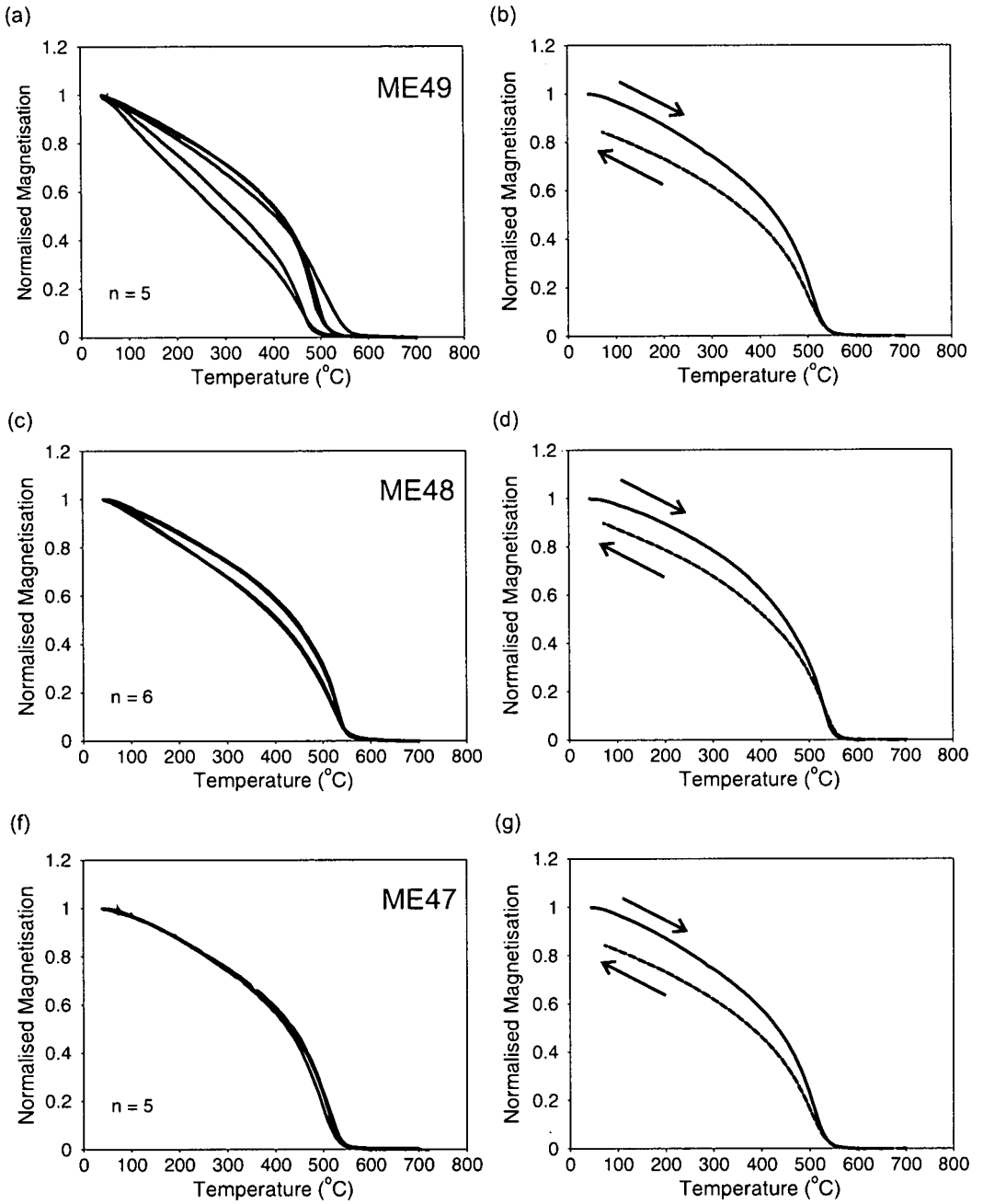


Fig. 3. Thermomagnetic heating curves for different samples from (a) ME49, (c) ME48, (e) ME47. $n$ is number of samples from each flow. An example of heating (solid line) and cooling curves (dashed line) from one sample from (b) ME49, (d) ME48, (f) ME47. Arrows indicate the direction of the temperature change.

### *3.3 FORC diagrams*

FORC distributions were calculated using the FORCLAB MATLAB code (Winklhofer and Zamanyi, 2006). Different smoothing factors were used during FORC measurement processing and are shown on Fig. 4, Fig. 5 and Fig. 6.

FORC diagrams from each flow have varying dependency of $\rho(H_c, H_u)$ on $H_c$ and $H_u$ that is manifested in a wide range of $H_c$ and $H_u$ as well as in the shape of the FORC contours. Variations of $\rho(H_c, H_u)$ are not only observed between 25 mm cores from the same flows (Fig. 6), they are also seen within 25 mm cores (Fig. 4). We have broadly classified our FORC diagrams into three types:

(1) The outermost five $\rho(H_c, H_u)$ contours meet the $H_u$ axis at a high angle (e.g. Fig. 4a and b).
(2) All contours have approximately the same width in the $H_u$ direction for all values of $H_c$ (e.g. Fig. 4c and Fig. 6).
(3) In the $H_u$ direction all contours are wider at lower $H_c$ and narrower at higher $H_c$, with the widest contours occurring at $H_c \geq 10$ mT (e.g. Fig. 5 and Fig. 6a and b).

The differences between the three types of FORC diagram result largely from variations in domain states. Type (1) FORC diagrams have previously been observed for synthetic and natural MD samples (Pike et al., 2001; Muxworthy and Dunlop, 2002). Type (2) FORC diagrams are characteristic of interacting SD particles (Egli, 2006). Type (3) has been observed for synthetic magnetite at the SD/pseudo single domain (PSD) boundary (Smirnov, 2006).

### *3.4 Distribution of interaction field and switching field of interacting SD particles*

As mentioned in section 3.3, type (2) FORC diagrams have a clear resemblance to previously observed FORC diagrams from dipolar magnetostatically interacting single-domain ferromagnetic particles. According to Egli (2006) and Chen et al. (2007), it is possible to quantitatively describe the interaction field distribution and to obtain a concentration of single domain particles by analysis of the FORC diagram based on Preisach-type formulism. Such analysis is of interest because it is the first step in accounting for the effect of dipolar magnetostatic interaction in the thermal remanence acquisition process.

For a sample consisting of homogeneous, uniaxial SD particles randomly distributed in space, its profile can be modelled using

$$g(H_u) = \frac{1}{w(H_c)} W\left(\frac{H_u - H_m}{w(H_c)}; p, \zeta\mu_s, \gamma\right) \tag{2}$$

where $\mu_s$ is the saturation magnetisation, $H_m$ is the mean interaction field, $p$ is the packing fraction, $\zeta$ is a the correction factor dependent on the switching mode, $\gamma$ is the average alignment of SD magnetic moment by the applied field,

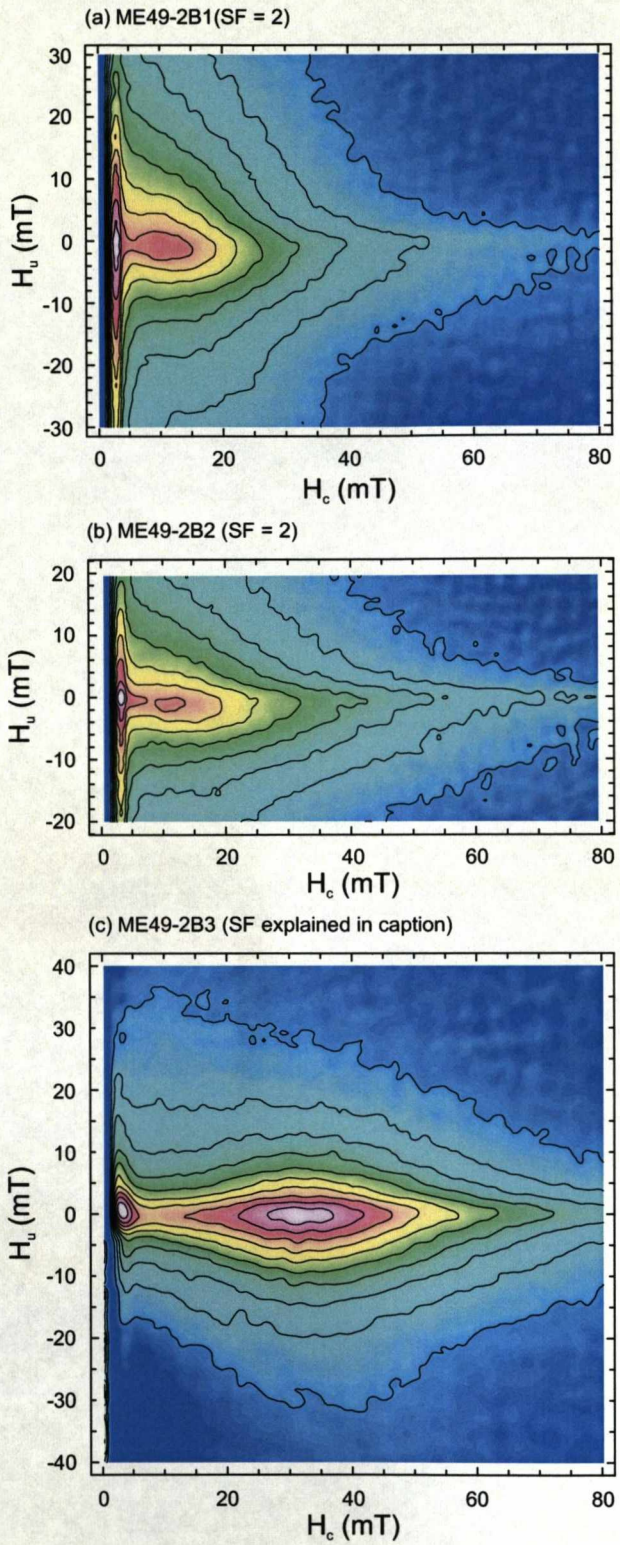


Fig. 4. FORC diagrams for three samples from the same 25 mm core from flow ME49. All $\rho(H_c, H_u)$ values are normalised to the maximum value. Ten contours are at intervals of 10% of maximum $\rho(H_c, H_u)$. (c) is a composite of four FORC diagrams covering different regions, with SF = 2 and SF = 3 for different sections.

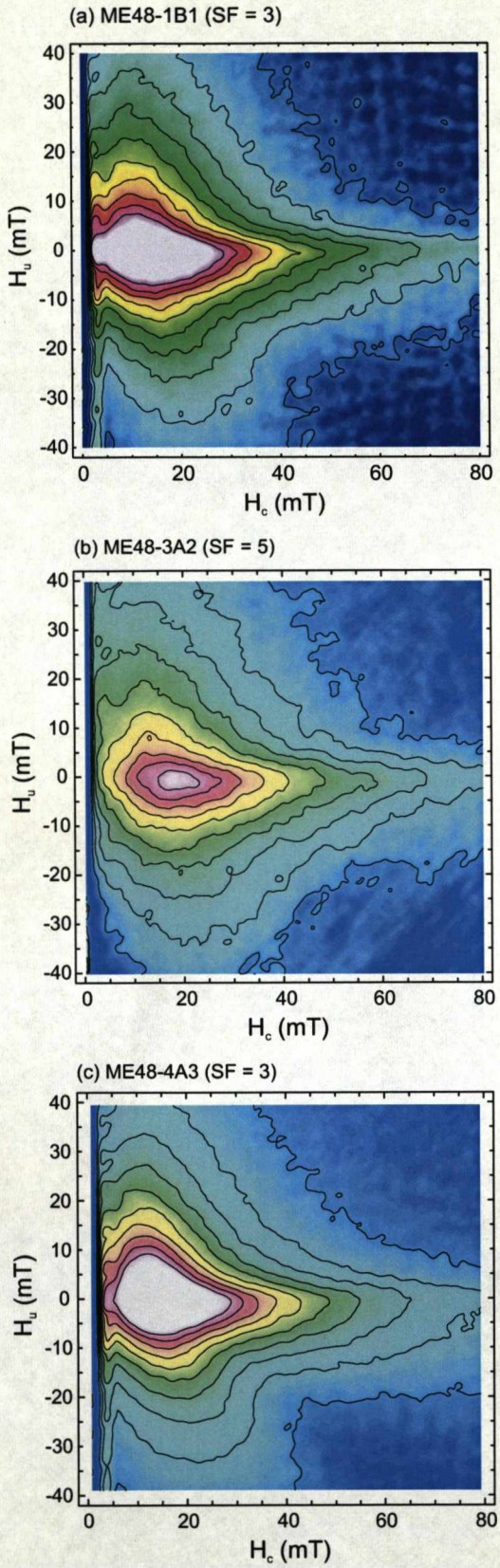


Fig. 5. FORC diagrams for three samples from different 25 mm cores from ME48. Normalisation and contouring explained in Fig. 5.

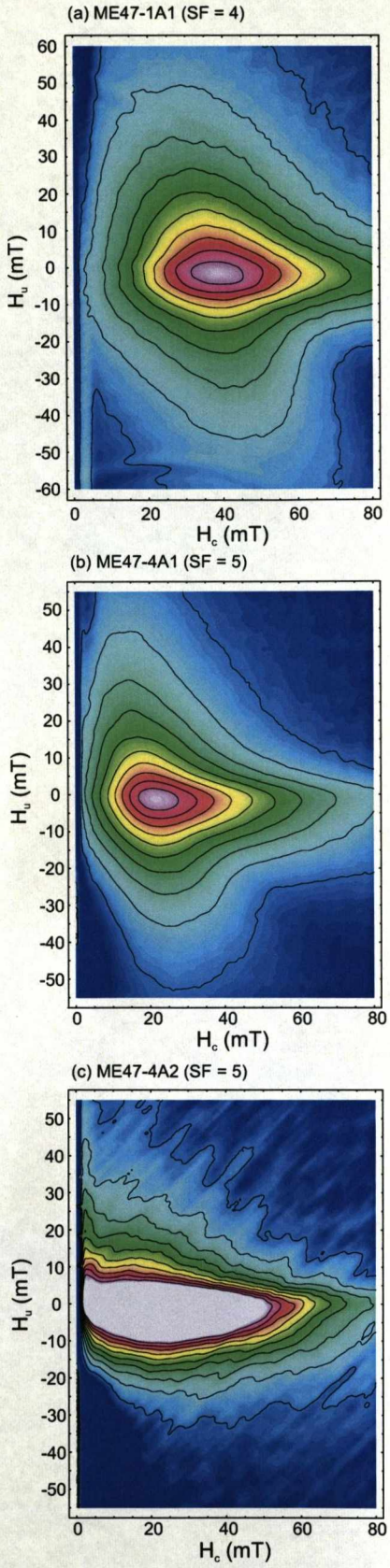


Fig. 6. FORC diagrams for three samples from different 25 mm cores from ME47. Normalisation and contouring explained in Fig. 4.

and $0 \leq w(H_c) \leq 1$ accounts for the magnetic moment that undergo reversible changes when cycled from $H_a$ and $H_b$. The function

$$W = \frac{e^{\alpha/\beta}}{\pi\beta\sqrt{1+H^2/\alpha^2}} K_1\left(\frac{\alpha}{\beta}\sqrt{1+H^2/\alpha^2}\right) \tag{3}$$

describes the statistical distribution of the interaction field, where $\alpha$ and $\beta$ are two constants that are a function of the magnetisation state, as well as $\gamma$; $K_1$ is in the form of modified Bessel function of the second kind (Egli, 2006). The model described here is constructed for a weak dipolar interaction system, where the width of the interaction field distribution is roughly less than the switching field distribution; although this model has performed well even for systems with stronger interactions (Egli, 2006). The switching field distribution is obtained by taking the marginal distribution

$$\rho(H_c) = \int_{-\infty}^{\infty} \rho(H_c, H_u) \mathrm{d}H_u \tag{4}$$

(Winklhofer and Zamanyi, 2006; Egli, 2006) and is shown in Fig. 7b and e, for ME47-4A2 and ME49-2B3, respectively. Note that both switching field distributions are asymmetric, with a peak at 20mT (for ME47-4A2) and 32mT (for ME49-4B3).

From Fig. 4c, Fig. 6c and Fig. 7b and e, the interaction field distribution is narrower than the switching field distribution for both ME47-4A2 and ME49-2B3; justifying he use of equation (2) to model the interaction field distribution. Of all the parameters needed to model $g(H_u)$ from the two FORC diagrams, we have assumed the values of the following parameters, so to optimise $p$ and $H_m$ for equation 2 without invalidating the model (as tested in both Egli (2006) and Chen et al. (2007)): $\zeta = 1.35$, $w(H_c) = 0.6$, $\gamma = 0.5$. Based on our best estimate for the composition for all flow considered (range between TM07 to TM18), we used $\mu_s = 456$ kA/m and $\mu_s = 420$ kA/m the upper and ower bounds for both samples, as $\mu_s$ is about 95% of that of $Fe_3O_4$ for $Fe_{\approx 2.93}Ti_{\approx 0.07}O_4$ and 87.5% for $Fe_{\approx 2.82}Ti_{\approx 0.18}O_4$ (Dunlop and Özdemir, 1997). The choice of $H_c$ from where $g(H_u)$ is taken is not arbitrary, rather, as shown by Egli (2006), should be as close to $H_c = 0$ as possible for as long as the normalised FORC distribution contours, defined by

$$\rho^*(H_c, H_u) = \frac{\rho(H_c, H_u)}{\max_{H_u} \rho(H_c, H_u)} \tag{5}$$

are all approximately parallel to the $H_c$ axis. Fig. 7a and d show the normalised FORC distribution as well as the location from where $g(H_u)$ profiles were

taken.

Results for ME47-4A2 are shown in Fig. 7c. Only one component is needed to model the $g(H_u)$ profile. We interpreted this sample as having one principle single-domain particle assemblage with compositions between TM07 and TM18 with packing fraction of 3.3 $\pm$ 0.5%. For ME49-2B3, two different components with distinct packing fractions (2.3 $\pm$ 0.5% and 10.9 $\pm$ 0.5 %) are needed to model the $g(H_u)$ profile. We interpret this sample to have one weakly interacting particle sub-assemblage and one strongly interacting particle sub-assemblage, both with a composition between TM07 and TM18. For both ME47-4A2 and ME49-2B3, the calculated packing fraction does not depend on the composition very strongly, with the difference between the packing fractions for the two composition end members (TM07 and TM18) well contained in the errors of the estimates

## 4 Discussion and implications

Large variations in microwave palaeointensity estimates and magnetic particle assemblages have been determined for all three flows. Importantly, both sets of variations are within 25 mm cores (see Fig. 2 and Fig. 4). Unfortunately, it is not possible to use the same samples for the FORC analyses and then for the microwave palaeointensity experiments without destroying the NRM of the samples. This means that we cannot empirically link a particular type of magnetic particle assemblage to a particular outcome of an individual Thellier type palaeointensity experiment; however, if within a sample set rock magnetic variations are present, then random sampling would result in palaeointensity experiments being performed on samples with a range of characteristics. It is a non-trivial task to relate the contribution to the FORC distribution to the contribution to the TRM. This is due to the unequal response of remanence carrying ferro-magnetic particles to the TRM process compared with the hysteresis process. Even non-remanence carrying particles can contribute to the FORC distribution.

Although the data set presented in Table 1 is small, we compare all palaeointensity estimates from the microwave and thermal Thllier techniques for ME47 and ME48. For this discussion we neglect data from ME49 as only two palaeointensity determinations were published in Valet et al. (1999). Both flows show very comparable flow mean palaeointensities when all estimates are considered; however, the range of microwave results is greater for both flows (see Table 1).

Using 25 mm cores for the thermal Thellier experiments may yield a weighted average of the samples intensity (weighted by the intensities recorded by dif-

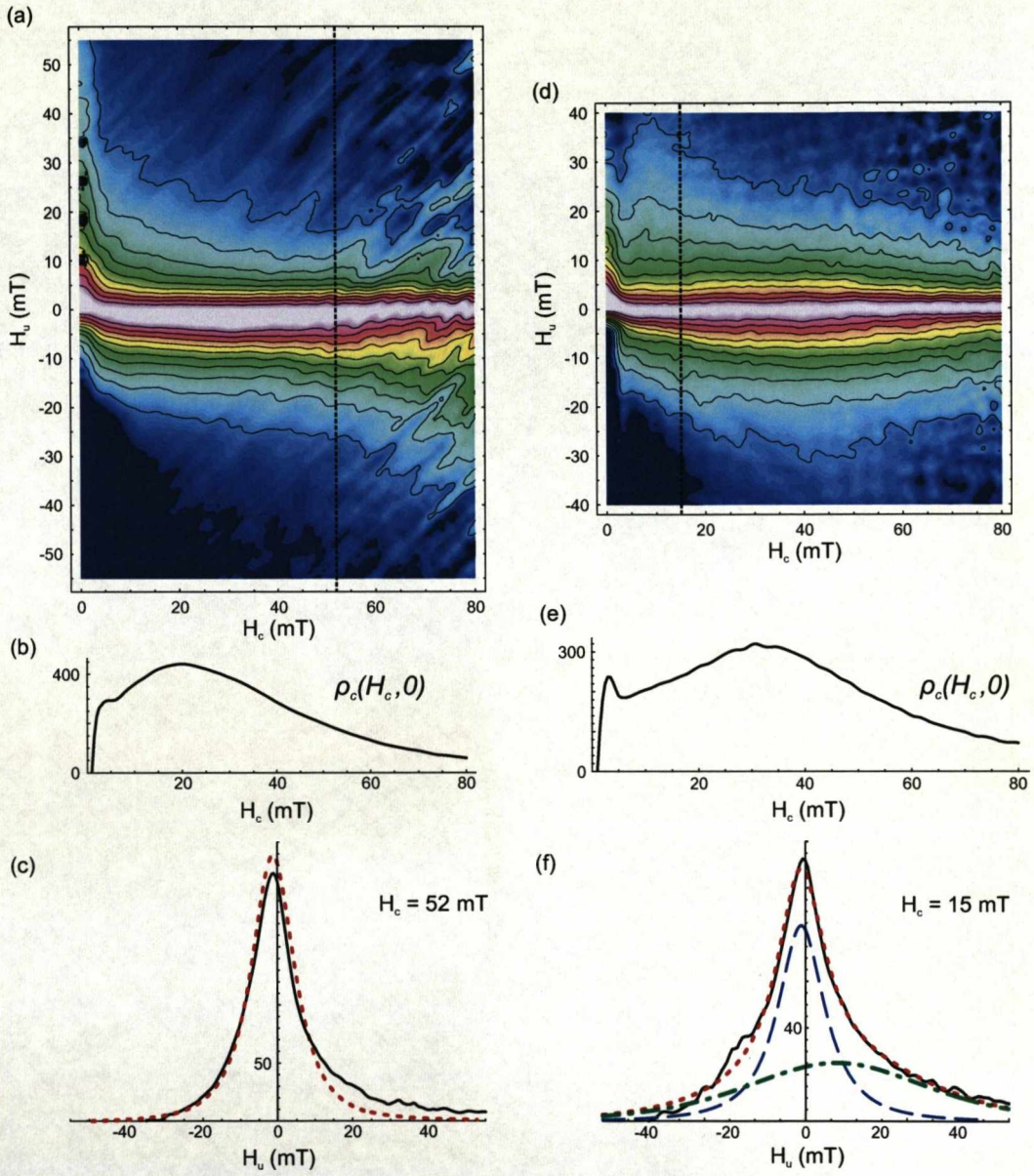


Fig. 7. Normalised FORC function defined by equation (5) for (a) ME47-4A2 and (d) ME49-2B3, dashed line indicates the location where the $H_u$ profile of the FORC function were taken. Marginal distribution for (b) ME47-4A2 and (e) ME49-2B3. $H_u$ profile (solid black line) of the FORC distribution at Profile of FORC function at (c) $H_c = 52$ mT for ME47-4A2 and (f) $H_c = 15$ mT for ME49-2B3. (c) one component (dotted red line) was used to model the profile using equation (2). (f) two components (dashed blue line and dot-dash green line) were used to model the profile using equation (2); the sum of the two component is shown is the dotted red line. For both (c) and (f), modeling assuming $\mu_s = 456$ KA/m is shown.

ferent magnetic particles). Since we have shown shown that 25 mm cores can have an inhomogeneous distrubtion of magnetic particle assemblages, using smaller samples that better represent the scale of this variation will produce a larger variation in palaeointensity within a given 25 mm core. We infer that the scale of variation in the magnetic partice assemblages is at least on the order of 5 mm spatially. This is a reflection of intrinsic differences in the samples and is not related to differences between the thermal and microwave excitation process. In other studies it has been demonstrated that thermal and microwave methods give comparable palaeointensity results and a low variation in palaeointensity (Hill and Shaw, 2000; Thomas et al., 2004; Gratton et al., 2005).

For this sample set the microwave palaeointensity technique produces results of two kinds: either Arai-Nagata plots show a straight line trend with large NRM fractions or they exhibit a concave-down increasing trend (failing when $r^2$ is too low to pass the selection criterion). The FORC diagrams show clear examples of MD dominated particle assemblages: however, the microwave technique has not produced concave-up increasing Arai-Nagata plots typical of MD contributions. Carvallo et al. (2006) found a different relationship between the MD contribution and the trend on the Arai-Nagata plot for a series of thermal Thellier experiments: the larger the MD contribution the greater the curvature in concave-up increasing trend. A possible explanation for the lack of curvature in the microwave experiments is that the microwaves may demagnetise the remanence held by the MD component at much low powers than is required to demagnetise the remanence held by the SD component. In the microwave experiment the cavity where the sample is held is tuned to a frequency at which there is minimum loss of microwave energy. This frequency is different for every experiment as the sample strongly effects the tuning frequency. During the experiment this frequency can also vary slightly and needs to be monitored, so a frequency sweep is performed before each microwave power application. To determine this optimum frequency a low amount of microwave power (1 W) is fed into the cavity, the microwave frequency is changed and the reflected power is monitored. This process takes approximately 10 s (10 joules of energy in total). The frequency at which the reflected power is a minimum is then chosen as the frequency at which the experiment will be performed at. It has been noted that the NRM for certain samples (and some samples from this study) often decreases after the very first tuning step (up to $\sim$ 10 %); however, it then requires a much greater amount of energy (microwave power and application time) to cause any further decrease in the remanence. This could relate to the coercivity distribution or, more likely, to the physical size of the grains and their relationship to ferromagnetic resonance.

For particles that are large (such as large PSD and MD magnetite particles in the $\mu$m range) microwave radiation will only penetrate to a certain depth. The skin depth (depth to 37% reduction of microwave radiation intensity) is

frequency dependent and for magnetite is about 5 $\mu$m (Griscom, 1974). For titanomagnetites, increasing Ti substitution will reduce electrical conductivity and increase skin depth (Fischer et al., 2007). If a magnetic particle is larger than the skin depth then the radio frequency (rf) field across the particle is not constant (Sparks, 1964). In this case nonzero wave-vector magnons are excited directly by the rf field (Ament and Rado, 1955) and will cause the particle to demagnetise. The samples studied here are all low Ti titanomagnetites so could have sufficiently low skin depth to be affected by this process. The way that the MD particles behave could be the same for each power step, retaining the linearity between NRM and $pT_MRM$. This is very different to how the MD component responds to thermal processes (Fabian, 2003) and highlights that our understanding of the microwave process needs considerable attention.

The results from this study suggest that large variations in rock magnetic properties can occur on the scale of a few mm. This is not only important for palaeointensity techniques that use single samples, but has implications for the multi-specimen parallel differential pTRM method (Dekkers and Böhnel, 2006). This method requires samples (usually 25 mm) that are as similar in their rock magnetic properties as possible and contain SD and large MD particle sizes over intermediate particle sizes (PSD or small MD particles) (Fabian and Leonhardt, 2007). Great care must be taken to ensure that both these conditions are fulfilled before palaeointensity estimates from non-historical flows using this method can be determined to be robust.

## 5 Conclusions

(1) All three flows have different magnetic particle assemblages and all show in-flow palaeointensity variation; they all have particles other than non-interacting single domain TRM carrieres.
(2) Both MD and interacting SD particles have been identified by FORC analyses within single 25 mm cores and in different 25 mm cores.
(3) As it is not possible to use the same 5 mm samples for the palaeointensity experiment and FORC measurement, we are unable to empirically link a particular type of magnetic particle assemblage to a particular outcome of an individual palaeointensity experiment.
(4) Nevertheless, FORC diagrams have successfully detected a range of small-scale variations and features that are not possible to determine using more standard rock magnetic analyses. Where interacting SD particles are present FORC measurements have allowed calculation of interaction field distributions and packing fractions of the particles.

Acknowledgements

MCB was funded by NERC grant NER/S/J/2004/13080 and a visiting fel-

lowship to the Institute for Rock Magnetism, University of Minnesota. The microwave instrumentation was funded by NERC grant NE/B50572X/1. The Institute for Rock Magnetism is supported by a grant from the Instruments and Facilities program, Earth Science Division, the National Science Foundation. Michael Winklhofer is thanked for providing us with the FORCLAB software. We would like to thank Yuhji Yamamoto, Mimi Hill, Neil Suttie, Ramon Egli, Valera Shcherbakov, John Shaw, Richard Holme and Mike Jackson for scientific discussion. John Share, Peat Sølheid and Brain Carter-Stiglitz are thanked for their experimental assistance.

## References

Ament, W. S., Rado, G. T., 1955. Electromagnetic effects of spin wave resonancein ferromagnetic metals. Phys. Rev. 97, 1558.

Biggin, A. J., Perrin, M., Dekkers, M. J., 2007a. A reliable absolute palaeointensity determination obtained from a non-ideal recorder. Earth Plant. Sci. Lett. 257, 545–563.

Biggin, A. J., Perrin, M., Shaw, J., 2007b. A comparison of a quasi-perpendicular method of palaeointensity determination with other thermal and microwave techniques. Earth Plant. Sci. Lett. 257, 564–581.

Bleil, U., Petersen, N., 1982. Magnetic properties of natural samples in *Numerical data and functional relationships in science and technology, Group V: Geophysics and space research*, edited by G. Angenheister. Springer, New York.

Böhnel, H., McIntosh, G., Sherwood, G., 2002. A parameter characterising the irreversibility of thermomagnetic curves. Phys. Chem. Earth 27, 1305–1309.

Brown, M. C., Gratton, M. N., Shaw, J., Holme, R., Soler, V., 2008. Microwave palaeointensity results from the Matuyama-Brunhes geomagnetic field reversal. *in prep.*

Carvallo, C., Roberts, A. P., Leonhardt, R., Laj, C., Kissel, C., Perrin, M., Camps, P., 2006. Increasing the efficiency of paleointensity analyses by selection of samples using first-order reversal curve diagrams. J. Geophys. Res. 111, B12103, doi:10.1029/2005JB004126.

Chen, A. P., Egli, R., Moskowitz, B. M., 2007. First-order reversal (FORC) diagrams of natural and cultured biogenic magnetic particles. J. Geophys. Res. 112, B08S90, doi:10,1029/2006JB004575.

Coe, R. S., 1967. Paleo-intensities of the Earth's magnetic field determined from Tertiary and Quaternary rocks. J. Geophys. Res. 72, 3247–3262.

Coe, R. S., Glatzmaier, G. A., 2006. Symmetry and stability of the geomagnetic field. Geophys. Res. Lett. 33, L21311, doi:10.1029/2006GL027903.

Coe, R. S., Grommé, S., Mankinen, E. A., 1978. Geomagnetic paleointensities from radiocarbon-dated lava flows on Hawaii and the question of the Pacific nondiple low. J. Geophys. Res. 83, 1740–1756.

Dekkers, M. J., Böhnel, H. N., 2006. Reliable absolute palaeointensities independent of magnetic domain state. Earth Plant. Sci. Lett. 248, 508–517.

Dunlop, D. J., Özdemir, O., 1997. Rock magnetism: Fundamentals and frontiers. Cambridge Univeristy Press.

Egli, R., 2006. Theoretical aspects of dipolar interactions and their appearance in first-order reversal curves of thermally activated single-domain particles. J. Geophys. Res. 111, B12S17, doi:10.1029/2006JB004567.

Fabian, K., 2003. Statistical theory of weak fieldthrmoremanenct magnetization in multidomain ensambles. Geophys. J. Int. 155, 479–488.

Fabian, K., Leonhardt, R., 2007. Testing multi specimen absolute paleointensity determination: theory and experiments (abstract). XXIV IUGG General Assembly, Perugia.

Fischer, H., Luster, J., Gehring, A. U., 2007. Epr evidence for maghemitization of magnetite in a tropical soil. Geophys. J. Int. 169, 909–916.

Gratton, M. N., Shaw, J., Herrero-Bervera, E., 2005. An absolute palaeointensity record from SOH1 lava core, Hawaii using the microwave technique. Phys. Earth Plant. Inter. 148, 193–214.

Griscom, D. L., 1974. Ferromagnetic resonance spectra of lunar fines: some implications of line shape analysis. Geochim. Cosmochim. Acta 38, 1509–1519.

Hill, M. J., Shaw, J., 2000. Magnetic field intensity study of the 1960 Kilauea lava flow, Hawaii, using the microwave palaeointensity technique. Geophys. J. Int. 142, 487–504.

Hill, M. J., Shaw, J., 2007. The use of the 'Kono perpendicular applied field method' in microwave palaeointensity experiments. Earth Planets Space 59, 711–716.

Kono, M., Roberts, P., 2002. Recent dynamo simulations and observations of the geomagnetic field. Rev. Geophys. 40, 4, doi:10/1029/2000RG000102.

Kono, M., Ueno, N., 1977. Paleointensity determination by a modified Thellier method. Phys. Earth Plant. Inter. 13, 305–314.

Korte, M., Constable, C. G., 2005. Continuous geomagnetic field models for the past 7 millenia: 2. CALS7K. Geochem. Geophys. Geosyst. 6, Q02H16, doi:10.1029/2004GC000801.

Lattard, D., Engelmann, R., Kontny, A., Sauerzapf, U., 2006. Curie tempertaures of synthetic titanomagnetites in the Fe-Ti-O system: Effects of composition, crystal chemistry, and thermomagnetic methods. J. Geophys. Res. 111, B12S28, doi:10.1029/2006JB004591.

Leonhardt, R., Fabian, K., 2007. Paleomagnetic reconstruction of the global geomagnetic field evolution during the Matuyama/Brunhes transition: iterative Bayesian inversion and independent verification. Earth Plant. Sci. Lett. 253, 172–195.

Mayergoyz, I. D., 1986. Mathematical modèls of hysteresis. Phys. Rev. Lett. 56, 1518–1561.

Moskowitz, B. M., 1981. Methods for estimating Curie temperatures of titanomaghemites from experimental Js-T data. Earth Plant. Sci. Lett. 52,

84–88.

Muxworthy, A. R., Dunlop, D., 2002. First-order reversal curve (FORC)diagrams for psuedo-single-domain magnetites at high temperature. Earth Plant. Sci. Lett. 203, 369–382.

Nagata, T., Arai, Y., Momose, K., 1963. Secular varaition of the geomagnetic force during the last 5000 years. J. Geophys. Res. 68, 5277–5281.

Néel, L., 1949. Théorie du traînage magnétique des ferromagnétiques en grains fins avec applications aux terre cuites. Ann. Géophys. 5, 99–136.

Pike, C. R., Roberts, A. P., Dekkers, M. J., Verosub, K. L., 2001. An investigation of multi-domain hysteresis mechanisms using forc diagrams. PEPI 126, 11–25.

Pike, C. R., Roberts, A. P., Verosub, K. L., 1999. Characterizing interactions in fine magnetic particl systems using first order reversal curves. J. Appl. Phys. 85, 6661–6667.

Selkin, P. A., Tauxe, L., 2000. Long-term varations in palaeointensity. Philos. Trans. R. Soc. Lond. A, 358, 1065–1088.

Shaw, J., Share, J. A., 2007. A new automated microwave demagnetiser/remagnetiser system for palaeointensity studies. Eos Trans. AGU Fall Meet. Suppl., Abstract, GP53C–1371.

Smirnov, A. V., 2006. Low temperature magnetic properties of magnetite using first-order revresal curve analysis: Implications for the pseudo-single-domain state. Geochem. Geophys. Geosyst. 7, Q11011, doi:10.1029/2006GC001397.

Sparks, M., 1964. Ferromagnetic-relaxation theory. Advanced Physics Monograph Series, McGraw-Hill Book Company.

Thellier, E., 1938. Sur l'aimantation des terres cuites et ses applications geophysiques. Ann. Inst. Globe Univ. Paris 16, 157–302.

Thomas, D. N., Hill, M. J., Garcia, A. S., 2004. Comparison of the Coe-Thellier-Thellier and microwave palaeointensity techniques using high-titanium titanomagnetites: results from a Tertiary basaltic intrusion from the Sydney Basin, New South Wales. Earth Plant. Sci. Lett. 229, 15–29.

Valet, J.-P., 2003. Time variations in geomagnetic intensity. Rev. Geophys. 41(1), 1004 doi:10/2001RG000104.

Valet, J.-P., Brassart, J., Quidelleur, X., Soler, V., Gillot, P.-Y., Hongre, L., 1999. Paleointensity variations across the last geomagnetic reversal at La Palma, Canary Islands, Spain. J. Geophys. Res. 104 (B4), 7577–7598.

Valet, J.-P., Kidane, T., Soler, V., Brassart, J., Courtillot, V., Meynadier, L., 1998. Remagnetization in lava flows recording pretransitional directions. J. Geophys. Res. 103, 9755–9775.

Wehland, F., Leonhardt, R., Vadeboin, F., Appel, E., 2005. Magnetic interaction analysis of basaltic samples and pre-selection for absolute palaeointensity measurements. Geophys. J. Int. 162, 315–320.

Winklhofer, M., Zamanyi, G. T., 2006. Extracting the intrinsic switching field distribution in perpendicular media: a comparative analysis. J. Appl. Phys. 99, O8E710.